https://ntrs.nasa.gov/search.jsp?R=19770021142 2020-03-22T07:46:23+00:00Z

NASA TECHNICAL MEMORANDUM

NASA TM X-3547

NASA TM X-3547

A COMPARISON OF THE EXPERIMENTAL AERODYNAMIC CHARACTERISTICS OF AN OBLIQUE WING WITH THOSE OF A SWEPT WING

Edward J. Hopkins and Sam C. Yee

Ames Research Center
Moffett Field, Calif. 94035

NATIONAL AERONAUTICS AND SPACE ADMINISTRATION • WASHINGTON, D. C. • JUNE 1977

1. Report No.	2. Government Accession No.	3. Recipient's Catalog No.
NASA TM X-3547		

4. Title and Subtitle	5. Report Date
A COMPARISON OF THE EXPERIMENTAL AERODYNAMIC CHARACTERISTICS OF AN OBLIQUE WING WITH THOSE OF A SWEPT WING	June 1977
	6. Performing Organization Code

7. Author(s)	8. Performing Organization Report No.
Edward J. Hopkins and Sam C. Yee*	A-6894
	10. Work Unit No.
	505-11-12
9. Performing Organization Name and Address	11. Contract or Grant No.
NASA Ames Research Center Moffett Field, California 94035	
	13. Type of Report and Period Covered
12. Sponsoring Agency Name and Address	Technical Memorandum
National Aeronautics and Space Administration Washington, D. C. 20546	14. Sponsoring Agency Code

15. Supplementary Notes

*Project Engineer, ARO, Inc., Moffett Field, Calif. 94035.

16. Abstract

Force and moment characteristics were measured for two trapezoidal oblique wings and a conventional swept wing mounted on a body of revolution at Mach numbers from 0.25 to 2.0. Both oblique wings had the same planform, but differed in profile and flexibility. One of the oblique wings was made of solid steel and had a maximum thickness-to-chord ratio of 4 percent. The other wing was built up by taking an aluminum wing (having a geometrically similar profile and planform to that of the steel wing) and adding epoxy material to the upper surface to increase the maximum thickness-to-chord ratio to 8.2 percent. The aspect ratio for both oblique wings when swept 45°, and for the swept wing with 45° of sweep was 4.1. Data were obtained at unit Reynolds numbers ranging from 3.3 to 8.2 million per meter in order to vary the dynamic pressure and to explore any flexibility effects. These data were compared with previously obtained data (ref. 5) on the aluminum wing before it was built up with epoxy.

Wing flexibility designed into the aluminum and built-up aluminum oblique wings increased the range of lift coefficients from 0.30 to 0.70 over which the pitching-moment curves were linear. However, flexibility did not improve the linearity of the rolling-moment curves and produced sizable side forces. At a Mach number of 0.95, the trapezoidal oblique wing had little or no improvement in the lift/drag ratios over those for a conventional swept wing of the same aspect ratio, sweep, and profile, probably because of the thinness of the wing profile. Thicker, highly cambered profiles previously investigated on oblique wings showed considerable improvement in the maximum lift/drag ratios over those for a conventional swept wing with the same profiles throughout a Mach number range from 0.6 to 1.2.

17. Key Words (Suggested by Author(s))	18. Distribution Statement
Oblique wing Swept wing Wing flexibility Wing flow separation	Unlimited STAR Category – 02

19. Security Classif. (of this report)	20. Security Classif. (of this page)	21. No. of Pages	22. Price*
Unclassified	Unclassified	474	$11.50

*For sale by the National Technical Information Service, Springfield, Virginia 22161

NOMENCLATURE

The axes systems and sign conventions are presented in figure 1. Lift, drag, and pitching moments are presented about the stability axes system; and the side force, rolling moments, and yawing moments are presented about the body axes system. Reference lengths and wing area are given in table 1.

A	aspect ratio
b	wing span ($\Lambda = 45°$)
C_L	lift coefficient, $\frac{\text{lift}}{qS}$
C_m	pitching-moment coefficient about moment center shown in figures 2(a) and 3(a), $\frac{\text{pitching moment}}{qS\bar{c}}$
C_n	yawing-moment coefficient, $\frac{\text{yawing moment}}{qSb}$
C_y	side-force coefficient, $\frac{\text{side force}}{qS}$
c	wing chord ($\Lambda = 0°$)
c_{root}	wing root chord ($\Lambda = 0°$)
$\bar{c}$	wing mean aerodynamic chord
C_D	drag coefficient, $\frac{\text{drag}}{qS}$
C_ℓ	rolling-moment coefficient, $\frac{\text{rolling moment}}{qSb}$
$\frac{L}{D}$	lift-to-drag ratio
M	Mach number
q, Q	free-stream dynamic pressure, N/m^2
r	body radius
$\frac{RN}{L}$	unit Reynolds number in millions per meter
S	wing area
$\left(\frac{t}{c}\right)_{max}$	maximum wing thickness-to-chord ratio

Preceding Page Blank

x	chordwise distance along airfoil
x_1	axial distance along body from the 57.45 cm longitudinal station
x_2, y_1, y_2	coordinates to define the wing tip (see figs. 2(b) and 3(b))
z	vertical distance from the chord plane of the airfoil
α	angle of attack, deg
Λ	sweep angle between a perpendicular to the body axis and the 0.25c line of the wing measured in a horizontal plane (right wing tip is forward for for positive (Λ's), deg

A COMPARISON OF THE EXPERIMENTAL AERODYNAMIC CHARACTERISTICS OF AN OBLIQUE WING WITH THOSE OF A SWEPT WING

Edward J. Hopkins and Sam C. Yee*

Ames Research Center

SUMMARY

Force and moment characteristics were measured for two trapezoidal oblique wings and a conventional swept wing mounted on a body of revolution at Mach numbers from 0.25 to 2.0. Both oblique wings had the same planform, but differed in profile and flexibility. One of the oblique wings was made of solid steel and had a maximum thickness-to-chord ratio of 4 percent. The other wing was built up by taking an aluminum wing (having a geometrically similar profile and planform to that of the steel wing) and adding epoxy material to the upper surface to increase the maximum thickness-to-chord ratio to 8.2 percent. The aspect ratio for both oblique wings when swept 45°, and for the swept wing with 45° of sweep was 4.1. Data were obtained at unit Reynolds numbers ranging from 3.3 to 8.2 million per meter in order to vary the dynamic pressure and to explore any flexibility effects. These data were compared with previously obtained data (ref. 5) on the aluminum wing before it was built up with epoxy.

Wing flexibility designed into the aluminum and built-up aluminum oblique wings increased the range of lift coefficients from 0.30 to 0.70 over which the pitching-moment curves were linear. However, flexibility did not improve the linearity of the rolling-moment curves and produced sizable side forces. At a Mach number of 0.95, the trapezoidal oblique wing had little or no improvement in the lift/drag ratios over those for a conventional swept wing of the same aspect ratio, sweep, and profile, probably because of the thinness of the wing profile. Thicker, highly cambered profiles previously investigated on oblique wings showed considerable improvement in the maximum lift/drag ratios over those for a conventional swept wing with the same profiles throughout a Mach number range from 0.6 to 1.2.

INTRODUCTION

An oblique wing for highly maneuverable aircraft, was investigated (refs. 1 and 2) as a possible means of improving both the maximum lift-to-drag ratios at transonic Mach numbers (with the wing swept), and the landing characteristics (with the wing unswept). At the high lift required for such aircraft, however, oblique wings incur asymmetric spanwise stalling resulting in nonlinear pitching-, rolling-, and yawing-moment curves. Several possible solutions to this problem were investigated: (a) fixed upward bending of the wing panels (refs. 2 and 3); (b) Krüger nose flaps (ref. 4); and (c) designed flexibility to give variable upward bending of the wing panels (ref. 5).

---

*Project Engineer, ARO, Inc., Moffett Field, Calif. 94035.

To obtain the desired flexibility (ref. 5), an oblique wing was made of solid aluminum with a maximum thickness-to-chord ratio of only 4 percent. It was found that at the design flow conditions, this aluminum wing had nearly linear moment curves indicating that as a result of wing flexibility, the wing was "self-relieving." However, because of the thinness of the profile, it is suspected that flow separation probably occurred near the wing leading edge at a low lift coefficient. In an attempt to alleviate this problem in the present investigation, the maximum thickness of the profile was approximately doubled and the leading-edge thickness was increased considerably more than double by reshaping the upper surface after an epoxy material was added. Wing flexibility was expected to be nearly the same as for the thin wing because of the low value of the modulus of elasticity for the added material.

In contrast to the elliptical wing planform used in references 1 through 4, the flexible aluminum wings tested in the present investigation had straight leading and trailing edges, and wing spans that were 15 percent greater than those for the ellipitcal wing previously tested. The planform of these flexible wings approximated the planform given by R. T. Jones (ref. 6) which specifies the optimum planform for minimum induced drag for a given lift and root bending moment. However, for these specified conditions (with the wing span as a free variable), the optimum planform is not elliptical.

The present experimental investigation was undertaken to study further the effects of wing flexibility on the forces and moments of oblique wings, and to compare the aerodynamic efficiency of such wings at transonic Mach numbers with that of a conventional swept wing having a maximum thickness of 4 percent chord. With the two oblique wings swept 45°, both wings have an aspect ratio of 4.1. The unit Reynolds number was varied from 3.3 to 8.2 million per meter in order to measure the effect of flexibility resulting from dynamic-pressure changes on the linearity of the moment curves. Results for the aluminum and the built-up aluminum oblique wings, and for the steel oblique wing are compared throughout the Mach number range from 0.25 to 2.0.

CONFIGURATION CODE

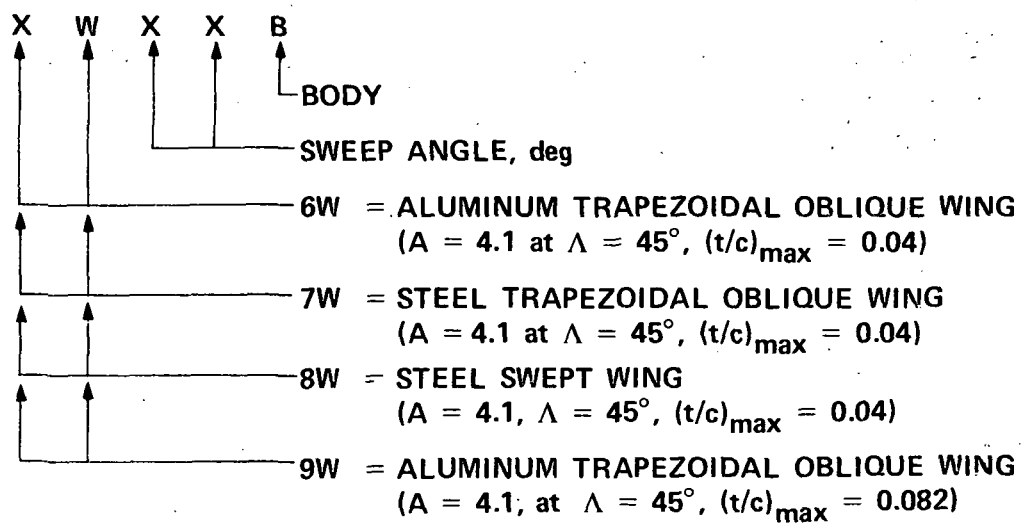

TEST FACILITY

The Ames 6- by 6-Foot Wind Tunnel is a variable pressure, continuous flow, closed return-type facility. The nozzle ahead of the test section consists of an asymmetric sliding block which permits a continuous variation of Mach number from 0.25 to 2.3. The test section has a perforated floor and ceiling for boundary-layer removal to permit transonic testing.

MODEL DESCRIPTION

The model consisted of a Sears-Haack body of revolution (designed to have minimum wave drag for a given length and volume) on which three different wings were mounted. Two of the three wings were trapezoidal which could be mounted on the body at different sweep angles. The third wing was a conventional swept wing having 45° of sweepback.

With different fairing blocks installed under the wings, the model could accommodate the oblique wings swept 0°, 45°, 50°, 55°, and 60° or the conventional swept wing as indicated in figures 2(a) and 3(a), respectively. Dimensional details of the body and the fairing blocks are given in table 3 of reference 1. The oblique wings had an aspect ratio of 7.9 ($\Lambda = 0°$) or 4.1 ($\Lambda = 45°$) and straight leading and trailing edges with modified elliptical wing tips as shown in figure 2(b). The swept wing had an aspect ratio of 4.1, its 0.25 chordline swept 45° and straight leading and trailing edges with modified elliptical tips as shown in figure 3(b). One oblique wing and the swept wing were made of stainless steel, had the NACA 65A204 profile perpendicular to their 0.25-chordlines, and had the same planform area. The other oblique wing was built up by taking an aluminum wing (geometrically similar in planform and thickness to that of the steel oblique wing) and adding epoxy material to the upper surface to make the maximum thickness-to-chord ratio 8.2 percent. This modified profile was developed on the Jameson-Hicks-Vanderplaats optimization program to be "shock free" at a Mach number of 0.6 and an angle of attack of 0°. The modified profile is compared with the NACA 65A204 in figure 4. This aluminum oblique wing with a modified profile was expected to have the same flexibility as the thin aluminum oblique wing investigated in reference 5, because the modulus of elasticity of the epoxy material is less than one-tenth that of aluminum. To prevent flaking of the epoxy material (fig. 5), slots (0.0635 cm in width) were cut in the epoxy material at various spanwise stations. Coordinates for the NACA 65A204 and the modified profile are presented in tables 2 and 3, respectively. The oblique wings had the same straight-edged planforms that approximated the R. T. Jones optimum planform (with curved edges) for a given area and root bending moment. The wing span was 15 percent greater than the wing span of the elliptical wing of references 1 and 2 in accordance with the Jones' concept of reference 6.

DATA REDUCTION AND TEST PROCEDURE

The model was sting supported through its base on a six-component electrical strain-gage balance as shown in figures 6 and 7. Measured drag forces were corrected to a condition corresponding to having the free-stream static pressure on the base of the model. Moment data are presented about moment centers located as shown in figures 2(a) and 3(a), $0.4c_{root}$ ($\Lambda = 0°$) for the oblique

wing and $0.25\bar{c}$ for the swept wing. Reference lengths and the wing area used in the reduction of the data are given in table 1.

Boundary-layer transition strips (0.1905 cm wide), consisting of random distribution of glass spheres 0.01905 cm in diameter, were placed on the upper and lower surface of the wing 0.762 cm downstream of the wing leading edge and on the body 2.54 cm behind its tip. Sublimation studies made on the elliptical oblique wing (ref. 1) at wing sweep angles of 0° and 45° indicate that the boundary layer was tripped near the transition strips at $\alpha = 0°$ and 10°. Estimates based on the size of the glass spheres required to cause transition at other sweep angles and Mach numbers in reference 1 indicate that the size chosen in the present investigation should be adequate.

Data were obtained for both the oblique wing and the swept wing at Mach numbers of 0.25, 0.4, 0.6, 0.8, 0.9, 0.95, 1.1, 1.2, 1.6, and 2.0. At each Mach number, the model was tested at unit Reynolds numbers ranging from 3.3×10^6/m to 8.2×10^6/m and throughout an angle-of-attack range of −3° to 22°. Angle of attack was indicated by an electrical dangleometer mounted in the model support strut located downstream of the sting. Corrections were applied to the indicated angle of attack for balance and sting deflections.

RESULTS AND DISCUSSION

Force and moment coefficients are presented for each of the wing-body combinations at each of the test Mach numbers. Table 4 shows the index of the figures for the various configurations. Results for the aluminum oblique wing with the modified NACA 65A204 profile are presented in figures 8 through 48, and the results for the steel oblique wing with the NACA 65A204 profile are presented in figures 49 through 89. Results for the steel swept wing with the NACA 65A204 profile are presented in figures 90 through 98. Finally, at a Mach number of 0.95 and a sweep angle of 45°, a comparison of the results for all of the above wings and the aluminum oblique wing with the NACA 65A204 profile (previously investigated in ref. 5) is presented in figure 99.

A comparison of the pitching-moment data for the aluminum oblique wings (with either profile) with that for the steel oblique wing is shown in figure 99(c). For the steel oblique wing, the pitching-moment curves were linear up to a $C_L \cong 0.3$ while the pitching-moment curves for the aluminum wings were linear up to a $C_L \cong 0.7$, indicating that wing flexibility increases the range of lift coefficients over which the pitching moment curves are linear. For reasonable center-of-gravity locations, the swept wing exhibited the usual "pitch-up" tendencies above a $C_L \cong 0.4$. Wing flexibility, which had a very small effect in linearizing the rolling-moment curves, produced sizable side forces as shown in figure 99(e). It is interesting to note that the oblique wing (7W45B) with the thinner wing profile had only a slightly higher maximum lift/drag ratio than the swept wing (8W45B), and that the lift/drag ratios for the thicker oblique wing (9W45B) were only superior to the swept wing (8W45B) between lift coefficients of about 0.4 and 0.6 as shown in figure 99(d). This result is different from the result shown previously in reference 2 for the elliptical wings for which the oblique wing configuration had considerably higher maximum lift/drag ratios than the conventional swept wing at all Mach numbers. This difference in result is believed related to the difference in the airfoils for the two investigations, the elliptical wings having a highly cambered thick airfoil ($(t/c)_{max} \cong 0.10$ along the wing span) and the trapezoidal wings having the thin NACA 65A204 airfoil with practically no camber. Therefore, it must be concluded that to provide

maximum aerodynamic efficiency, the oblique-wing concept has application primarily to wings designed with relatively thick and cambered airfoils.

Ames Research Center
National Aeronautics and Space Administration
Moffett Field, Calif. 94035, January 25, 1977

REFERENCES

1. Hopkins, Edward J.; Meriwether, Frank D.; and Pena, Douglas F.: Experimental Aerodynamic Characteristics of Low Aspect Ratio Swept and Oblique Wings at Mach Numbers Between 0.6 and 1.4. NASA TM X-62,317, 1973.

2. Hopkins, Edward J.; and Levin, Alan D.: Study of Low Aspect Ratio Swept and Oblique Wings. J. Aircraft, vol. 12, no. 8, August 1975, pp. 648–652.

3. Hopkins, Edward J.: Effects of Wing Bend on the Aerodynamic Characteristics of a Low Aspect Ratio Oblique Wing. AIAA Preprint 75-995, AIAA 1975 Aircraft Systems and Technology Meeting, Los Angeles, Calif., August 4–7, 1975.

4. Hopkins, Edward J.; and Lovette, George H.: Effect of Krüger Nose Flaps on the Experimental Force and Moment Characteristics of an Oblique Wing. NASA TM X-3372, 1976.

5. Hopkins, Edward J.; and Yee, Sam C.: Effect of Wing Flexibility on the Experimental Aerodynamic Characteristics of an Oblique Wing. NASA TM X-3460, 1977.

6. Jones, Robert T.: The Spanwise Distribution of Lift for Minimum Induced Drag of Wings Having a Given Lift and a Given Bending Moment. NACA TN-2249, 1950.

TABLE 1.– MODEL GEOMETRY, REFERENCE LENGTHS AND AREAS

Body	
Radius	$r = 3.856\{1 - [1 - (2x_1/114.91)]^2\}^{3/4}$ cm
Length	
Closed	114.91 cm
Cutoff	91.44 cm
Maximum diameter	7.71 cm
Straight-tapered oblique wings	
Span ($\Lambda = 0°$)	104.08 cm
Span (reference), b	74.80 cm
Area (reference) S	1365.09 cm^2
Mean aerodynamic chord (reference), c	21.62 cm
Aspect ratio ($\Lambda = 0°$)	7.9
Aspect ratio ($\Lambda = 45°$)	4.1
Root chord	22.51 cm
Tip chord (projected)	3.81 cm
Taper ratio	0.169
Incidence relative to body centerline	0°
Profiles perpendicular to the 0.25c line	NACA 65A204 or modified NACA 65A204 (see tables 2 and 3 and fig. 4)
Straight-tapered swept wing	
Span (reference), b	74.80 cm
Area (reference), S	1365.09 cm^2
Mean aerodynamic chord (reference), $\bar{c}$	21.62 cm
Aspect ratio	4.1
Root chord	31.83 cm
Tip chord (projected)	4.67 cm
Taper ratio	0.147
Incidence relative to body centerline	0°
Profile perpendicular to 0.25c line	NACA 65A204 (see table 2 and fig. 4)

TABLE 2.– COORDINATES FOR THE NACA 65A204 PROFILE

x/c	z/c	x/c	z/c
0	0	0	0
.00040	.00111	.00060	−.00096
.00086	.00160	.00114	−.00132
.00133	.00198	.00167	−.00158
.00180	.00231	.00220	−.00180
.00228	.00211	.00272	−.00199
.00276	.00287	.00324	−.00215
.00324	.00312	.00376	−.00229
.00421	.00356	.00479	−.00253
.00519	.00395	.00581	−.00273
.00617	.00431	.00683	−.00291
.00716	.00464	.00784	−.00306
.00815	.00496	.00885	−.00320
.00914	.00525	.00986	−.00333
.01013	.00554	.01087	−.00345
.01112	.00581	.01188	−.00356
.01212	.00607	.01288	−.00366
.01958	.00776	.02042	−.00423
.02456	.00871	.02544	−.00449
.02955	.00956	.03045	−.00469
.03454	.01033	.03546	−.00484
.03953	.01106	.04047	−.00497
.04453	.01174	.04547	−.00508
.04952	.01241	.05048	−.00519
.05452	.01305	.05548	−.00531
.05951	.01369	.06049	−.00542
.06451	.01431	.06549	−.00554
.06951	.01491	.07049	−.00566
.07450	.01549	.07550	−.00577
.07950	.01606	.08050	−.00587
.08450	.01660	.08550	−.00597
.08950	.01713	.09050	−.00605
.09450	.01764	.09550	−.00614
.09950	.01814	.10050	−.00622
.14952	.02243	.15048	−.00682
.19956	.02579	.20044	−.00719
.24961	.02841	.25039	−.00738
.29968	.03041	.30033	−.00744
.34975	.03185	.35026	−.00737
.39982	.03275	.40018	−.00717
.44990	.03309	.45010	−.00680
.49998	.03282	.50002	−.00622
.55005	.03193	.54995	−.00541
.60012	.03043	.59988	−.00440
.65019	.02839	.64981	−.00329
.70024	.02583	.69976	−.00217
.75029	.02273	.75971	−.00113
.80035	.01903	.79965	−.00034
.85034	.01453	.84966	−.00010
.90024	.00983	.89976	−.00002
.95012	.00491	.94988	−.00001
1.00000	.00000	1.00000	.00000

TABLE 3.– COORDINATES FOR THE MODIFIED NACA 65A204 PROFILE

x/c	z/c	x/c	z/c
0	0	0	0
.00040	.00449	.00060	−.00096
.00080	.00578	.00114	−.00132
.00100	.00632	.00167	−.00158
.00200	.00839	.00220	−.00180
.00300	.00995	.00272	−.00199
.00400	.01123	.00376	−.00229
.00500	.01232	.00479	−.00253
.01000	.01661	.00986	−.00333
.02000	.02259	.02042	−.00423
.03000	.02702	.03045	−.00469
.04000	.03076	.04047	−.00497
.05000	.03409	.05048	−.00519
.06000	.03713	.06049	−.00542
.07000	.03993	.07049	−.00566
.08000	.04252	.08050	−.00587
.10000	.04715	.10050	−.00622
.15000	.05664	.15048	−.00682
.20000	.06403	.20044	−.00719
.25000	.06983	.25039	−.00738
.30000	.07434	.30033	−.00744
.35000	.07774	.35026	−.00737
.40000	.08005	.40018	−.00717
.45000	.08137	.45010	−.00680
.50000	.08165	.50002	−.00622
.55000	.08087	.54995	−.00541
.60000	.07887	.59988	−.00440
.65000	.07547	.64981	−.00329
.70000	.07037	.69976	−.00217
.75000	.06259	.75971	−.00113
.80000	.05178	.79965	−.00034
.85000	.03925	.84966	−.00010
.90000	.02536	.89976	−.00002
.95000	.01126	.94988	−.00001
1.00000	.00000	1.00000	.00000

TABLE 4.– INDEX OF DATA FIGURES

Mach number, M	Sweep, Λ, deg	Wing configuration	Figure
0.4 – 2.0	45	Aluminum oblique, modified NACA 65A204 profile	8 – 16
.4 – 2.0	50	Aluminum oblique, modified NACA 65A204 profile	17 – 25
.4 – 2.0	55	Aluminum oblique, modified NACA 65A204 profile	26 – 34
.4 – 2.0	60	Aluminum oblique, modified NACA 65A204 profile	35 – 43
.4 – .95	0	Aluminum oblique, modified NACA 65A204 profile	44 – 48
.4 – 2.0	45	Steel oblique, NACA 65A204 profile	49 – 57
.4 – 2.0	50	Steel oblique, NACA 65A204 profile	58 – 66
.4 – 2.0	55	Steel oblique, NACA 65A204 profile	67 – 75
.4 – 2.0	60	Steel oblique, NACA 65A204 profile	76 – 84
.4 – .95	0	Steel oblique, NACA 65A204 profile	85 – 89
.4 – 2.0	45	Steel swept, NACA 65A204 profile	90 – 98
.95	45	a. Aluminum oblique, NACA 65A204 profile. b. Aluminum oblique, modified NACA 65A204 profile c. Steel oblique, NACA 65A204 profile d. Steel swept, NACA 65A204 profile	99

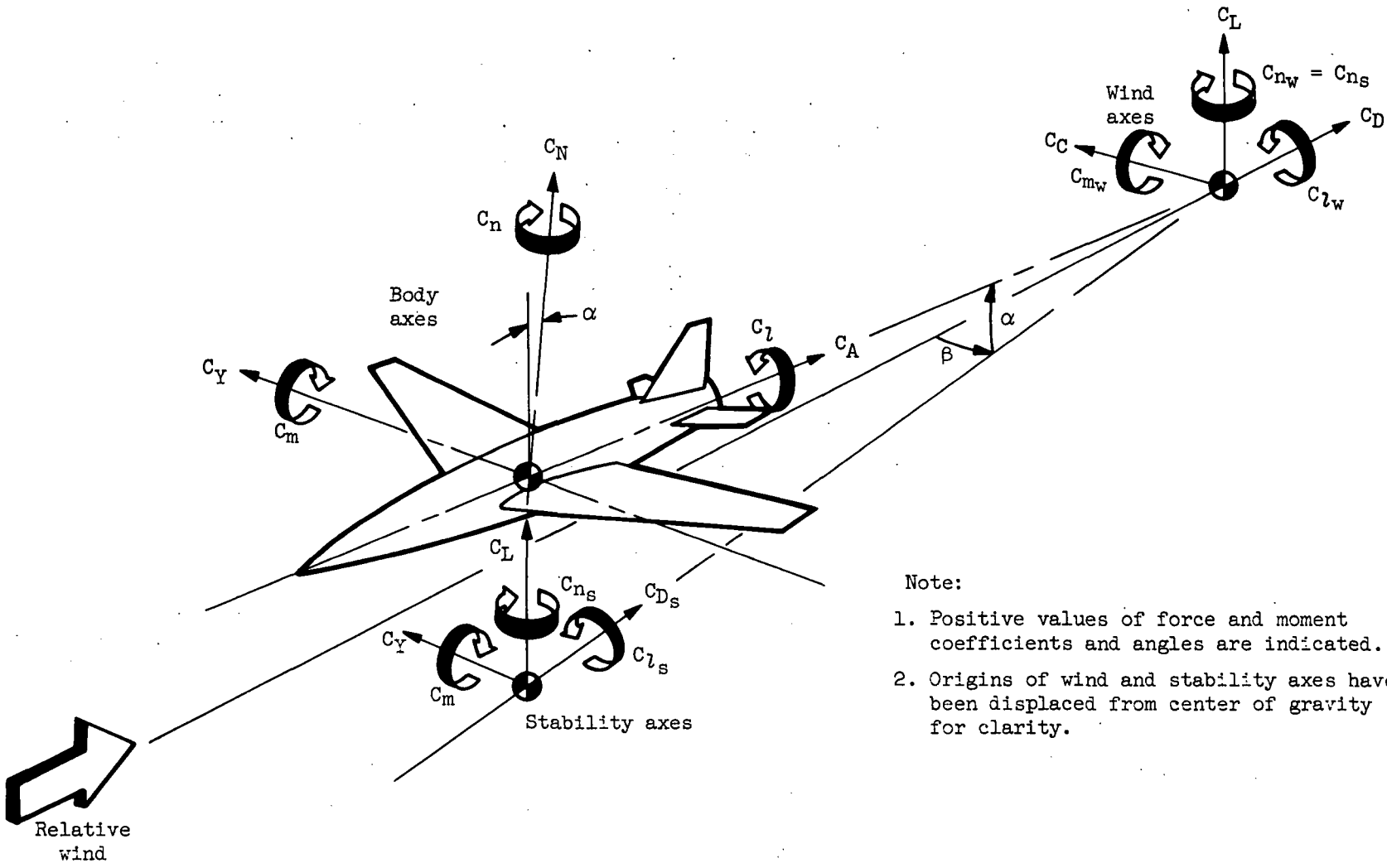

Figure 1.– Axes systems.

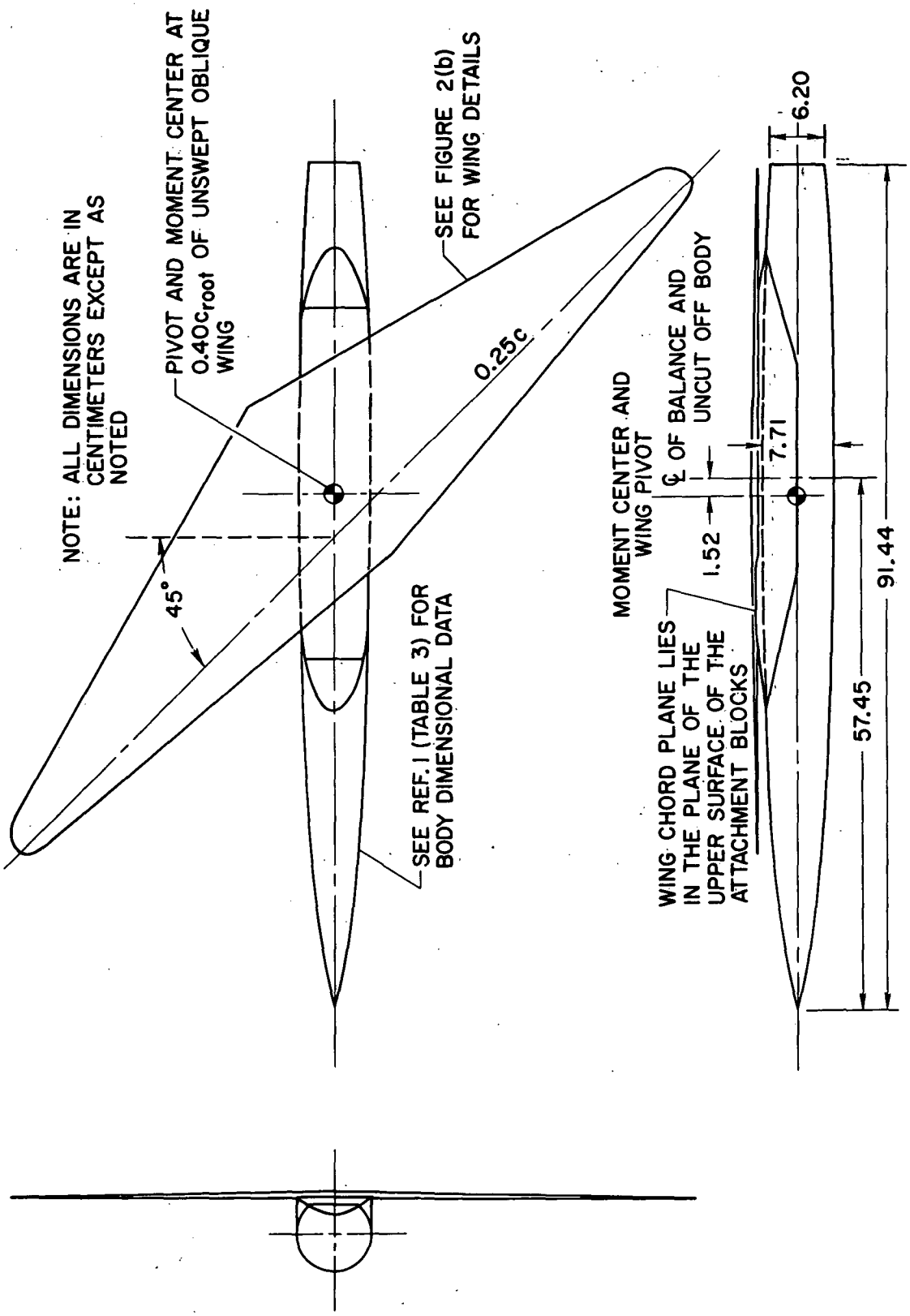

(a) Wing mounted on top of body.

Figure 2.– Straight-tapered oblique wing and body details.

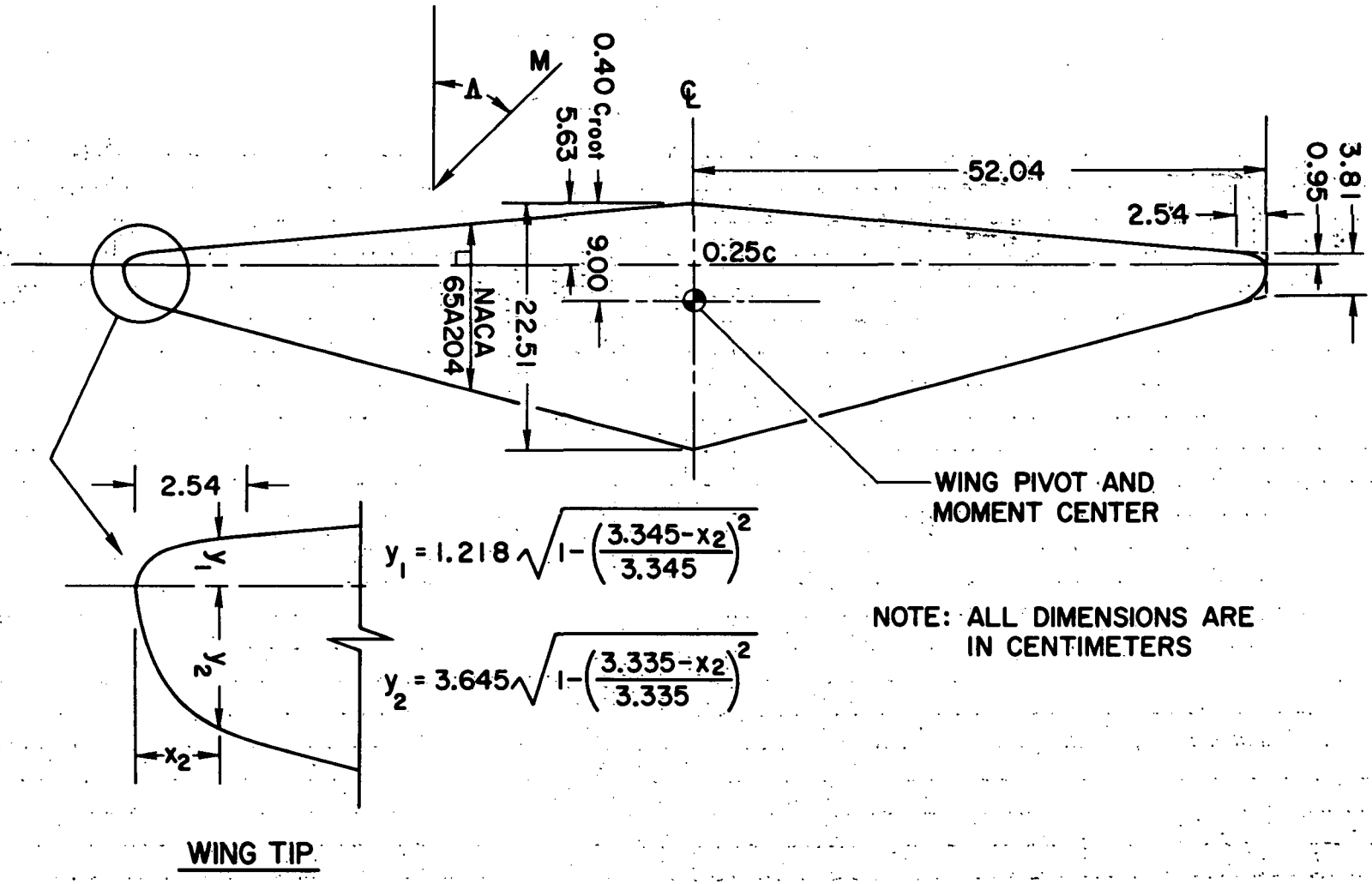

(b) Wing planform.

Figure 2.– Concluded.

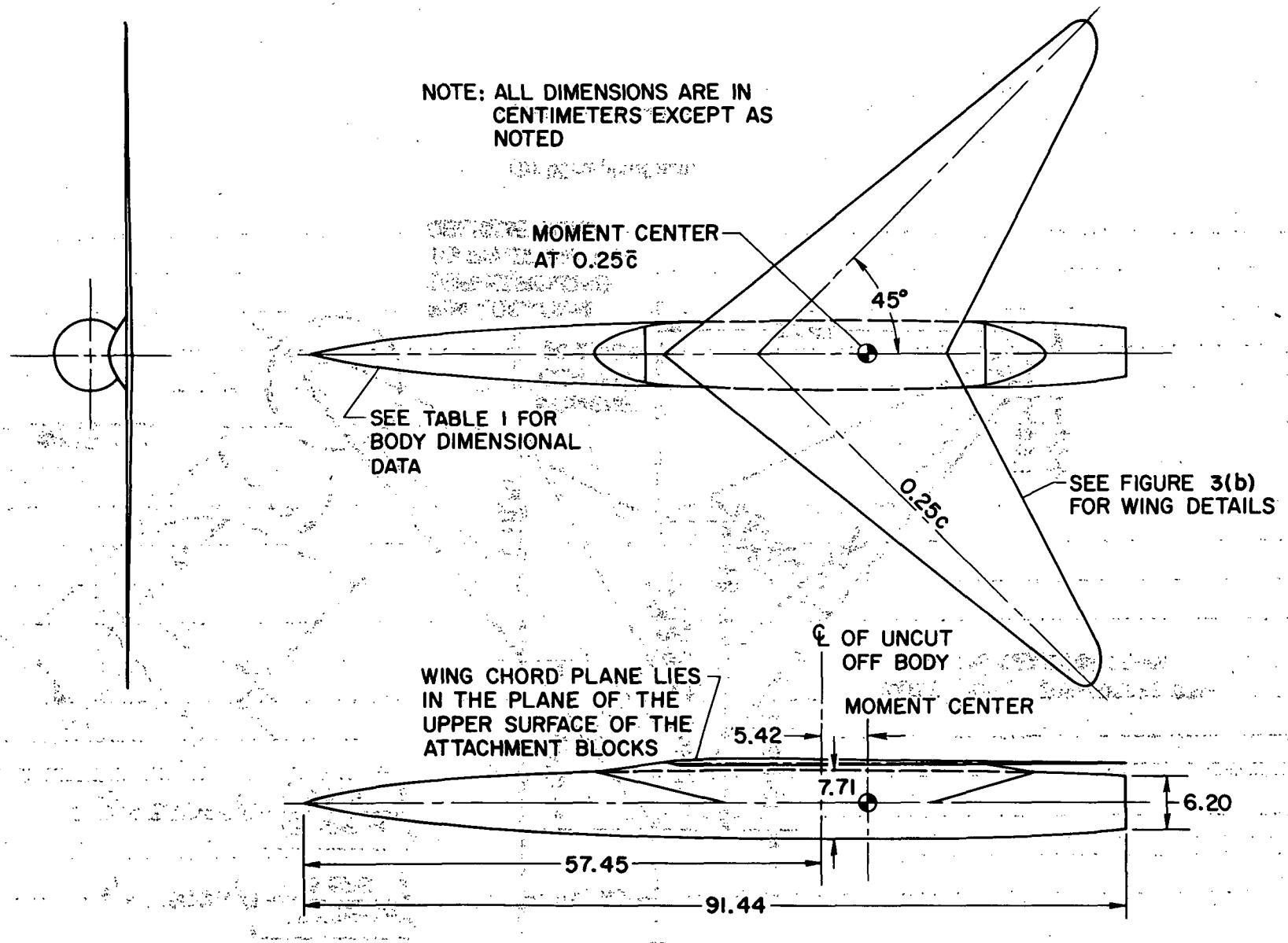

(a) Wing mounted on top of body.

Figure 3.– Swept wing and body details.

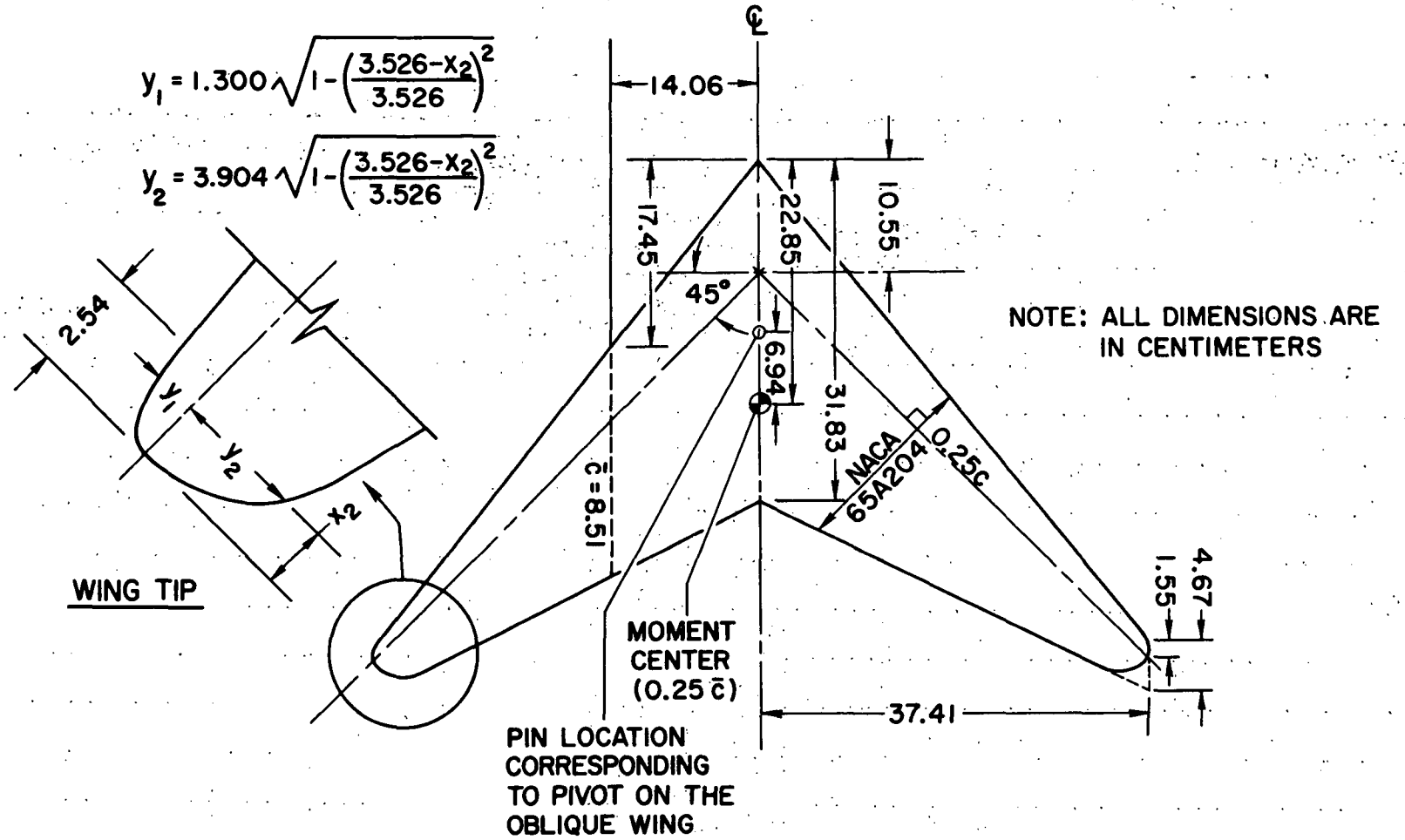

(b) Wing planform.

Figure 3.– Concluded.

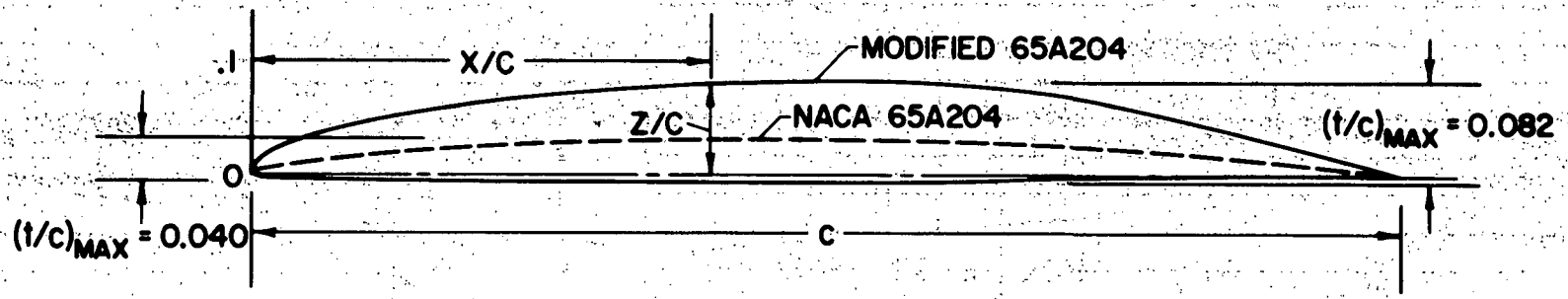

Figure 4.– Comparison between the NACA 65A204 and the modified NACA 65A204 profiles.

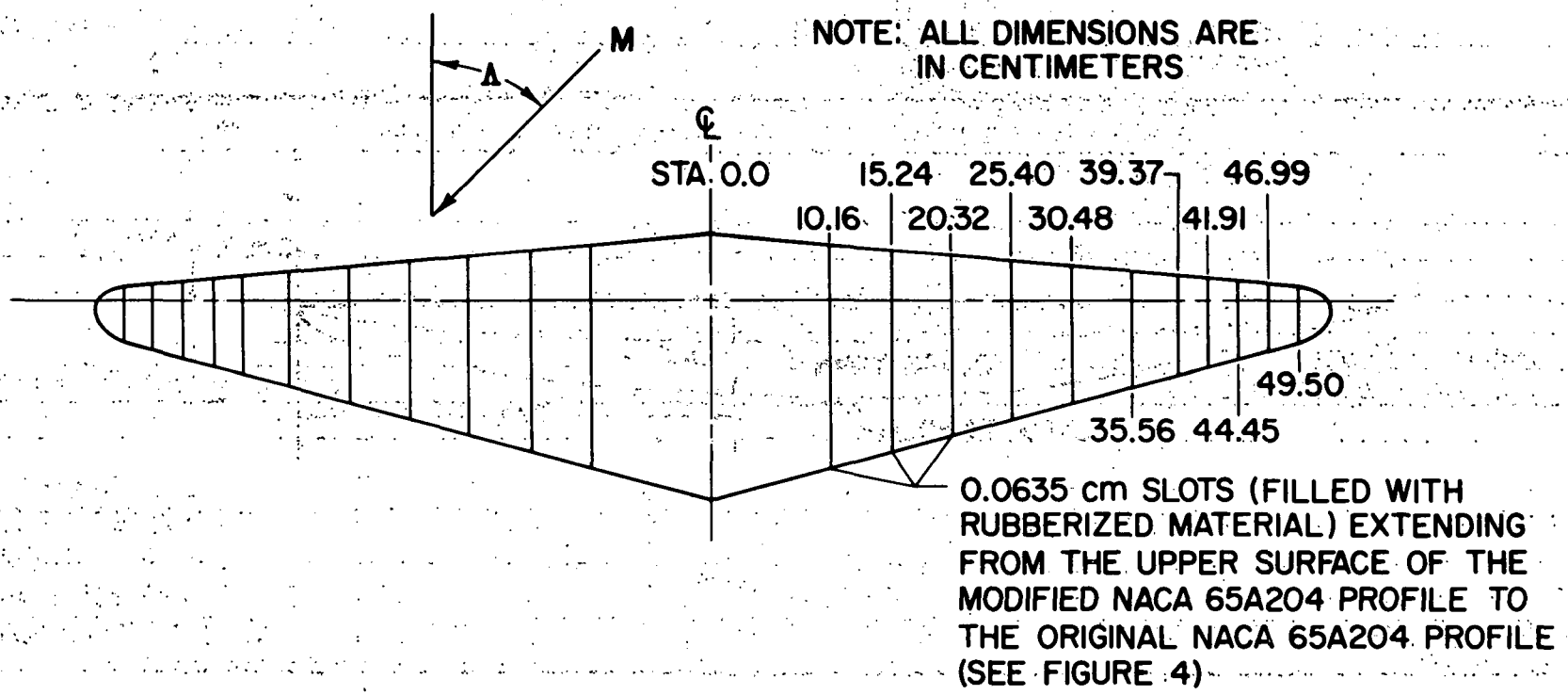

Figure 5.— Slot details for the oblique wing with the modified NACA 65A204 profile.

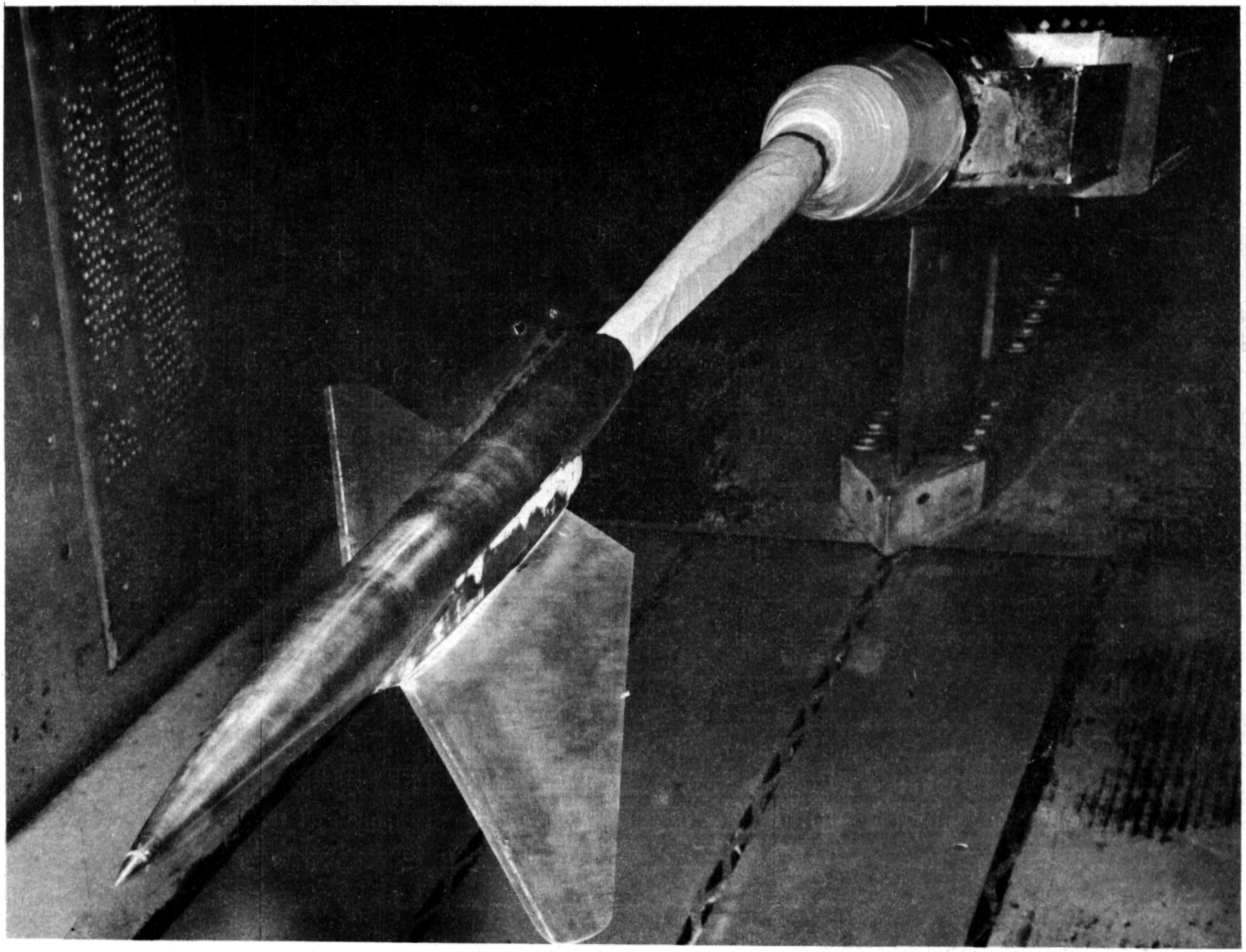

Figure 6.– Photograph of the oblique wing ($\Lambda = 45°$) mounted on top of the body of revolution (model is pitched in the $+\alpha$ direction toward the test section floor).

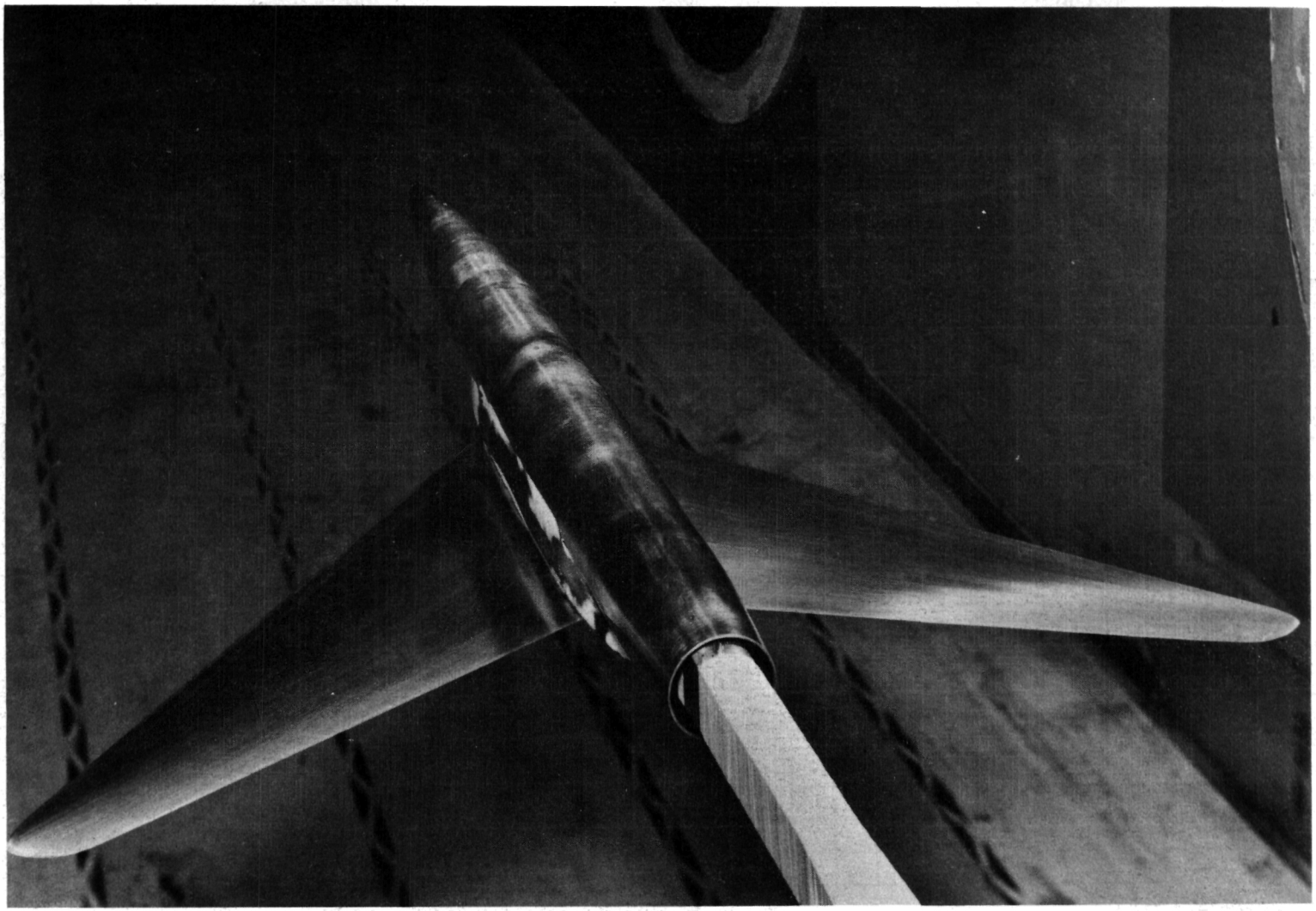

Figure 7.– Photograph of the swept wing with 45° of sweep mounted on top of the body of revolution.

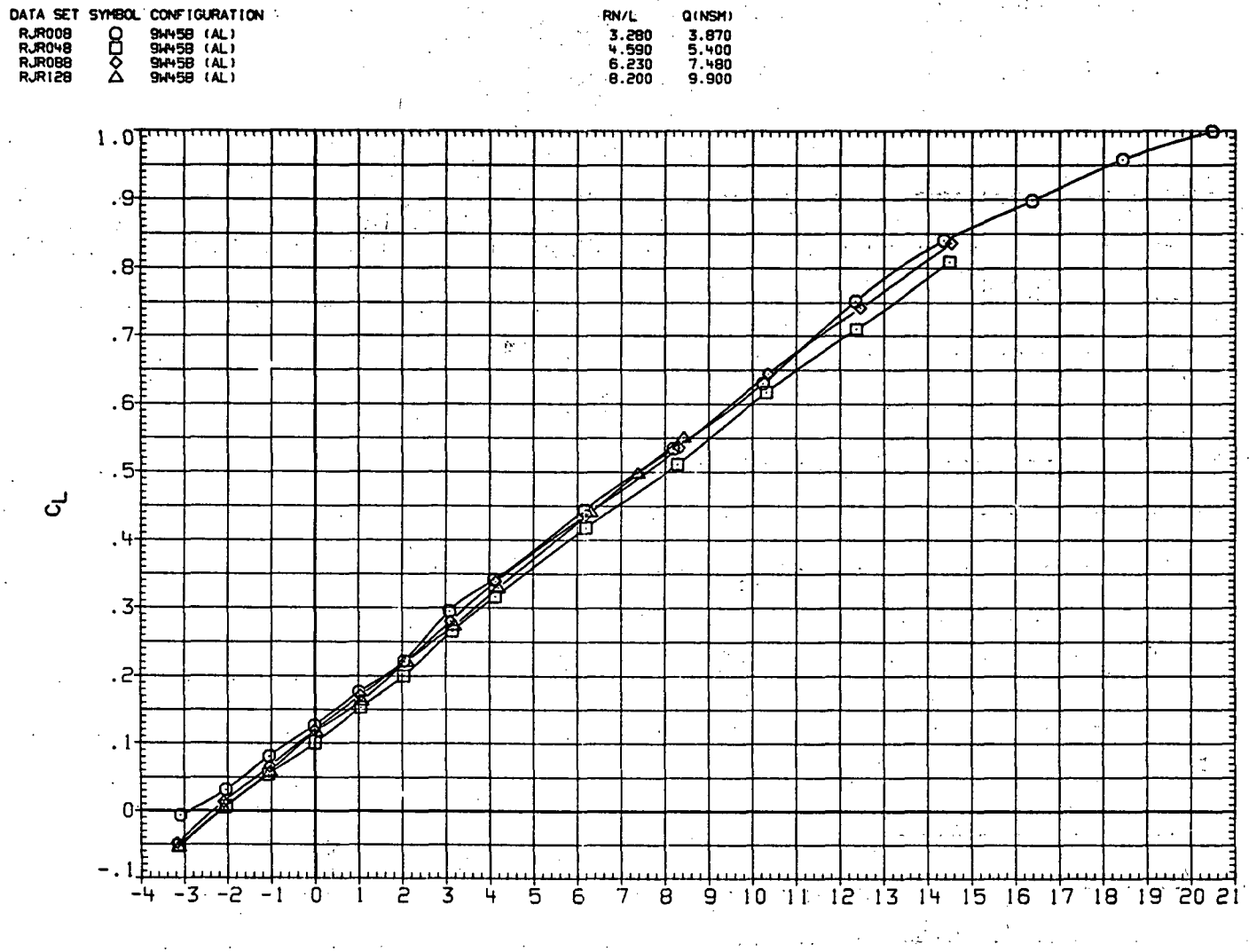

(a) C_L vs α.

Figure 8.– Dynamic-pressure effects on the aerodynamic characteristics of the aluminum trapezoidal oblique wing-body combination ($\Lambda = 45°$, $M = 0.4$ and the modified NACA 65A204 airfoil).

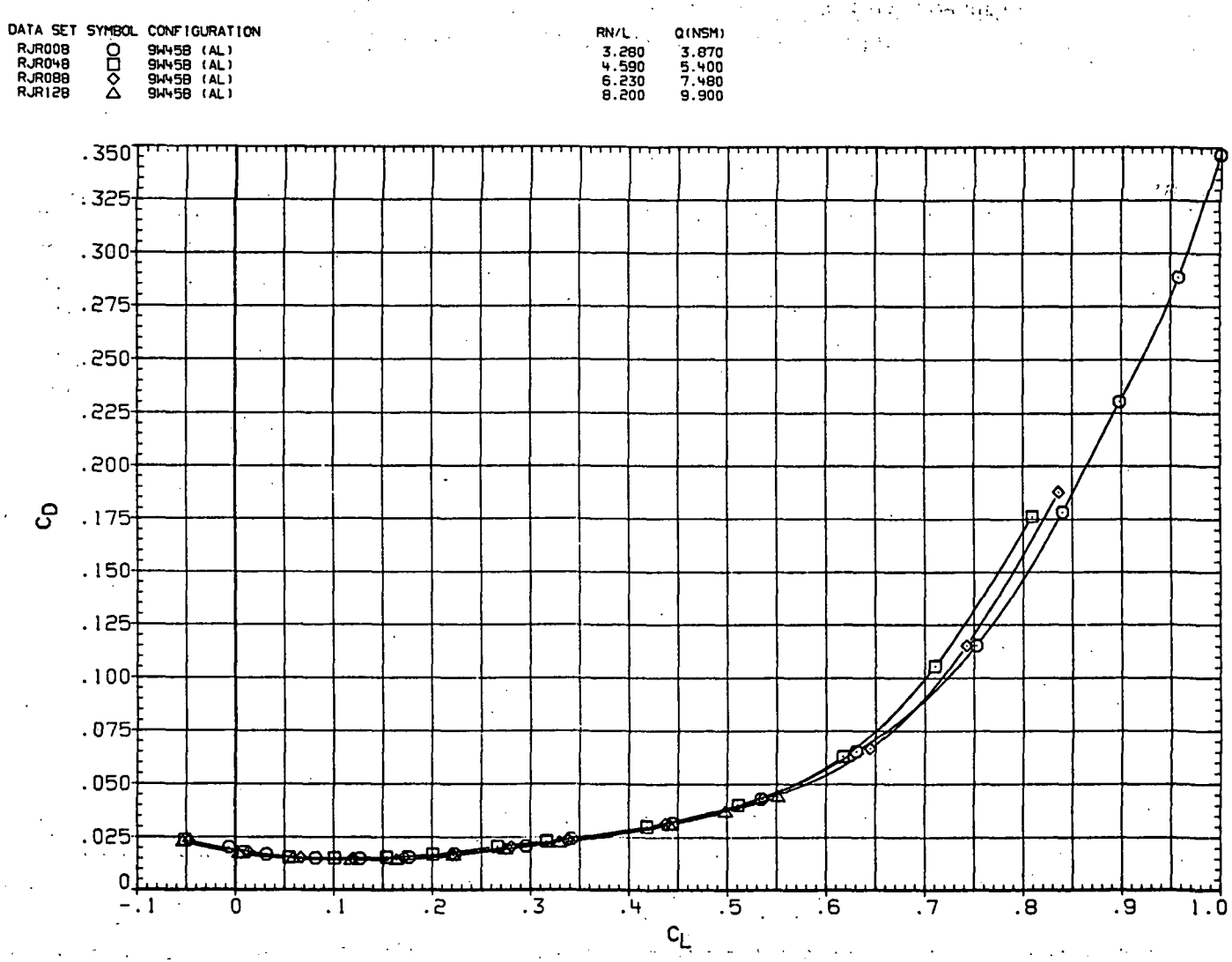

(b) C_D vs C_L.

Figure 8.– Continued.

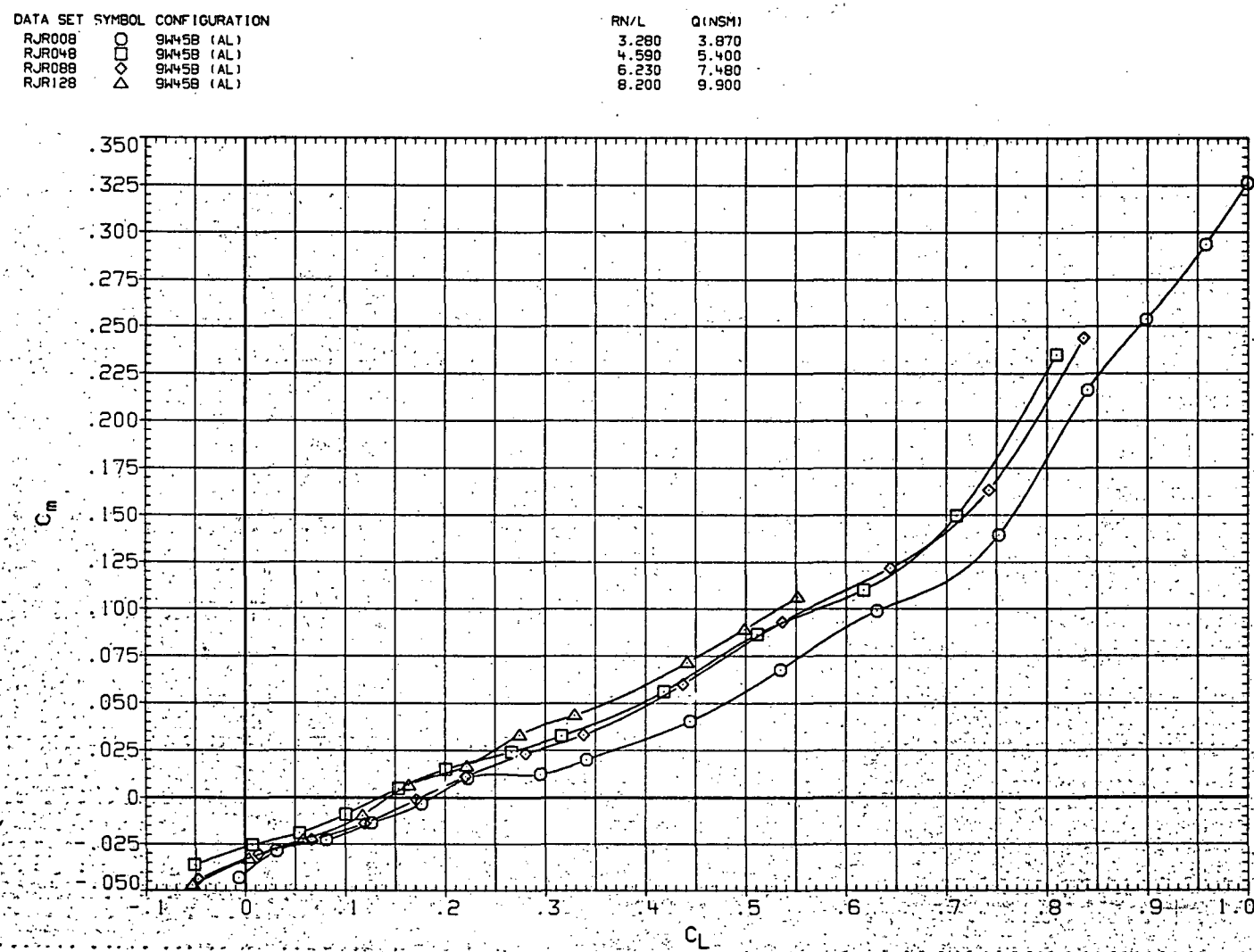

(c) C_m vs C_L

Figure 8.– Continued.

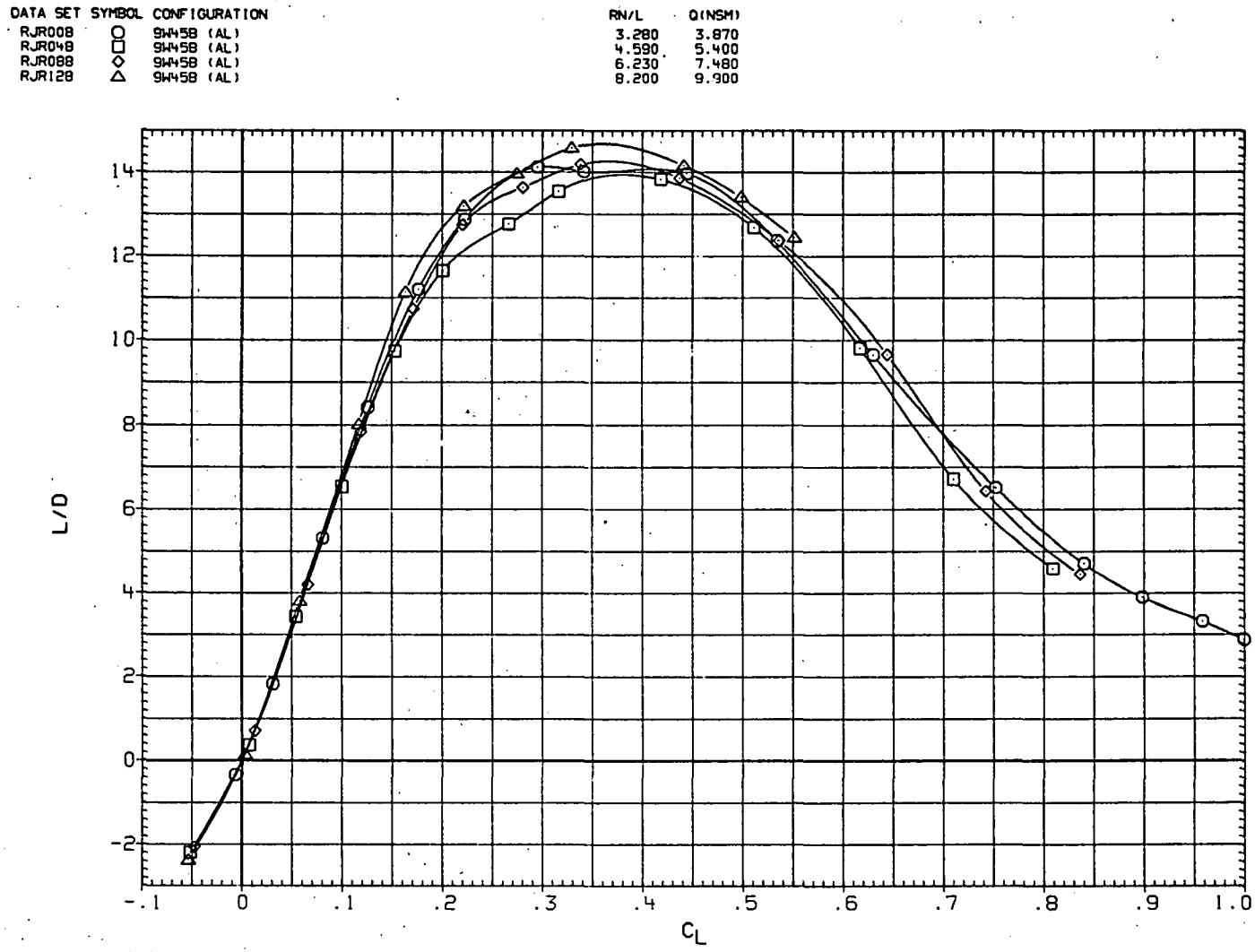

(d) L/D vs C_L.

Figure 8.– Continued.

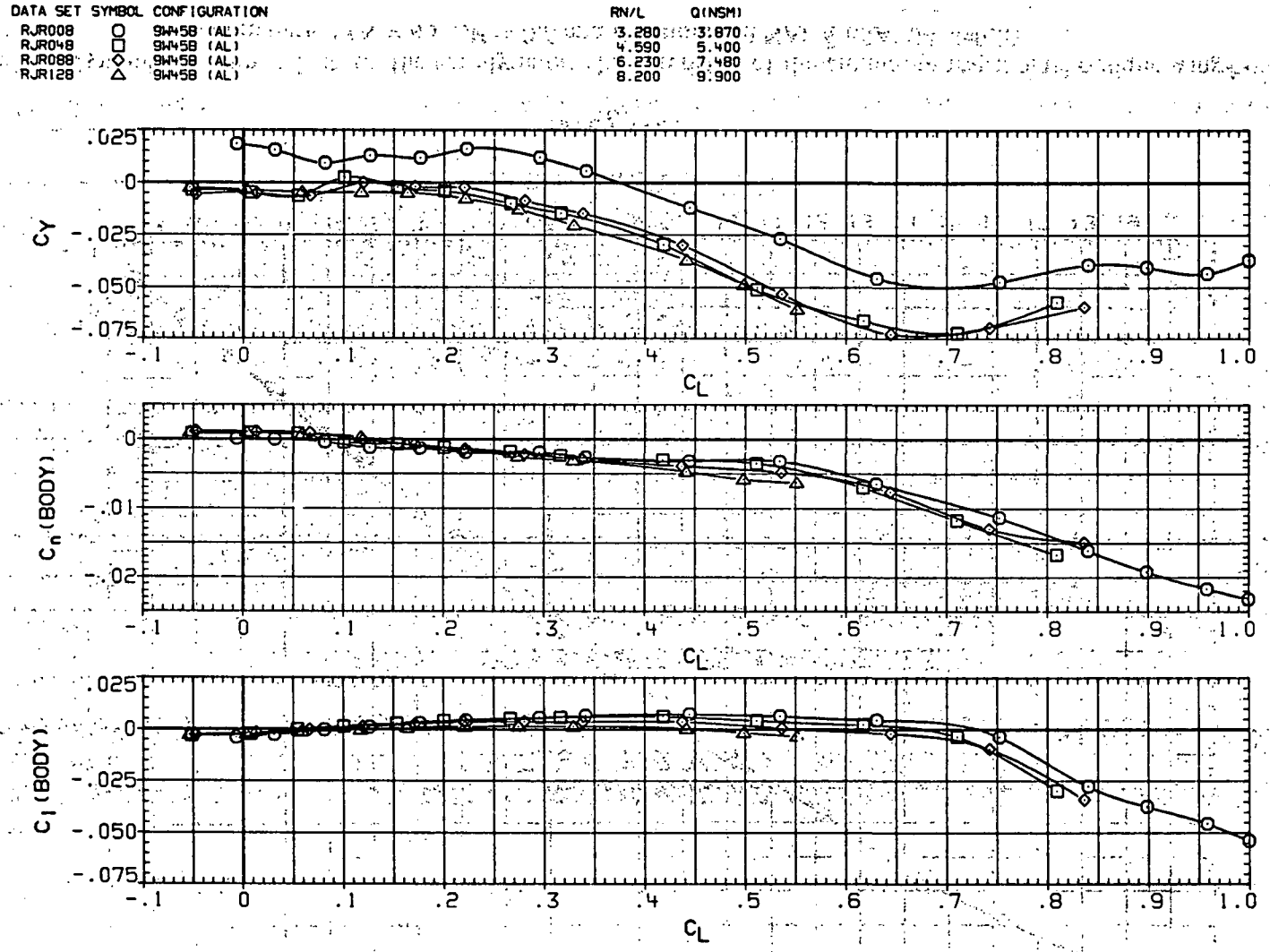

(e) C_Y, C_n and C_ℓ vs C_L.

Figure 8.– Concluded.

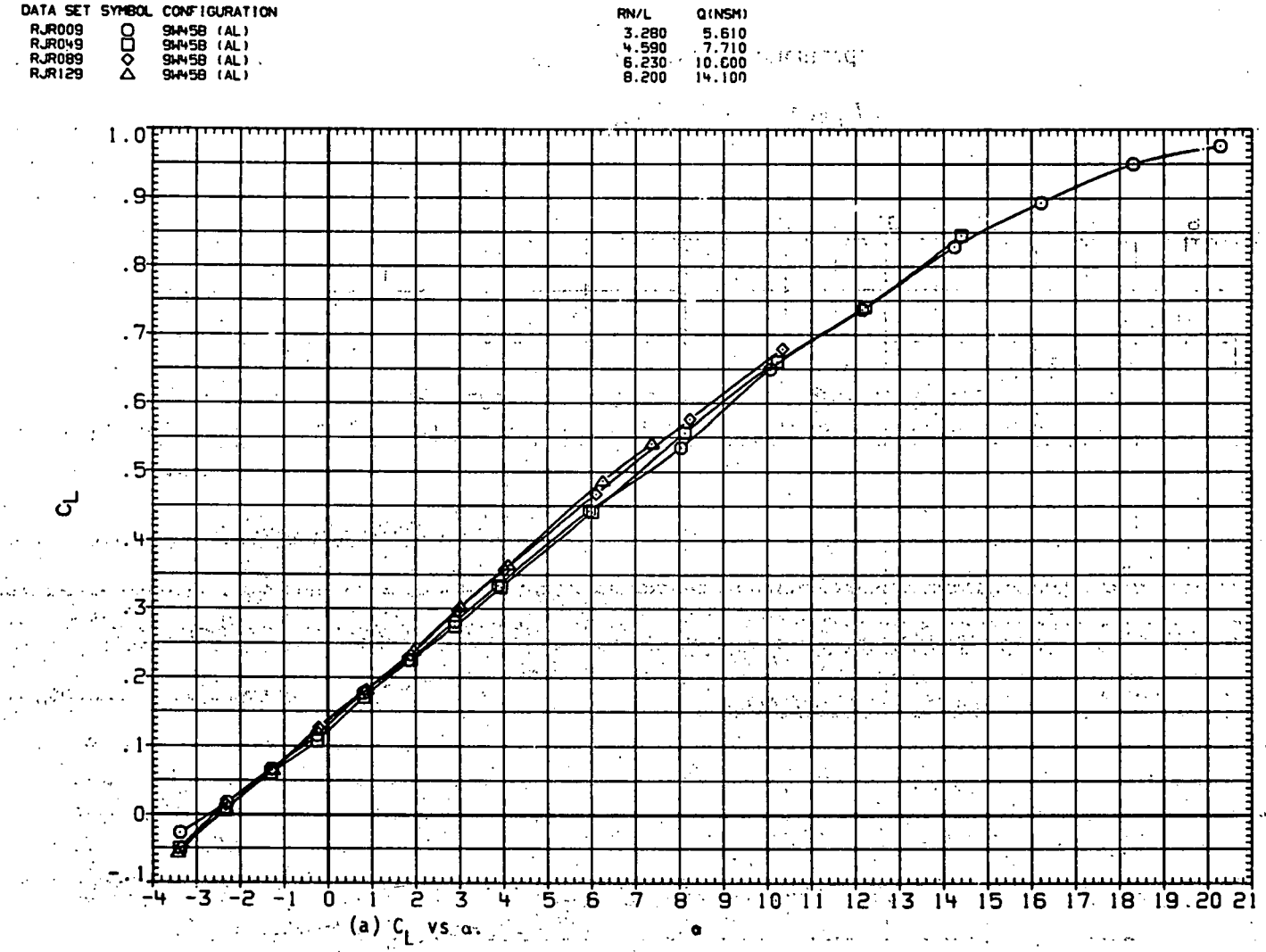

(a) C_L vs α.

Figure 9.– Dynamic-pressure effects on the aerodynamic characteristics of the aluminum trapezoidal oblique wing-body combination ($\Lambda = 45°$, $M = 0.6$ and the modified NACA 65A204 airfoil).

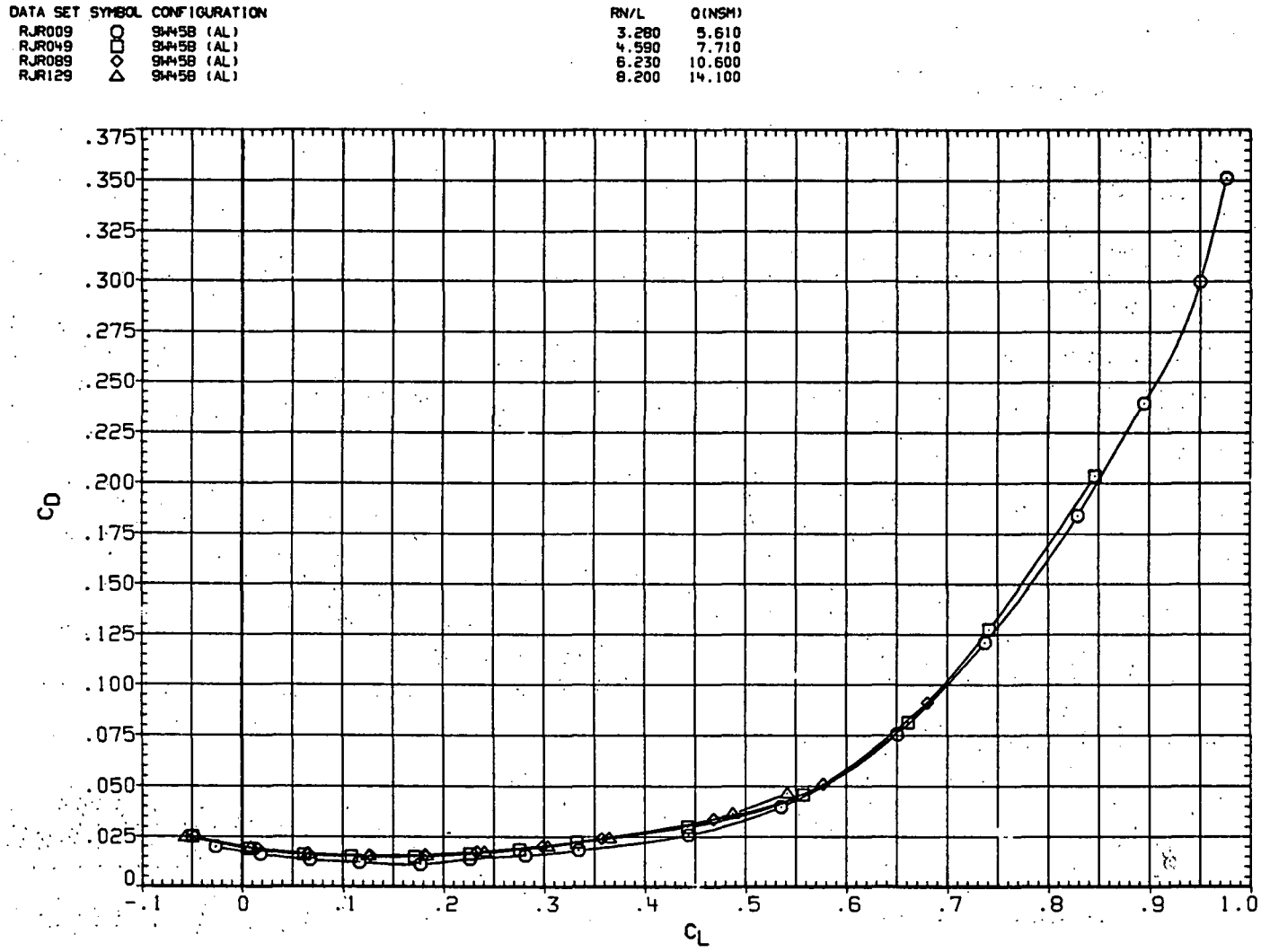

(b) C_D vs C_L.

Figure 9.– Continued.

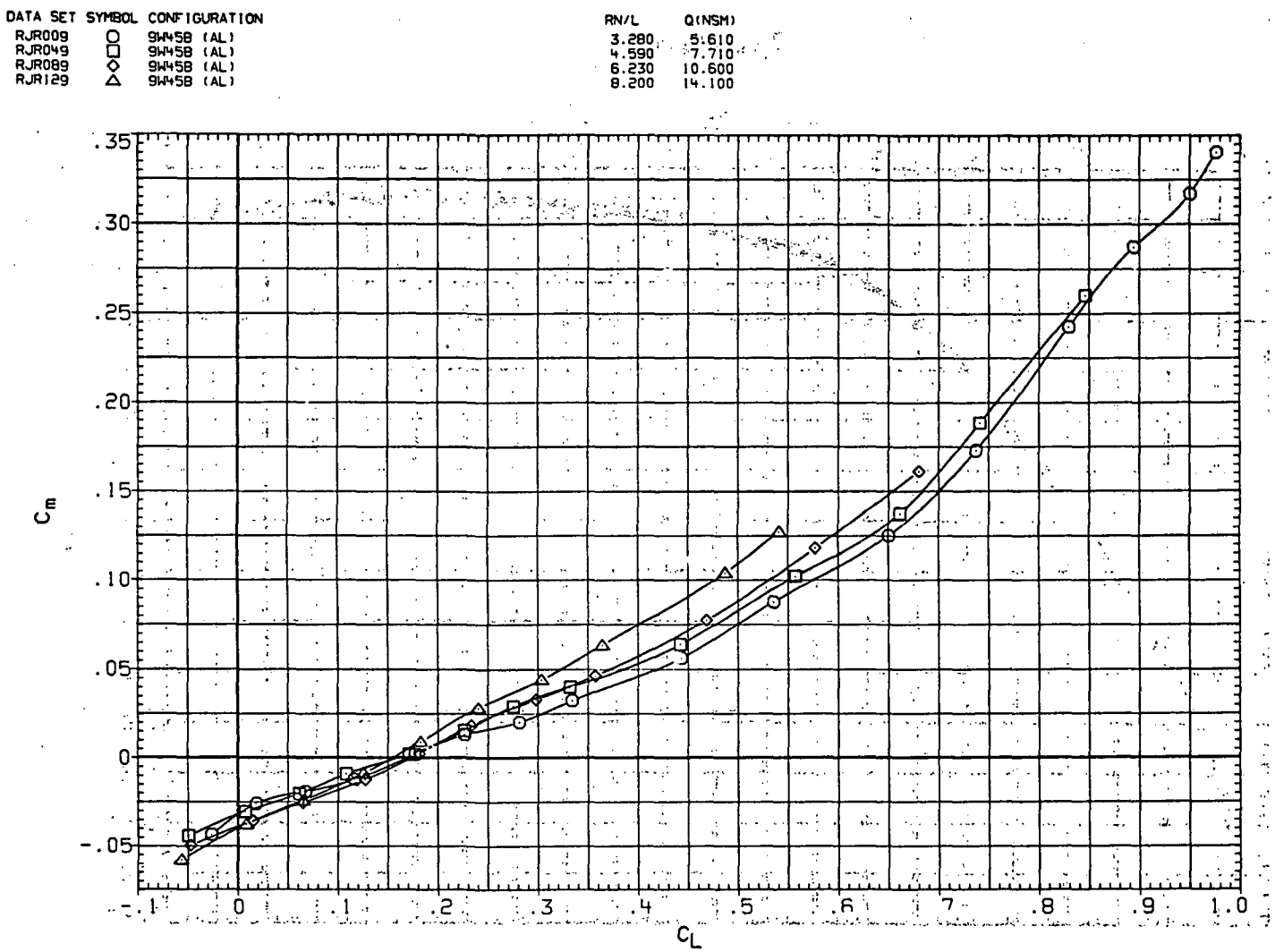

(c) C_m vs C_L.

Figure 9.– Continued.

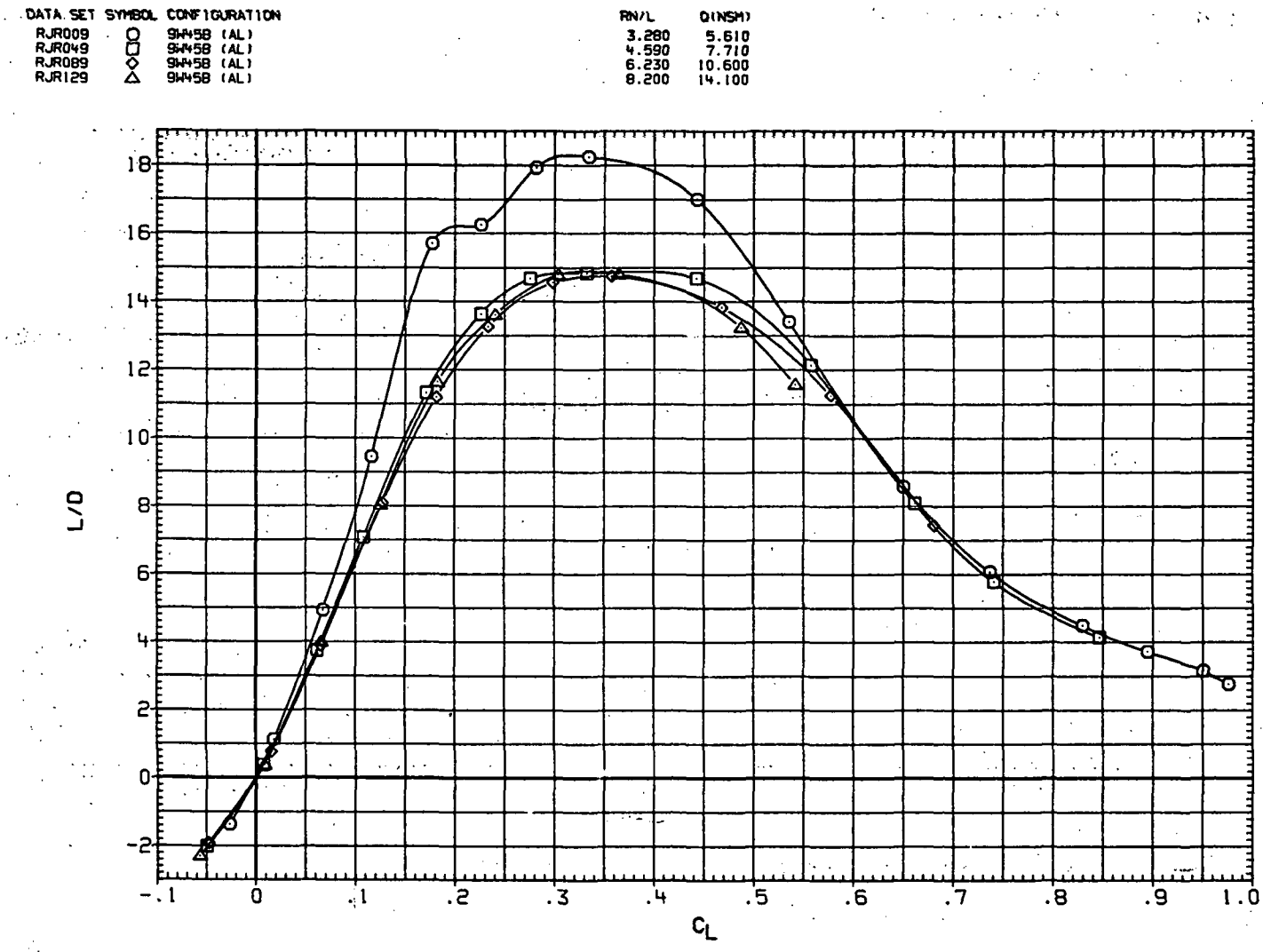

(d) L/D vs C_L.

Figure 9.– Continued.

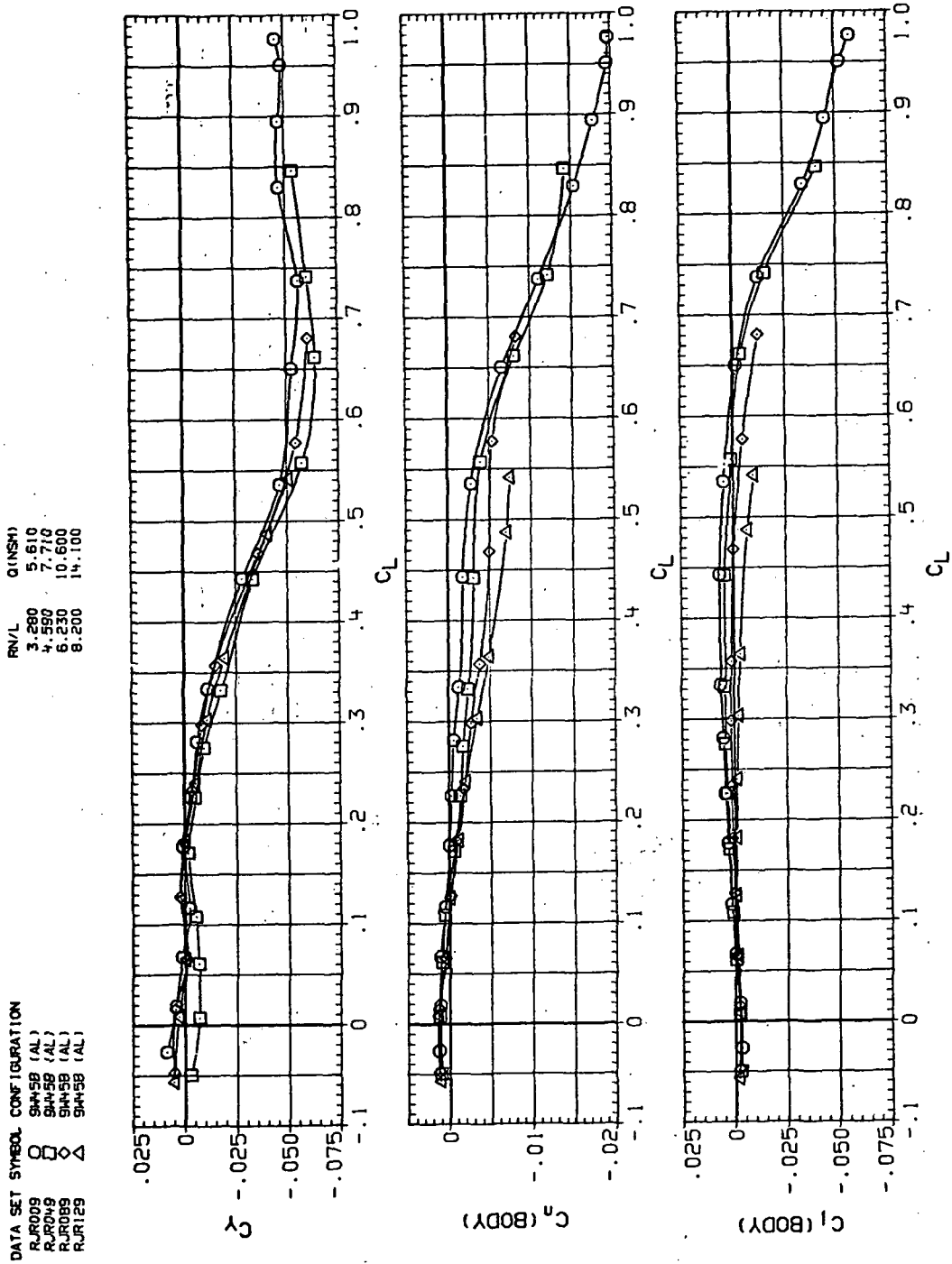

(e) C_Y, C_n and C_ℓ vs C_L.

Figure 9.– Concluded.

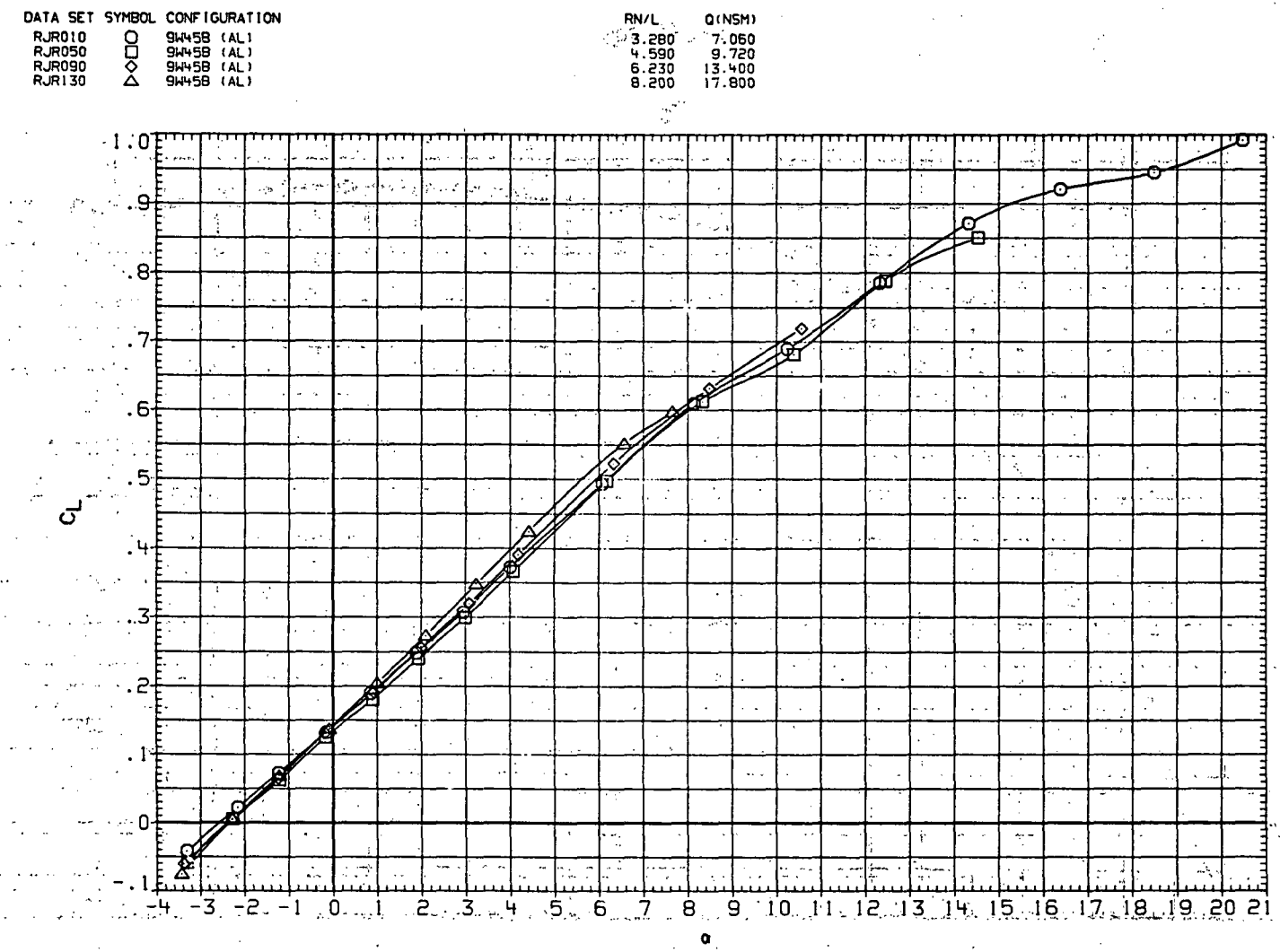

(a) C_L vs α.

Figure 10.– Dynamic-pressure effects on the aerodynamics characteristics of the aluminum trapezoidal oblique wing-body combination ($\Lambda = 45°$, $M = 0.8$ and the modified NACA 65A204 airfoil).

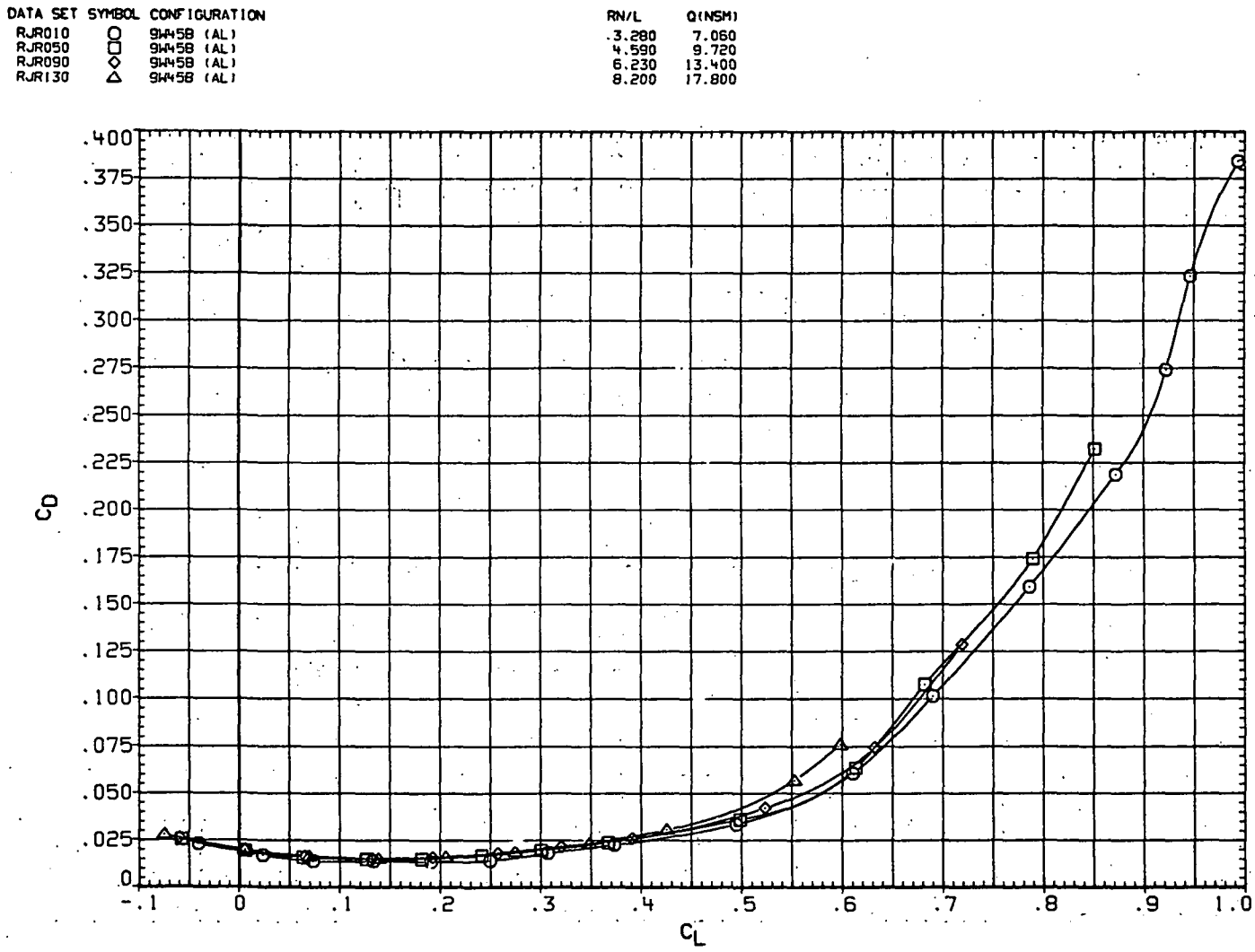

(b) C_D vs C_L.

Figure 10.– Continued.

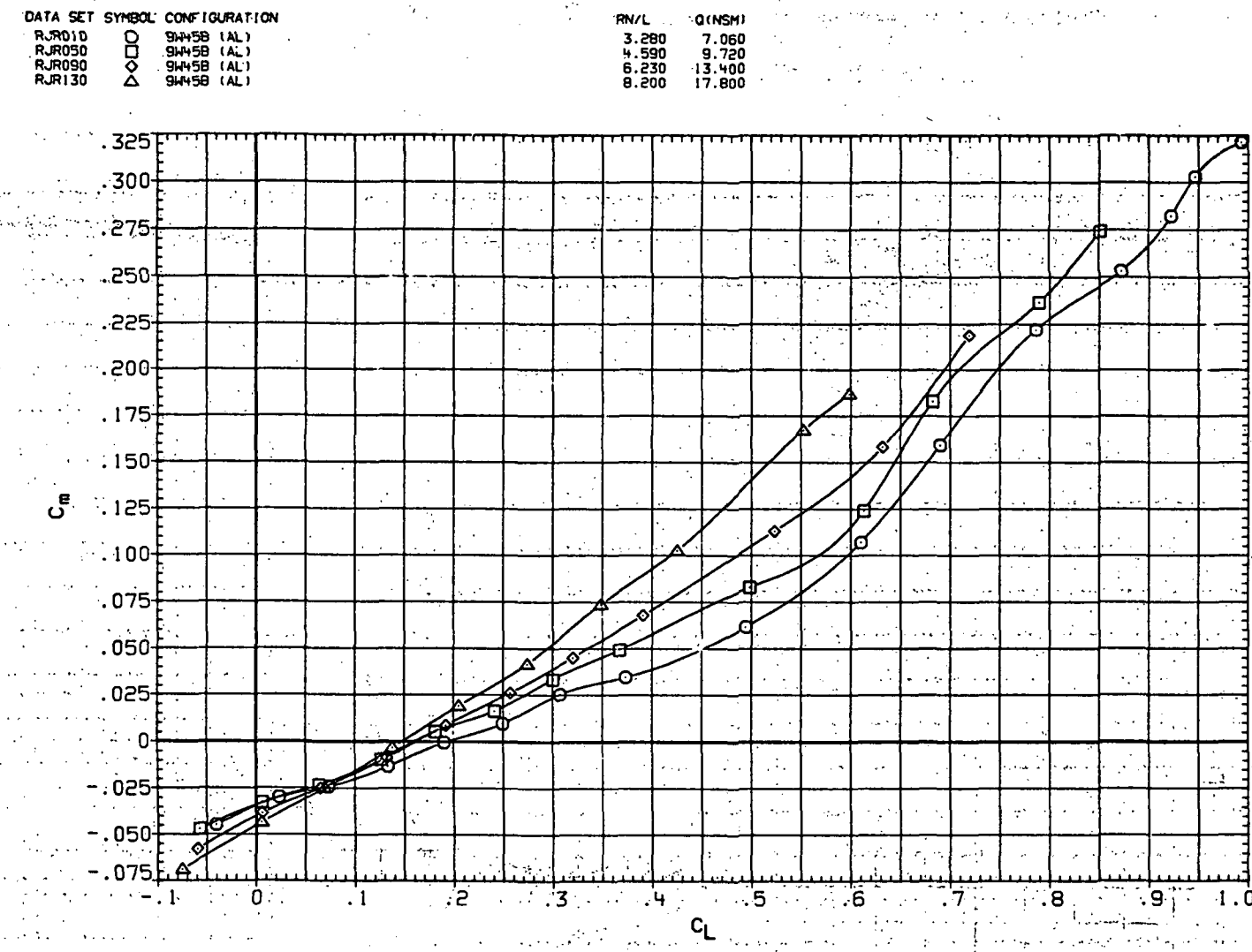

(c) C_m vs C_L.

Figure 10.– Continued.

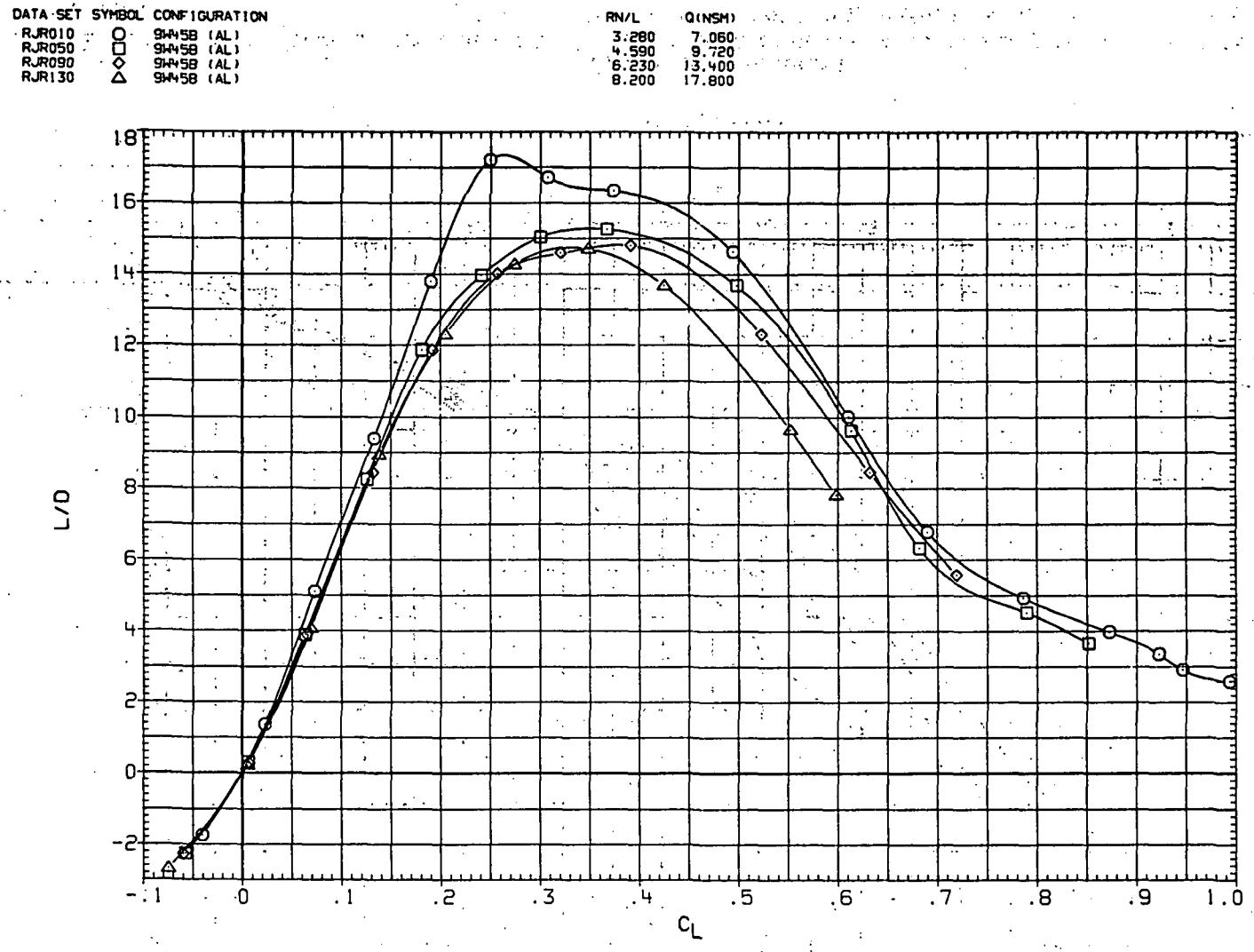

(d) L/D vs C_L.

Figure 10.– Continued.

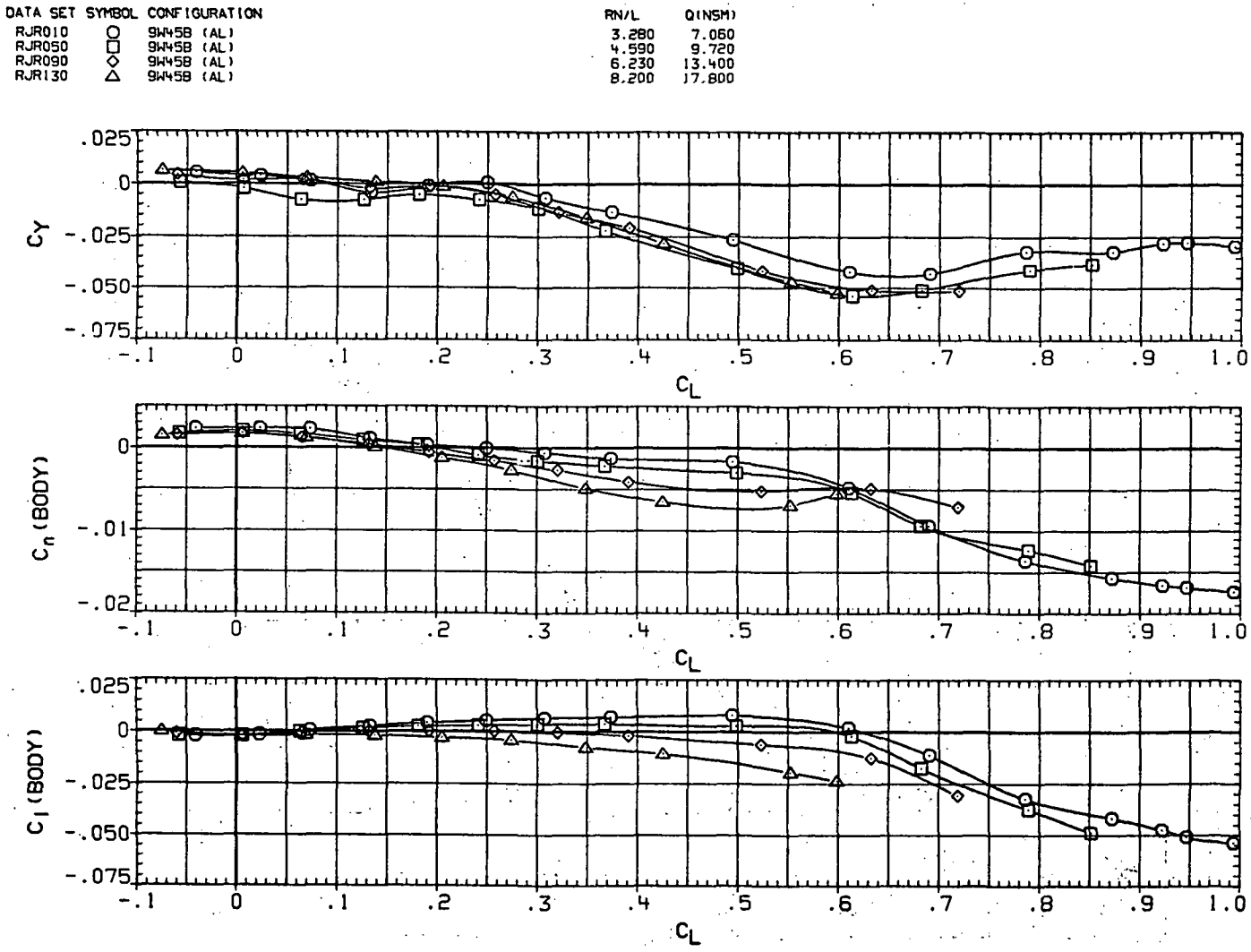

(e) C_Y, C_n and C_ℓ and C_L.

Figure 10.– Concluded.

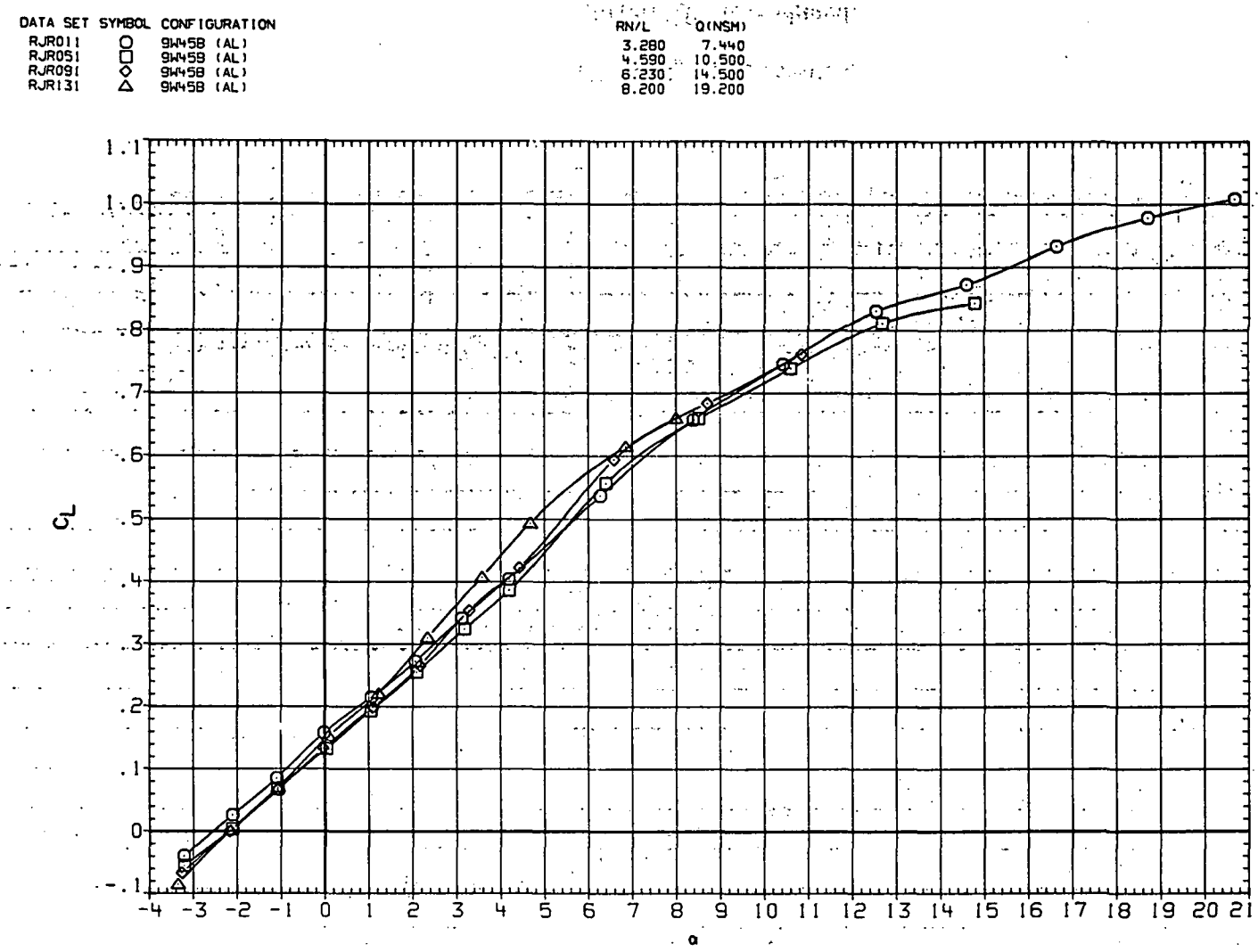

(a) C_L vs α.

Figure 11.– Dynamic-pressure effects on the aerodynamic characteristics of the aluminum trapezoidal oblique wing-body combination ($\Lambda = 45°$, $M = 0.9$ and the modified NACA 65A204 airfoil).

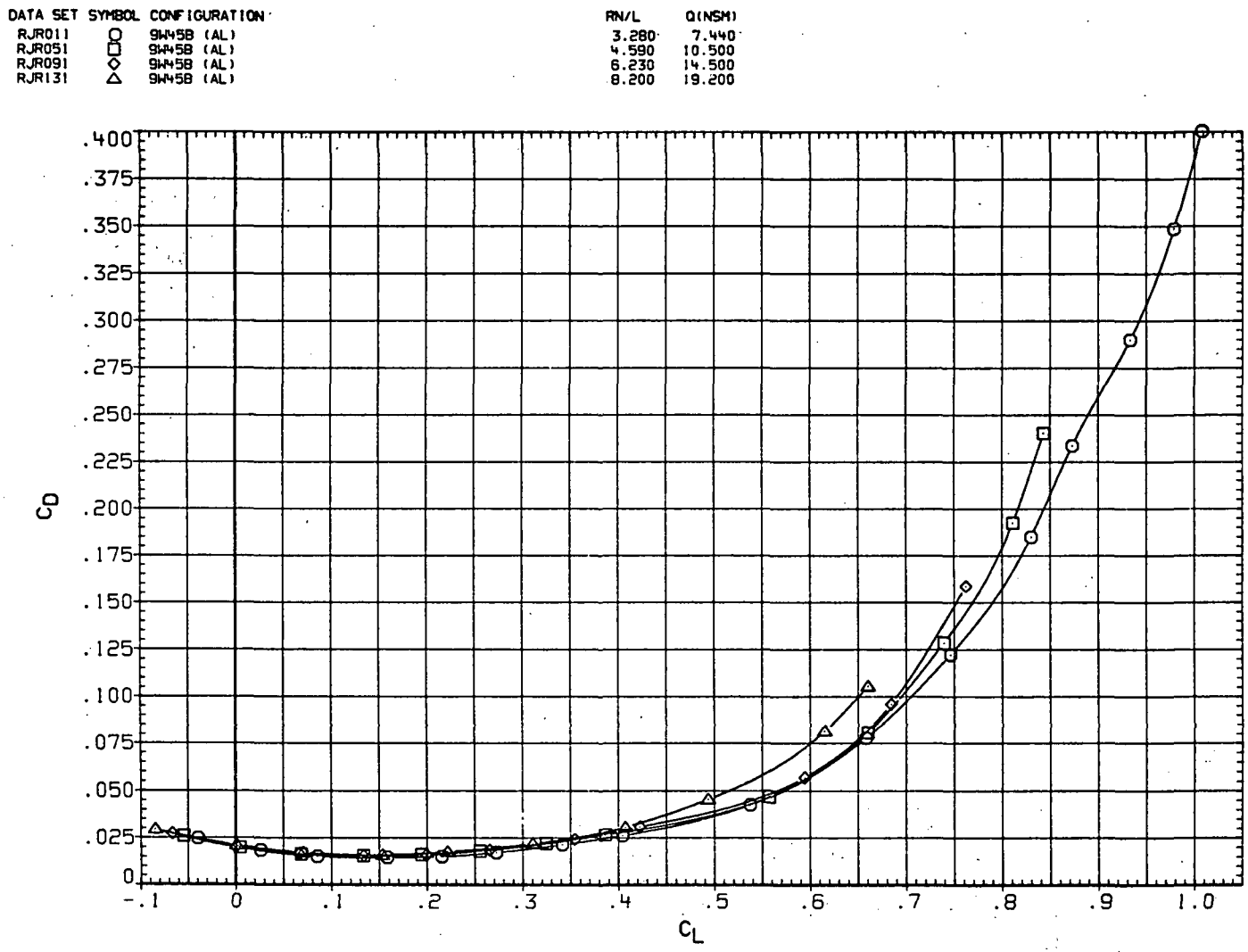

(b) C_D vs C_L.

Figure 11.– Continued.

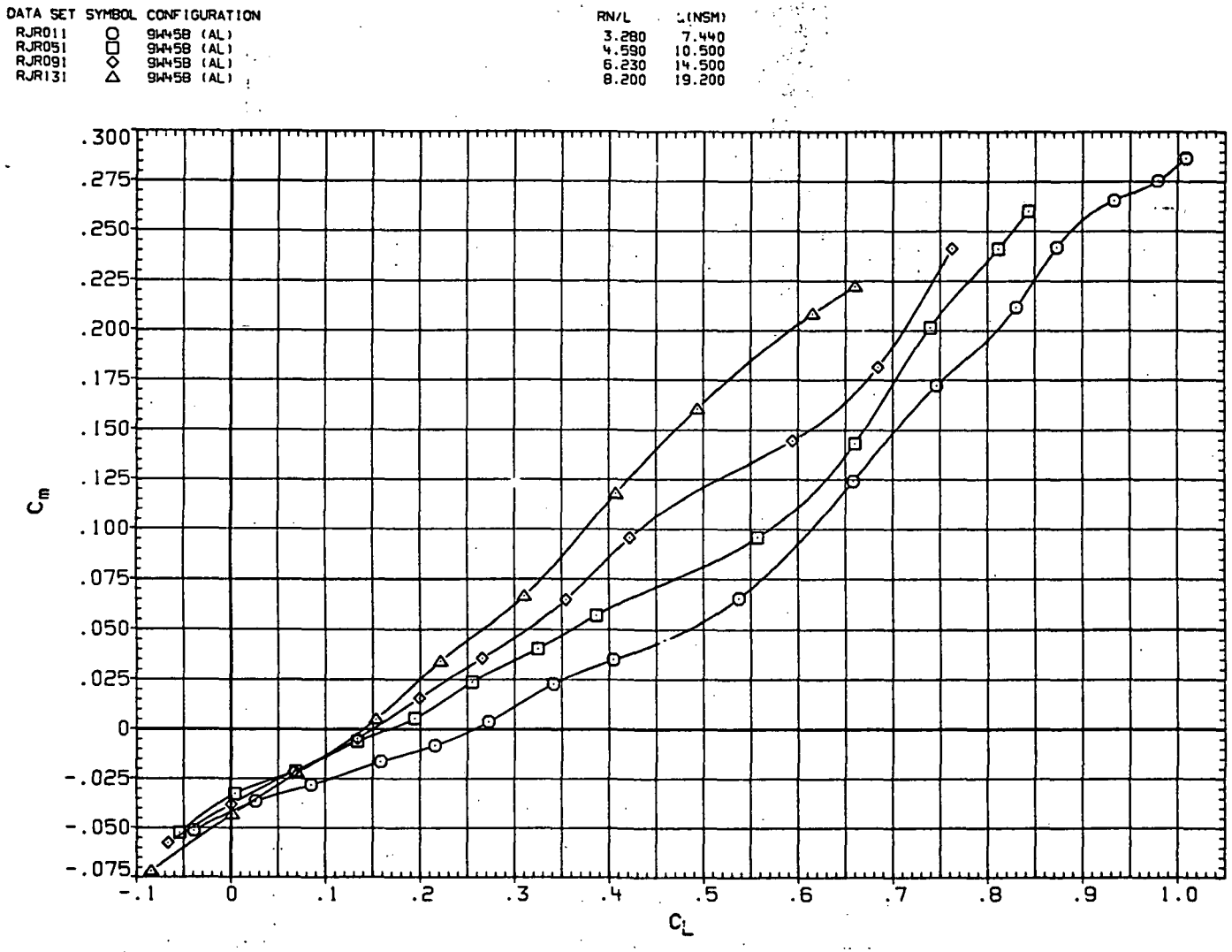

(c) C_m vs C_L.

Figure 11.– Continued.

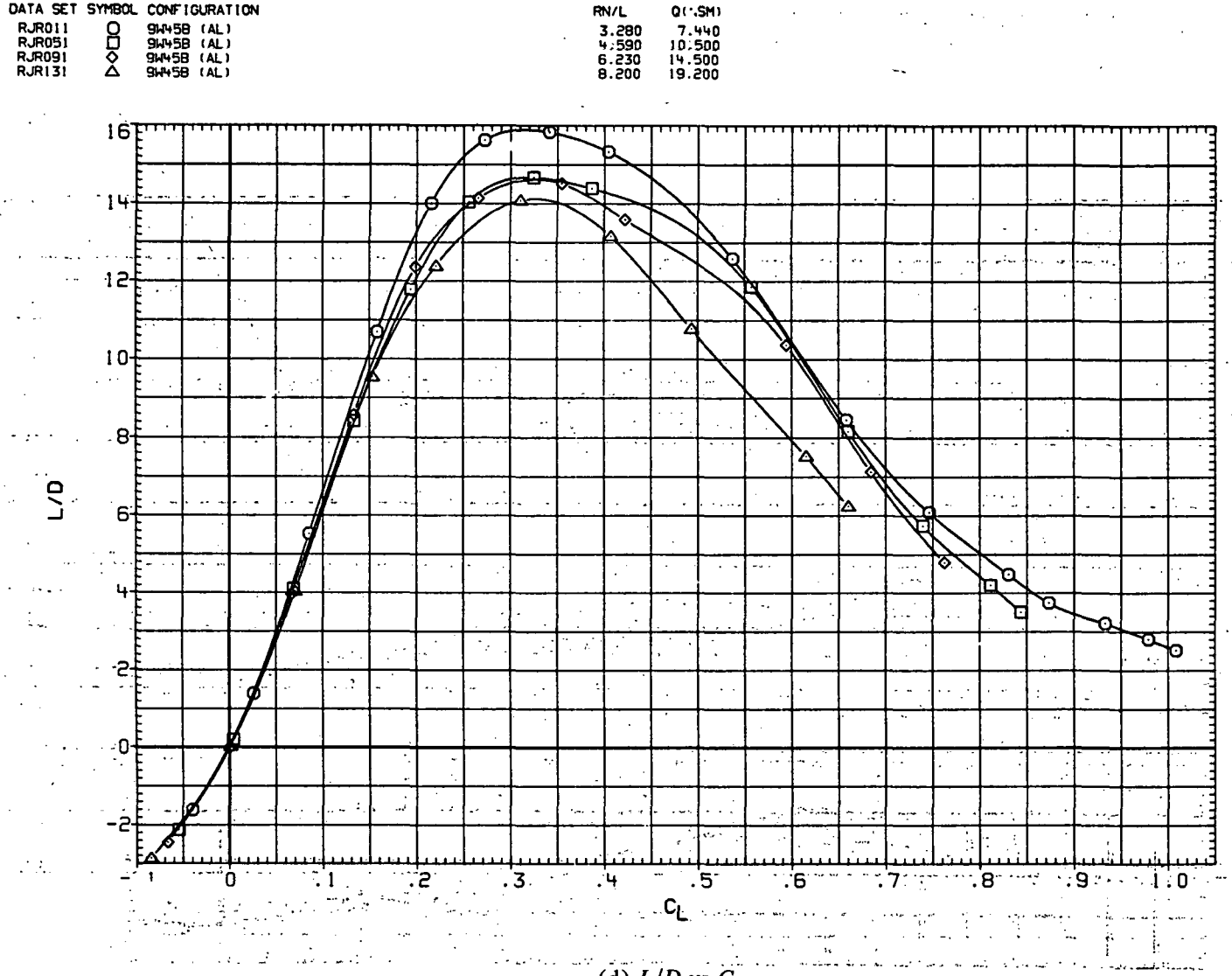

(d) L/D vs C_L.

Figure 11.– Continued.

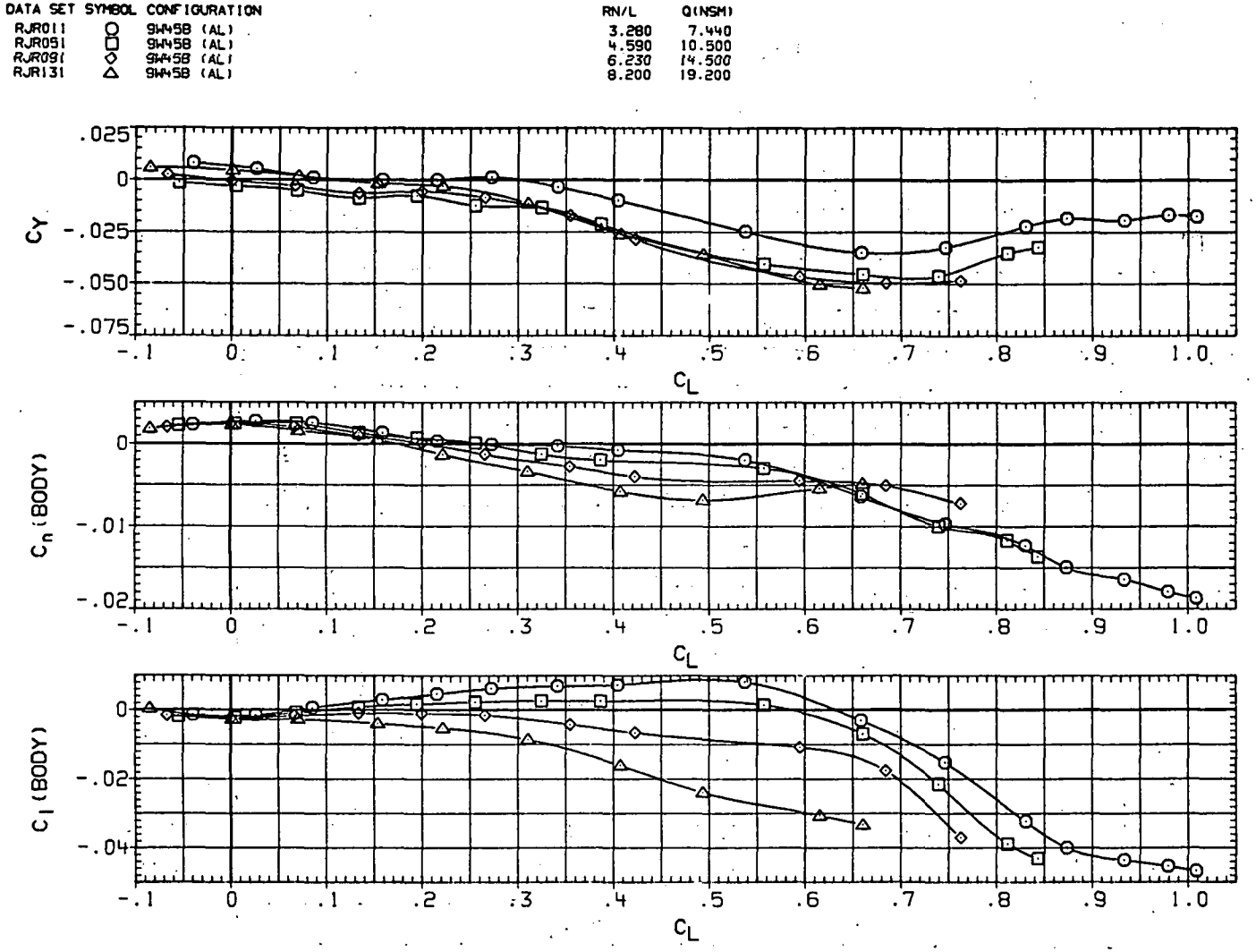

(e) C_Y, C_n and C_ℓ vs C_L.

Figure 11.– Concluded.

DATA SET	SYMBOL	CONFIGURATION	RN/L	Q(NSM)
RJR012	○	9W45B (AL)	3.280	7.960
RJR052	□	9W45B (AL)	4.590	10.900
RJR092	◇	9W45B (AL)	6.230	15.000
RJR132	△	9W45B (AL)	8.200	19.900

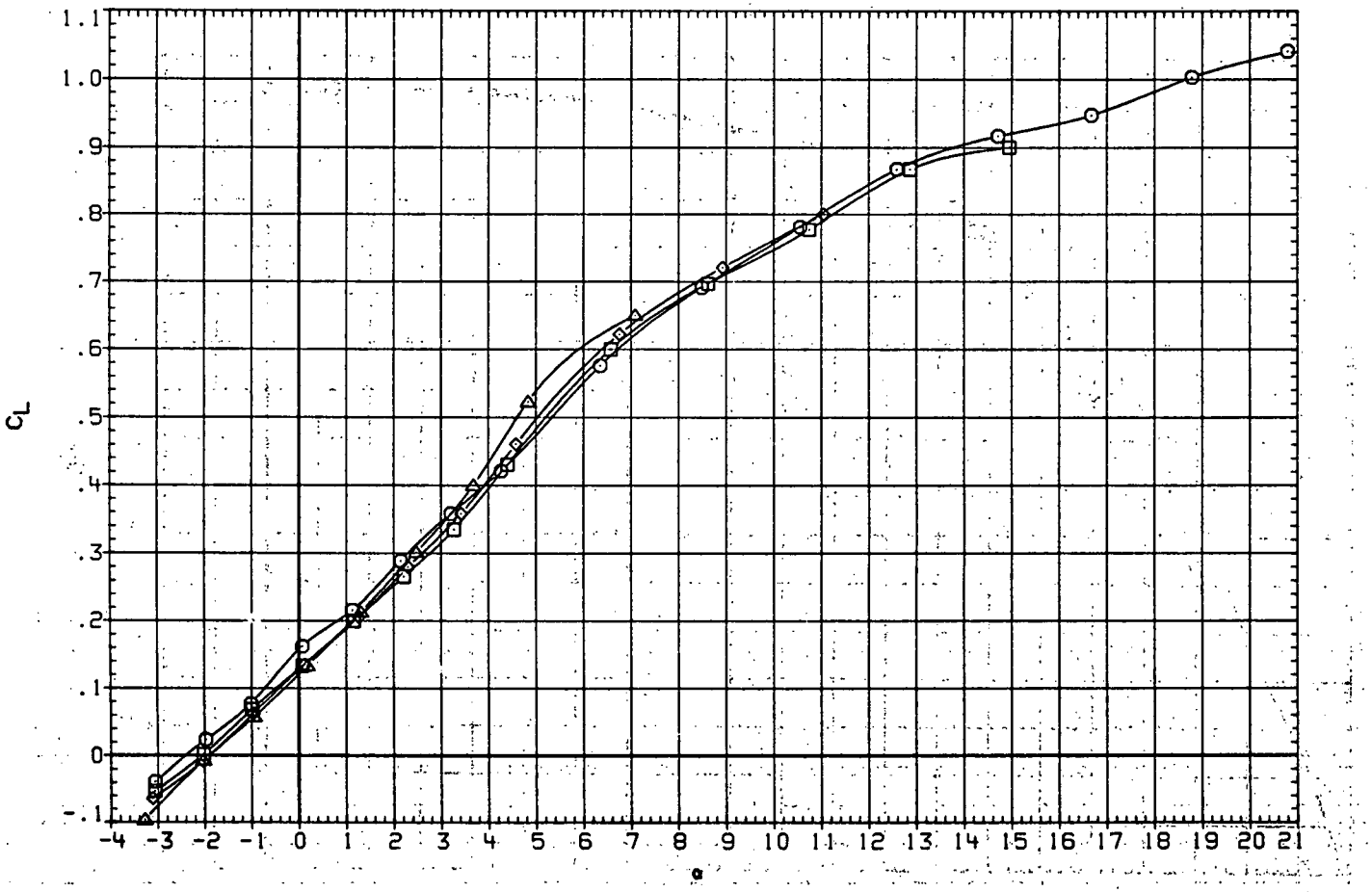

(a) C_L vs α.

Figure 12.– Dynamic-pressure effects on the aerodynamic characteristics of the aluminum trapezoidal oblique wing-body combination ($\Lambda = 45°$, $M = 0.95$ and the modified NACA 65A204 airfoil).

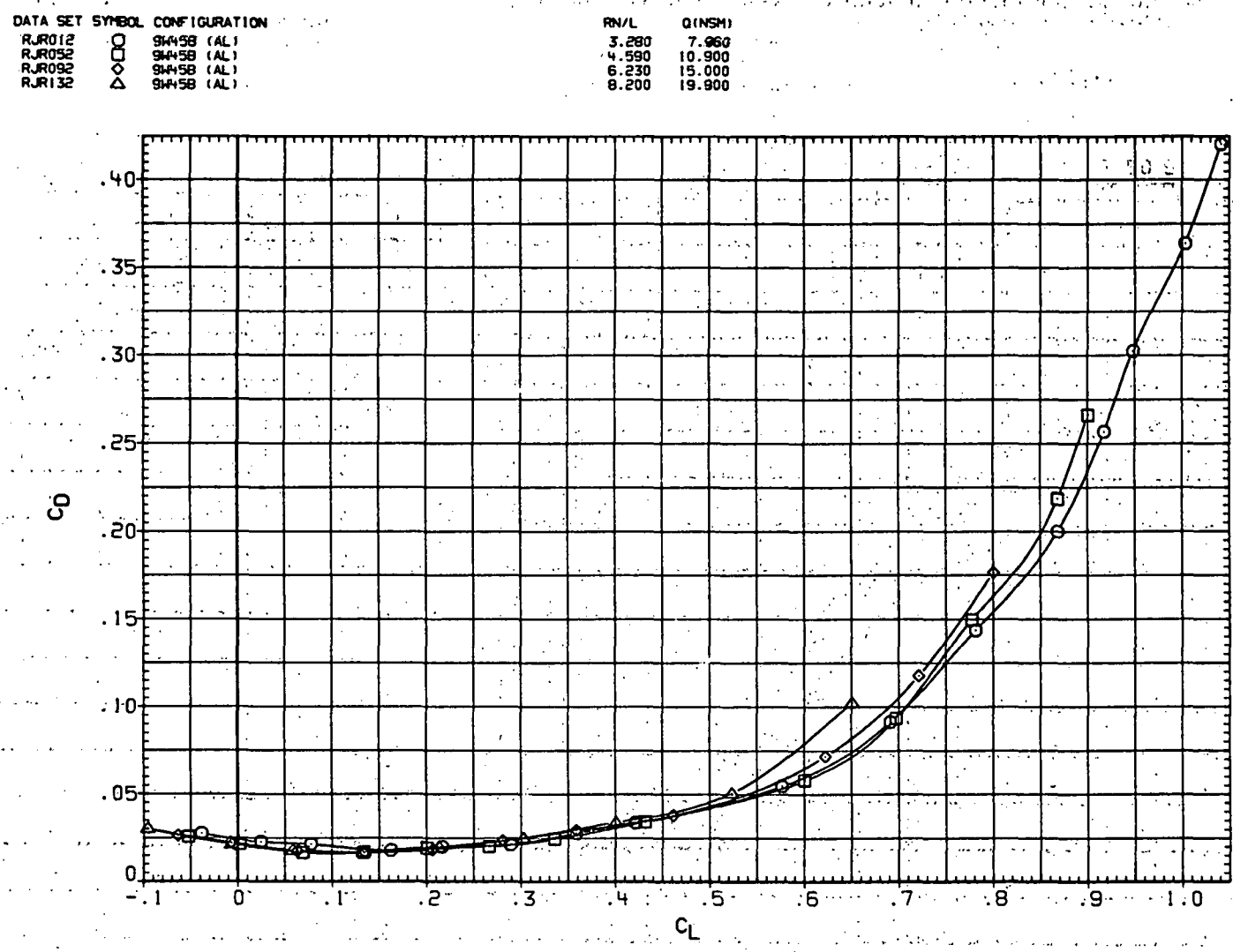

(b) C_D vs C_L.

Figure 12.– Continued.

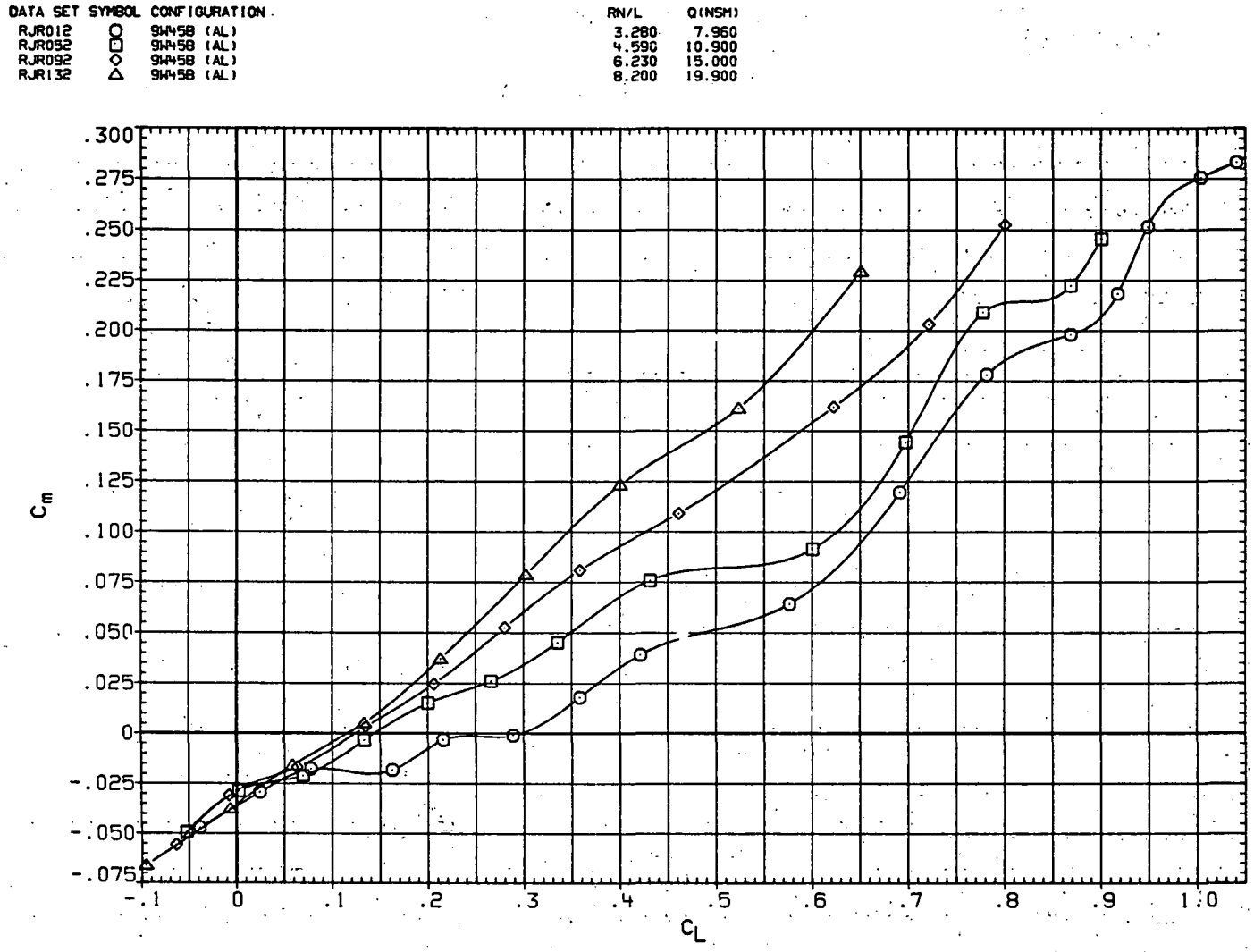

(c) C_m vs C_L.

Figure 12.– Continued.

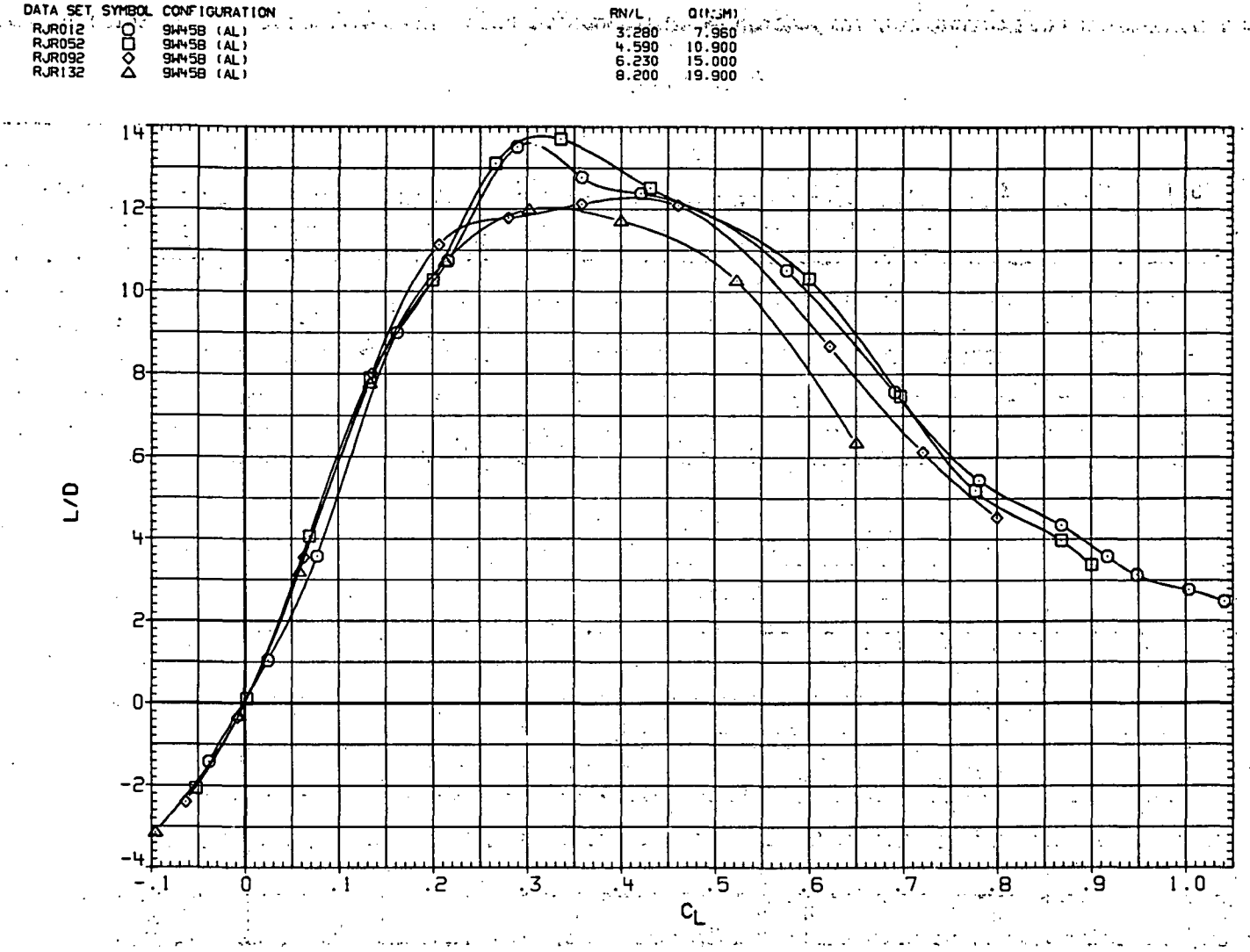

(d) L/D vs C_L.

Figure 12.– Continued.

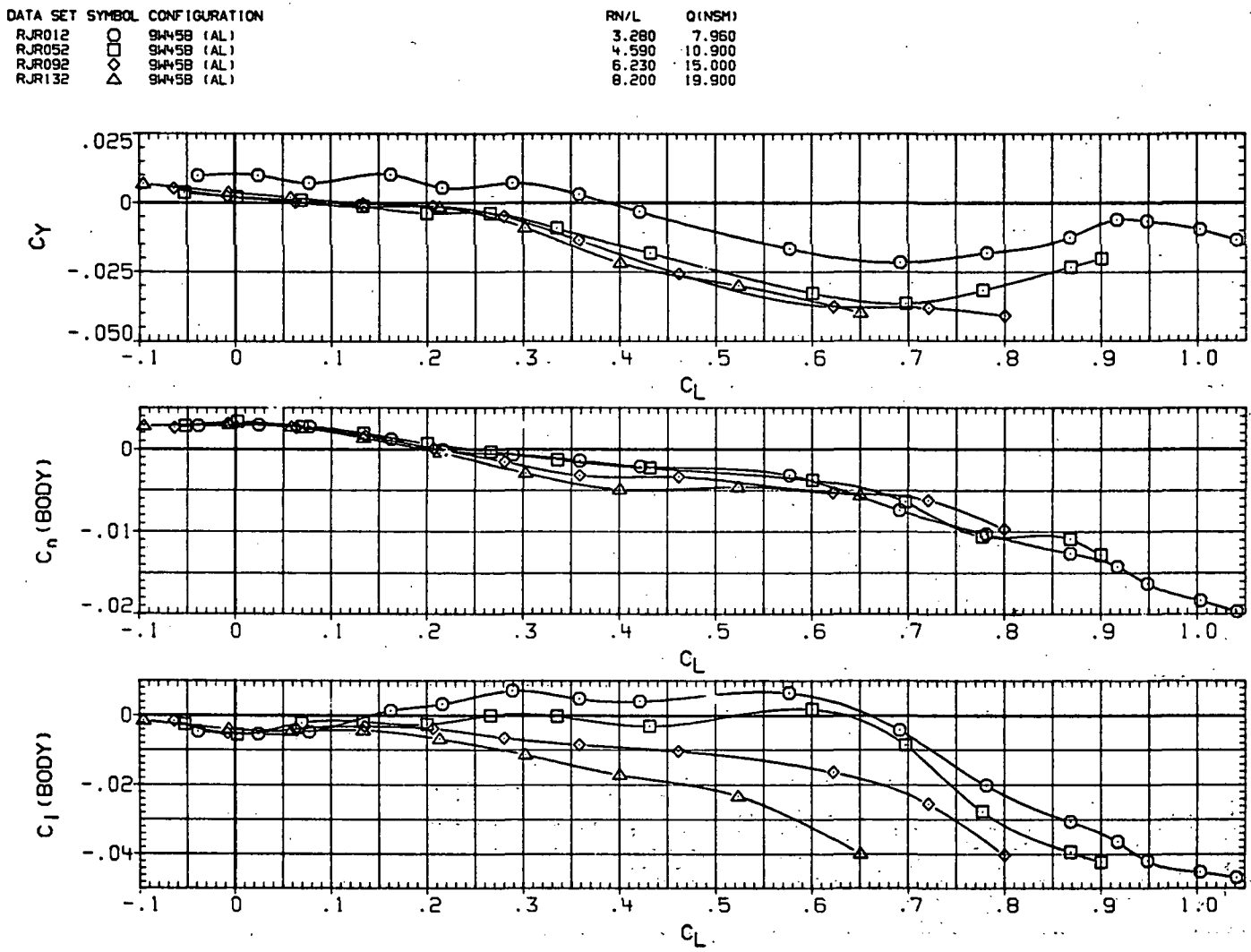

(e) C_Y, C_n and C_ℓ vs C_L.

Figure 12.– Concluded.

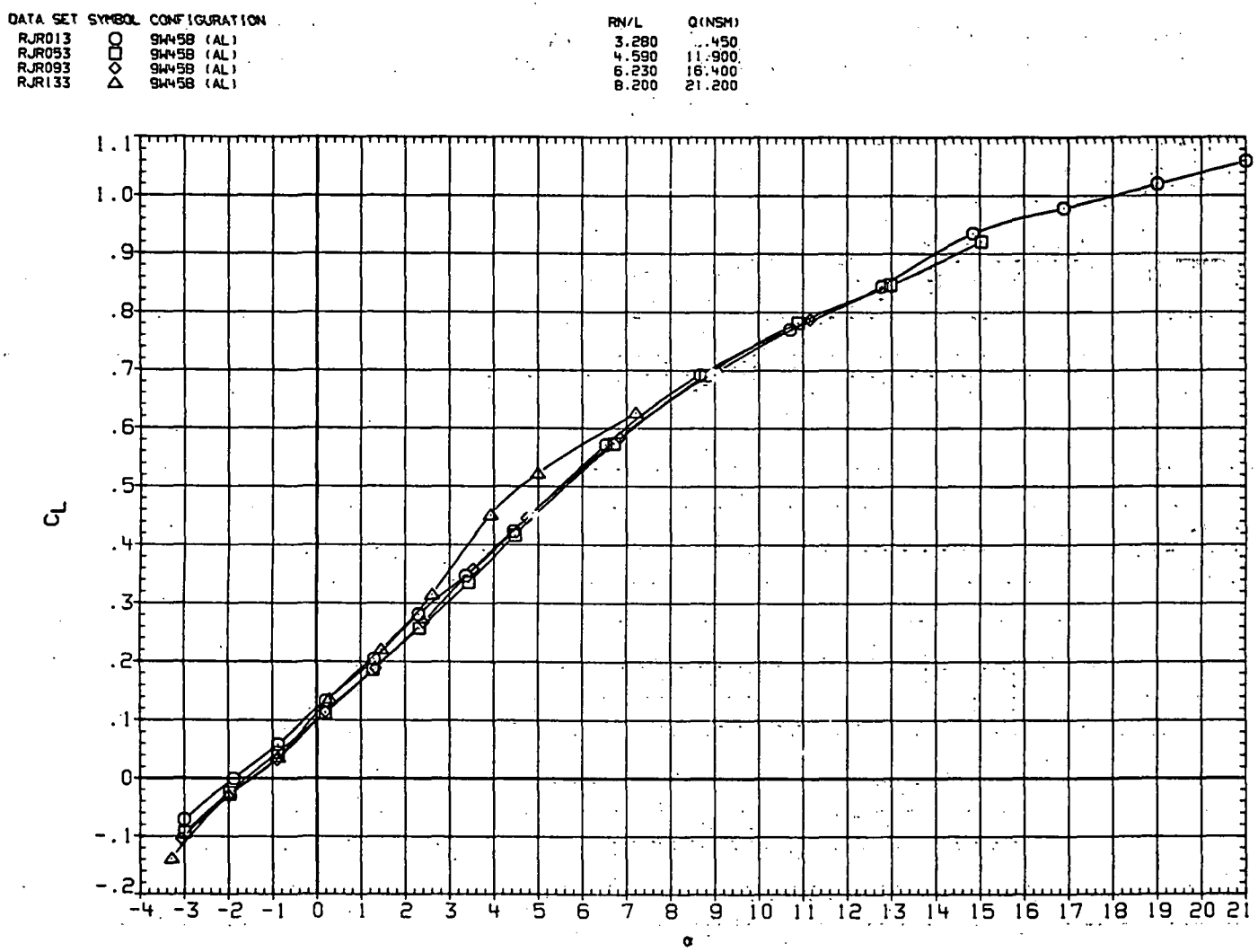

(a) C_L vs α.

Figure 13.– Dynamic-pressure effects on the aerodynamic characteristics of the aluminum trapezoidal oblique wing-body combination ($\Lambda = 45°, M = 1.1$ and the modified NACA 65A204 airfoil).

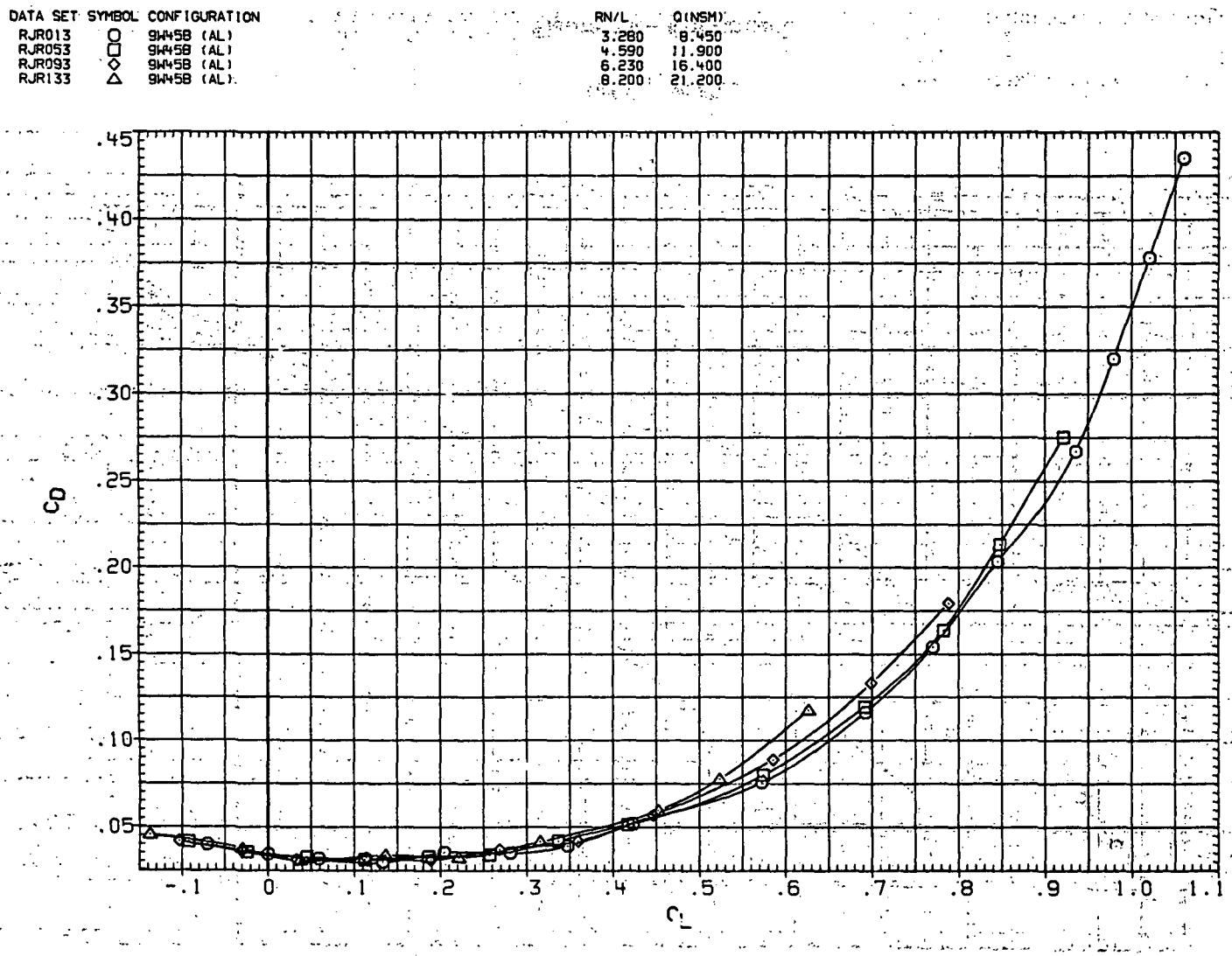

(b) C_D vs C_L.

Figure 13.– Continued.

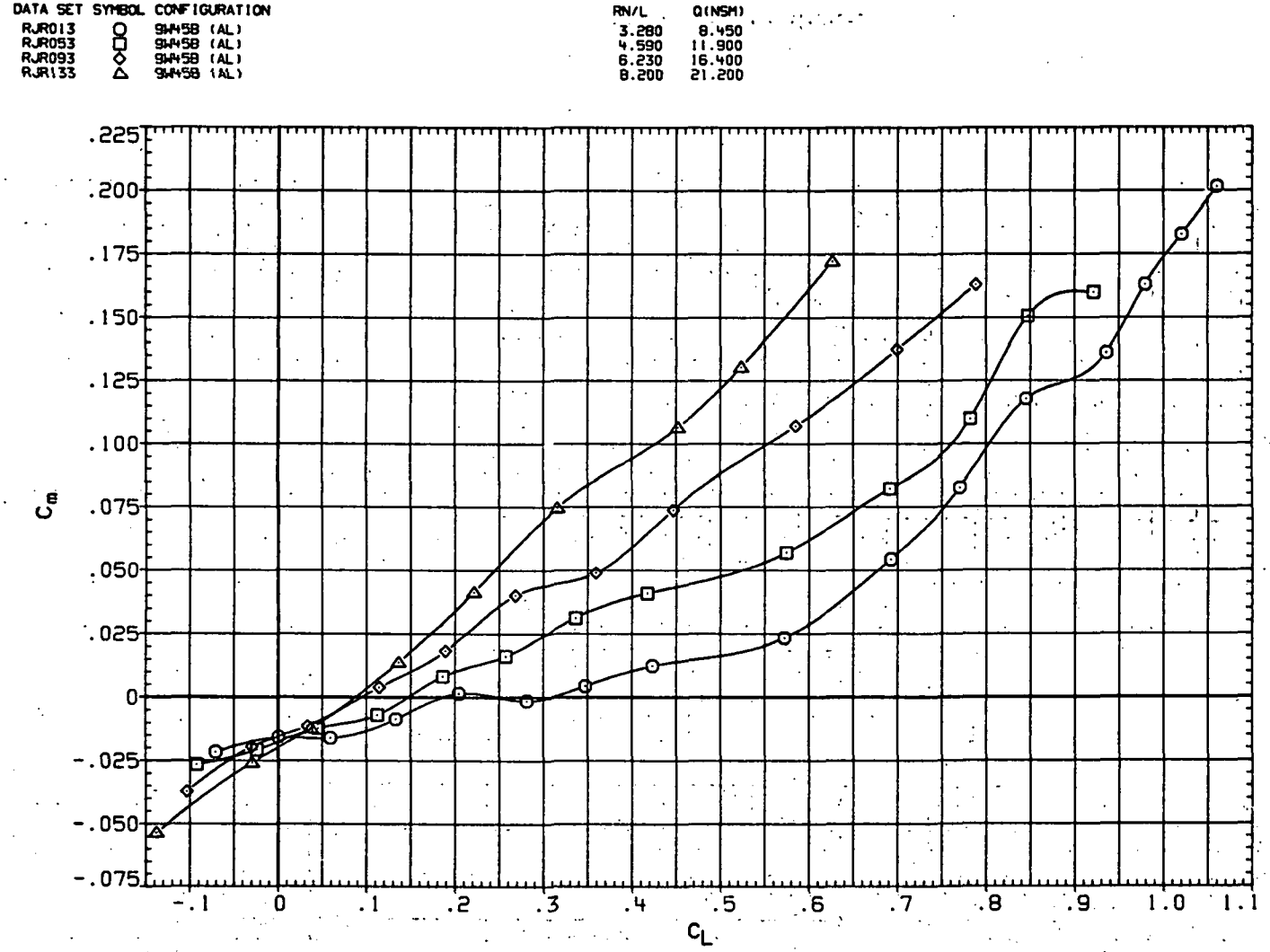

(c) C_m vs C_L.

Figure 13.– Continued.

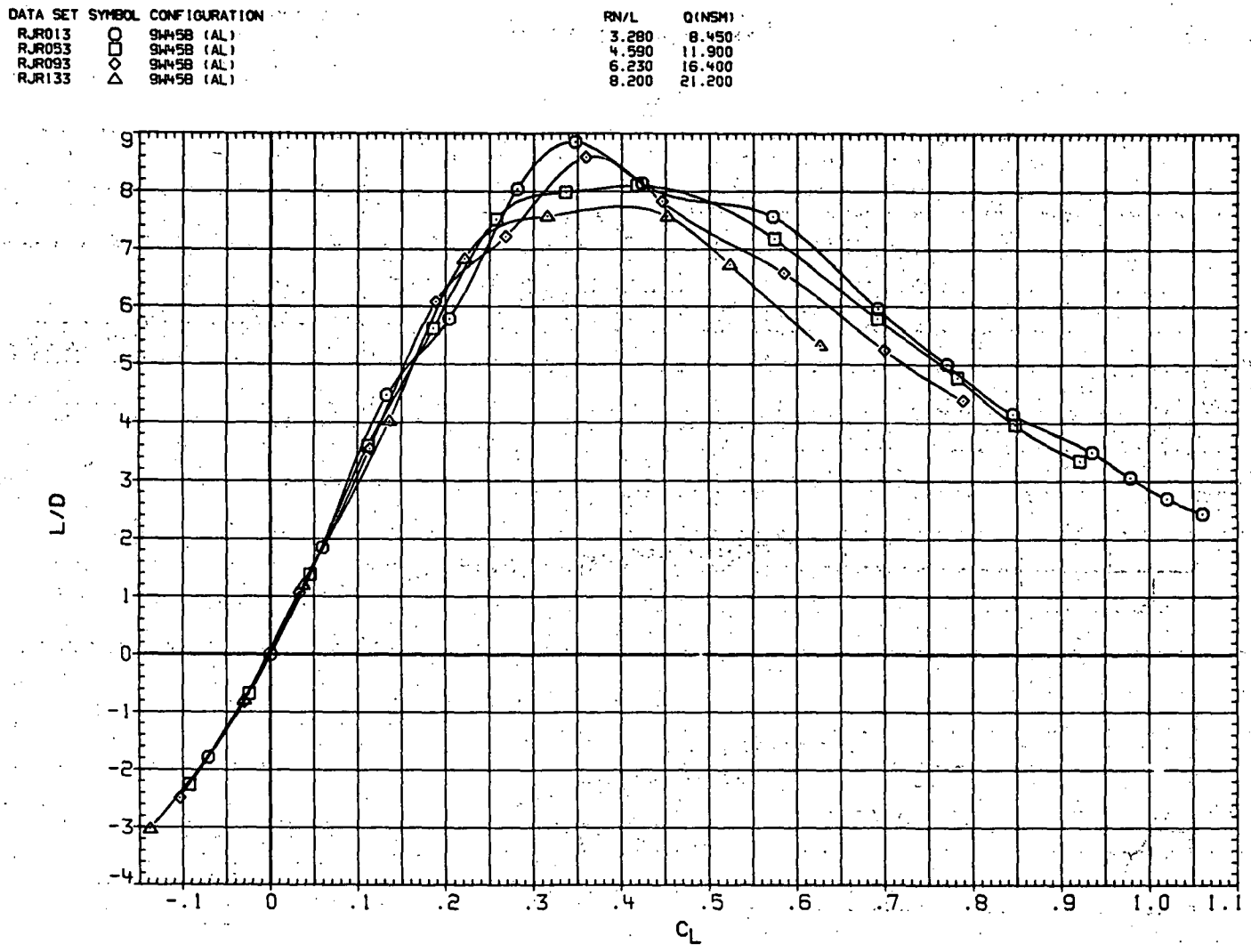

(d) L/D vs C_L.

Figure 13.– Continued.

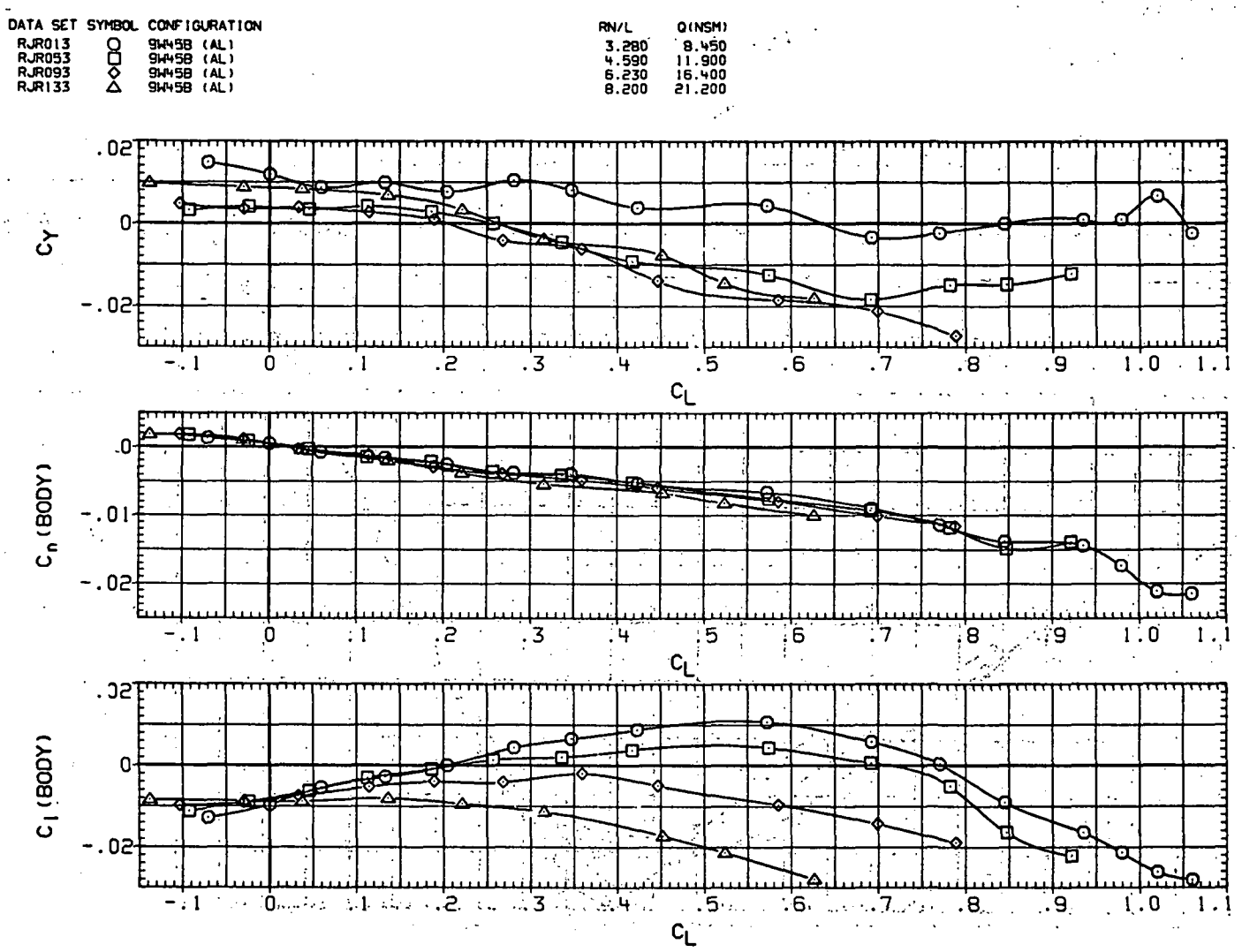

(e) C_Y, C_n and C_ℓ vs C_L.

Figure 13.– Concluded.

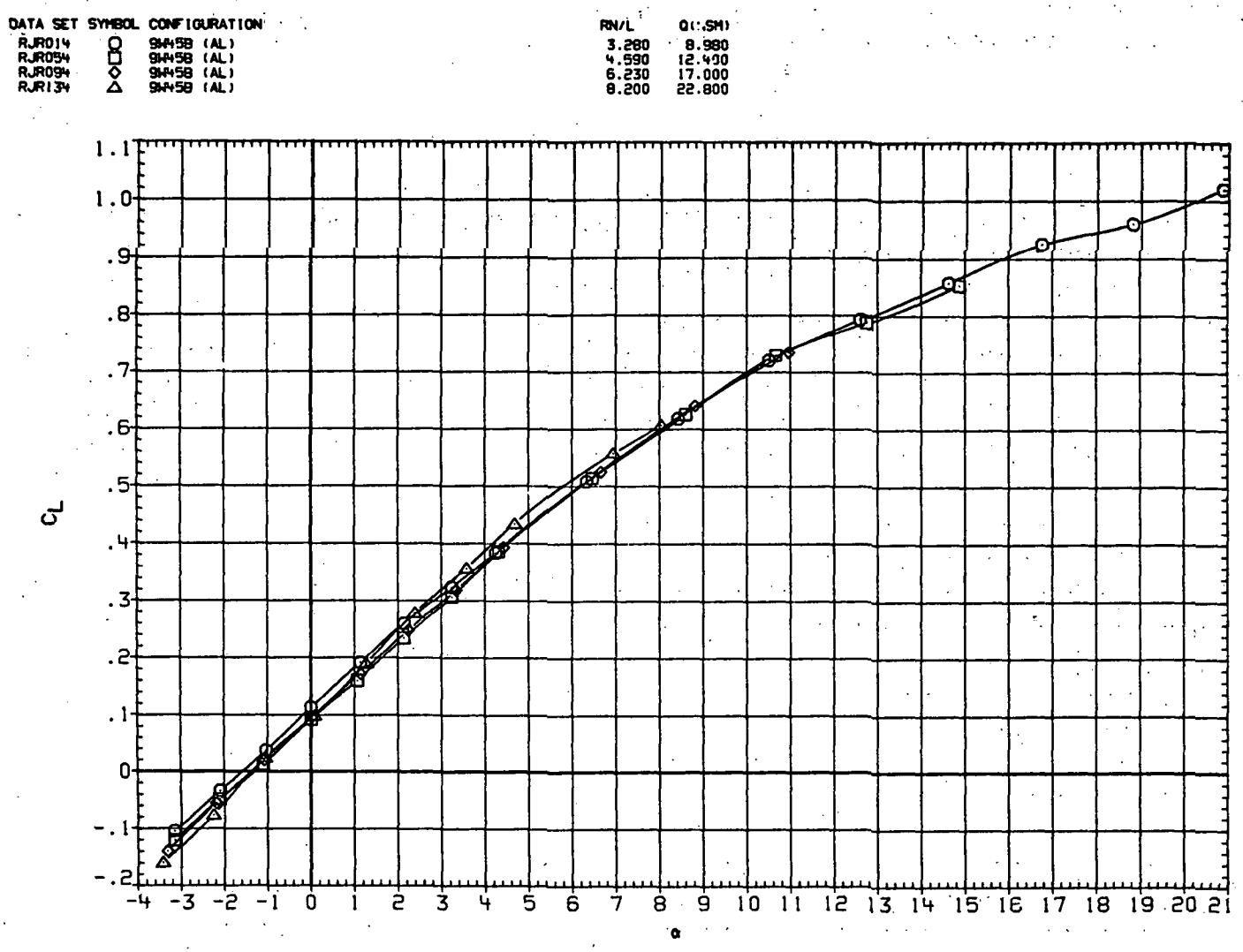

(a) C_L vs α.

Figure 14.– Dynamic-pressure effects on the aerodynamic characteristics of the aluminum trapezoidal oblique wing-body combination ($\Lambda = 45°$, $M = 1.2$ and the modified NACA 65A204 airfoil).

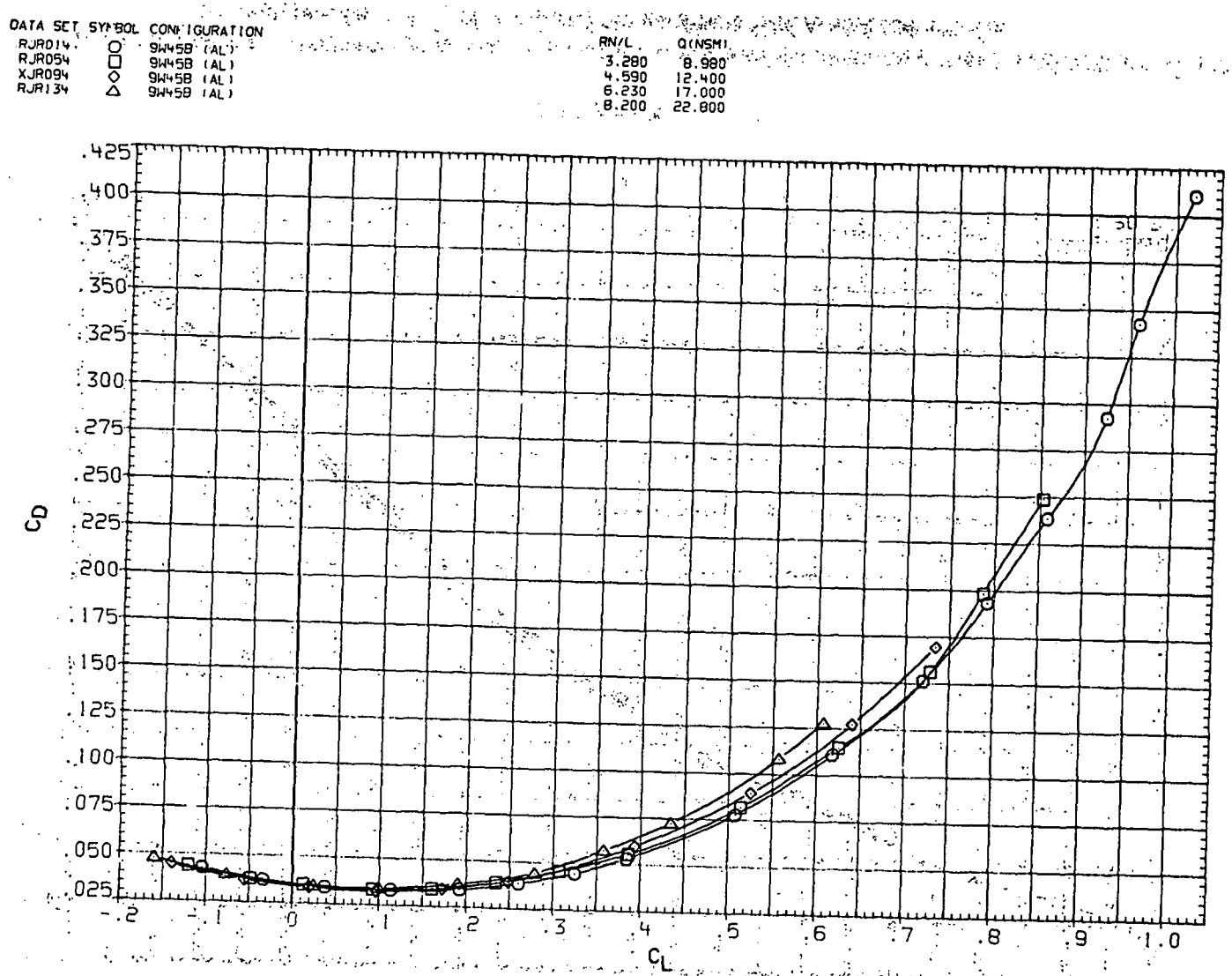

(b) C_D vs C_L.

Figure 14.– Continued.

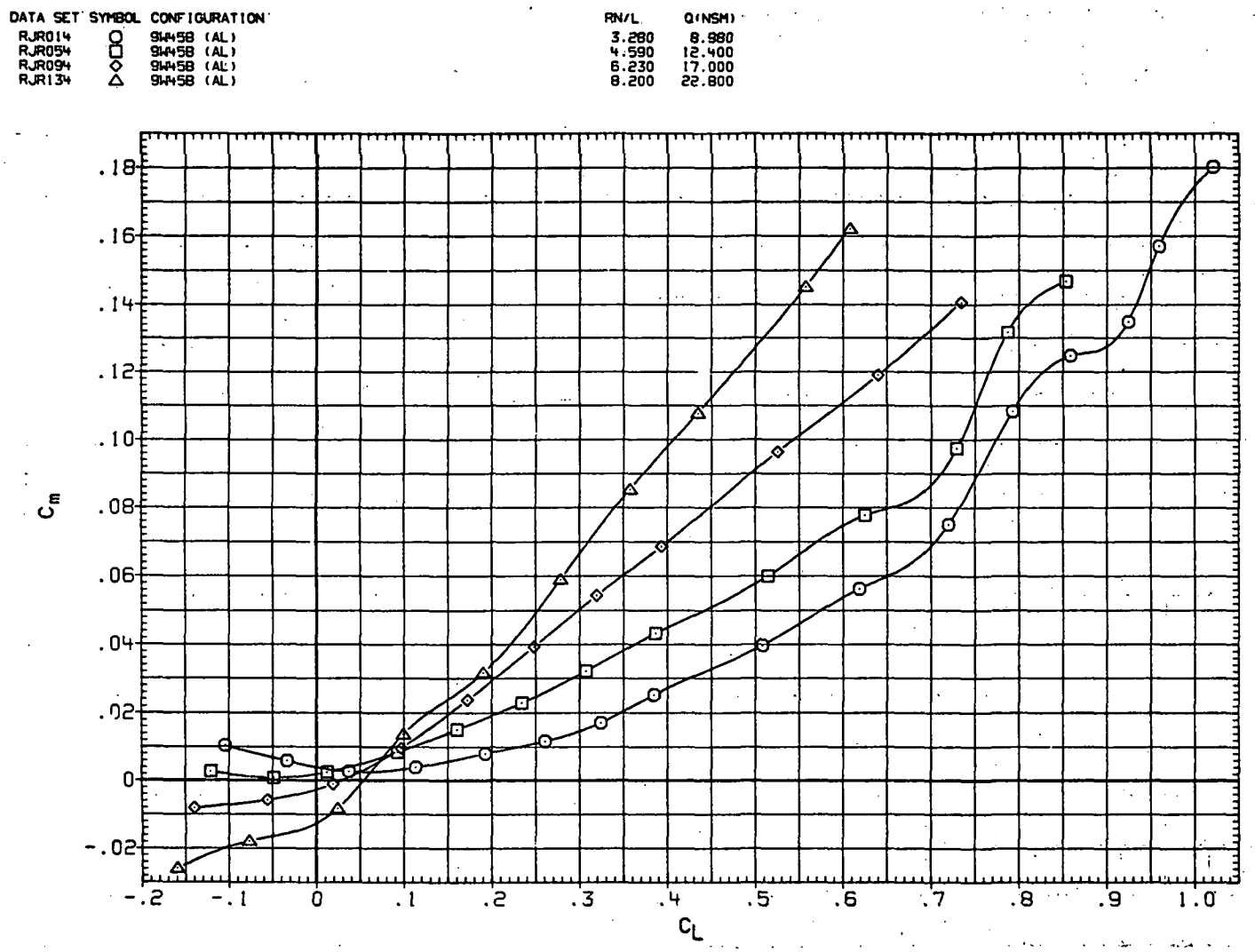

(c) C_m vs C_L.

Figure 14.– Continued.

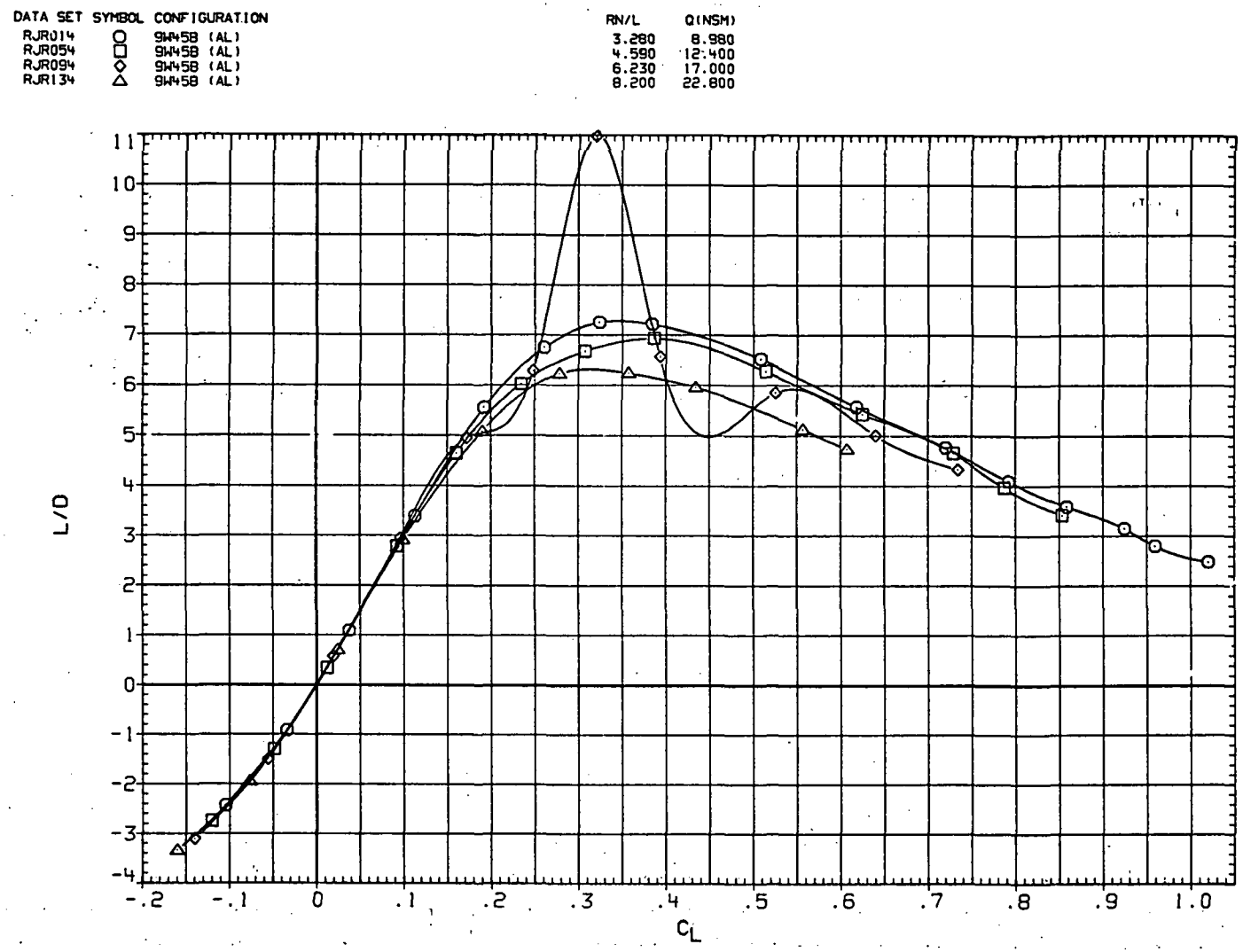

(d) L/D vs C_L.

Figure 14.– Continued.

DATA SET	SYMBOL	CONFIGURATION	RN/L	Q(NSM)
RJR014	○	9W45B (AL)	3.280	8.980
RJR054	□	9W45B (AL)	4.590	12.400
RJR094	◇	9W45B (AL)	6.230	17.000
RJR134	△	9W45B (AL)	8.200	22.800

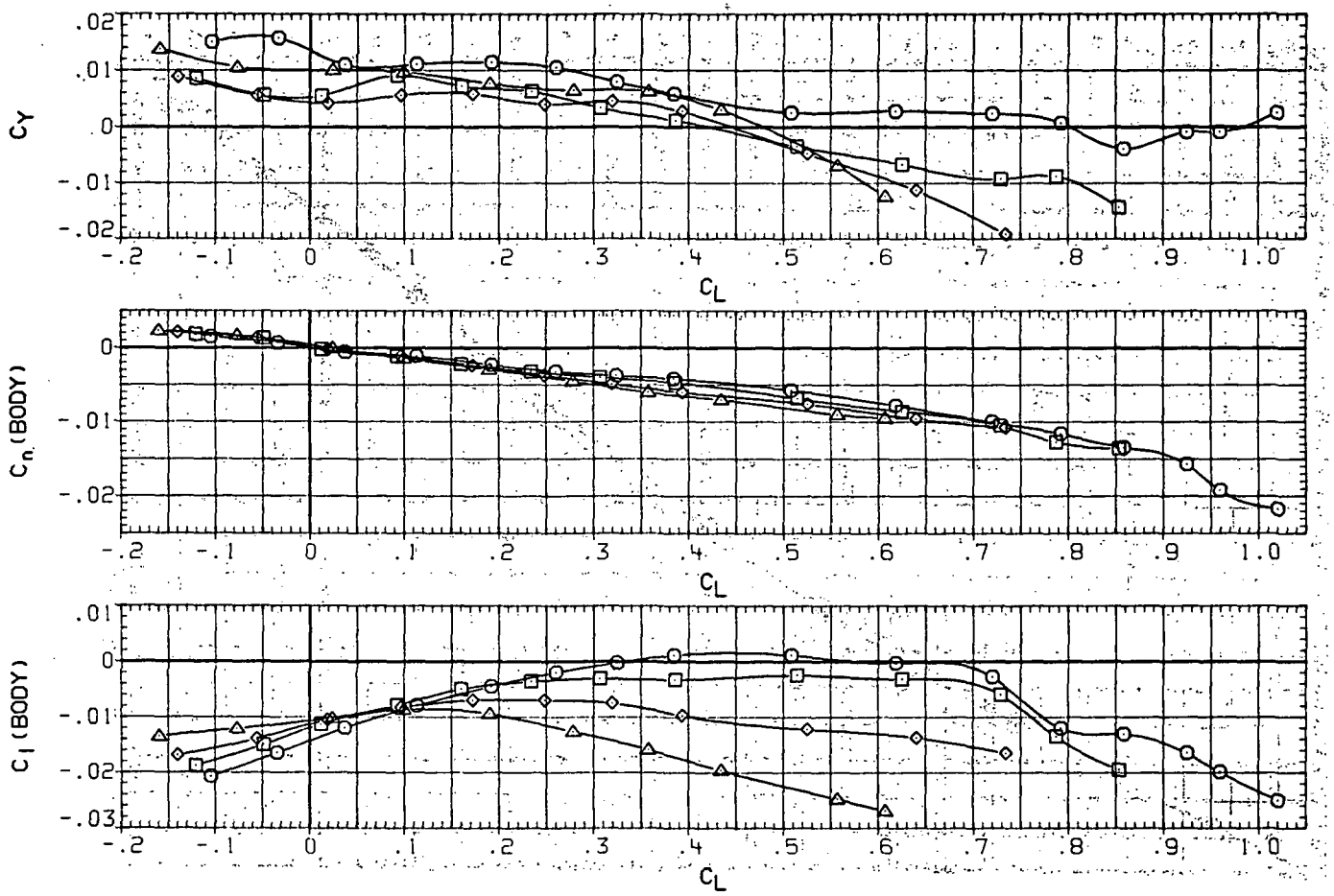

(e) C_Y, C_n and C_ℓ vs C_L.

Figure 14.– Concluded.

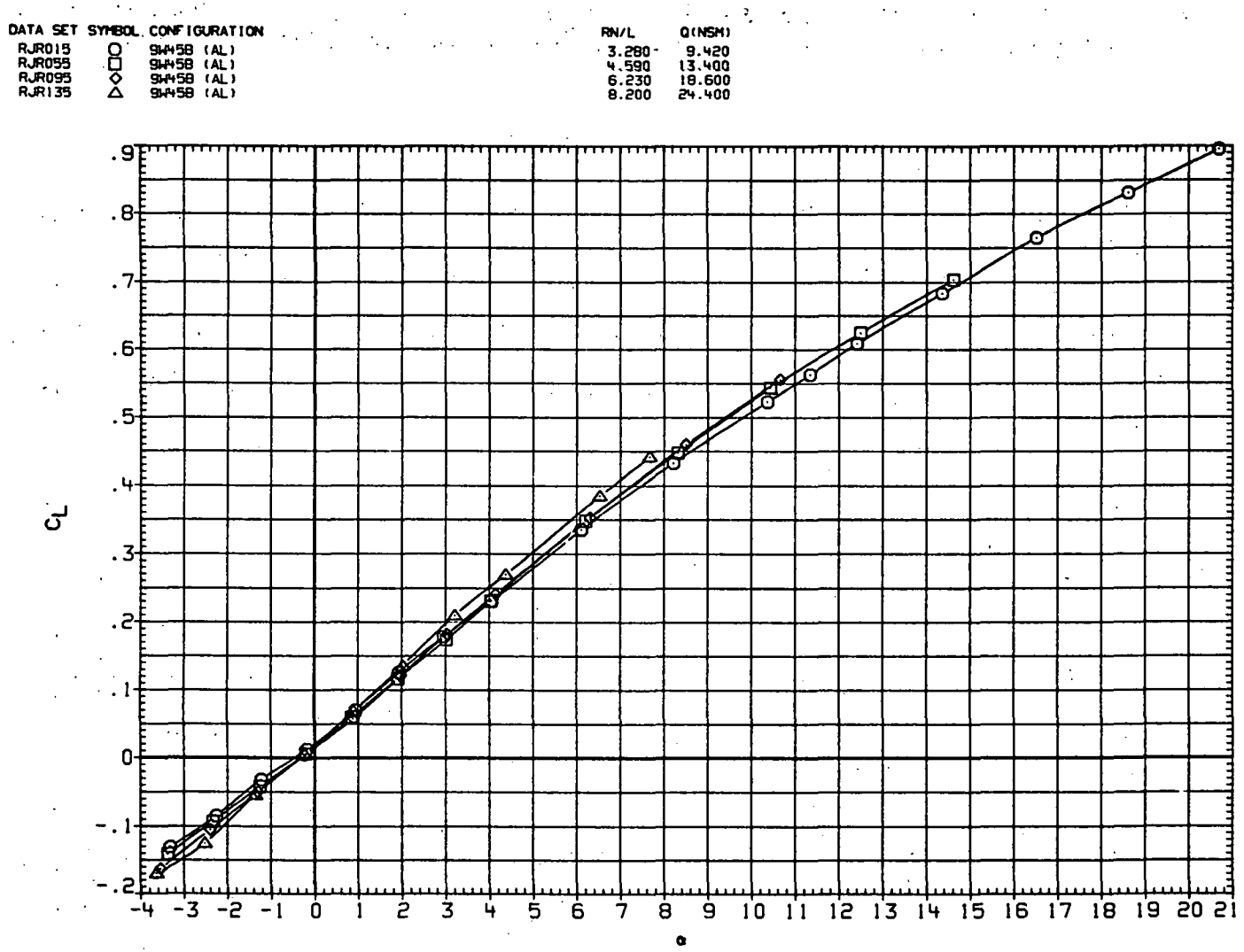

(a) C_L vs α.

Figure 15.– Dynamic-pressure effects on the aerodynamic characteristics of the aluminum trapezoidal oblique wing-body combination ($\Lambda = 45°, M = 1.6$ and the modified NACA 65A204 airfoil).

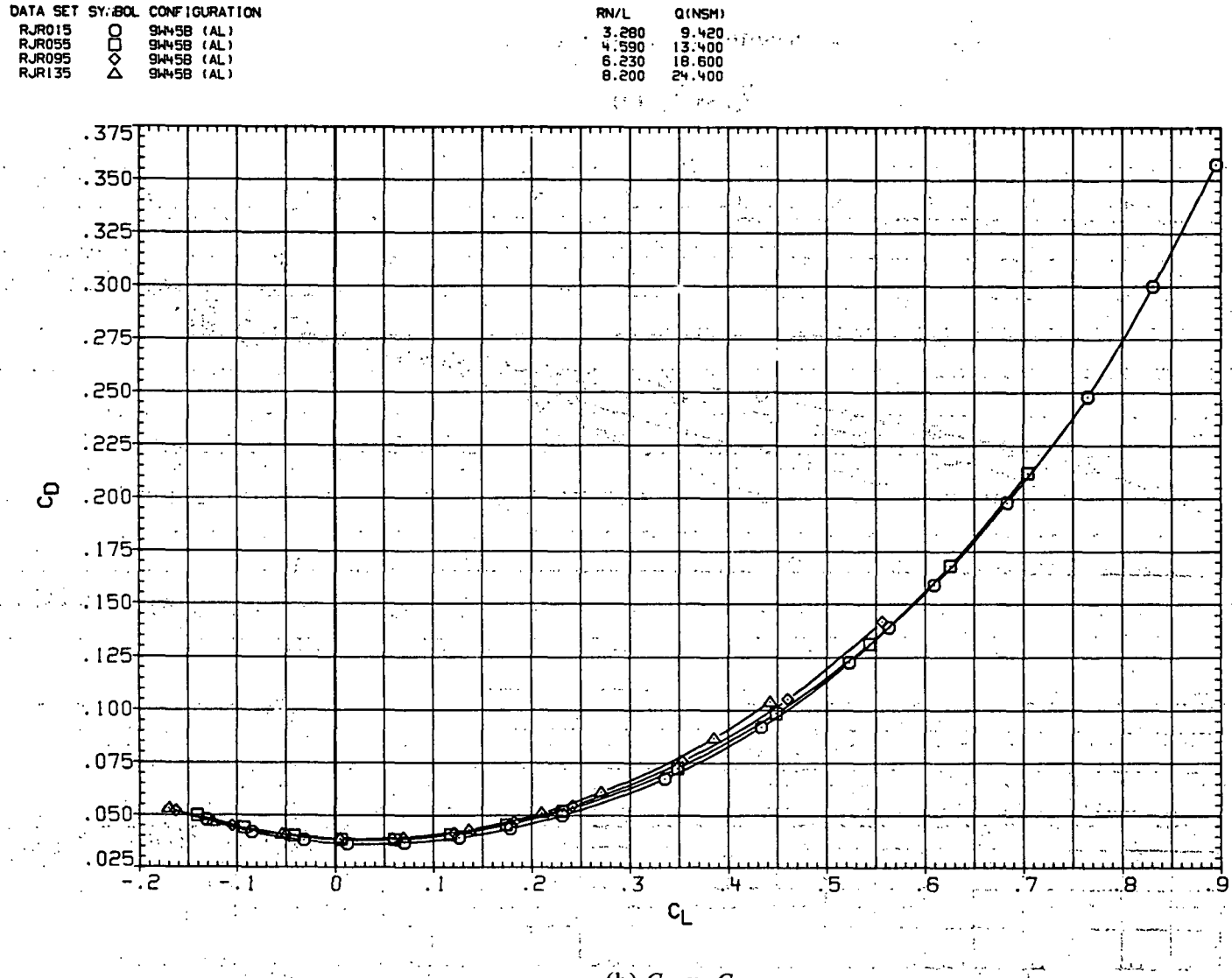

(b) C_D vs C_L.

Figure 15.– Continued.

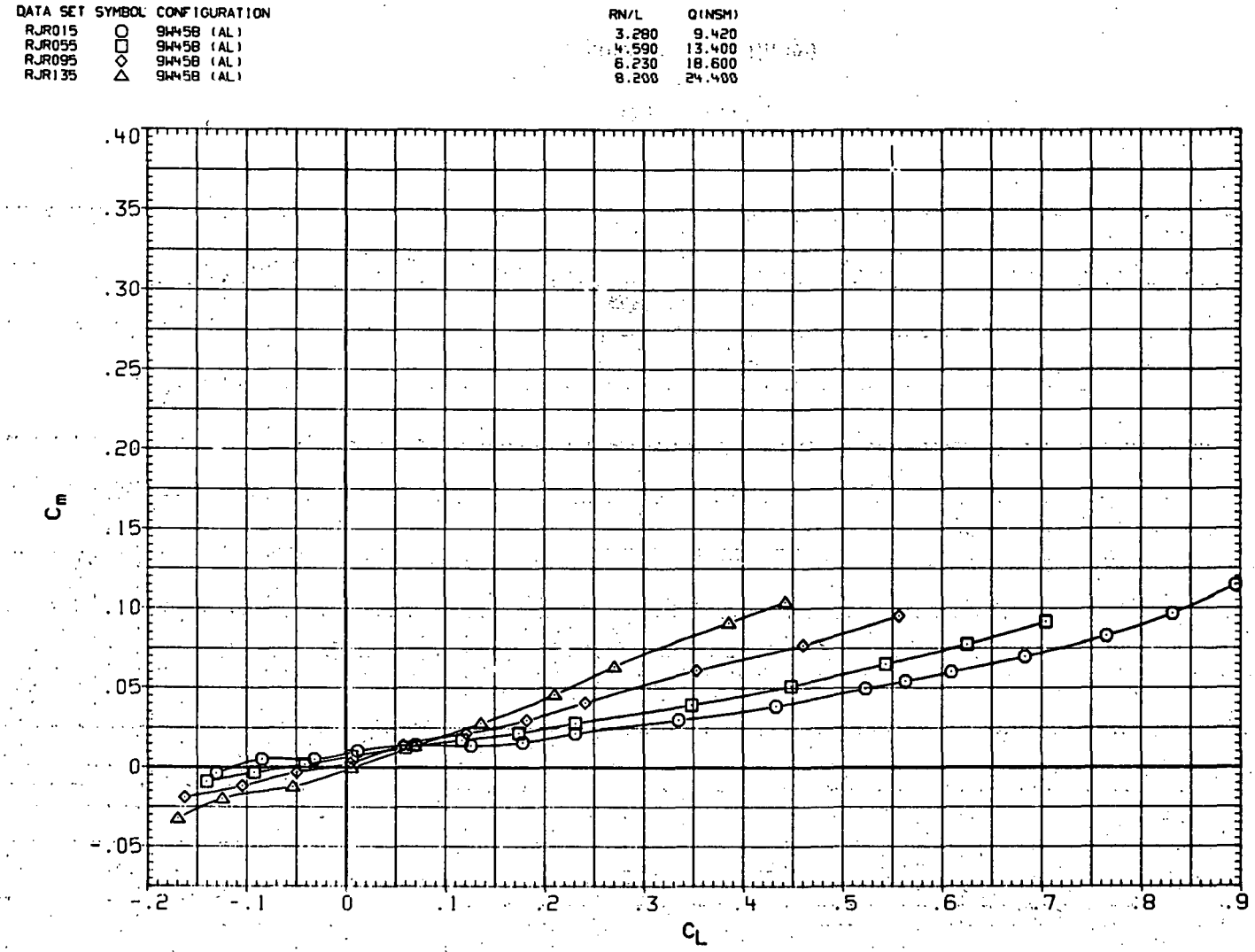

(c) C_m vs C_L.

Figure 15.– Continued.

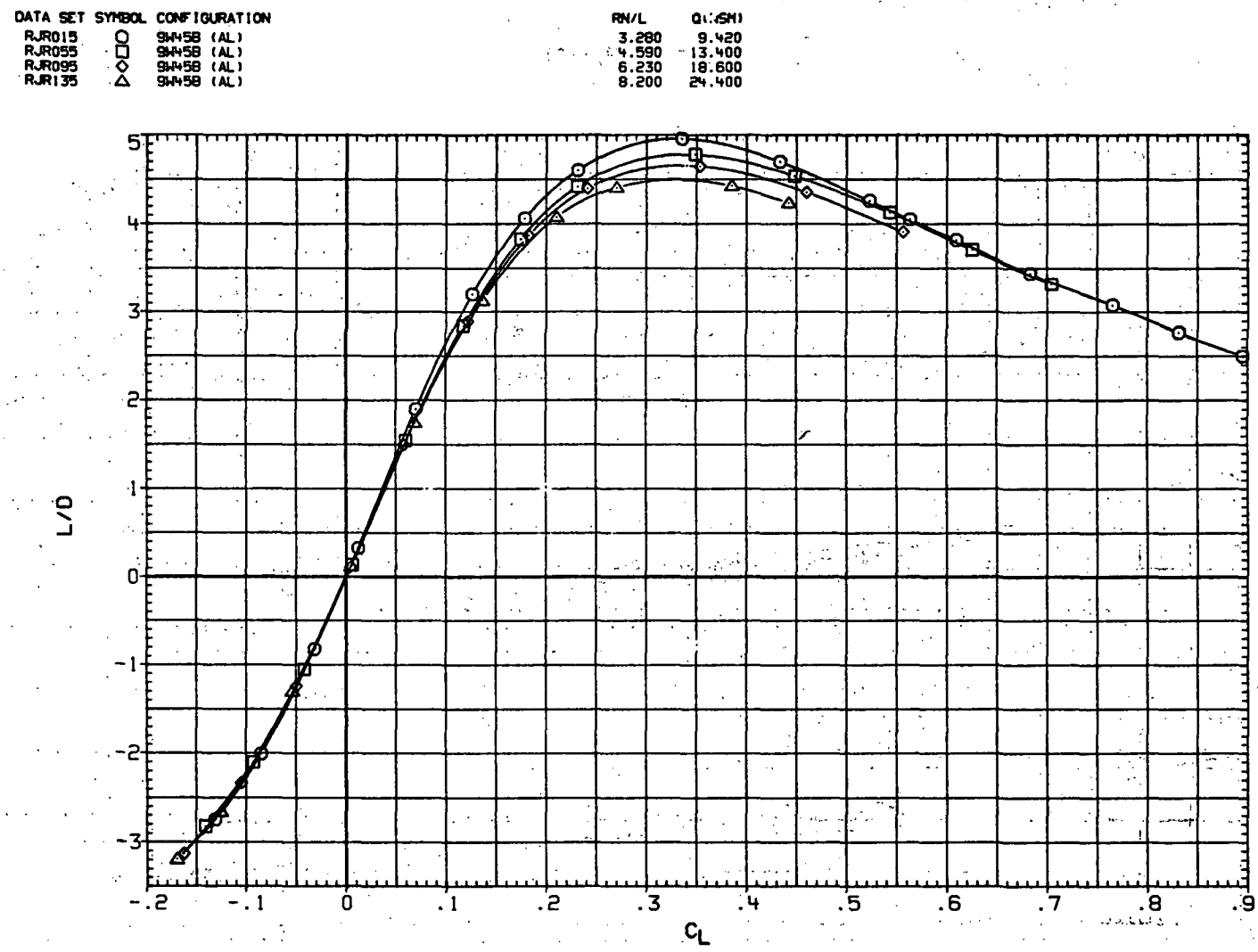

(d) L/D vs C_L.

Figure 15.– Continued.

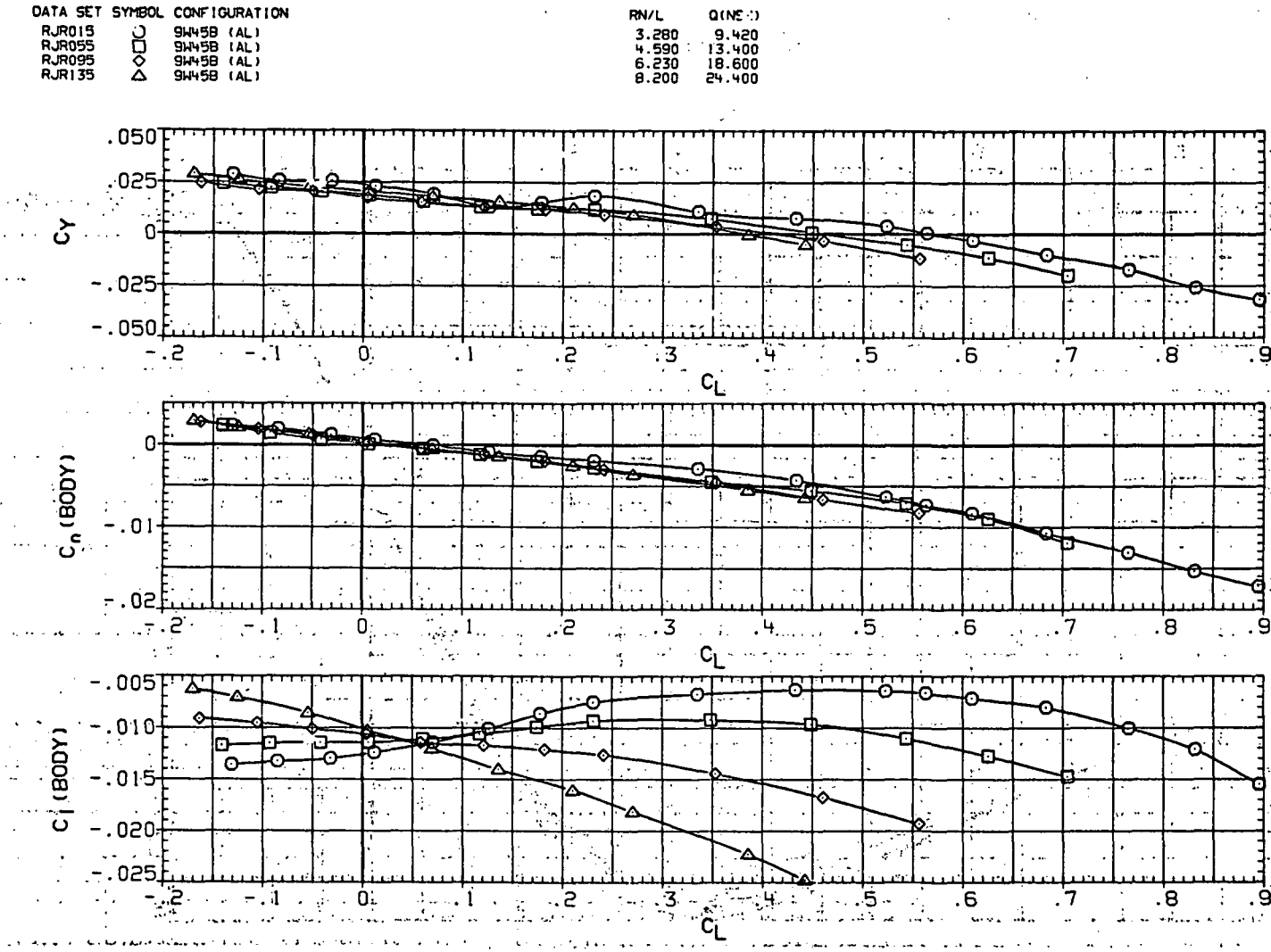

(e) C_Y, C_n and C_ℓ vs C_L.

Figure 15.– Concluded.

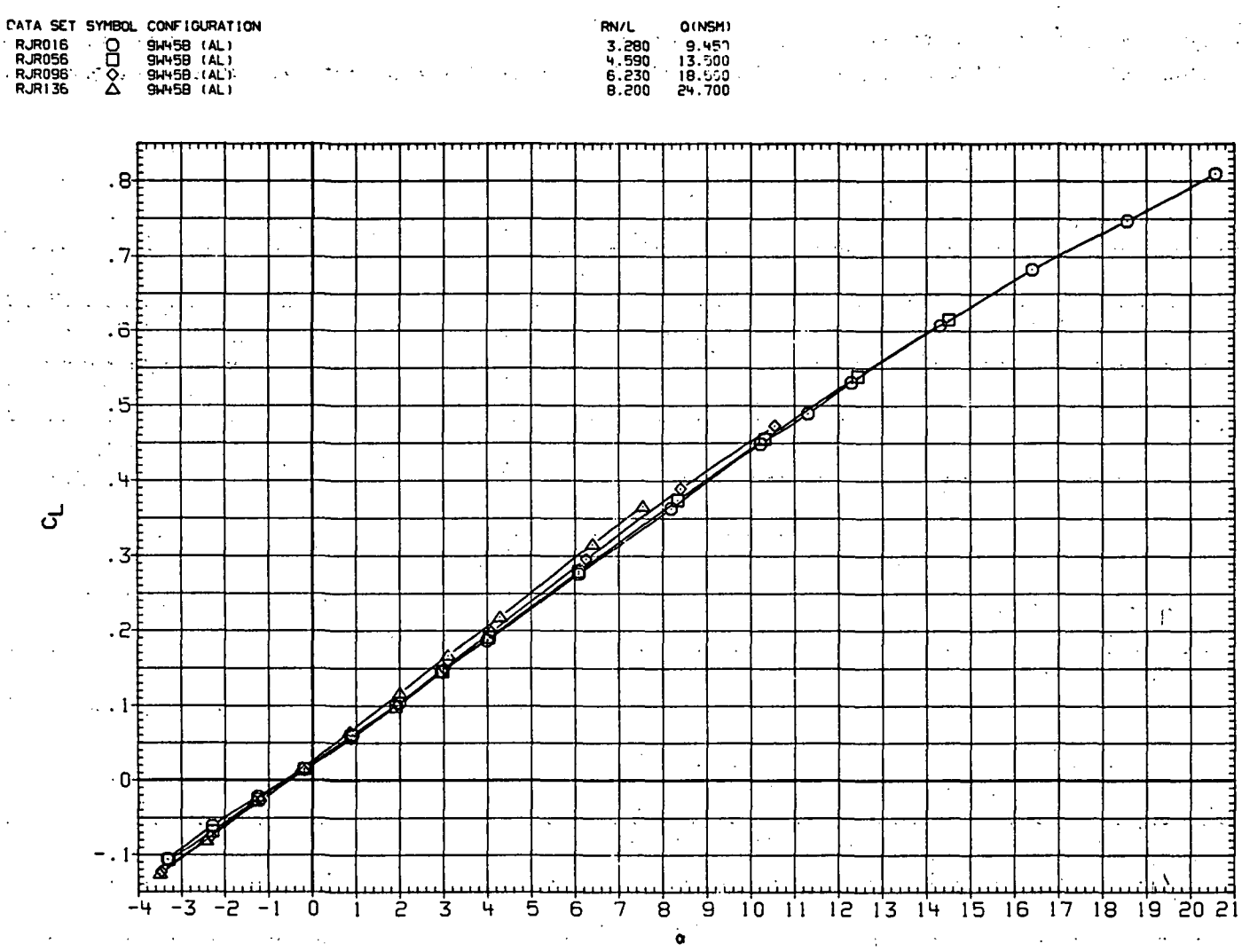

(a) C_L vs α.

Figure 16.– Dynamic-pressure effects on the aerodynamic characteristics of the aluminum trapezoidal oblique wing-body combination ($\Lambda = 45°$, $M = 2.0$ and the modified NACA 65A204 airfoil).

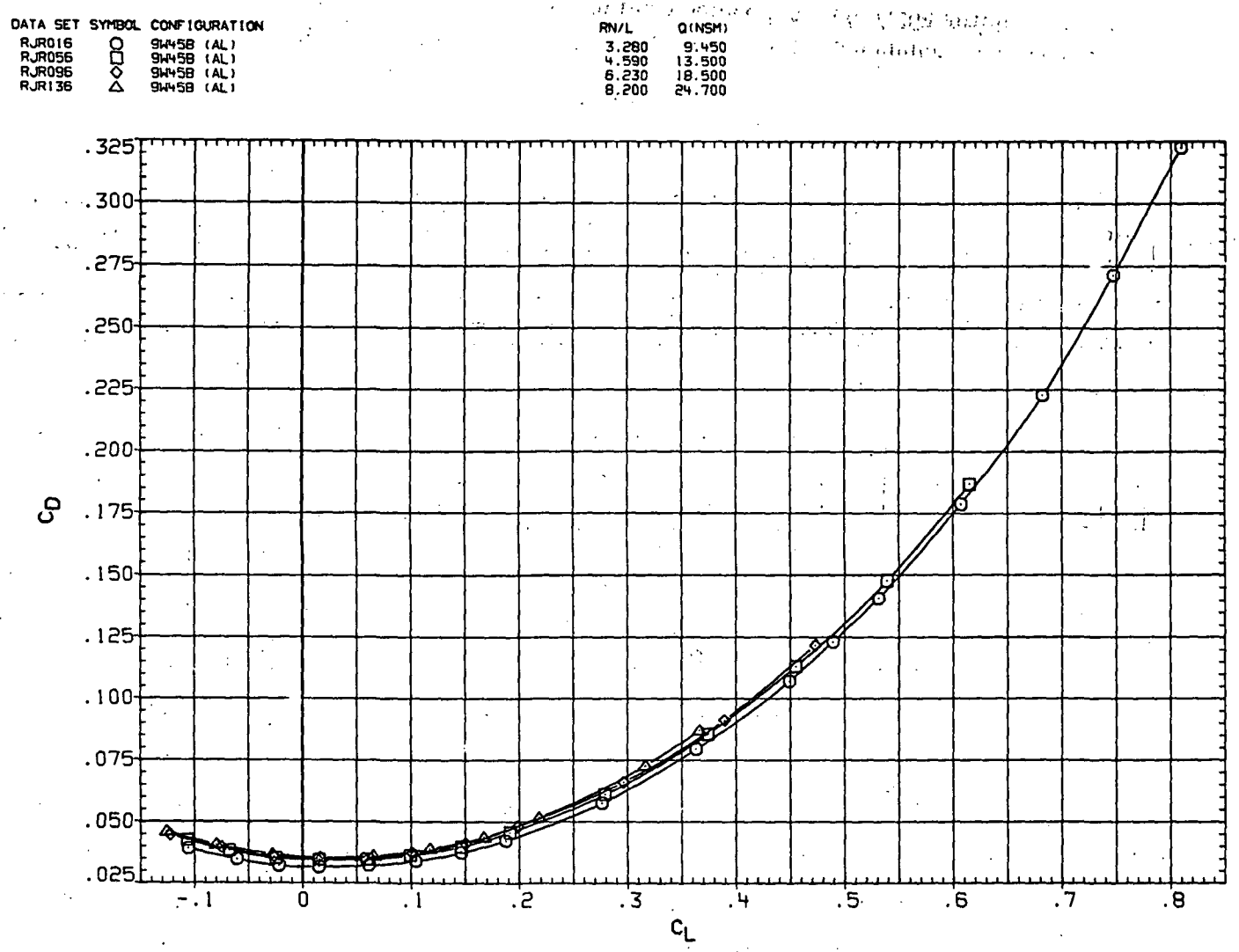

(b) C_D vs C_L.

Figure 16.– Continued.

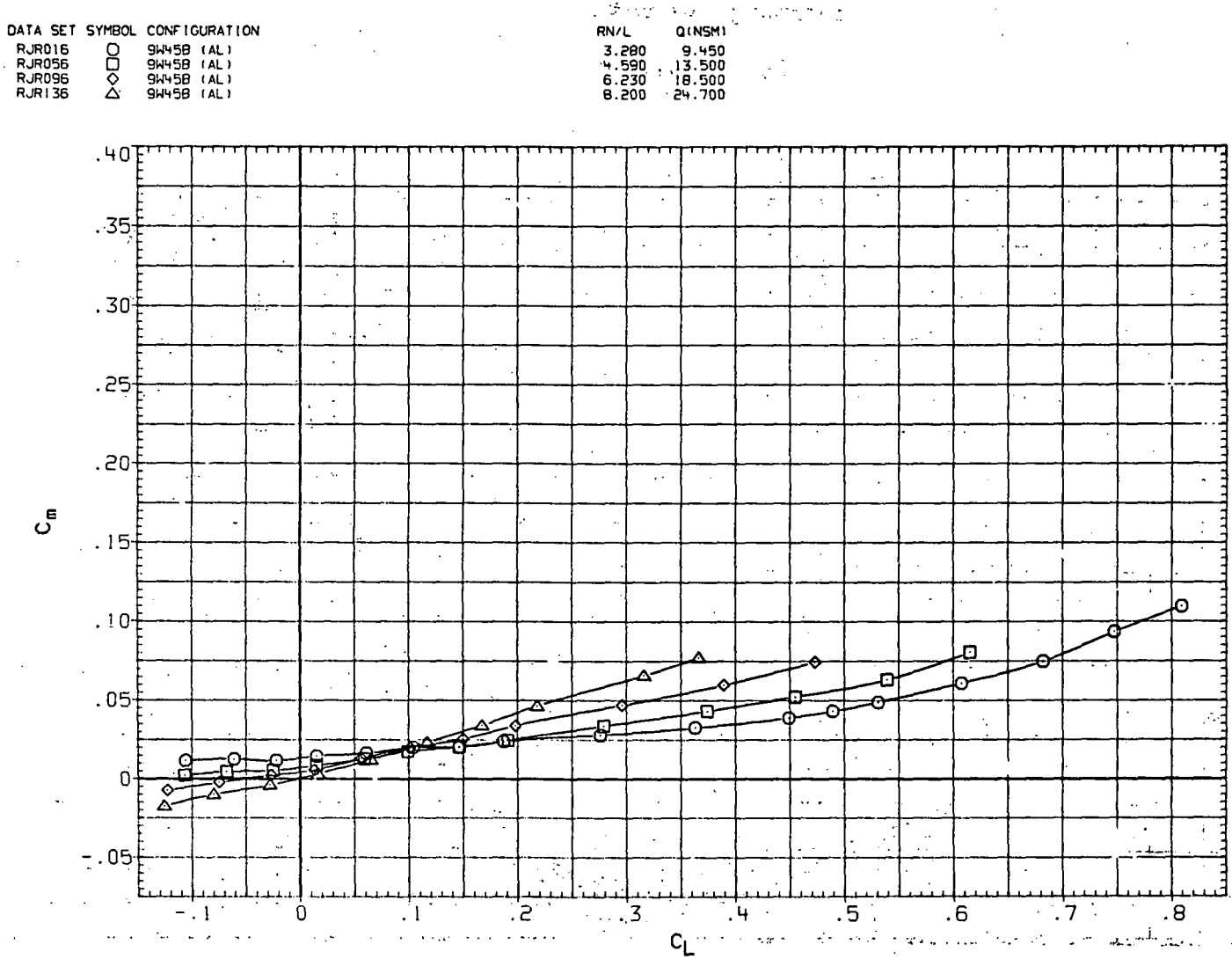

(c) C_m vs C_L.

Figure 16.– Continued.

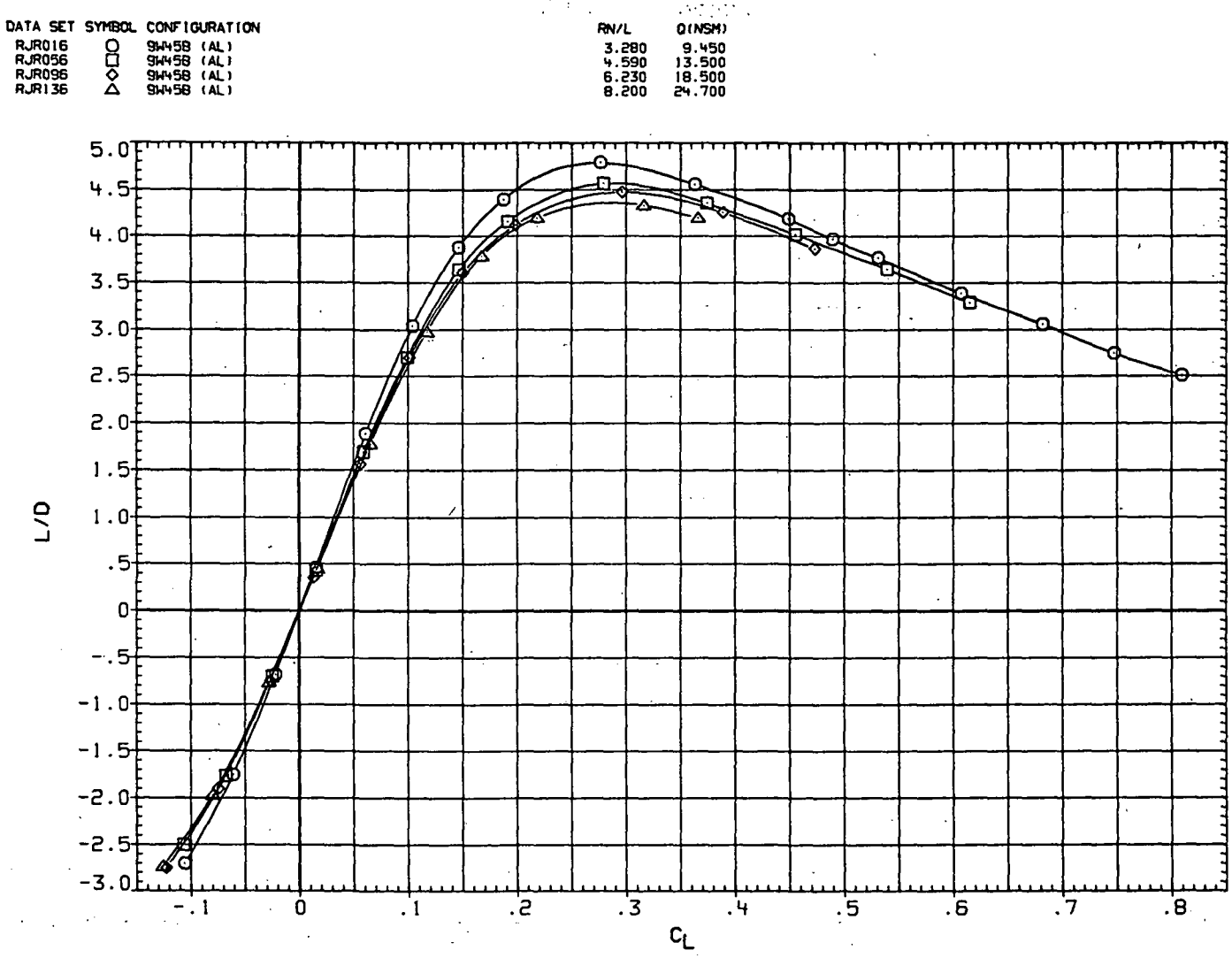

(d) L/D vs C_L.

Figure 16.– Continued.

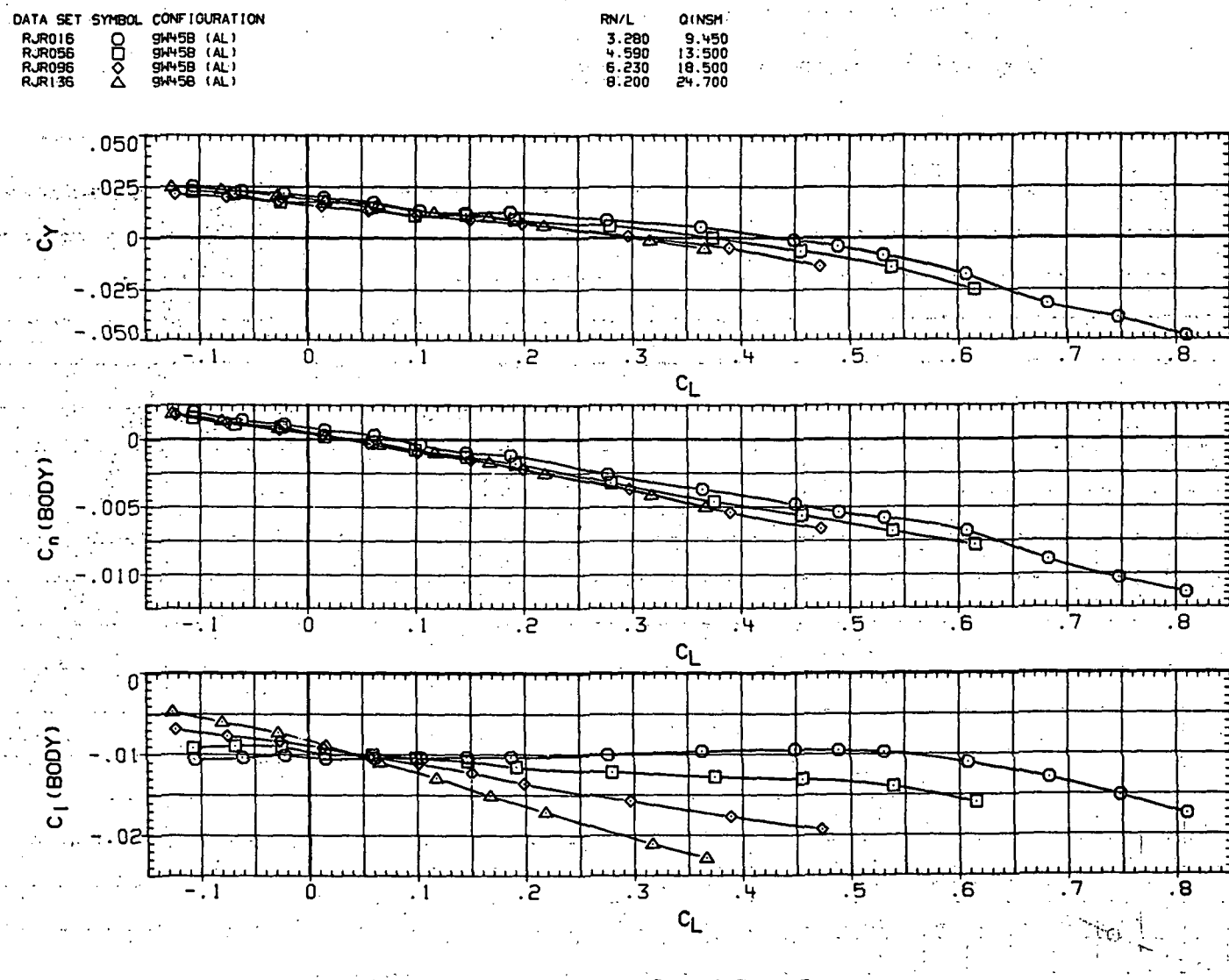

(e) C_Y, C_n and C_ℓ vs C_L.

Figure 16.– Concluded.

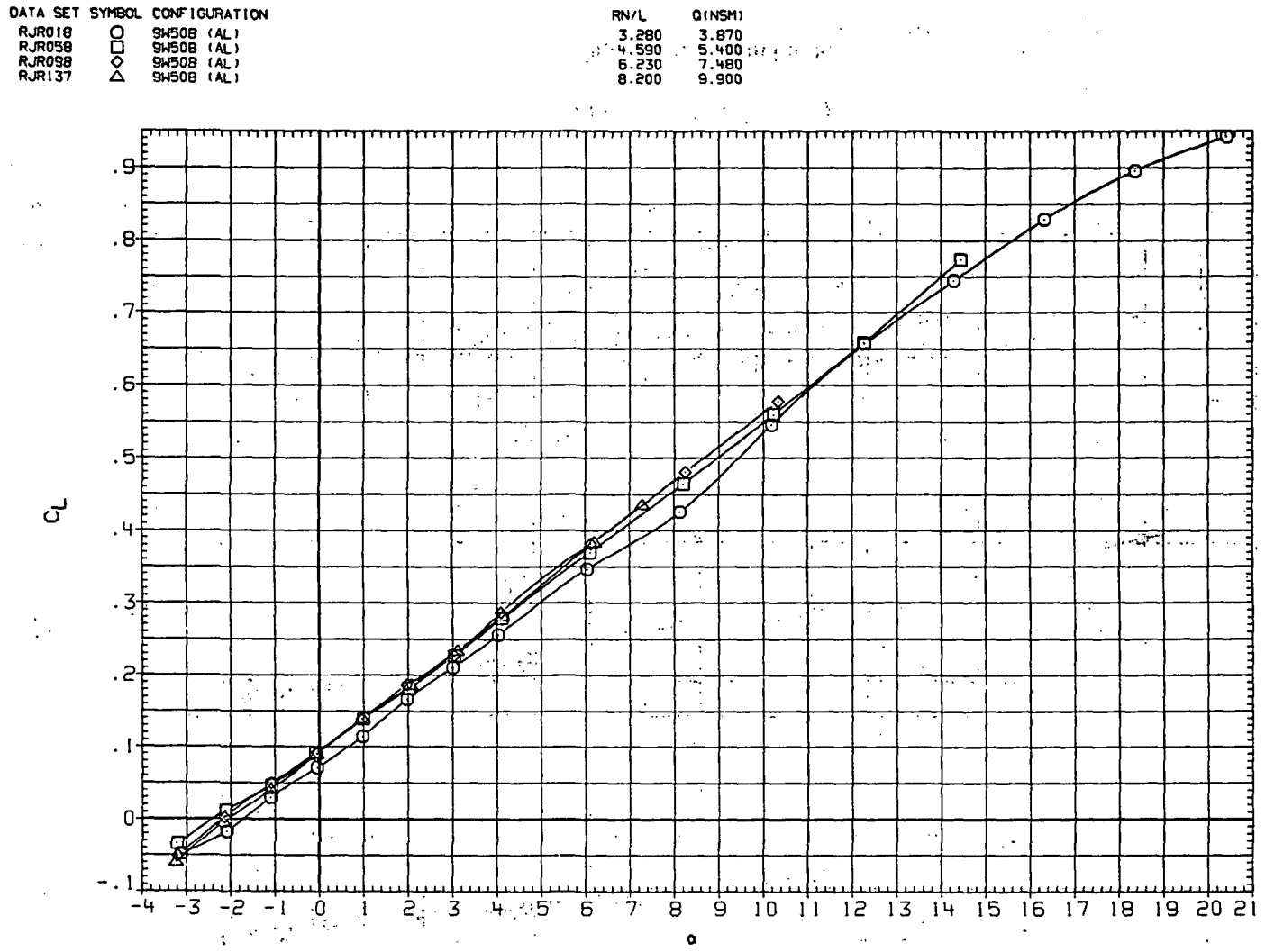

(a) C_L vs α.

Figure 17.– Dynamic-pressure effects on the aerodynamic characteristics of the aluminum trapezoidal oblique wing-body combination ($\Lambda = 50°$, $M = 0.4$ and the modified NACA 65A204 airfoil).

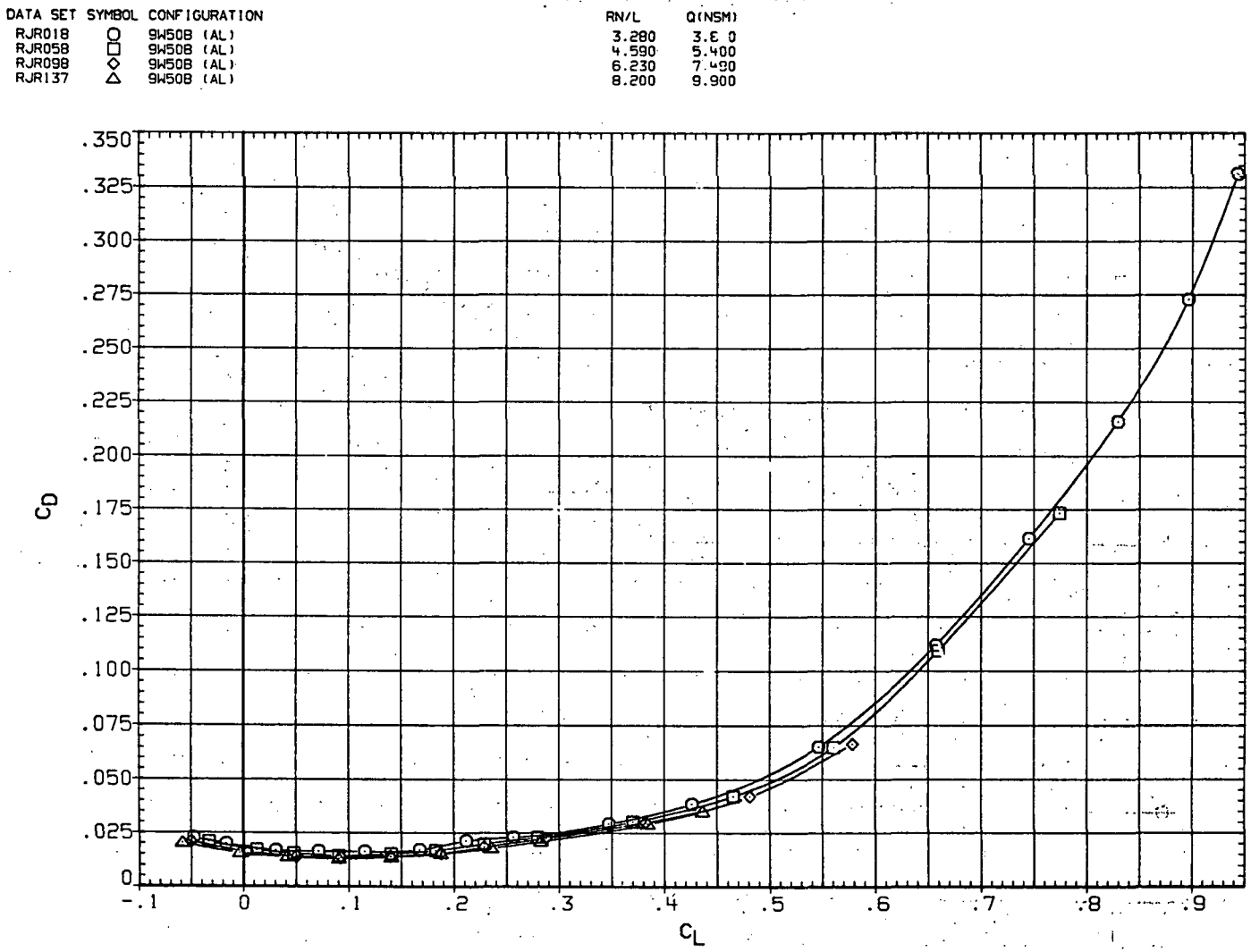

(b) C_D vs C_L.

Figure 17.– Continued.

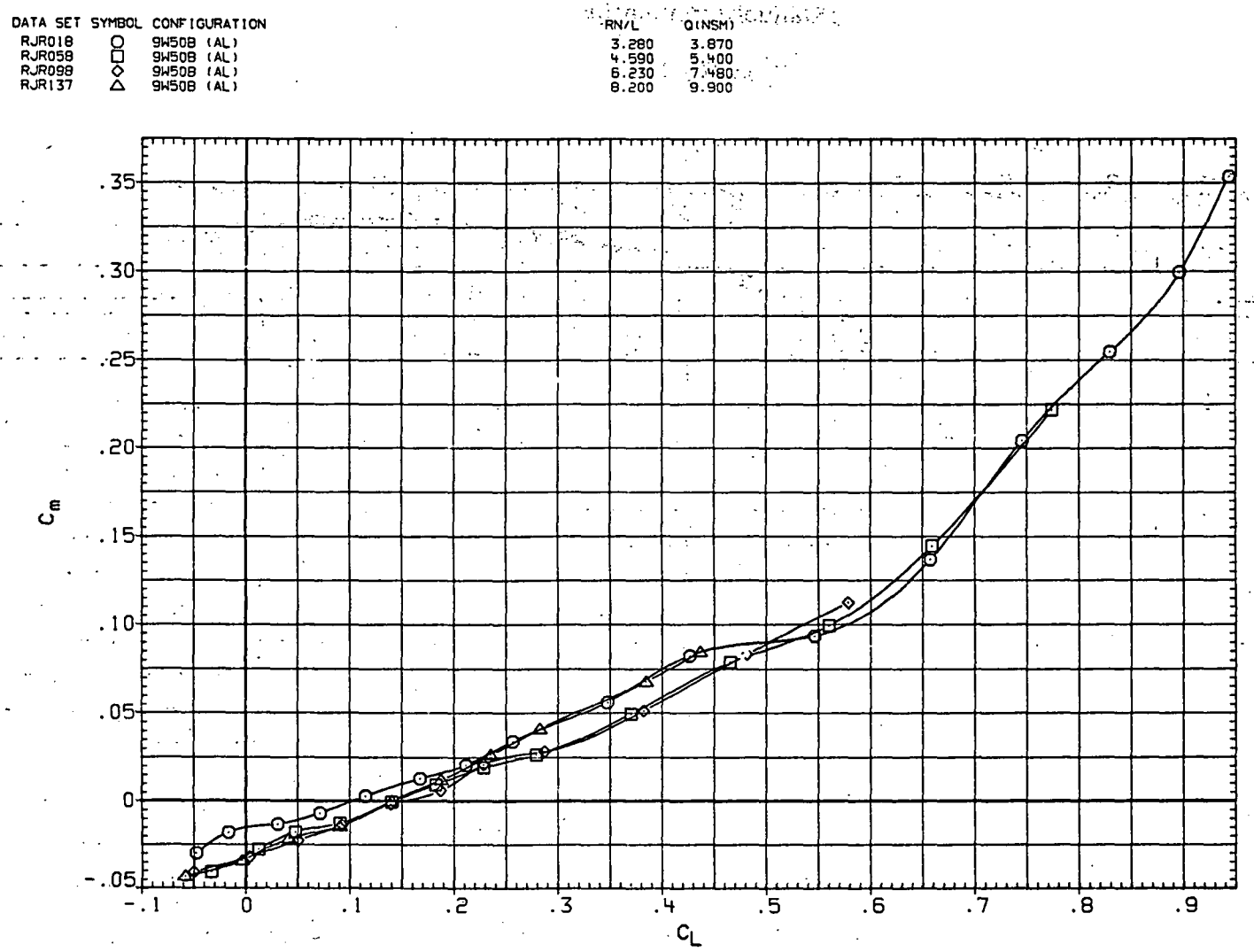

(c) C_m vs C_L.

Figure 17.– Continued.

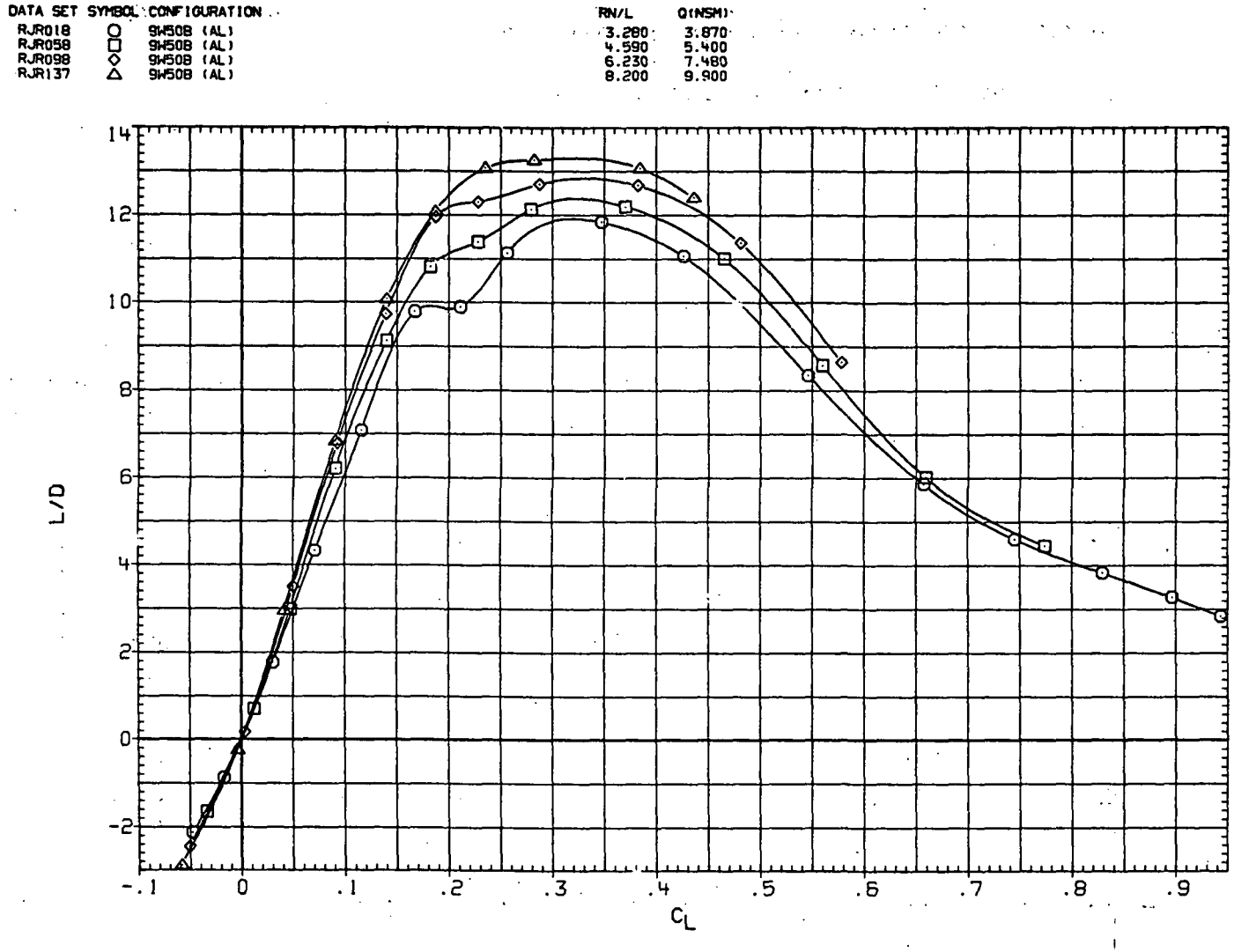

(d) L/D vs C_L.

Figure 17.– Continued.

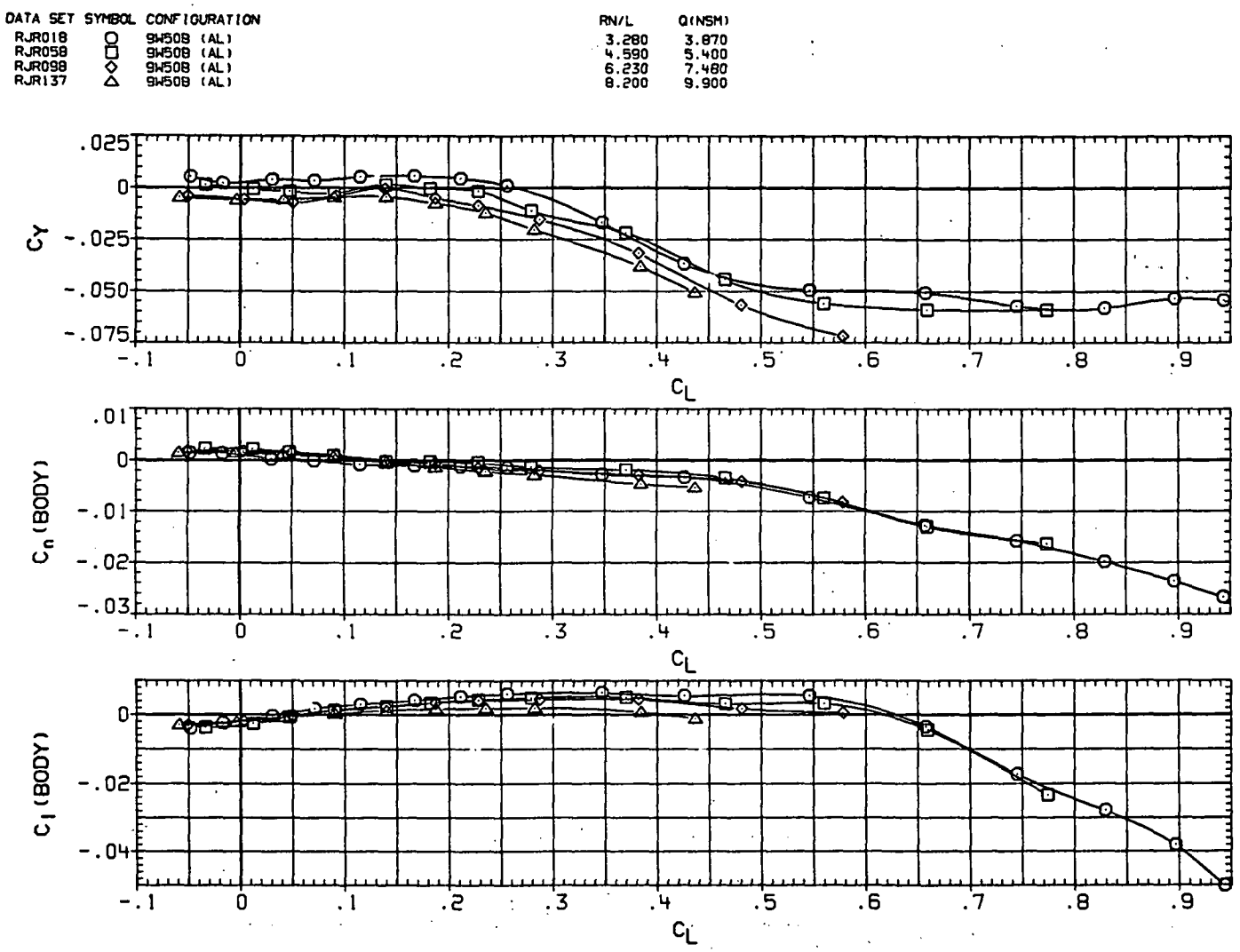

(e) C_Y, C_n and C_ℓ vs C_L.

Figure 17.– Concluded.

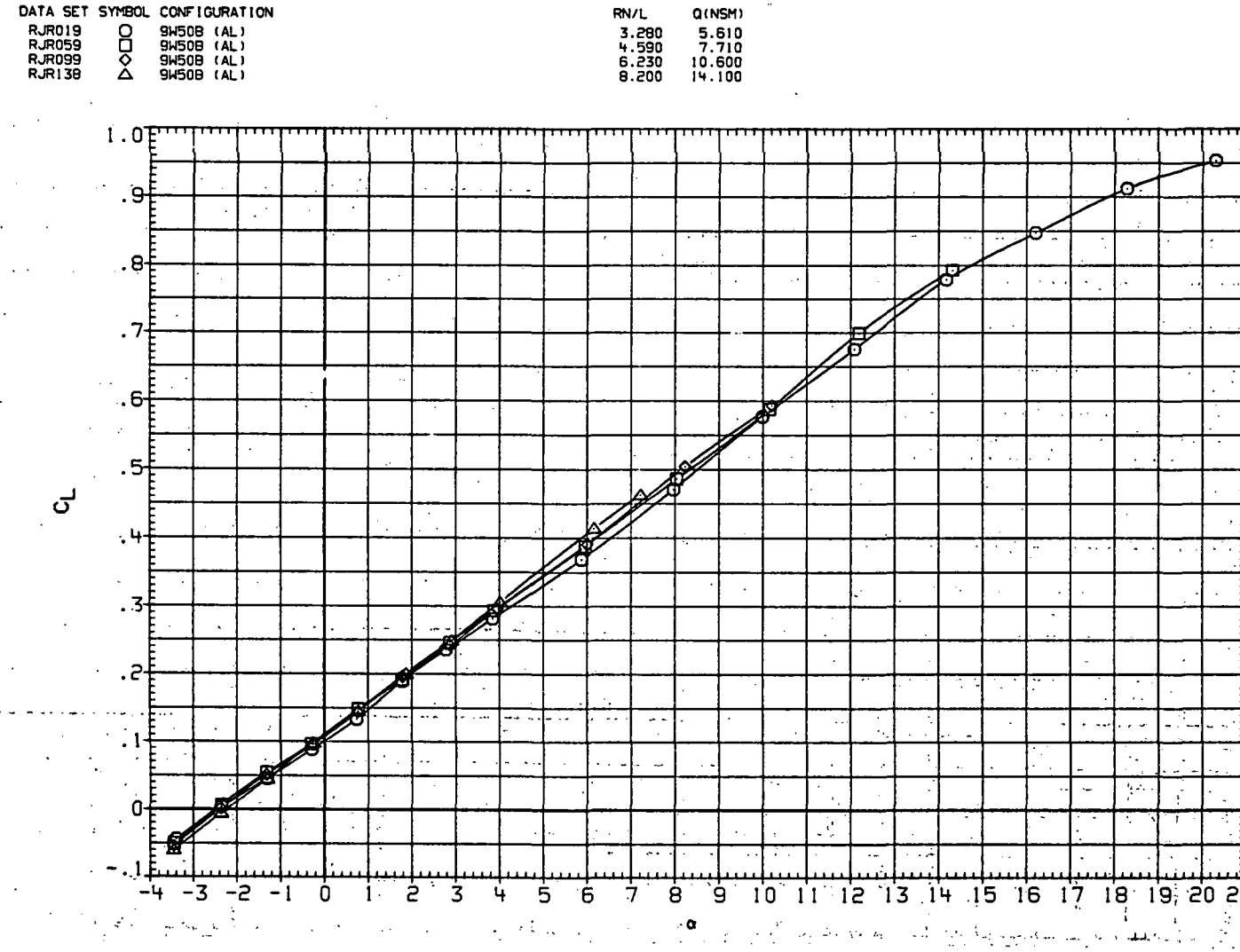

(a) C_L vs α.

Figure 18.– Dynamic-pressure effects on the aerodynamic characteristics of the aluminum trapezoidal oblique wing-body combination ($\Lambda = 50°$, $M = 0.6$ and the modified NACA 65A204 airfoil).

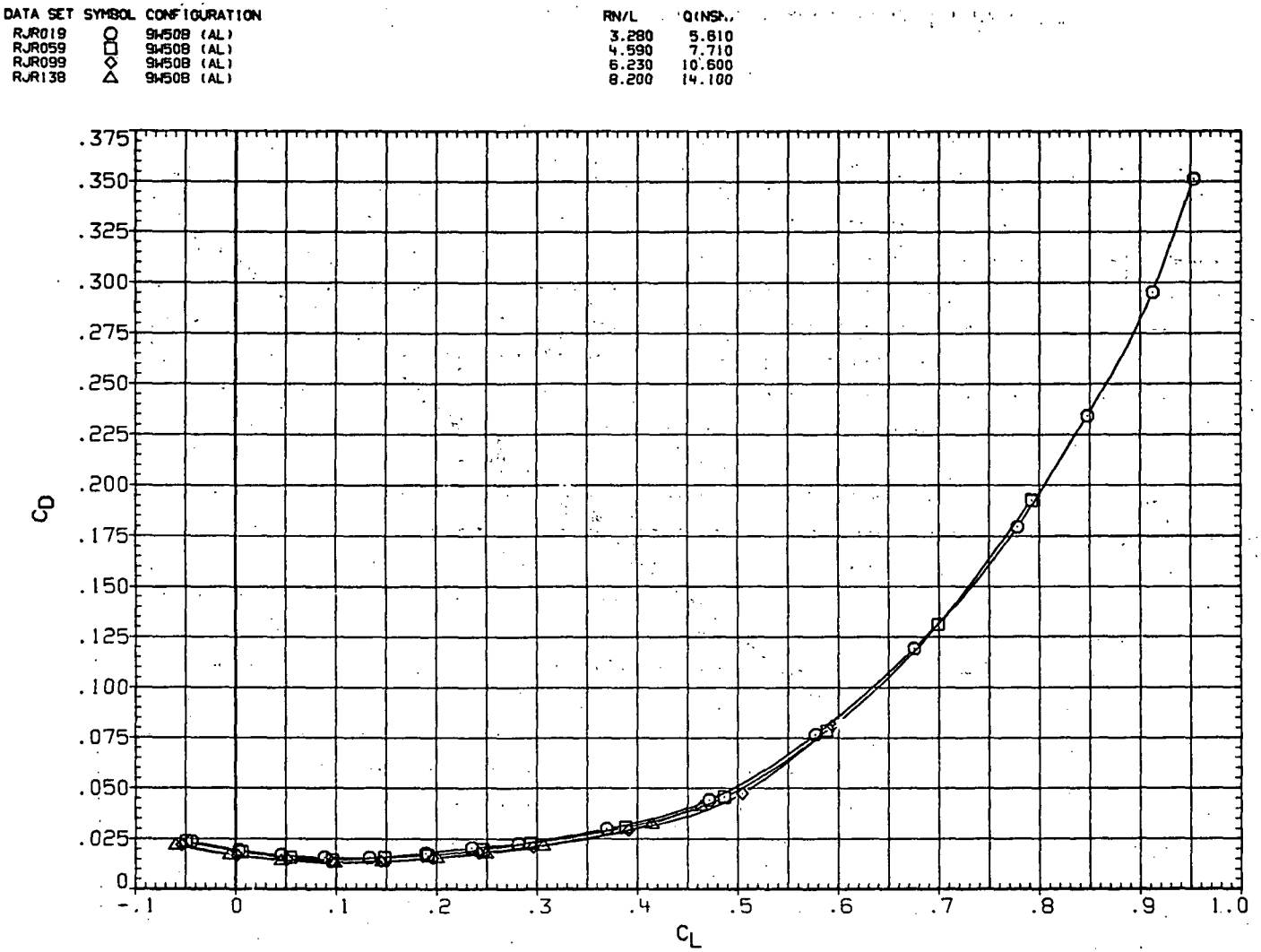

(b) C_D vs C_L.

Figure 18.– Continued.

DATA SET	SYMBOL	CONFIGURATION	RN/L	Q(NSM)
RJR019	○	9W50B (AL)	3.280	5.610
RJR059	□	9W50B (AL)	4.590	7.710
RJR099	◇	9W50B (AL)	6.230	10.600
RJR138	△	9W50B (AL)	8.200	14.100

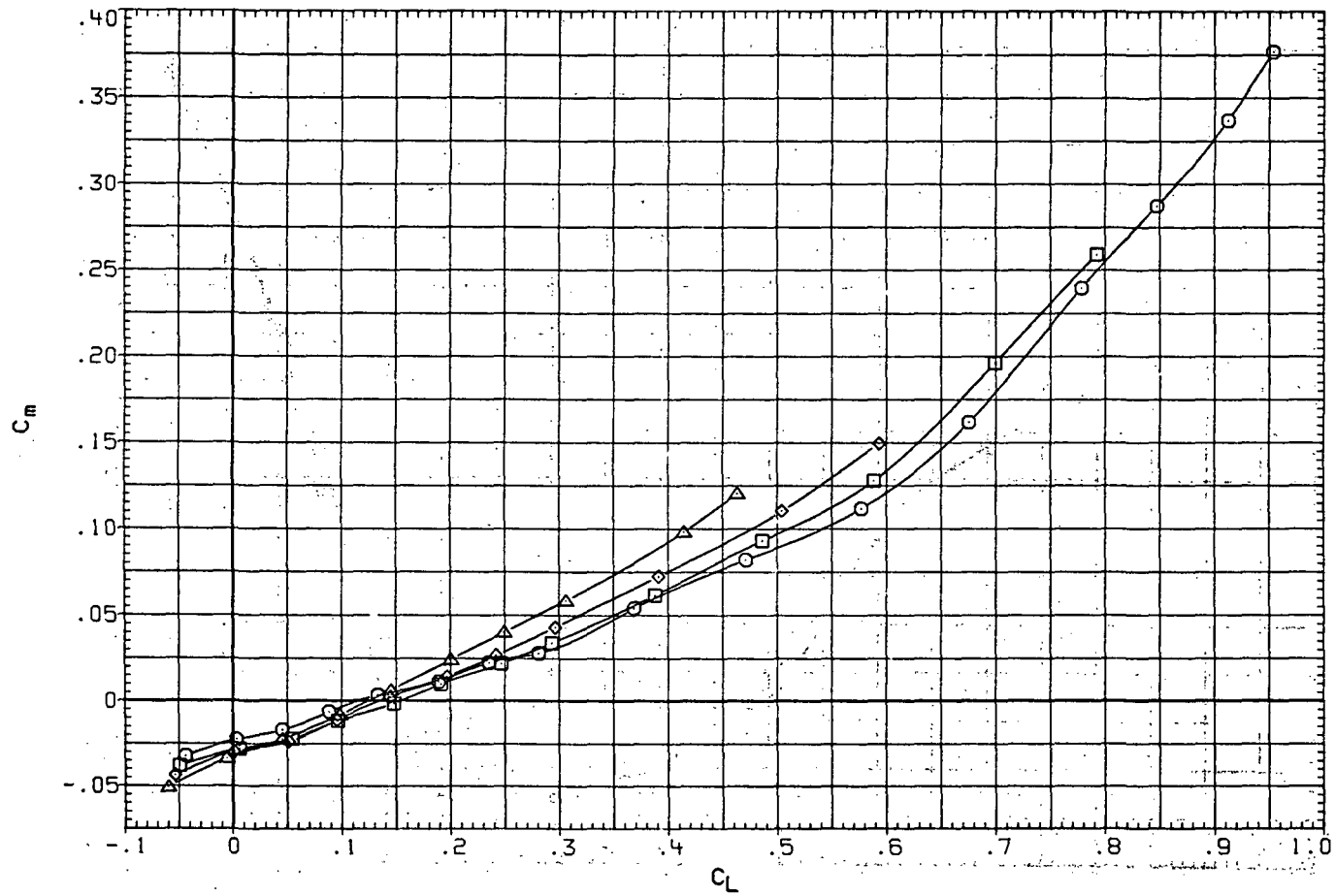

(c) C_m vs C_L.

Figure 18.– Continued.

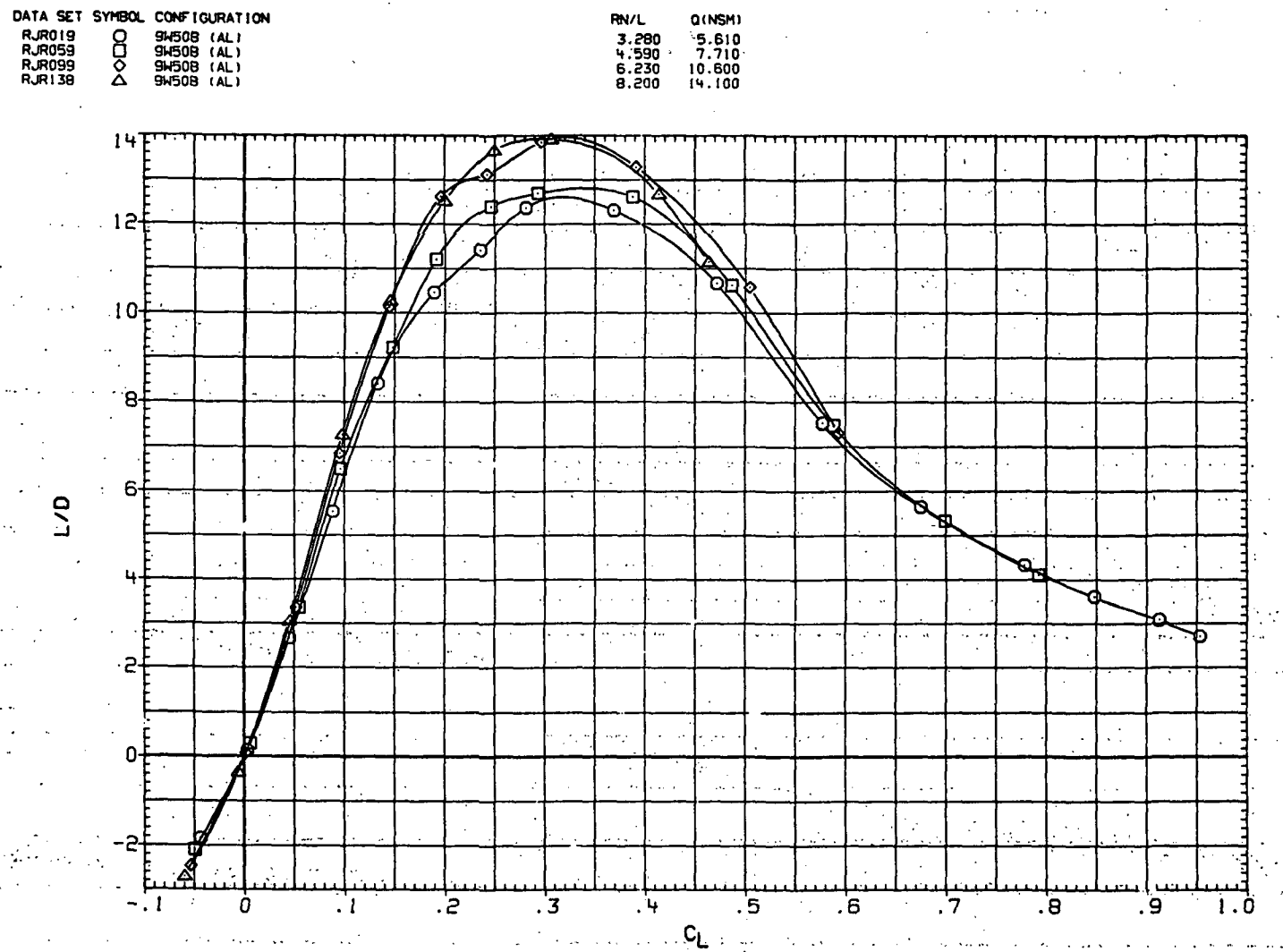

(d) L/D vs C_L.

Figure 18.– Continued.

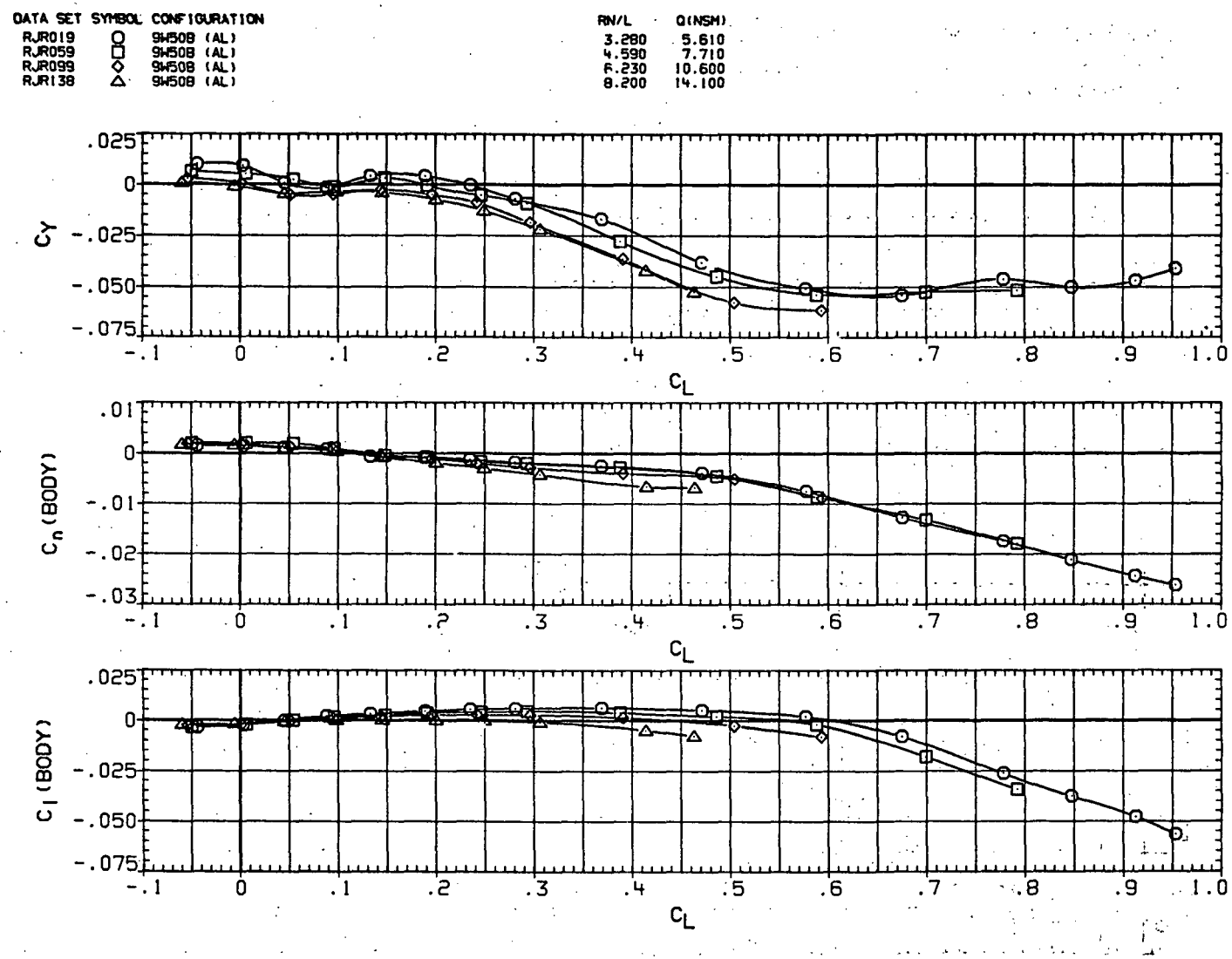

(e) C_Y, C_n and C_ℓ vs C_L.

Figure 18.– Concluded.

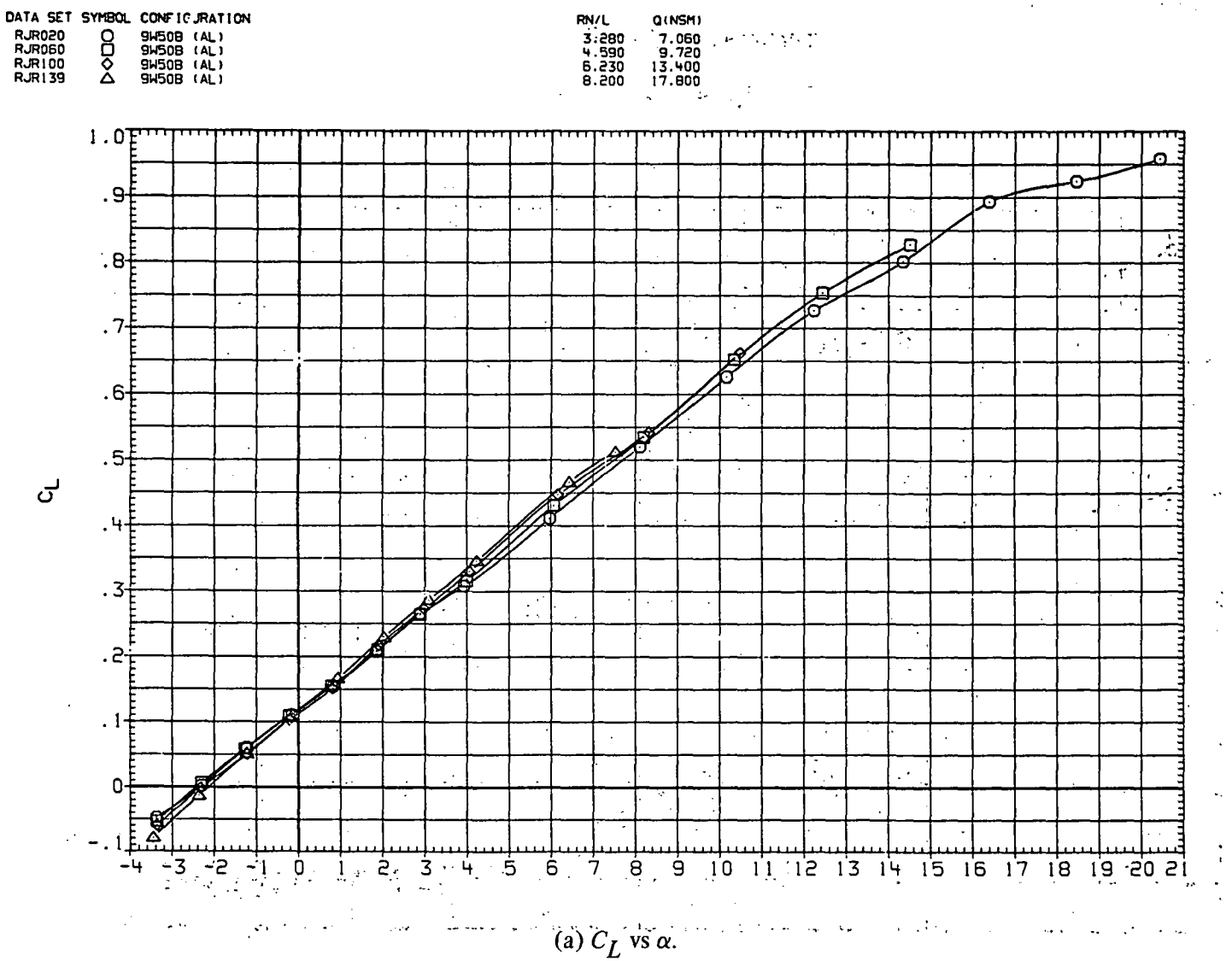

(a) C_L vs α.

Figure 19.– Dynamic-pressure effects on the aerodynamic characteristics of the aluminum trapezoidal oblique wing-body combination ($\Lambda = 50°$, $M = 0.8$ and the modified NACA 65A204 airfoil).

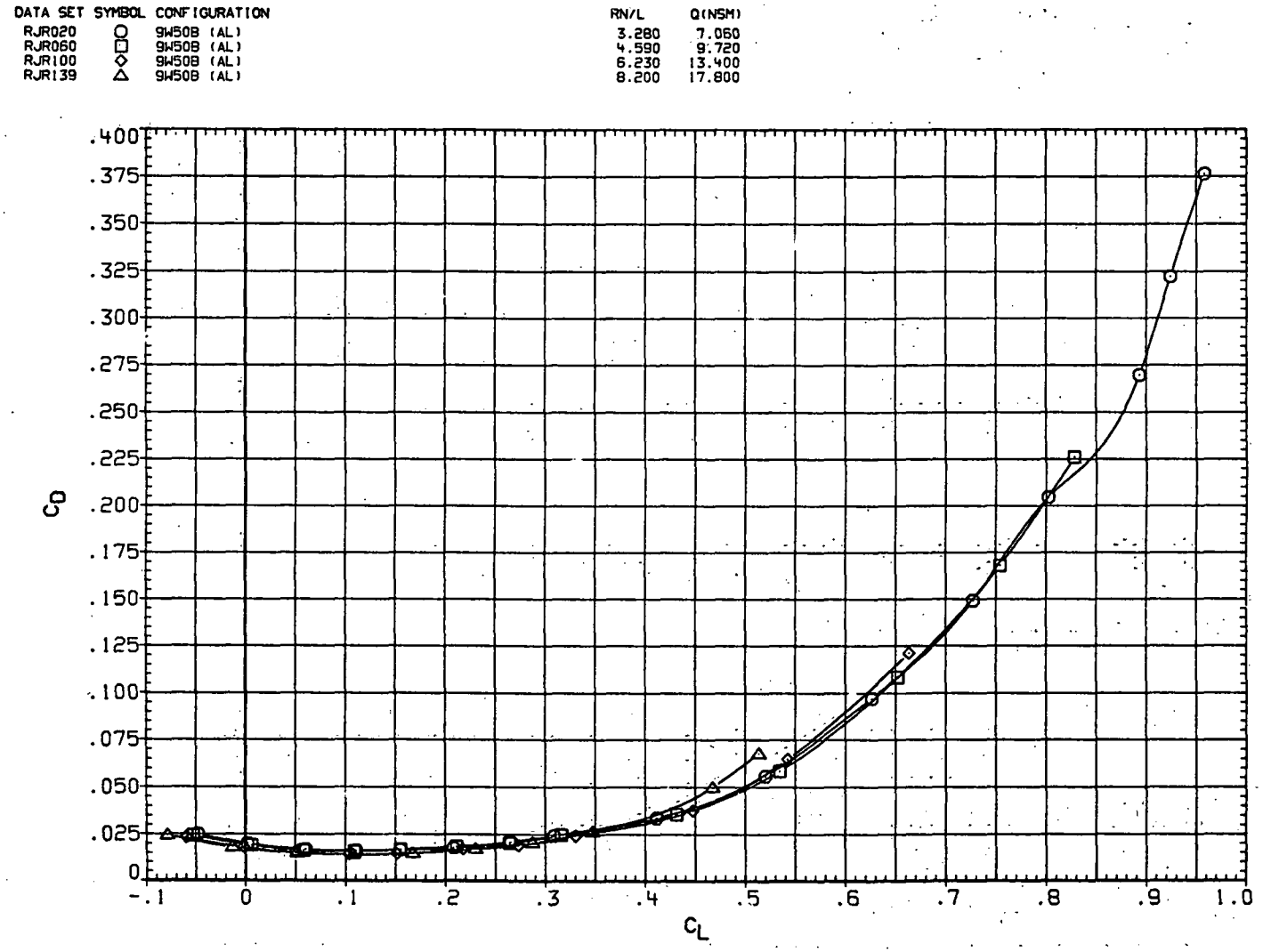

(b) C_D vs C_L.

Figure 19.– Continued.

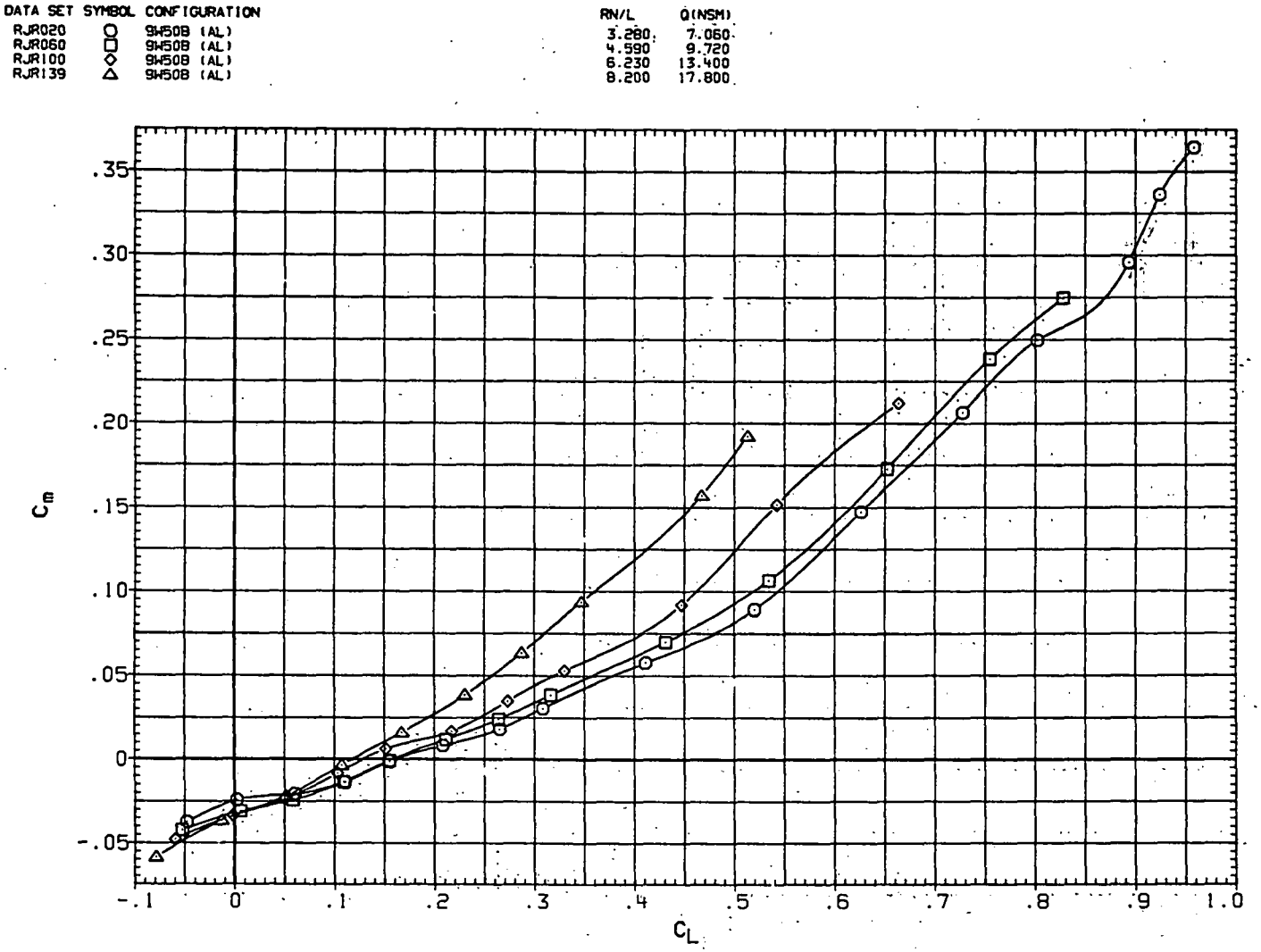

(c) C_m vs C_L.

Figure 19.– Continued.

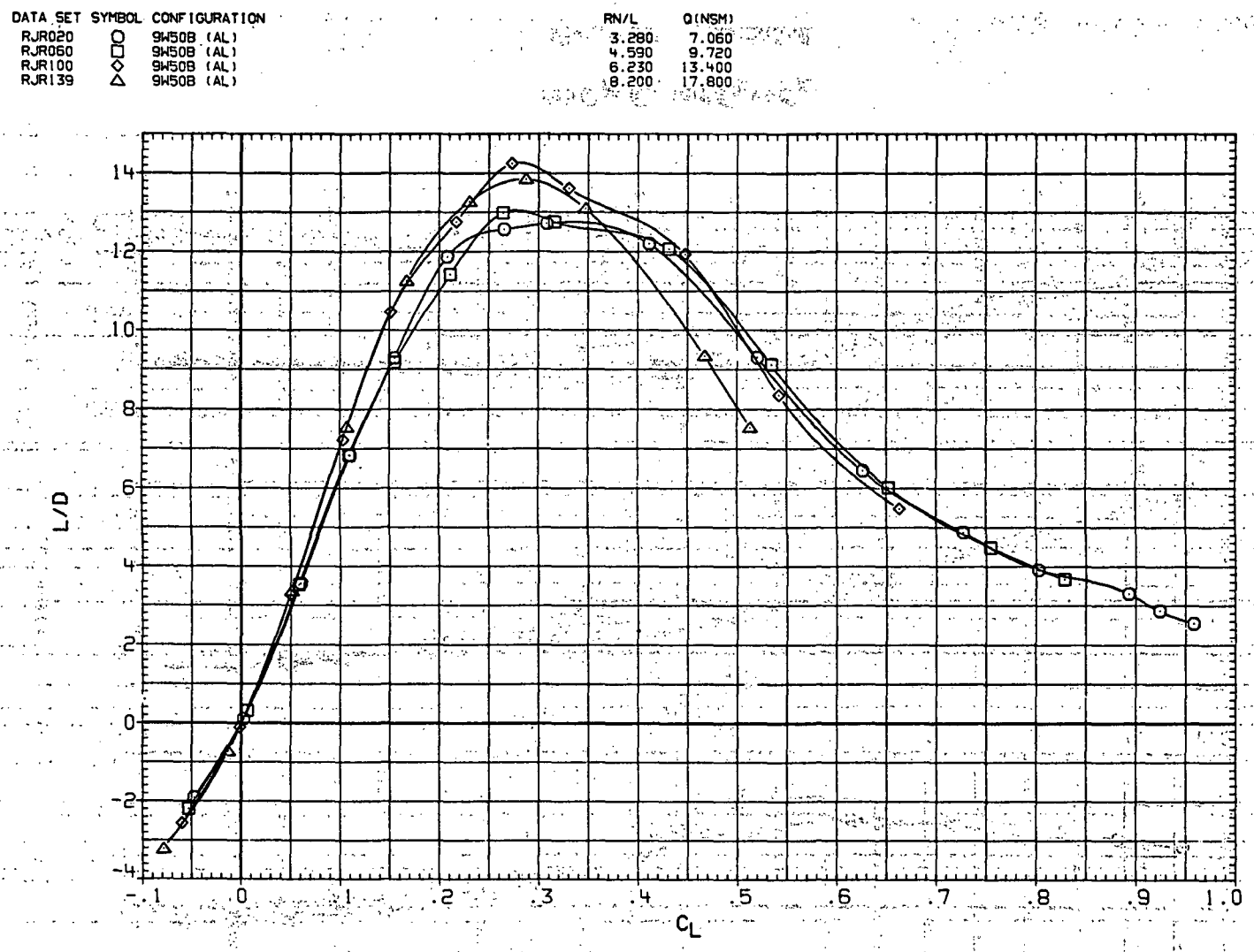

(d) L/D vs C_L.

Figure 19.– Continued.

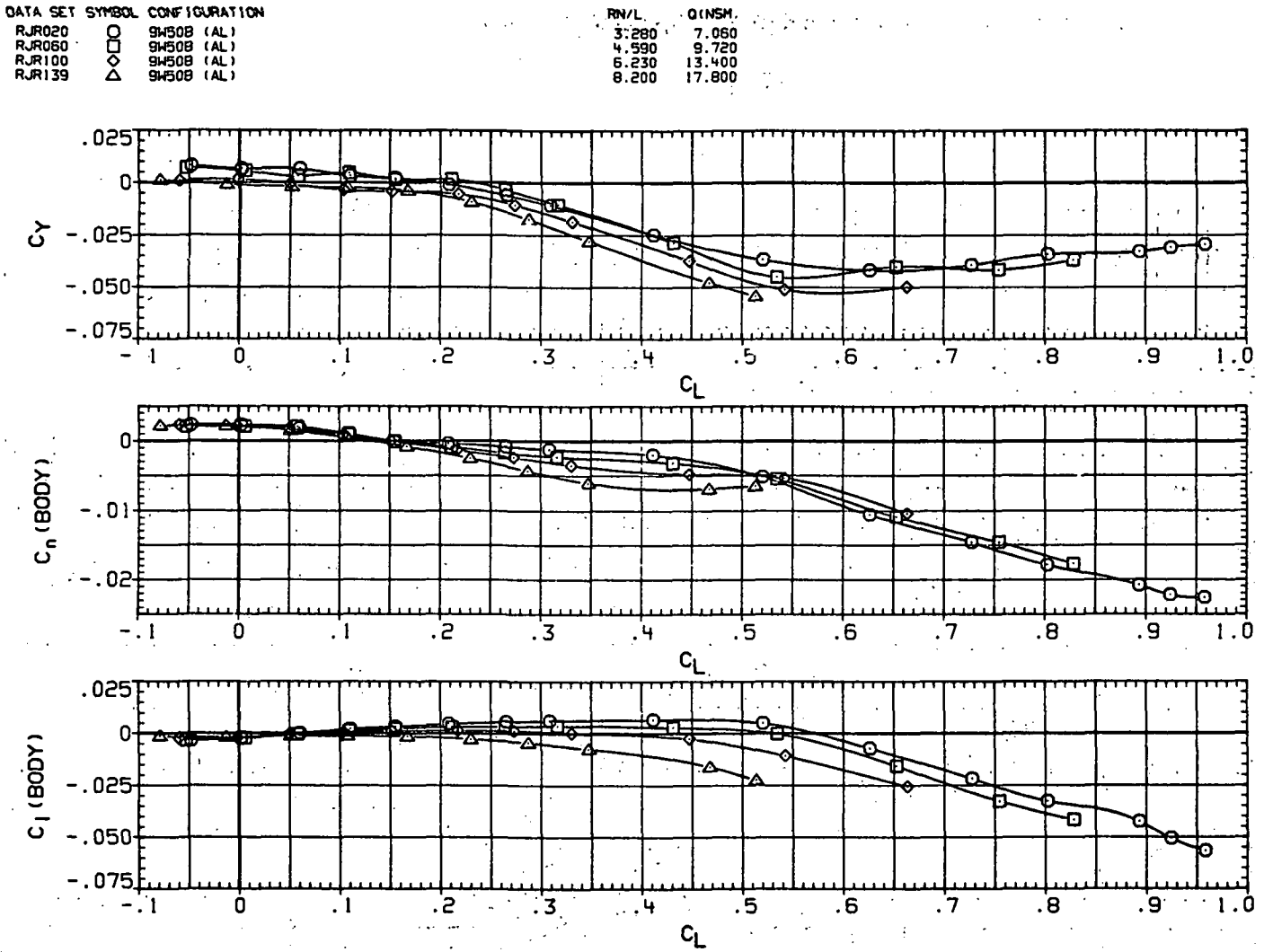

(e) C_Y, C_n and C_ℓ vs C_L.

Figure 19.– Concluded.

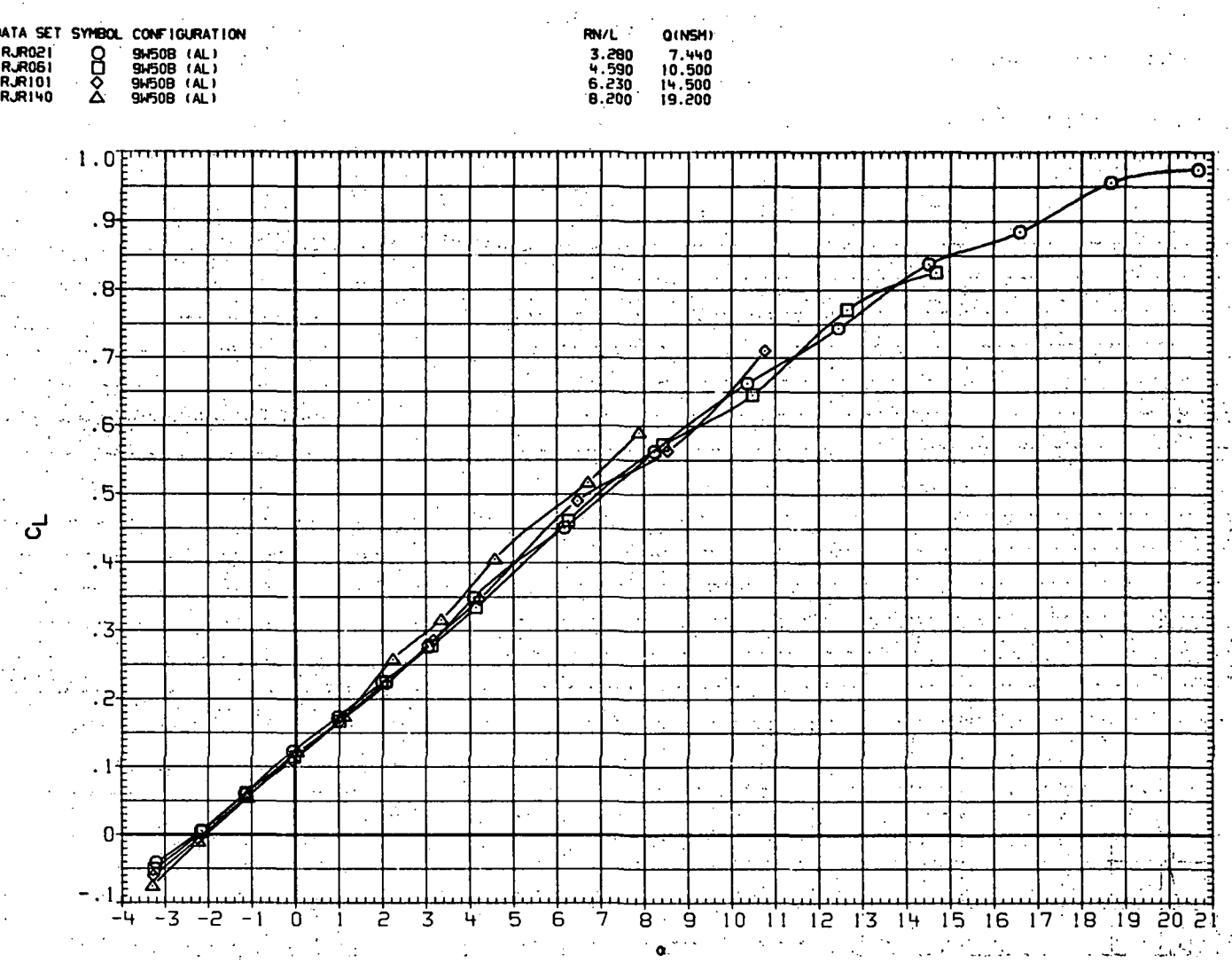

(a) C_L vs α.

Figure 20.– Dynamic-pressure effects on the aerodynamic characteristics of the aluminum trapezoidal oblique wing-body combination ($\Lambda = 50°$, $M = 0.9$ and the modified NACA 65A204 airfoil).

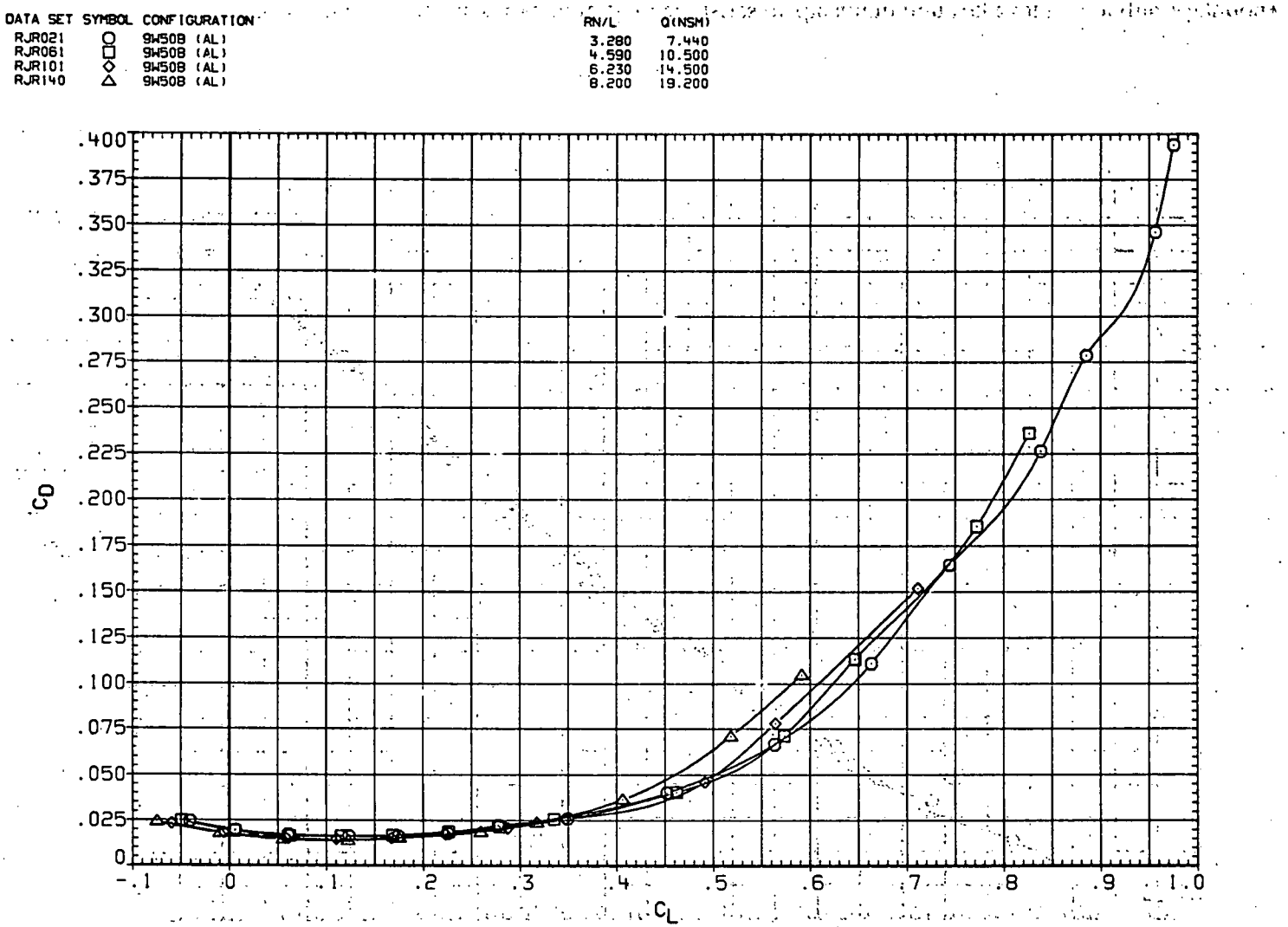

(b) C_D vs C_L.

Figure 20.– Continued.

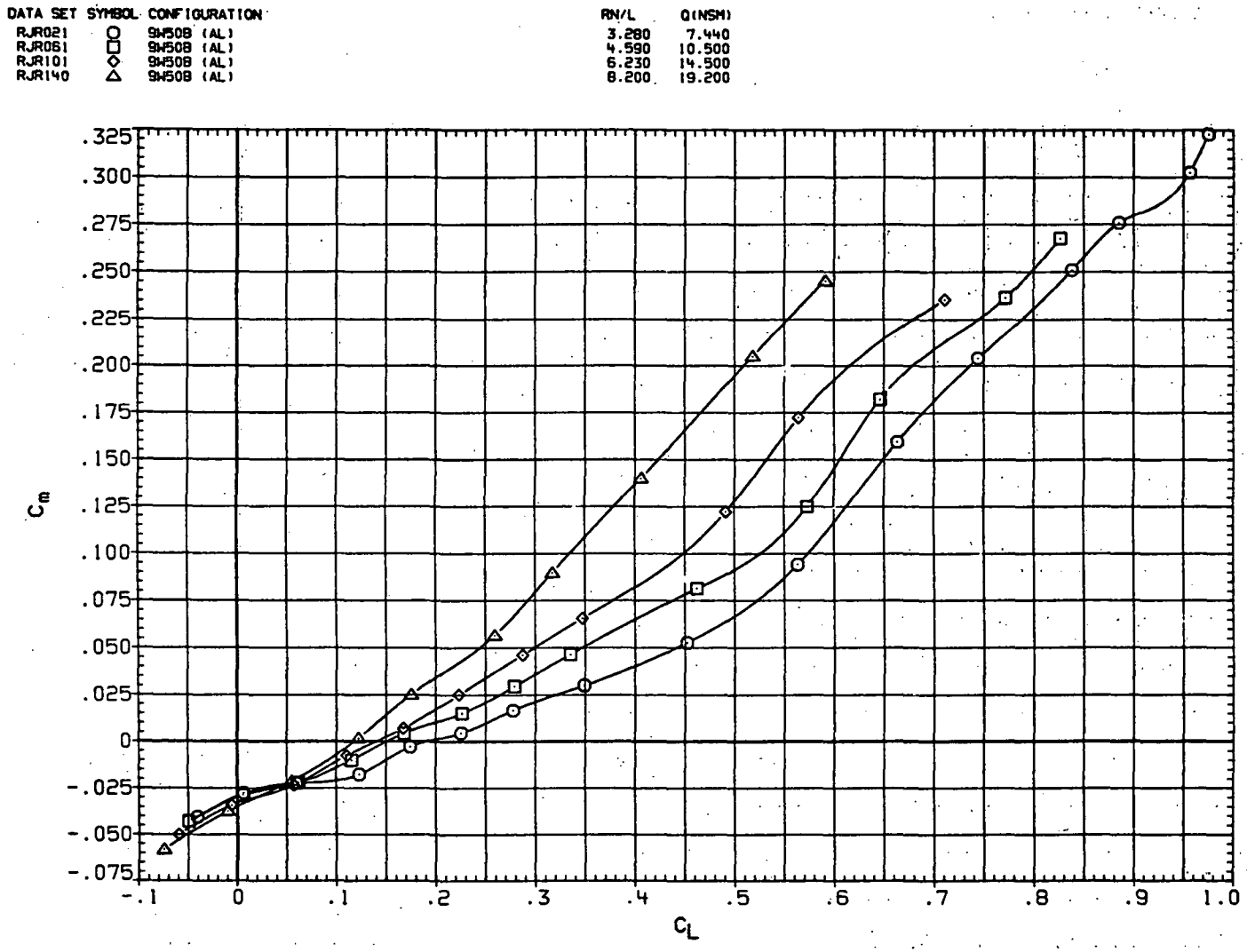

(c) C_m vs C_L.

Figure 20.– Continued.

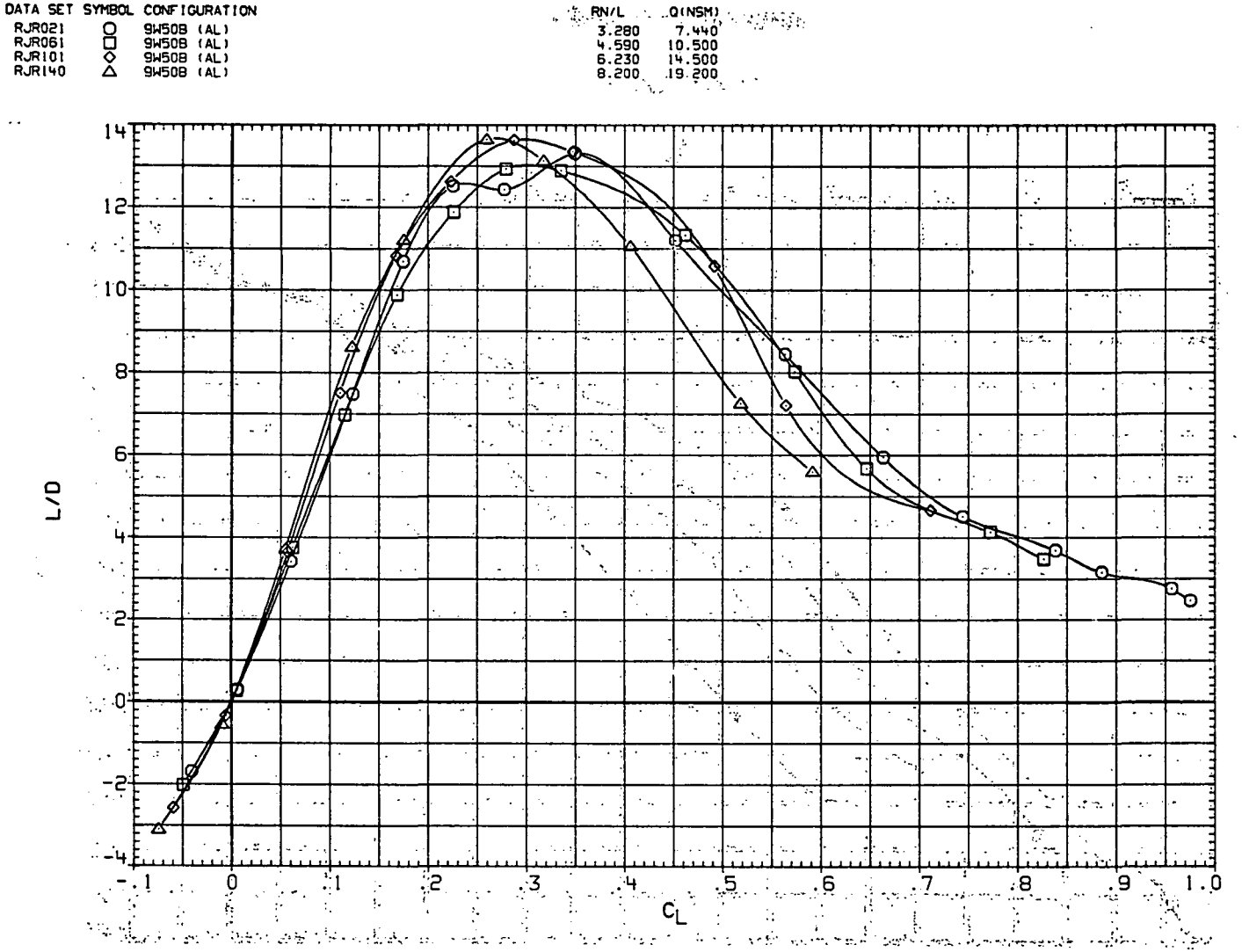

(d) L/D vs C_L.

Figure 20.– Continued.

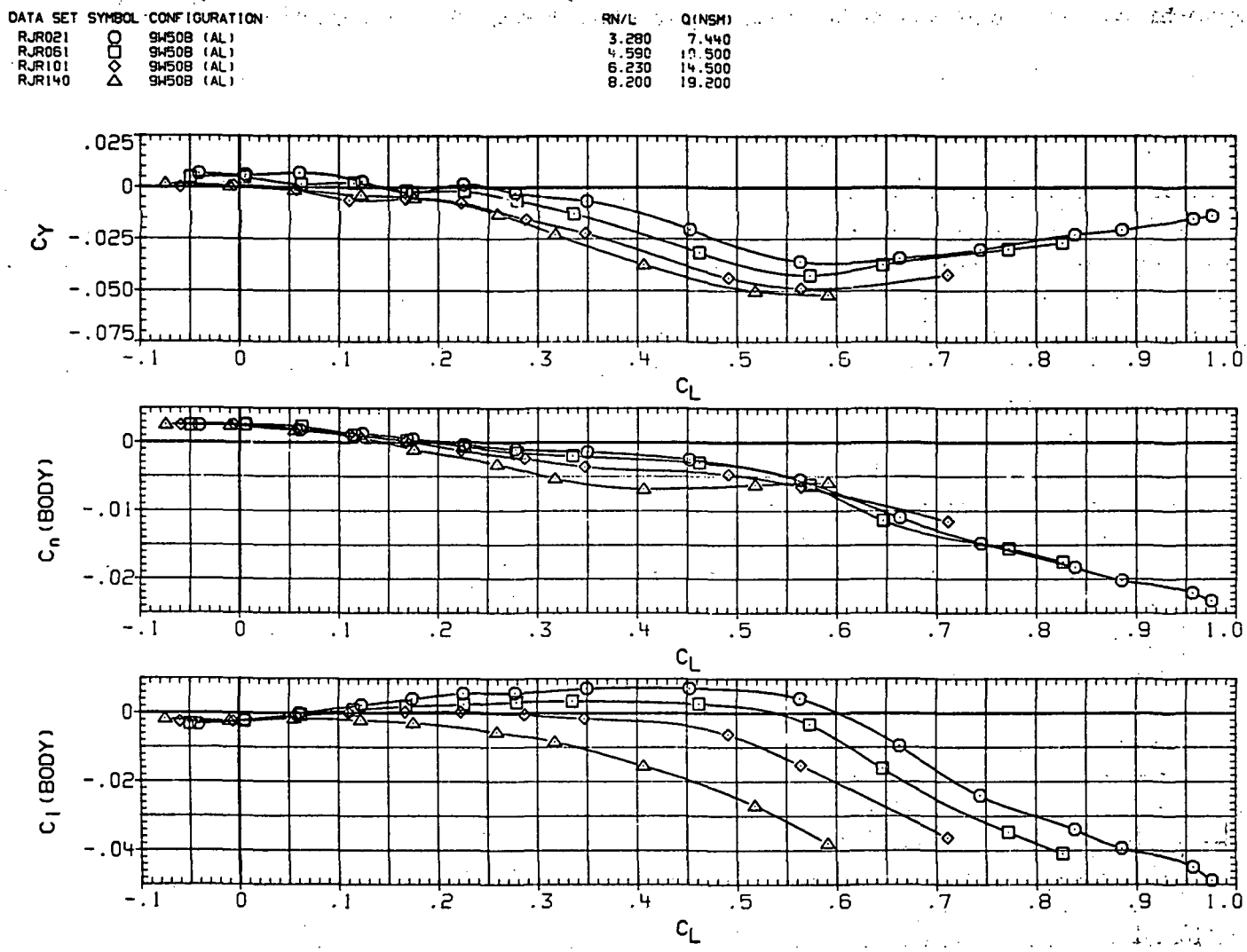

(e) C_Y, C_n and C_ℓ vs C_L.

Figure 20.– Concluded.

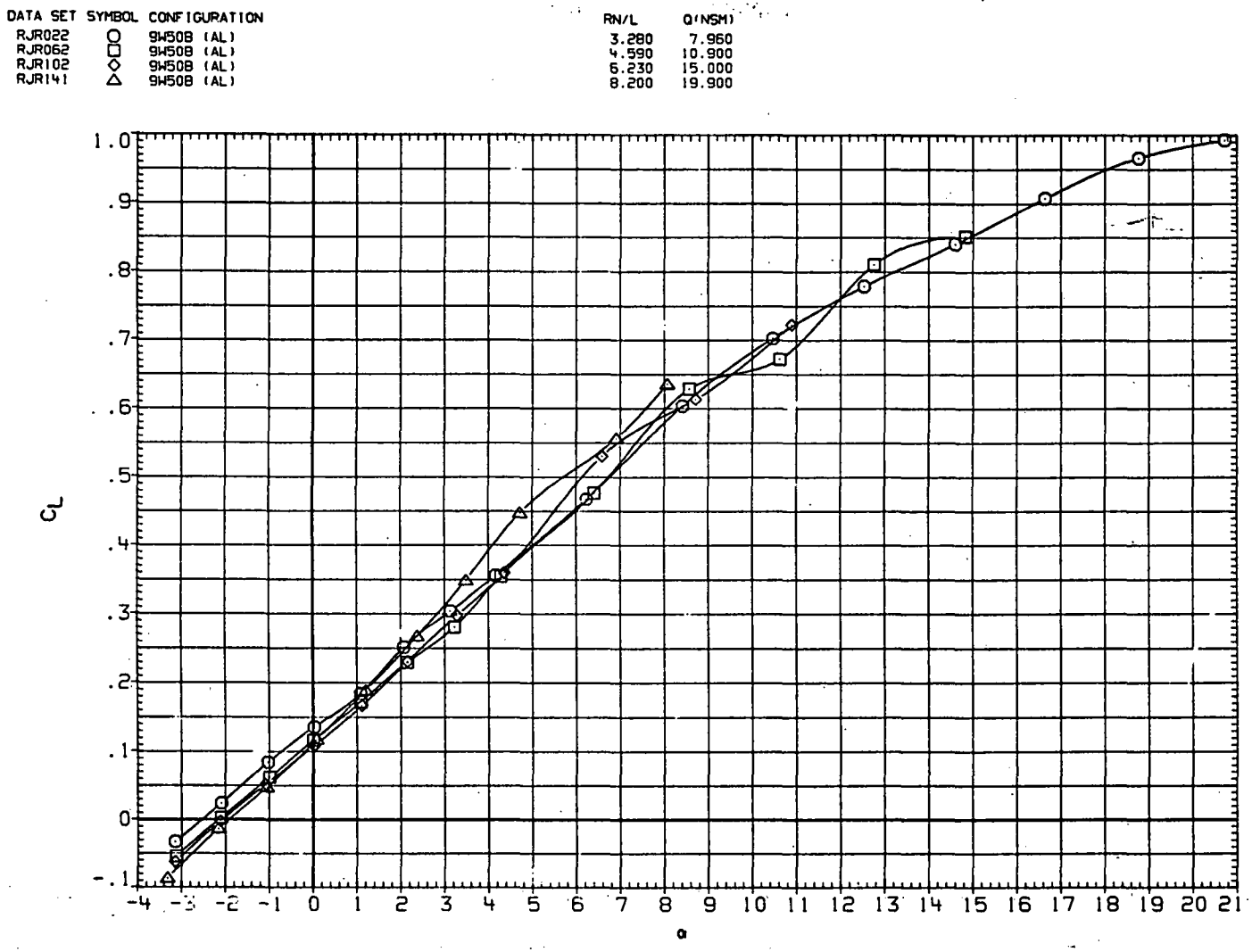

(a) C_L vs α.

Figure 21.– Dynamic-pressure effects on the aerodynamic characteristics of the aluminum trapezoidal oblique wing-body combination ($\Lambda = 50°, M = 0.95$ and the modified NACA 65A204 airfoil).

DATA SET	SYMBOL	CONFIGURATION
RJR022	○	9W50B (AL)
RJR062	□	9W50B (AL)
RJR102	◇	9W50B (AL)
RJR141	△	9W50B (AL)

RN/L	Q(NSM)
3.280	7.960
4.590	10.900
6.230	15.000
8.200	19.900

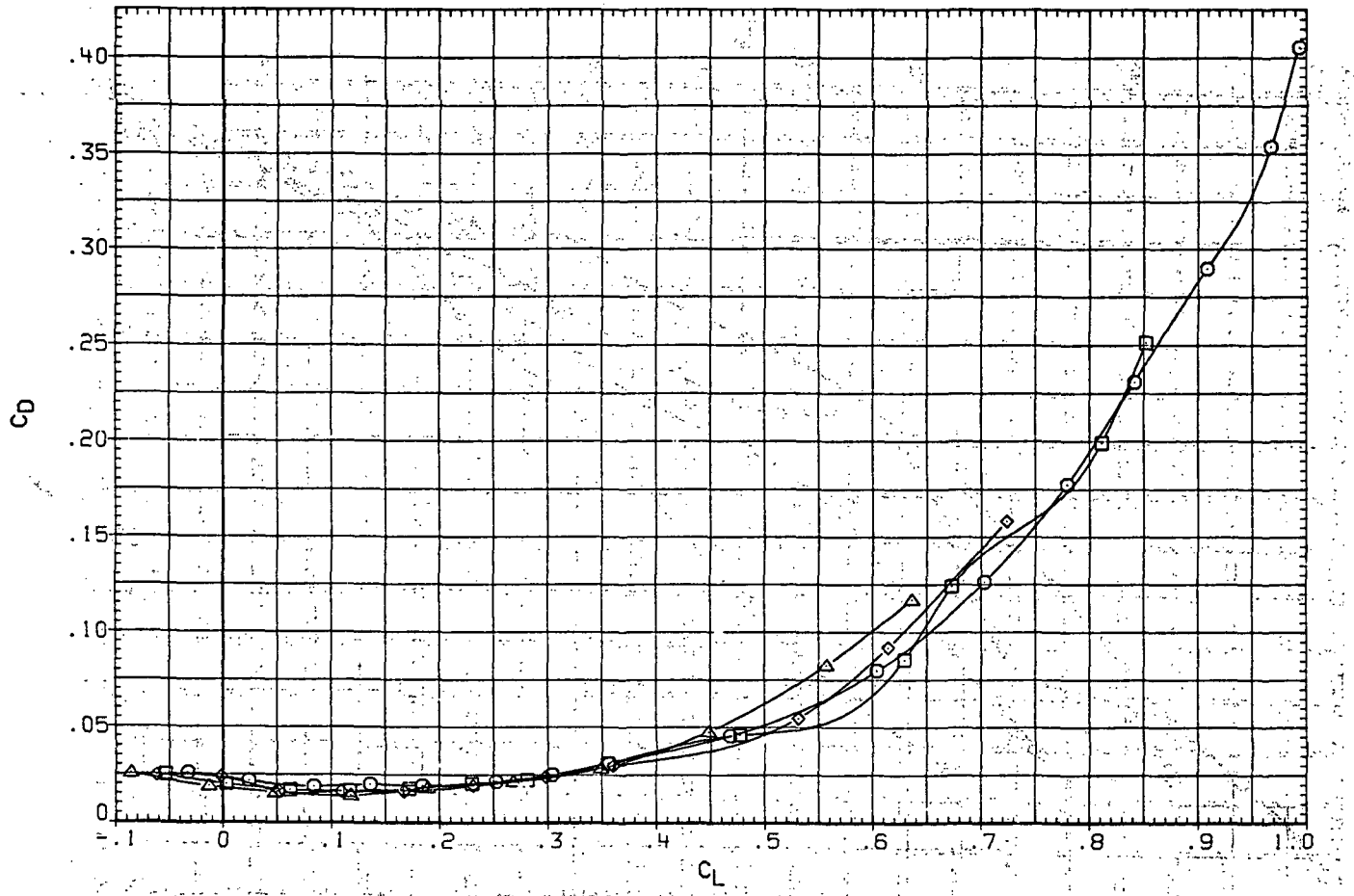

(b) C_D vs C_L.

Figure 21.– Continued.

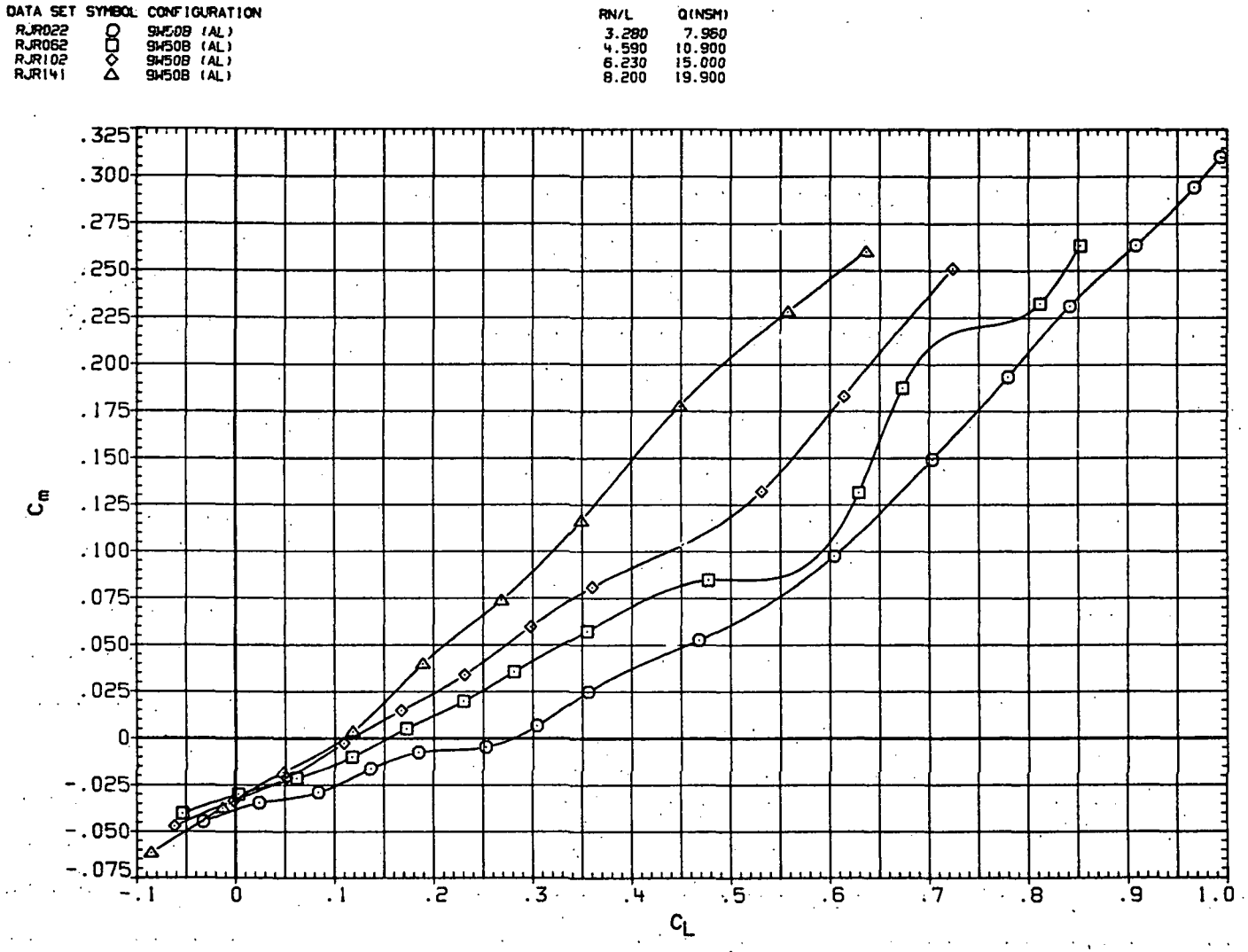

(c) C_m vs C_L.

Figure 21.—Continued.

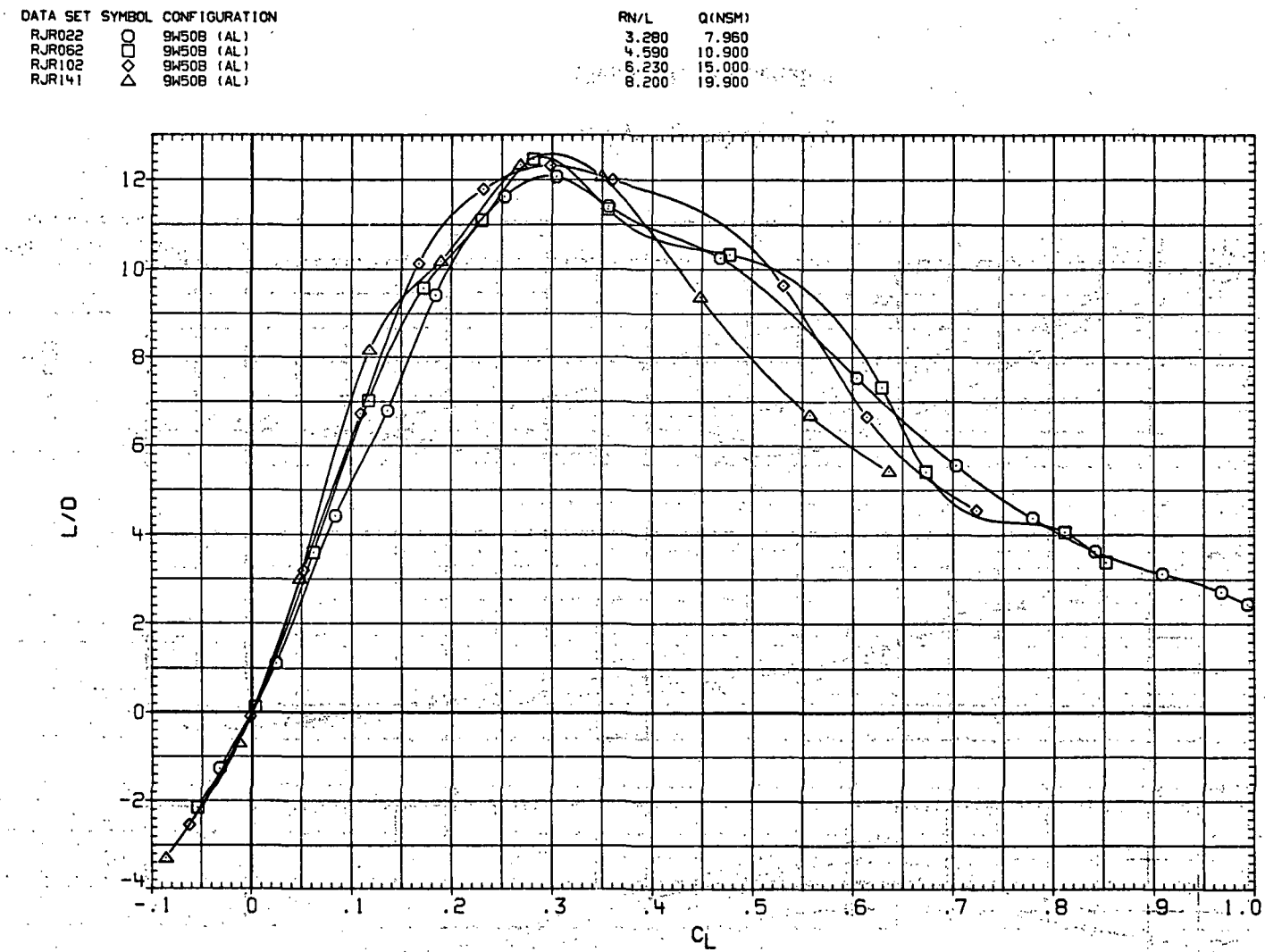

(d) L/D vs C_L.

Figure 21.– Continued.

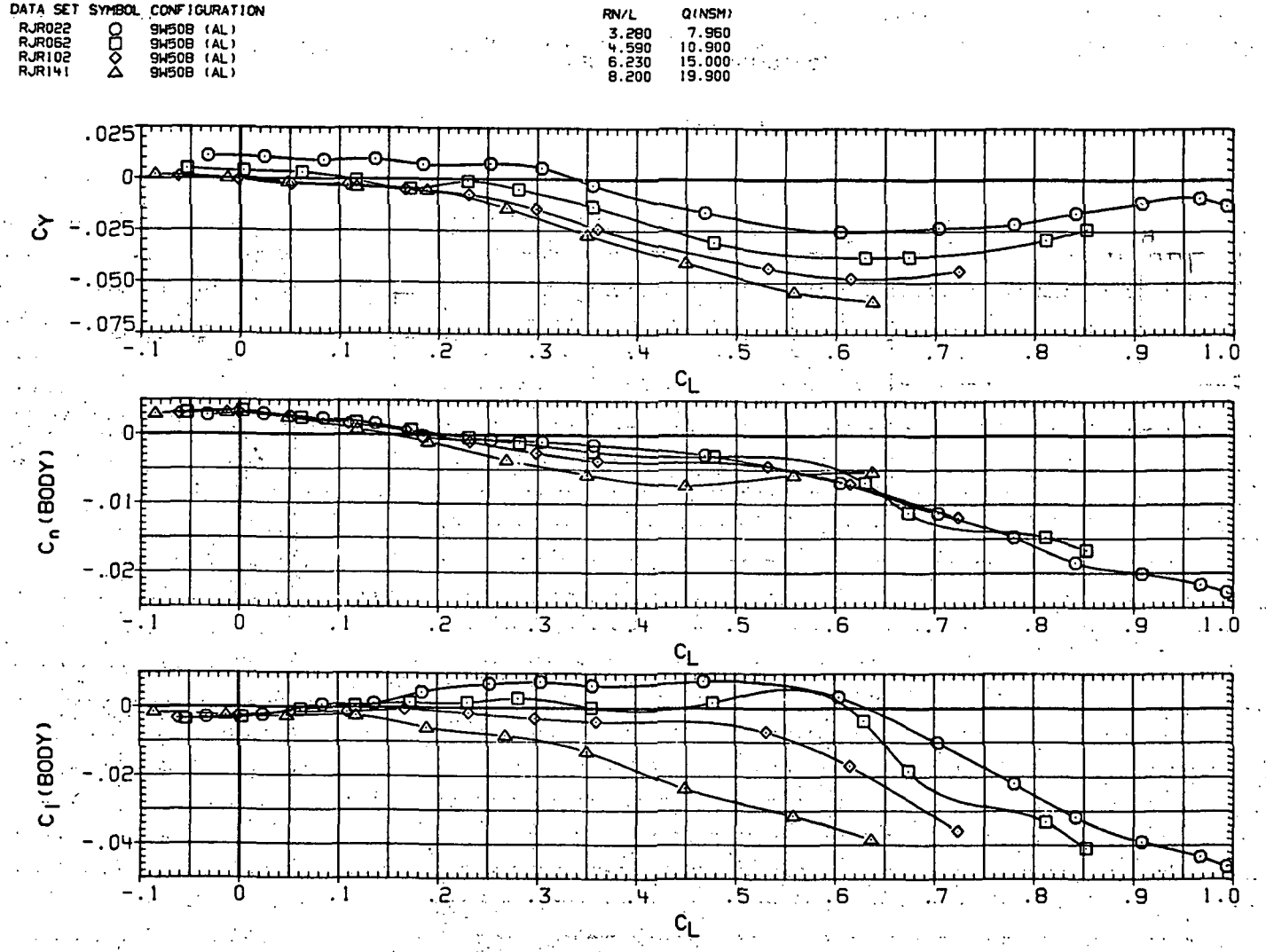

(e) C_Y, C_n and C_ℓ vs C_L.

Figure 21.– Concluded.

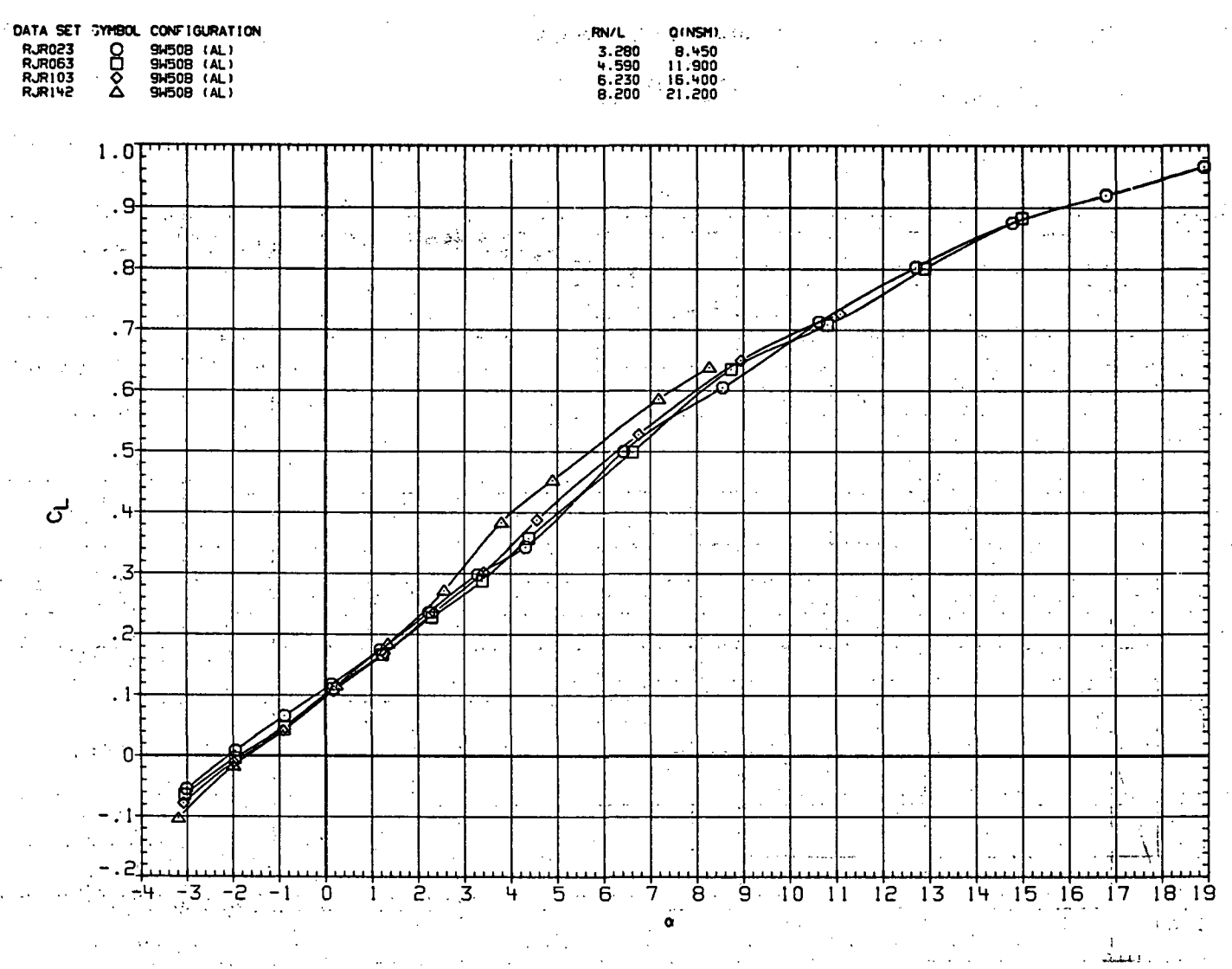

(a) C_L vs α.

Figure 22.– Dynamic-pressure effects on the aerodynamic characteristics of the aluminum trapezoidal oblique wing-body combination ($\Lambda = 50°$, $M = 1.1$ and the modified NACA 65A204 airfoil).

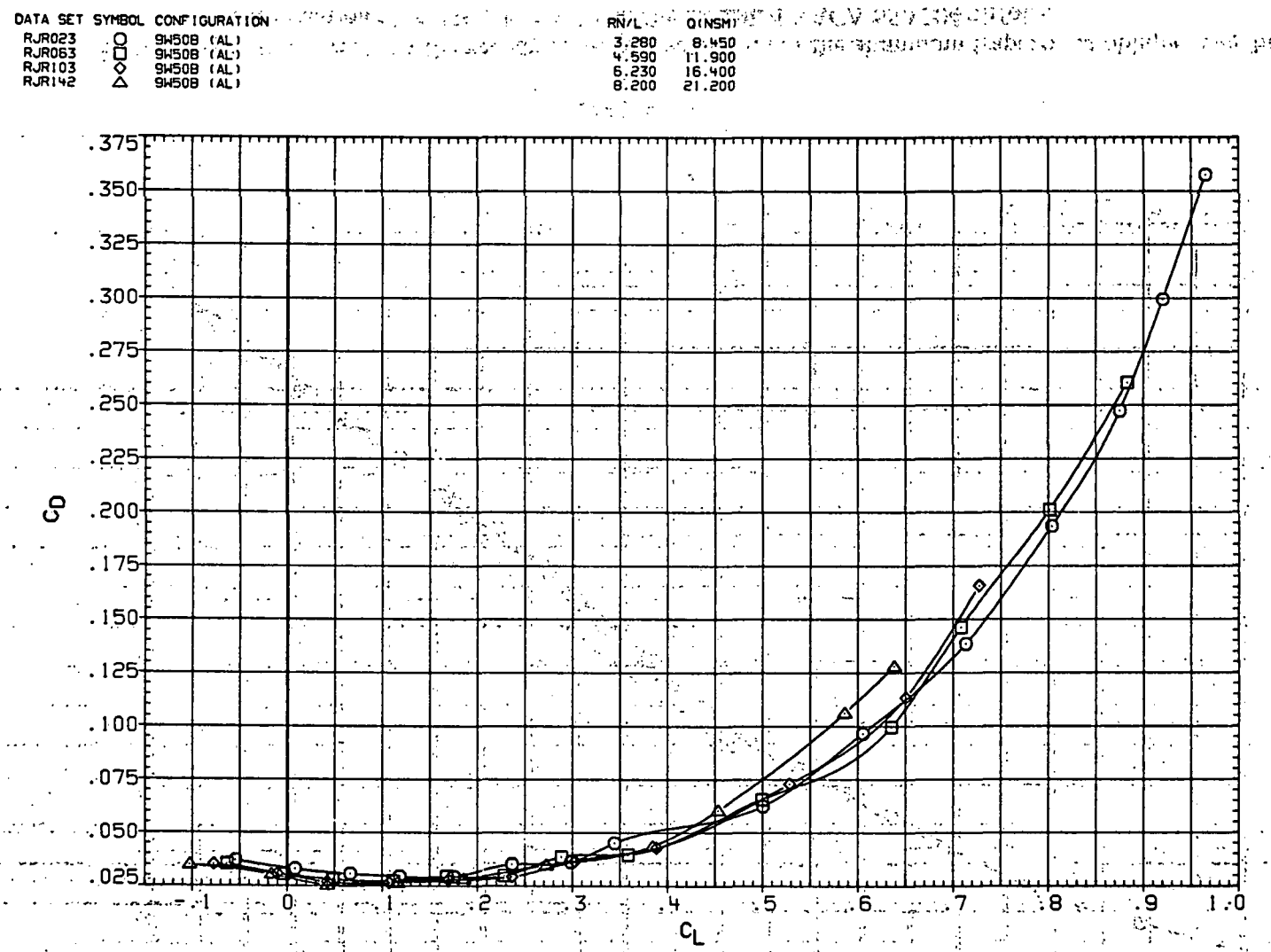

(b) C_D vs C_L.

Figure 22.– Continued.

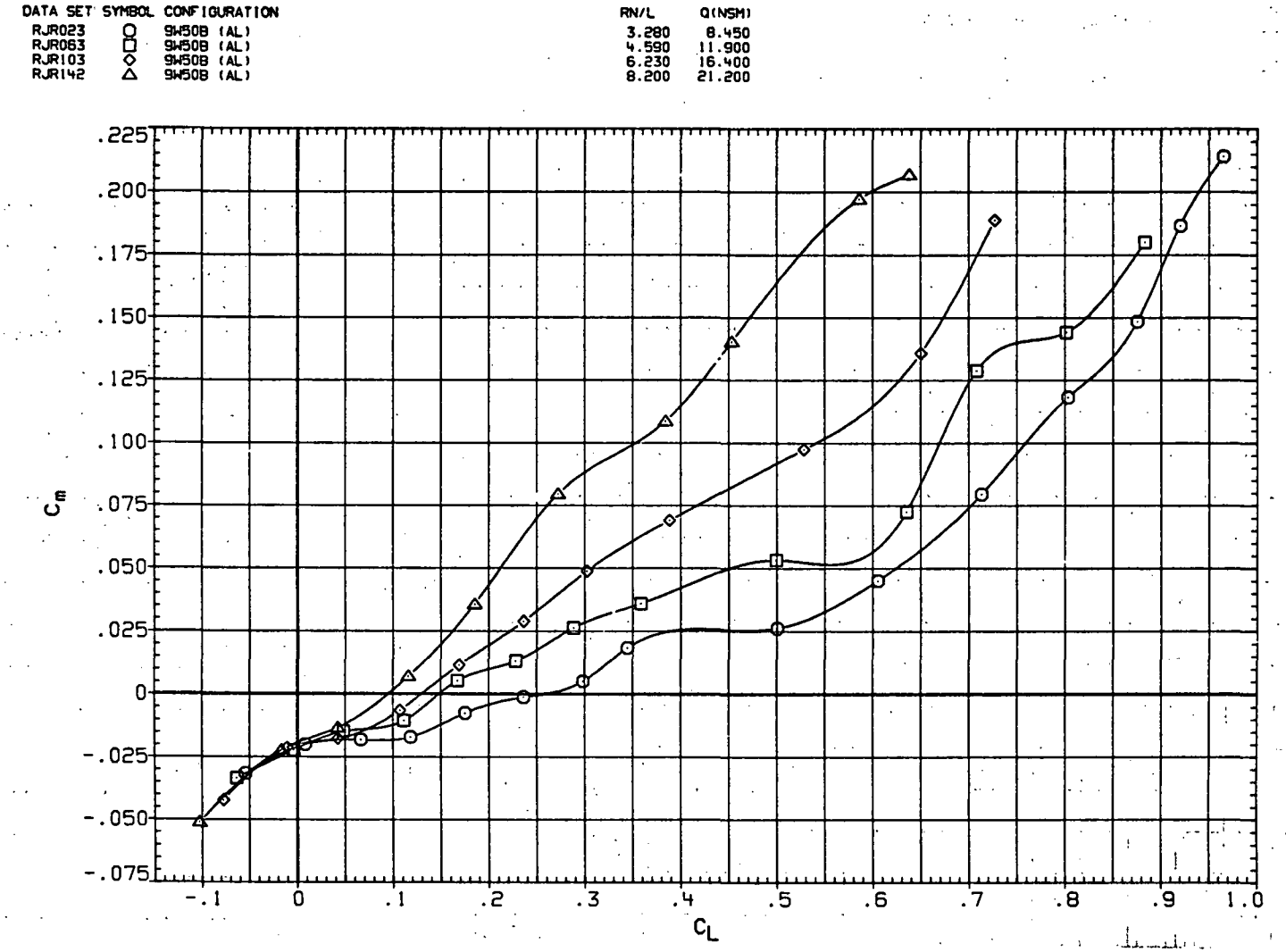

(c) C_m vs C_L.

Figure 22.– Continued.

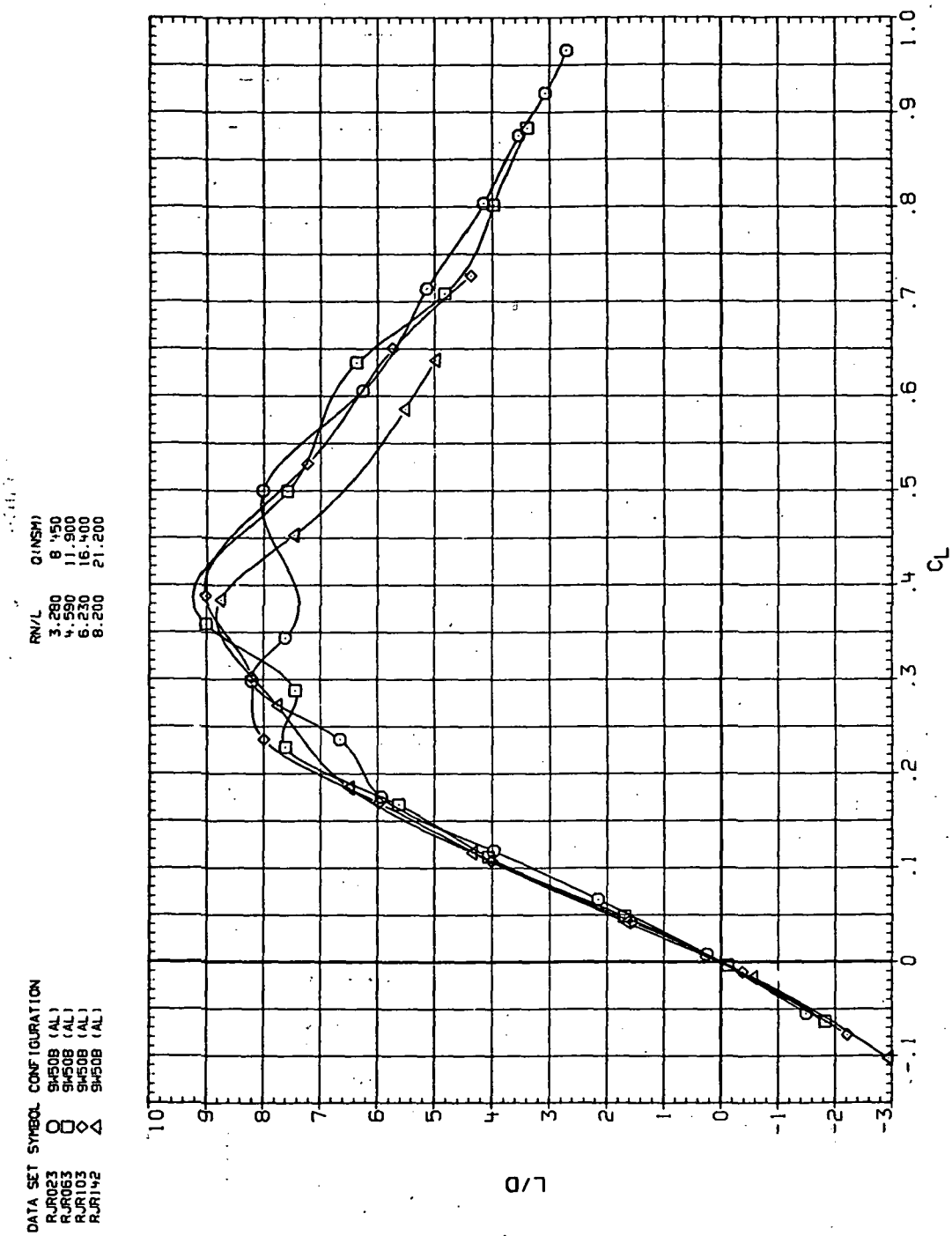

(d) L/D vs C_L.

Figure 22.– Continued.

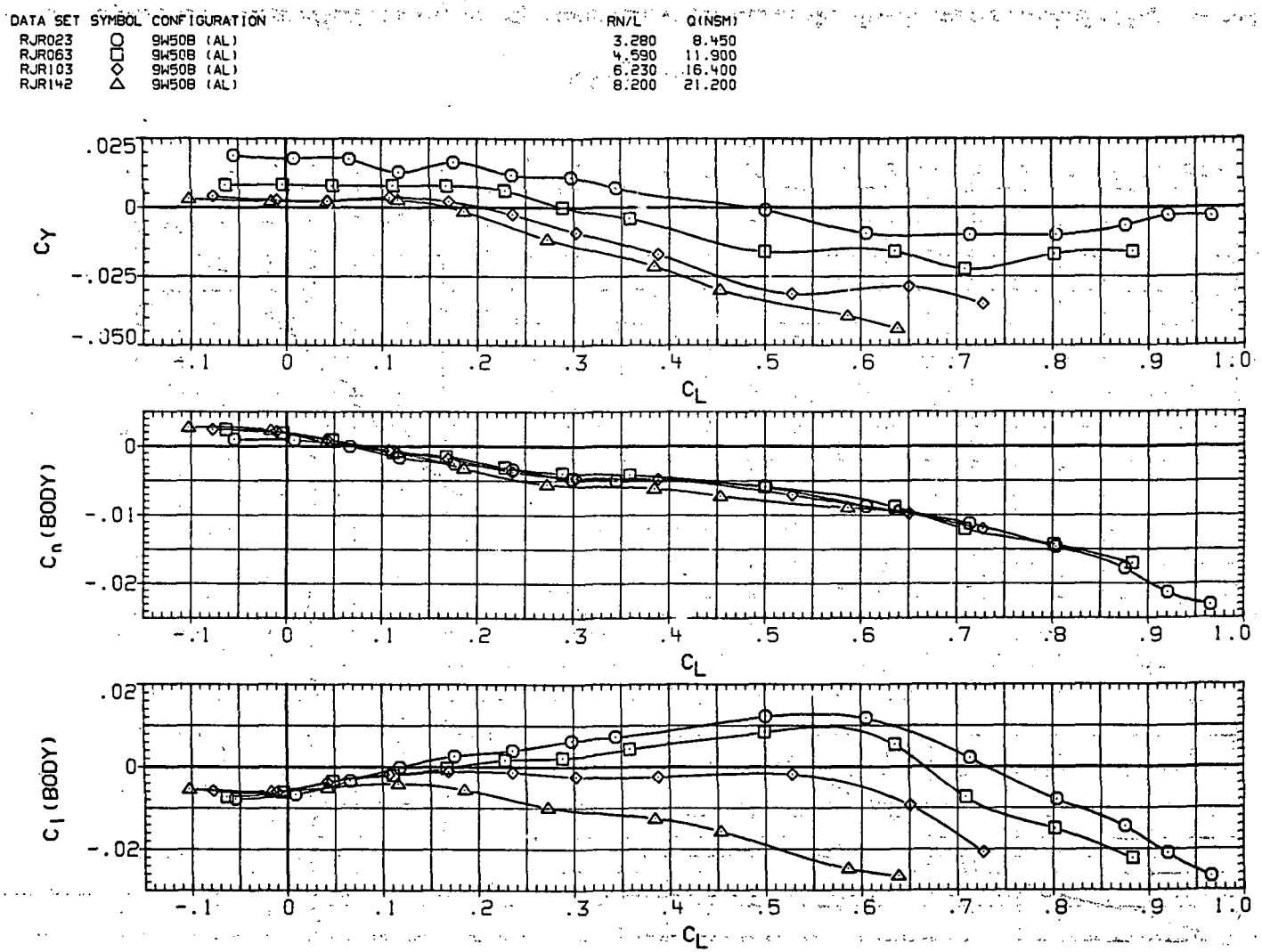

(e) C_Y, C_n and C_ℓ vs C_L.

Figure 22.– Concluded.

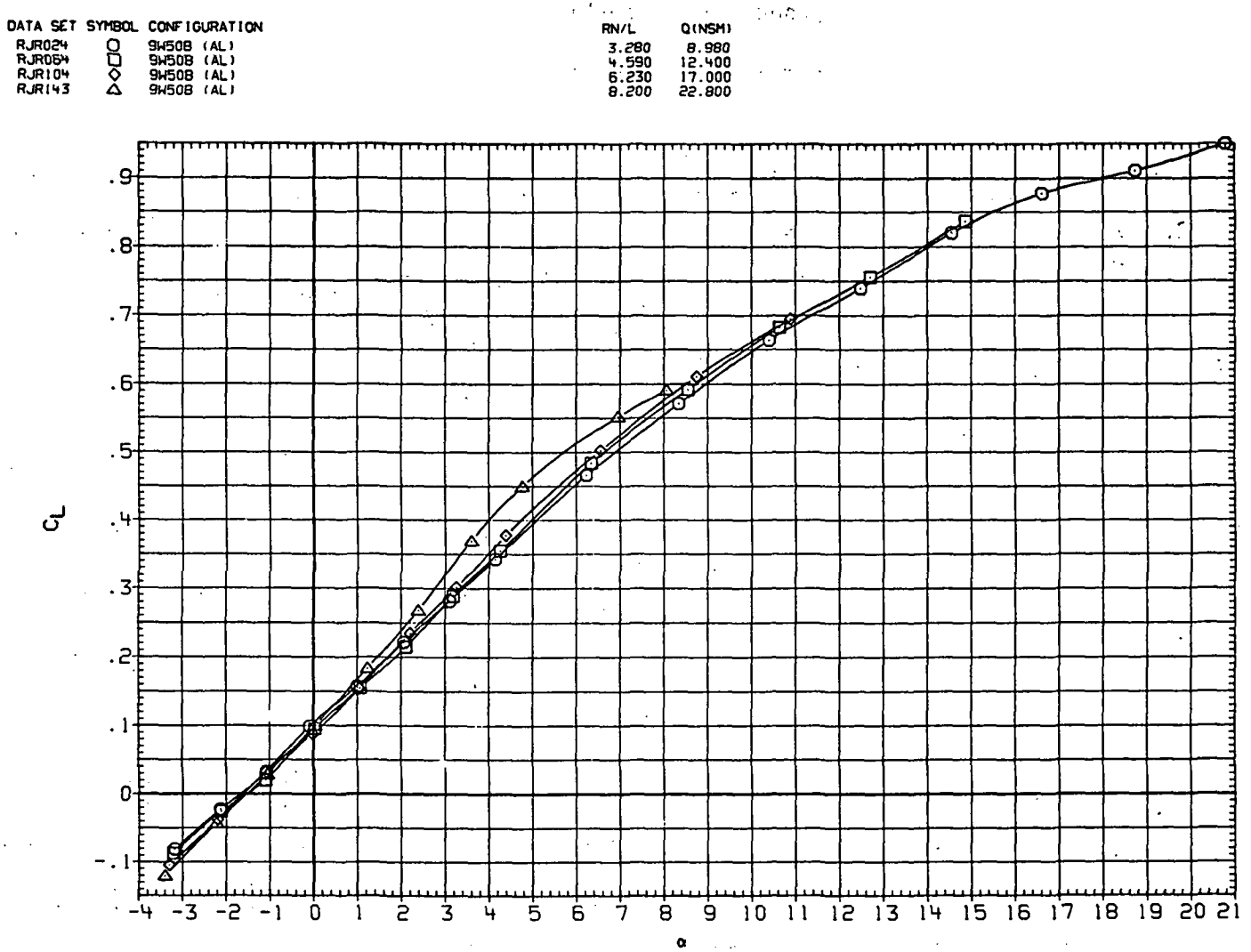

(a) C_L vs α.

Figure 23.– Dynamic-pressure effects on the aerodynamic characteristics of the aluminum trapezoidal oblique wing-body combination ($\Lambda = 50°$, $M = 1.2$ and the modified NACA 65A204 airfoil).

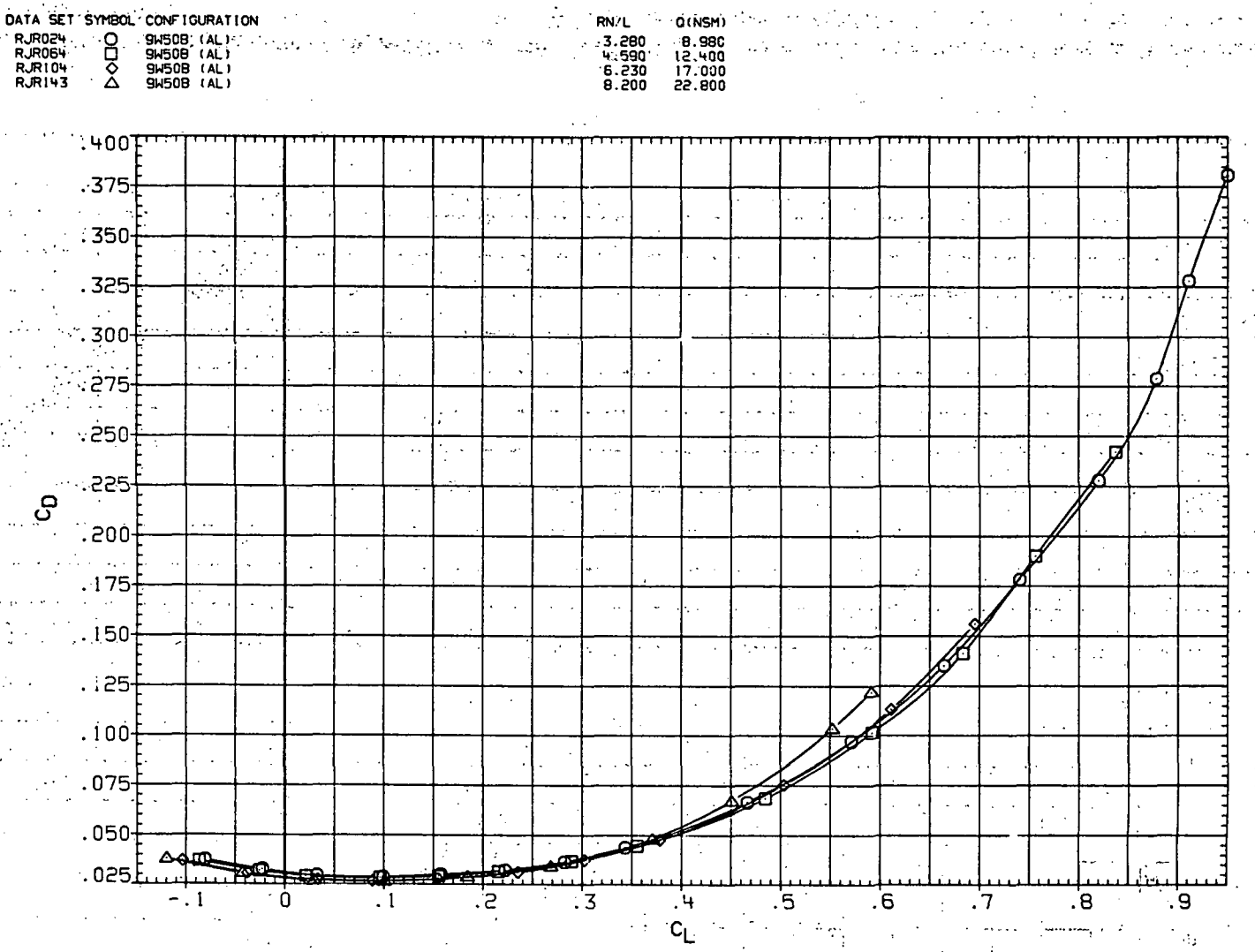

(b) C_D vs C_L.

Figure 23.– Continued.

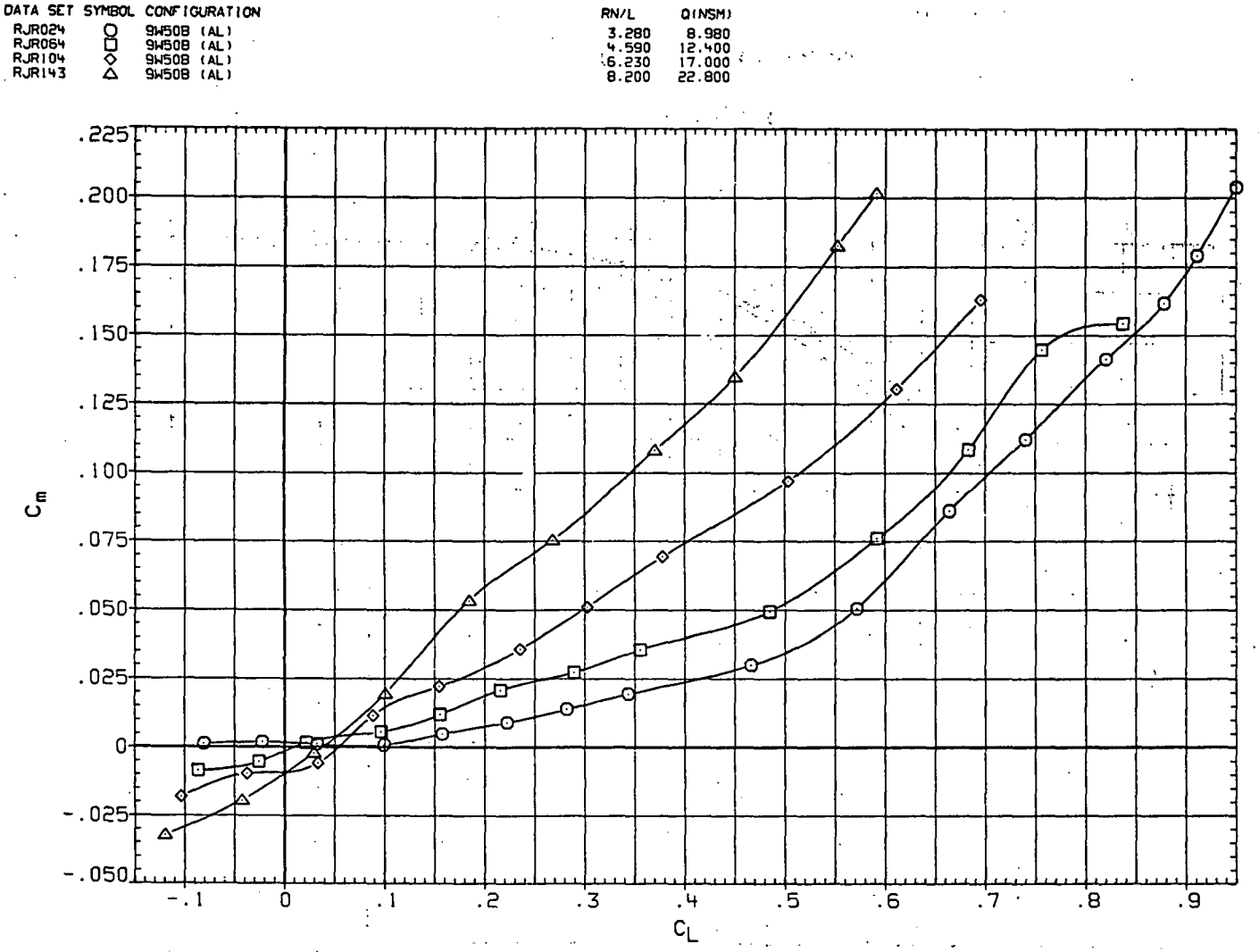

(c) C_m vs C_L.

Figure 23.– Continued.

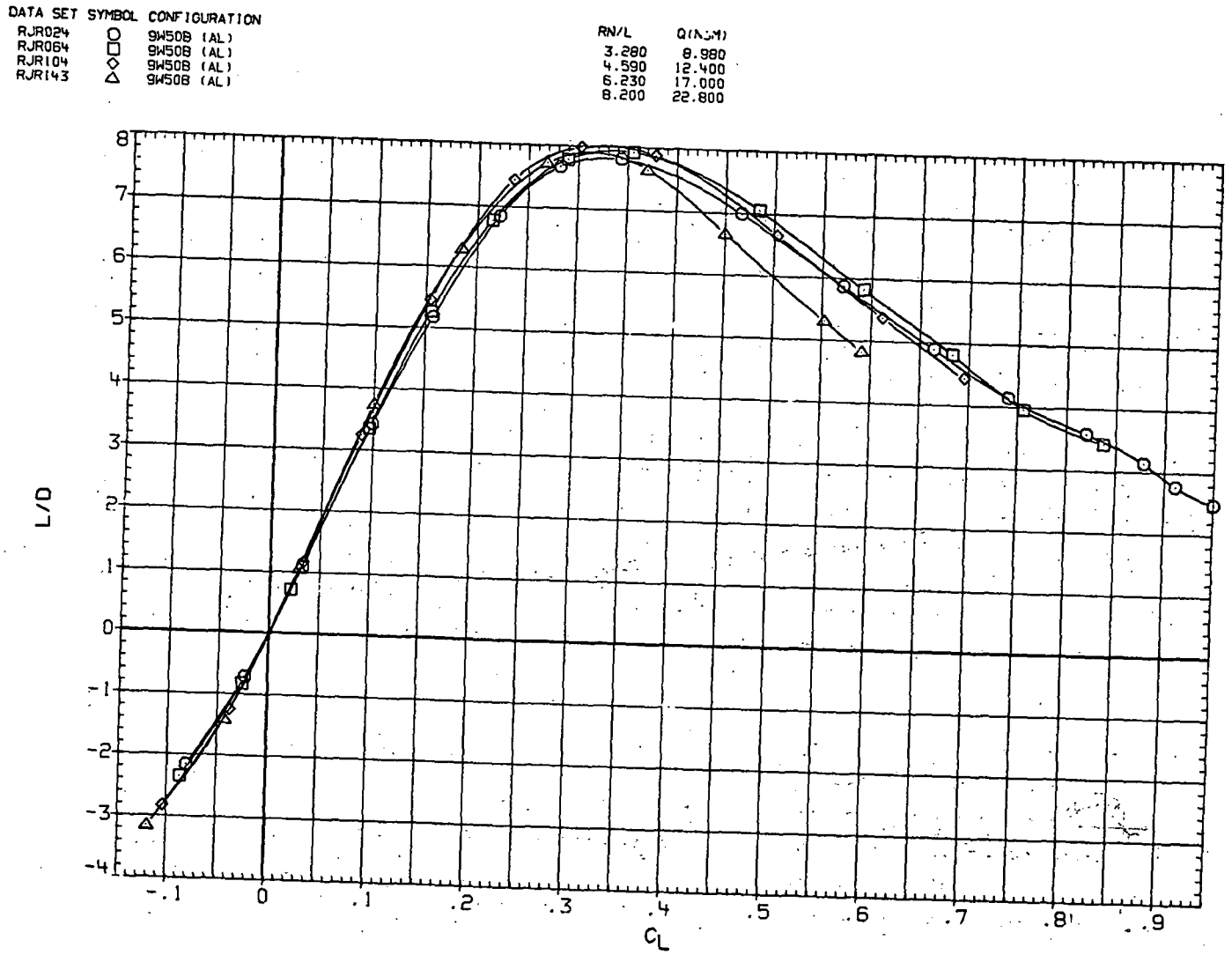

(d) L/D vs C_L.

Figure 23.– Continued.

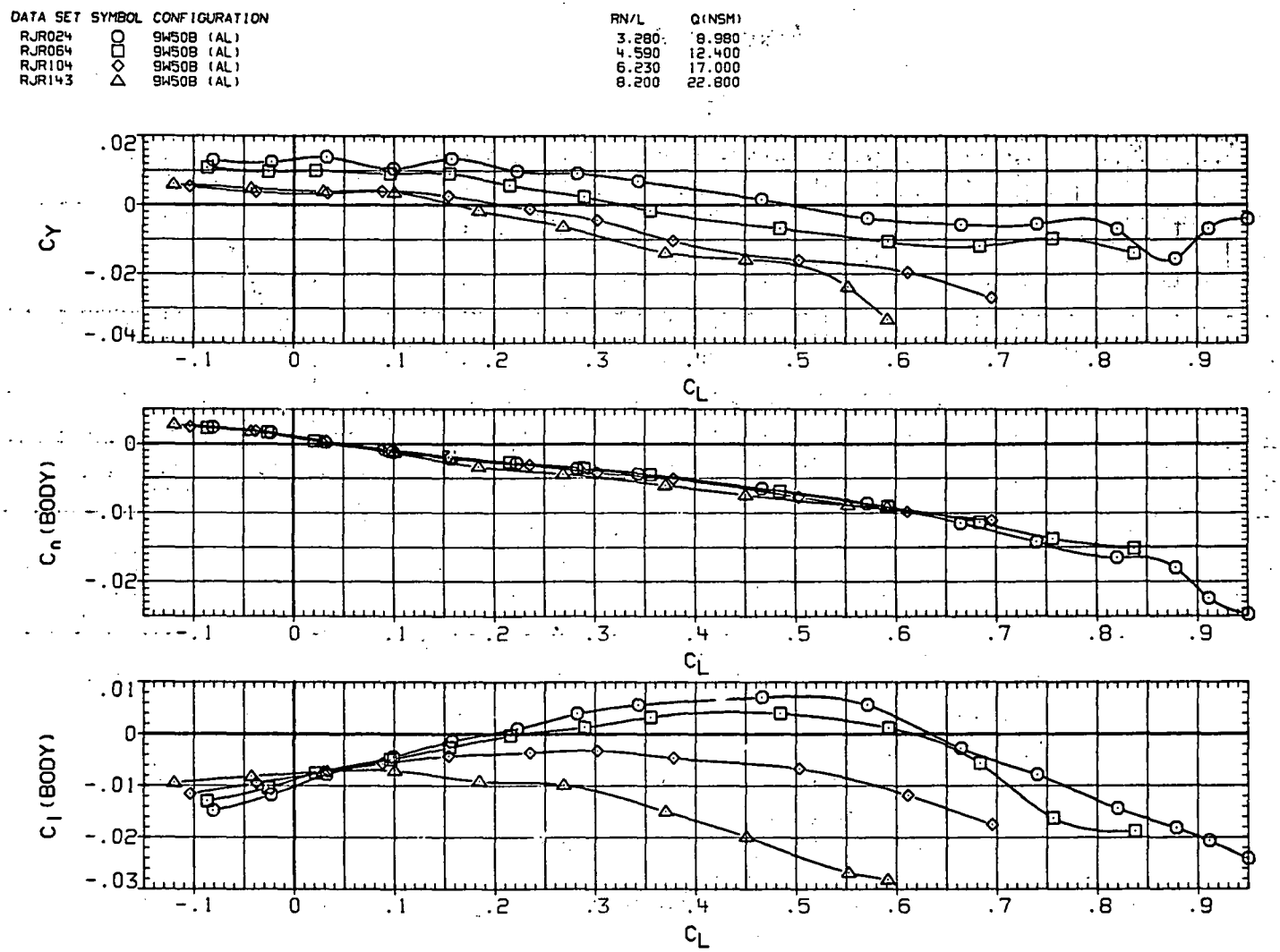

(e) C_Y, C_n and C_ℓ vs C_L.

Figure 23.– Concluded.

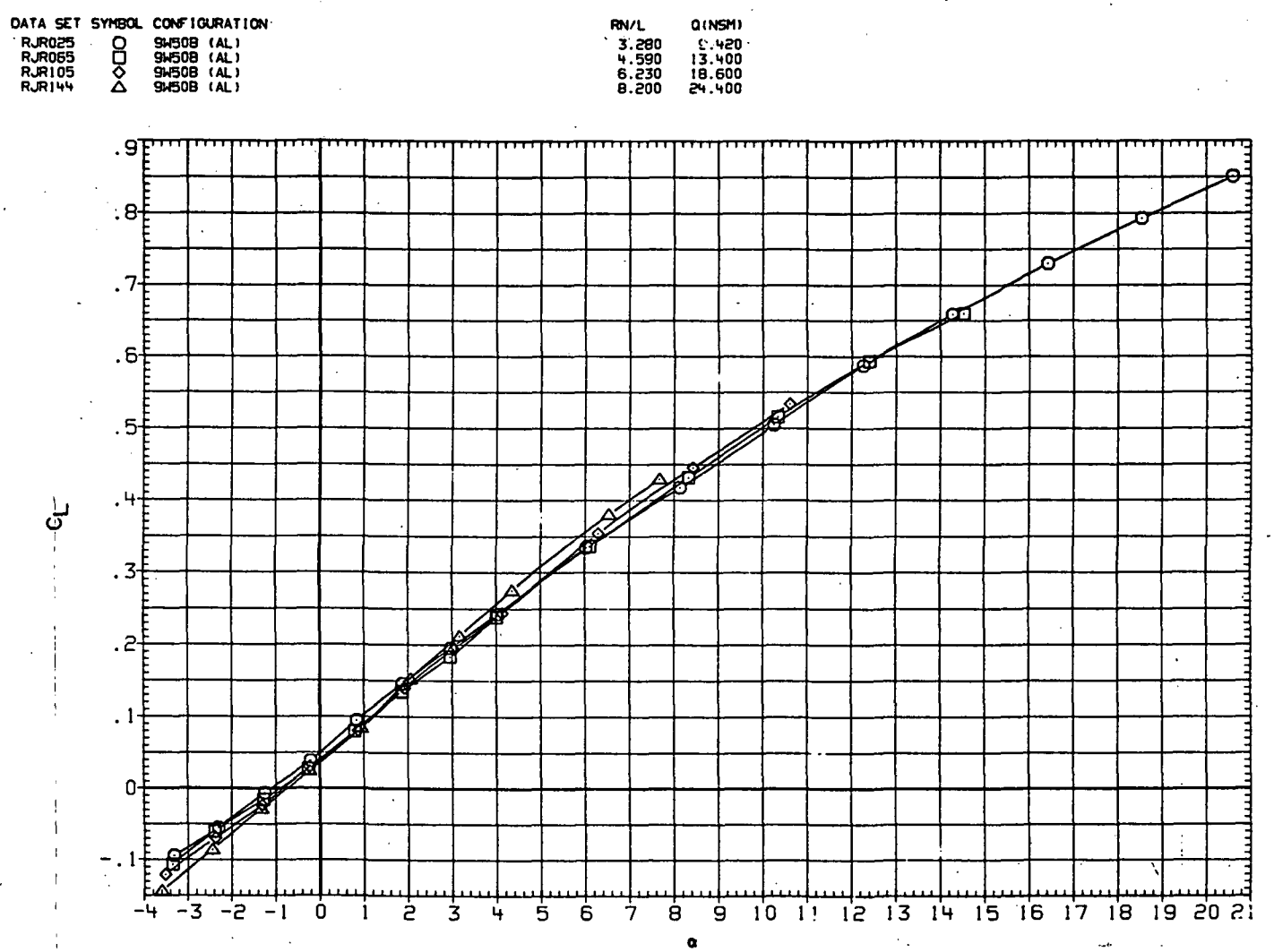

(a) C_L vs α.

Figure 24.– Dynamic-pressure effects on the aerodynamic characteristics of the aluminum trapezoidal oblique wing-body combination ($\Lambda = 50°$, $M = 1.6$ and the modified NACA 65A204 airfoil).

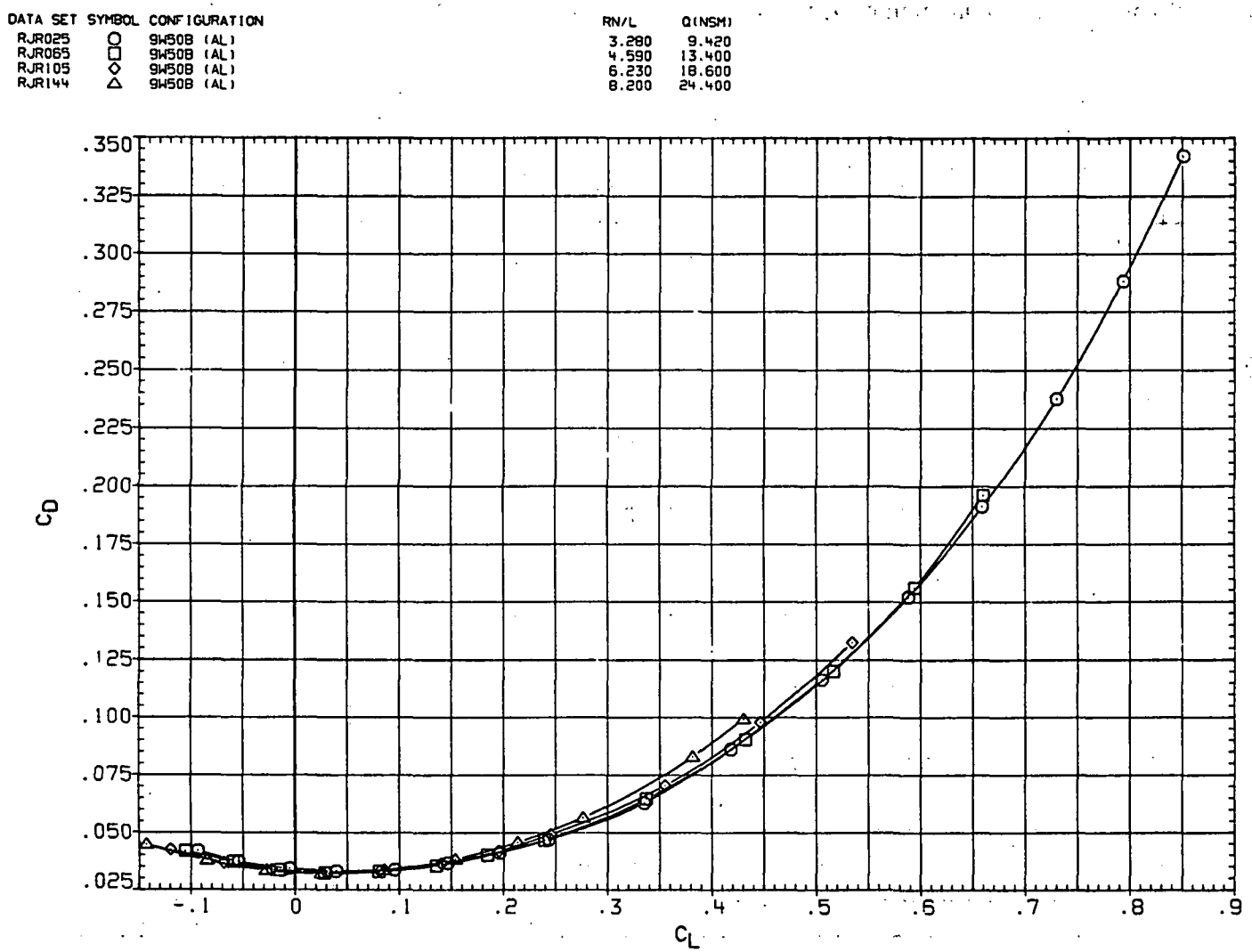

(b) C_D vs C_L.

Figure 24.– Continued.

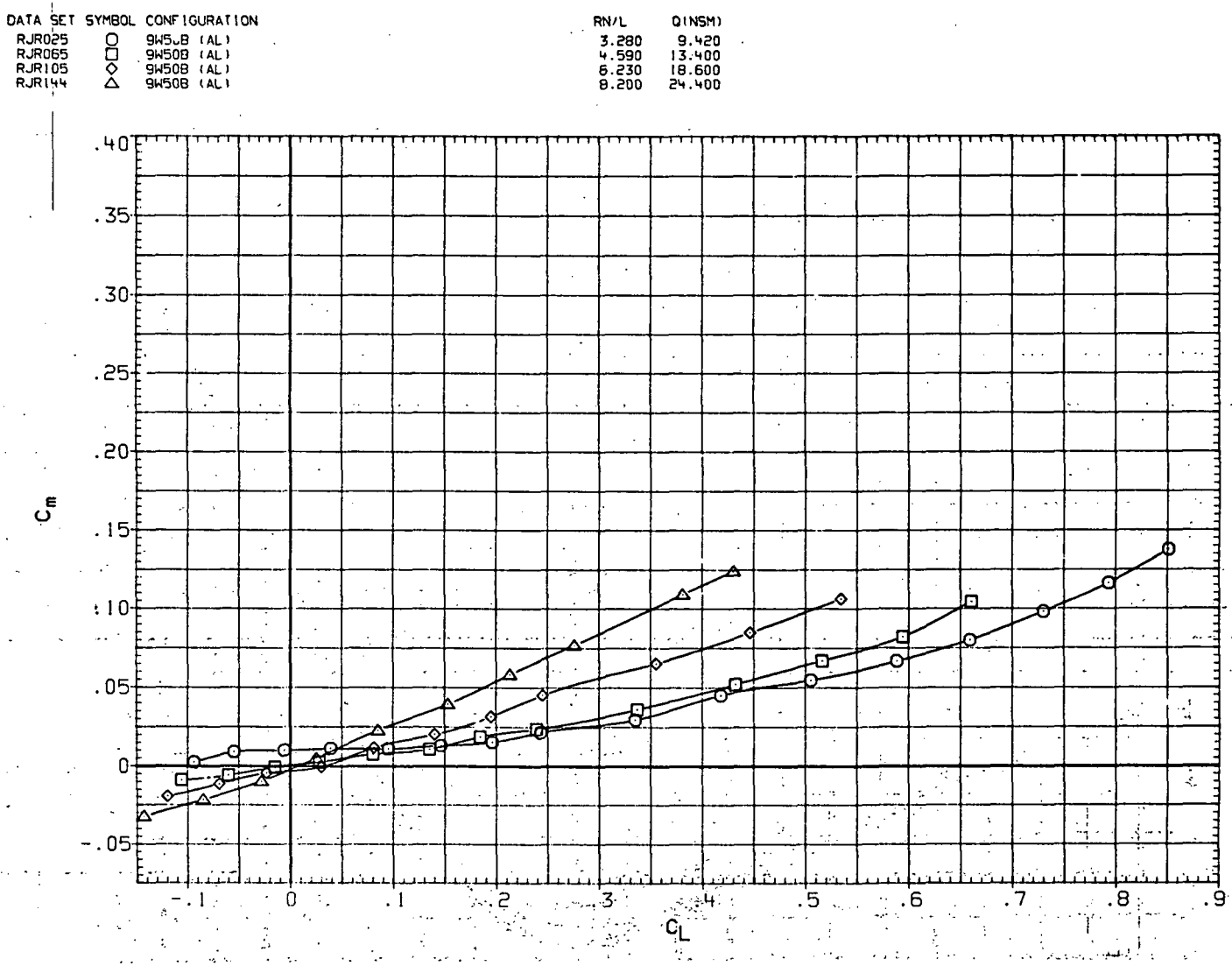

(c) C_m vs C_L.

Figure 24.– Continued.

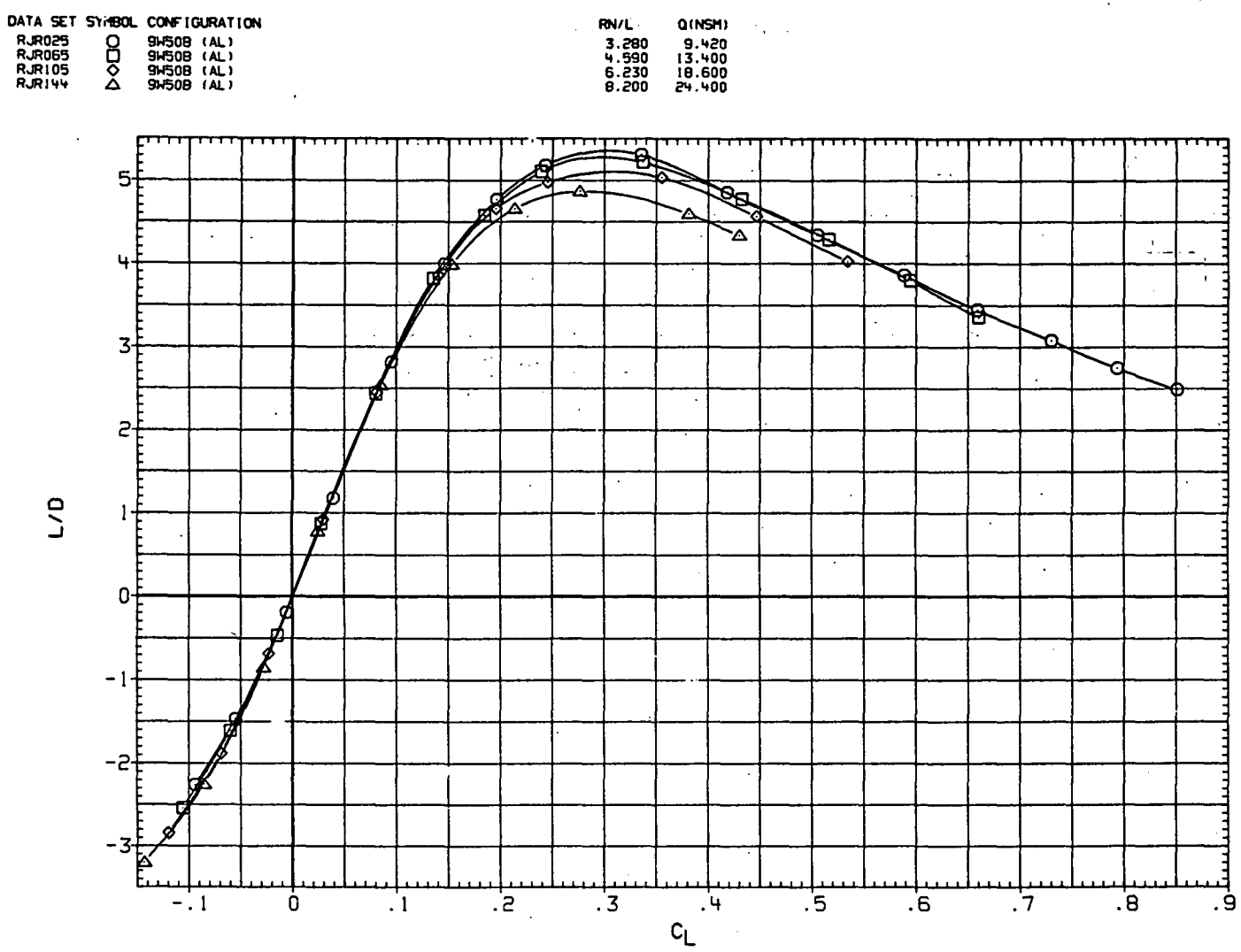

(d) L/D vs C_L.

Figure 24.– Continued.

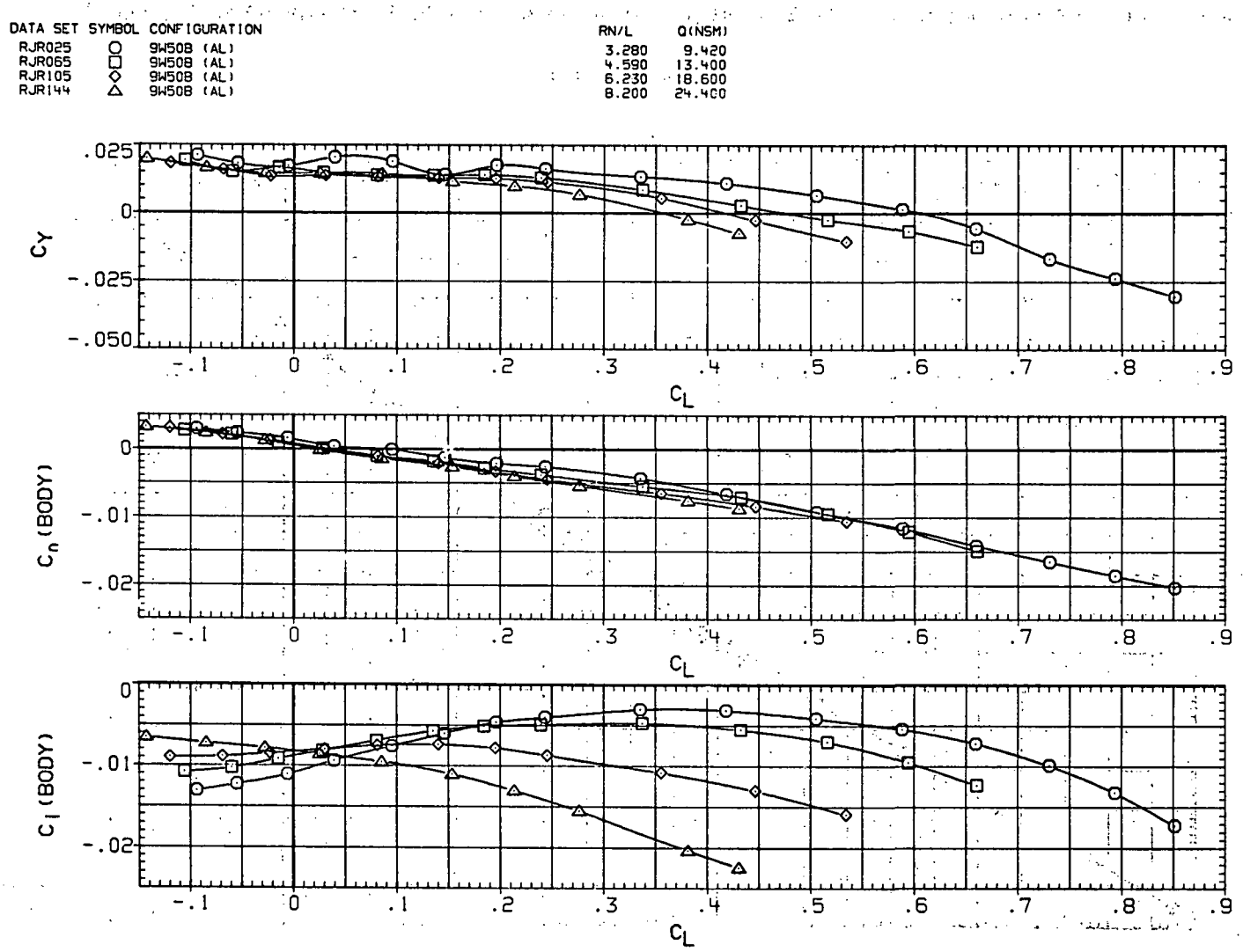

(e) C_Y, C_n and C_ℓ vs C_L.

Figure 24.– Concluded.

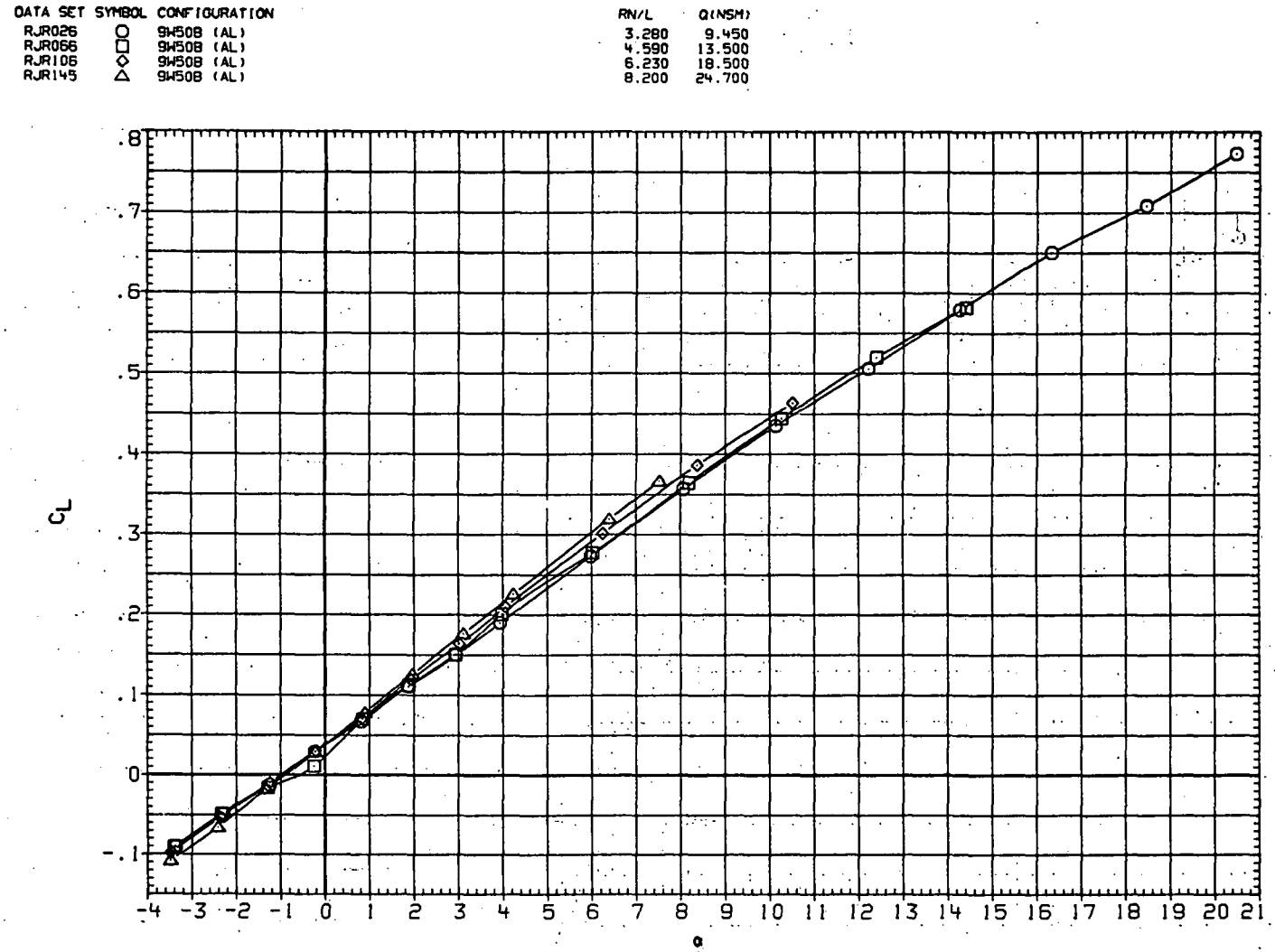

(a) C_L vs α.

Figure 25.– Dynamic-pressure effects on the aerodynamic characteristics of the aluminum trapezoidal oblique wing-body combination ($\Lambda = 50°$, $M = 2.0$ and the modified NACA 65A204 airfoil).

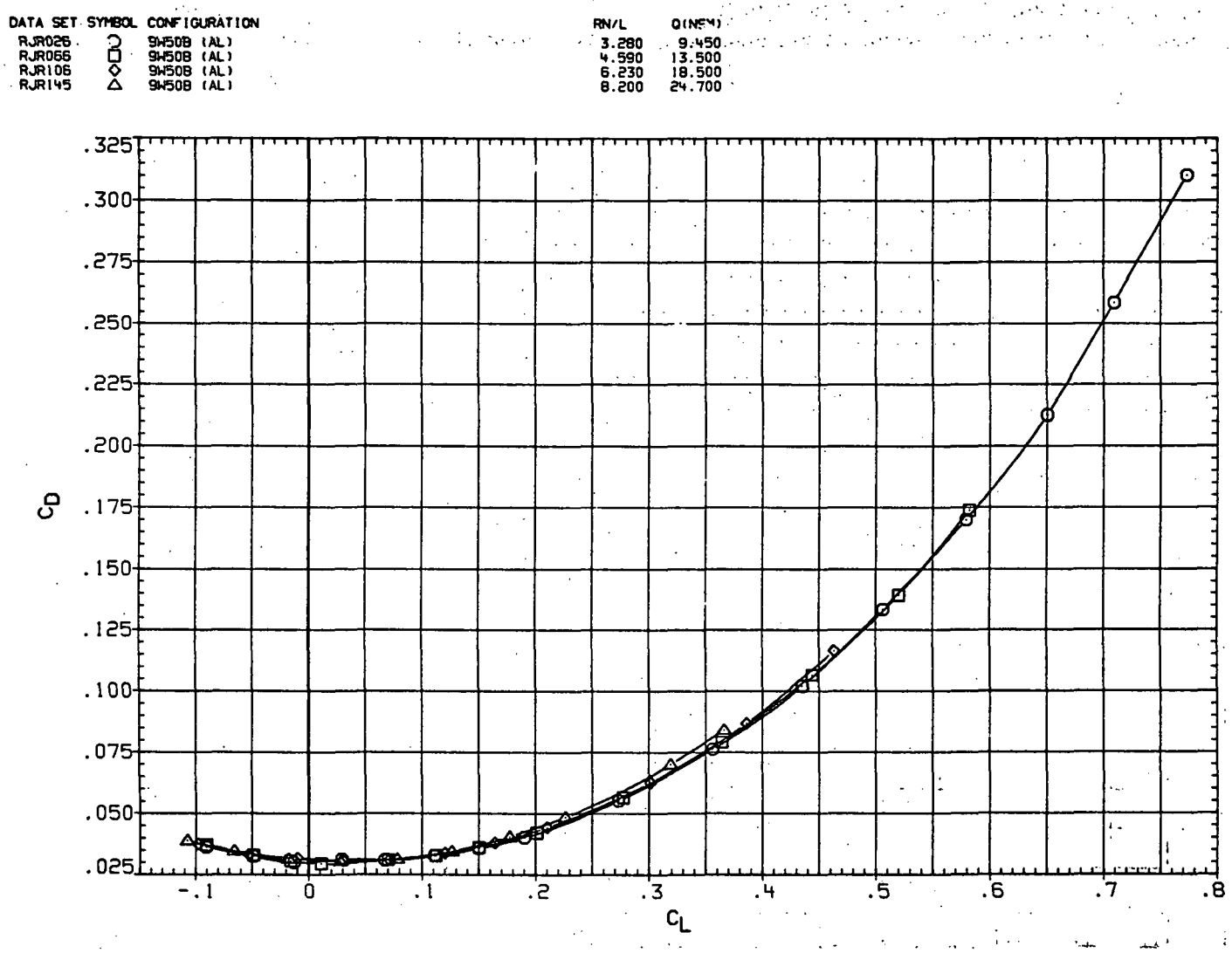

(b) C_D vs C_L.

Figure 25.– Continued.

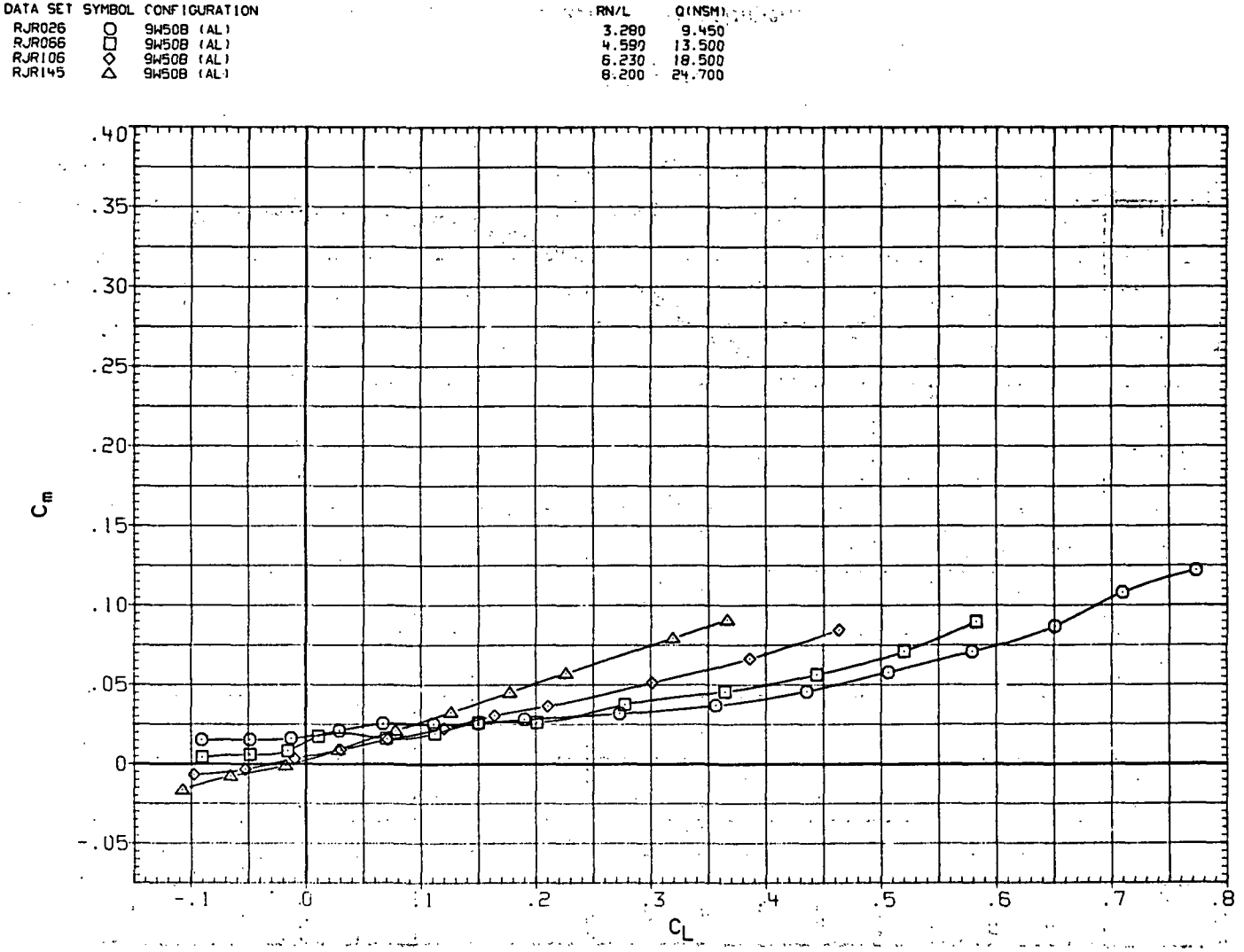

(c) C_m vs C_L.

Figure 25.– Continued.

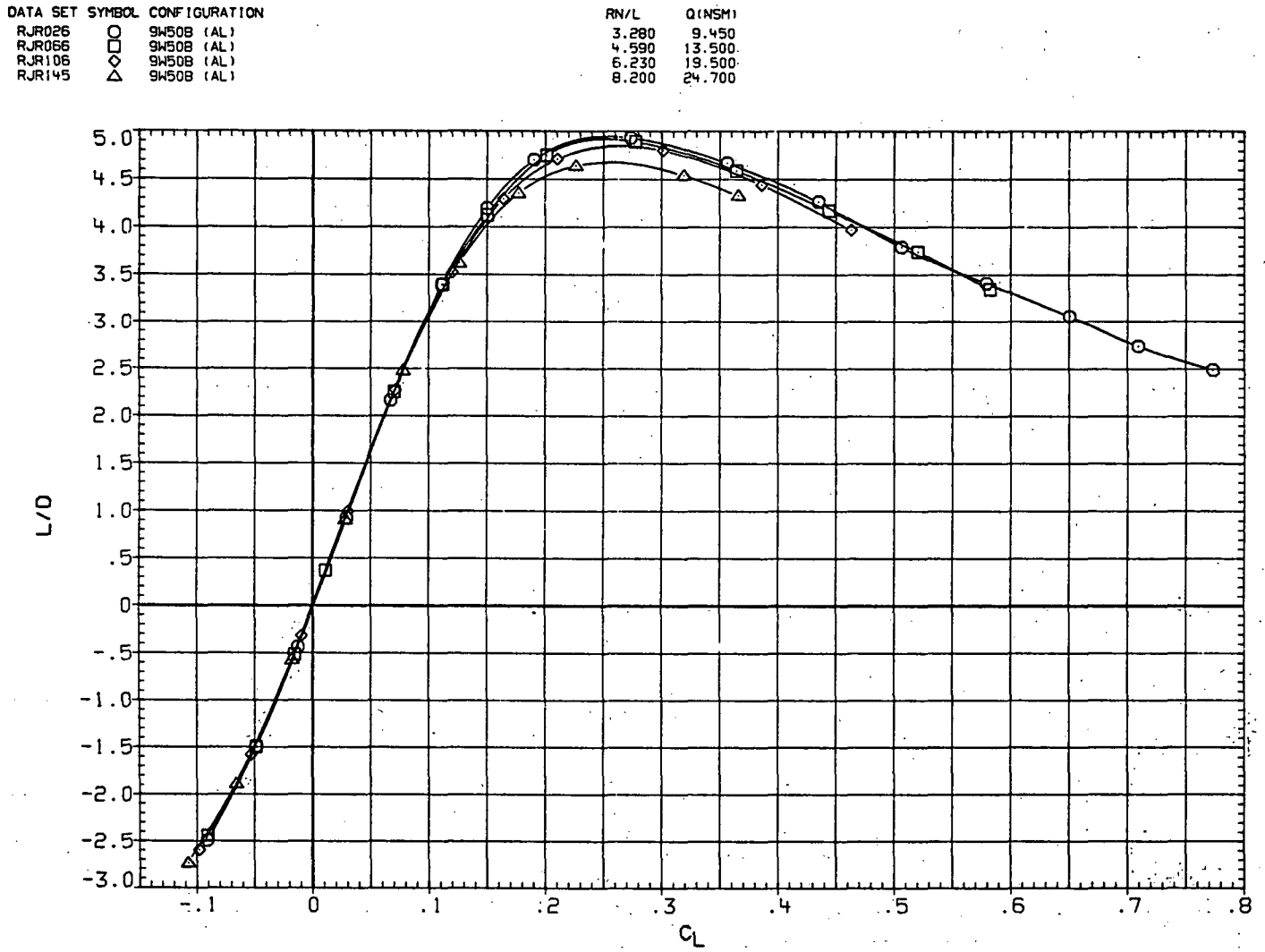

(d) L/D vs C_L.

Figure 25.– Continued.

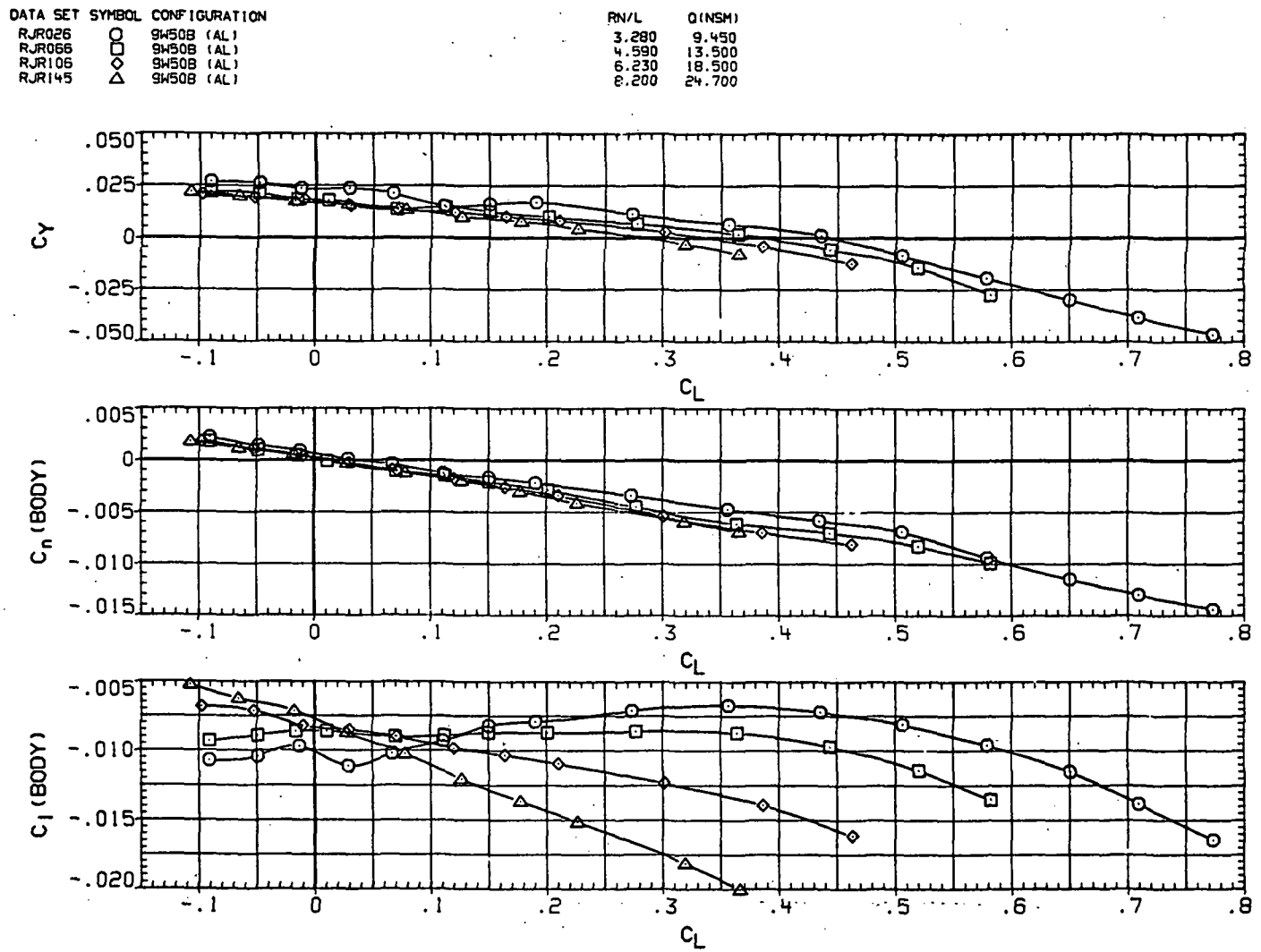

(e) C_Y, C_n and C_ℓ vs C_L.

Figure 25.– Concluded.

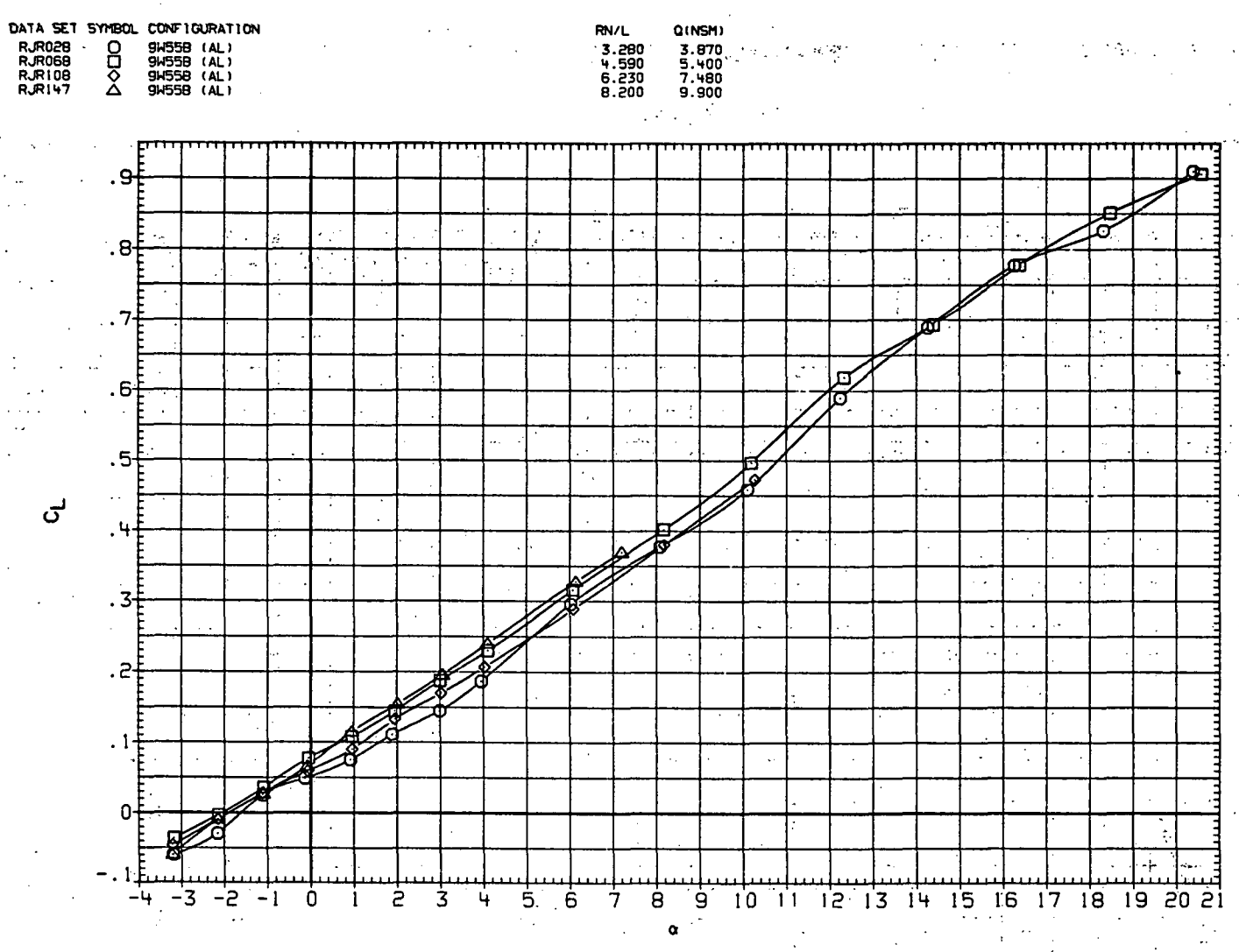

(a) C_L vs α.

Figure 26.– Dynamic-pressure effects on the aerodynamic characteristics of the aluminum trapezoidal oblique wing-body combination ($\Lambda = 55°$, $M = 0.4$ and the modified NACA 65A204 airfoil).

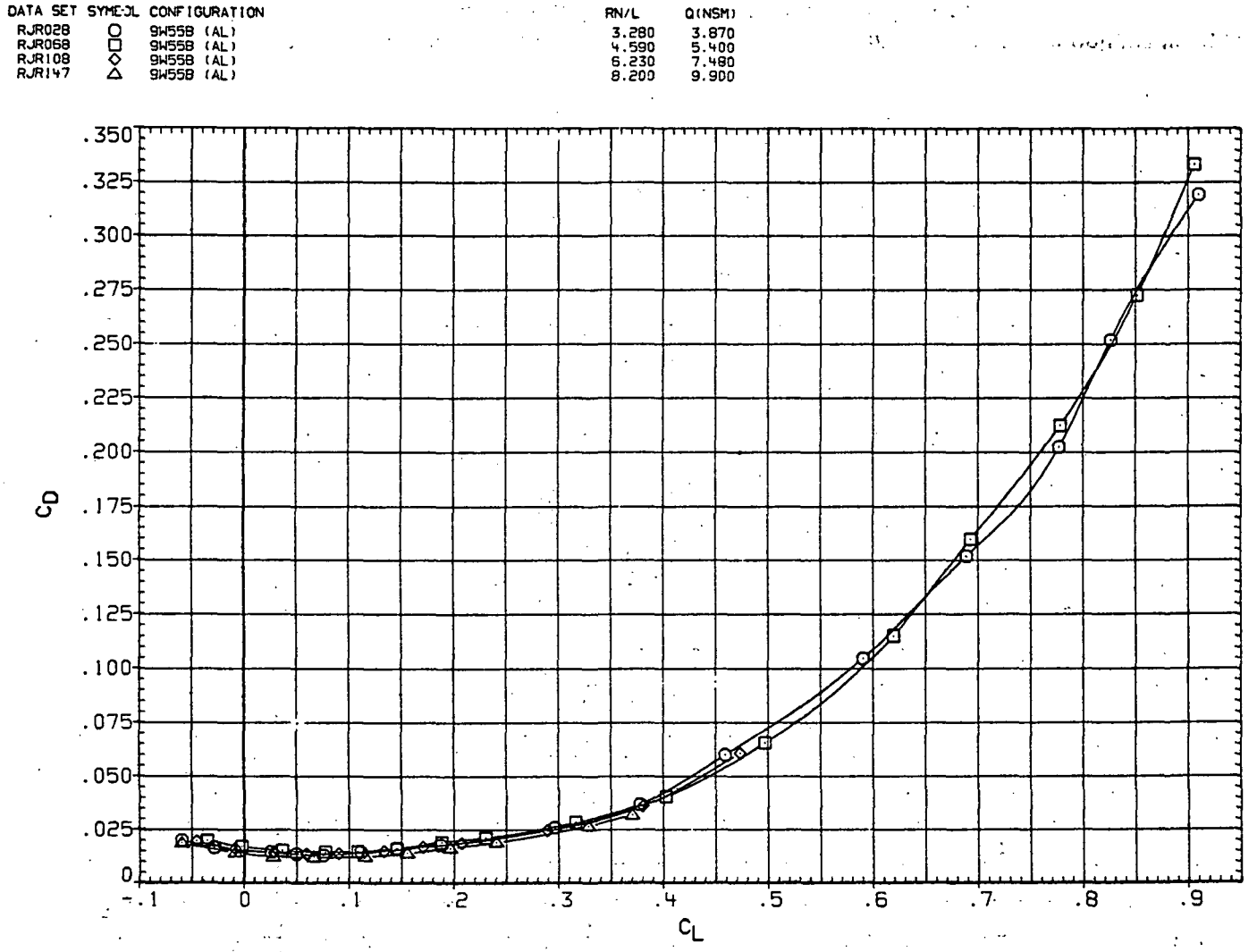

(b) C_D vs C_L

Figure 26.– Continued.

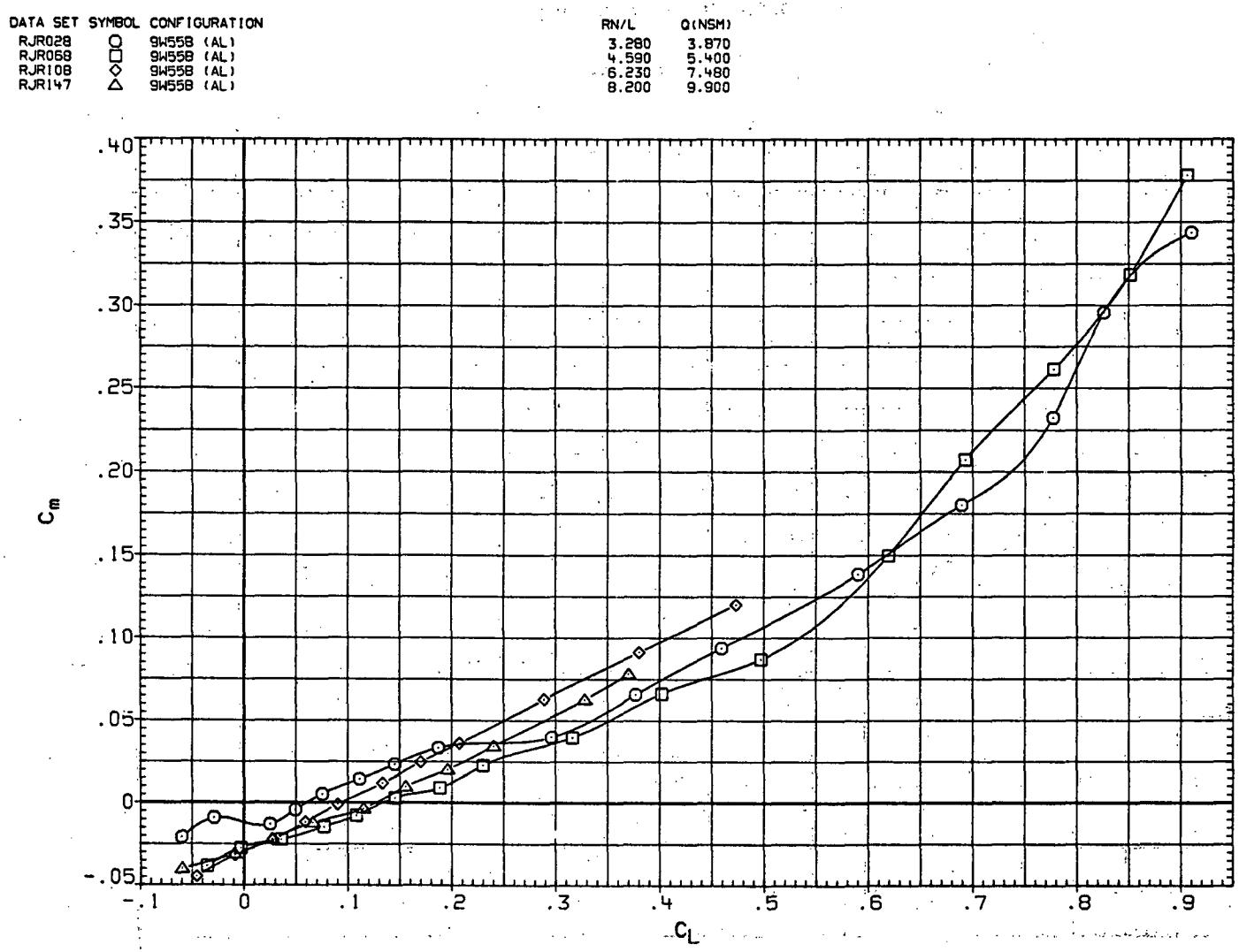

(c) C_m vs C_L.

Figure 26.– Continued.

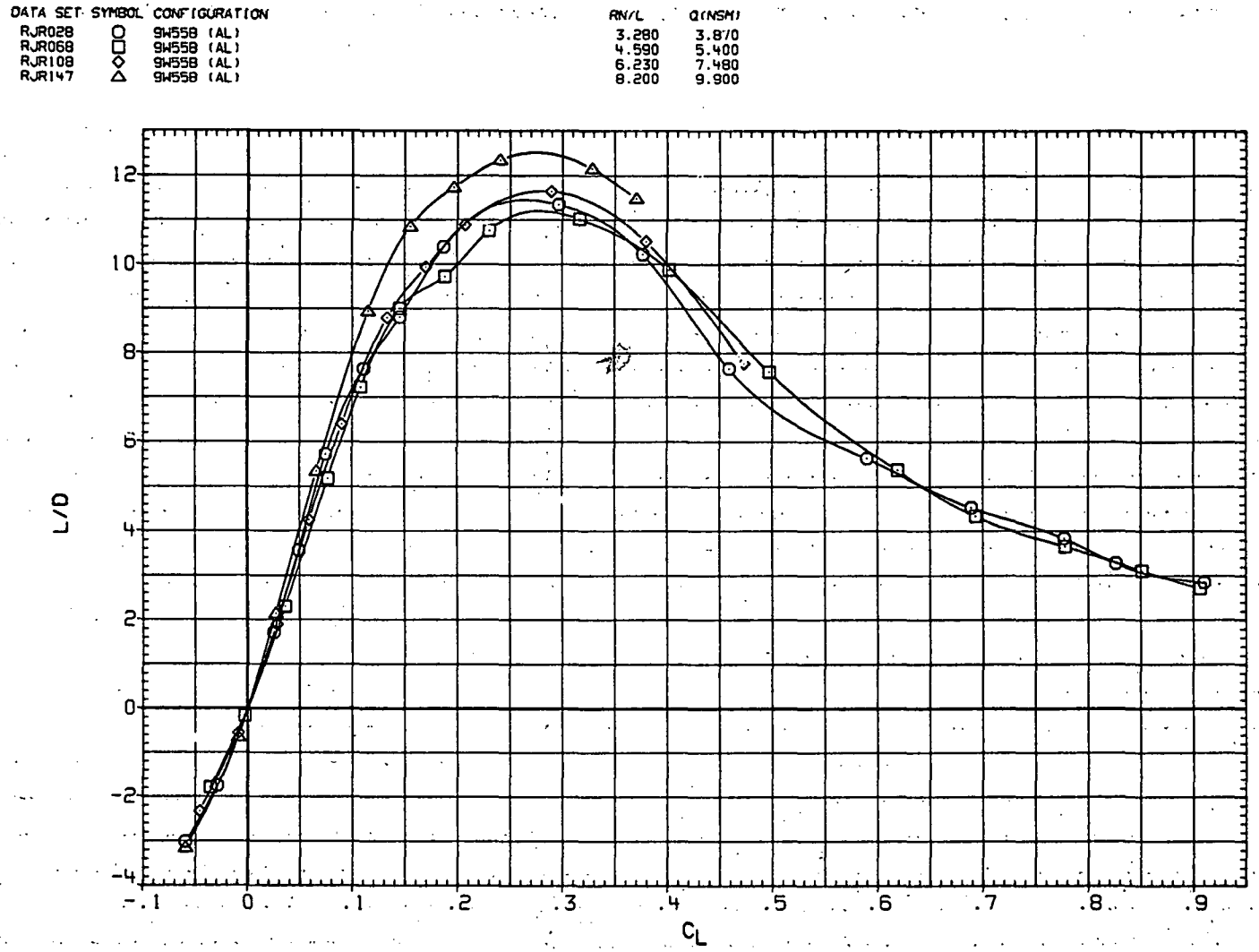

(d) L/D vs C_L.

Figure 26.– Continued.

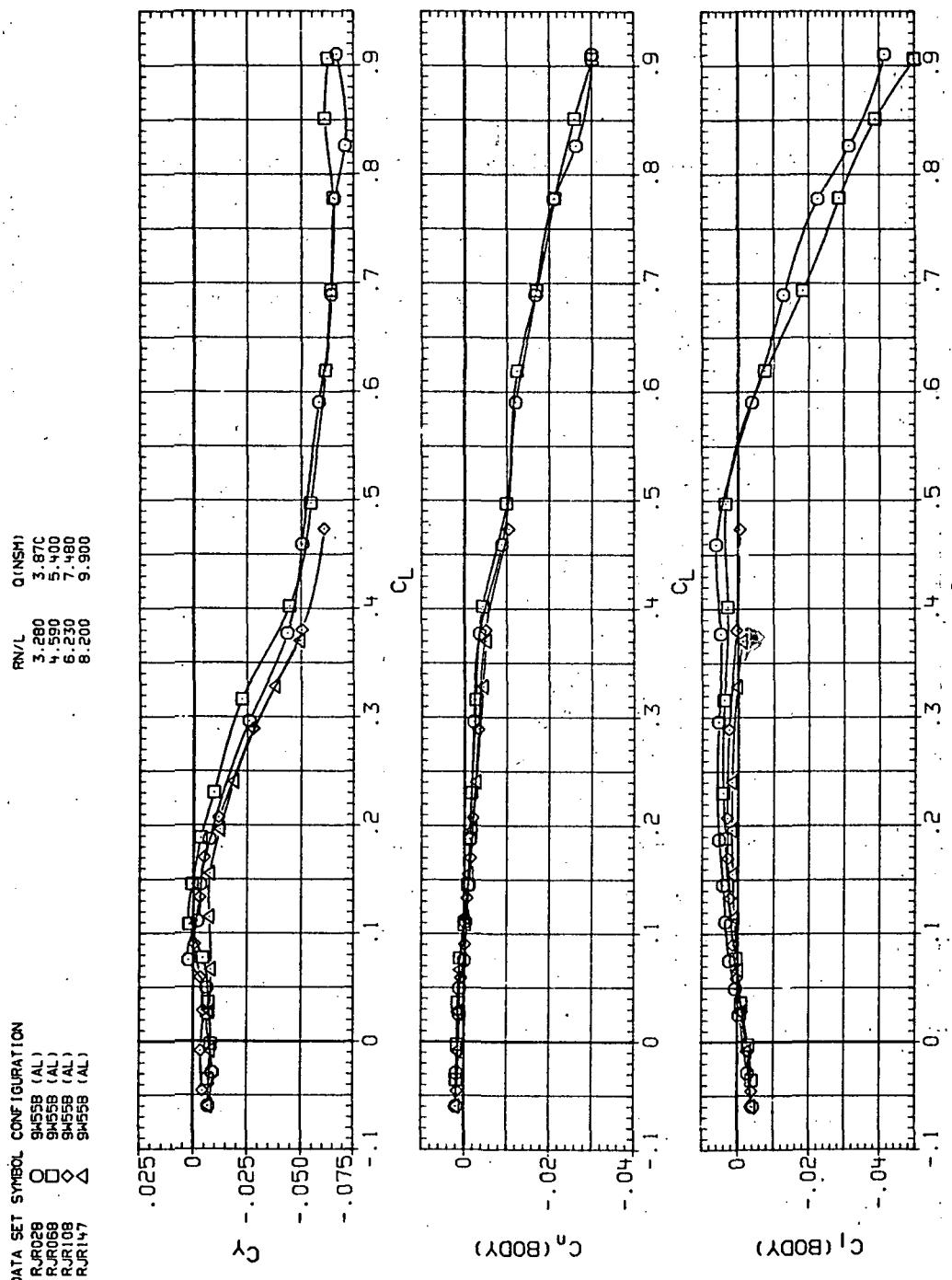

(e) C_Y, C_n and C_ℓ vs C_L.

Figure 26.– Concluded.

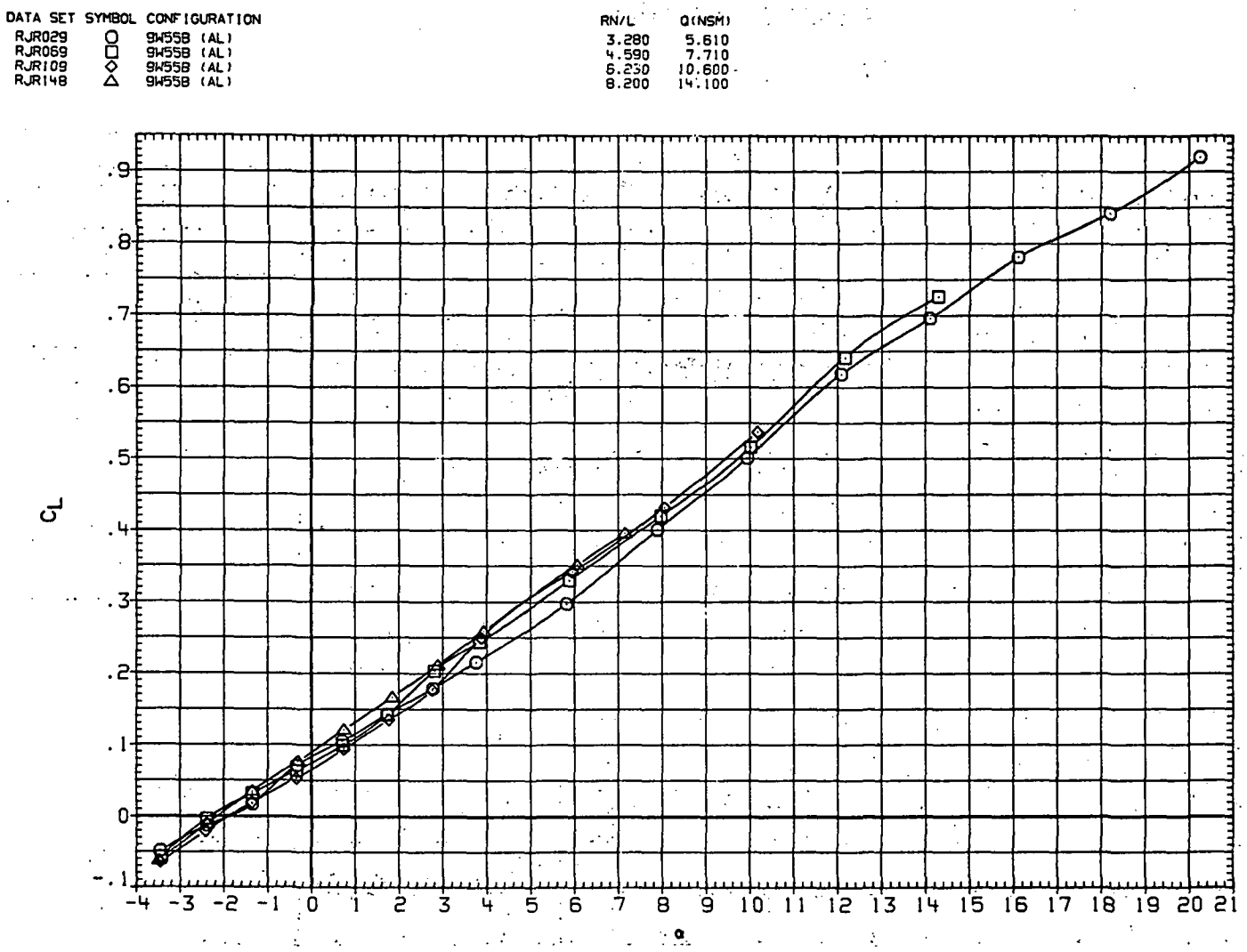

(a) C_L vs α.

Figure 27.– Dynamic-pressure effects on the aerodynamic characteristics of the aluminum trapezoidal oblique wing-body combination ($\Lambda = 55°$, $M = 0.6$ and the modified NACA 65A204 airfoil).

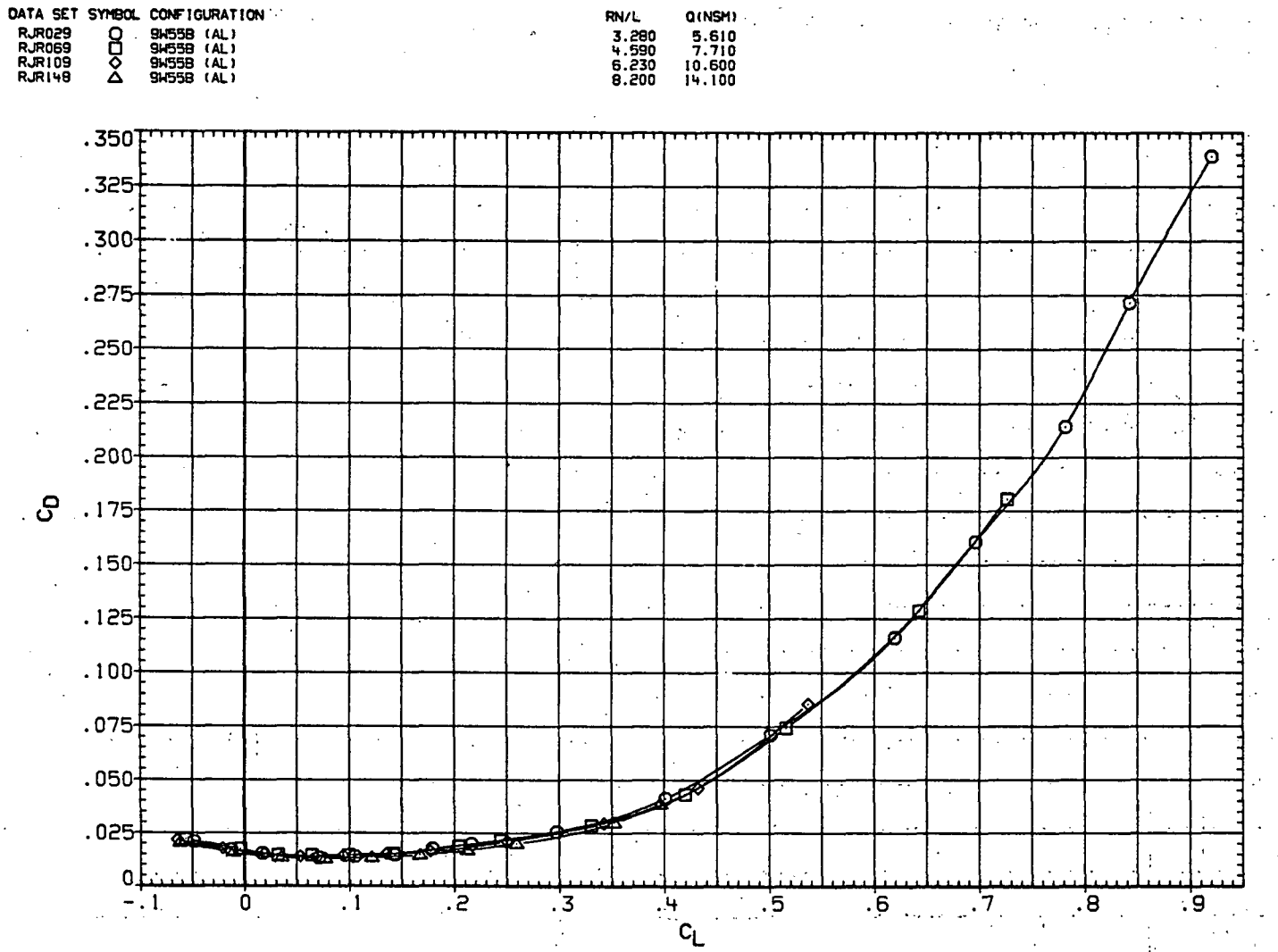

(b) C_D vs C_L.

Figure 27.– Continued.

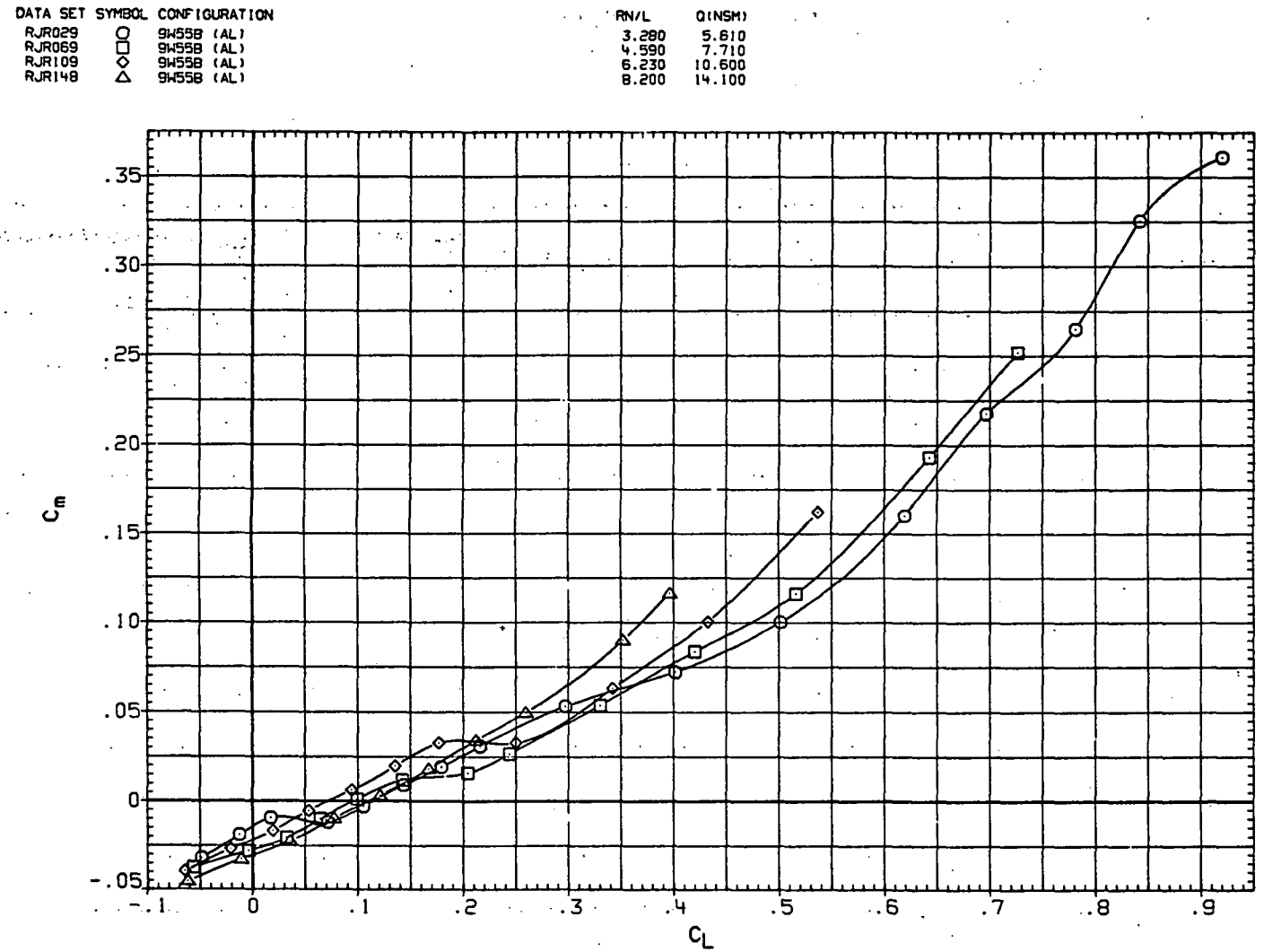

(c) C_m vs C_L.

Figure 27.– Continued.

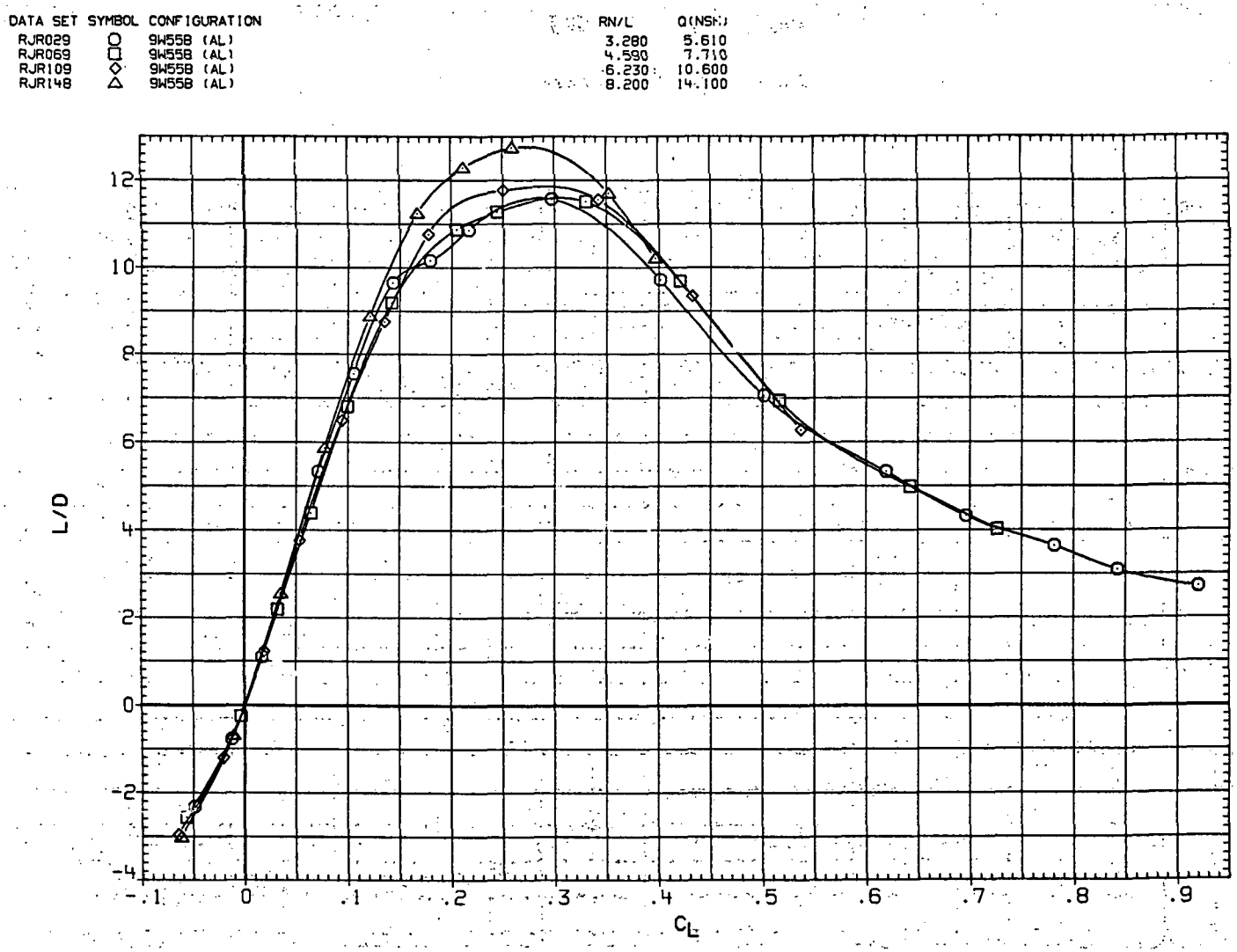

(d) L/D vs C_L.

Figure 27.—Continued.

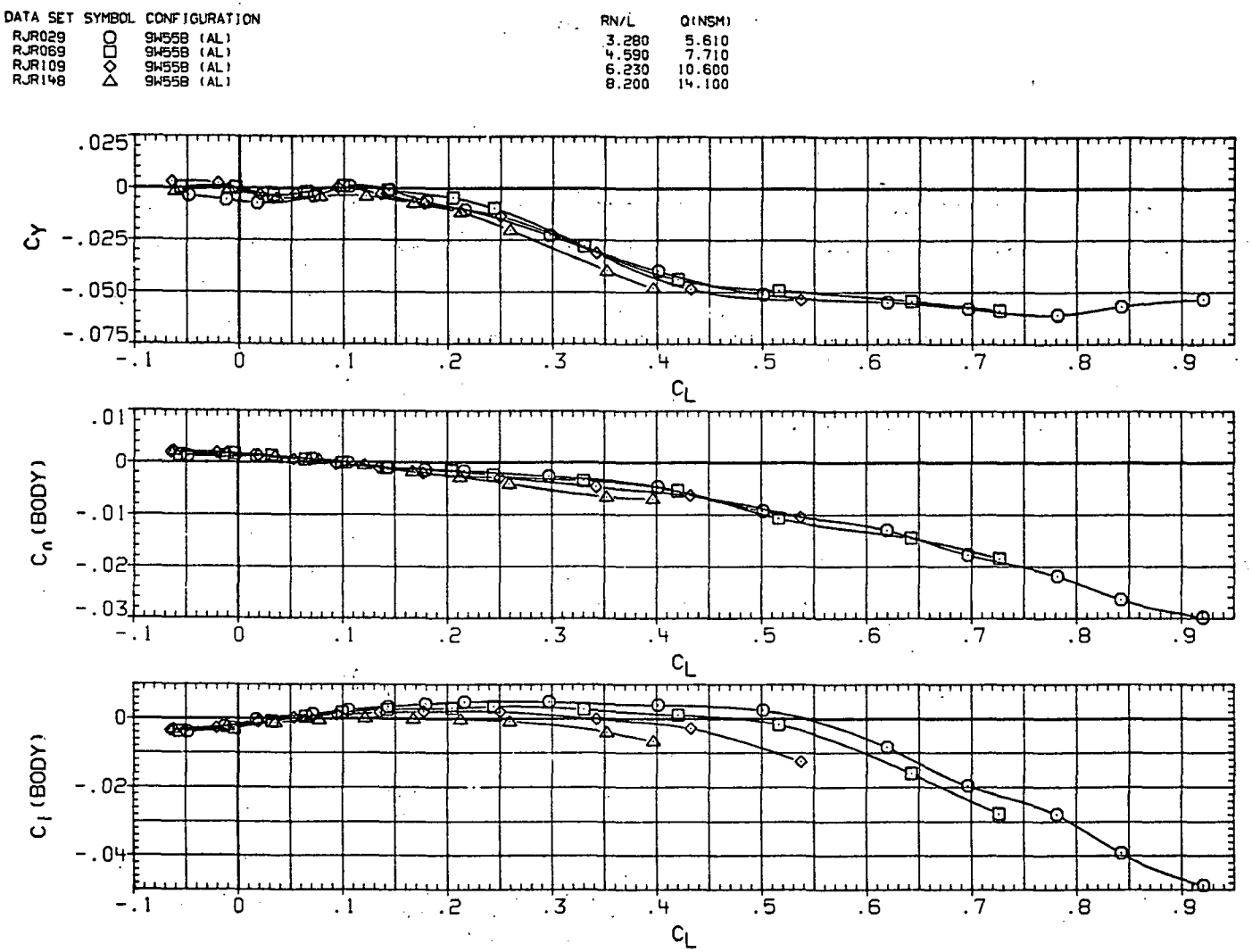

(e) C_Y, C_n and C_ℓ vs C_L.

Figure 27.– Concluded.

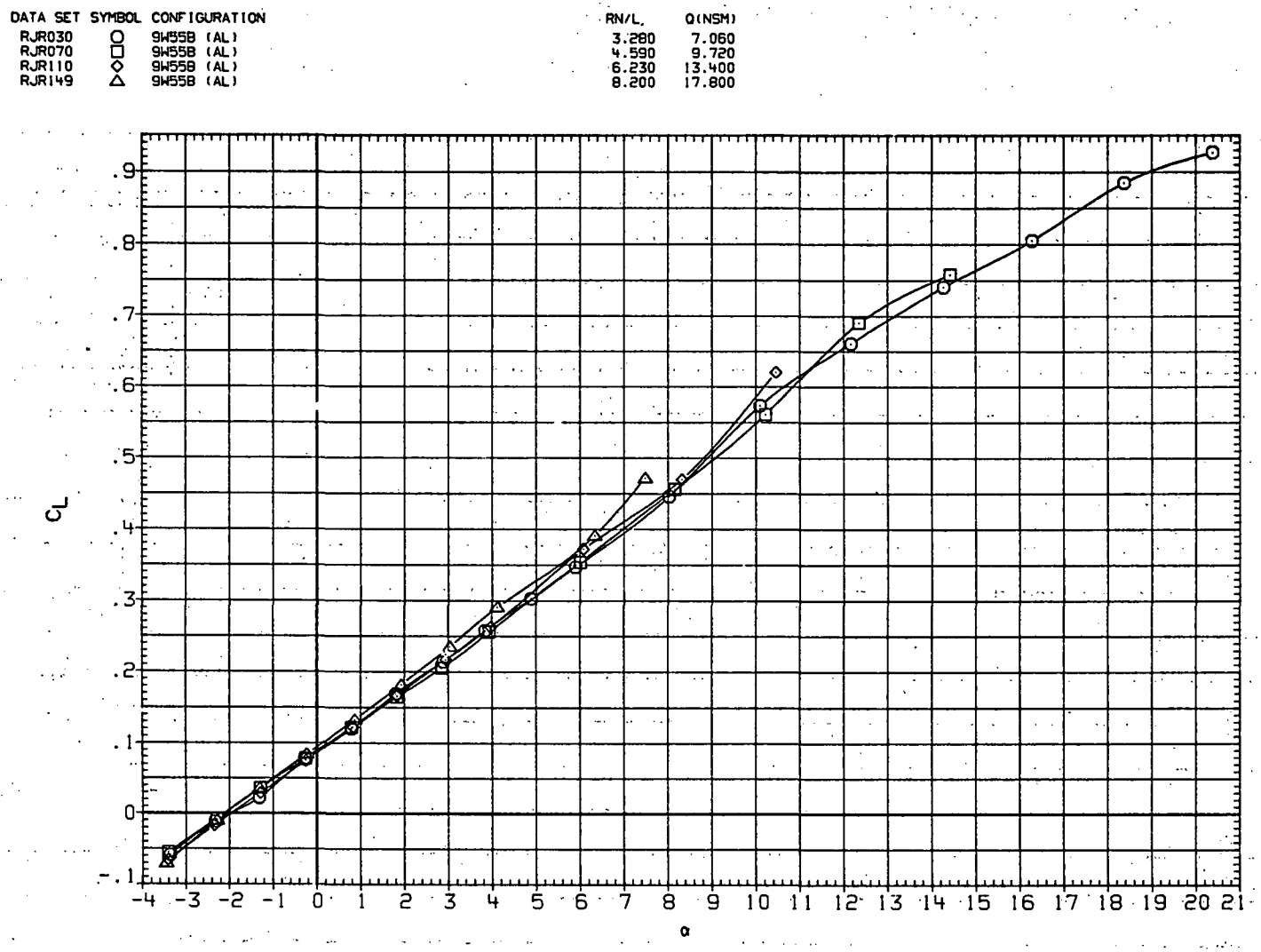

(a) C_L vs α.

Figure 28.– Dynamic-pressure effects on the aerodynamic characteristics of the aluminum trapezoidal oblique wing-body combination ($\Lambda = 55°, M = 0.8$ and the modified NACA 65A204 airfoil).

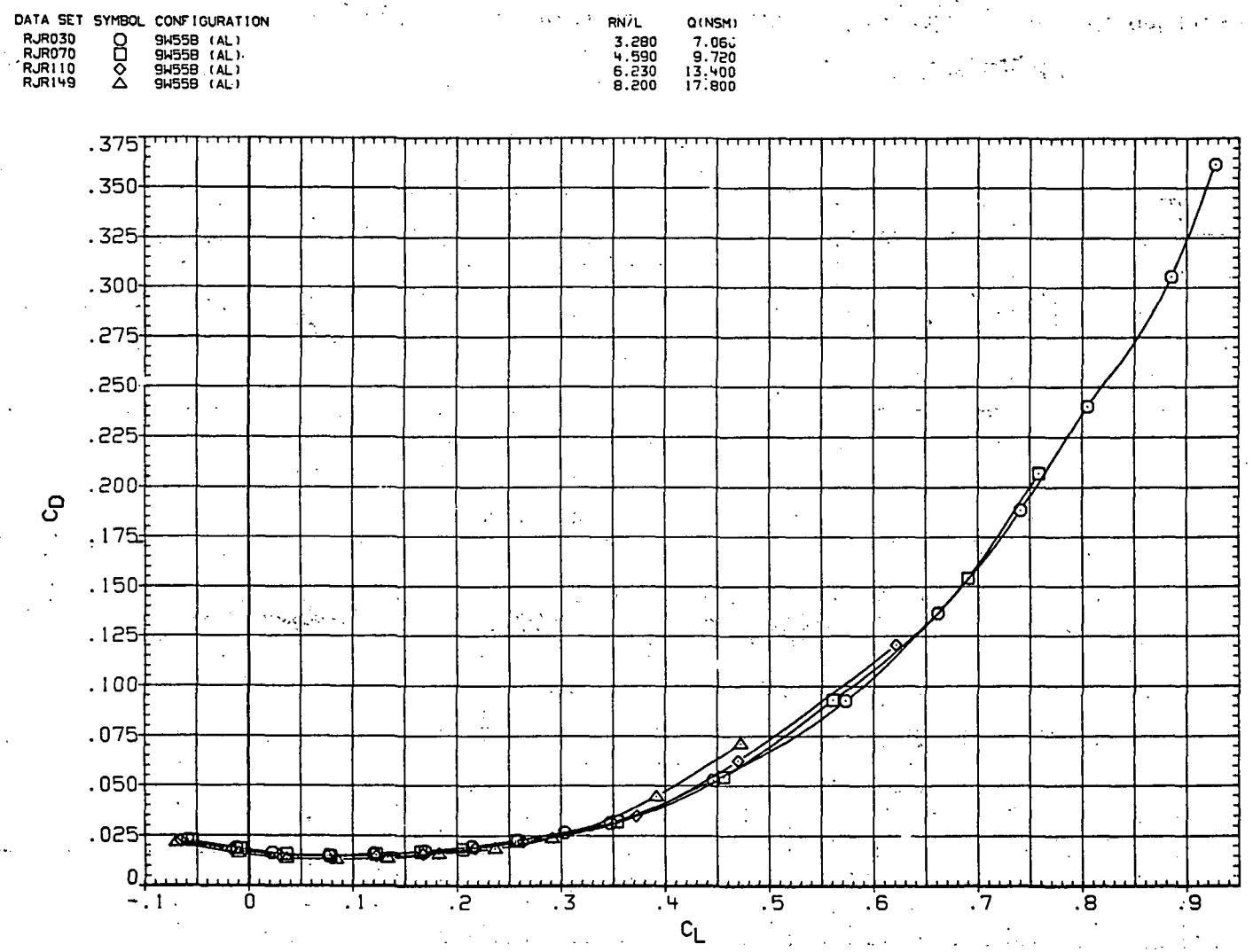

(b) C_D vs C_L.

Figure 28.– Continued.

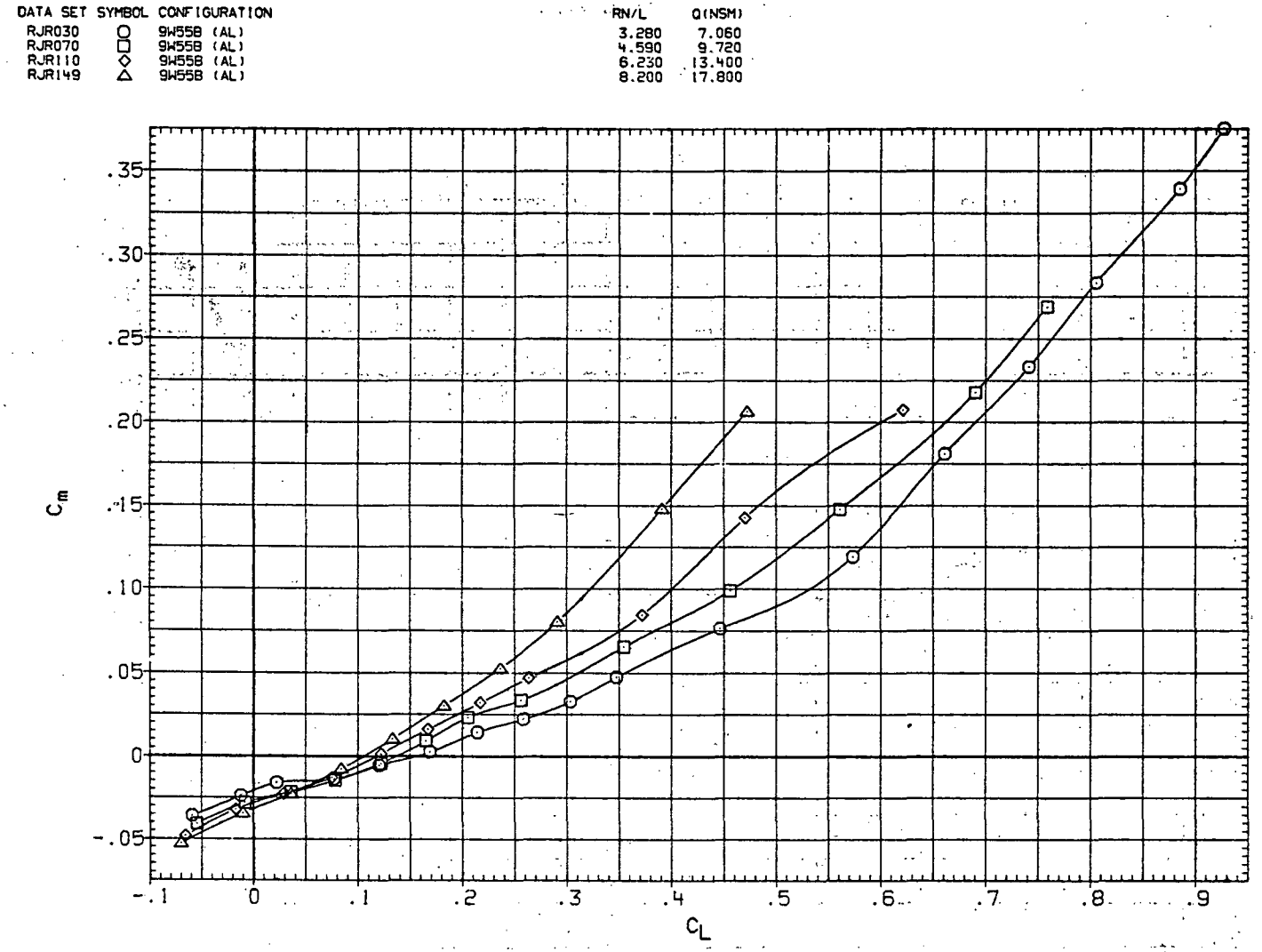

(c) C_m vs C_L.

Figure 28.– Continued.

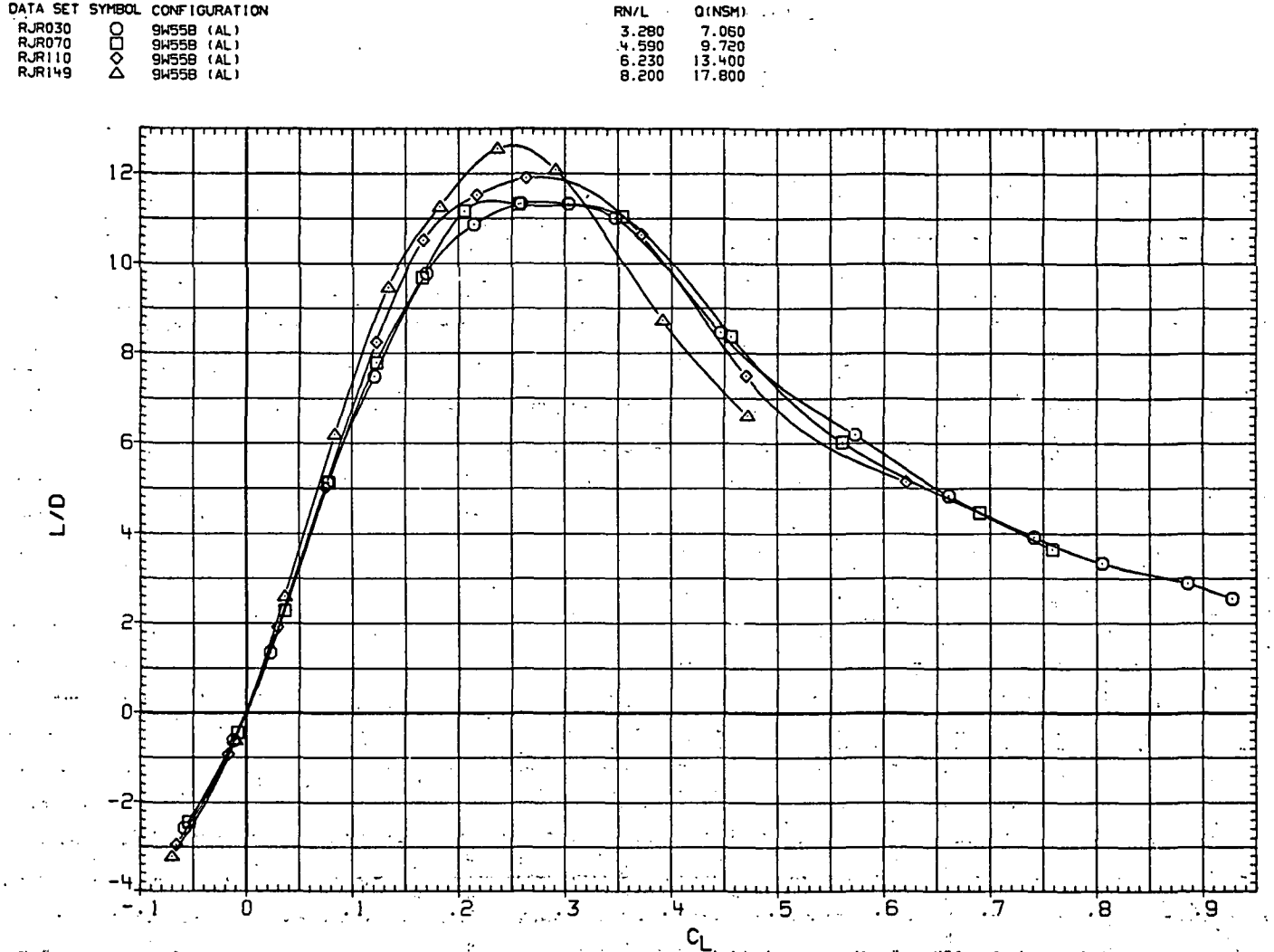

(d) L/D vs C_L.

Figure 28.– Continued.

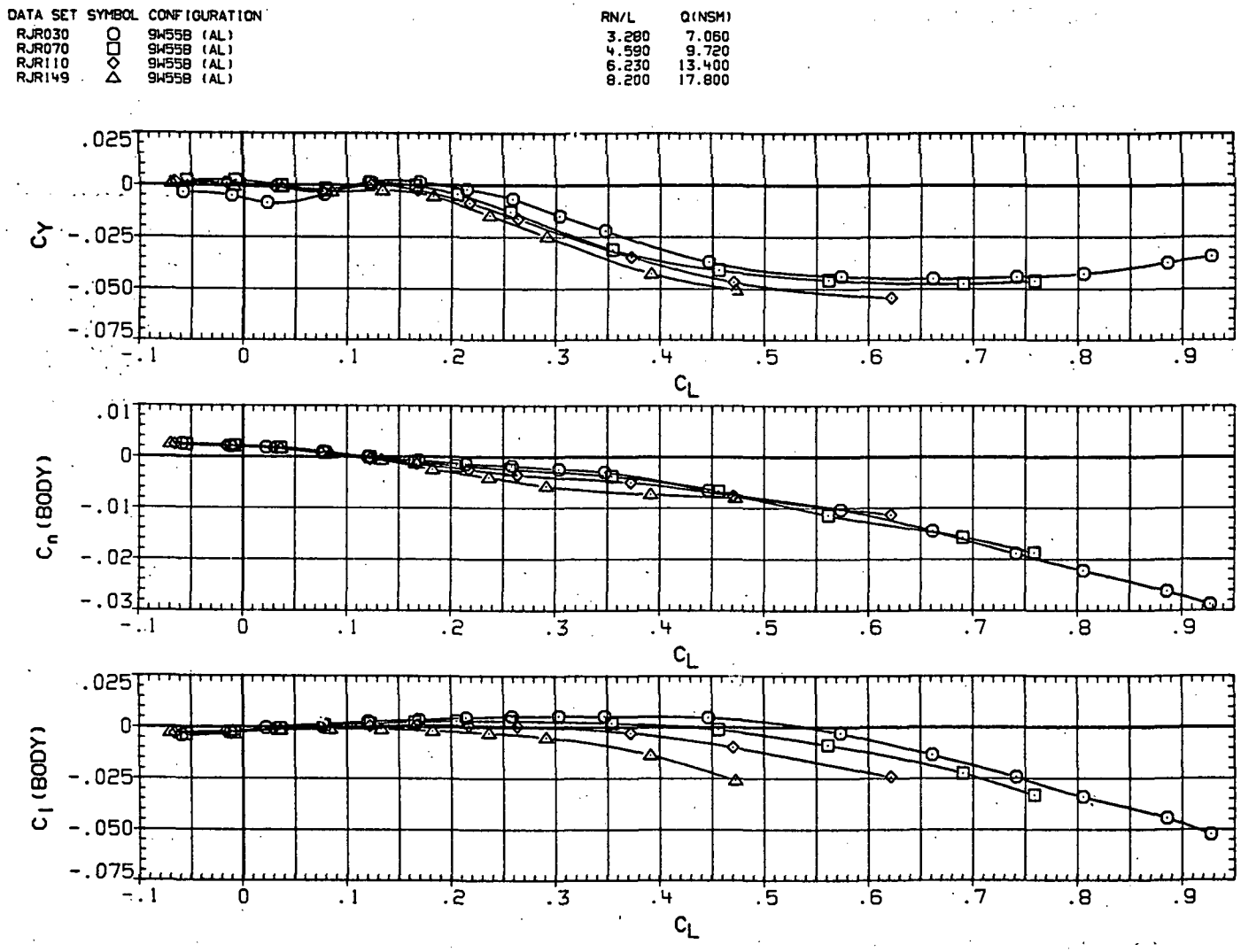

(e) C_Y, C_n and C_ℓ vs C_L.

Figure 28.– Concluded.

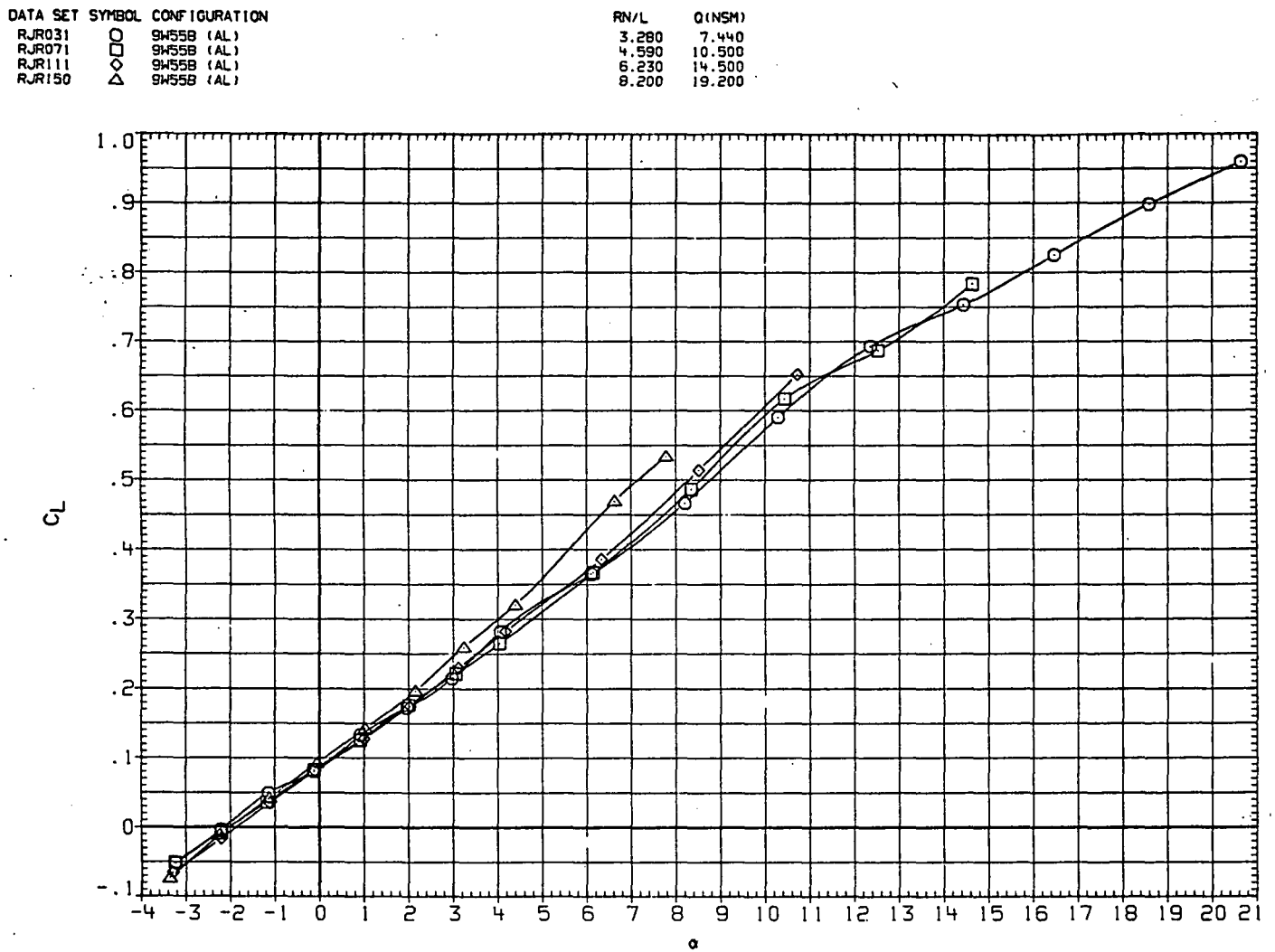

(a) C_L vs α.

Figure 29.– Dynamic-pressure effects on the aerodynamic characteristics of the aluminum trapezoidal oblique wing-body combination ($\Lambda = 55°, M = 0.9$ and the modified NACA 65A204 airfoil).

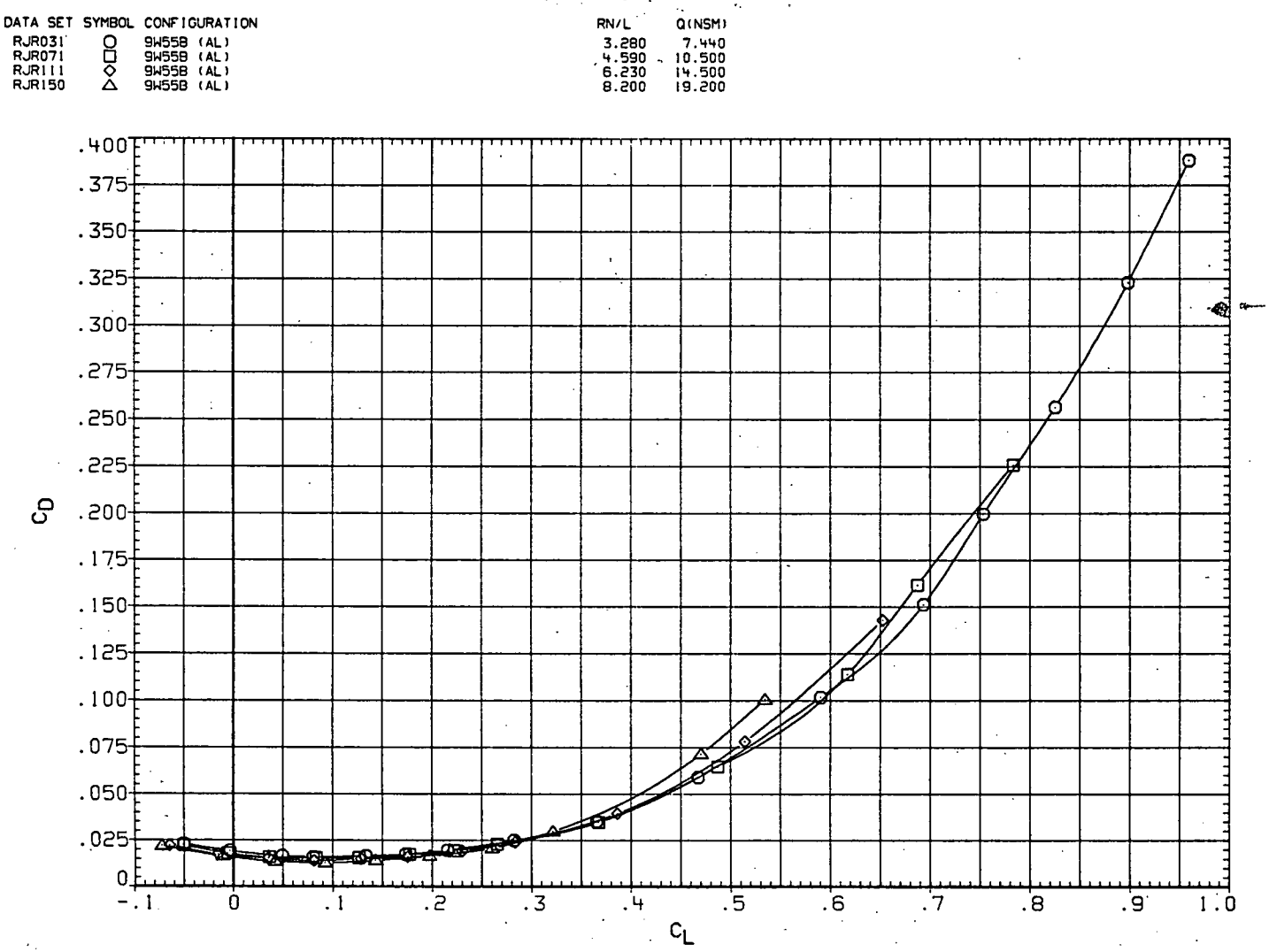

(b) C_D vs C_L.

Figure 29.– Continued.

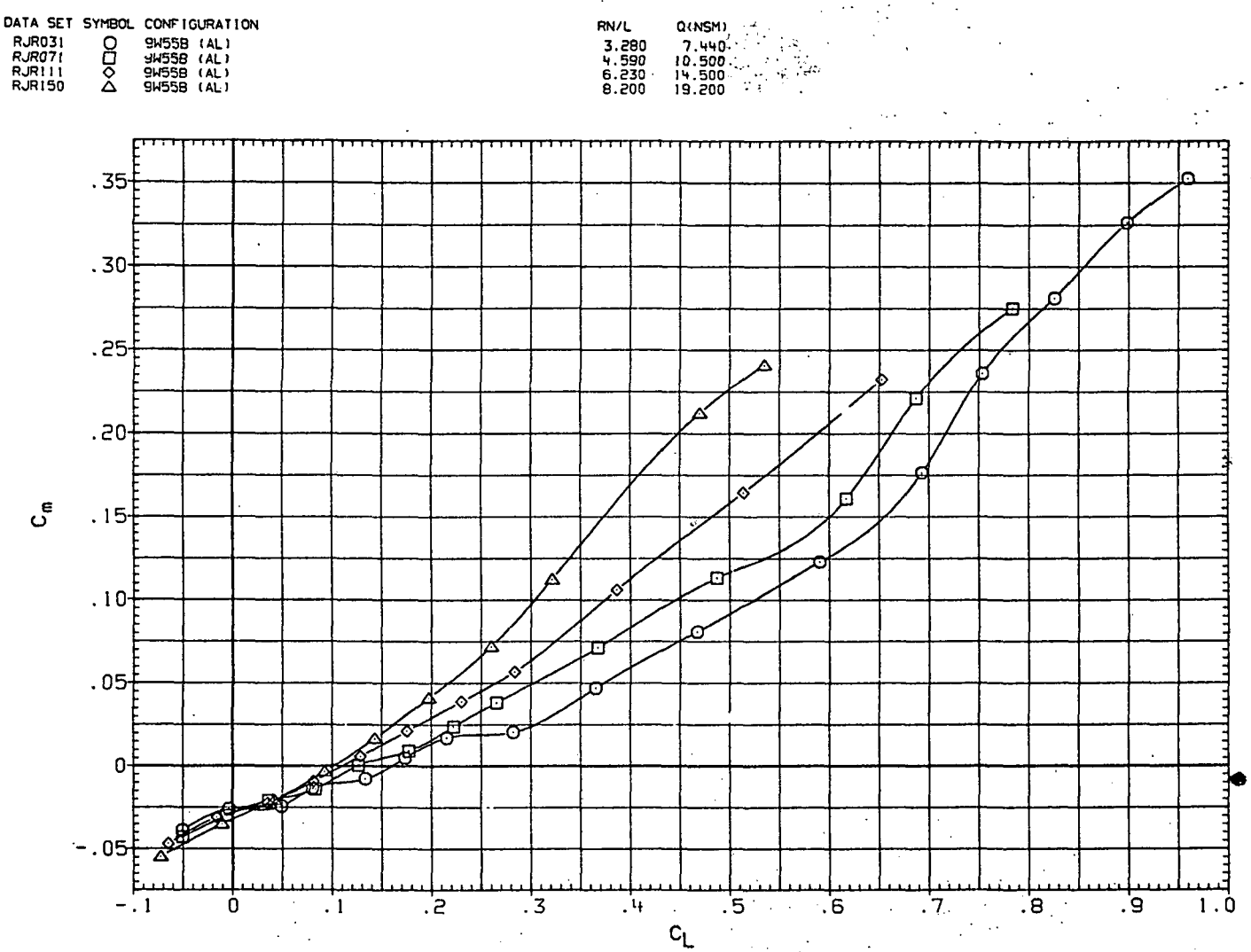

(c) C_m vs C_L.

Figure 29.– Continued.

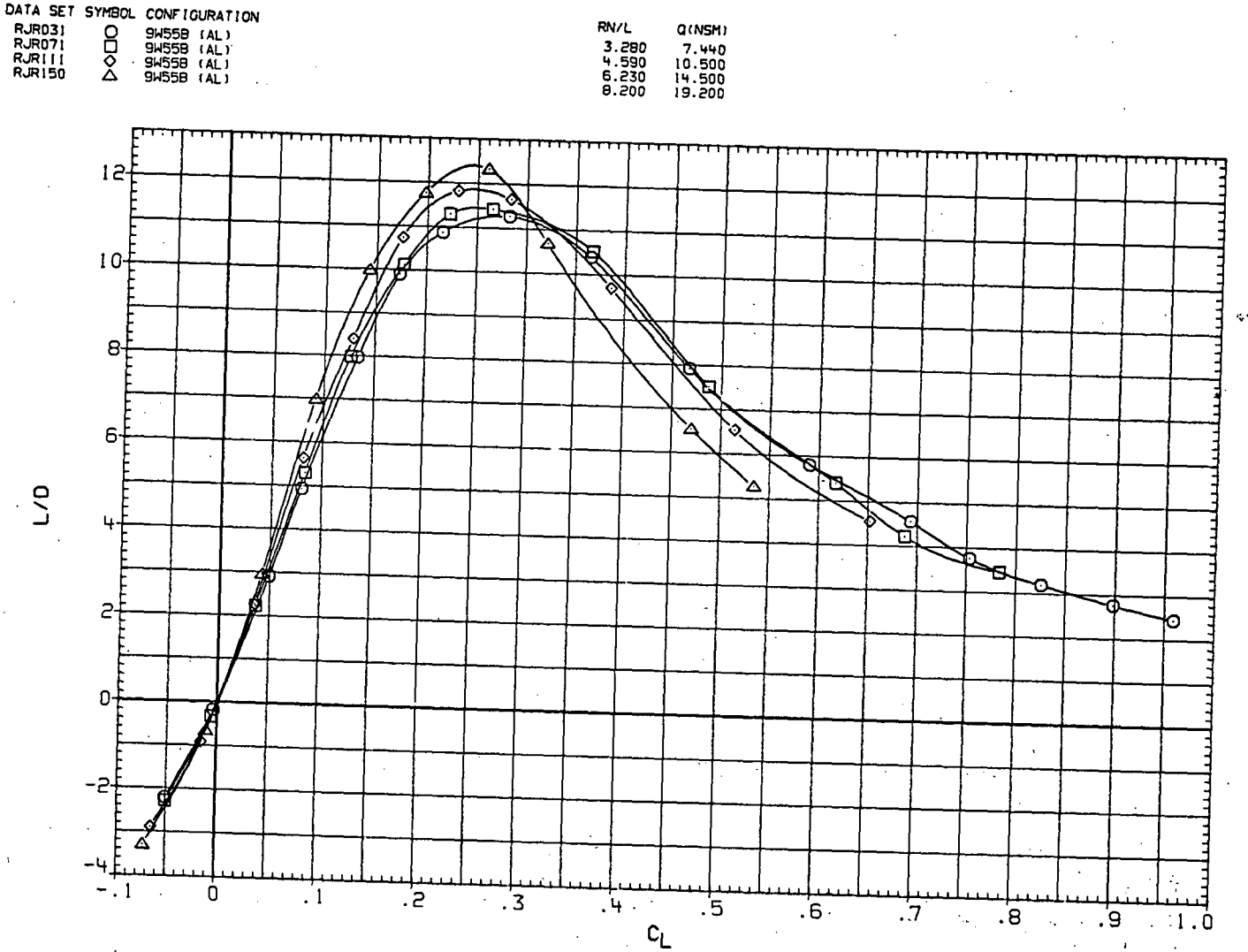

(d) L/D vs C_L.

Figure 29.– Continued.

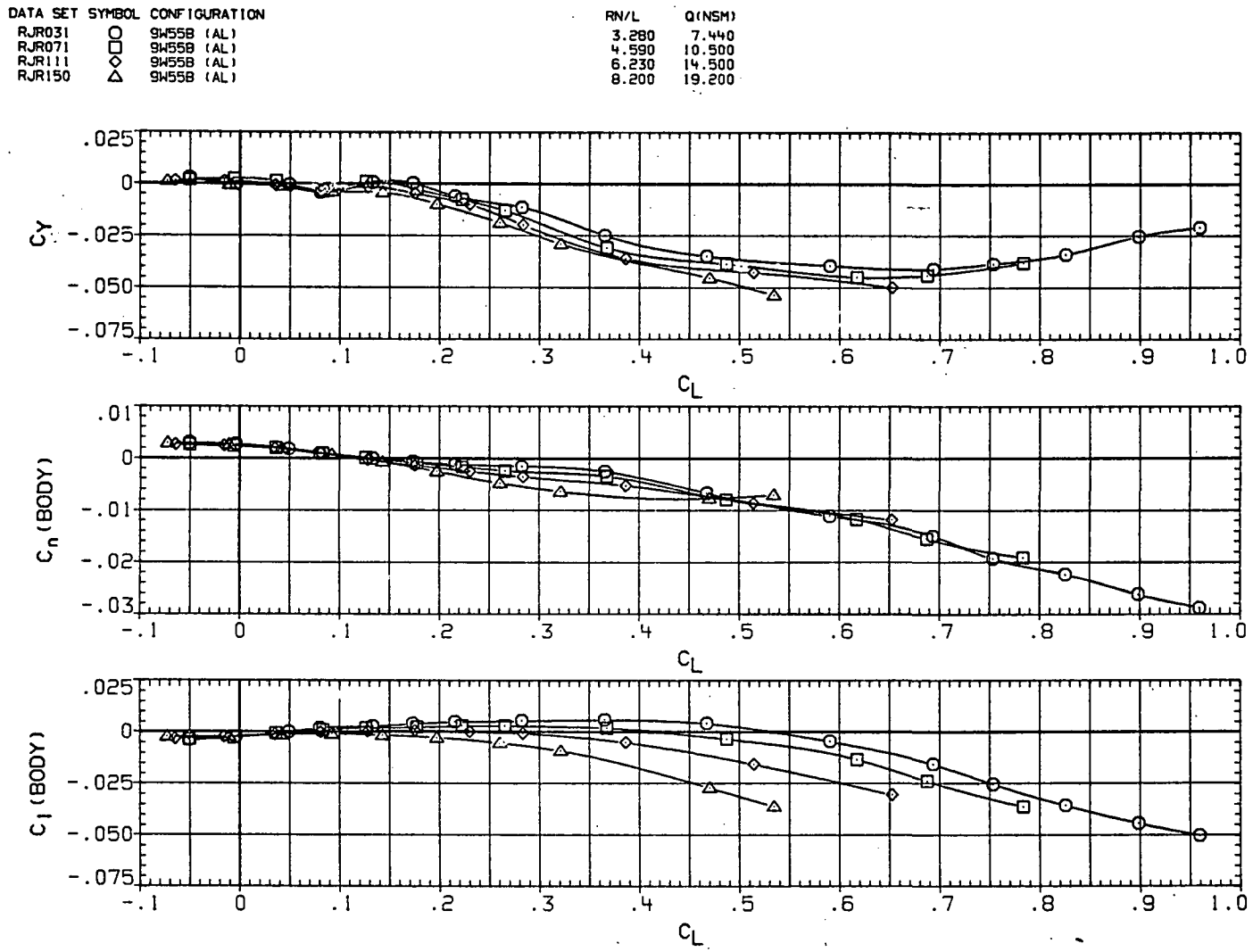

(e) C_Y, C_n and C_ℓ vs C_L.

Figure 29.– Concluded.

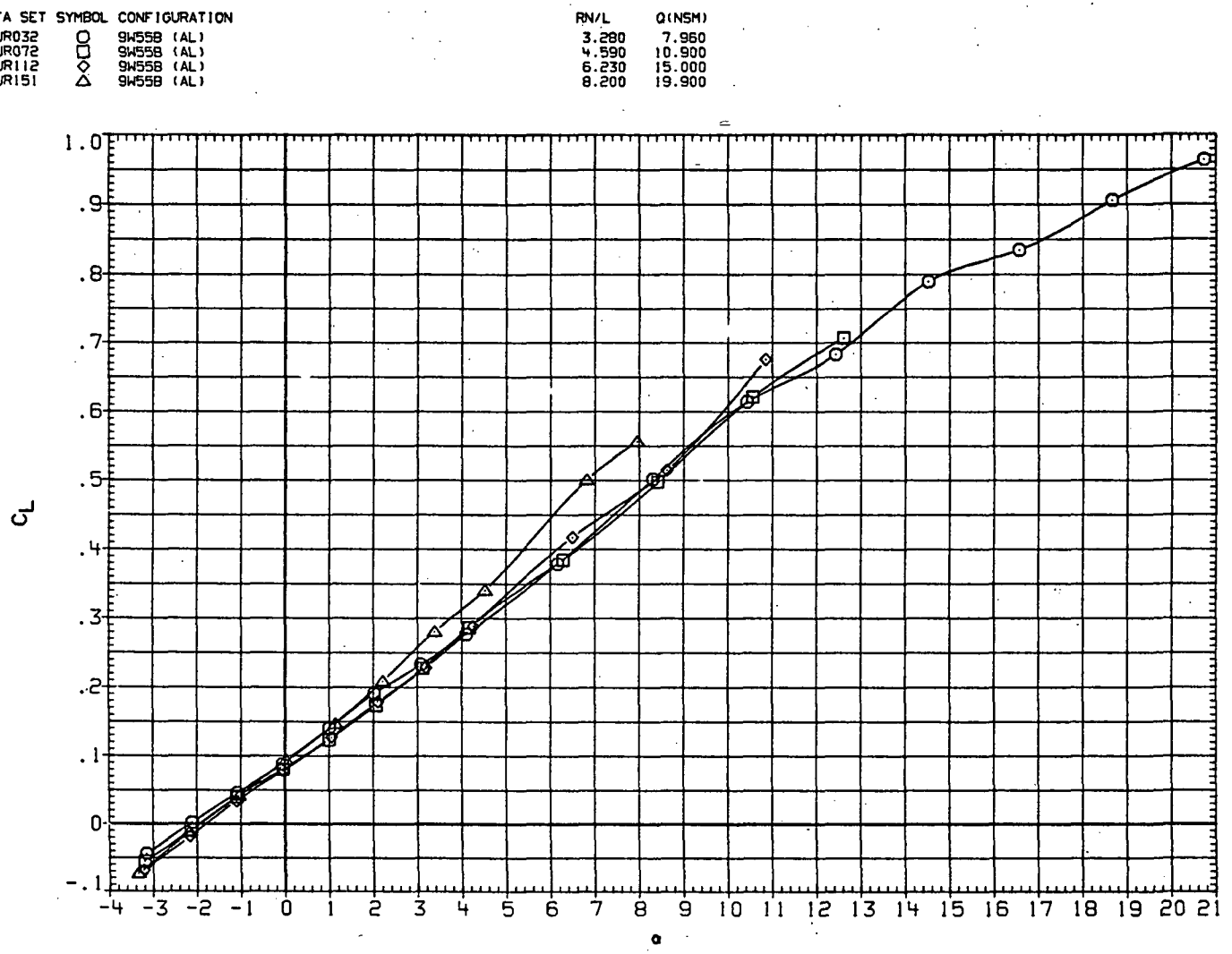

(a) C_L vs α.

Figure 30.– Dynamic-pressure effects on the aerodynamic characteristics of the aluminum trapezoidal oblique wing-body combination ($\Lambda = 55°, M = 0.95$ and the modified NACA 65A204 airfoil).

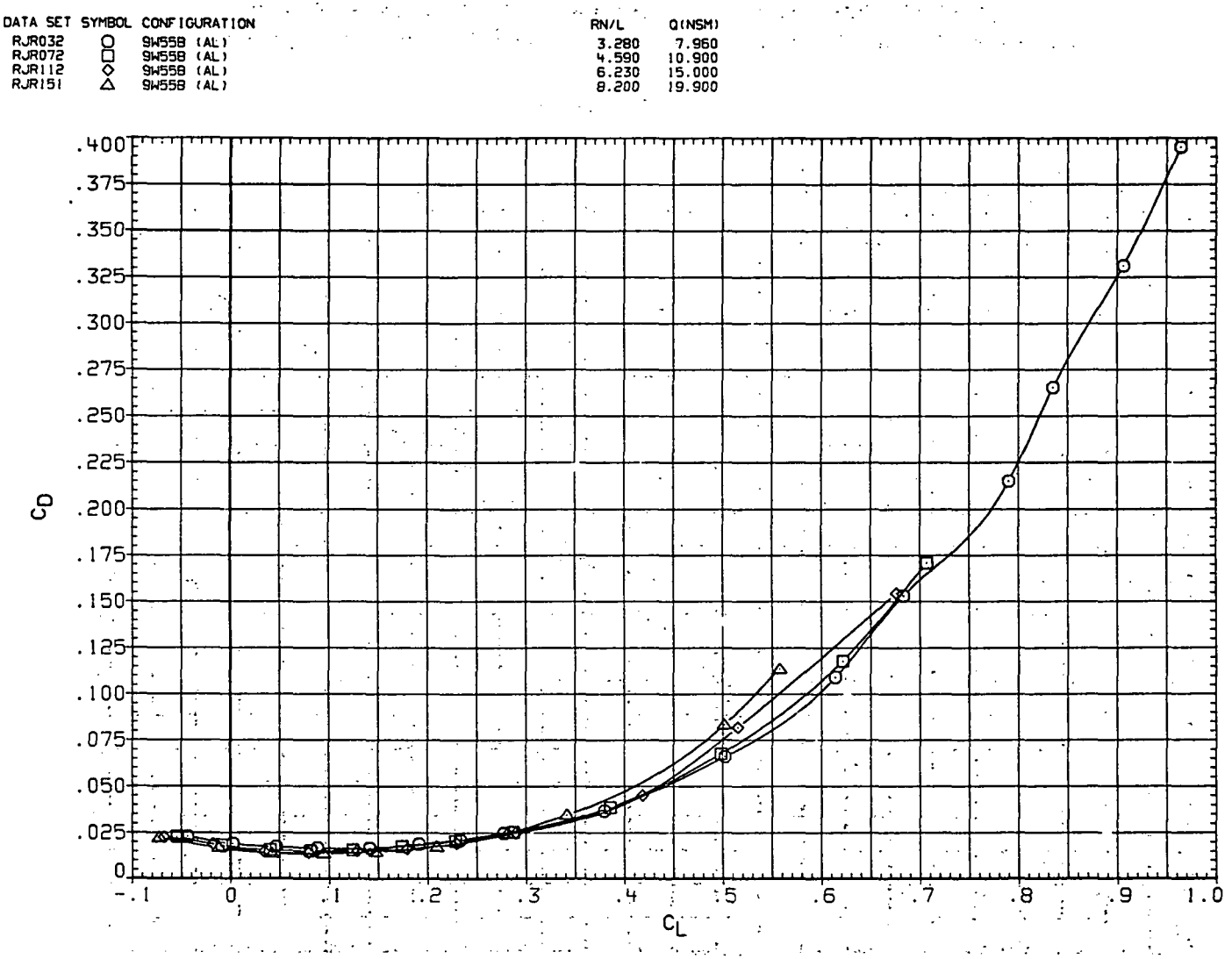

(b) C_D vs C_L.

Figure 30.– Continued.

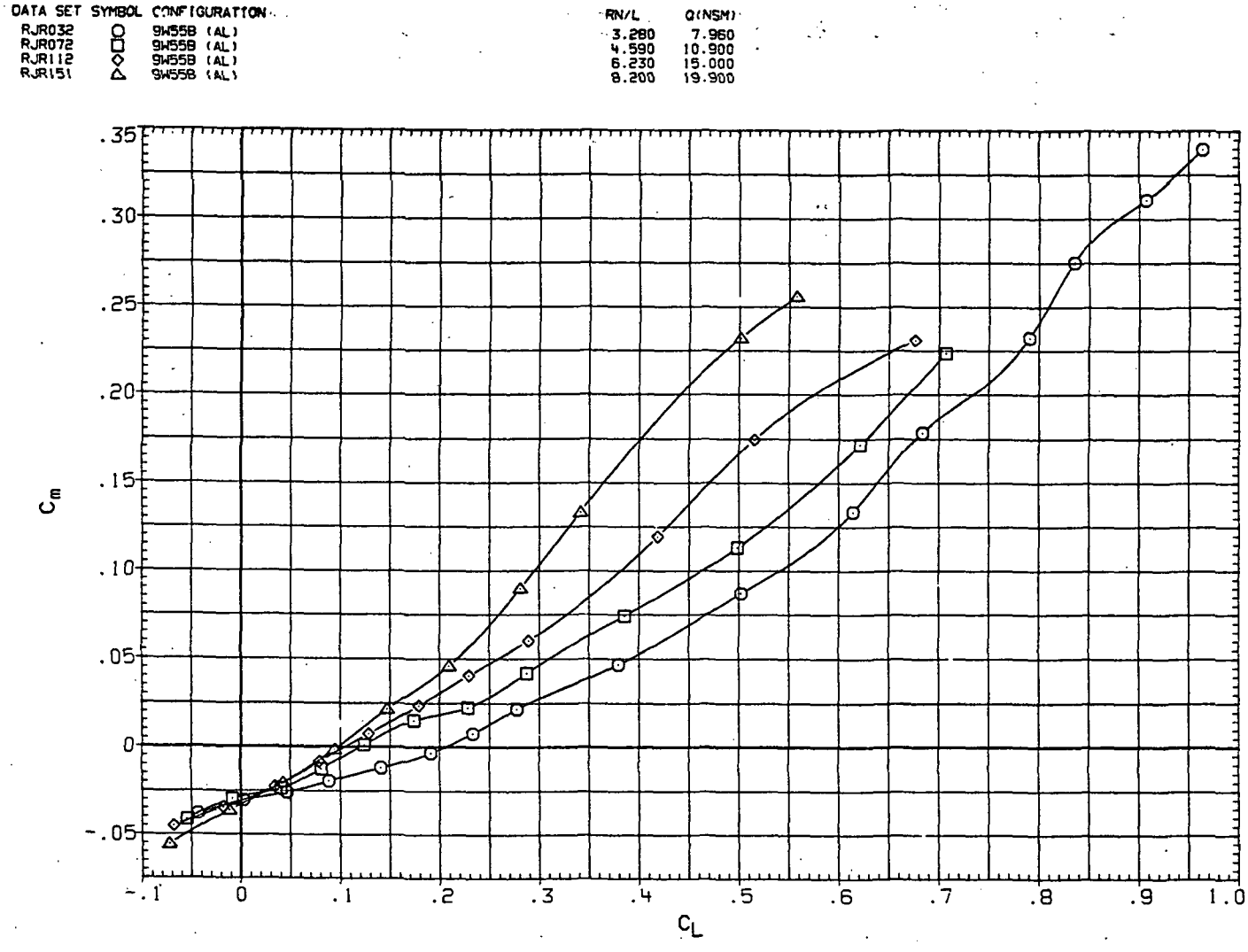

(c) C_m vs C_L.

Figure 30.– Continued.

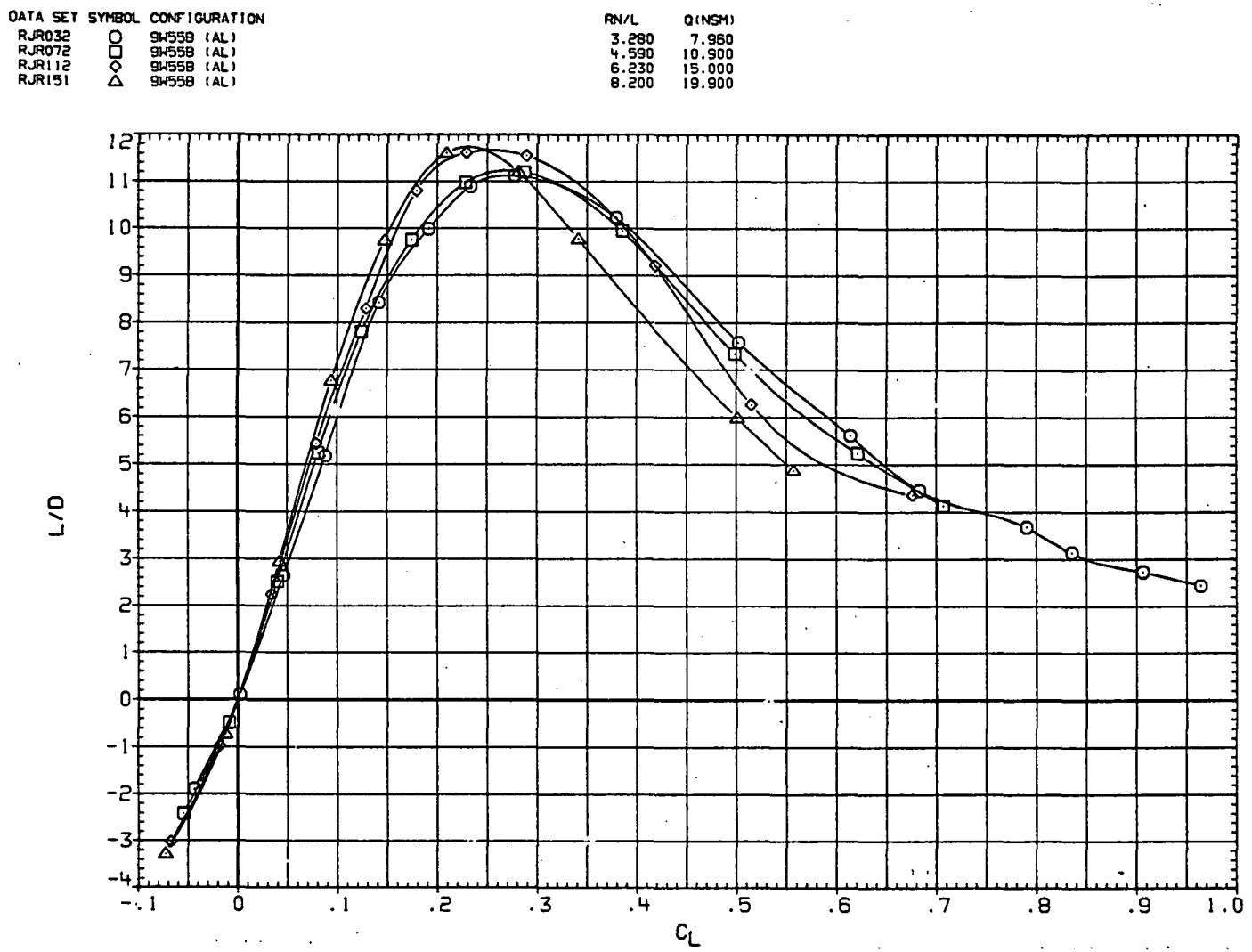

(d) L/D vs C_L.

Figure 30.– Continued.

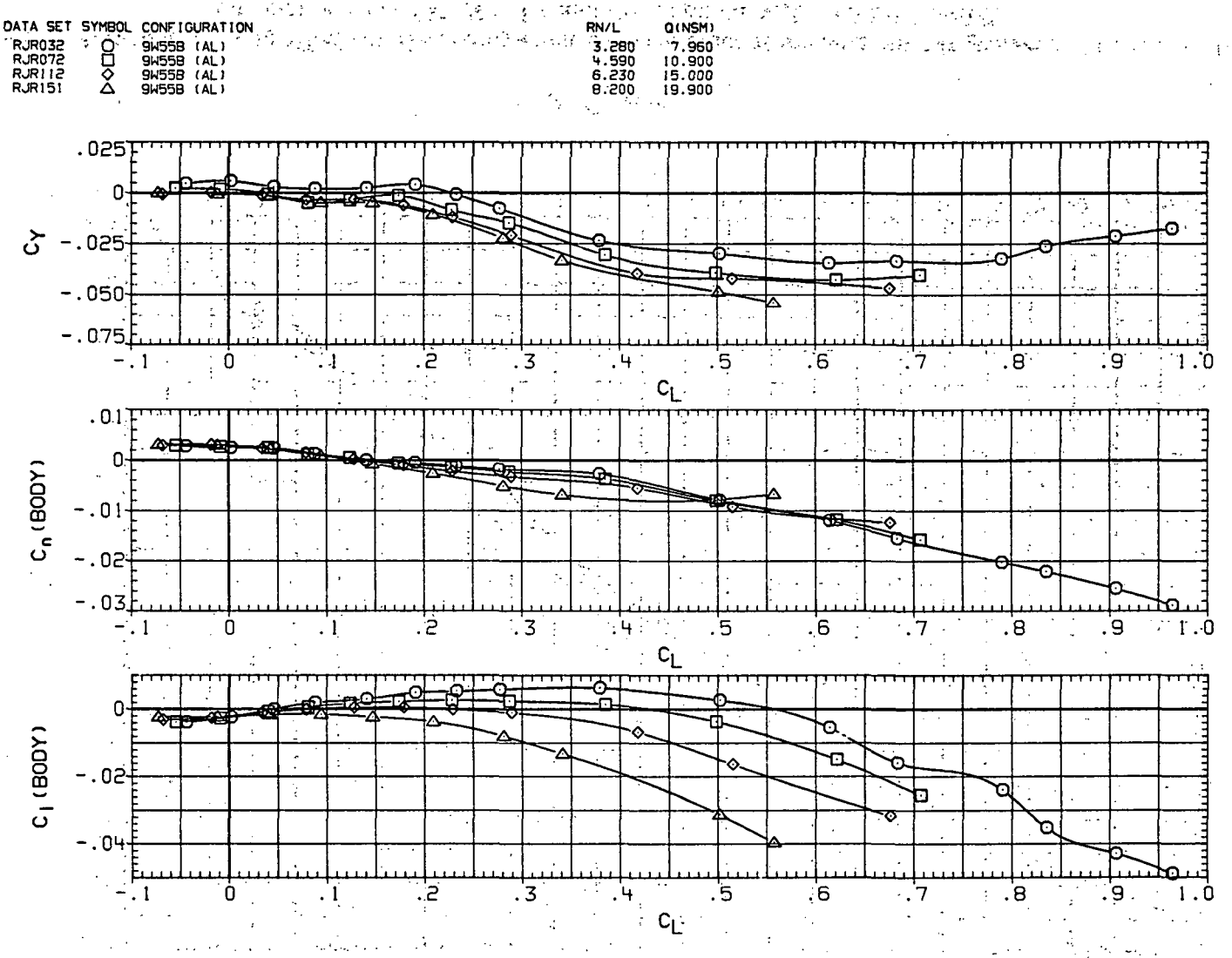

(e) C_Y, C_n and C_ℓ vs C_L.

Figure 30.– Concluded.

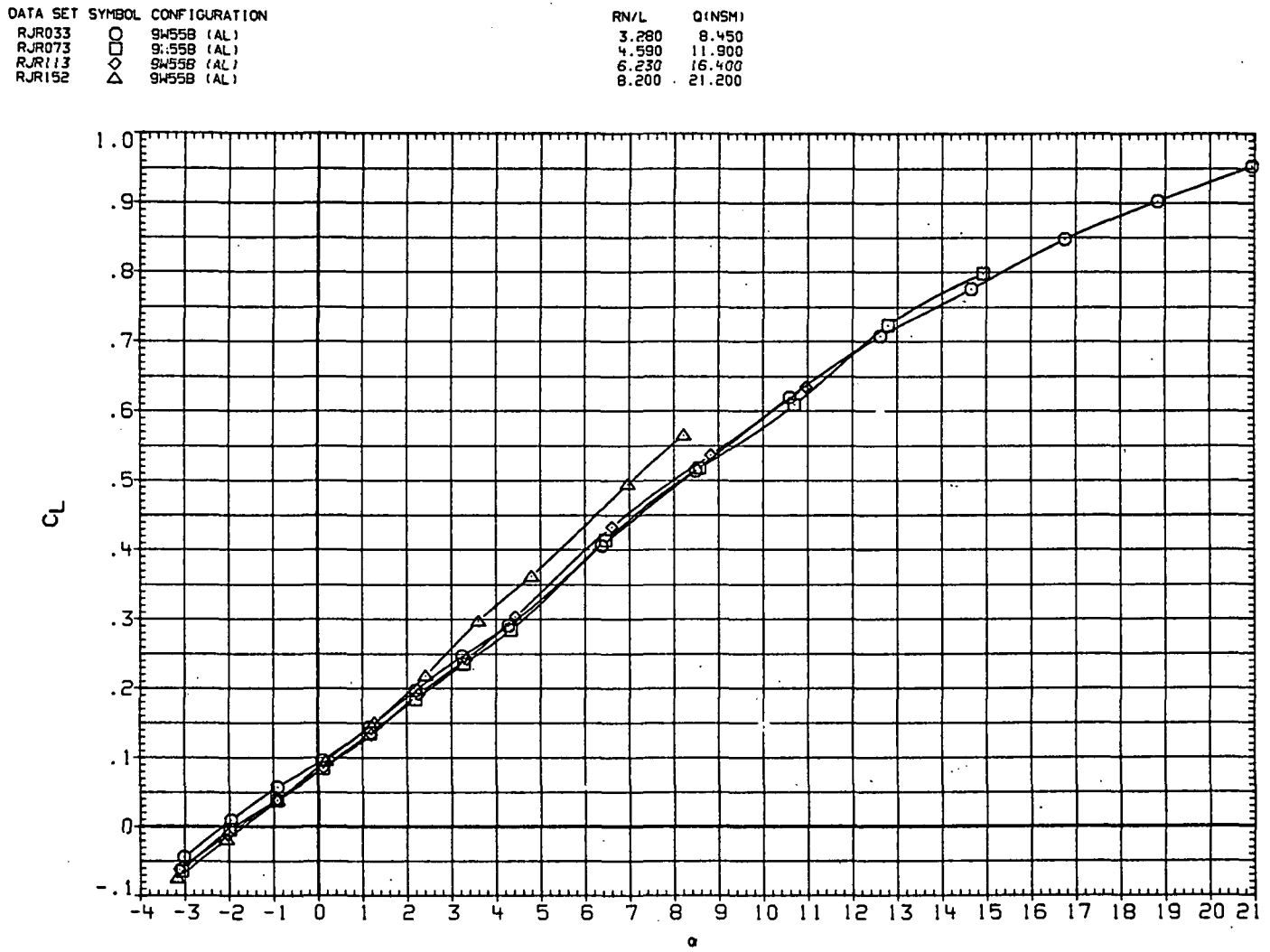

(a) C_L vs α.

Figure 31.– Dynamic-pressure effects on the aerodynamic characteristics of the aluminum trapezoidal oblique wing-body combination ($\Lambda = 55°, M = 1.1$ and the modified NACA 65A204 airfoil).

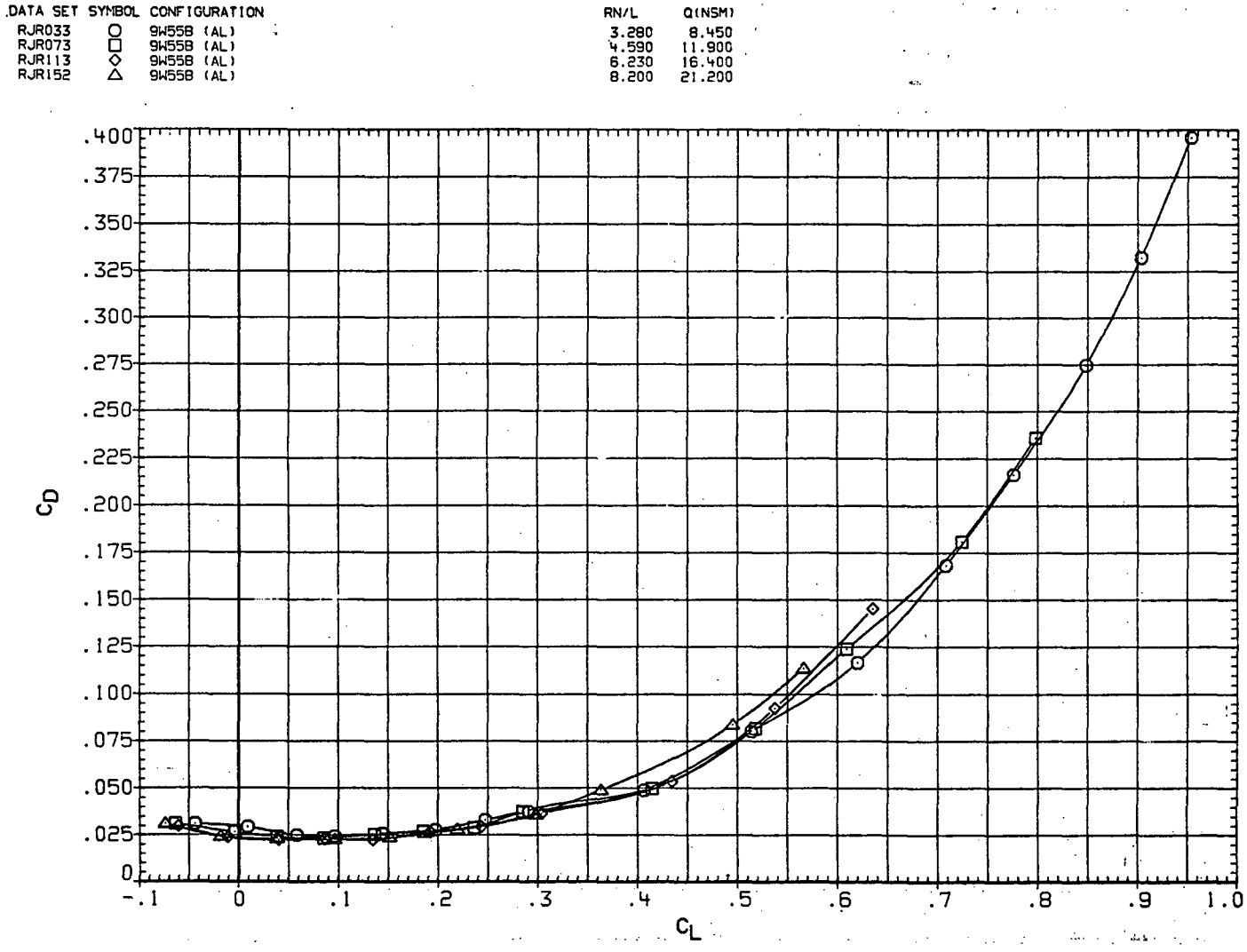

(b) C_D vs C_L.

Figure 31.– Continued.

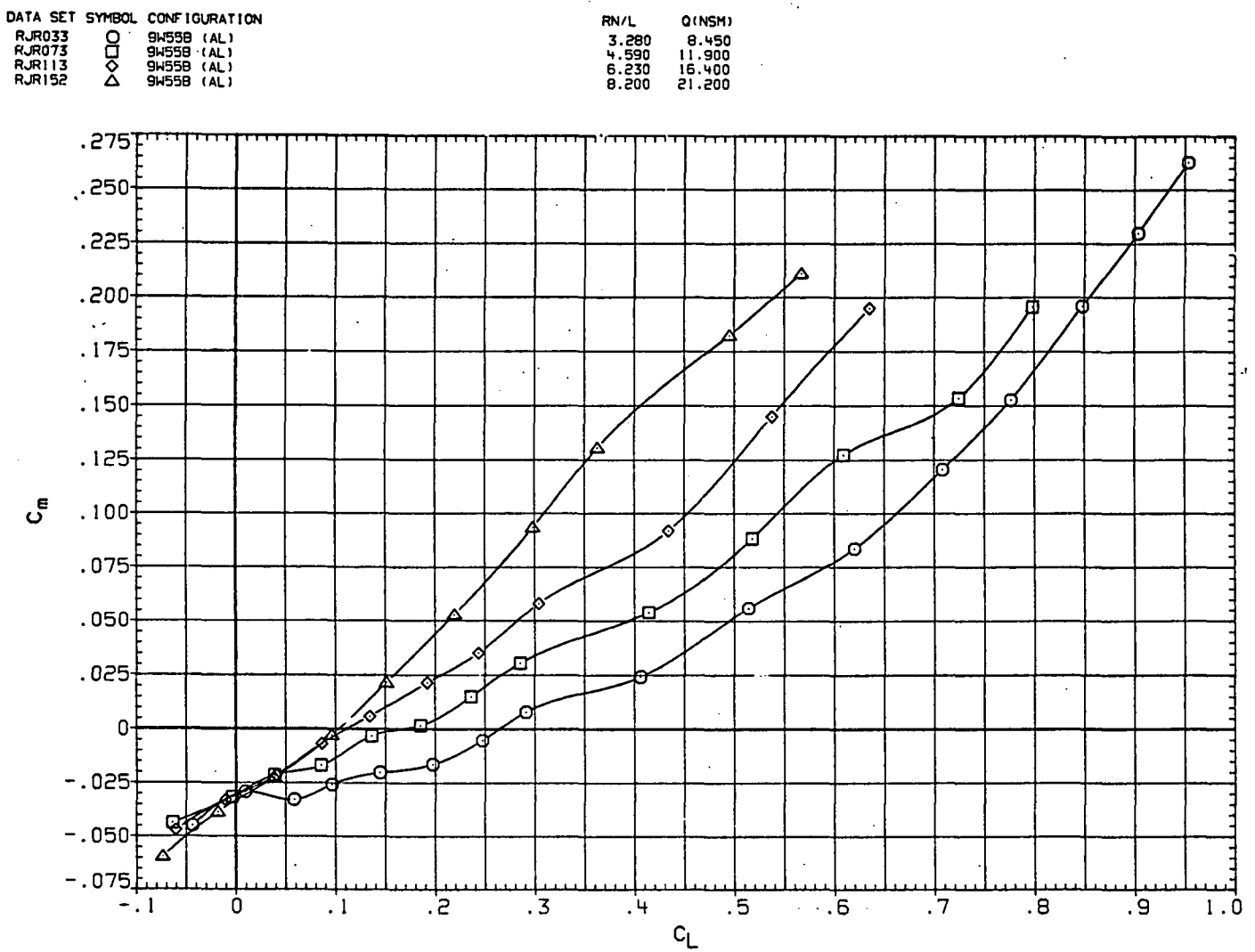

(c) C_m vs C_L.

Figure 31.– Continued.

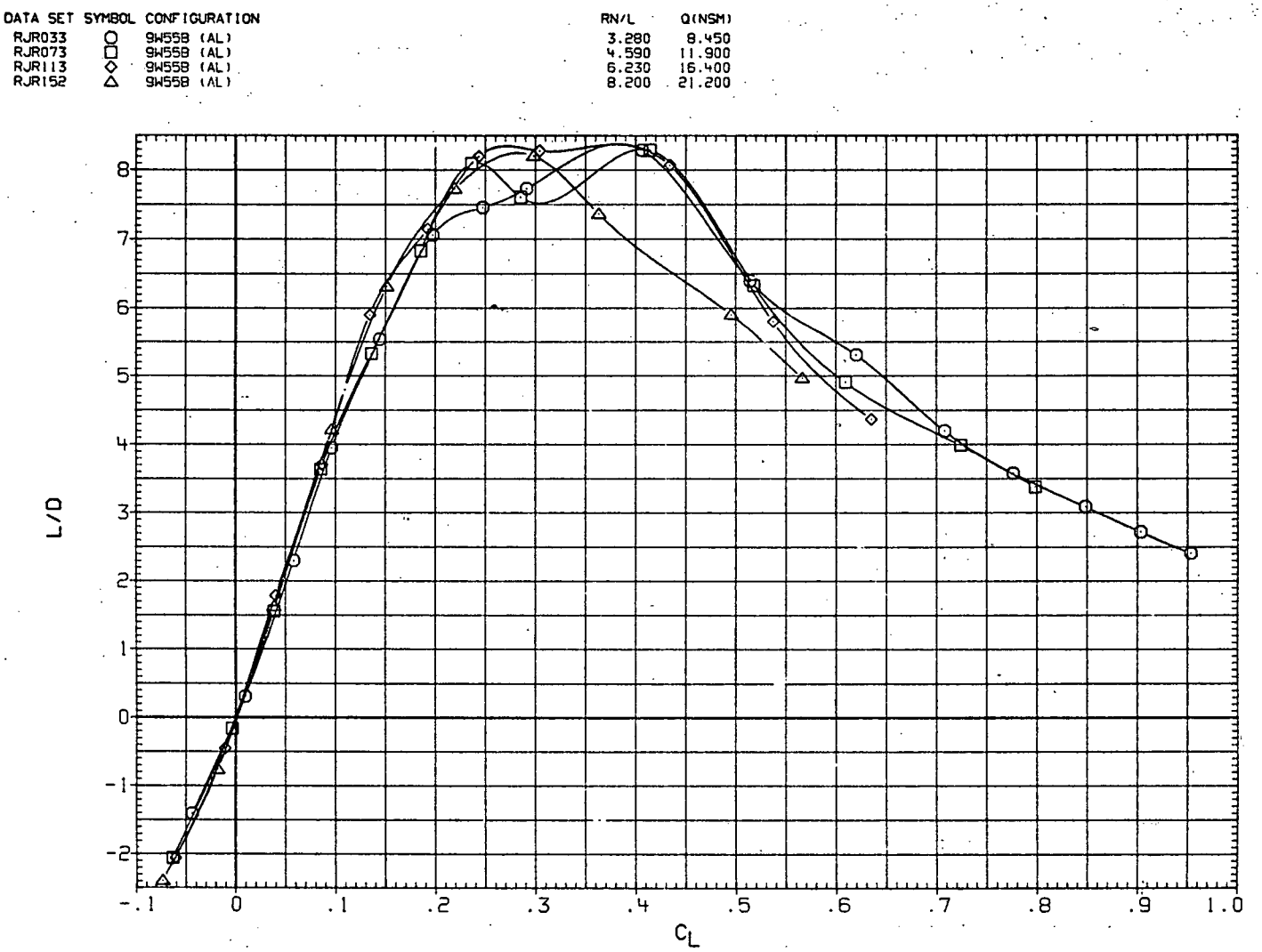

(d) L/D vs C_L.

Figure 31.– Continued.

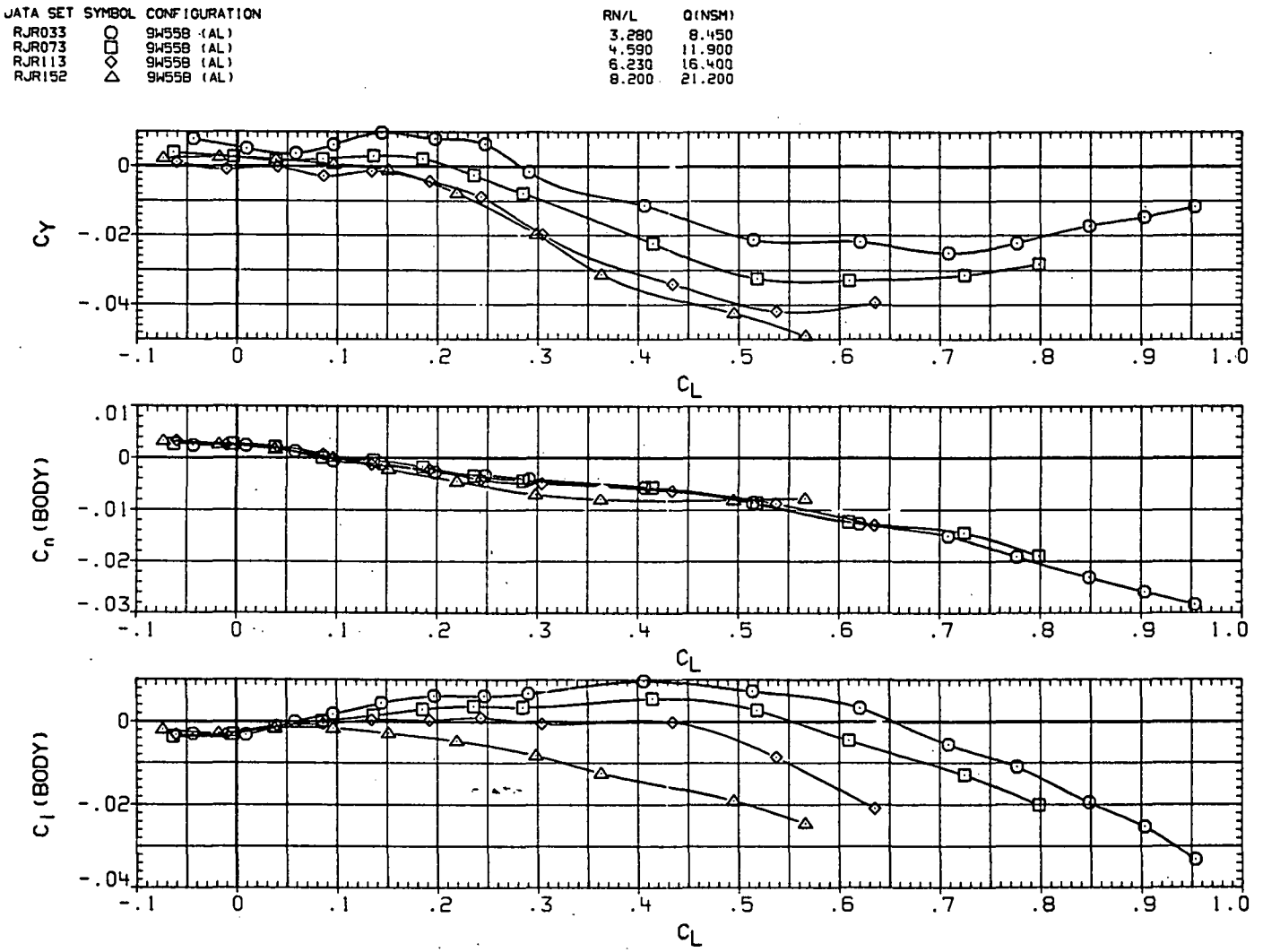

(e) C_Y, C_n and C_ℓ vs C_L.

Figure 31.– Concluded.

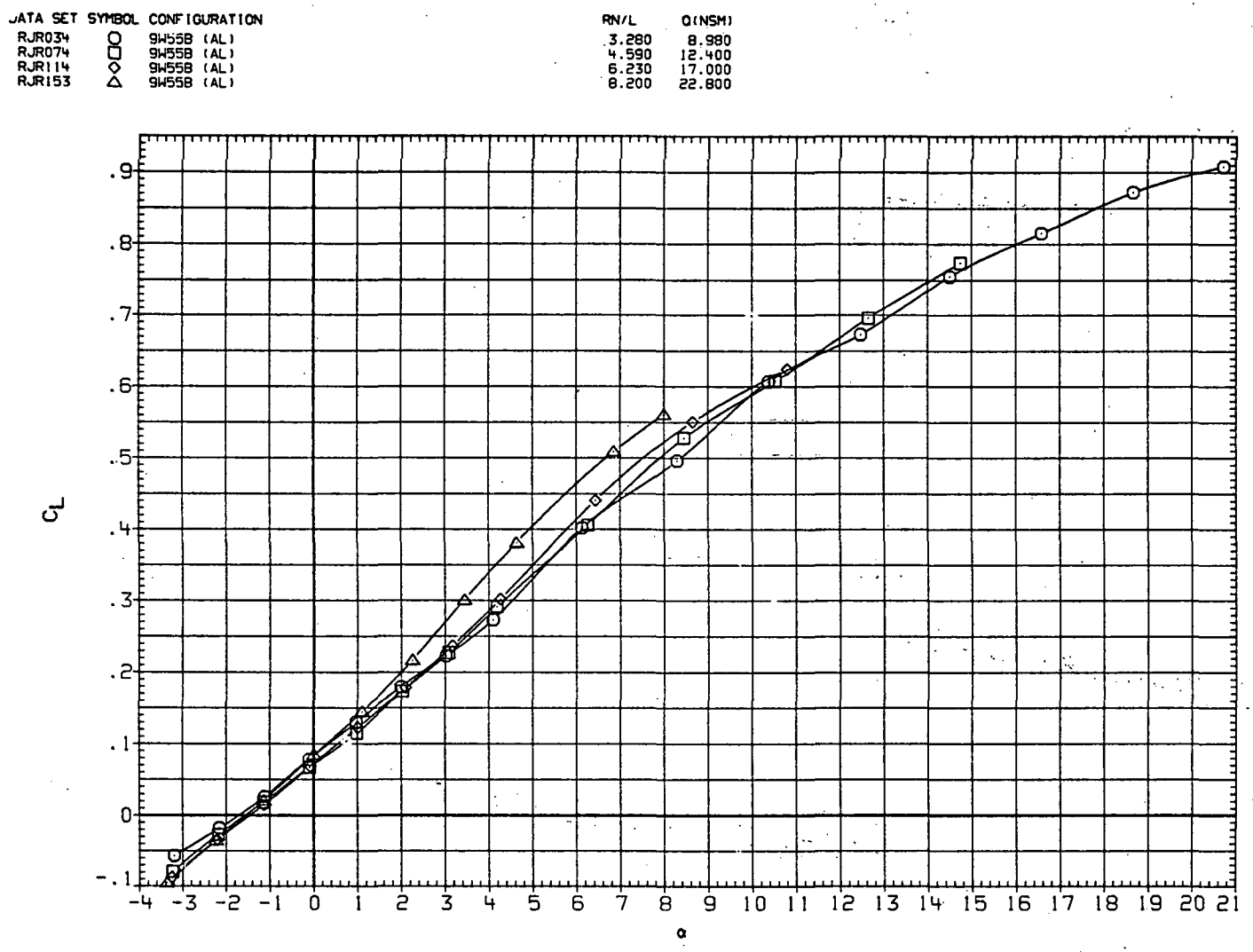

(a) C_L vs α.

Figure 32.– Dynamic-pressure effects on the aerodynamic characteristics of the aluminum trapezoidal oblique wing-body combination ($\Lambda = 55°, M = 1.2$ and the modified NACA 65A204 airfoil).

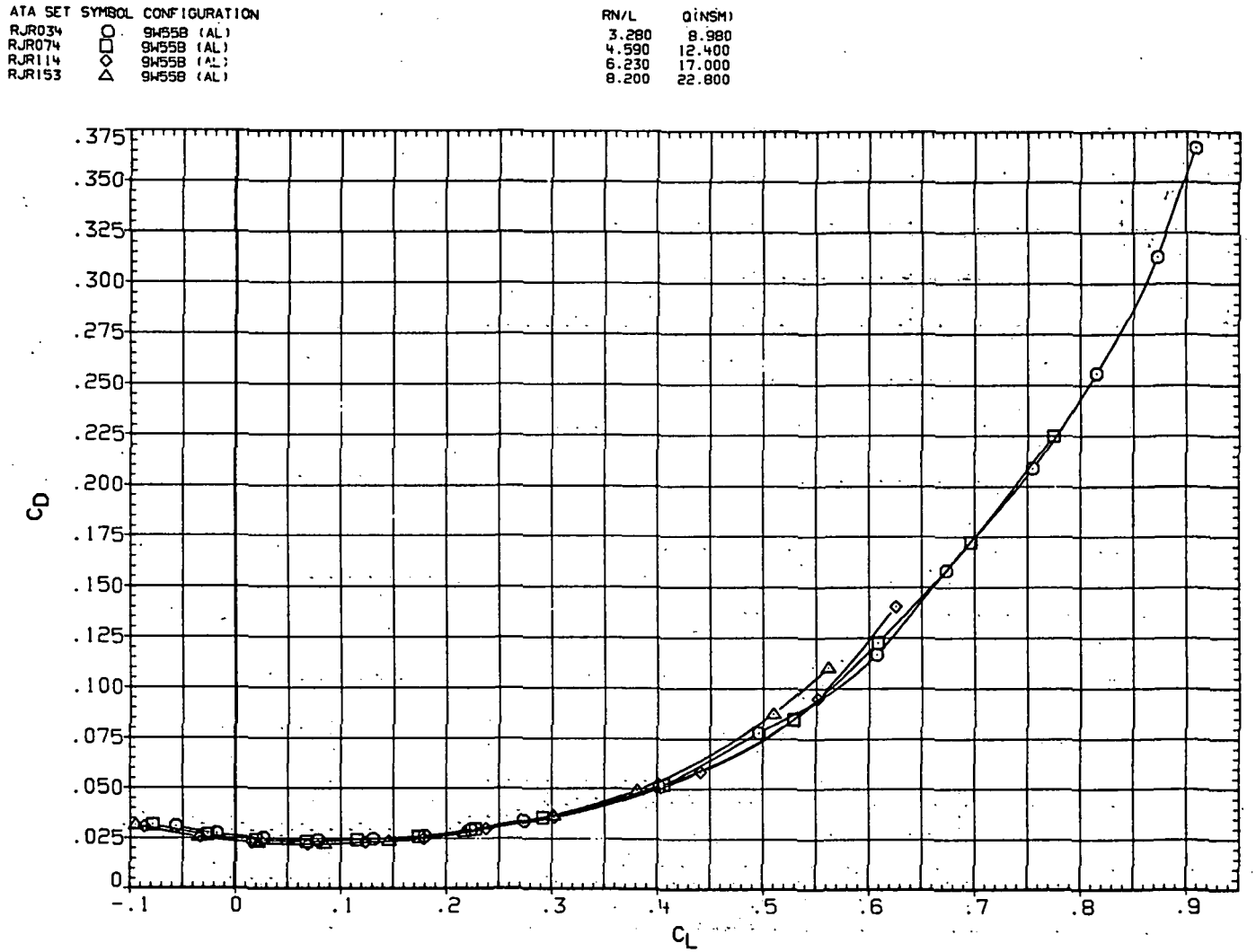

(b) C_D vs C_L.

Figure 32.– Continued.

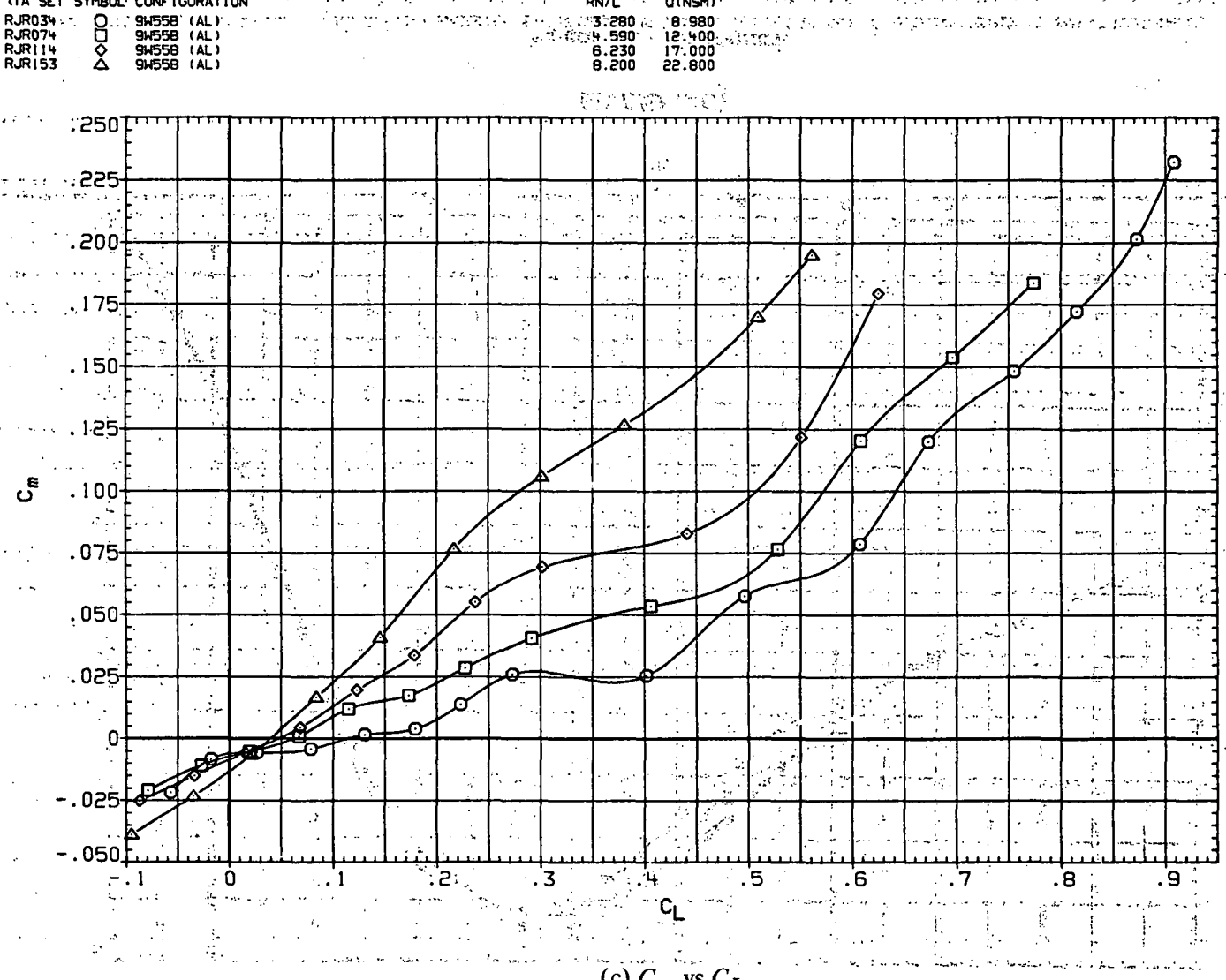

(c) C_m vs C_L.

Figure 32. – Continued.

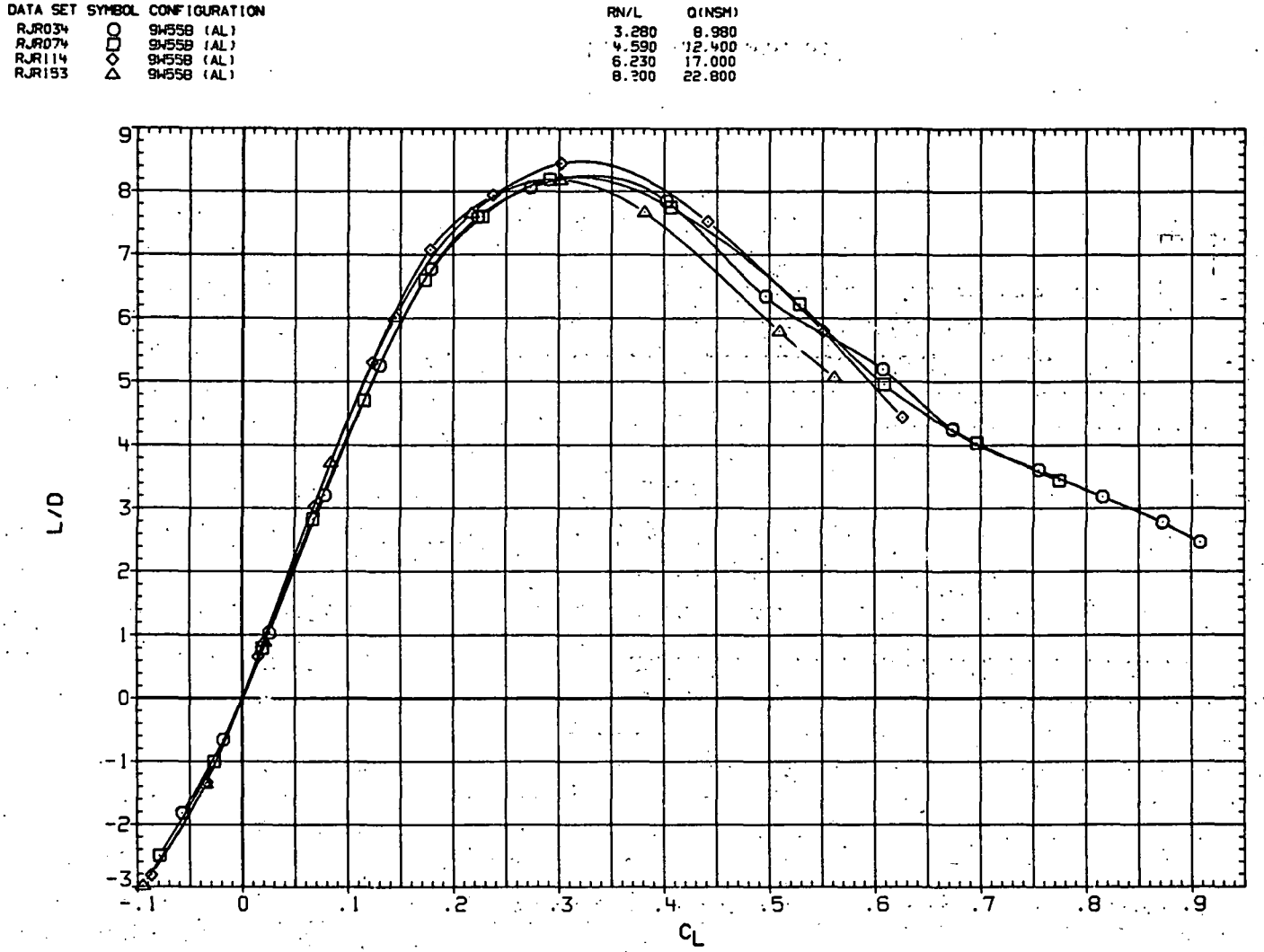

(d) L/D vs C_L.

Figure 32.– Continued.

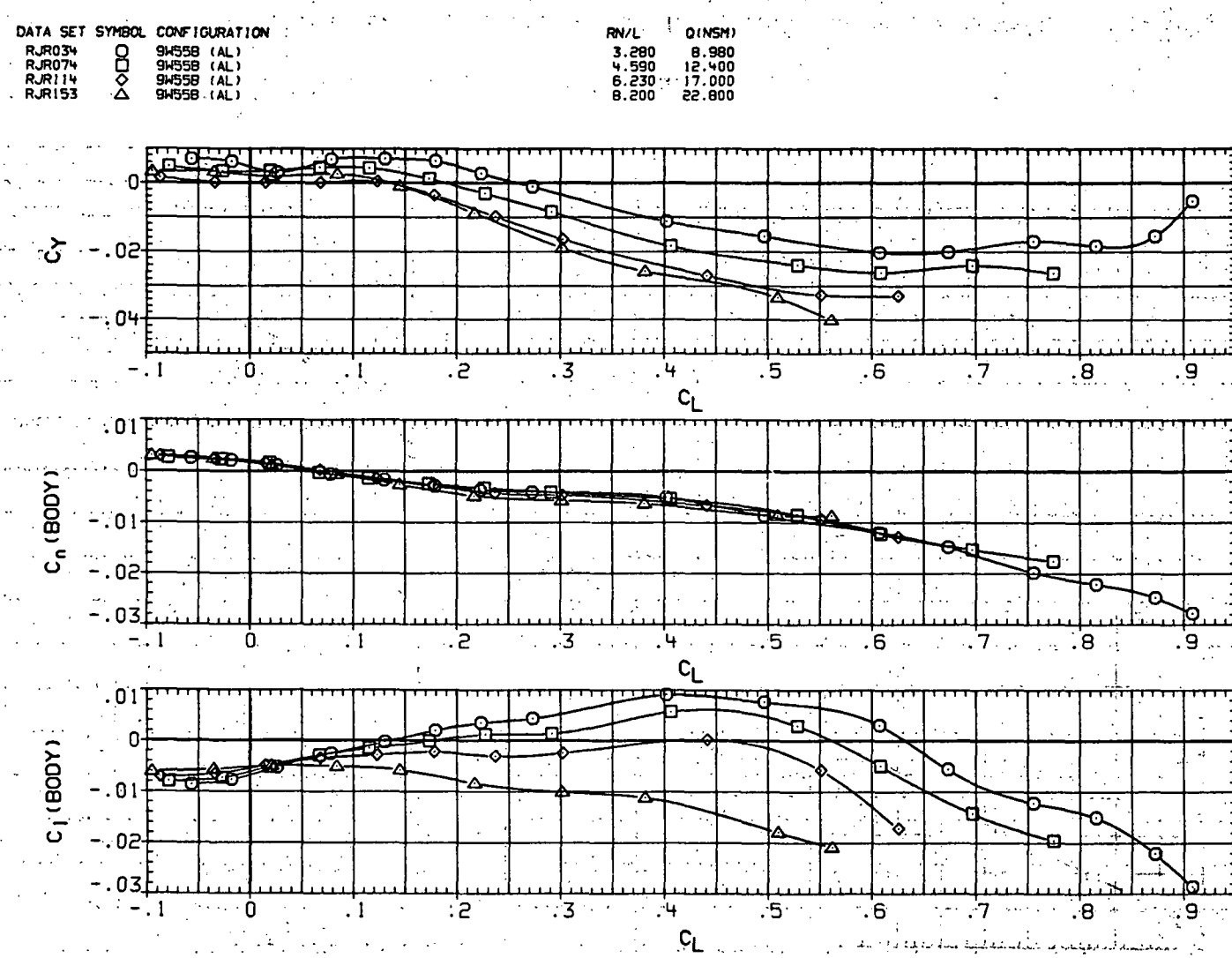

(e) C_Y, C_n and C_ℓ vs C_L.

Figure 32.– Concluded.

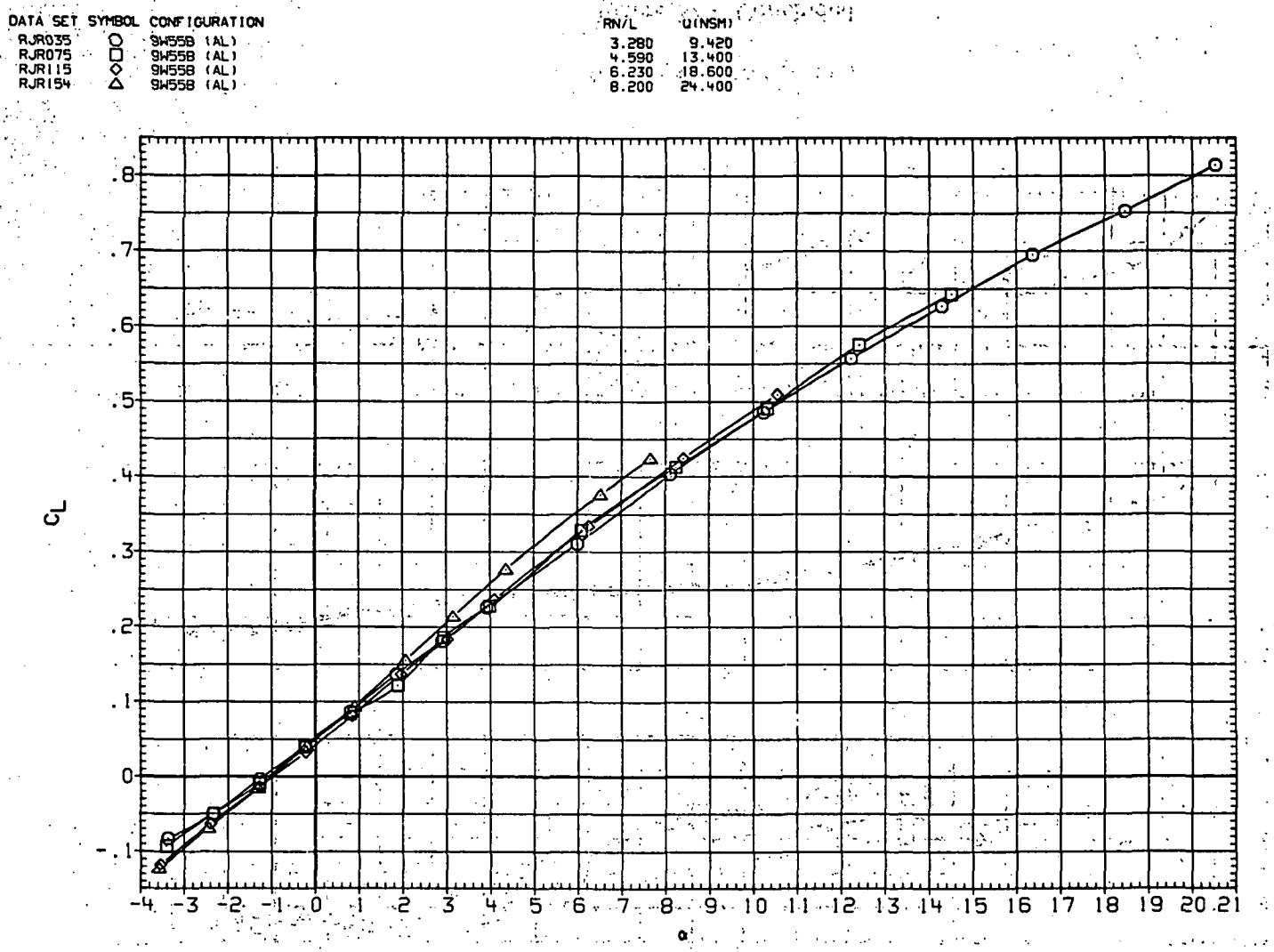

(a) C_L vs.α.

Figure 33.– Dynamic-pressure effects on the aerodynamic characteristics of the aluminum trapezoidal oblique wing-body combination ($\Lambda = 55°, M = 1.6$ and the modified NACA 65A204 airfoil).

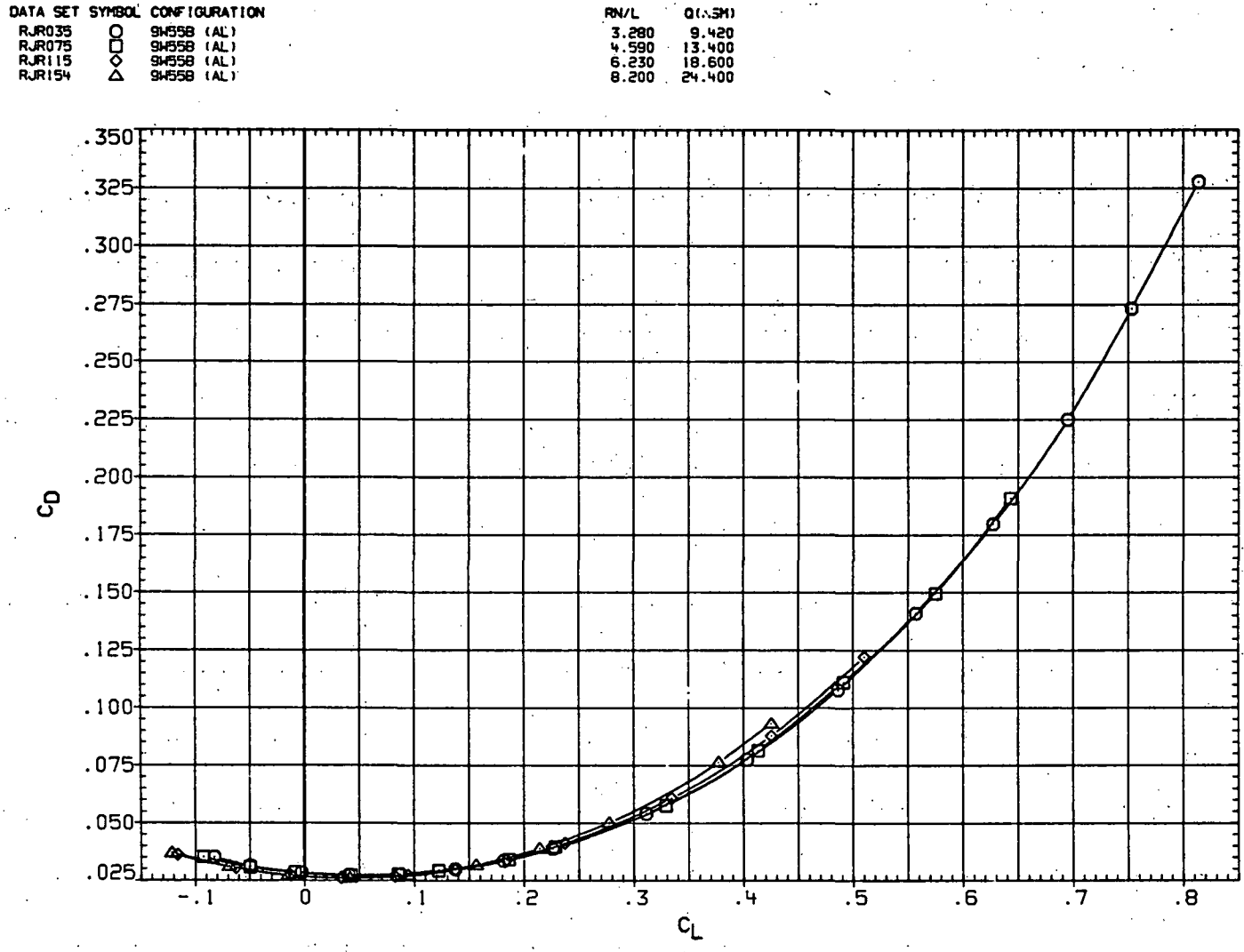

(b) C_D vs C_L.

Figure 33.– Continued.

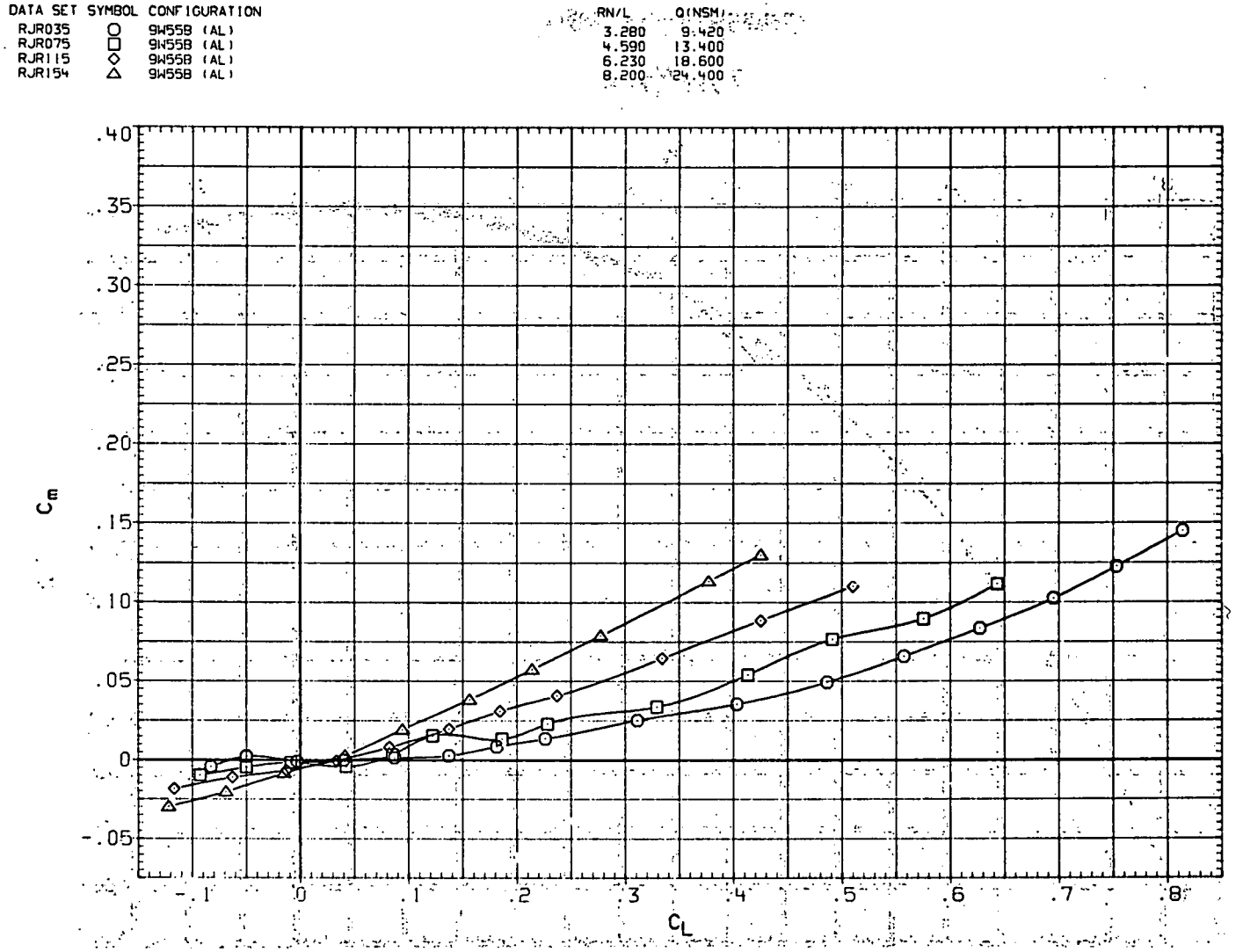

(c) C_m vs C_L.

Figure 33.—Continued.

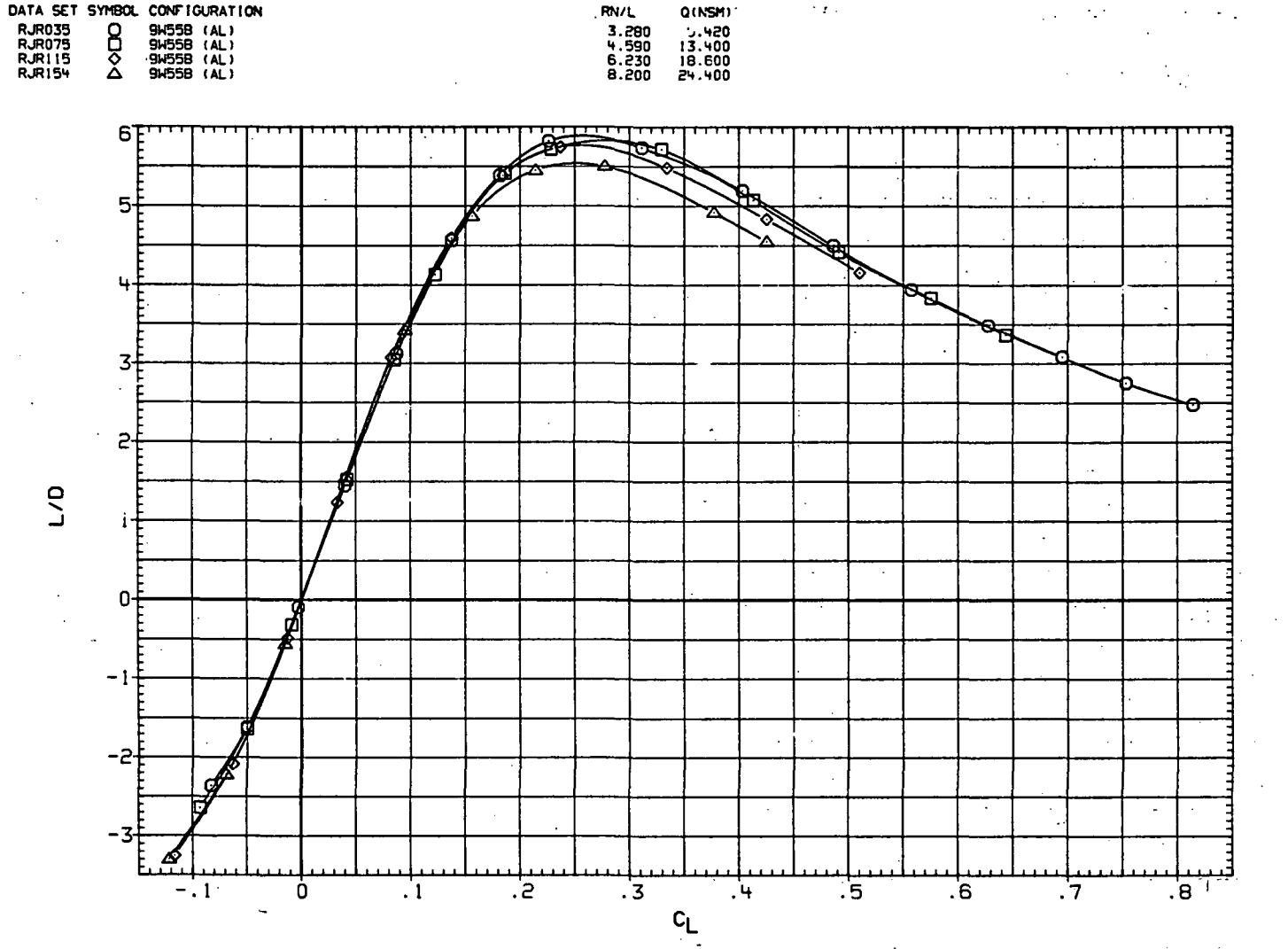

(d) L/D vs C_L.

Figure 33.– Continued.

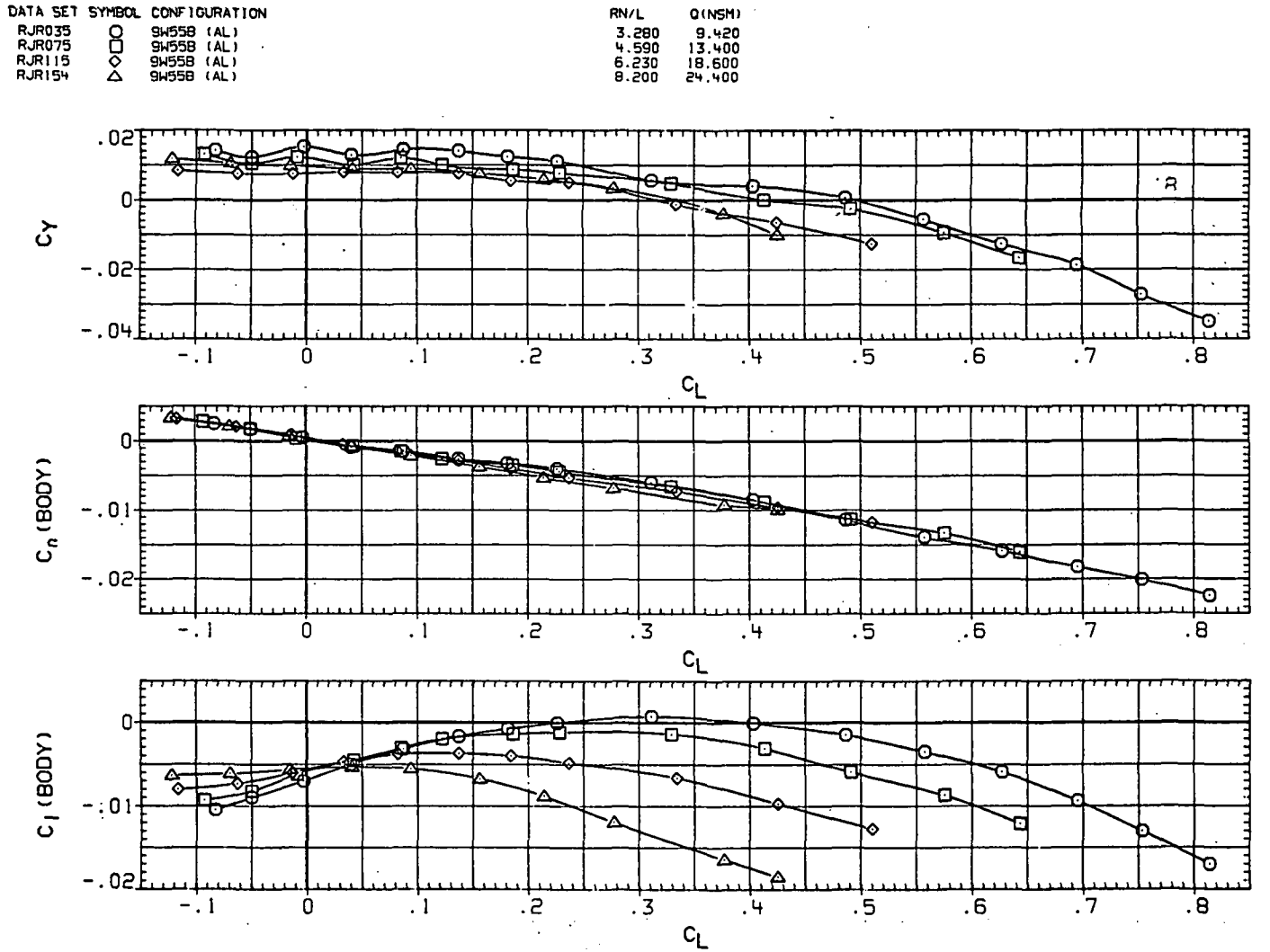

(e) C_Y, C_n and C_ℓ vs C_L.

Figure 33.– Concluded.

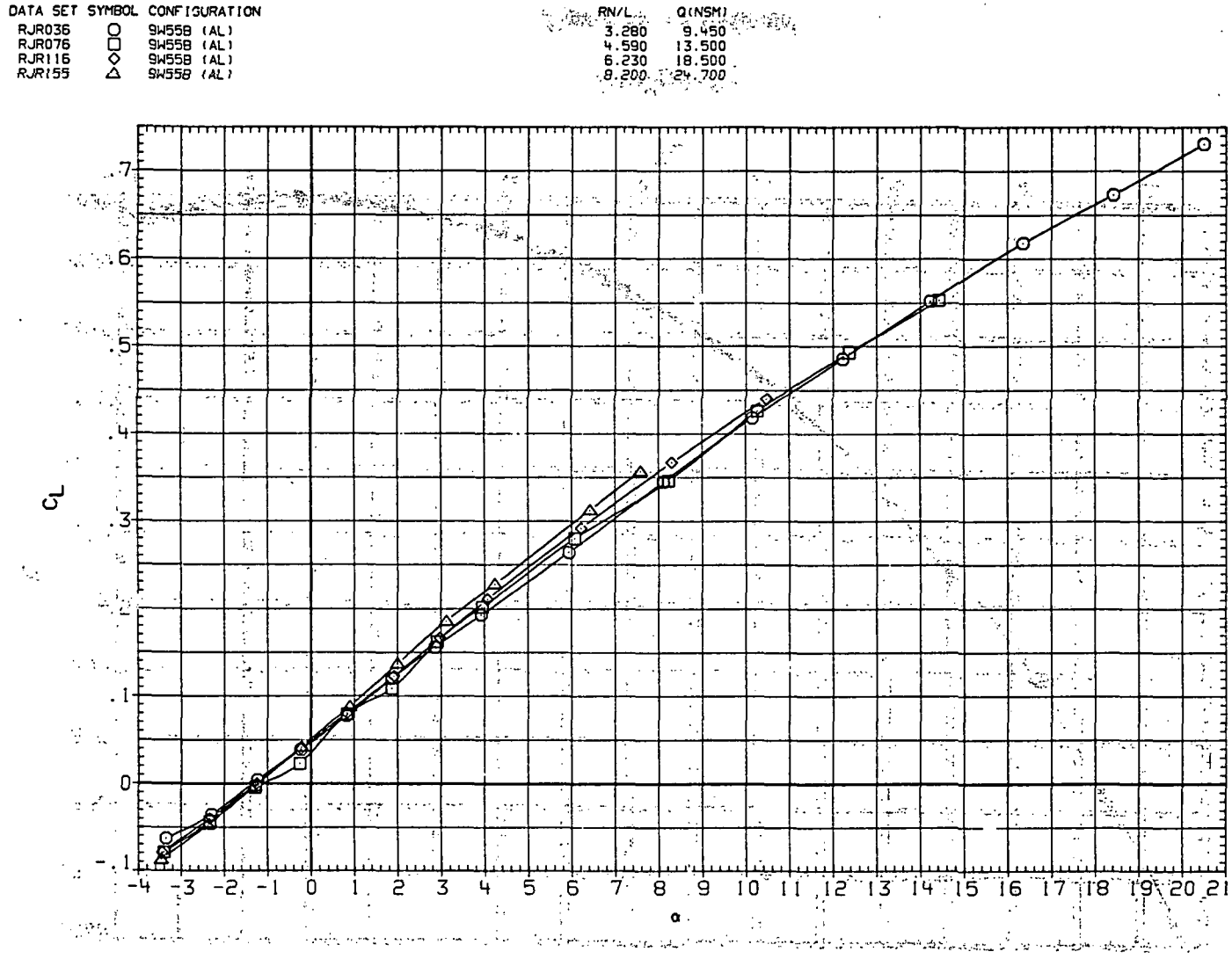

(a) C_L vs α.

Figure 34.– Dynamic-pressure effects on the aerodynamic characteristics of the aluminum trapezoidal oblique wing-body combination ($\Lambda = 55°$, $M = 2.0$ and the modified NACA 65A204 airfoil).

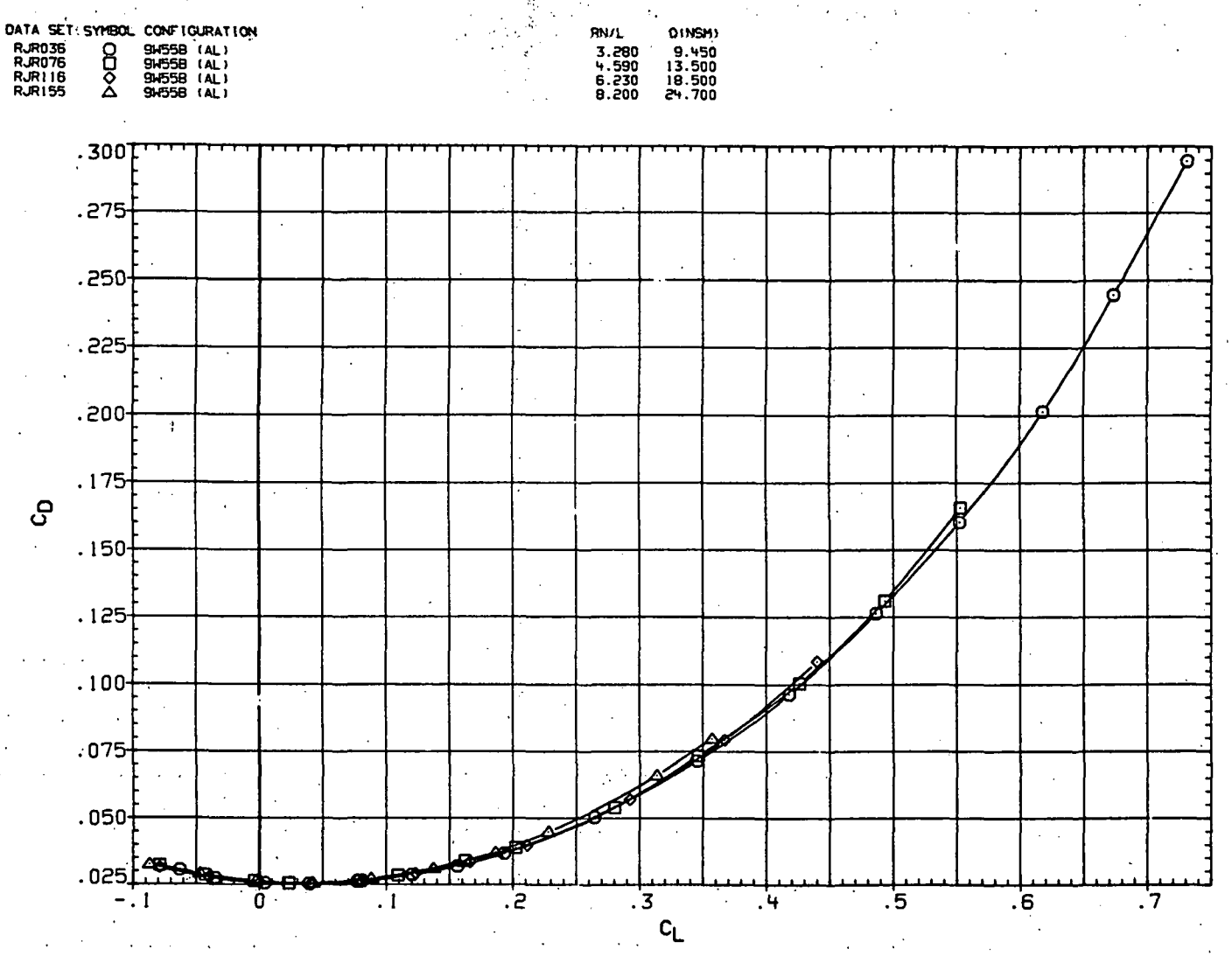

(b) C_D vs C_L.

Figure 34.– Continued.

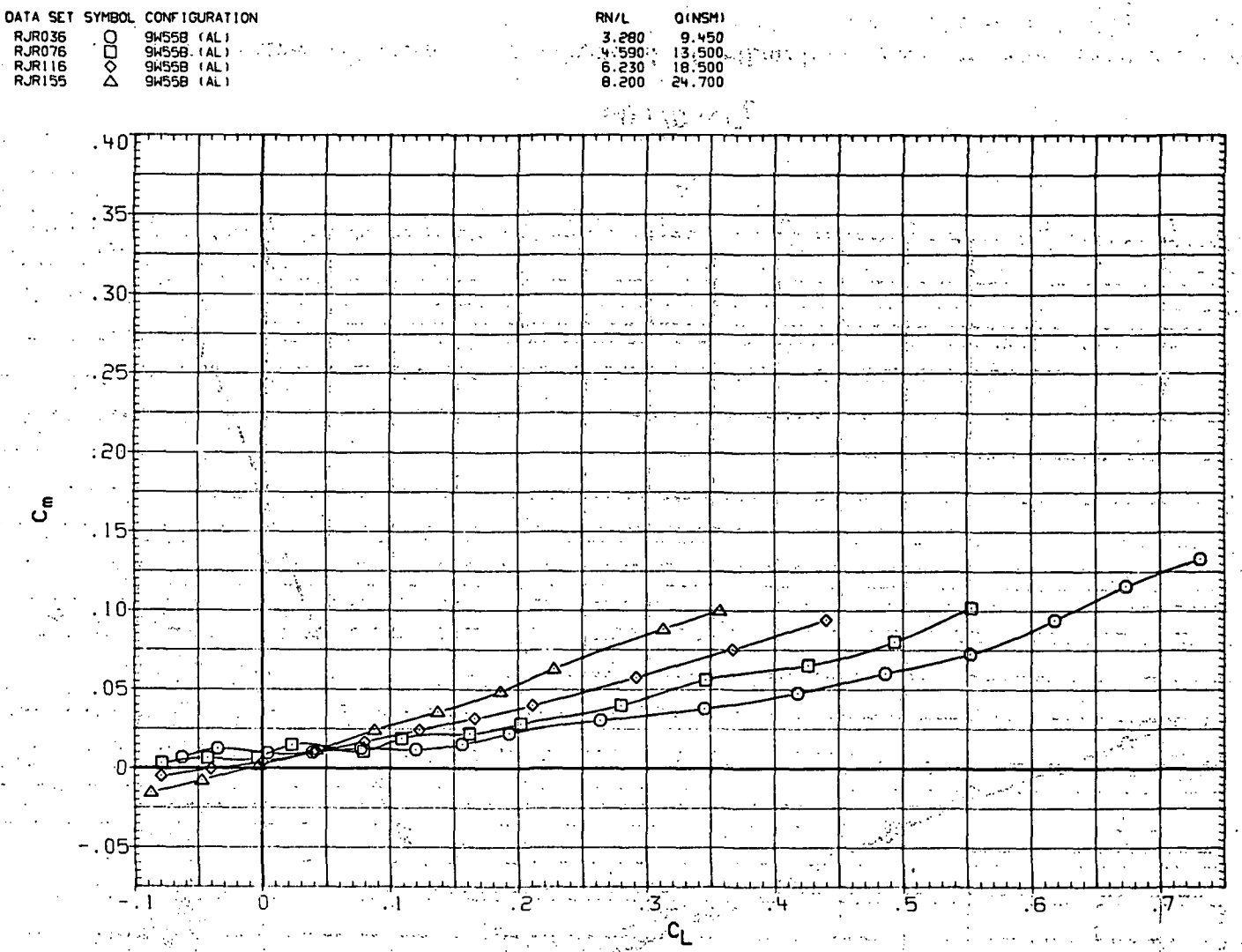

(c) C_m vs C_L.

Figure 34.– Continued.

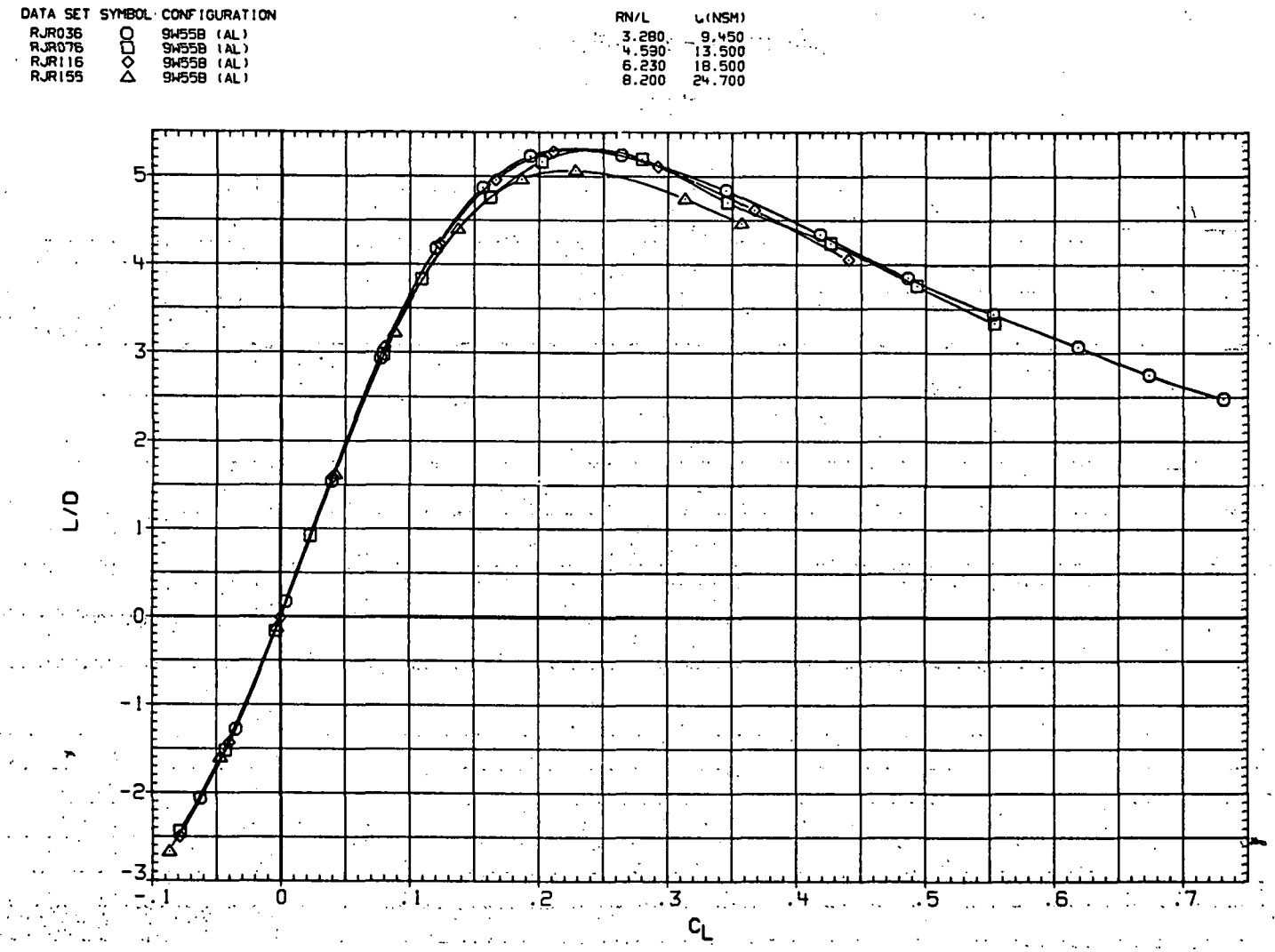

(d) L/D vs C_L.

Figure 34.– Continued.

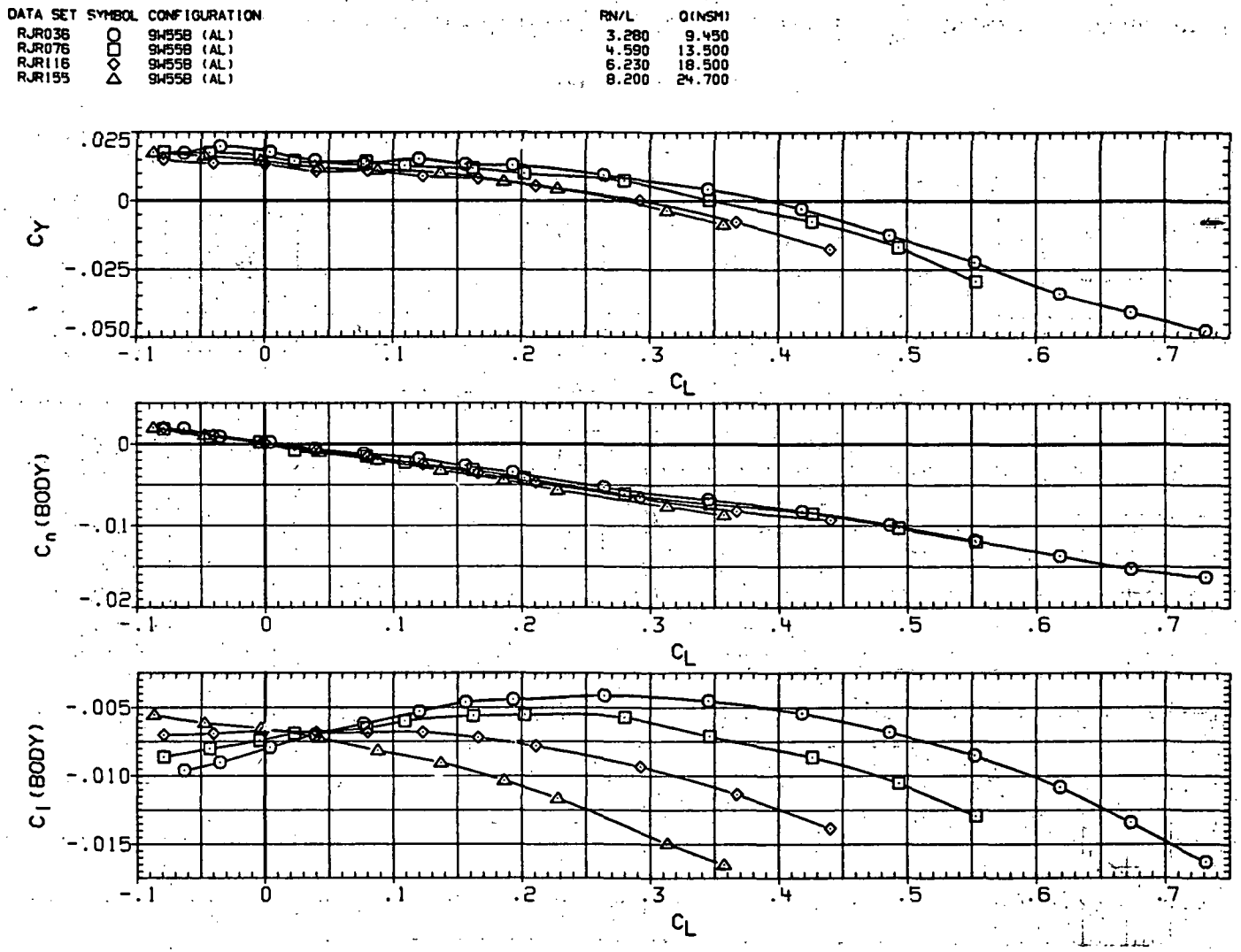

(e) C_Y, C_n and C_ℓ vs C_L.

Figure 34.– Concluded.

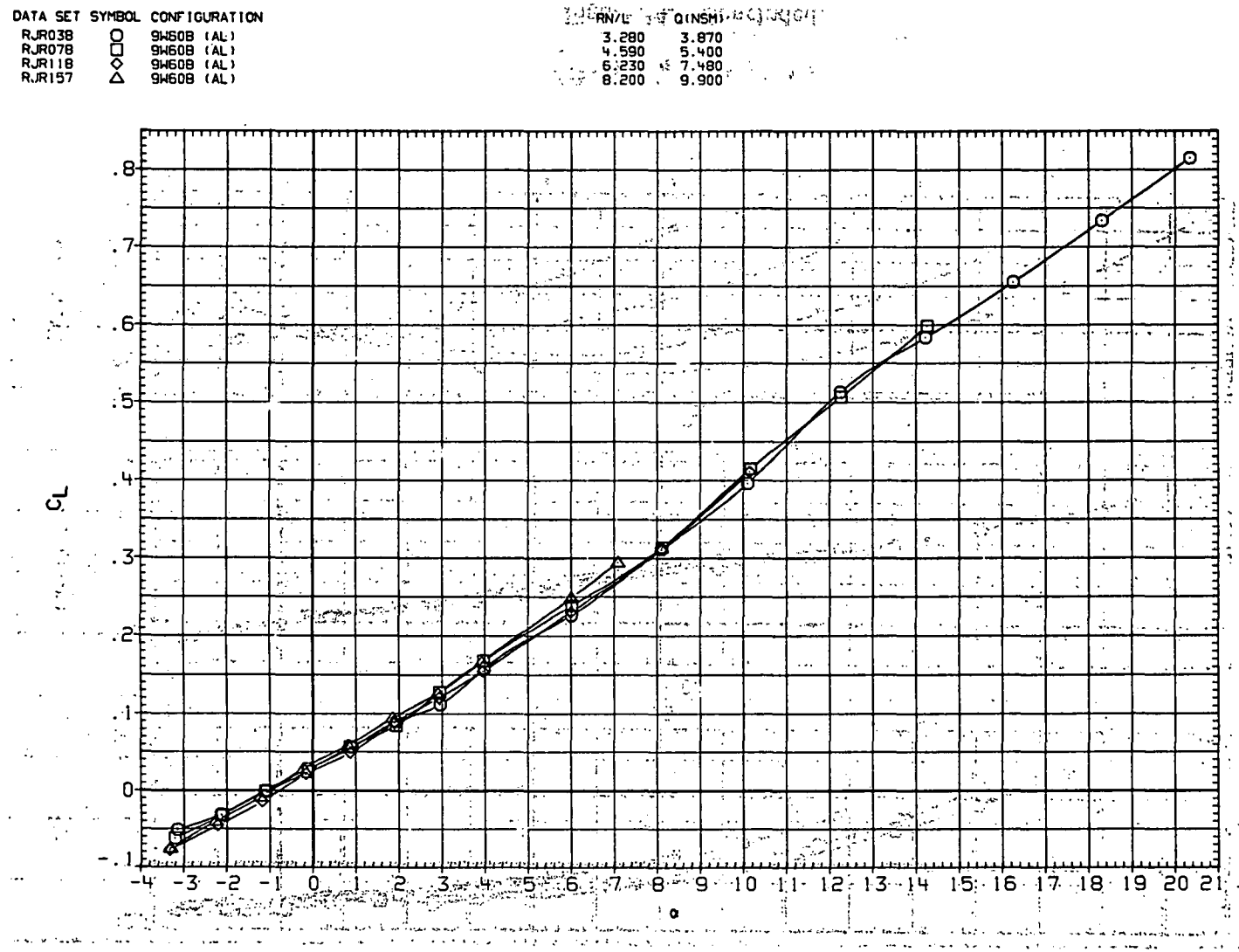

(a) C_L vs. α.

Figure 35. – Dynamic-pressure effects on the aerodynamic characteristics of the aluminum trapezoidal oblique wing-body combination ($\Lambda = 60°$, $M = 0.4$ and the modified NACA 65A204 airfoil).

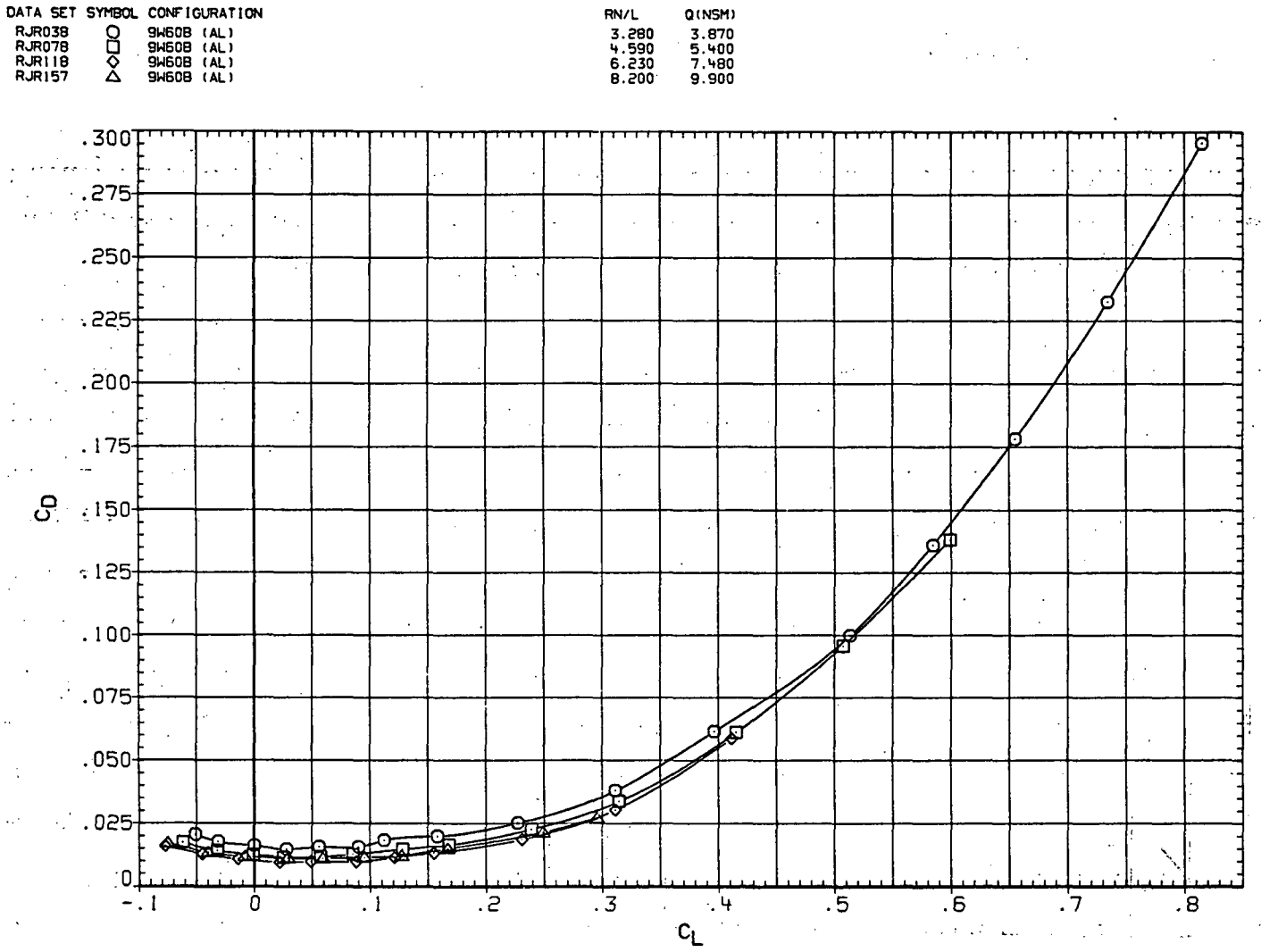

(b) C_D vs C_L.

Figure 35.– Continued.

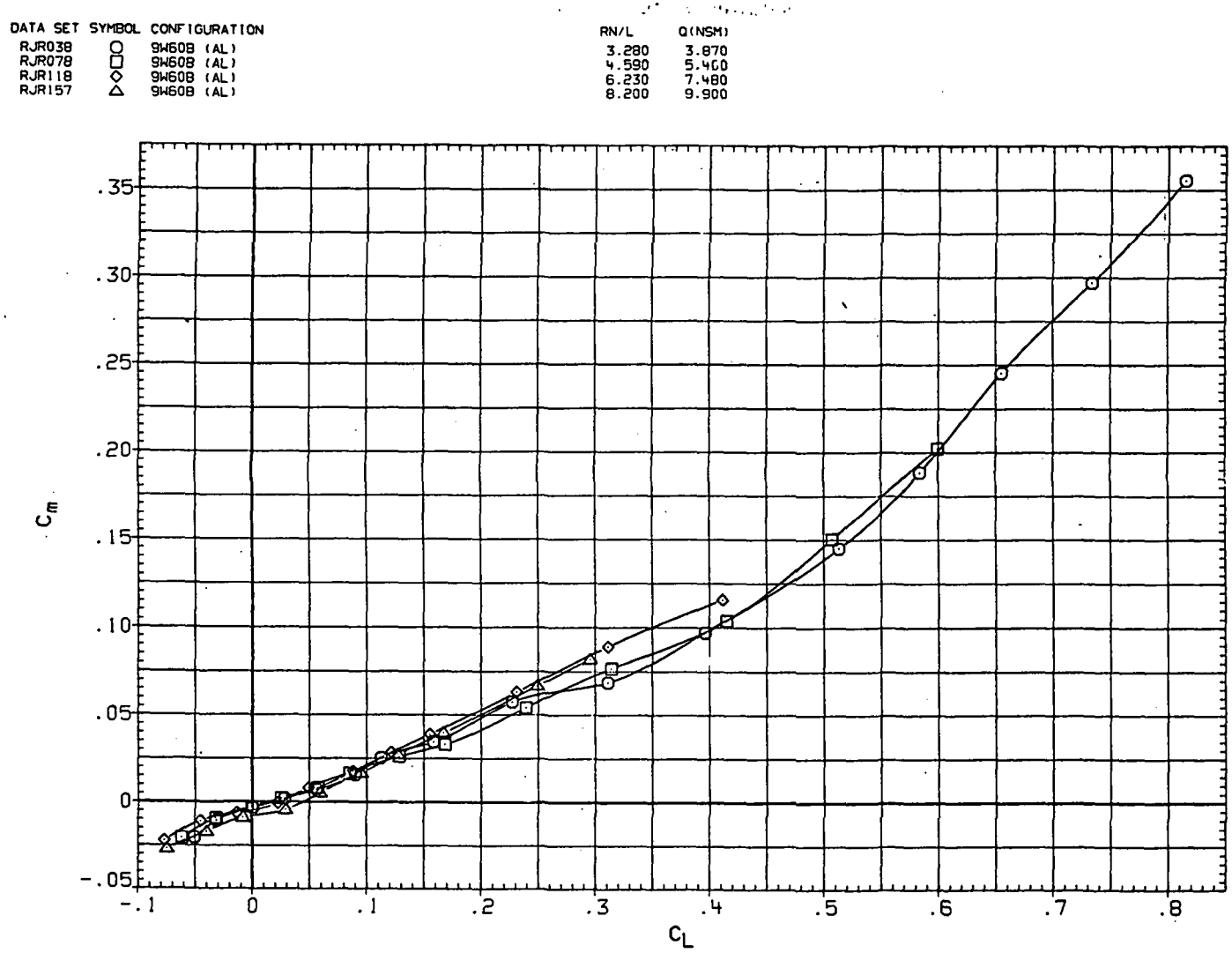

(c) C_m vs C_L.

Figure 35.– Continued.

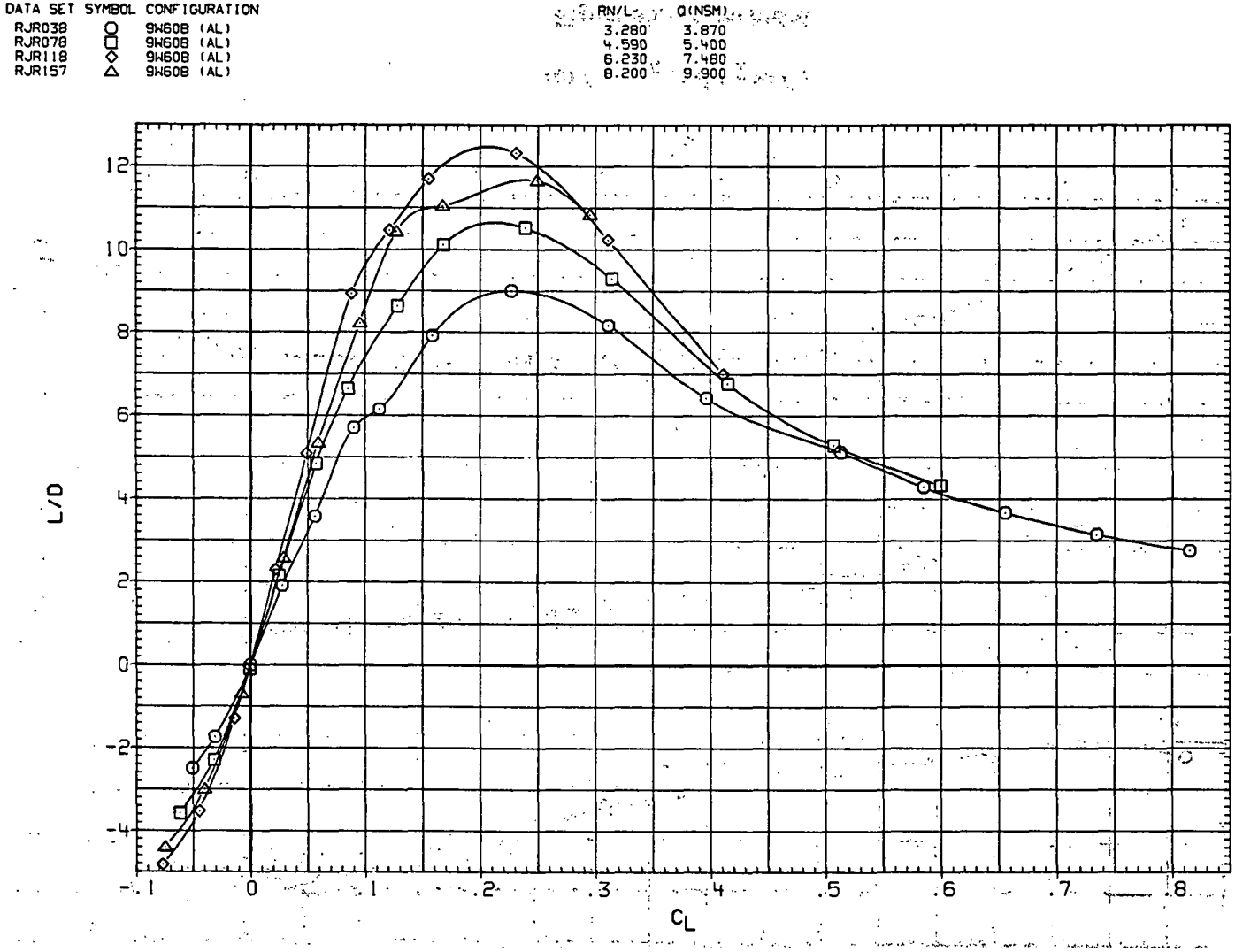

(d) L/D vs C_L.

Figure 35.—Continued.

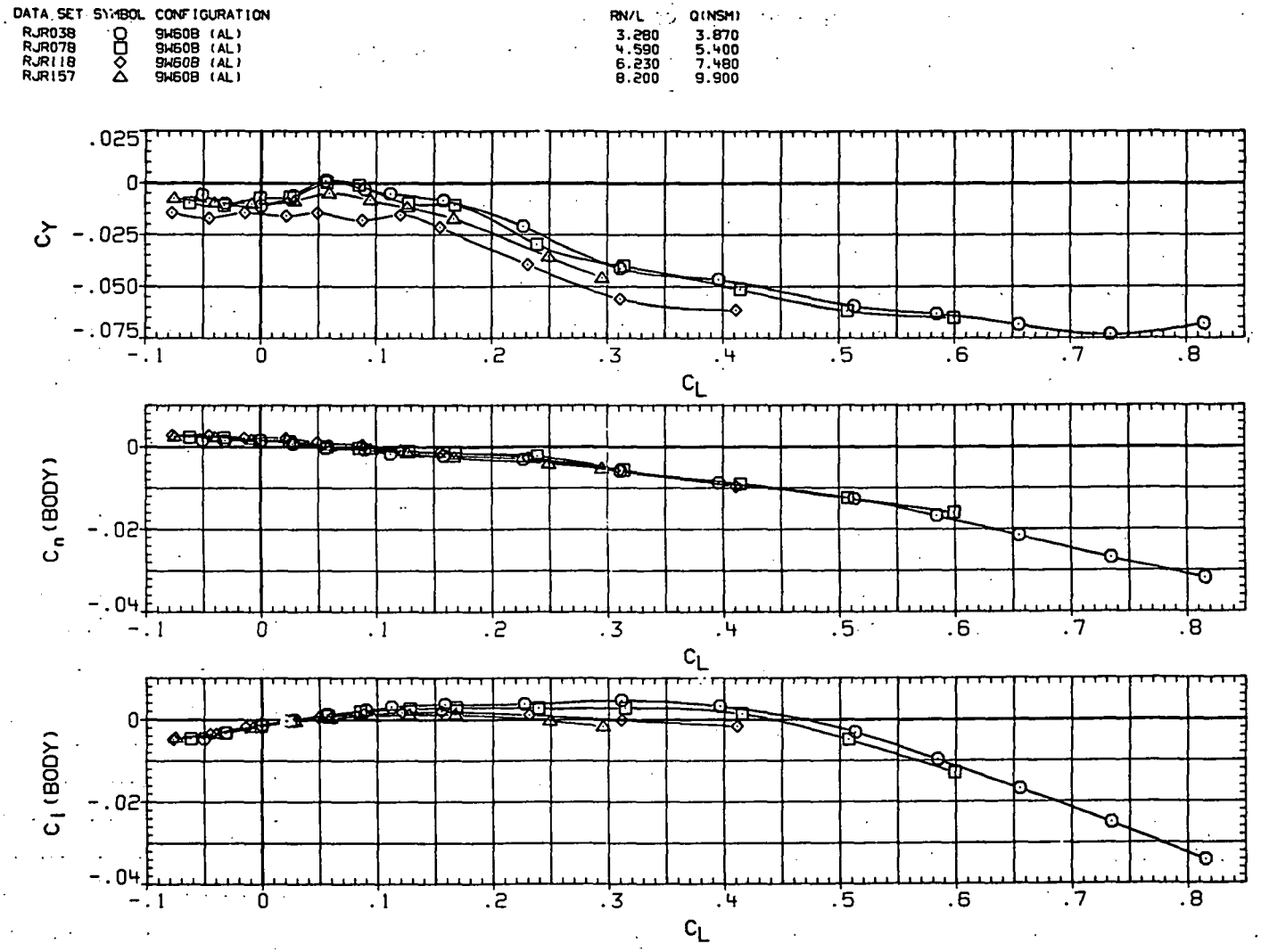

(e) C_Y, C_n and C_ℓ vs C_L.

Figure 35.– Concluded.

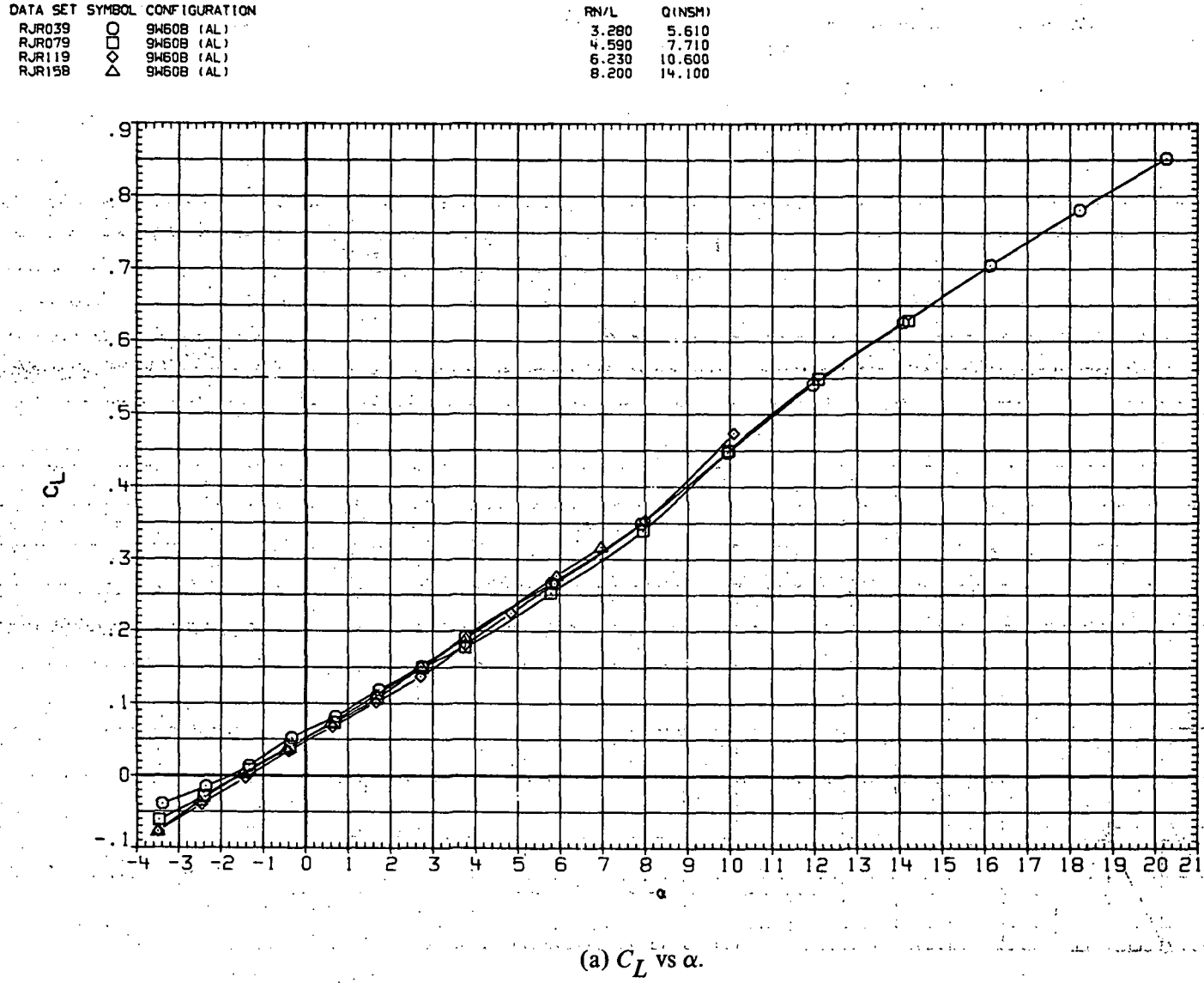

(a) C_L vs α.

Figure 36.– Dynamic-pressure effects on the aerodynamic characteristics of the aluminum trapezoidal oblique wing-body combination ($\Lambda = 60°$, $M = 0.6$ and the modified NACA 65A204 airfoil).

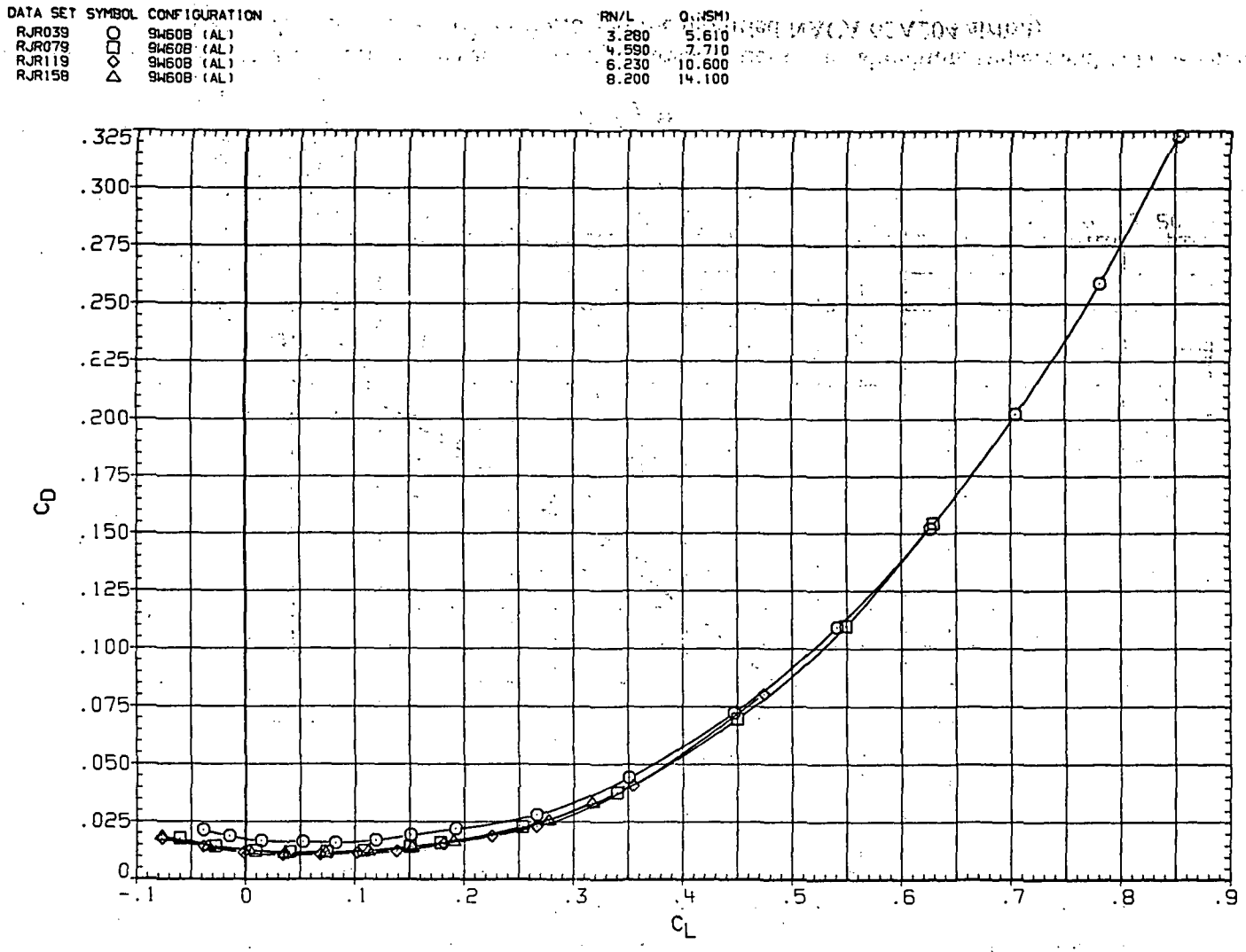

(b) C_D vs C_L.

Figure 36.– Continued.

DATA SET	SYMBOL	CONFIGURATION
RJR039	○	9W60B (AL)
RJR079	□	9W60B (AL)
RJR119	◇	9W60B (AL)
RJR158	△	9W60B (AL)

RN/L	Q(NT·I)
3.280	5.610
4.590	7.710
6.230	10.600
8.200	14.100

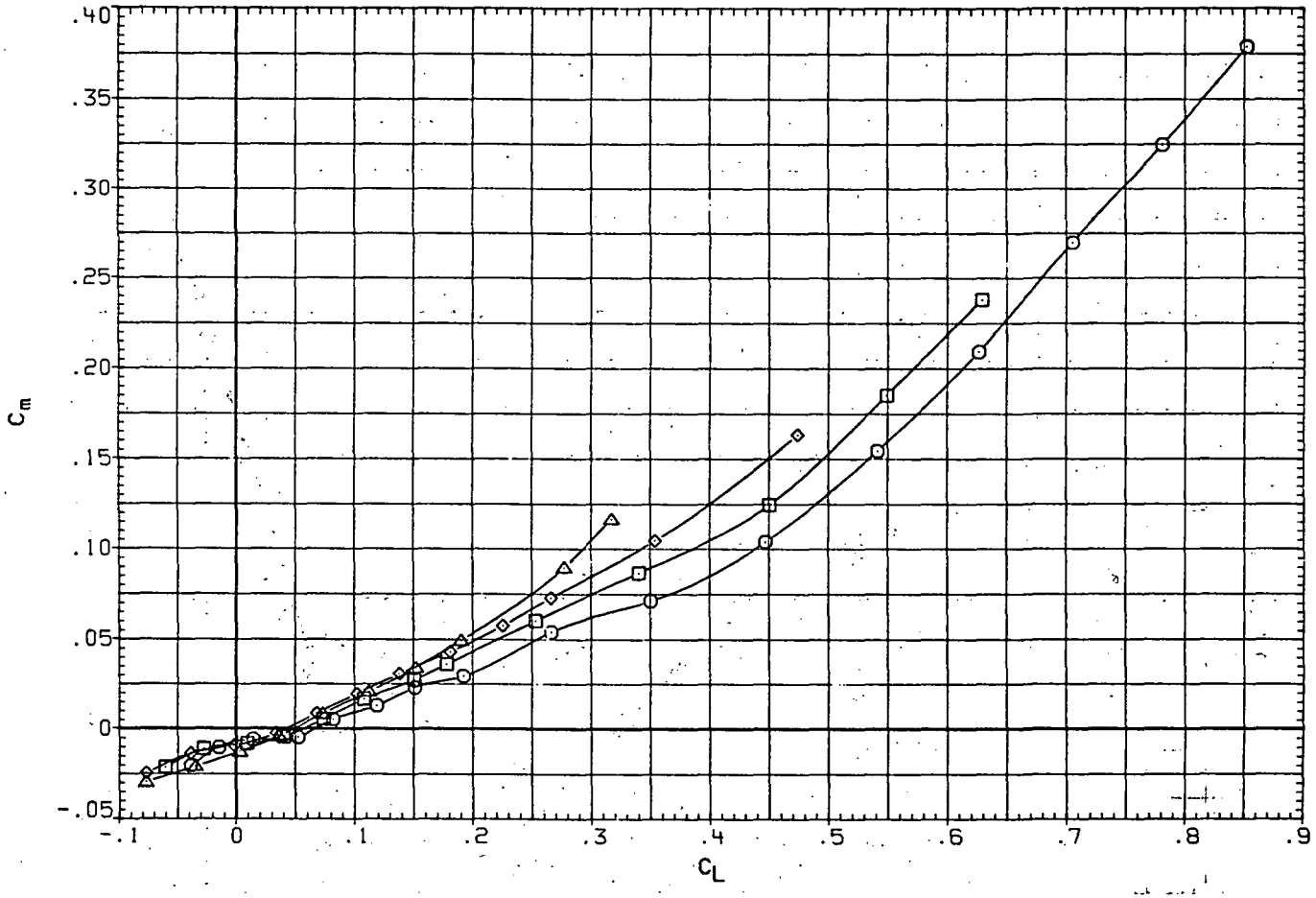

(c) C_m vs C_L.

Figure 36.– Continued.

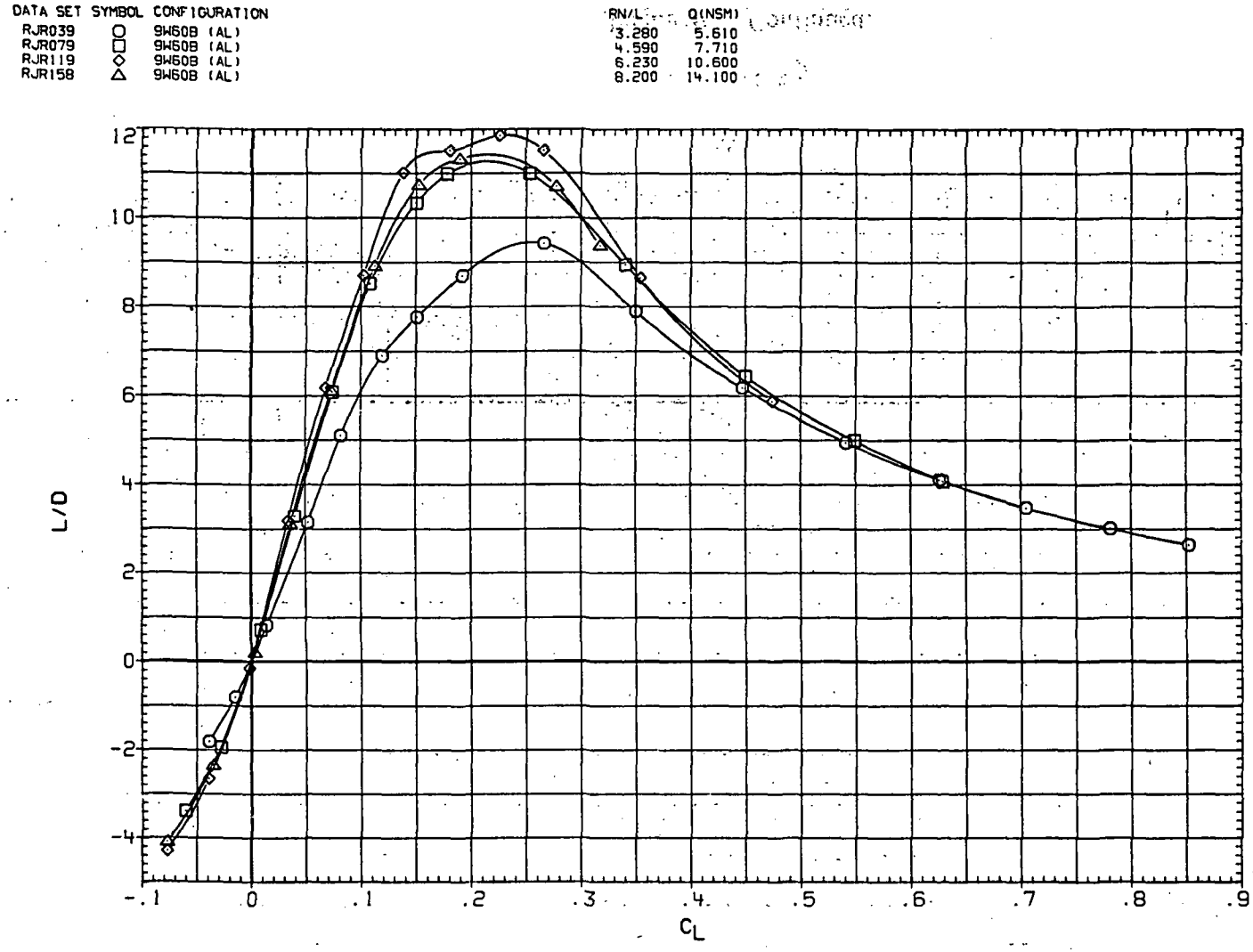

(d) L/D vs C_L.

Figure 36.– Continued.

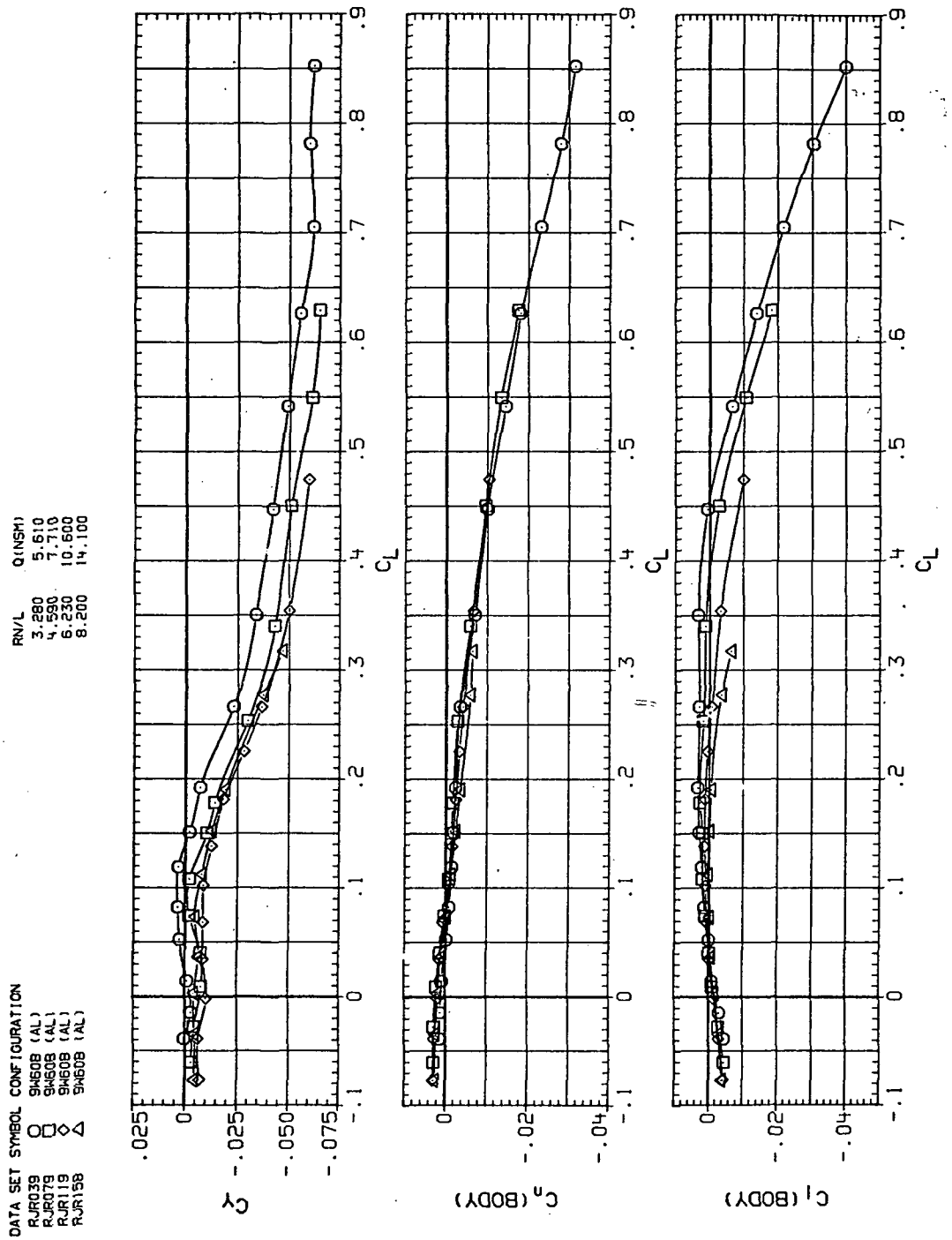

(e) C_Y, C_n and C_ℓ vs C_L.

Figure 36.– Concluded.

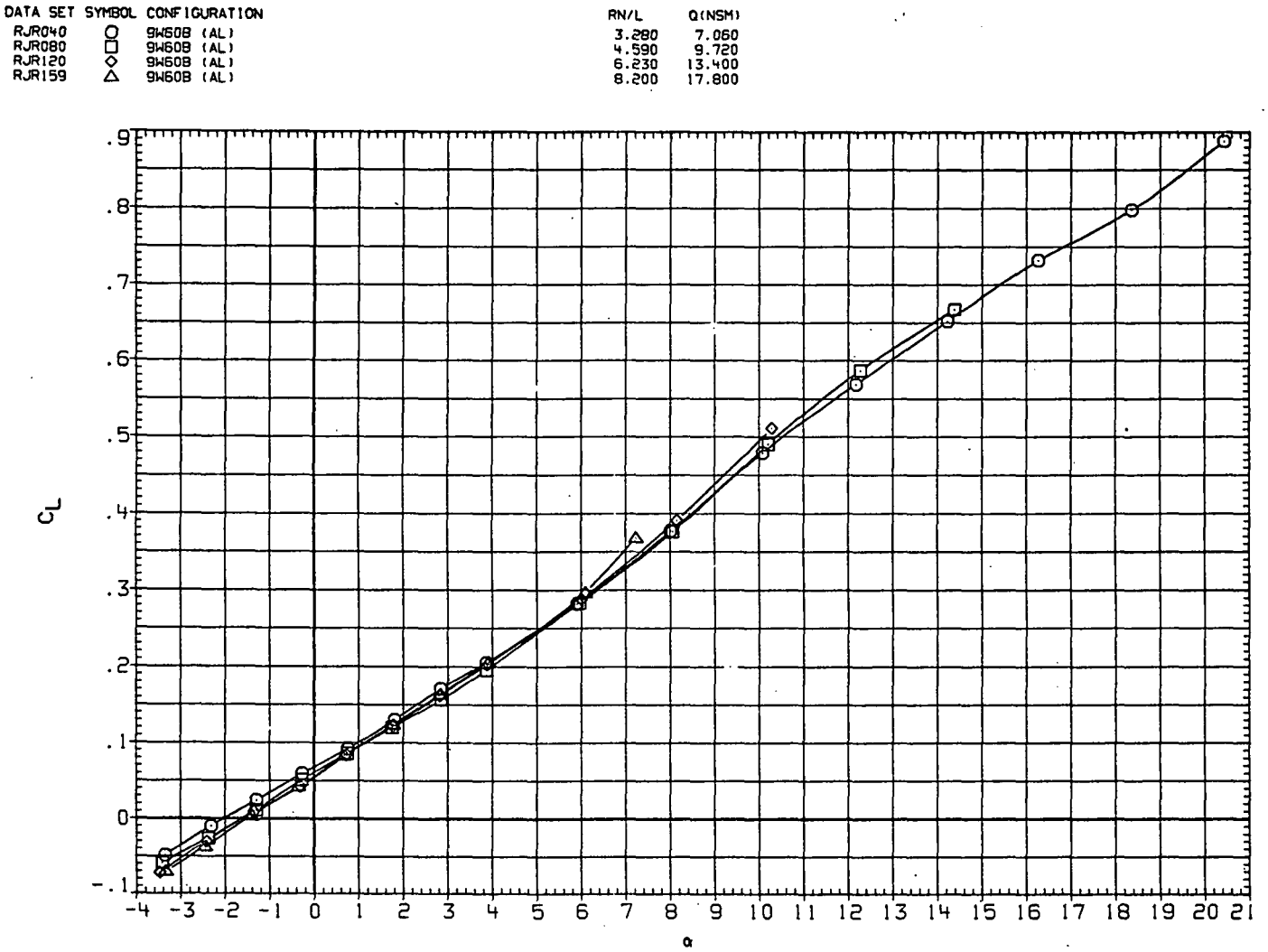

(a) C_L vs α.

Figure 37.– Dynamic-pressure effects on the aerodynamic characteristics of the aluminum trapezoidal oblique wing-body combination ($\Lambda = 60°$, $M = 0.8$ and the modified NACA 65A204 airfoil).

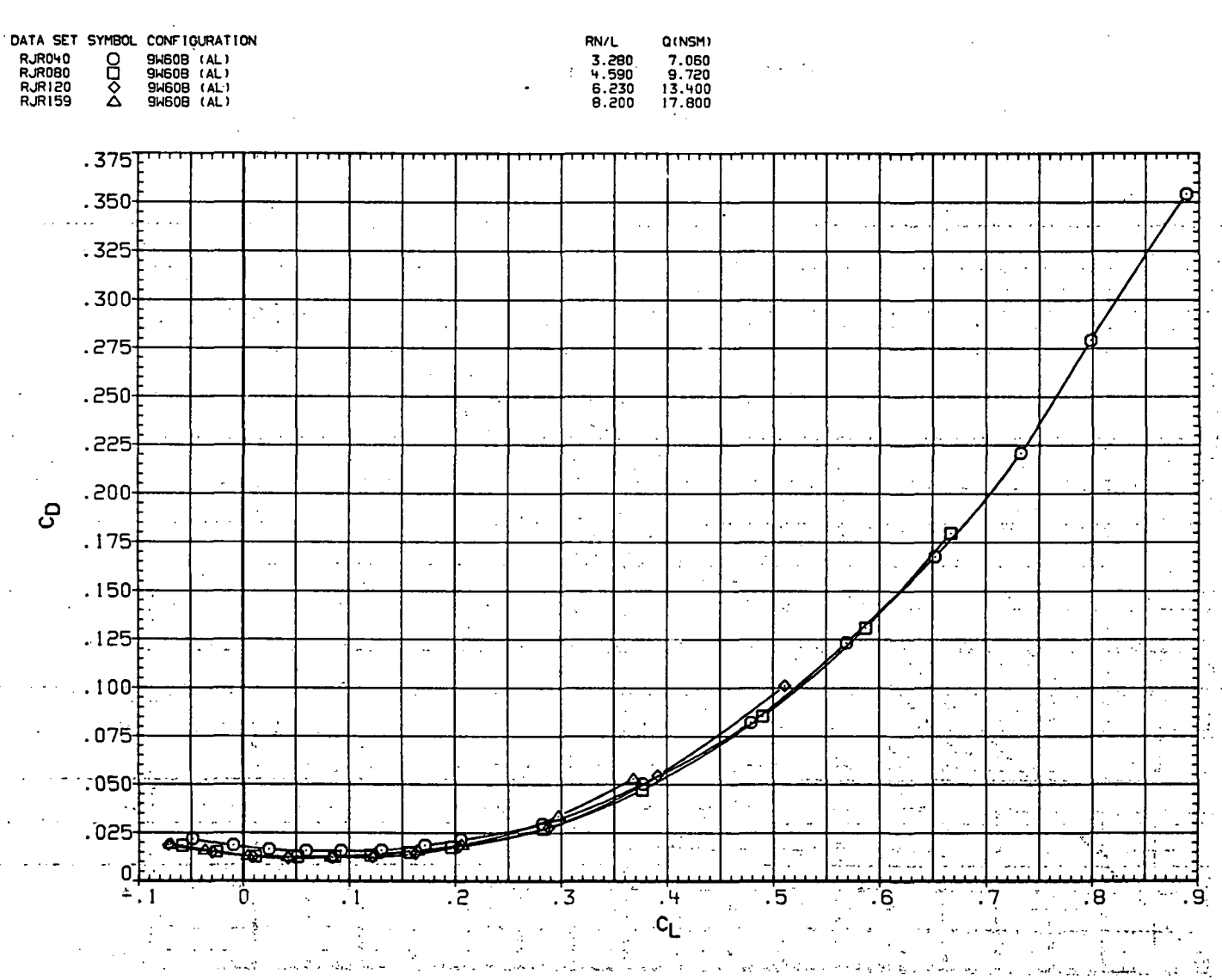

(b) C_D vs C_L.

Figure 37.– Continued.

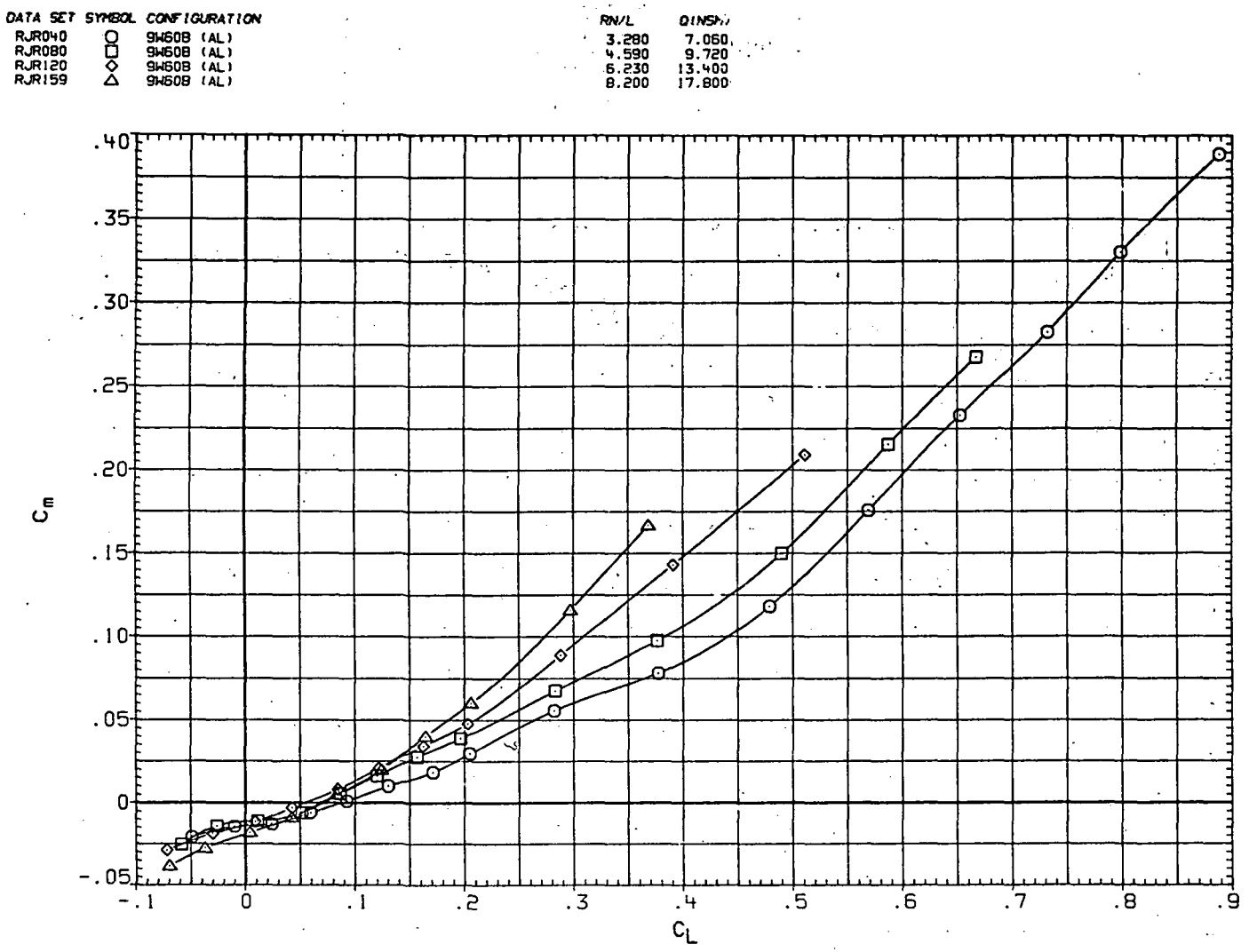

(c) C_m vs C_L.

Figure 37.– Continued.

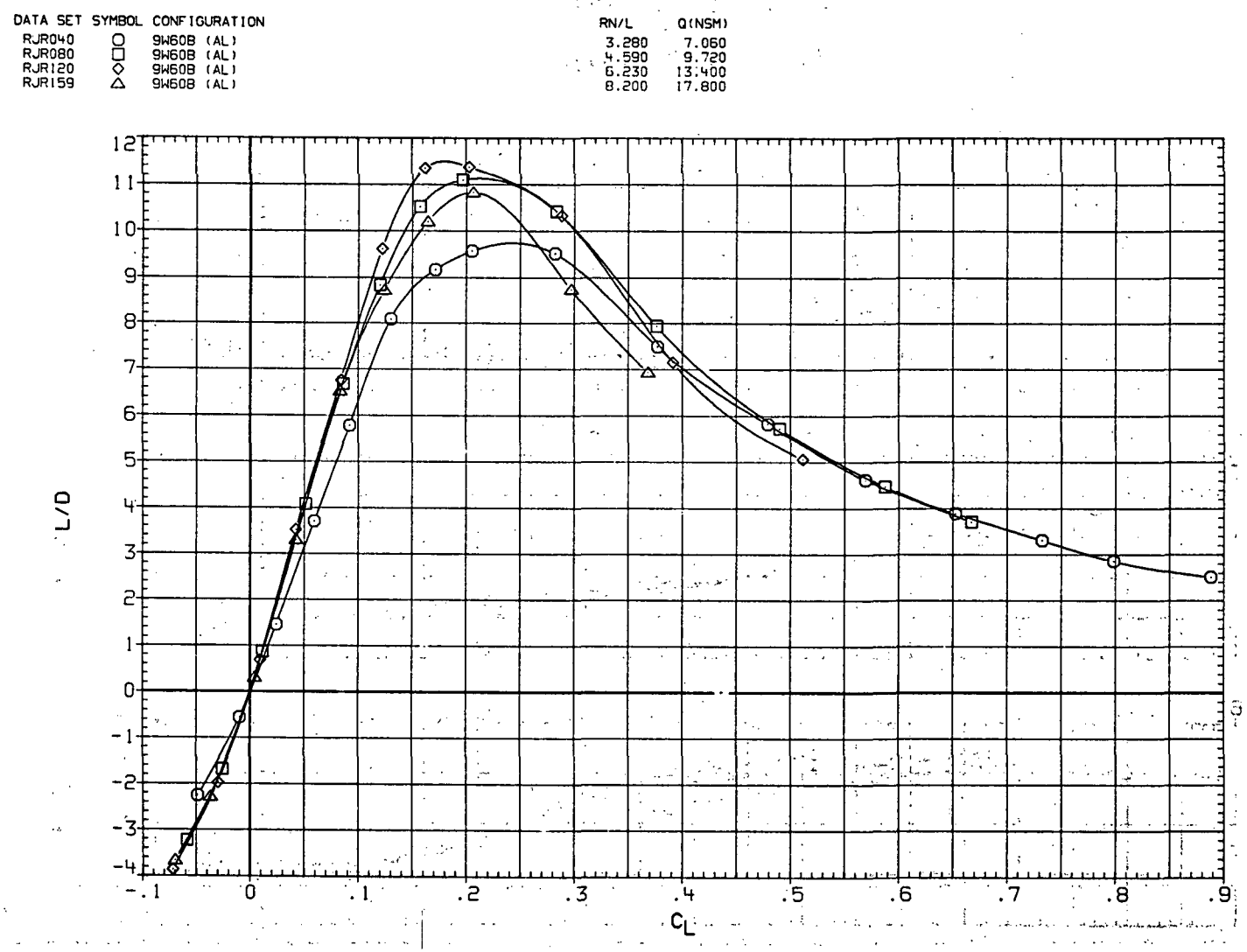

(d) L/D vs C_L.

Figure 37.– Continued.

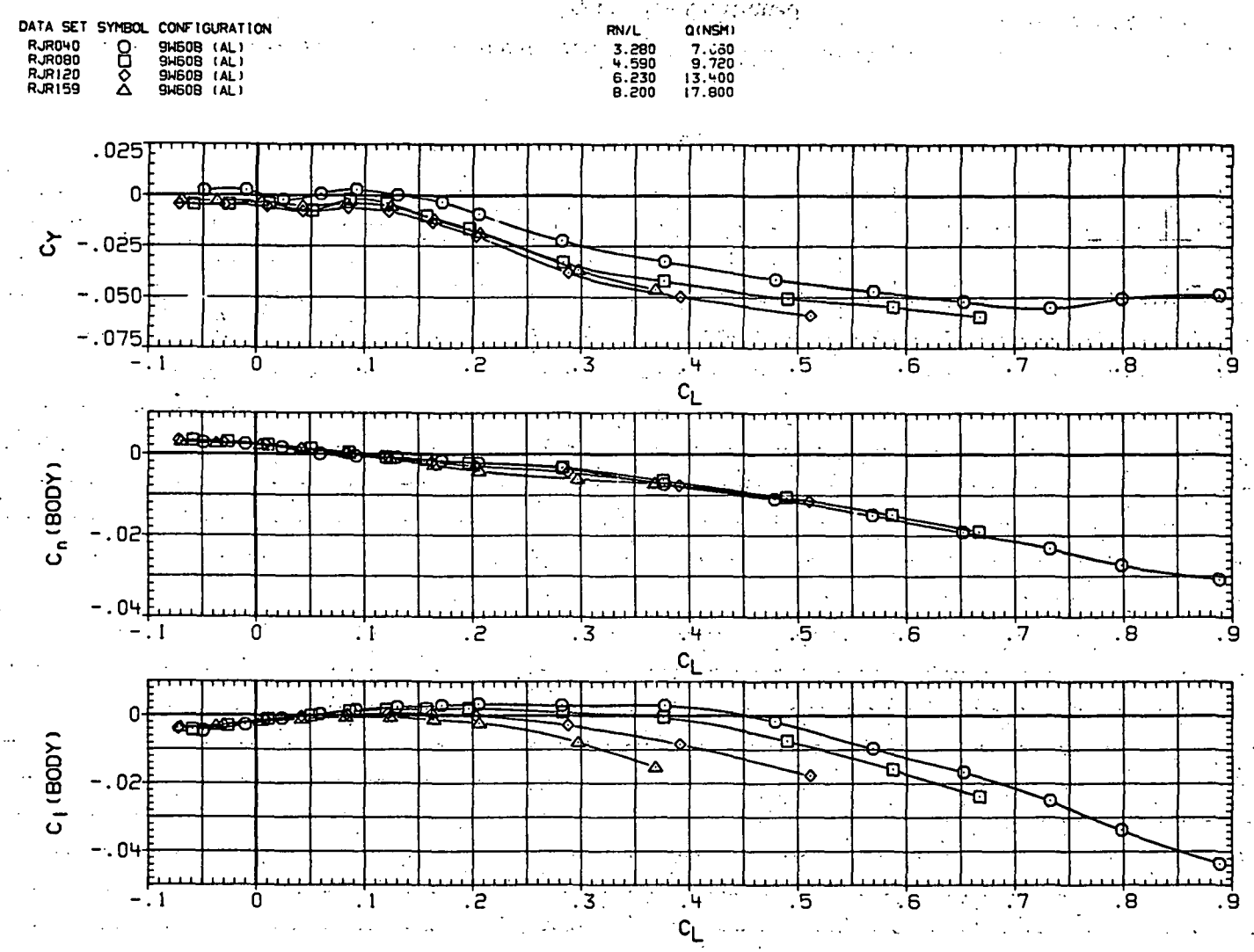

(e) C_Y, C_n and C_ℓ vs C_L.

Figure 37.– Concluded.

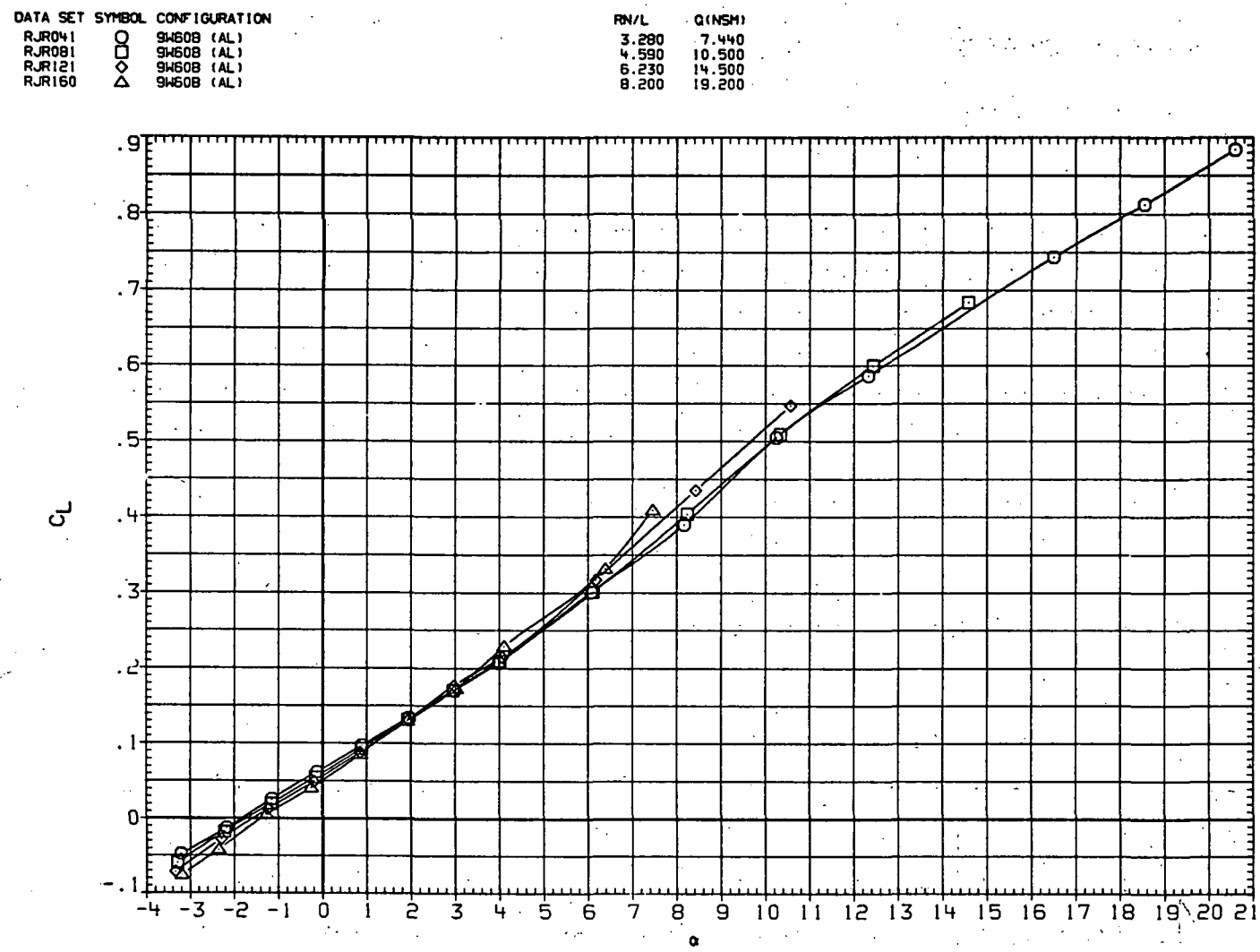

(a) C_L vs α.

Figure 38.– Dynamic-pressure effects on the aerodynamic characteristics of the aluminum trapezoidal oblique wing-body combination ($\Lambda = 60°$, $M = 0.9$ and the modified NACA 65A204 airfoil).

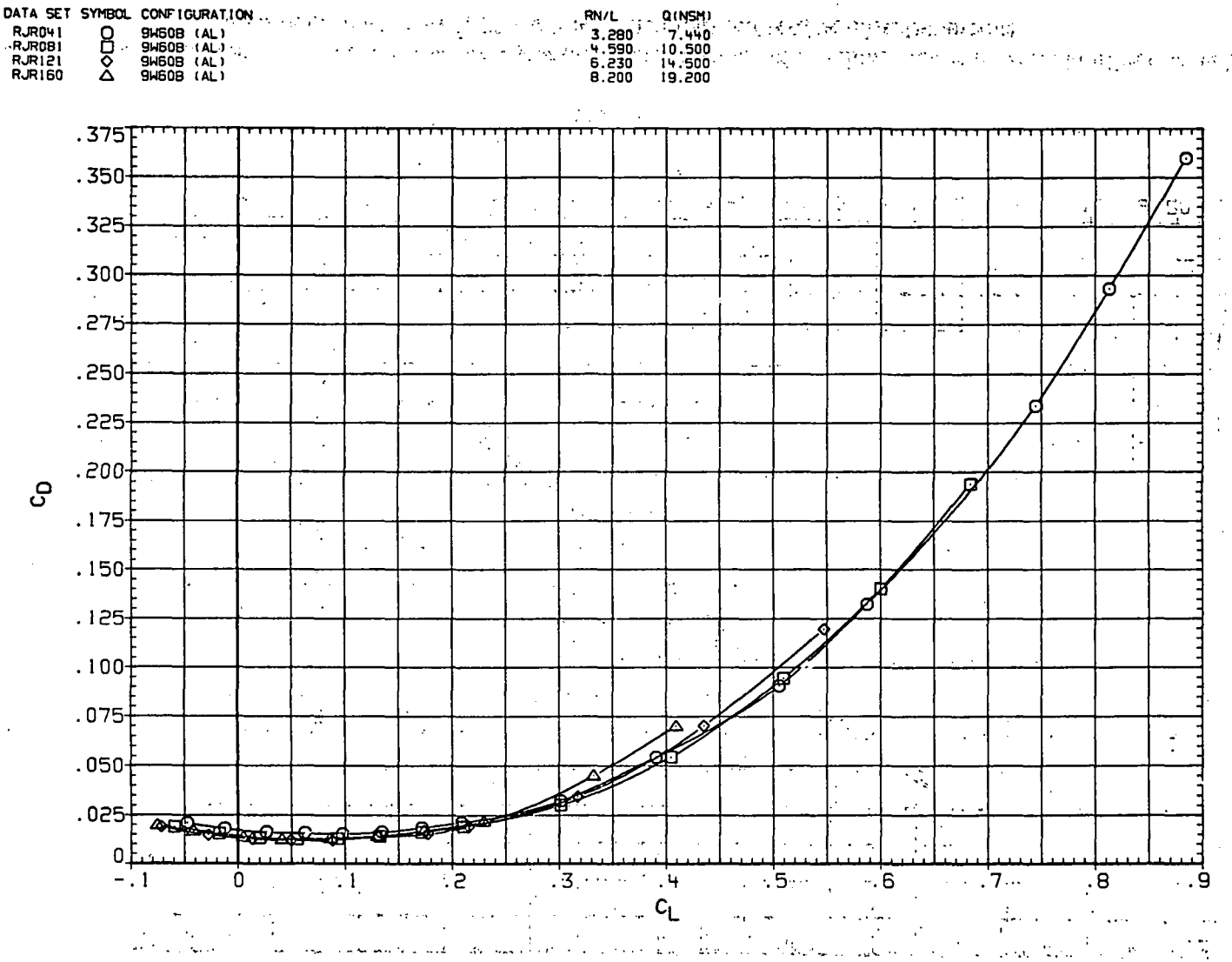

(b) C_D vs C_L.

Figure 38 – Continued.

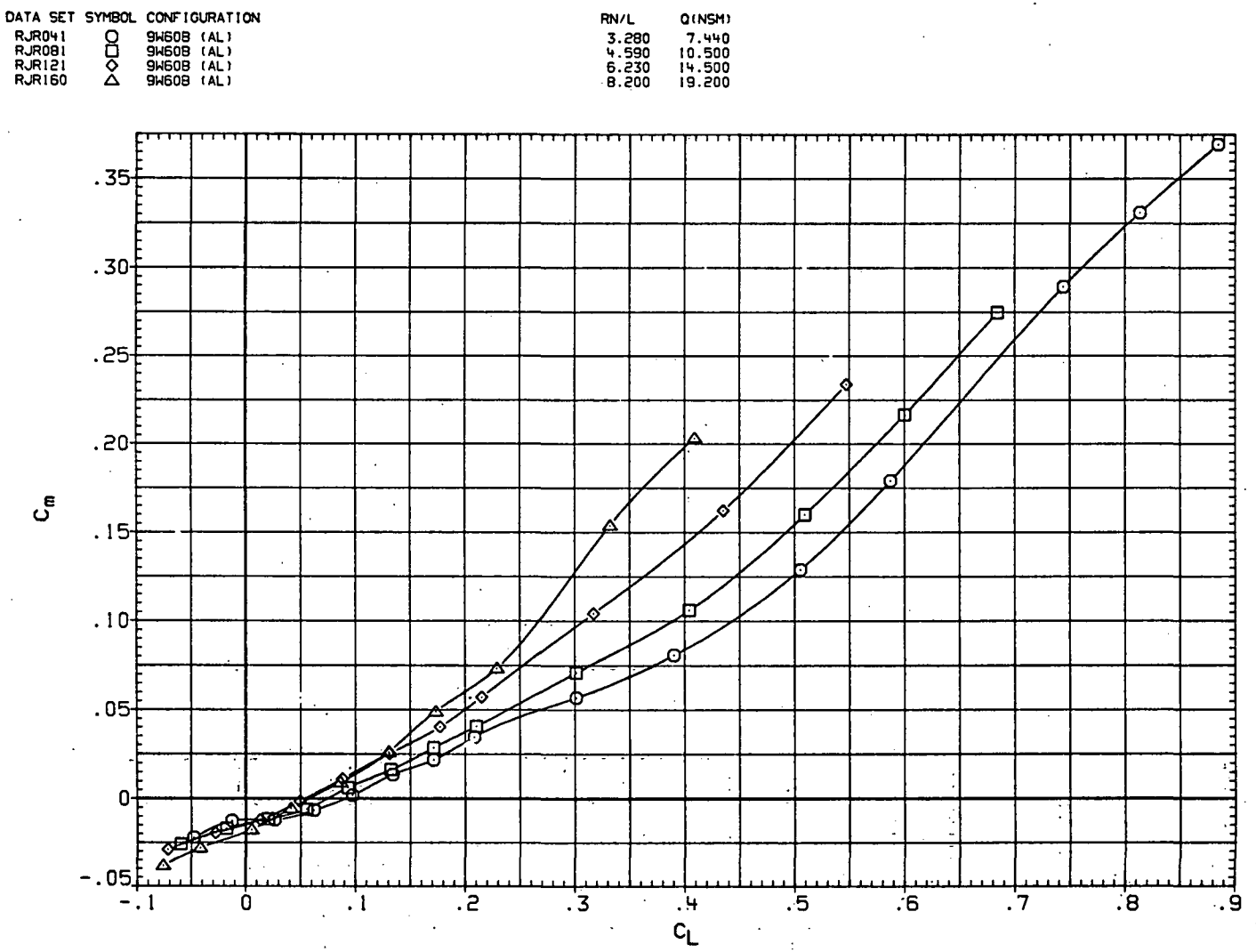

(c) C_m vs C_L.

Figure 38.—Continued.

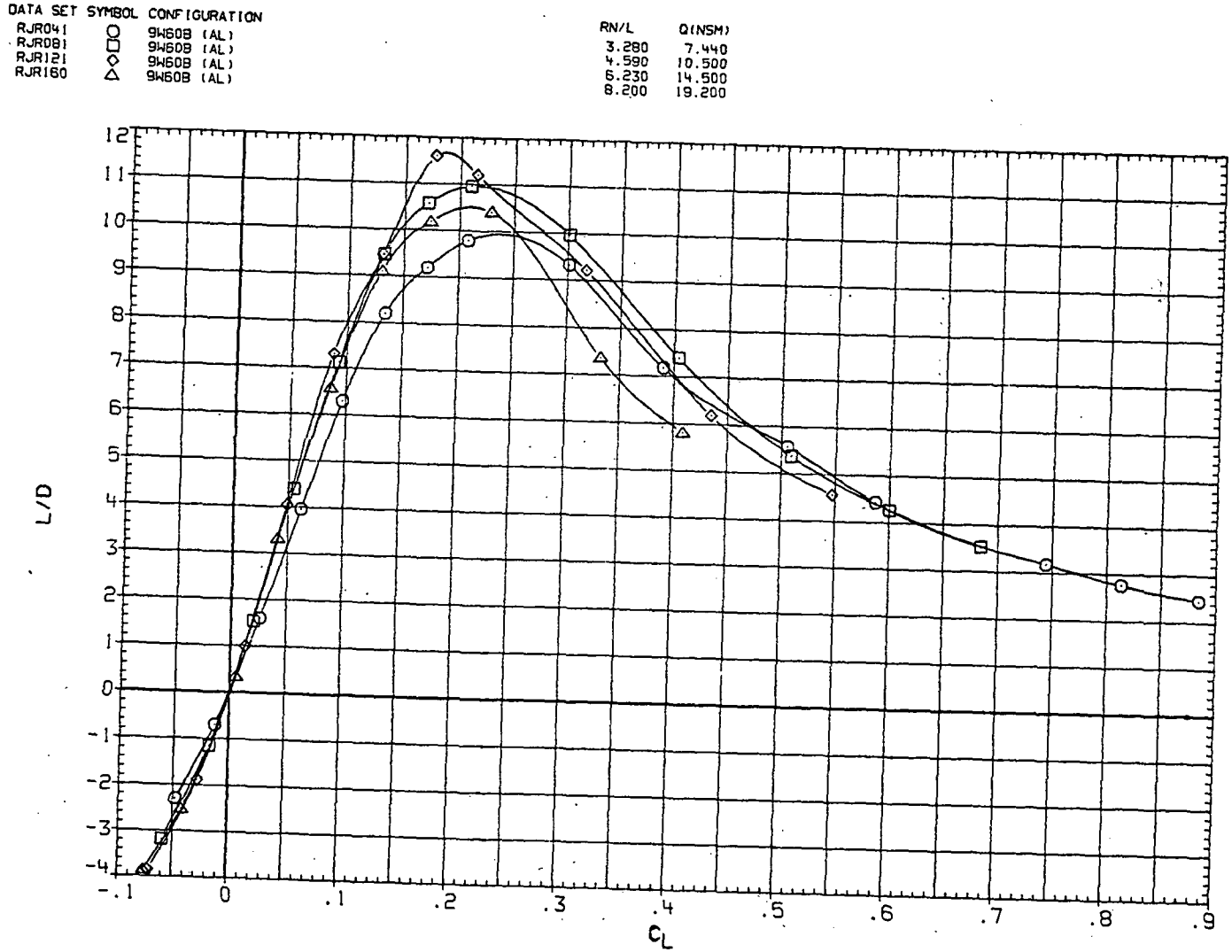

(d) L/D vs C_L.

Figure 38.– Continued.

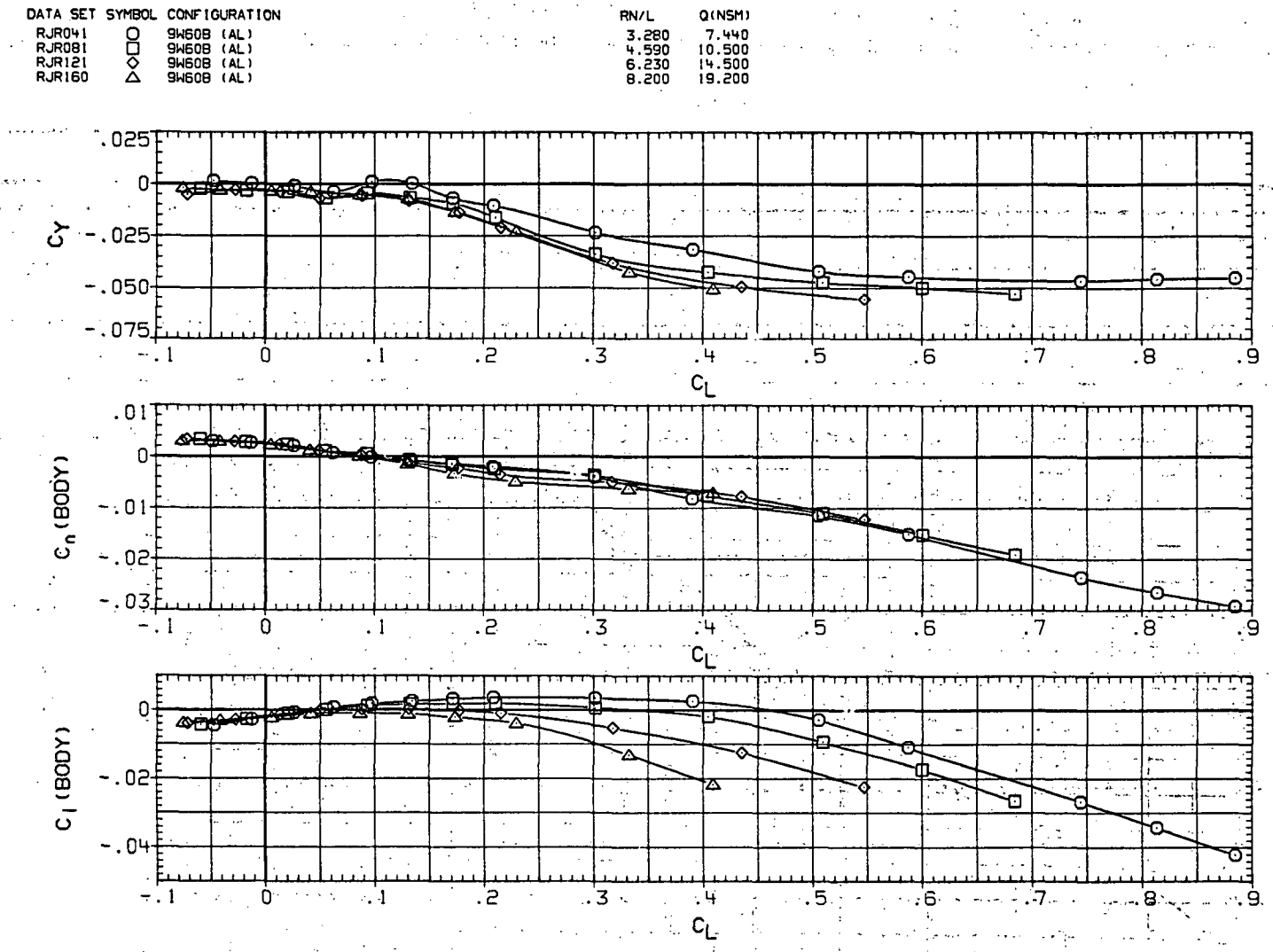

(e) C_Y, C_n and C_ℓ vs C_L.

Figure 38.– Concluded.

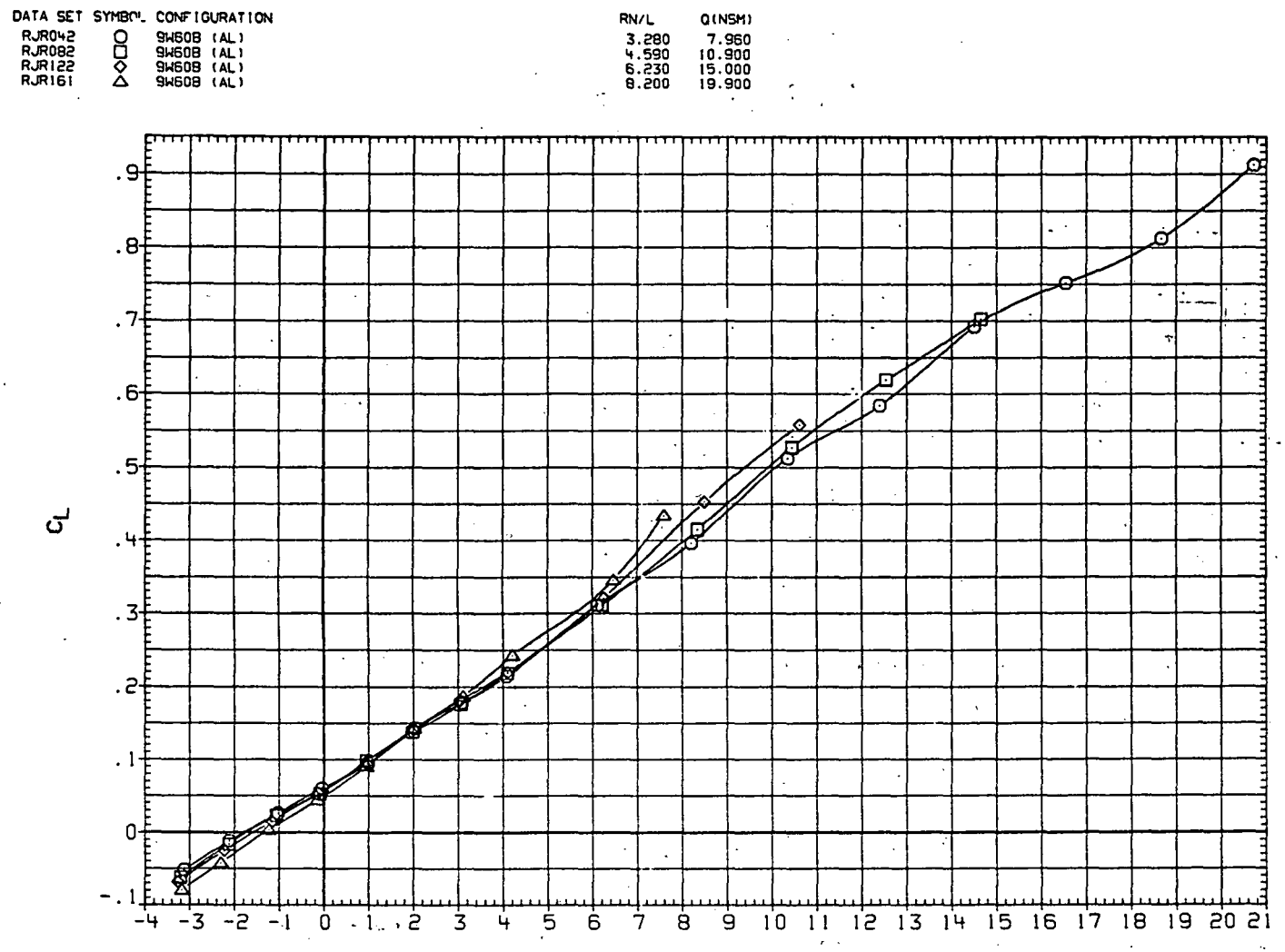

(a) C_L vs α.

Figure 39.– Dynamic-pressure effects on the aerodynamic characteristics of the aluminum trapezoidal oblique wing-body combination ($\Lambda = 60°$, $M = 0.95$ and the modified NACA 65A204 airfoil).

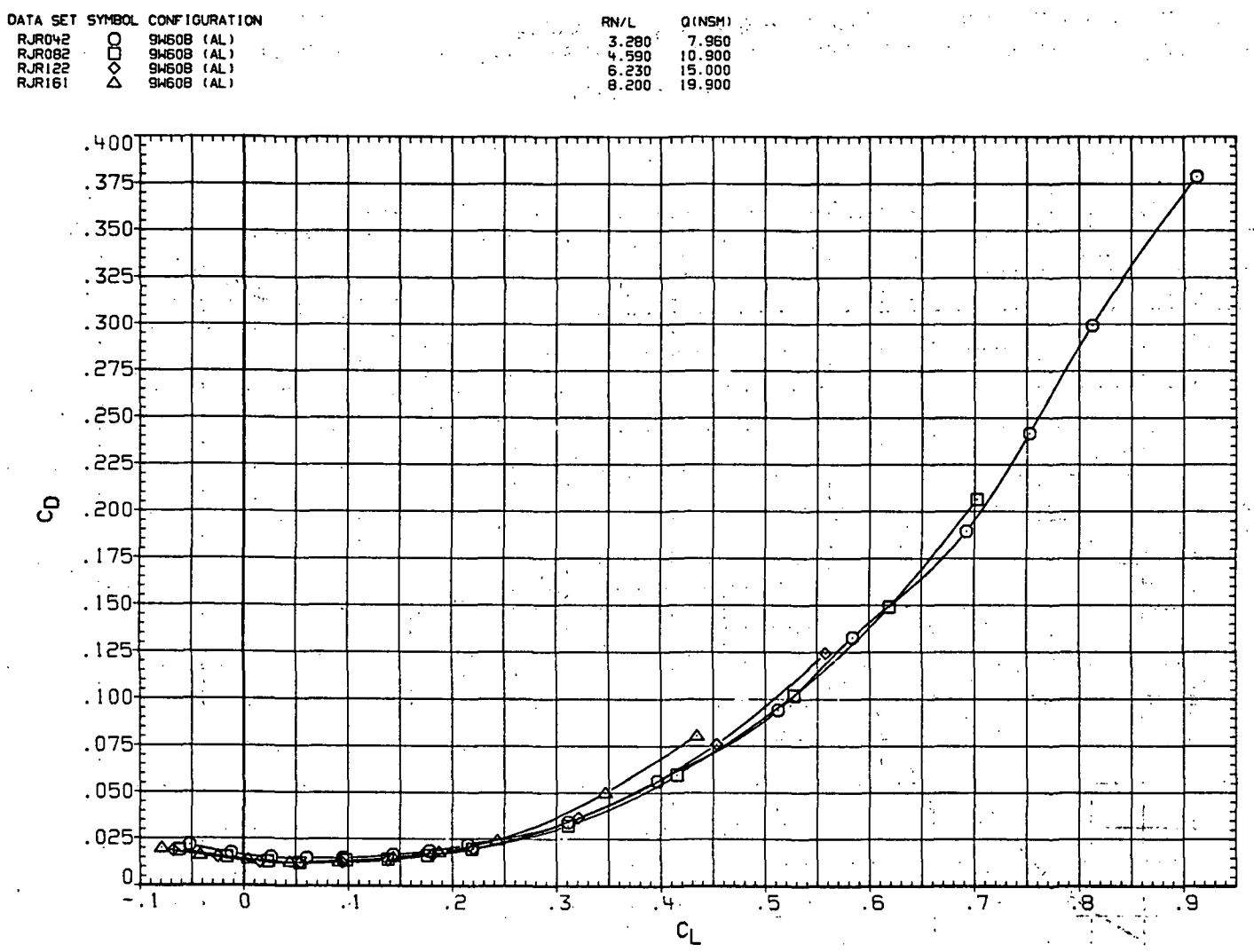

(b) C_D vs C_L.

Figure 39.– Continued.

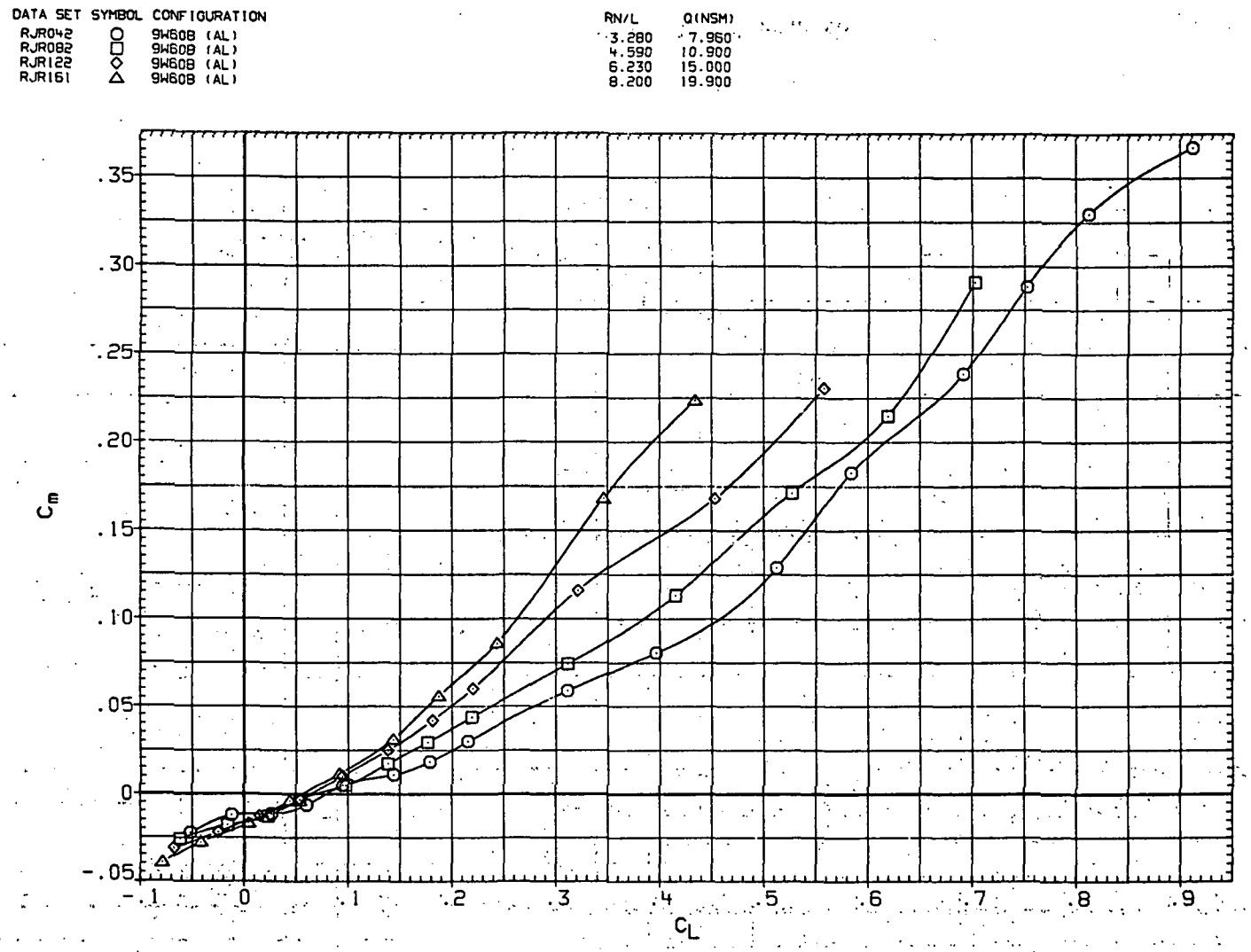

(c) C_m vs C_L.

Figure 39.– Continued.

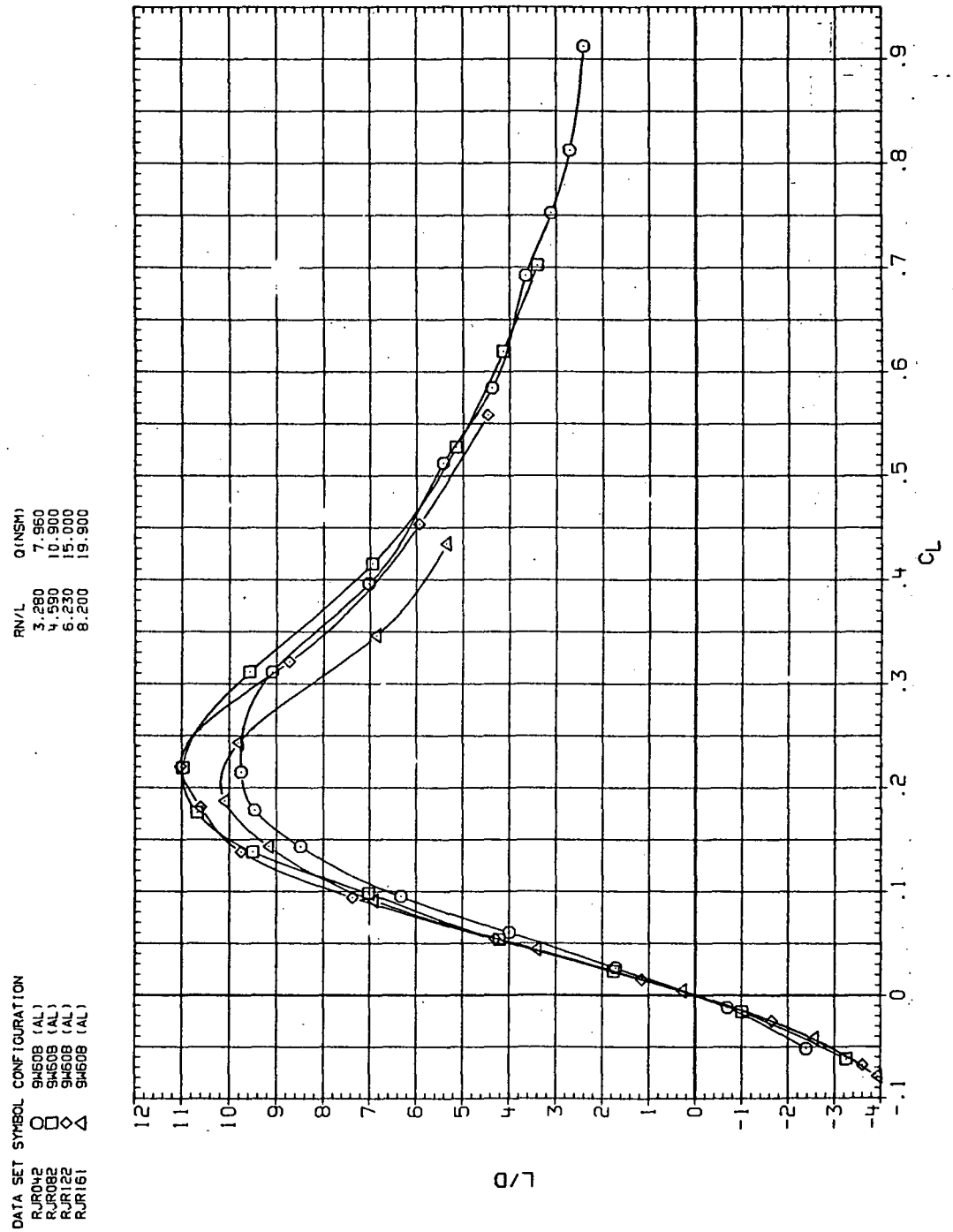

(d) L/D vs C_L.

Figure 39.– Continued.

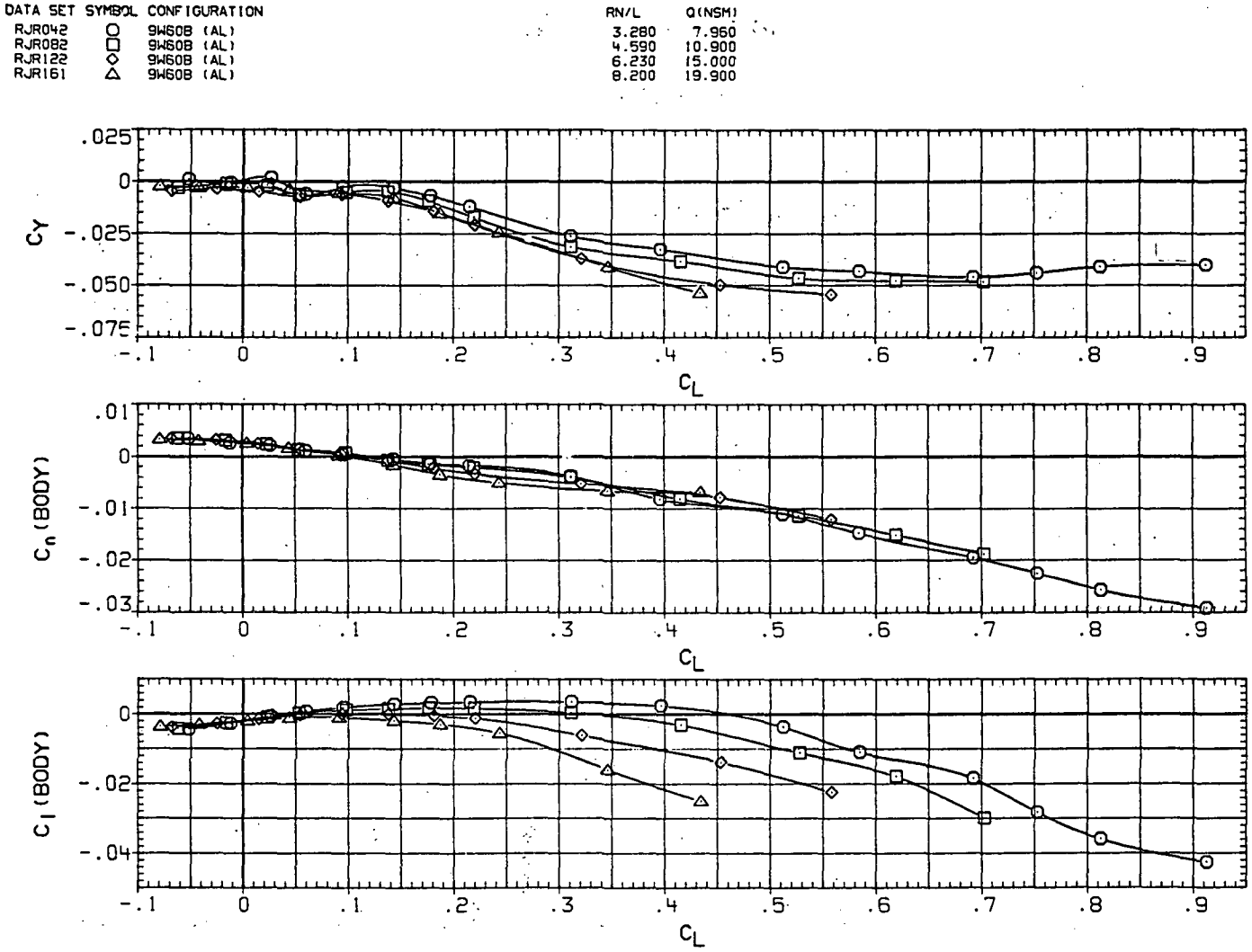

(e) C_Y, C_n and C_ℓ vs C_L.

Figure 39.– Concluded.

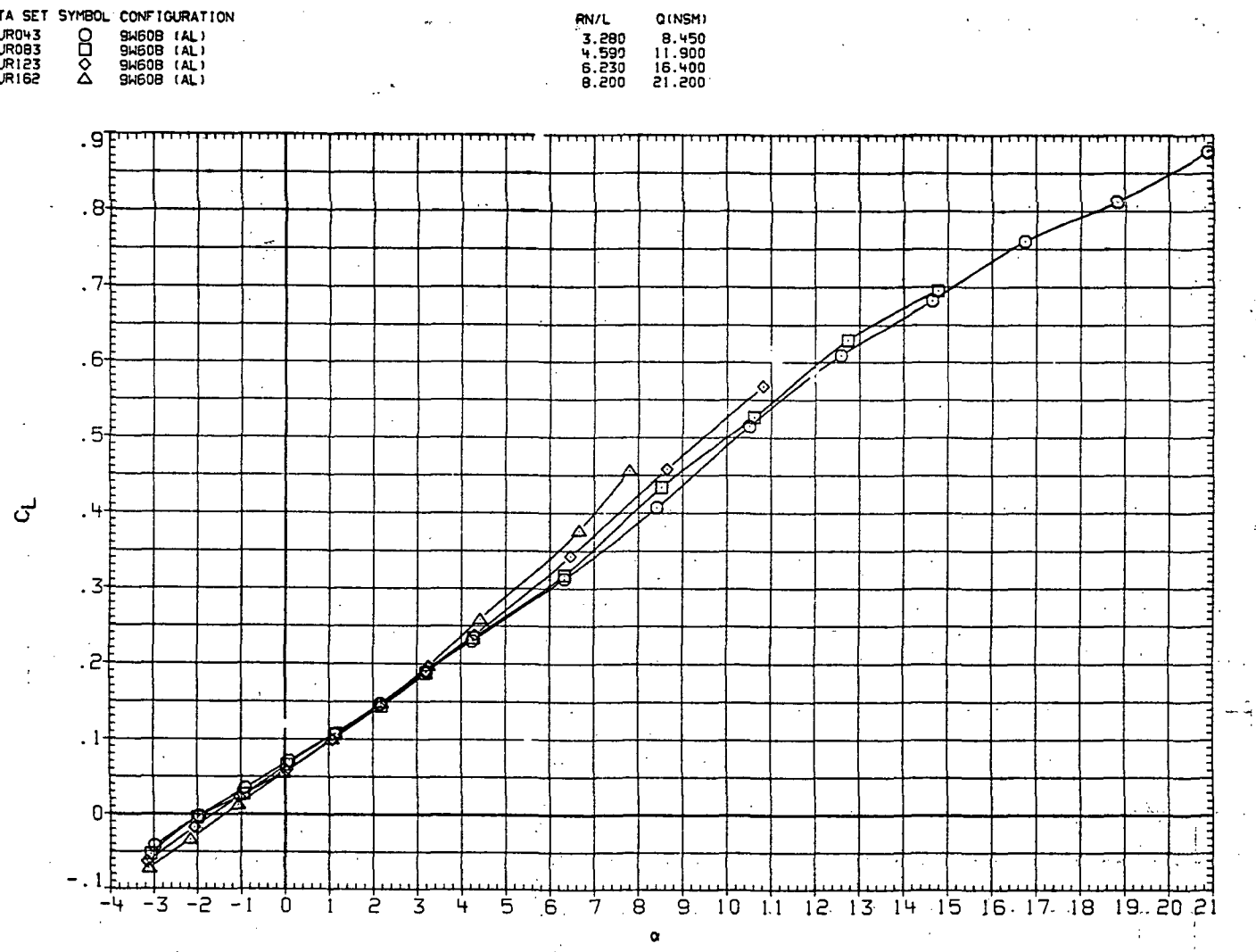

(a) C_L vs α.

Figure 40.– Dynamic-pressure effects on the aerodynamic characteristics of the aluminum trapezoidal oblique wing-body combination ($\Lambda = 60°, M = 1.1$ and the modified NACA 65A204 airfoil).

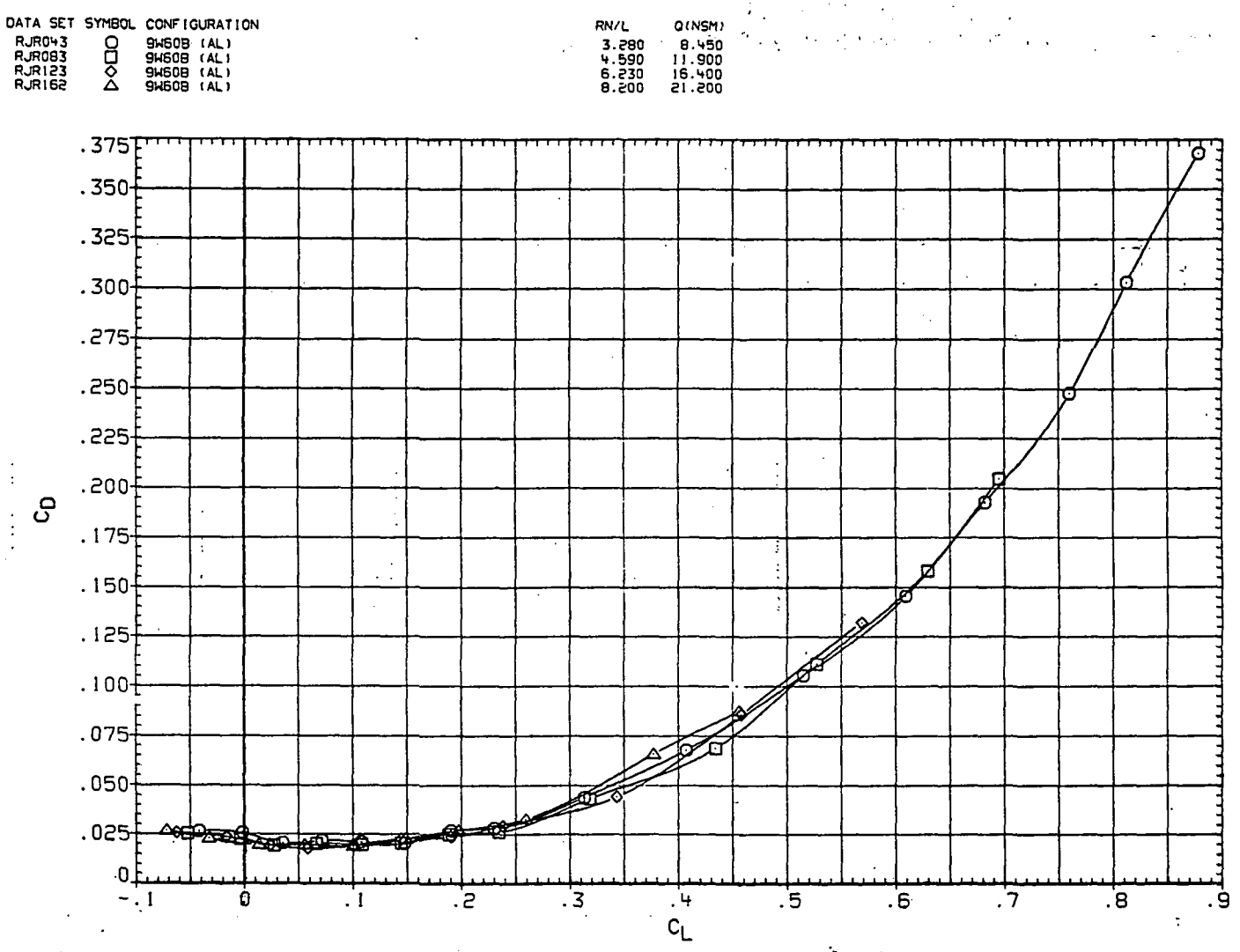

(b) C_D vs C_L.

Figure 40.– Continued.

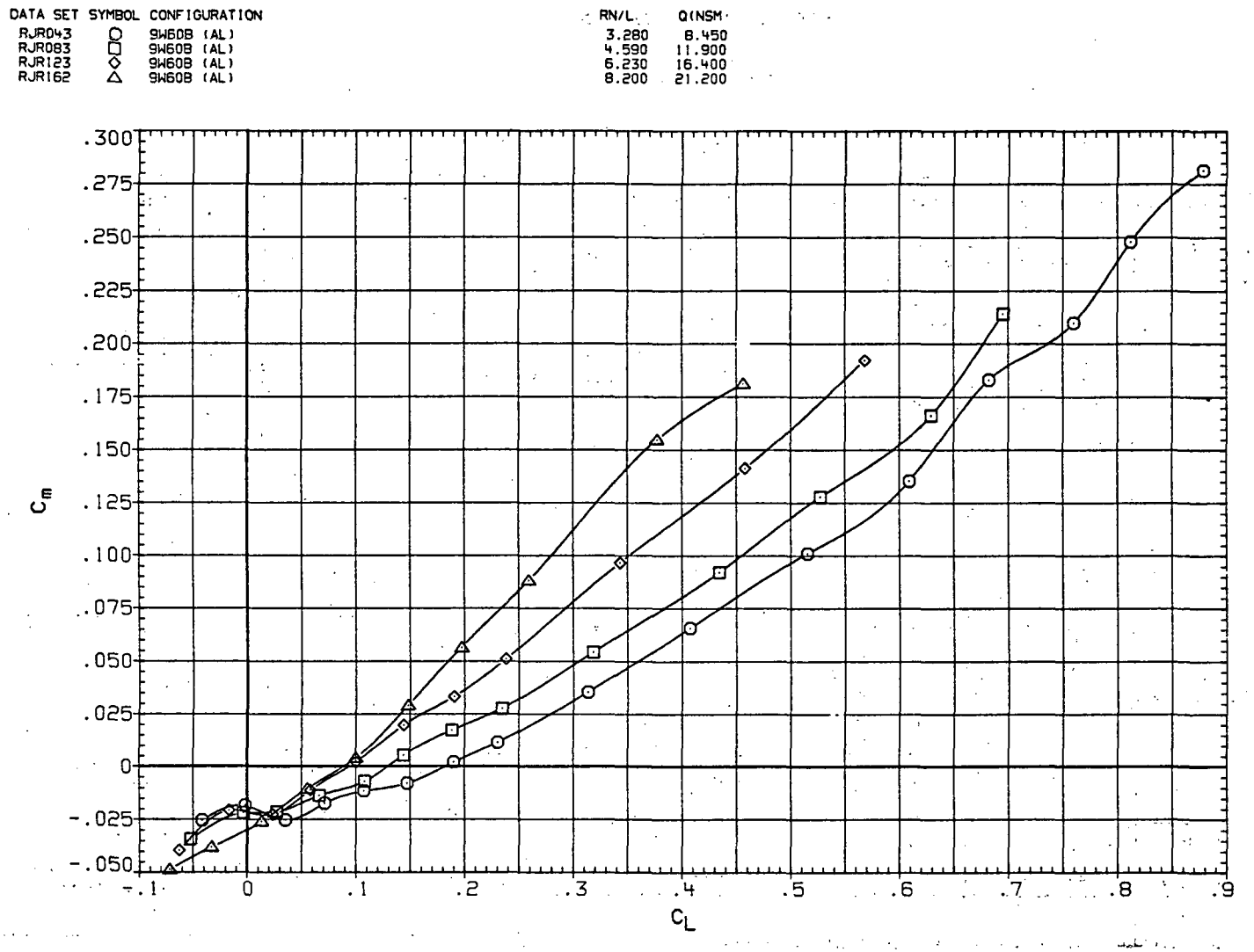

(c) C_m vs C_L.

Figure 40.– Continued.

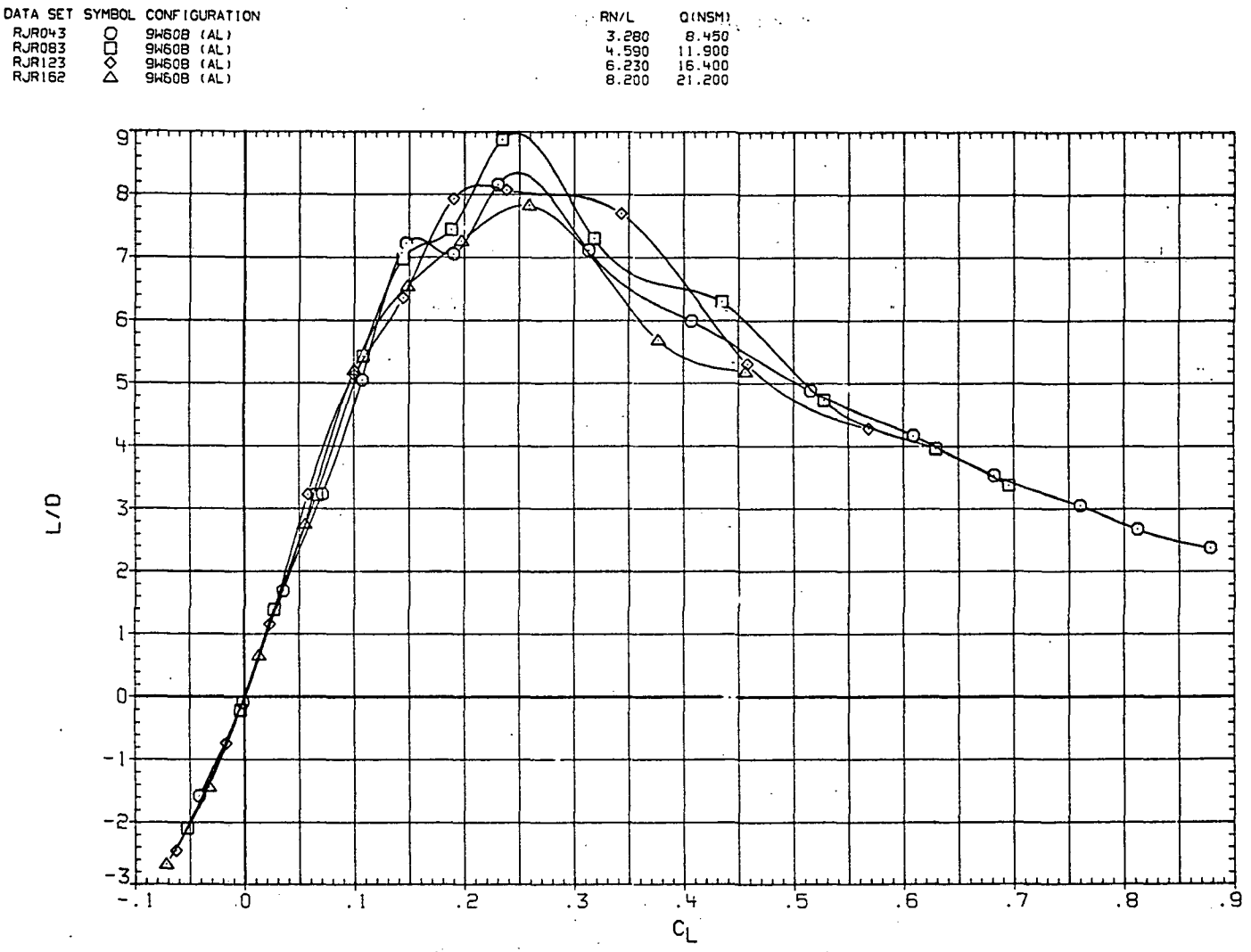

(d) L/D vs C_L.

Figure 40.– Continued.

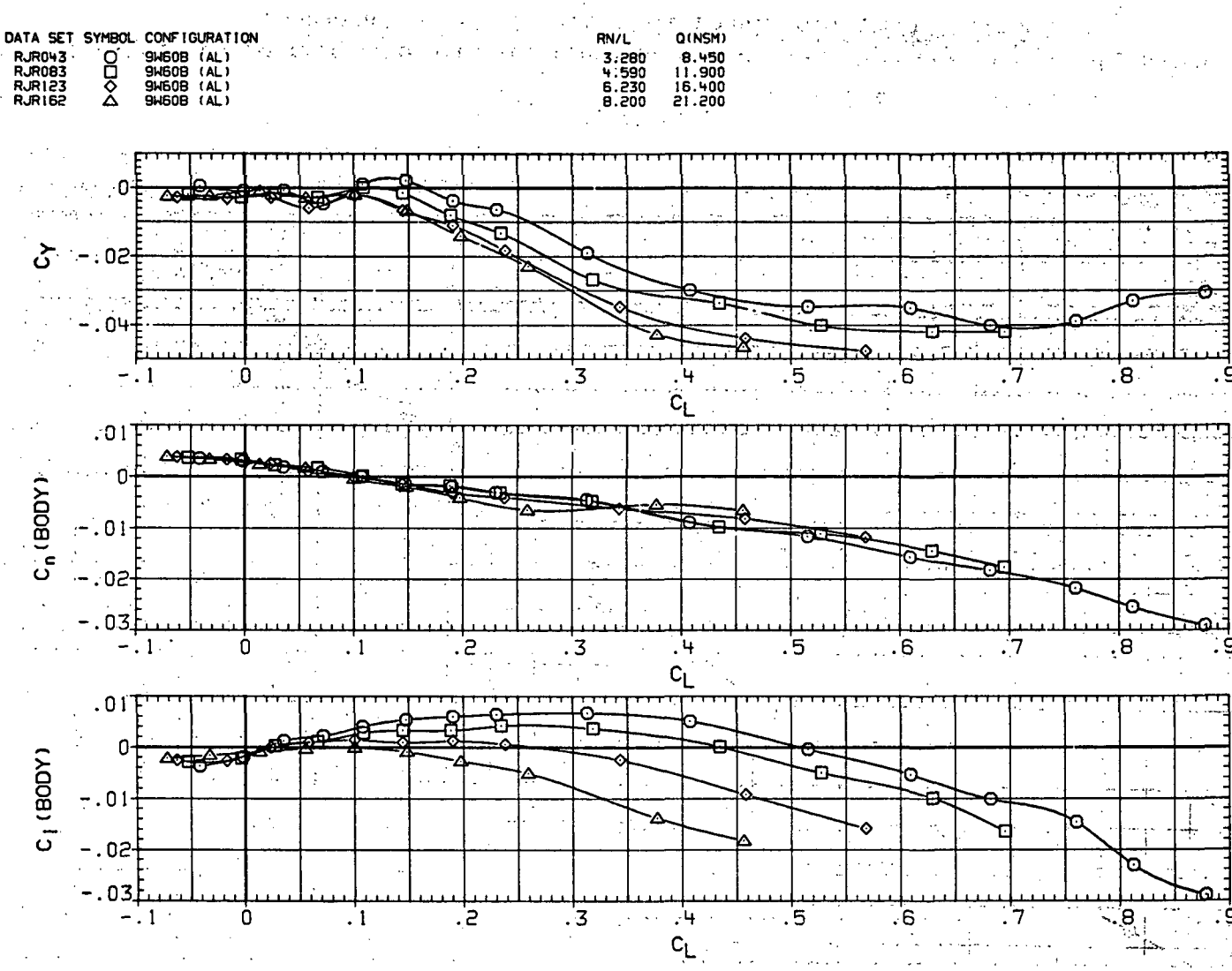

(e) C_Y, C_n and C_ℓ vs C_L.

Figure 40.– Concluded.

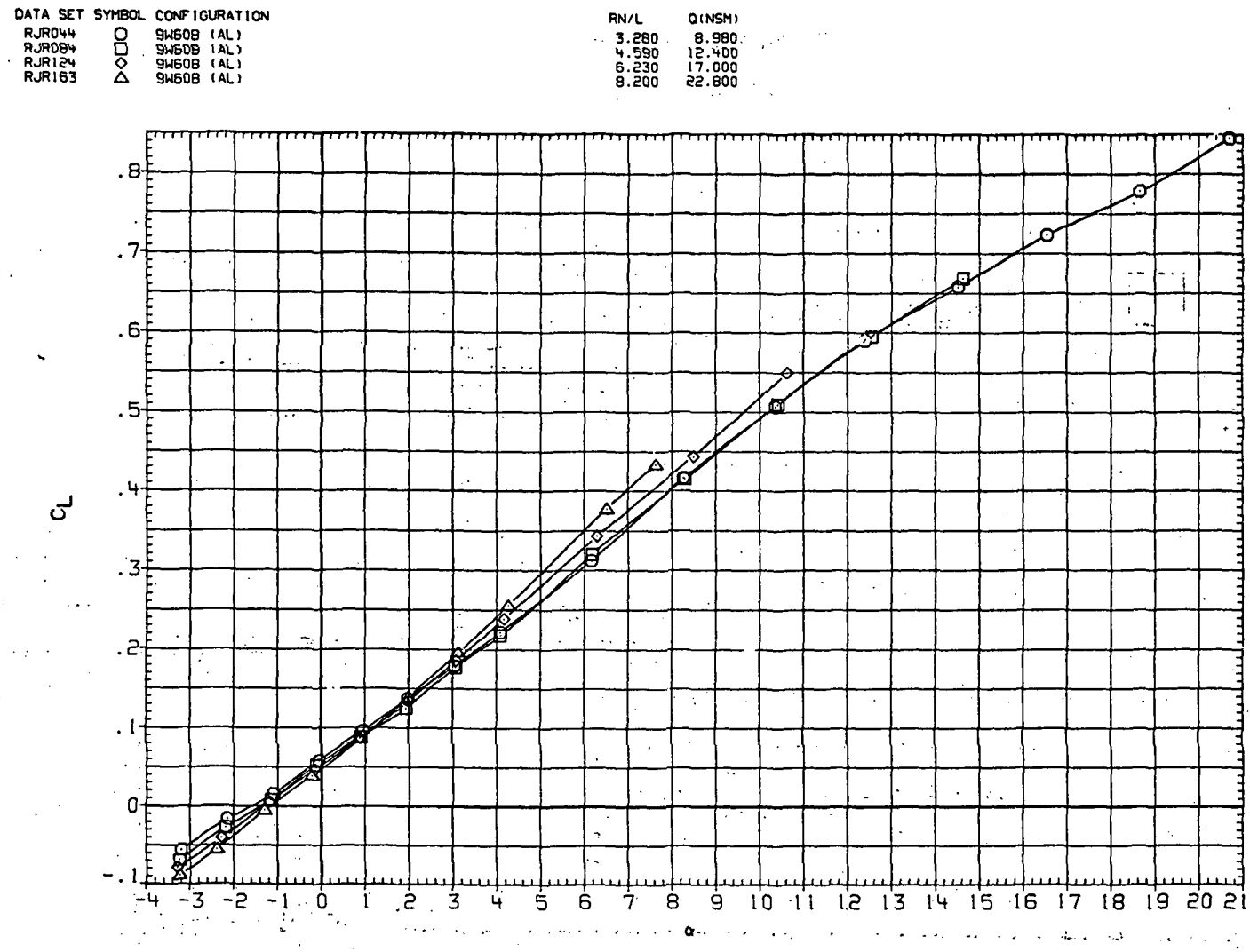

(a) C_L vs α.

Figure 41.– Dynamic-pressure effects on the aerodynamic characteristics of the aluminum trapezoidal oblique wing-body combination ($\Lambda = 60°$, $M = 1.2$ and the modified NACA 65A204 airfoil).

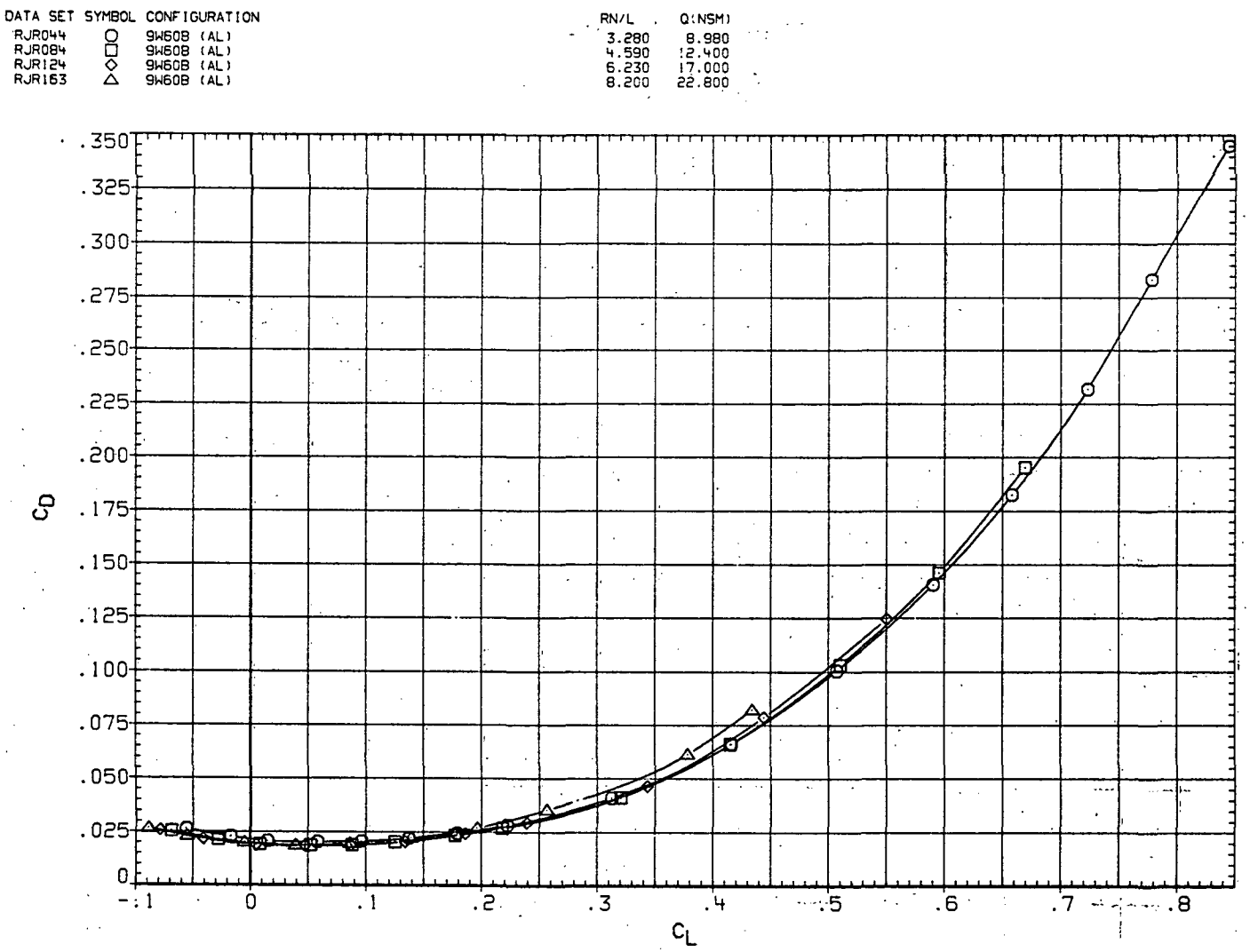

(b) C_D vs C_L.

Figure 41.– Continued.

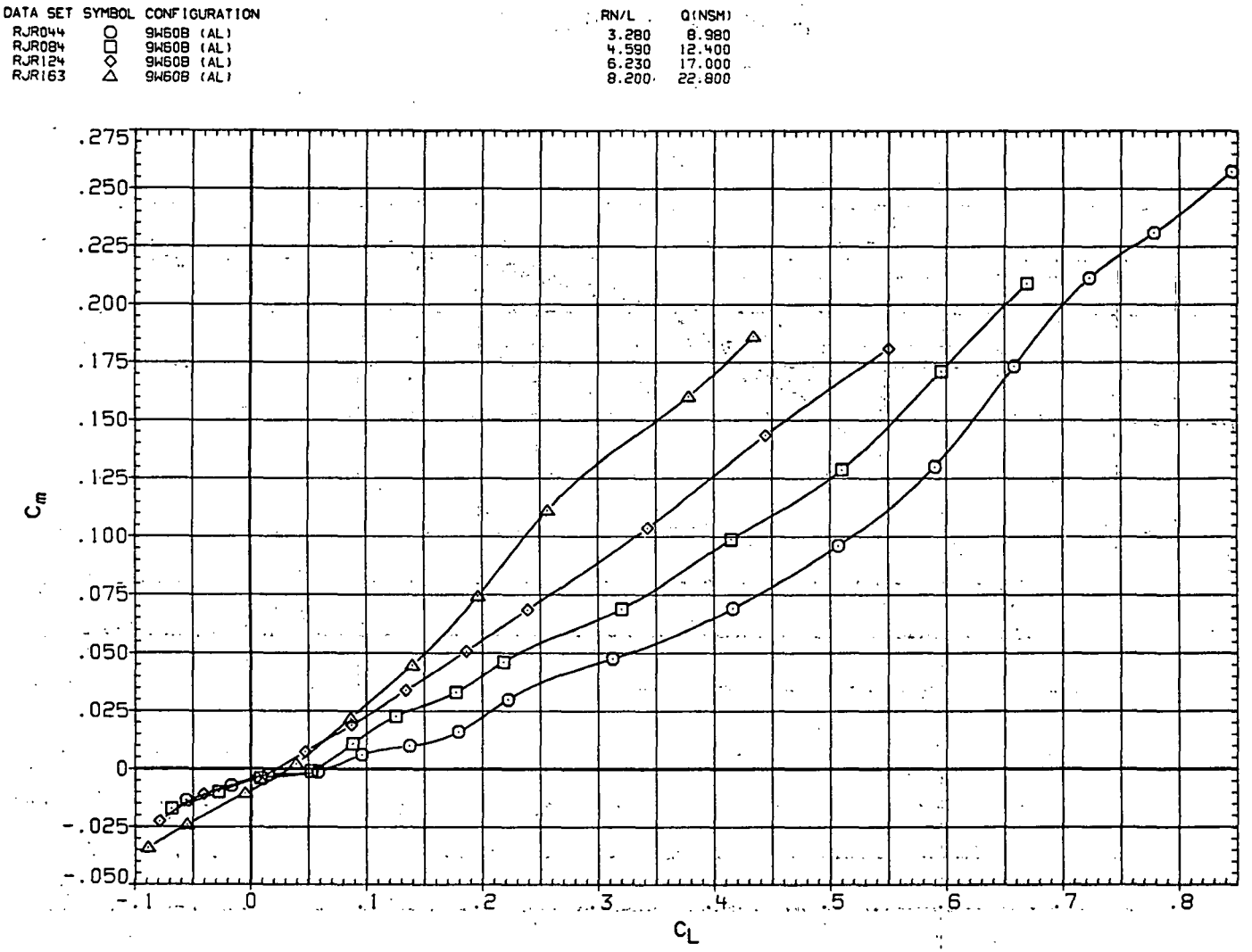

(c) C_m vs C_L.

Figure 41.– Continued.

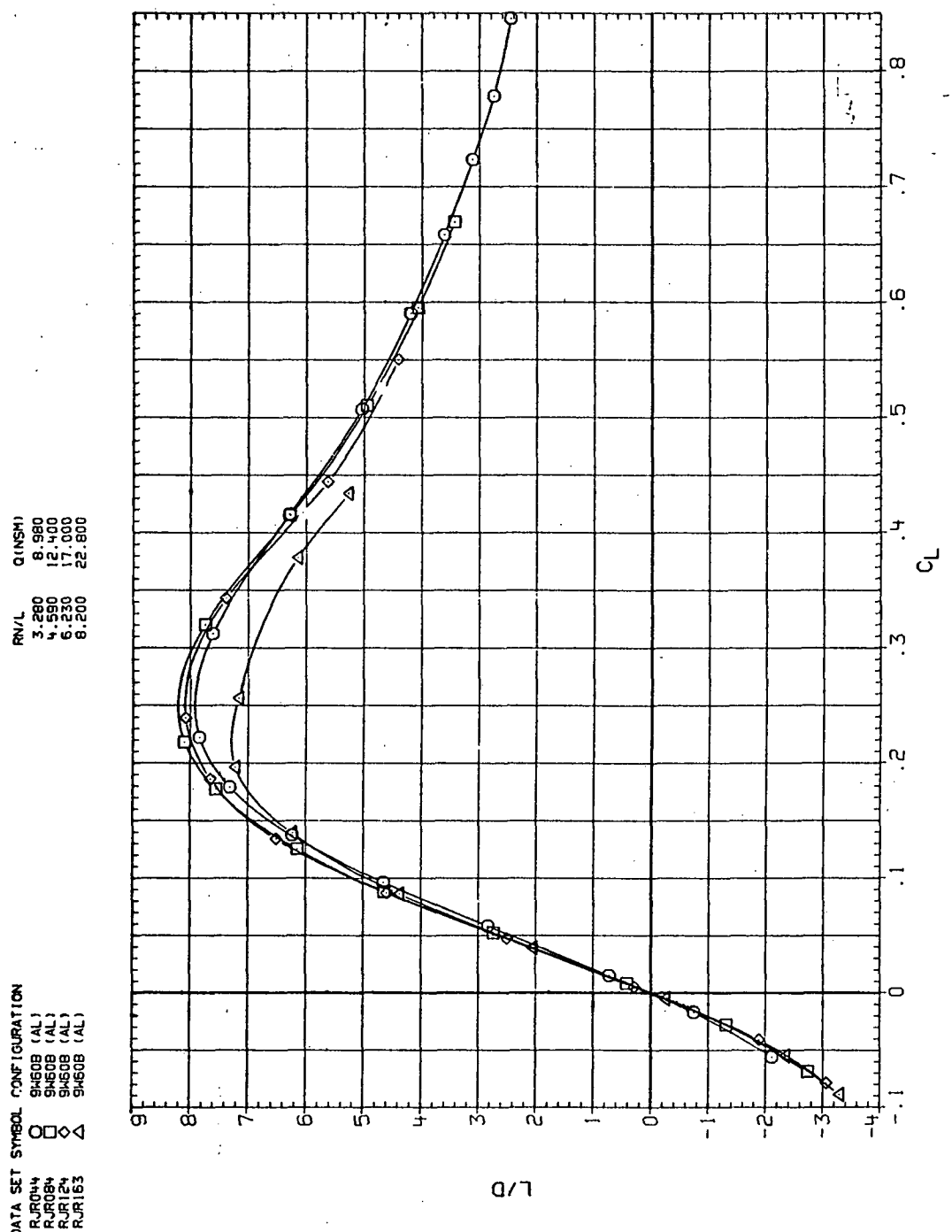

(d) L/D vs C_L.

Figure 41.– Continued.

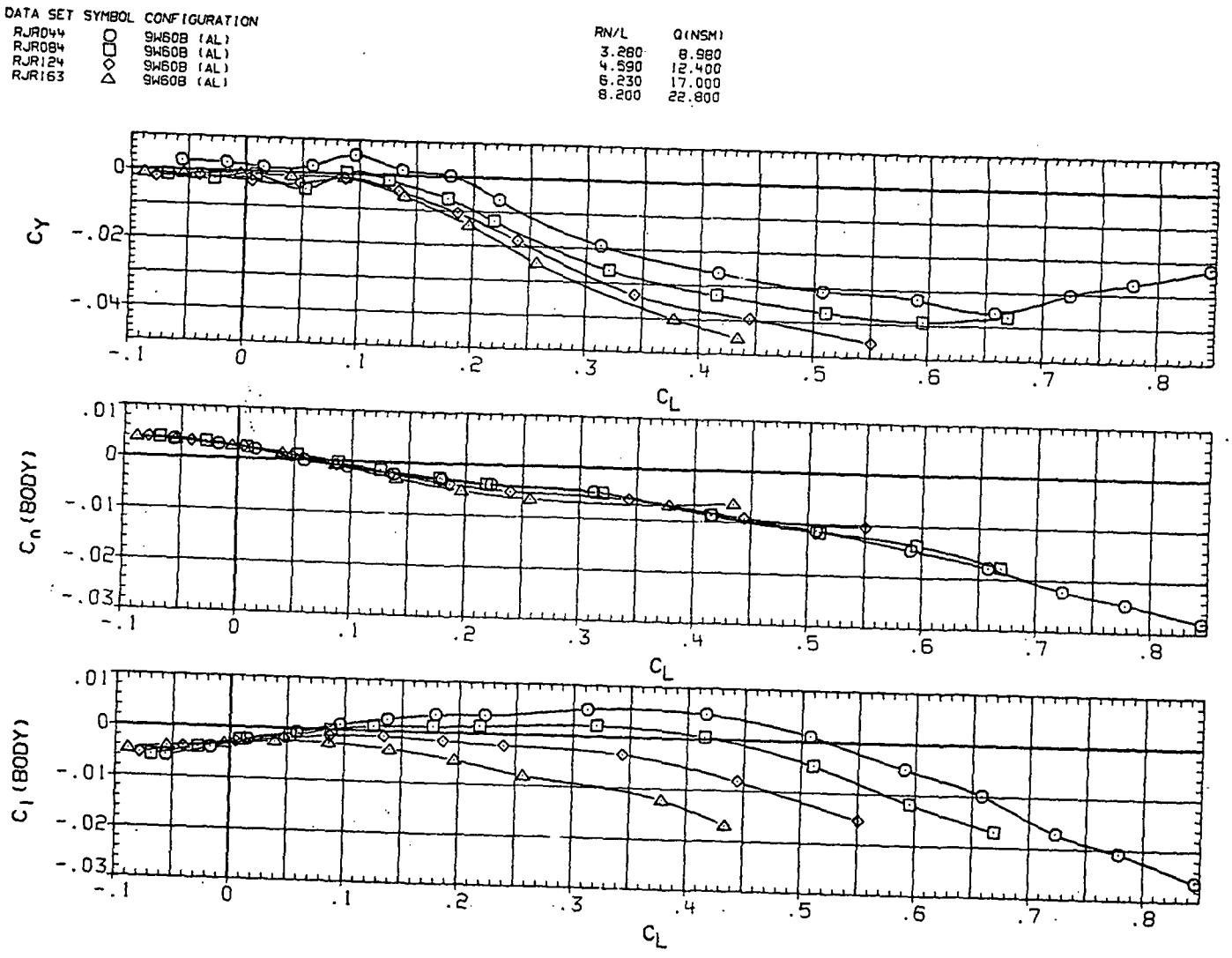

(e) C_Y, C_n and C_ℓ vs C_L.

Figure 41.– Concluded.

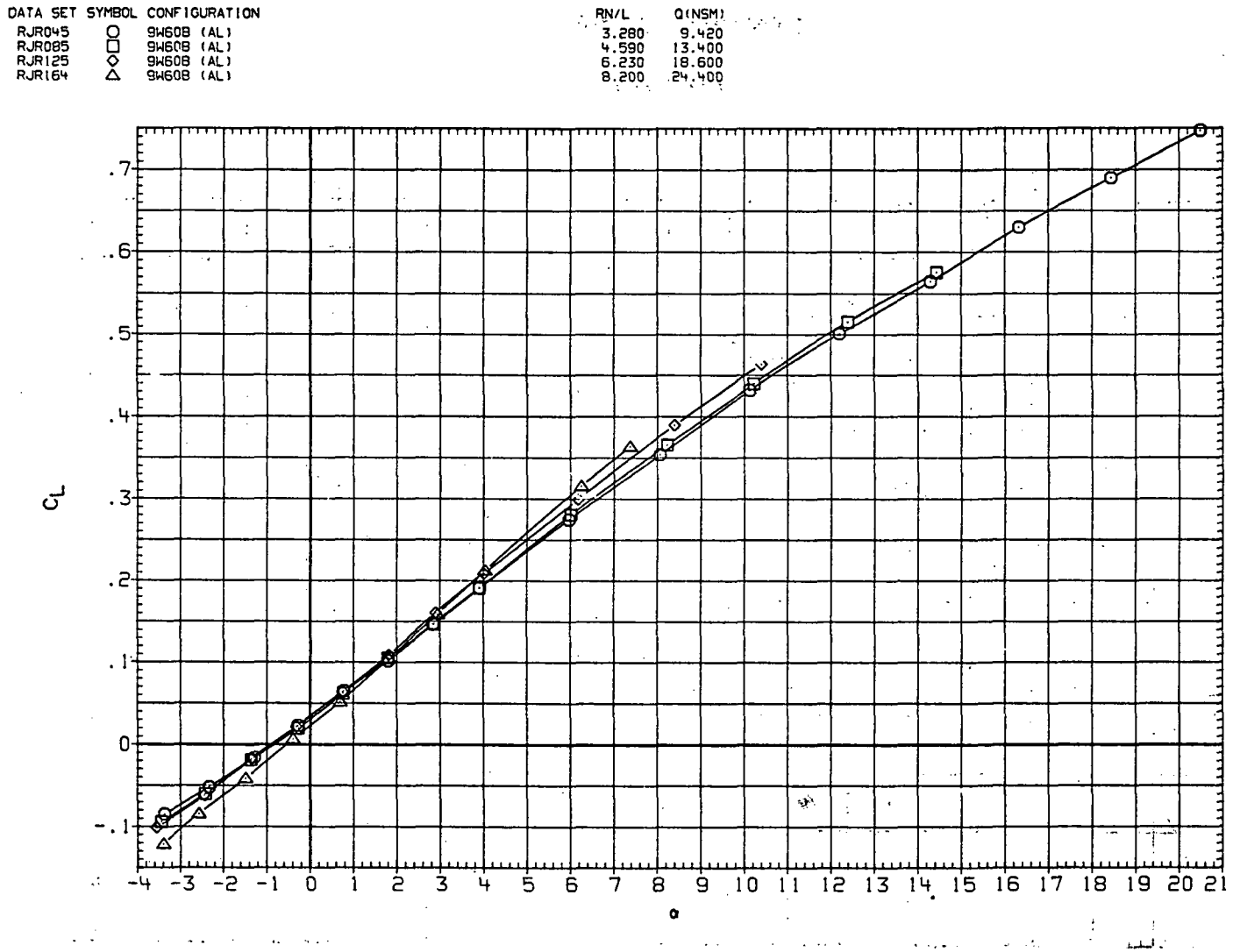

(a) C_L vs α.

Figure 42.– Dynamic-pressure effects on the aerodynamic characteristics of the aluminum trapezoidal oblique wing-body combination ($\Lambda = 60°$, $M = 1.6$ and the modified NACA 65A204 airfoil).

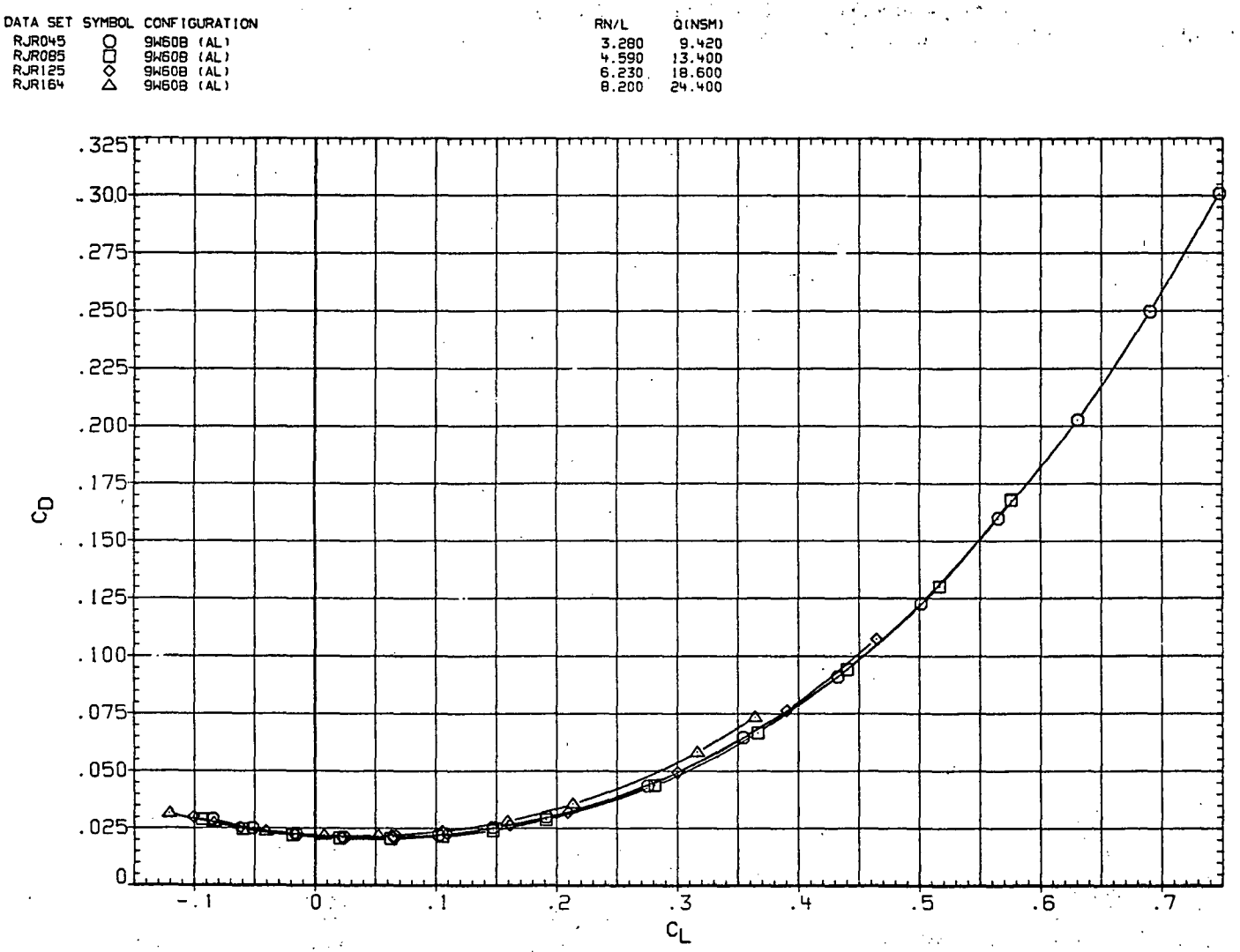

(b) C_D vs C_L.

Figure 42.– Continued.

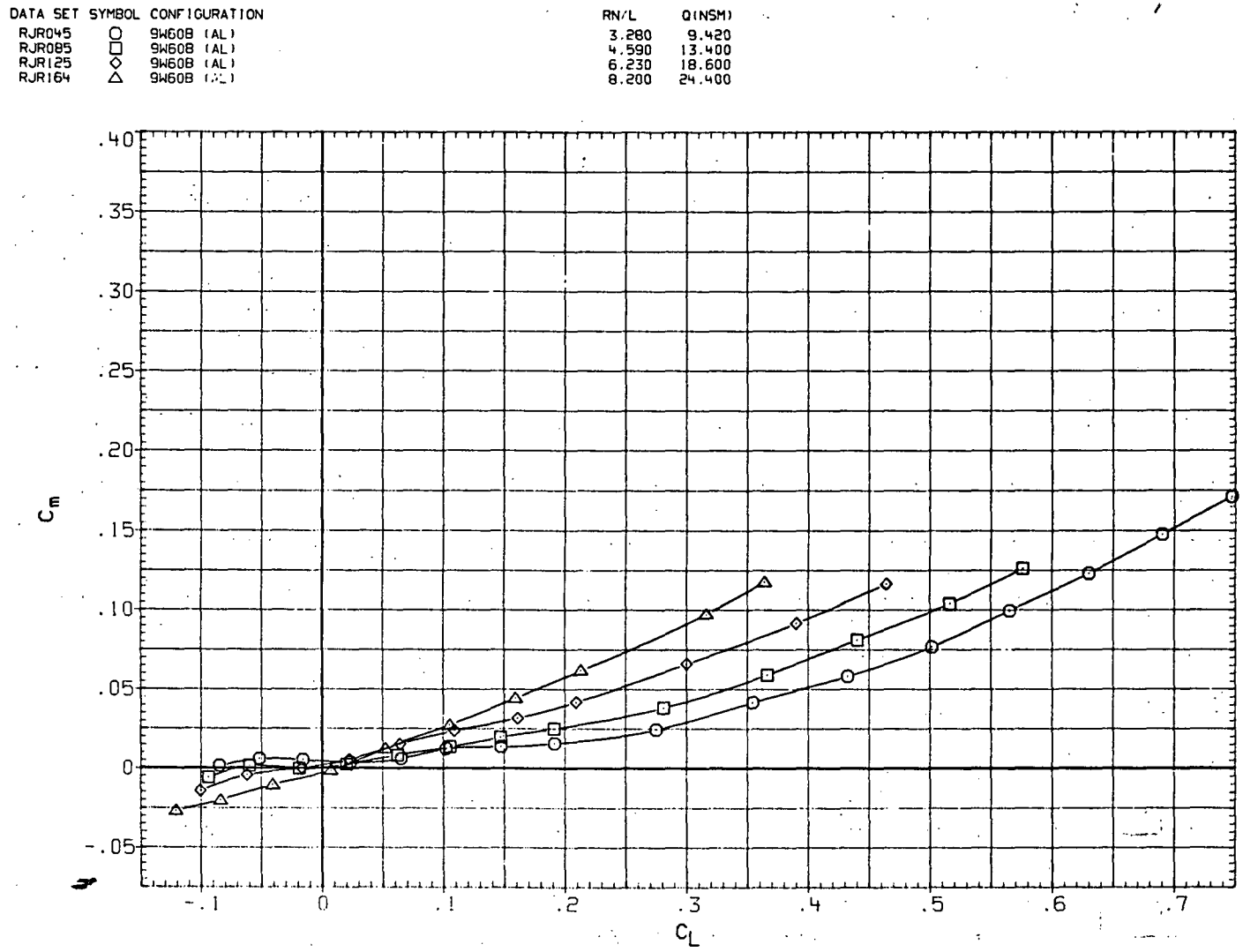

(c) C_m vs C_L.

Figure 42.– Continued.

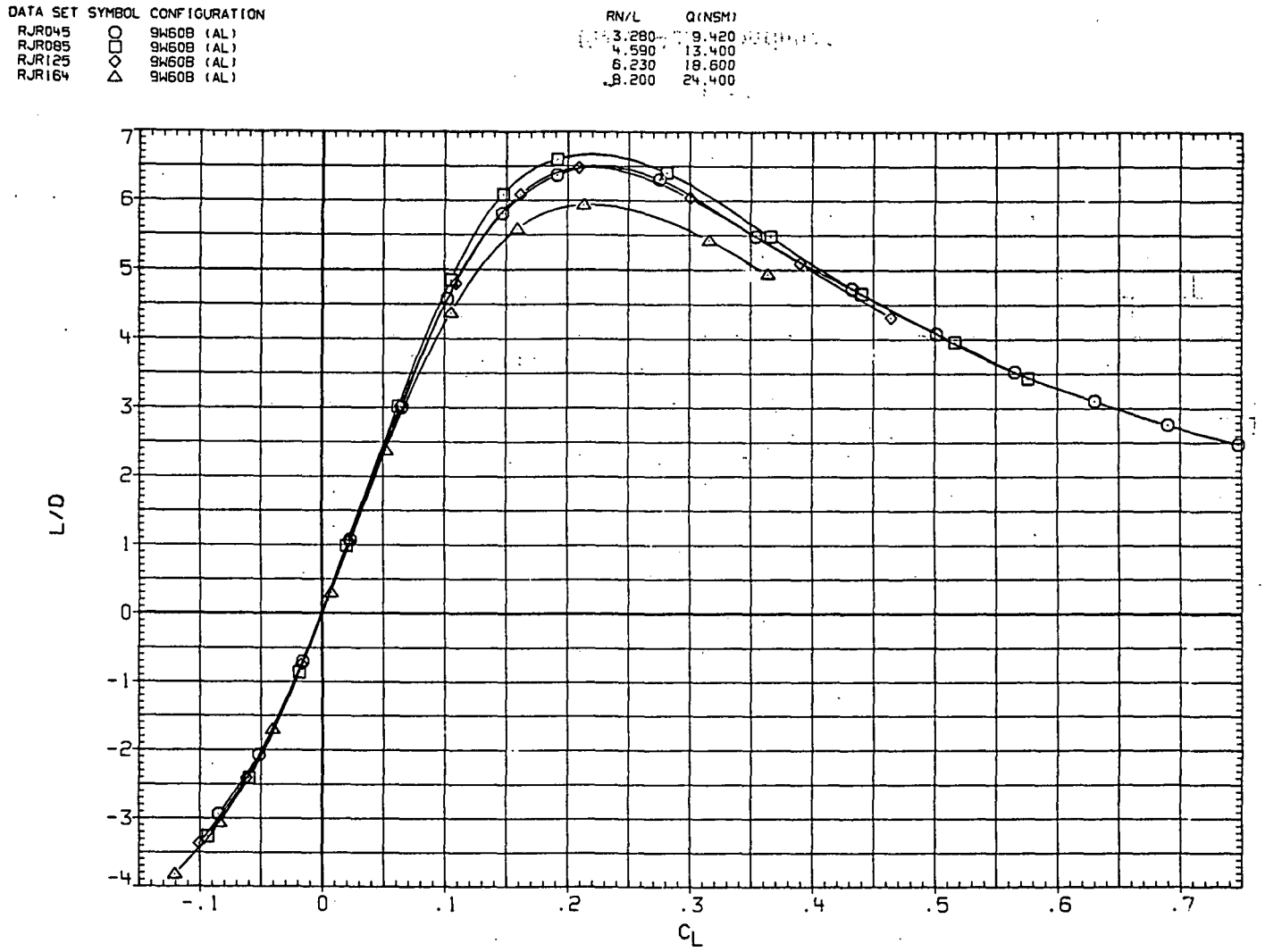

(d) L/D vs C_L.

Figure 42.– Continued.

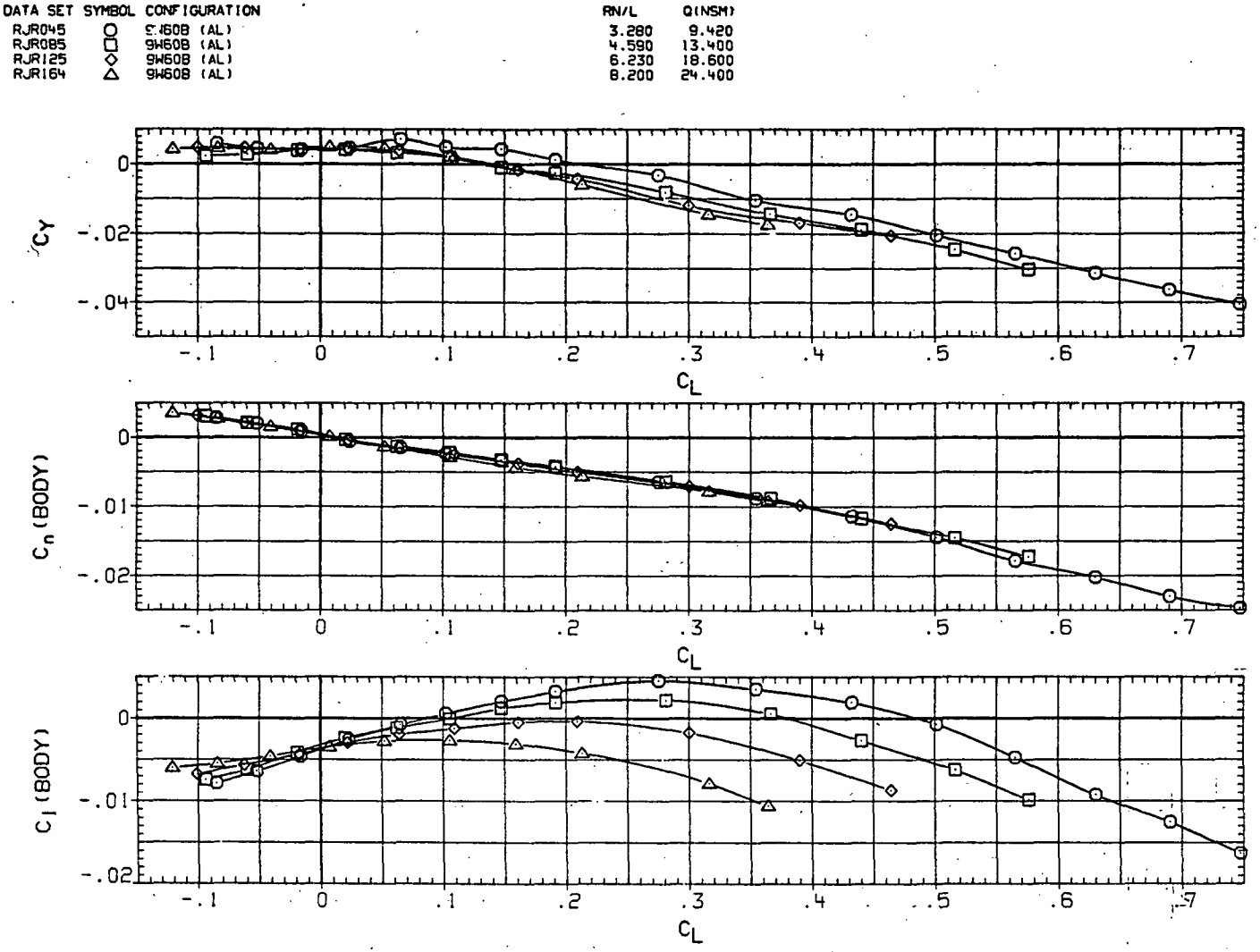

(e) $\bar{C_Y}$, C_n and C_ℓ vs C_L.

Figure 42.– Concluded.

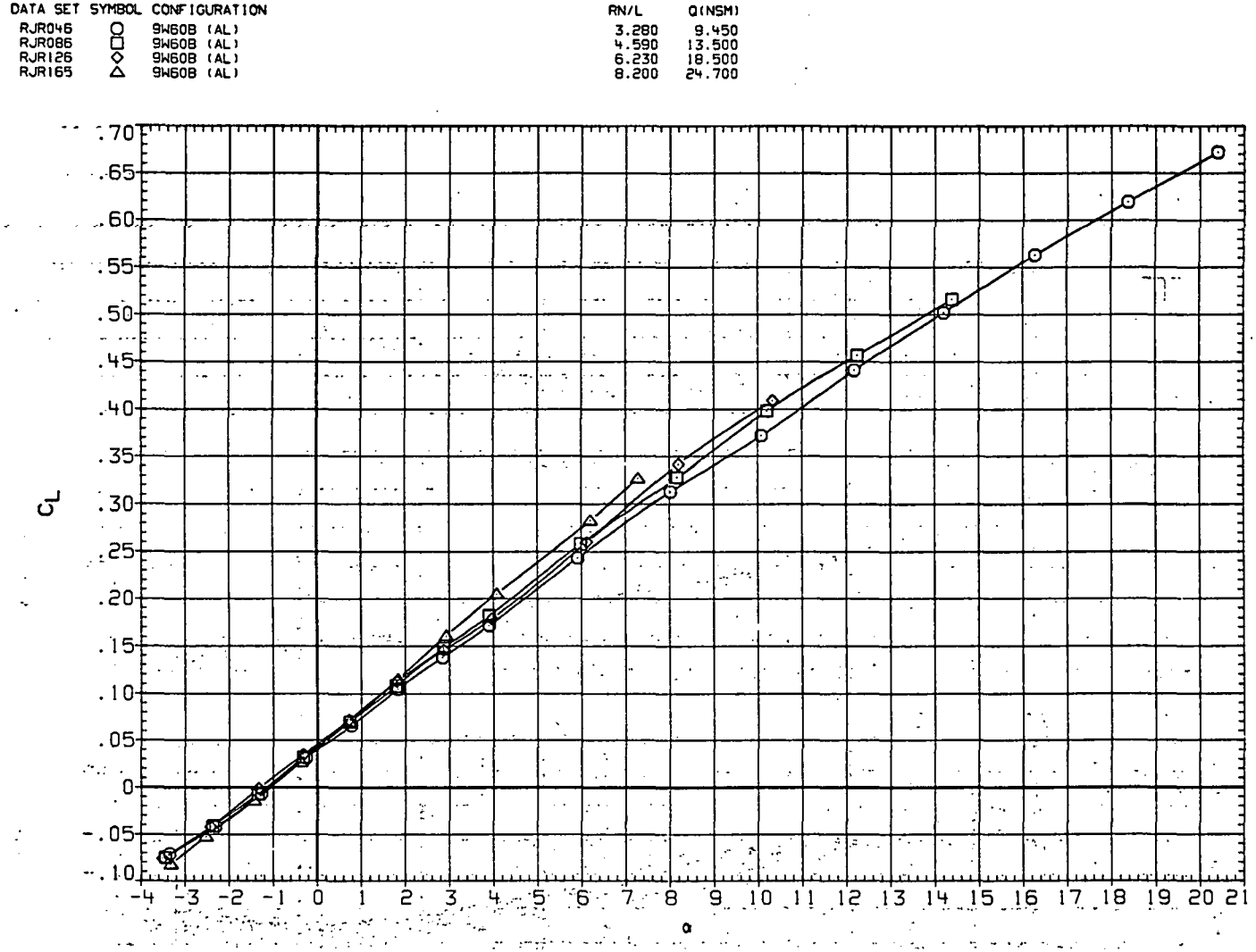

(a) C_L vs α.

Figure 43.– Dynamic-pressure effects on the aerodynamic characteristics of the aluminum trapezoidal oblique wing-body combination ($\Lambda = 60°$, $M = 2.0$ and the modified NACA 65A204 airfoil).

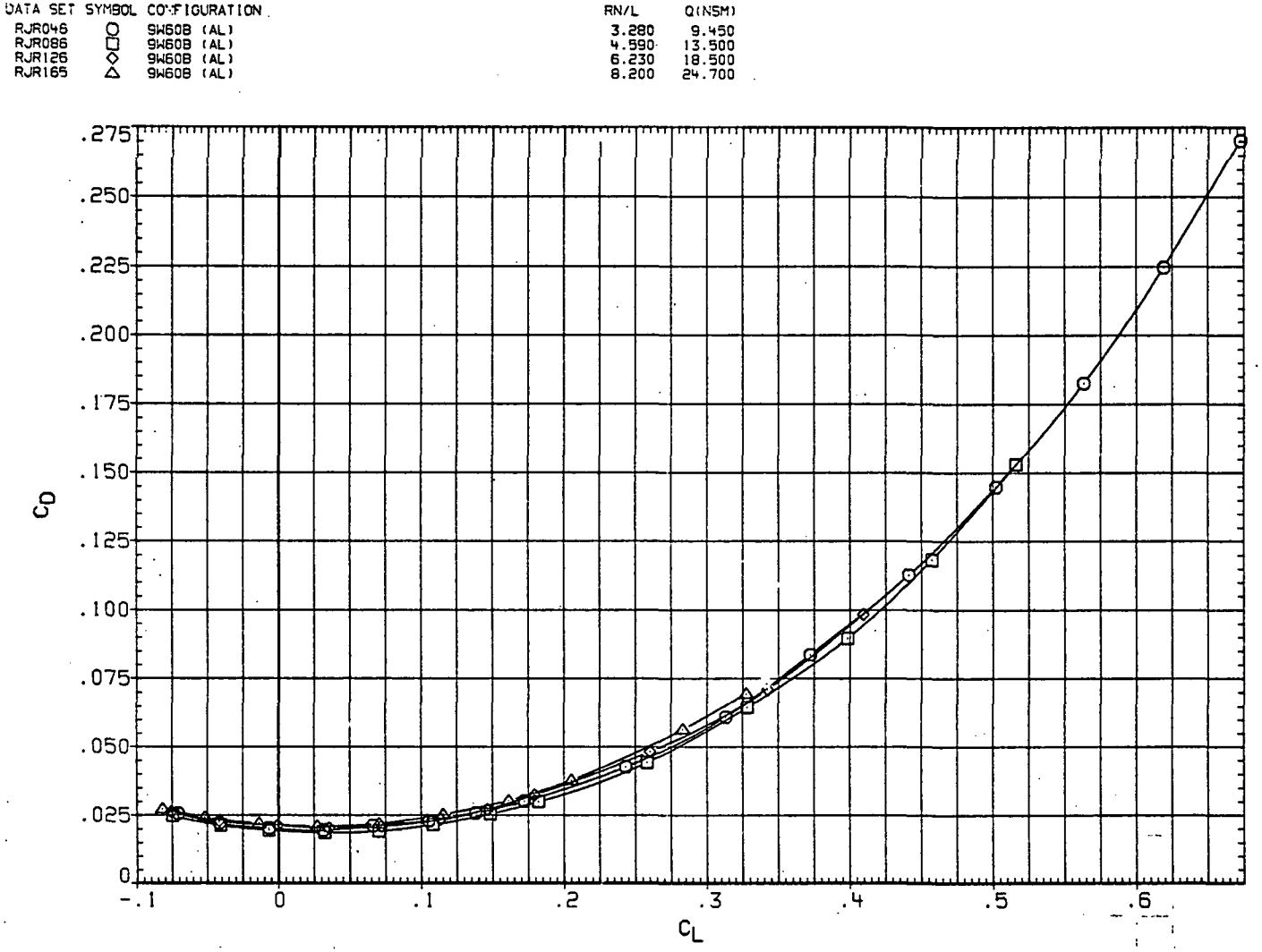

(b) C_D vs C_L.

Figure 43.– Continued.

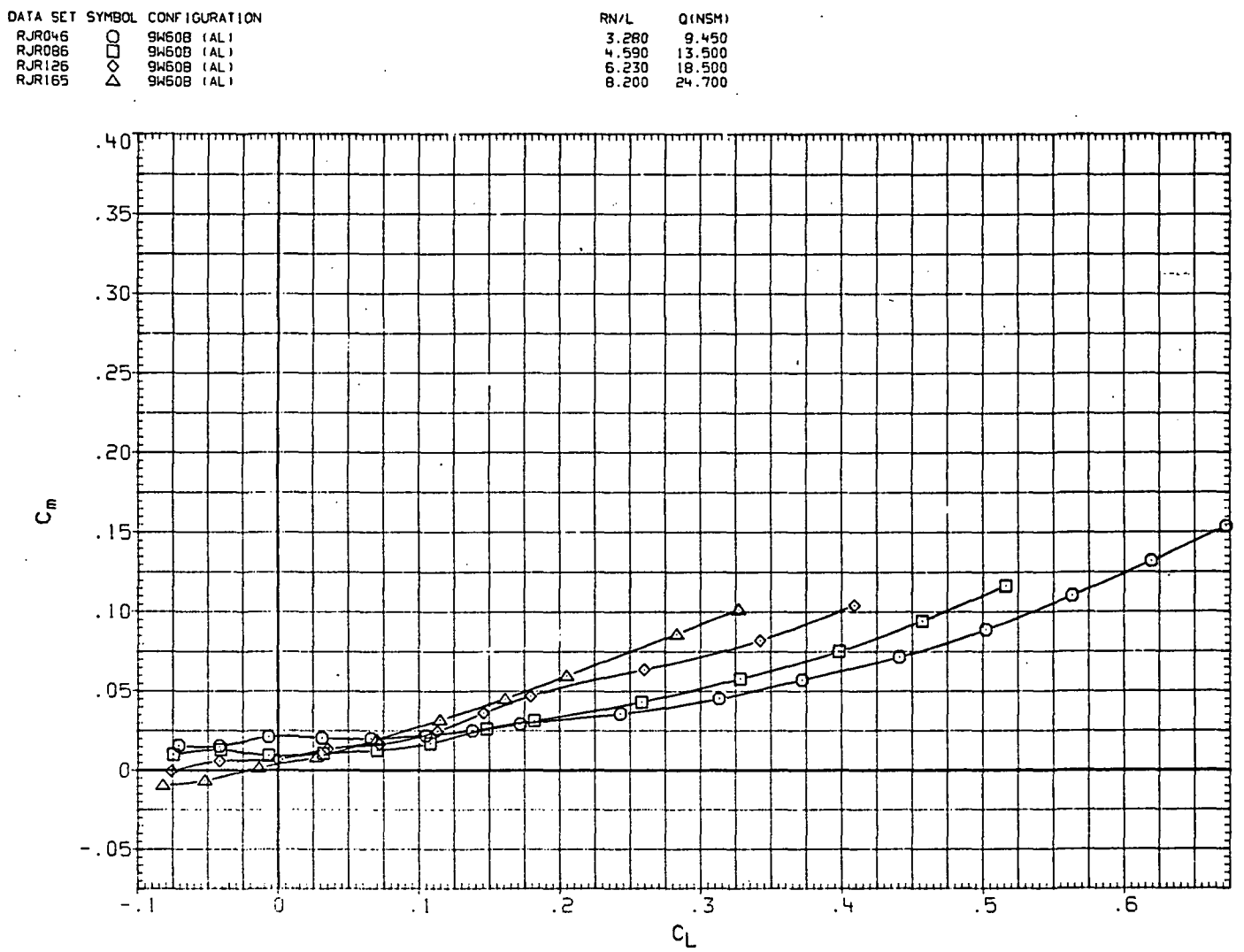

(c) C_m vs C_L.

Figure 43.– Continued.

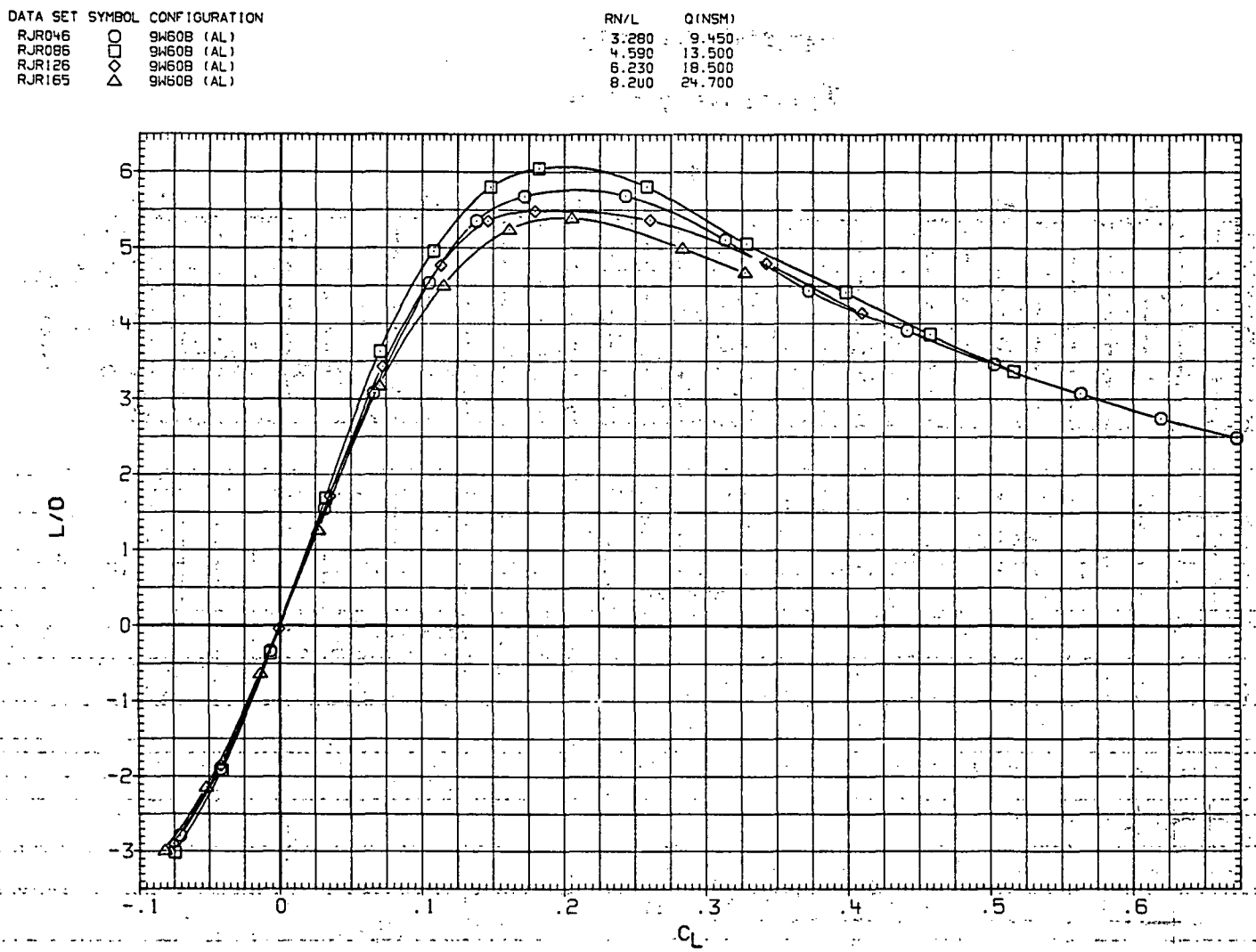

(d) L/D vs C_L.

Figure 43.– Continued.

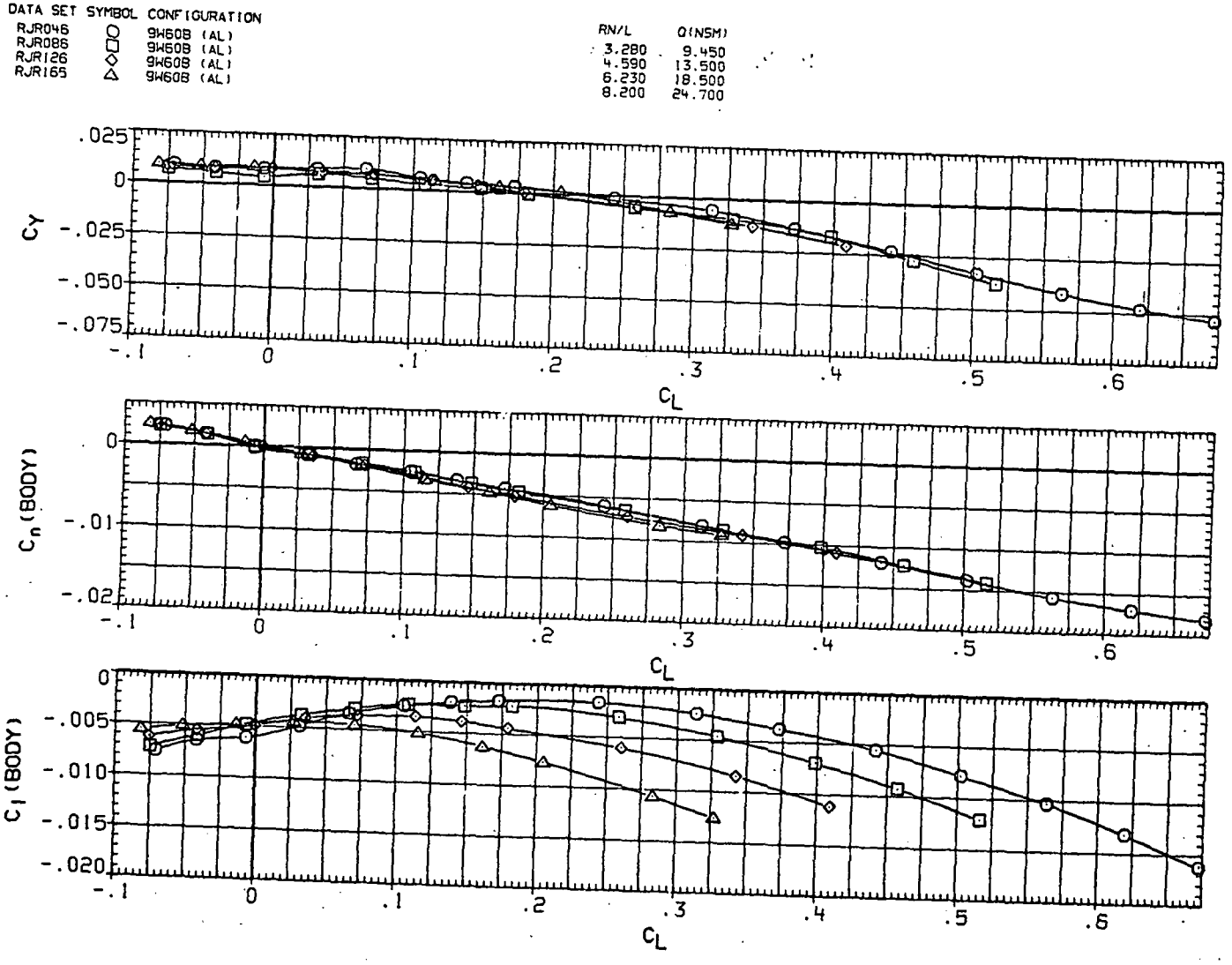

(e) C_Y, C_n and C_ℓ vs C_L.

Figure 43.– Concluded.

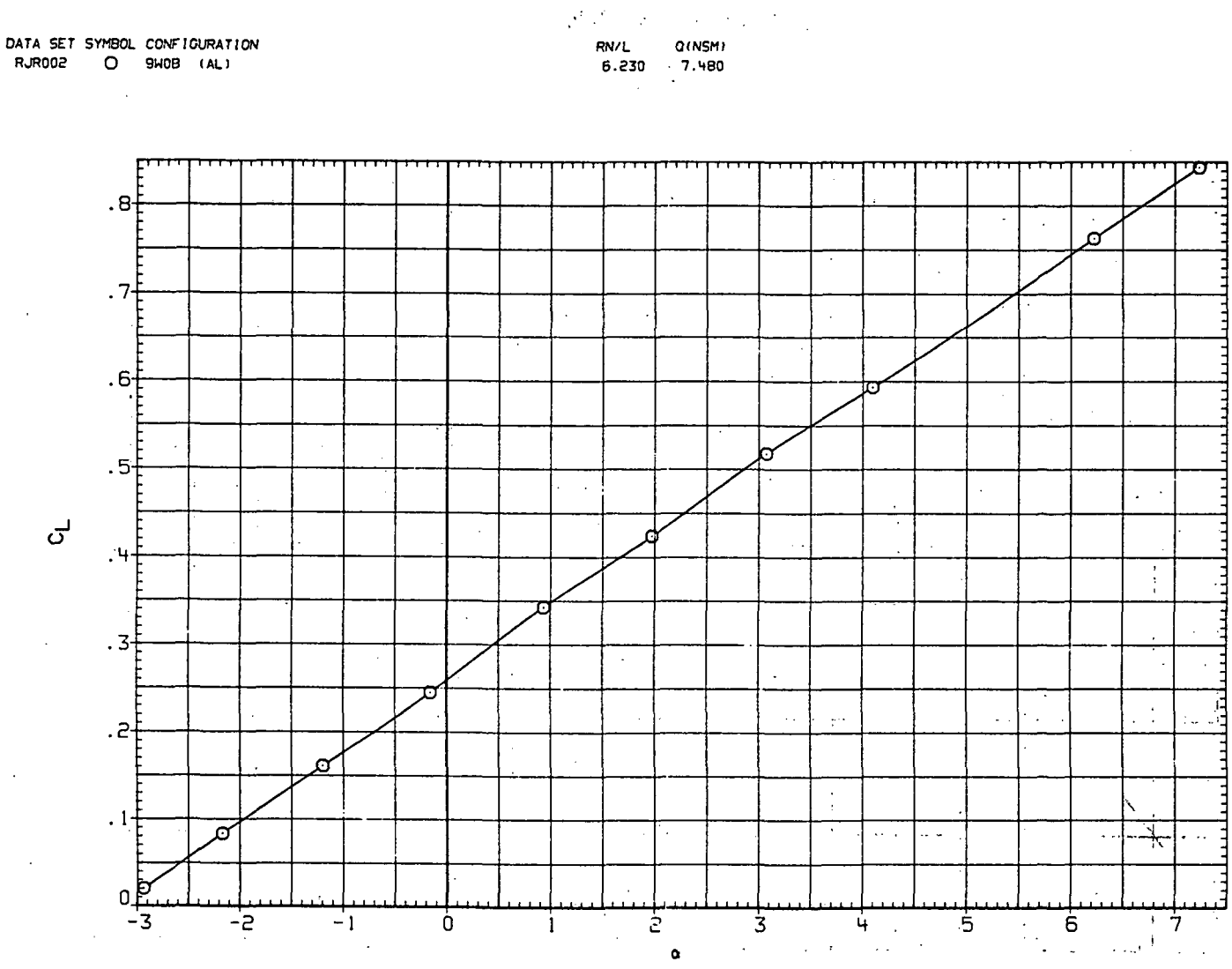

(a) C_L vs α.

Figure 44.– Aerodynamic characteristics of the aluminum trapezoidal oblique wing-body combination ($\Lambda = 0$, $M = 0.4$ and the modified NACA 65A204 airfoil).

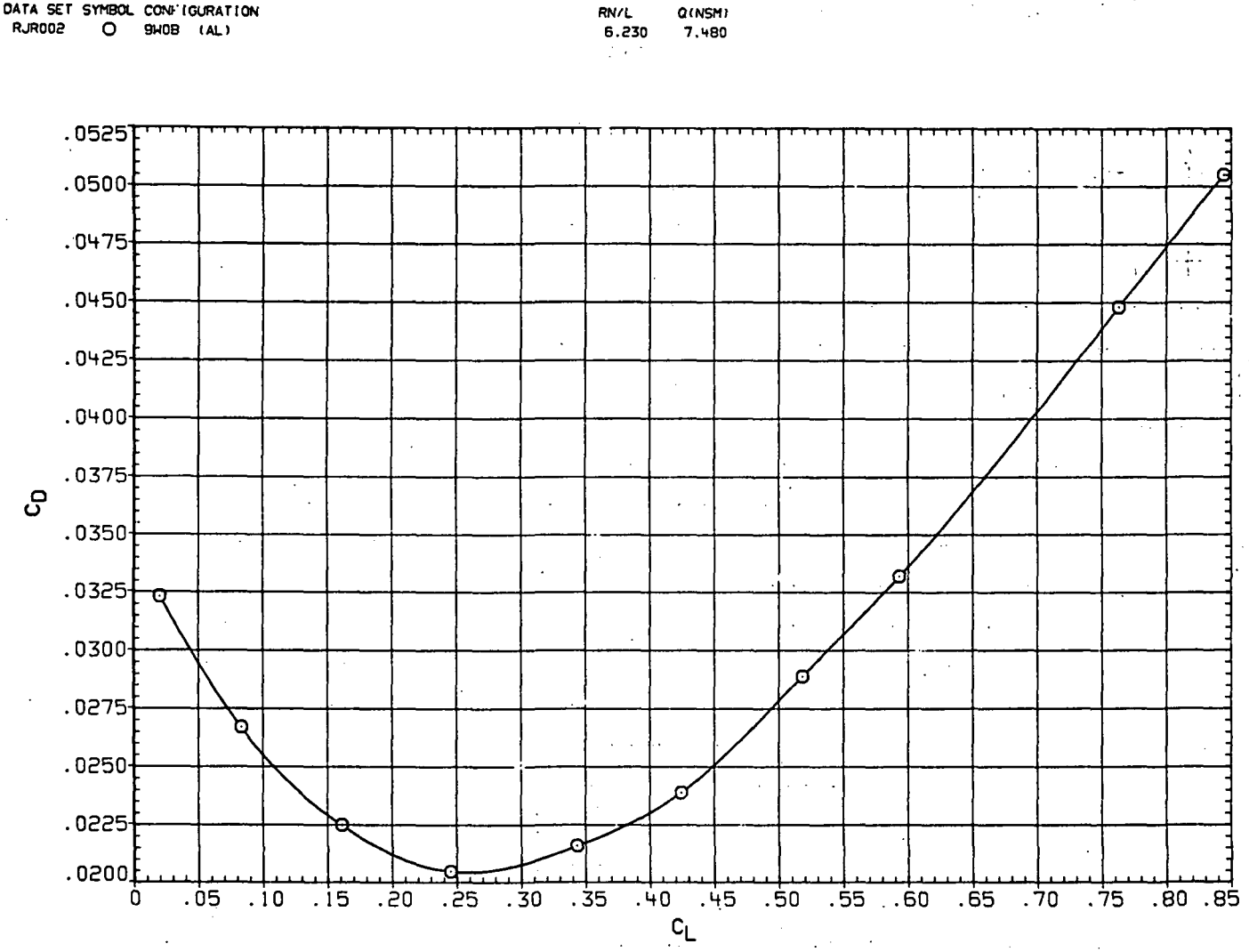

(b) C_D vs C_L.

Figure 44.– Continued.

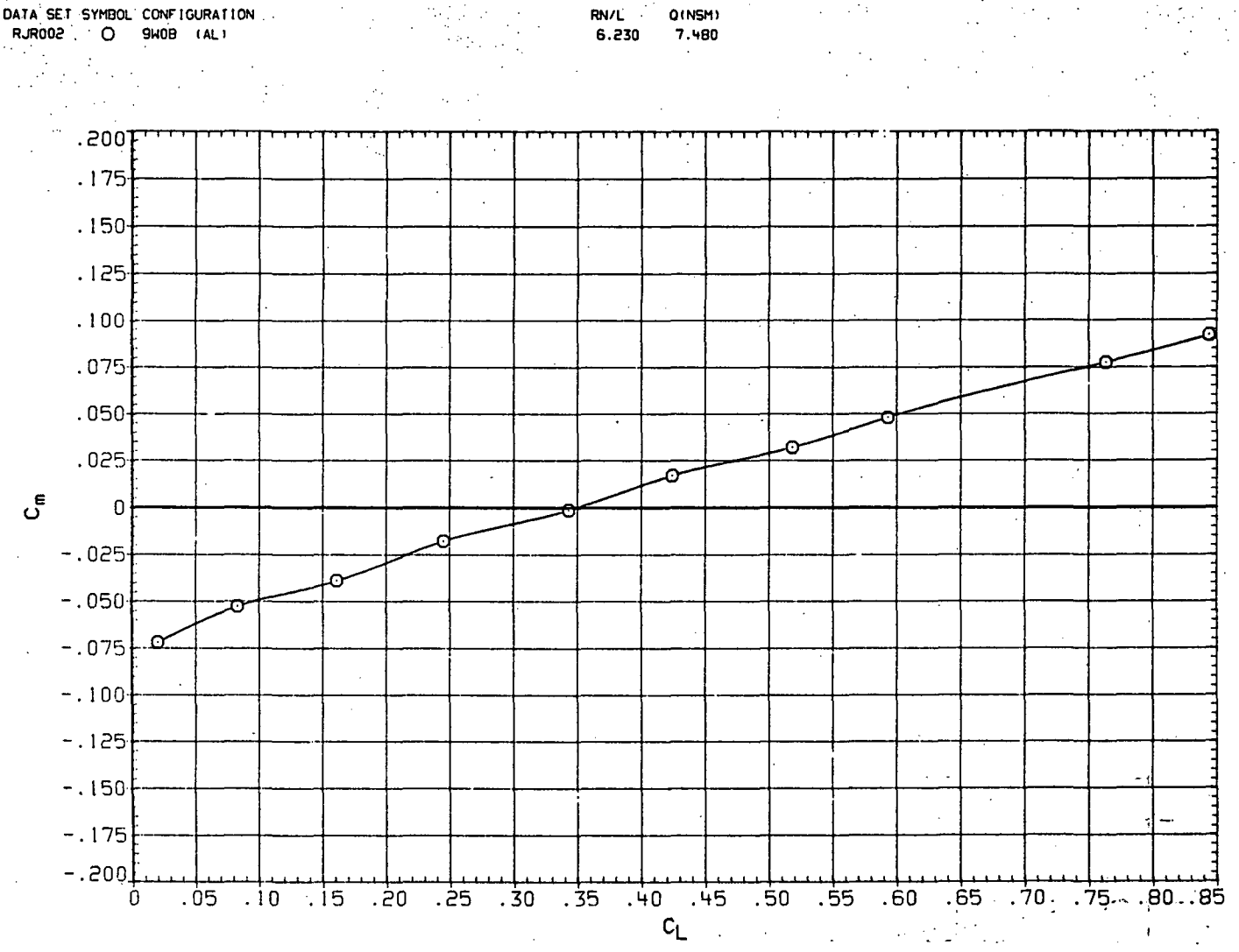

(c) C_m vs C_L.

Figure 44.– Continued.

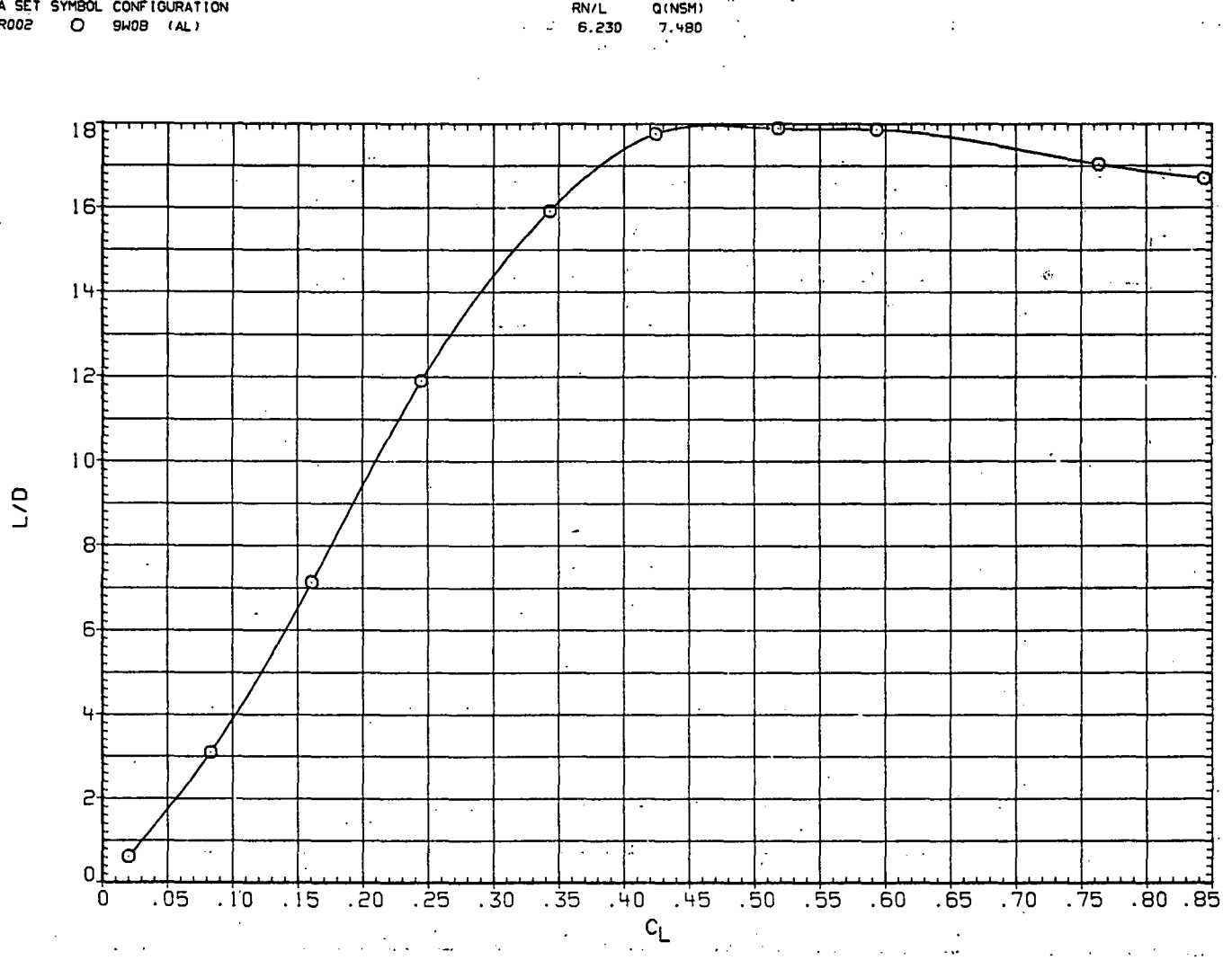

(d) L/D vs C_L.

Figure 44.– Continued.

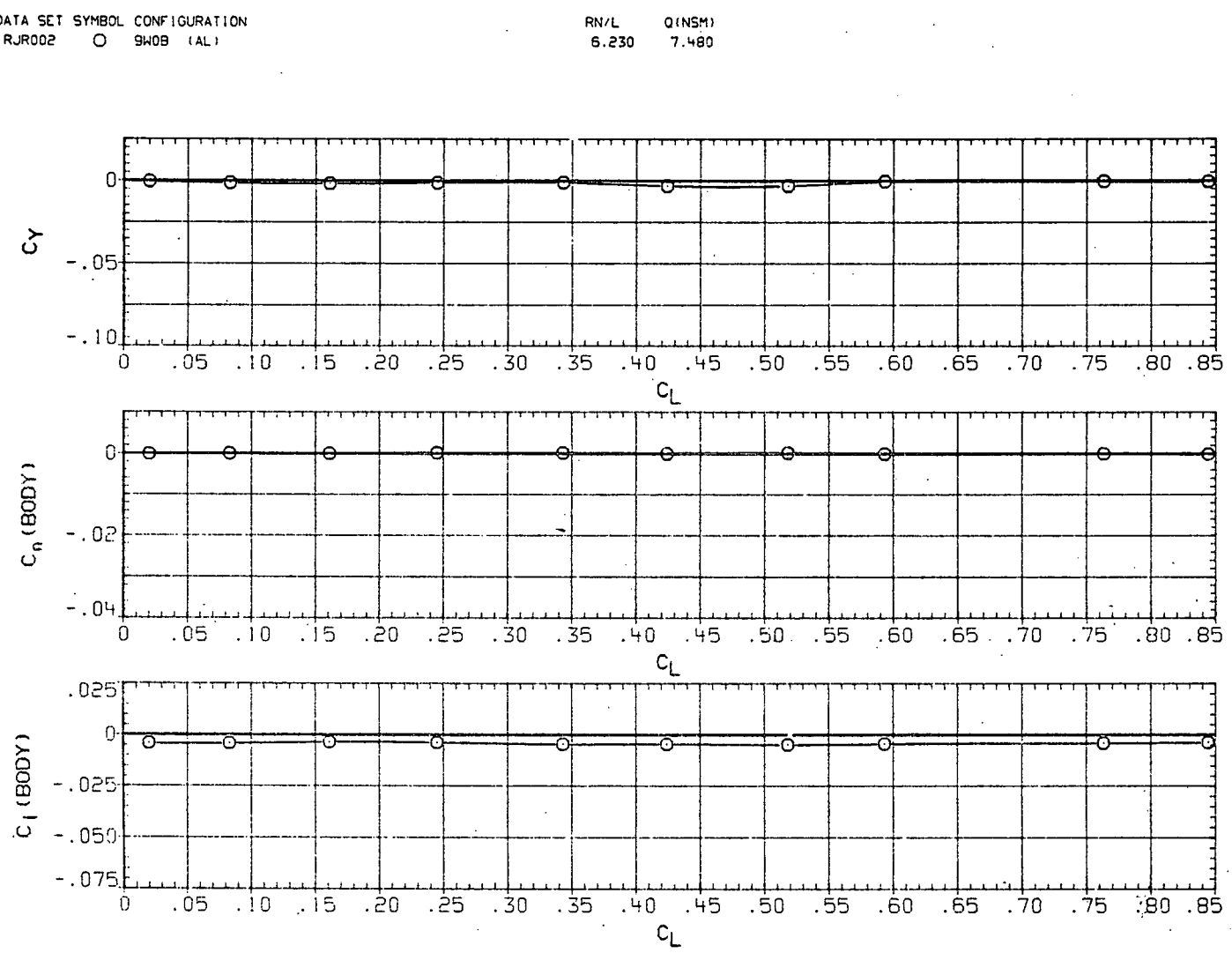

(e) C_Y, C_n and C_ℓ vs C_L.

Figure 44.– Concluded.

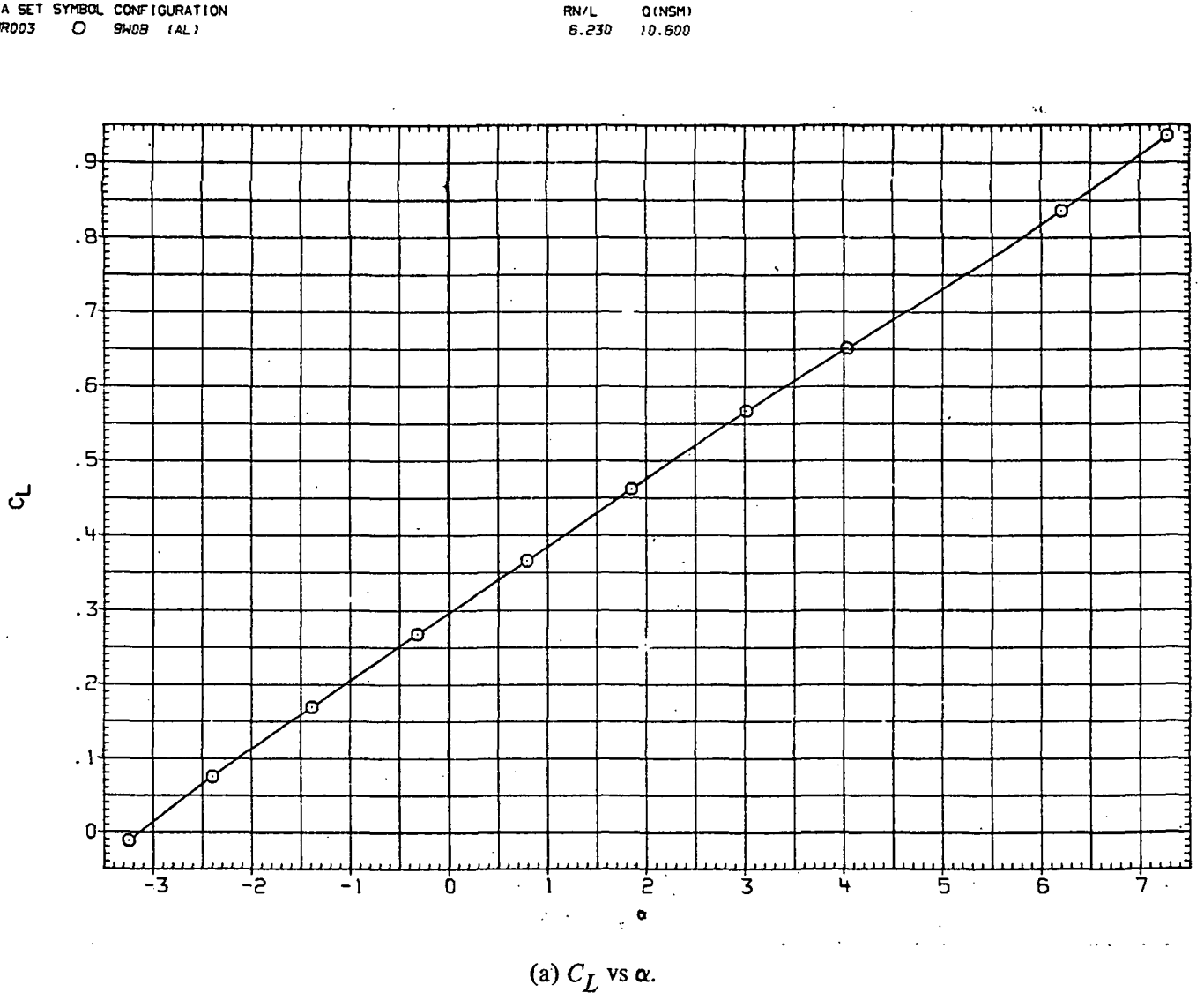

(a) C_L vs α.

Figure 45.– Aerodynamic characteristics of the aluminum trapezoidal oblique wing-body combination ($\Lambda = 0$, $M = 0.6$ and the modified NACA 65A204 airfoil).

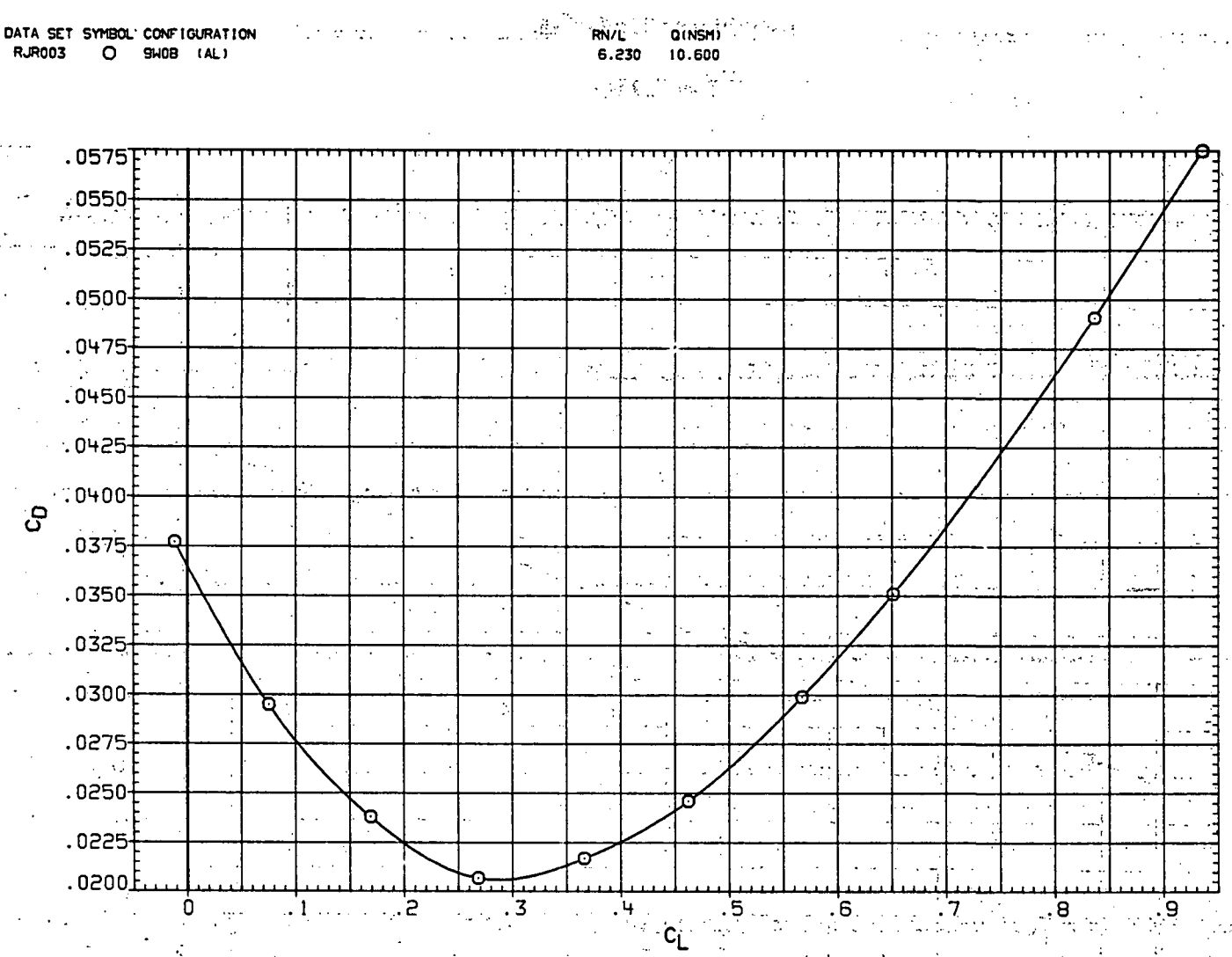

(b) C_D vs C_L.

Figure 45.– Continued.

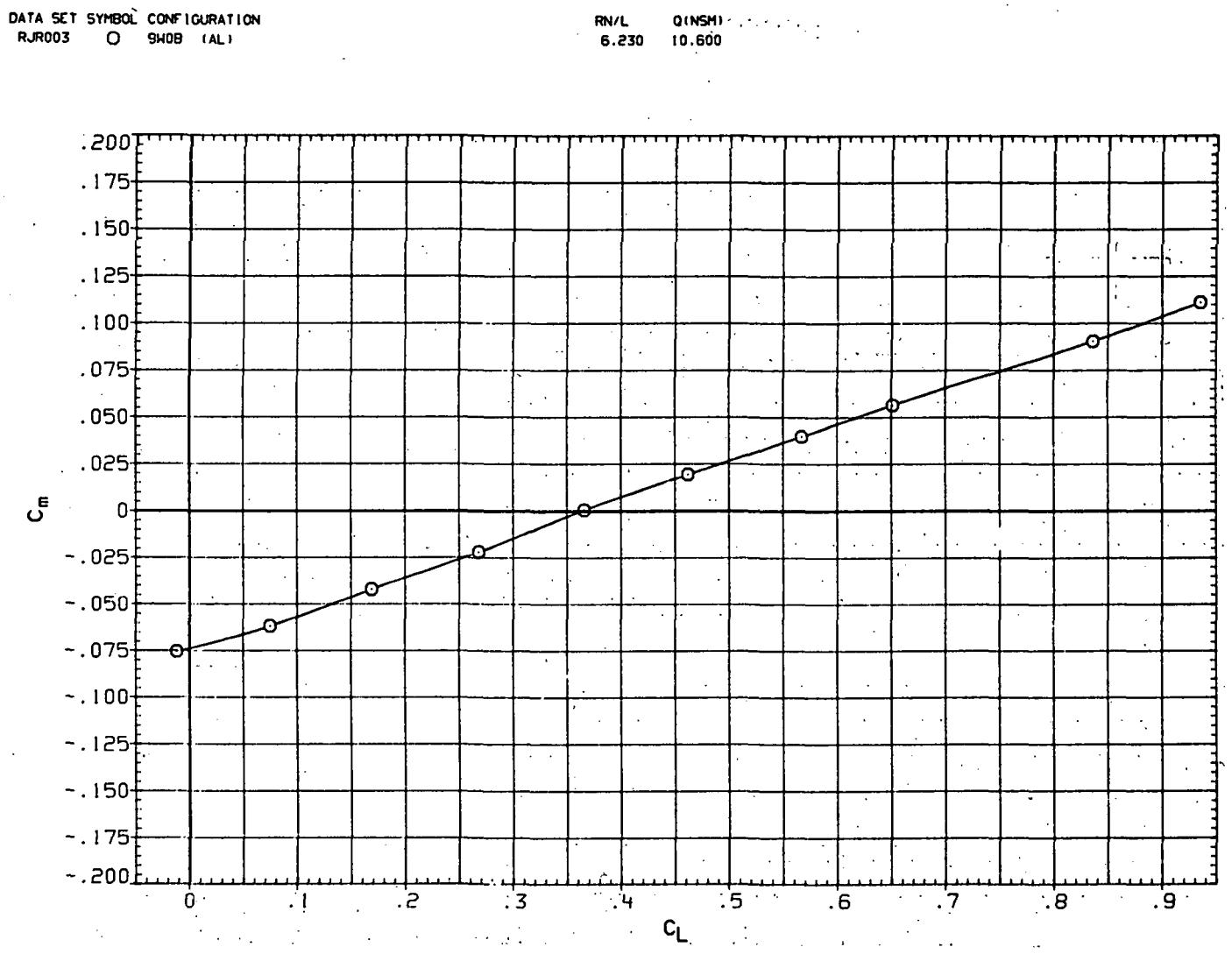

(c) C_m vs C_L.

Figure 45.– Continued.

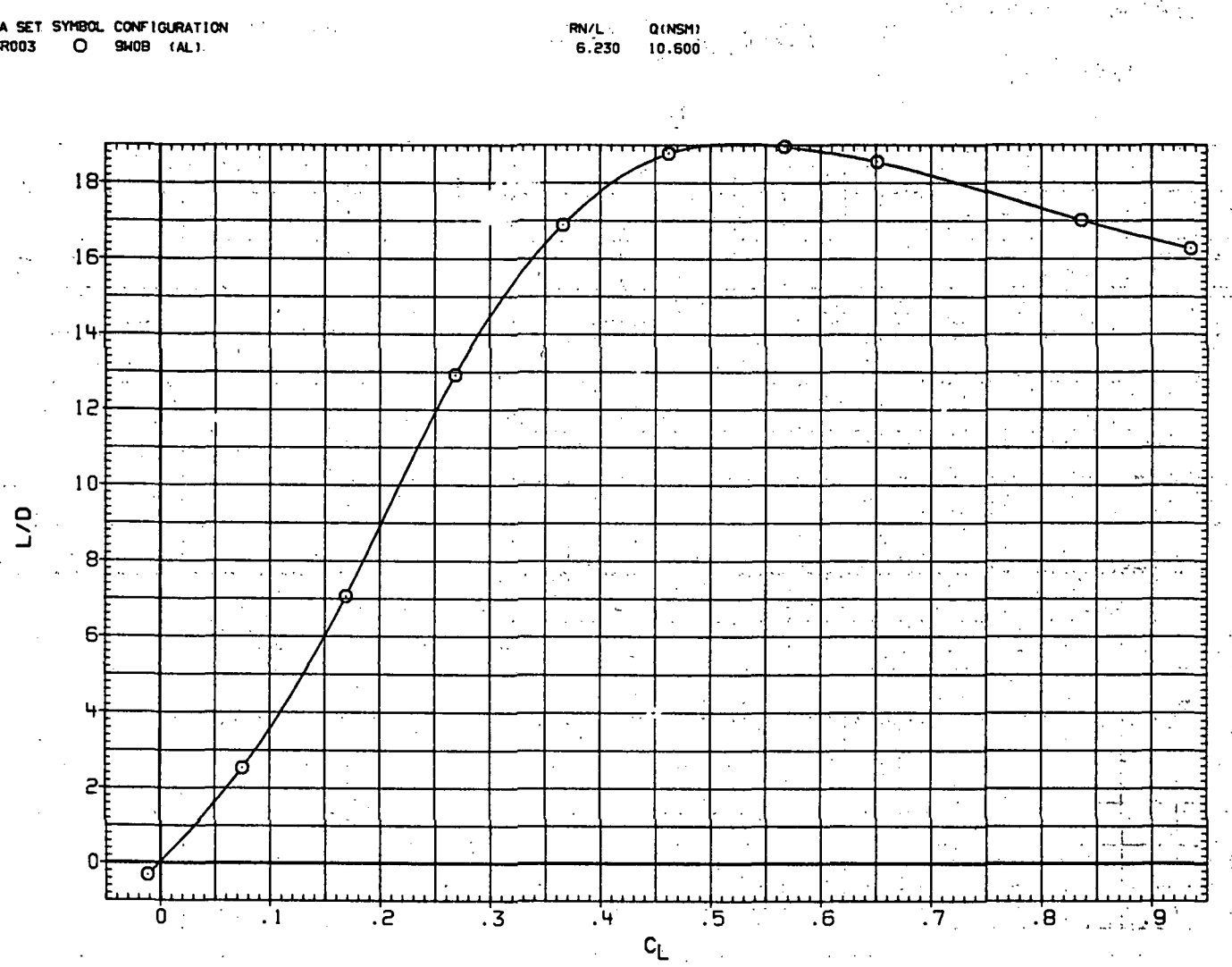

(d) L/D vs C_L.

Figure 45.– Continued.

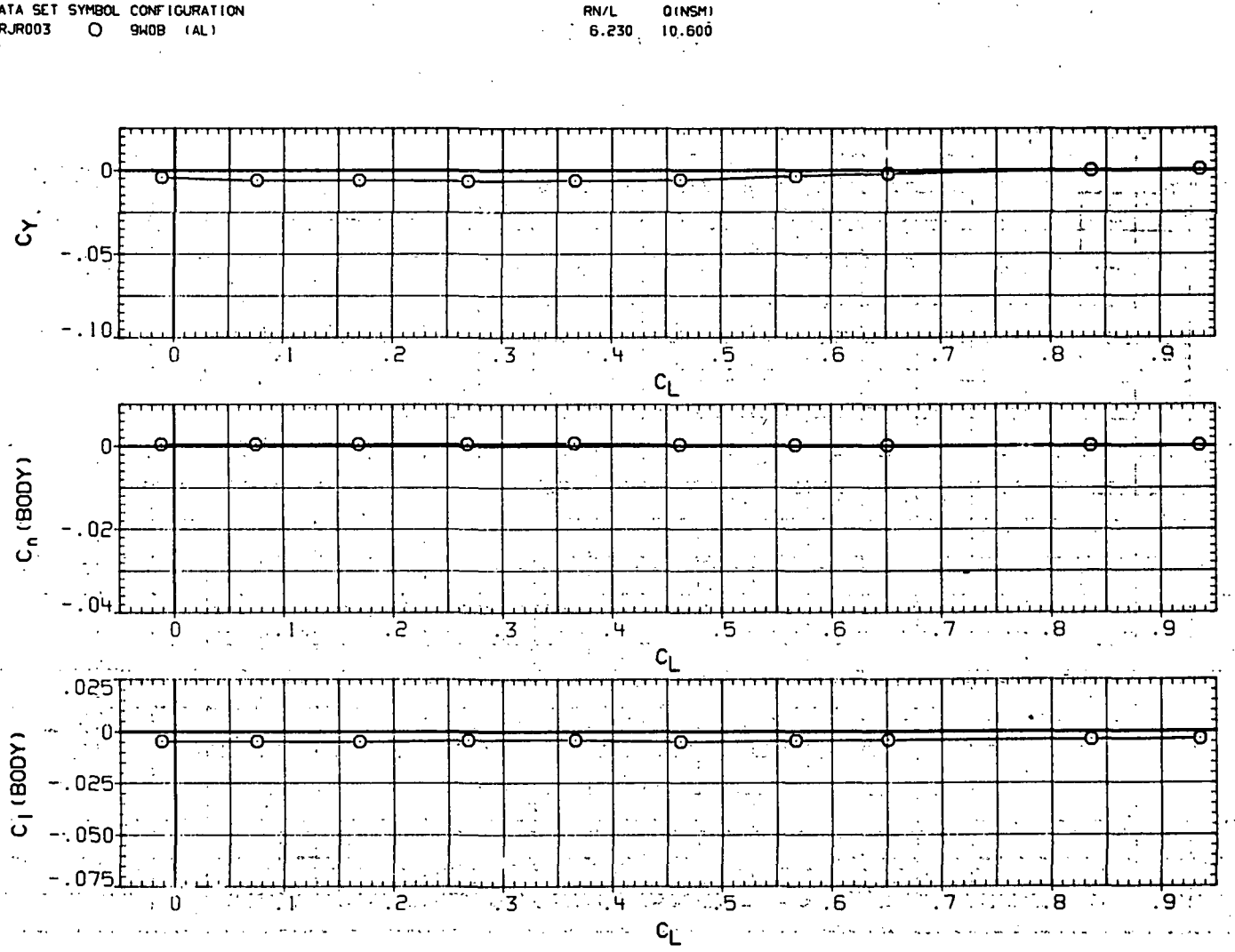

(e) C_Y, C_n and C_ℓ vs C_L.

Figure 45.– Concluded.

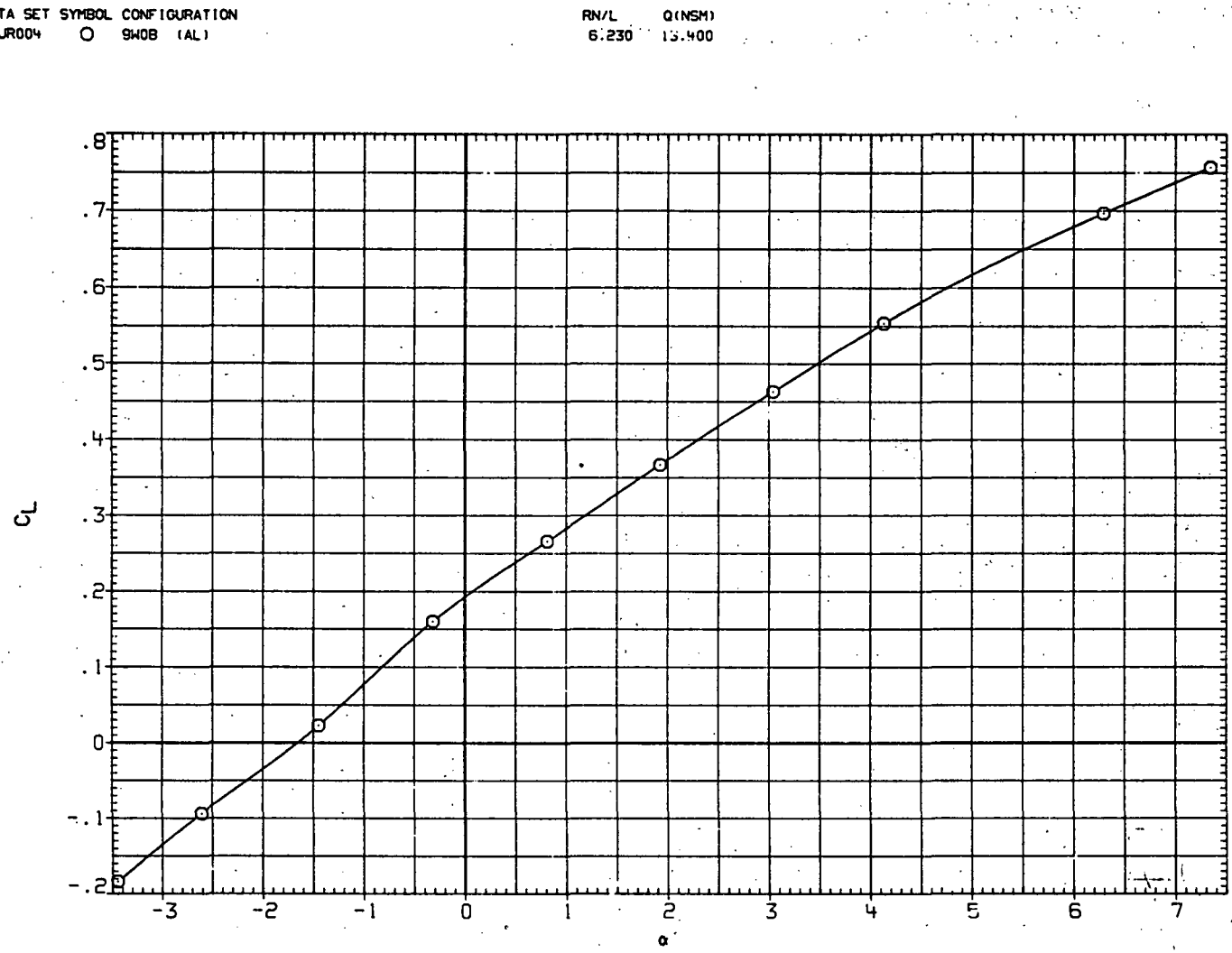

(a) C_L vs α.

Figure 46.– Aerodynamic characteristics of the aluminum trapezoidal oblique wing-body combination ($\Lambda = 0$, $M = 0.8$ and the modified NACA 65A204 airfoil).

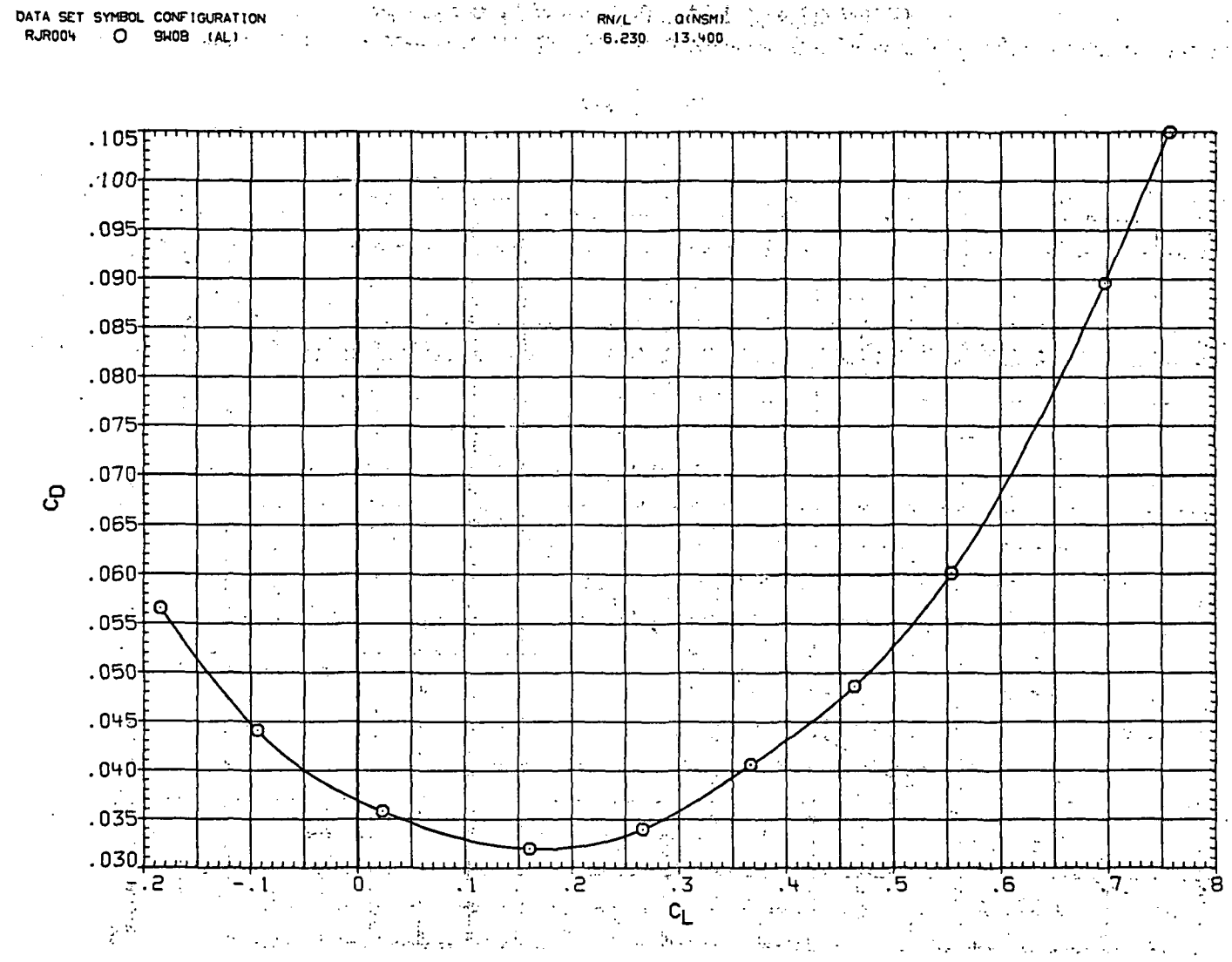

(b) C_D vs C_L.

Figure 46.– Continued.

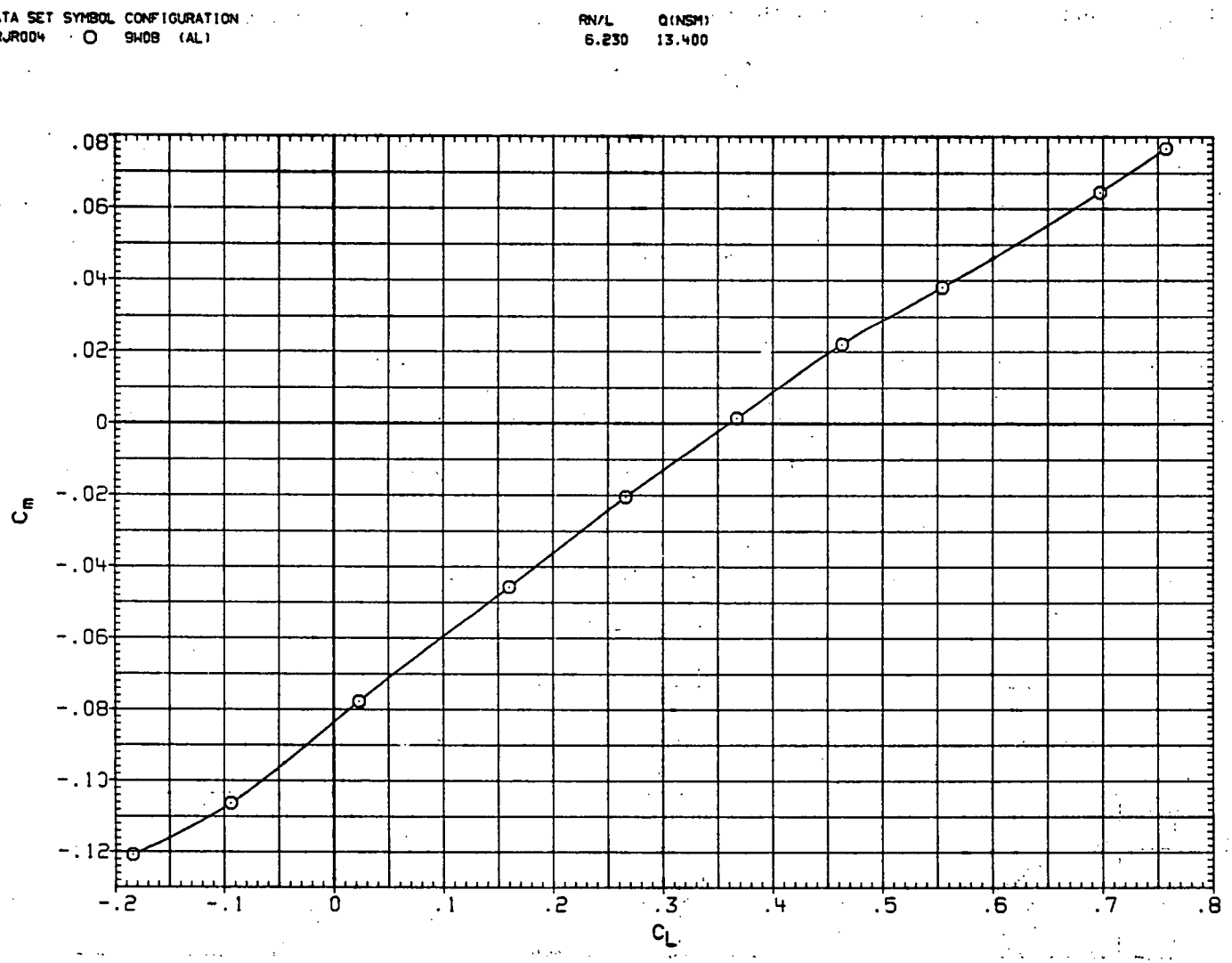

(c) C_m vs C_L.

Figure 46.– Continued.

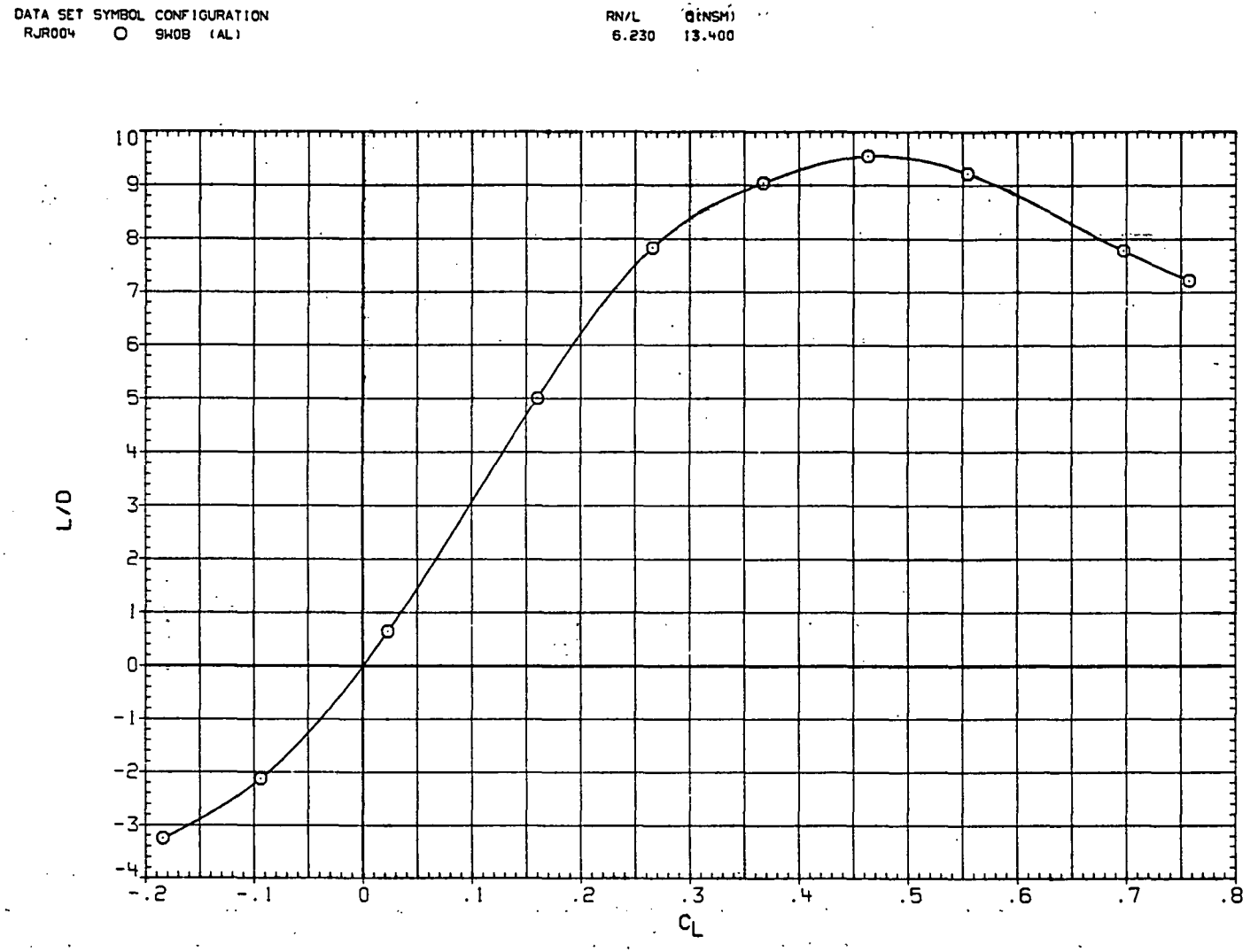

(d) L/D vs C_L.

Figure 46.– Continued.

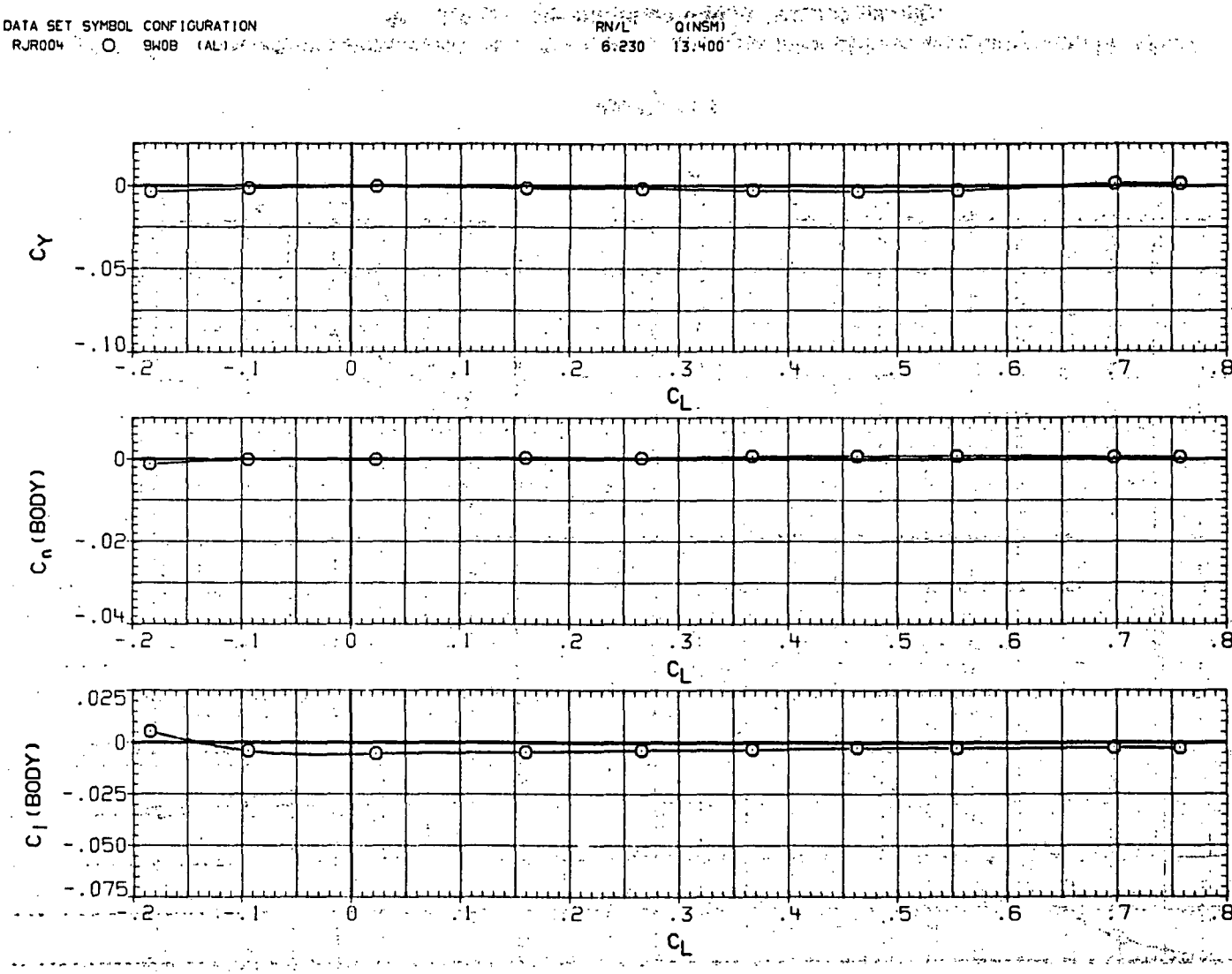

(e) C_Y, C_n and C_ℓ vs C_L.

Figure 46.– Concluded.

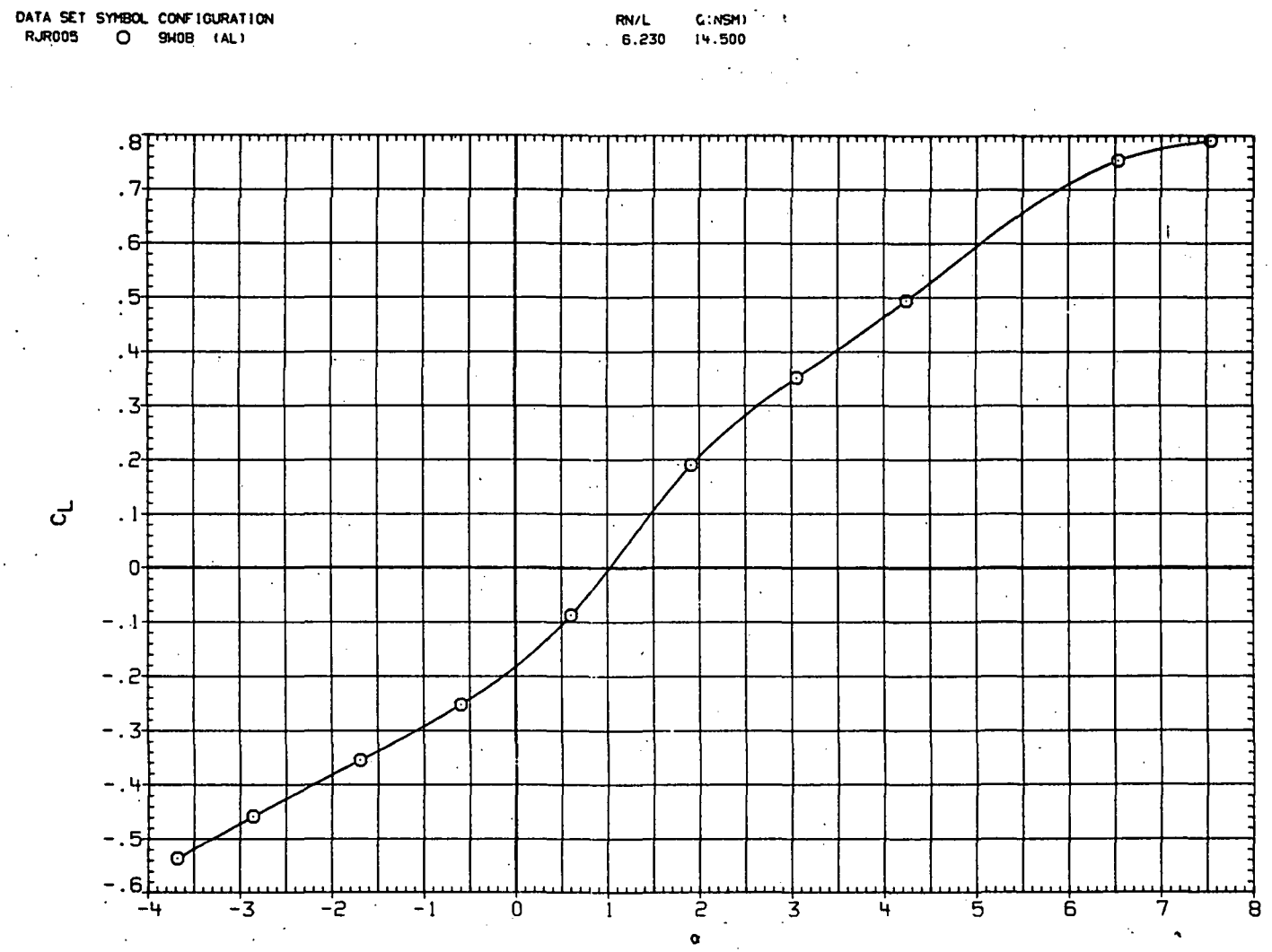

(a) C_L vs α.

Figure 47.– Aerodynamic characteristics of the aluminum trapezoidal oblique wing-body combination ($\Lambda = 0$, $M = 0.9$ and the modified NACA 65A204 airfoil).

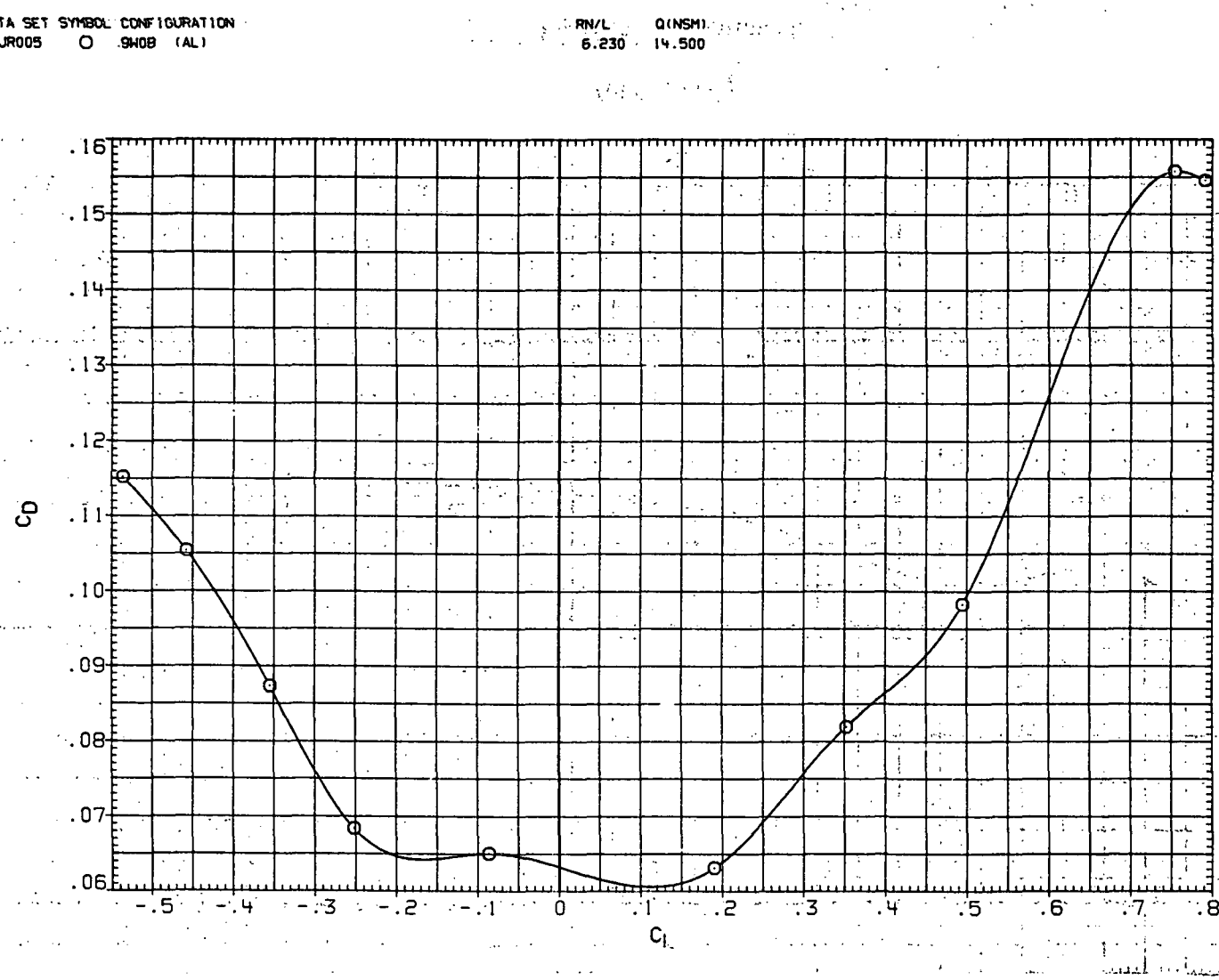

(b) C_D vs C_L.

Figure 47.– Continued.

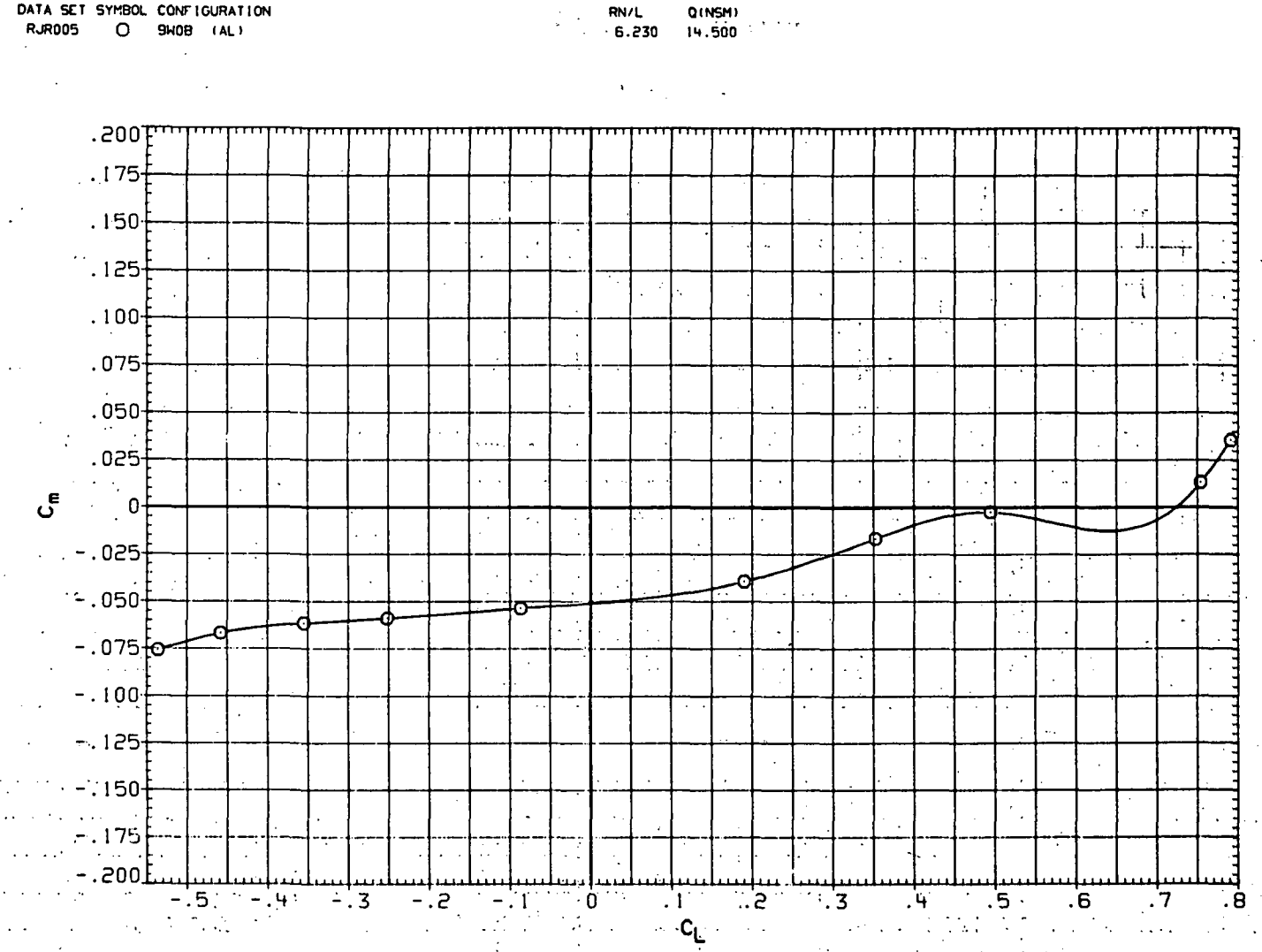

(c) C_m vs C_L.

Figure 47.– Continued.

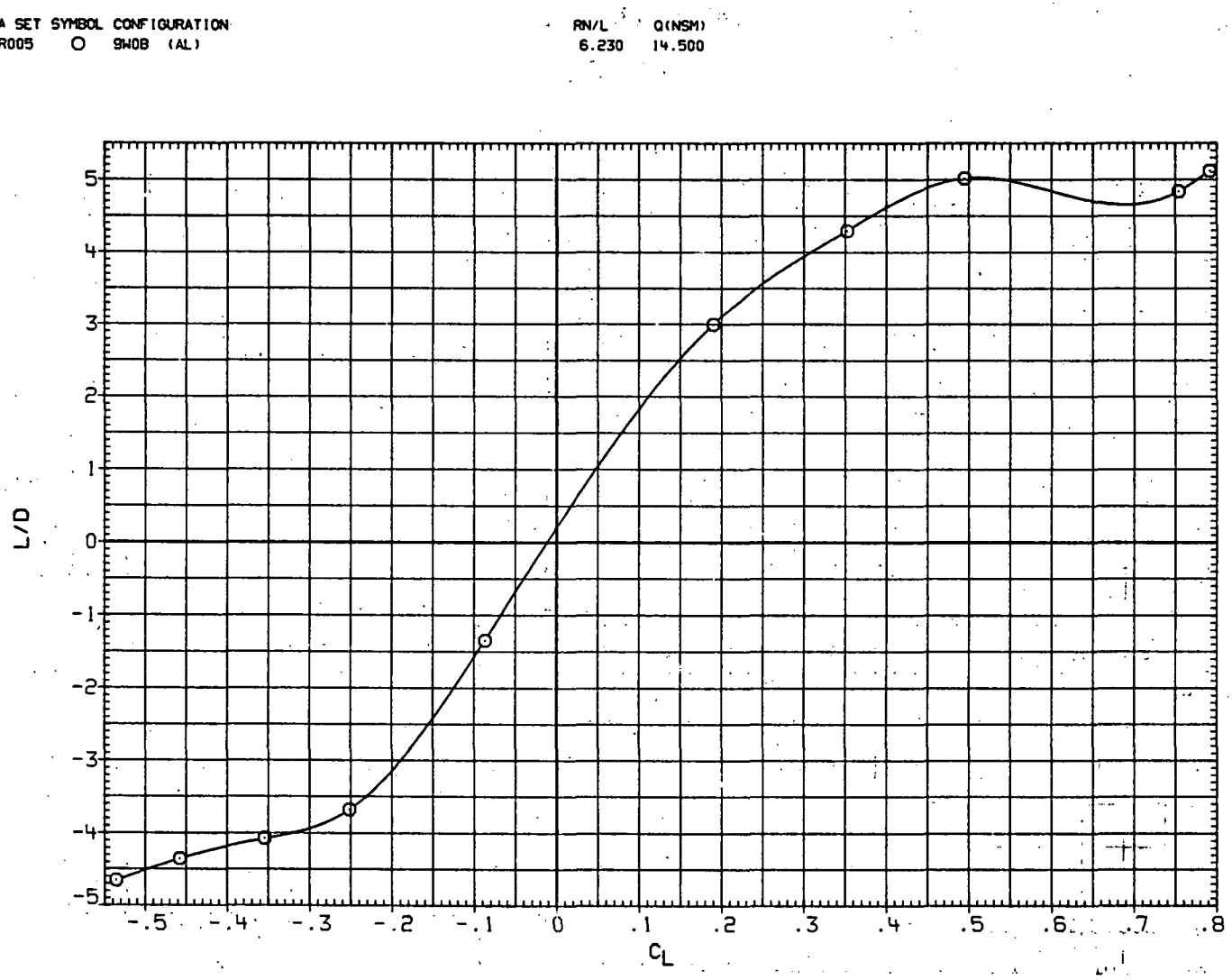

(d) L/D vs C_L.

Figure 47.– Continued.

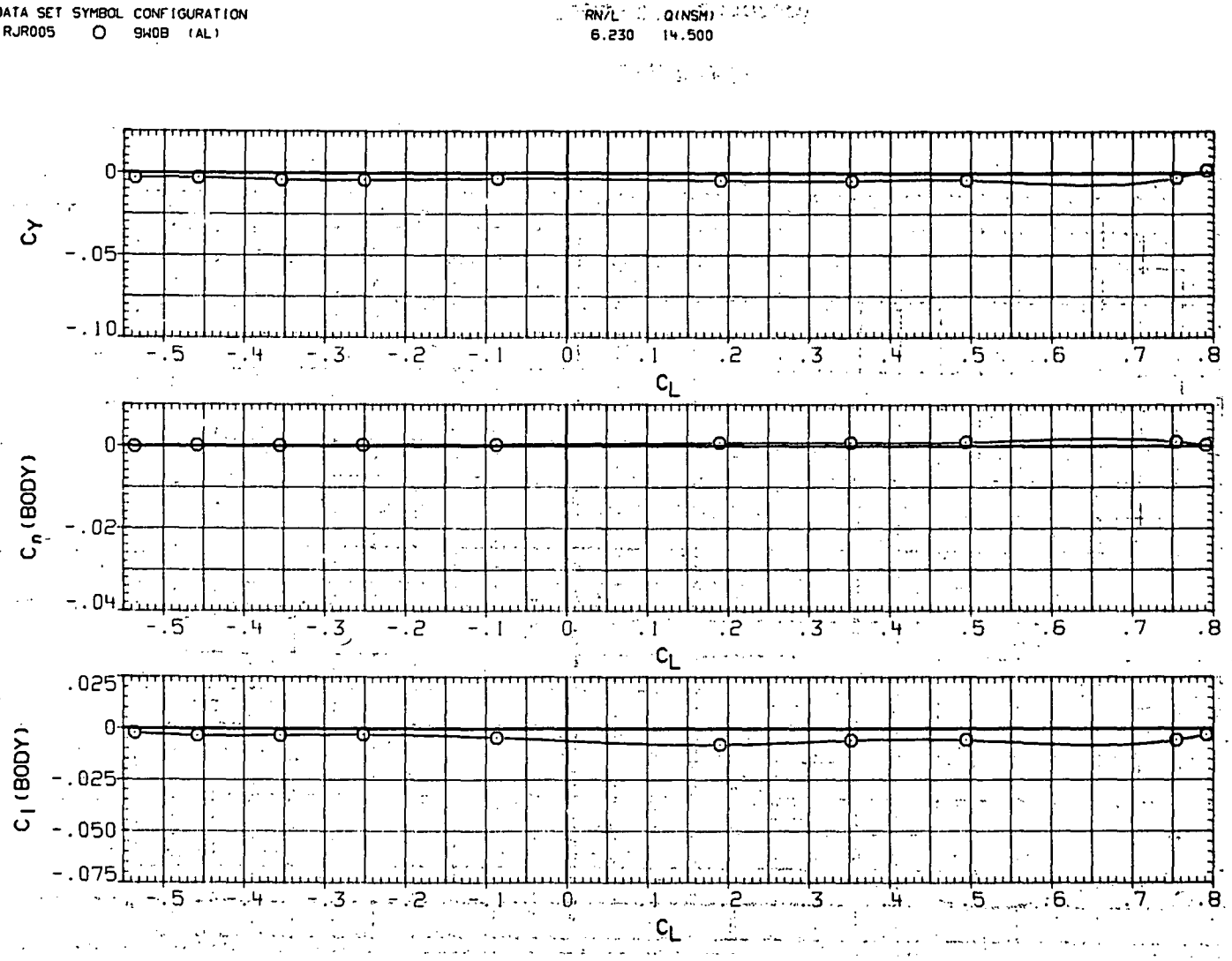

(e) C_Y, C_n and C_ℓ vs C_L.

Figure 47.– Concluded.

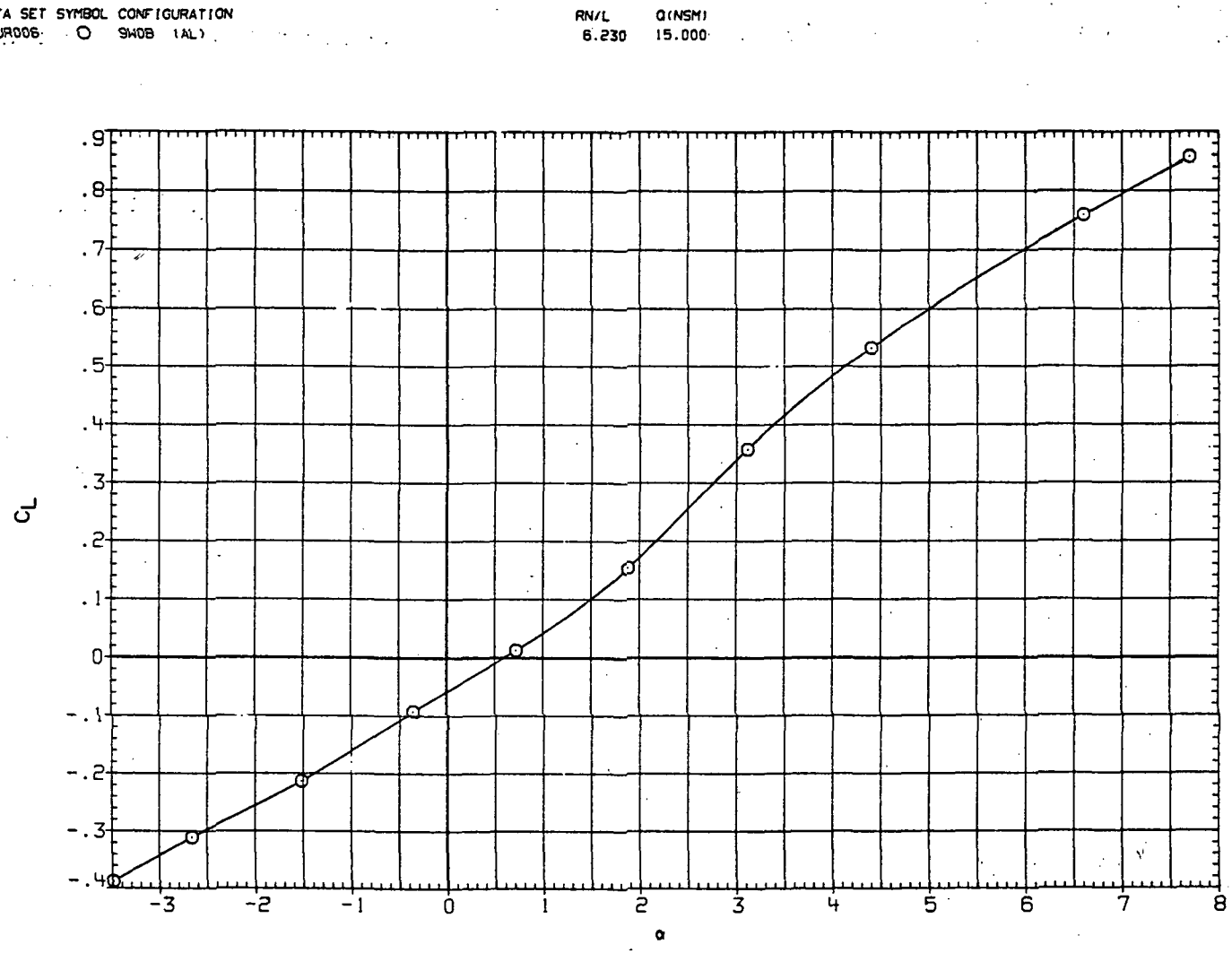

(a) C_L vs α.

Figure 48.– Aerodynamic characteristics of the aluminum trapezoidal oblique wing-body combination ($\Lambda = 0$, $M = 0.95$ and the modified NACA 65A204 airfoil).

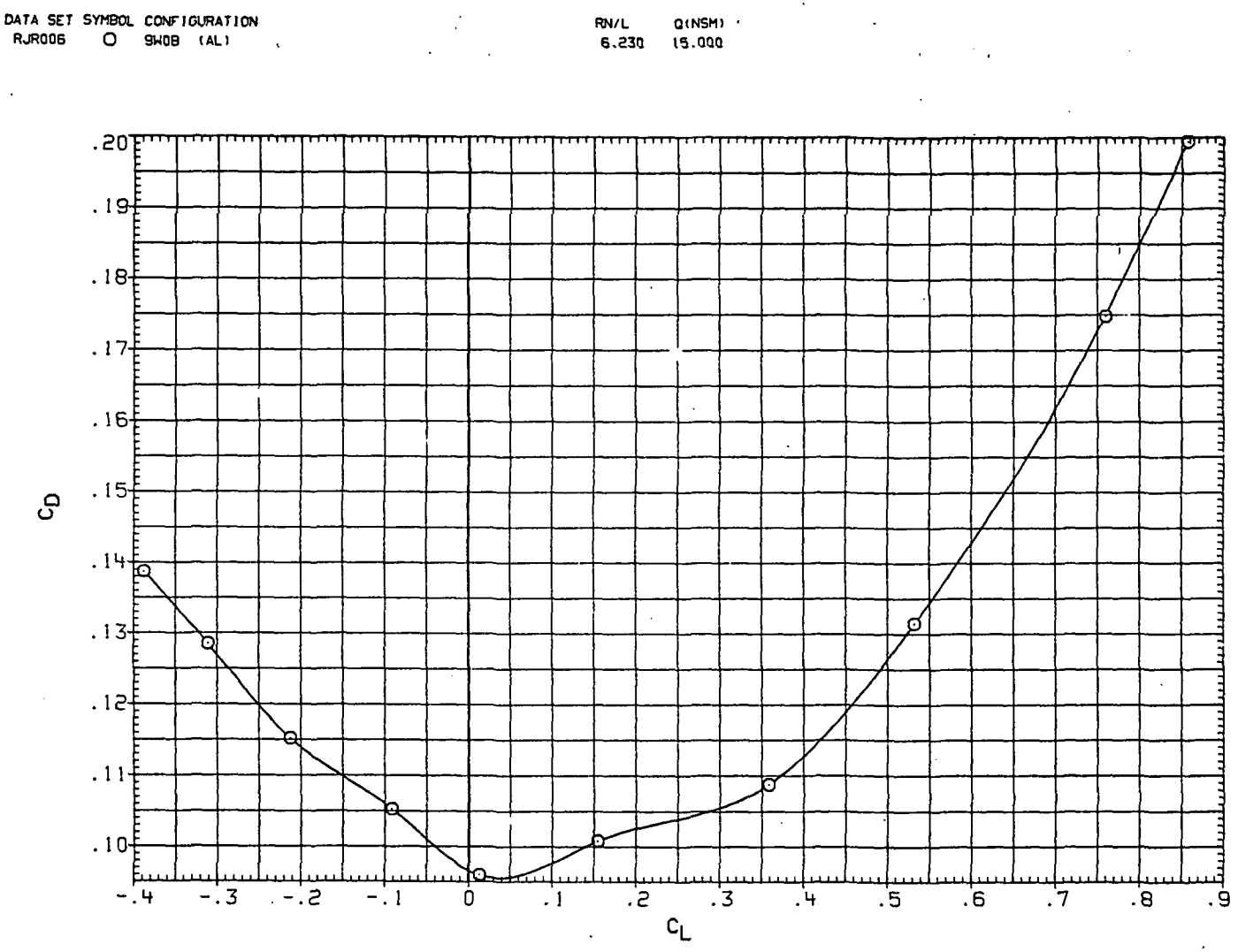

(b) C_D vs C_L.

Figure 48.– Continued.

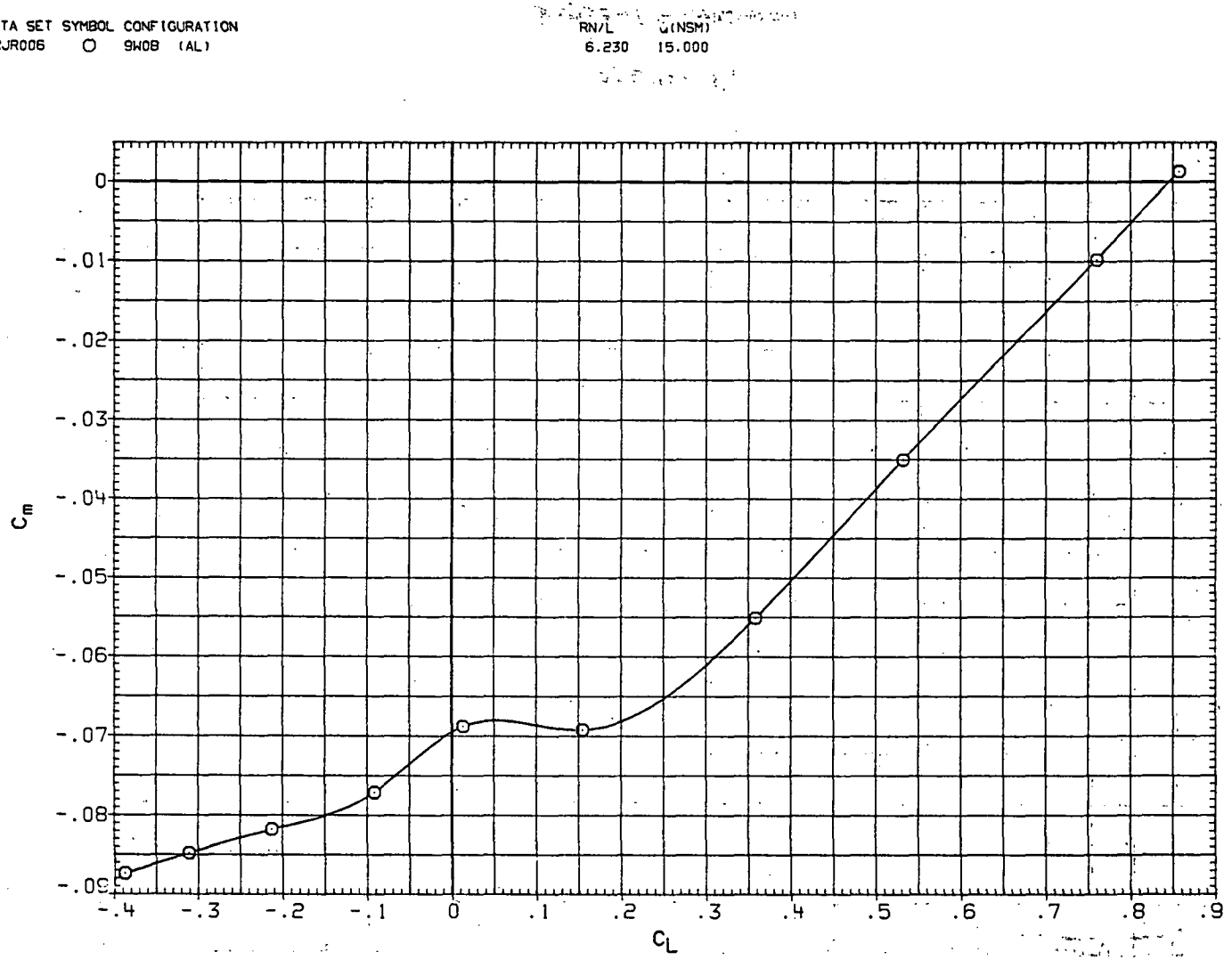

(c) C_m vs C_L.

Figure 48.– Continued.

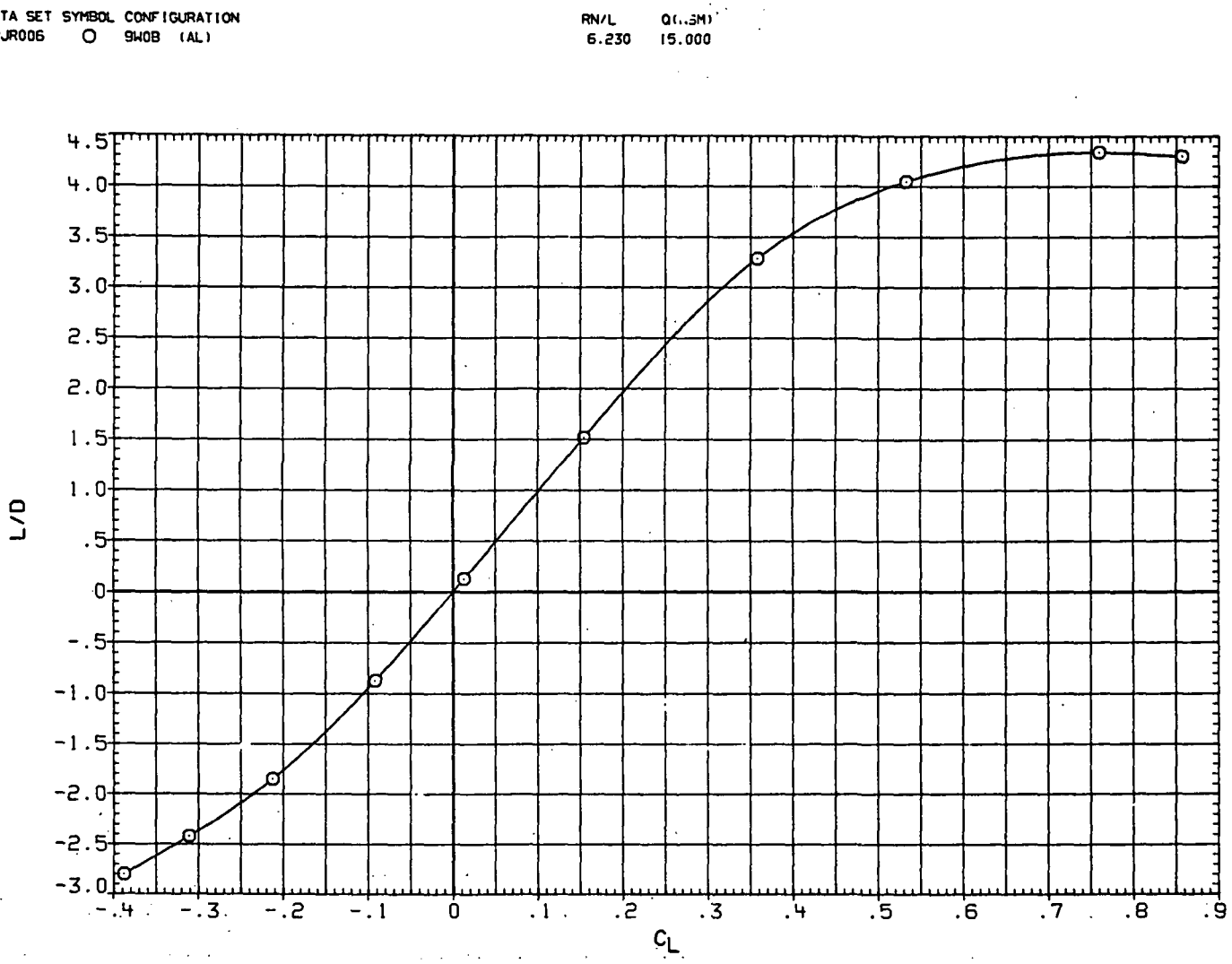

(d) L/D vs C_L.

Figure 48.– Continued.

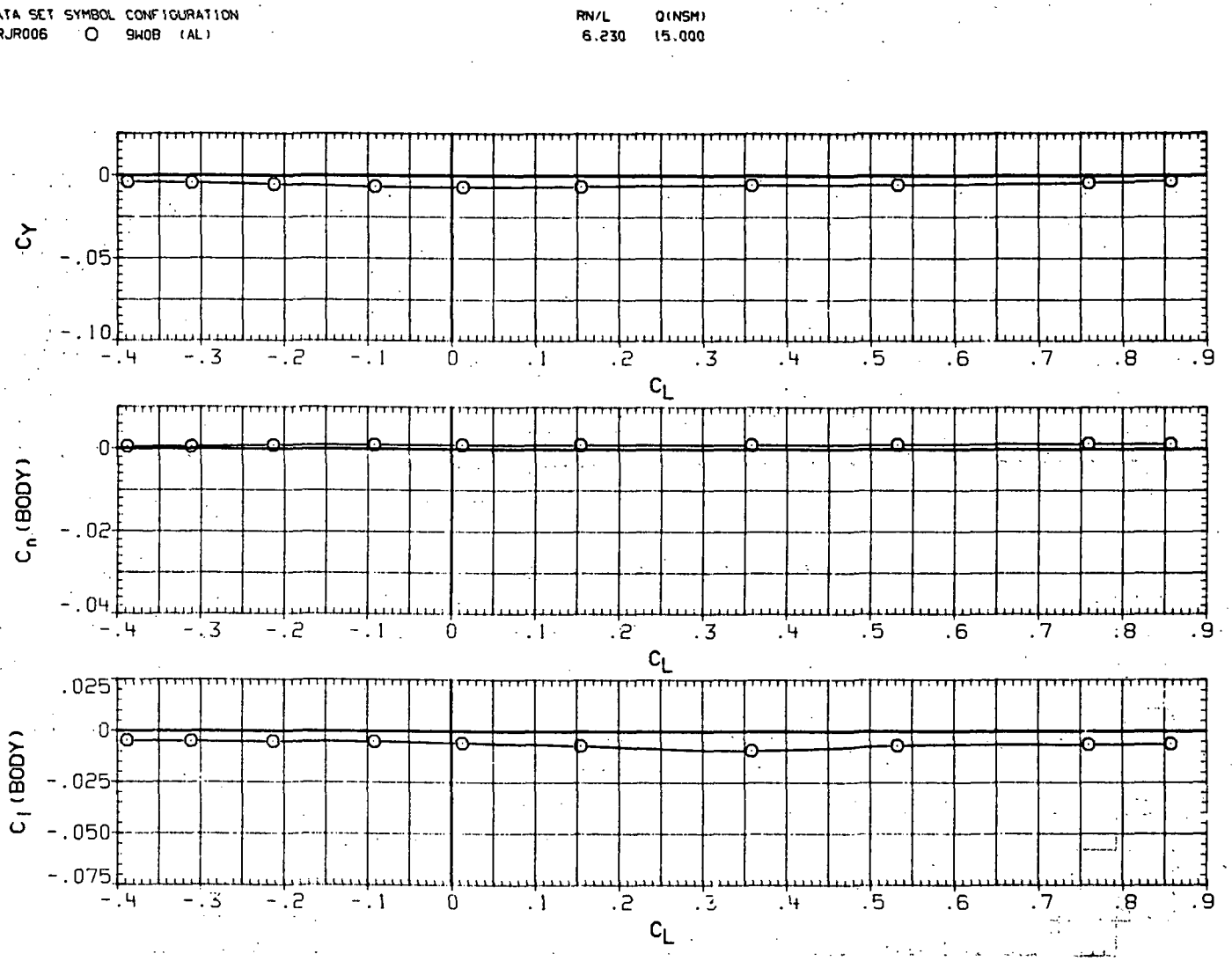

(e) C_Y, C_n and C_ℓ vs C_L.

Figure 48.– Concluded.

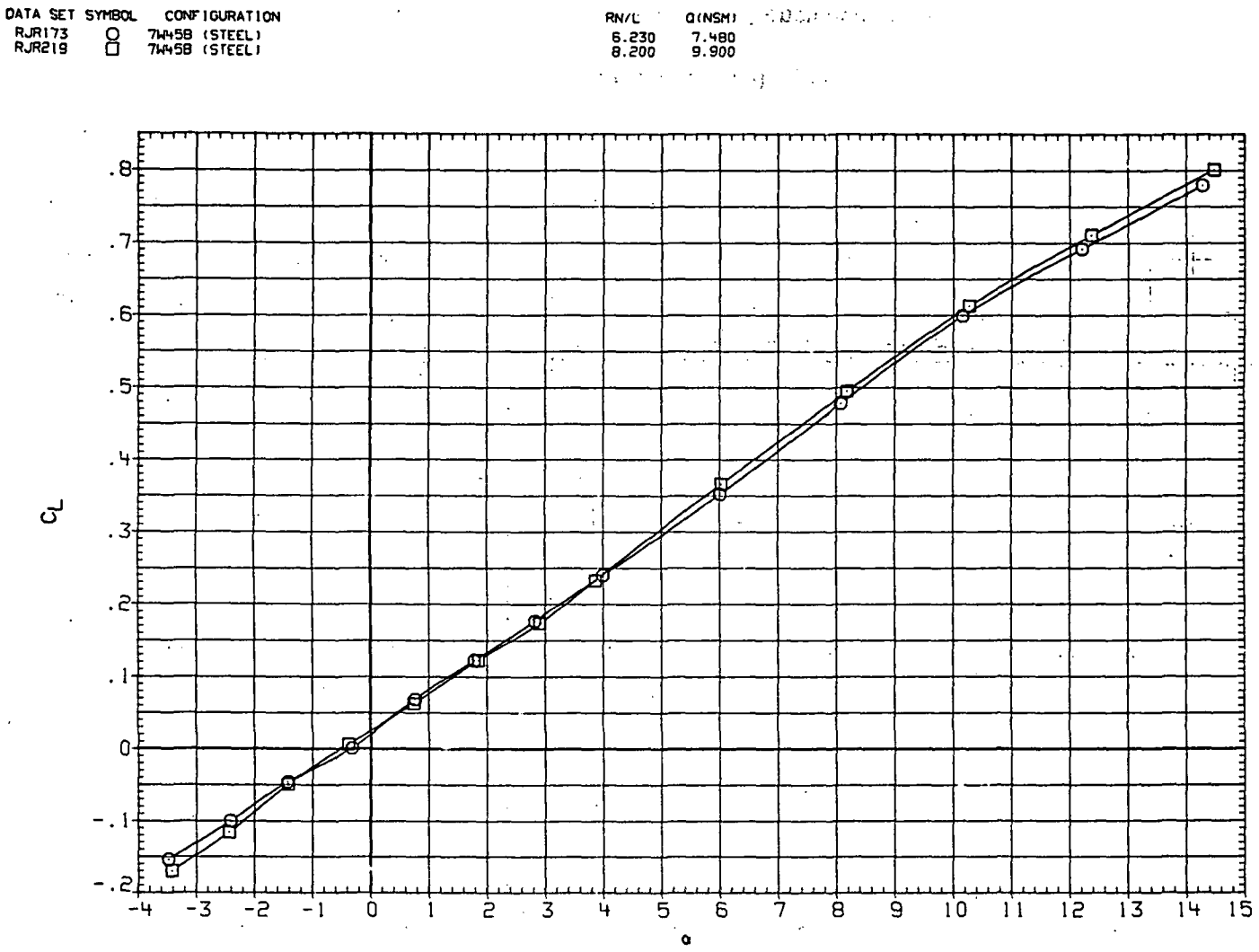

(a) C_L vs α.

Figure 49.– Dynamic-pressure effects on the aerodynamic characteristics of the steel trapezoidal oblique wing-body combination ($\Lambda = 45°$, $M = 0.4$ and the NACA 65A204 airfoil).

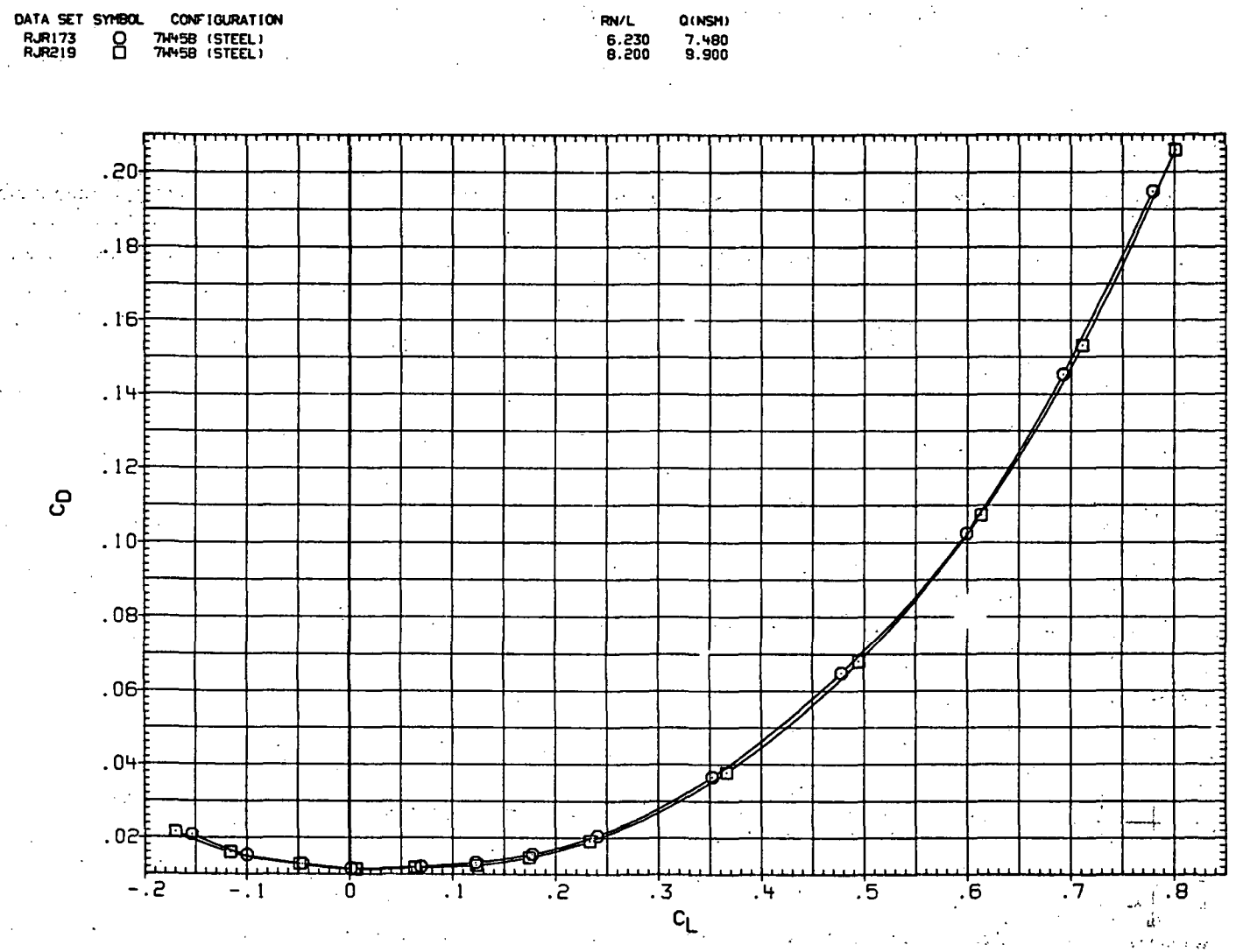

(b) C_D vs C_L.

Figure 49.– Continued.

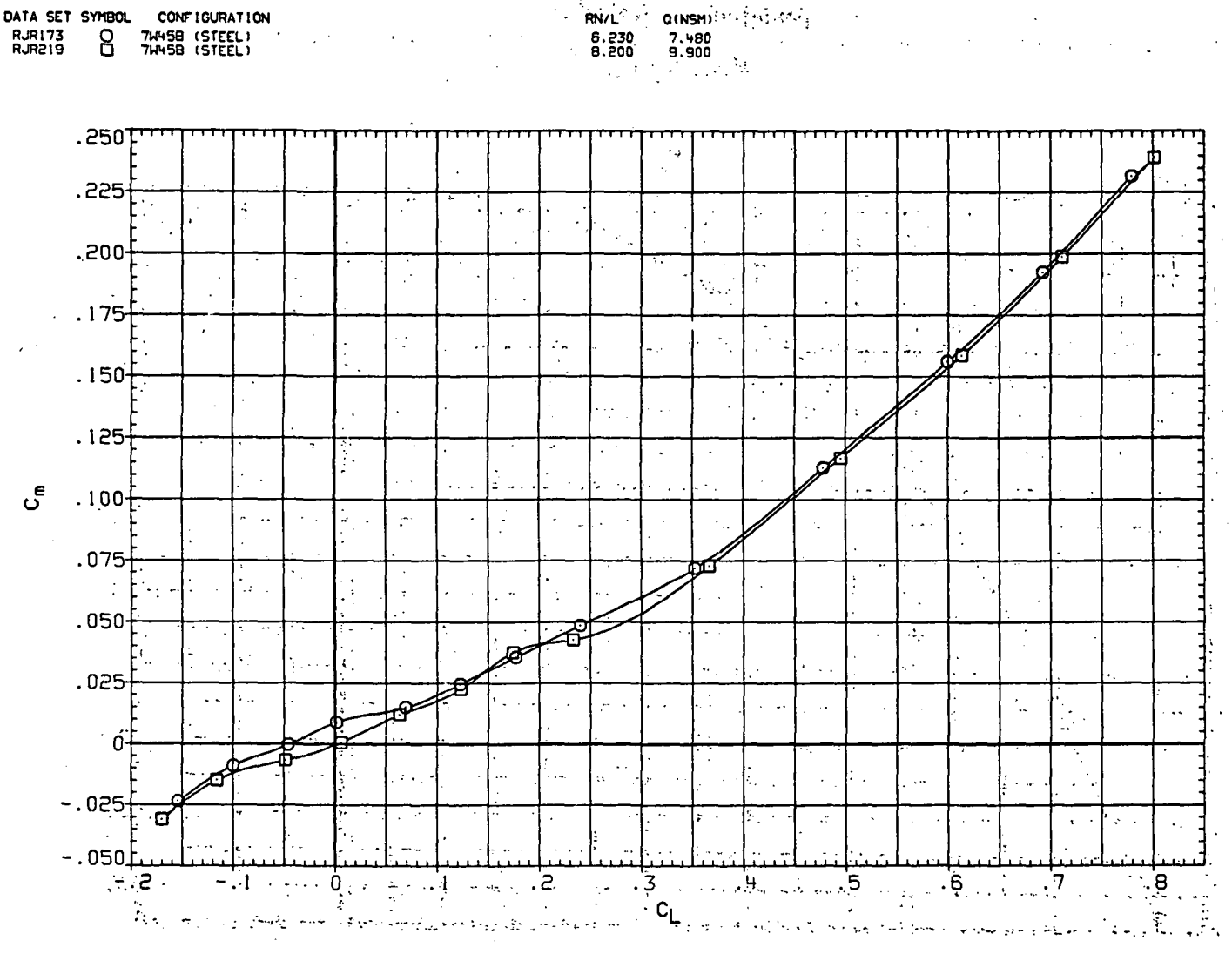

(c) C_m vs C_L.

Figure 49.– Continued.

(d) L/D vs C_L.

Figure 49.– Continued.

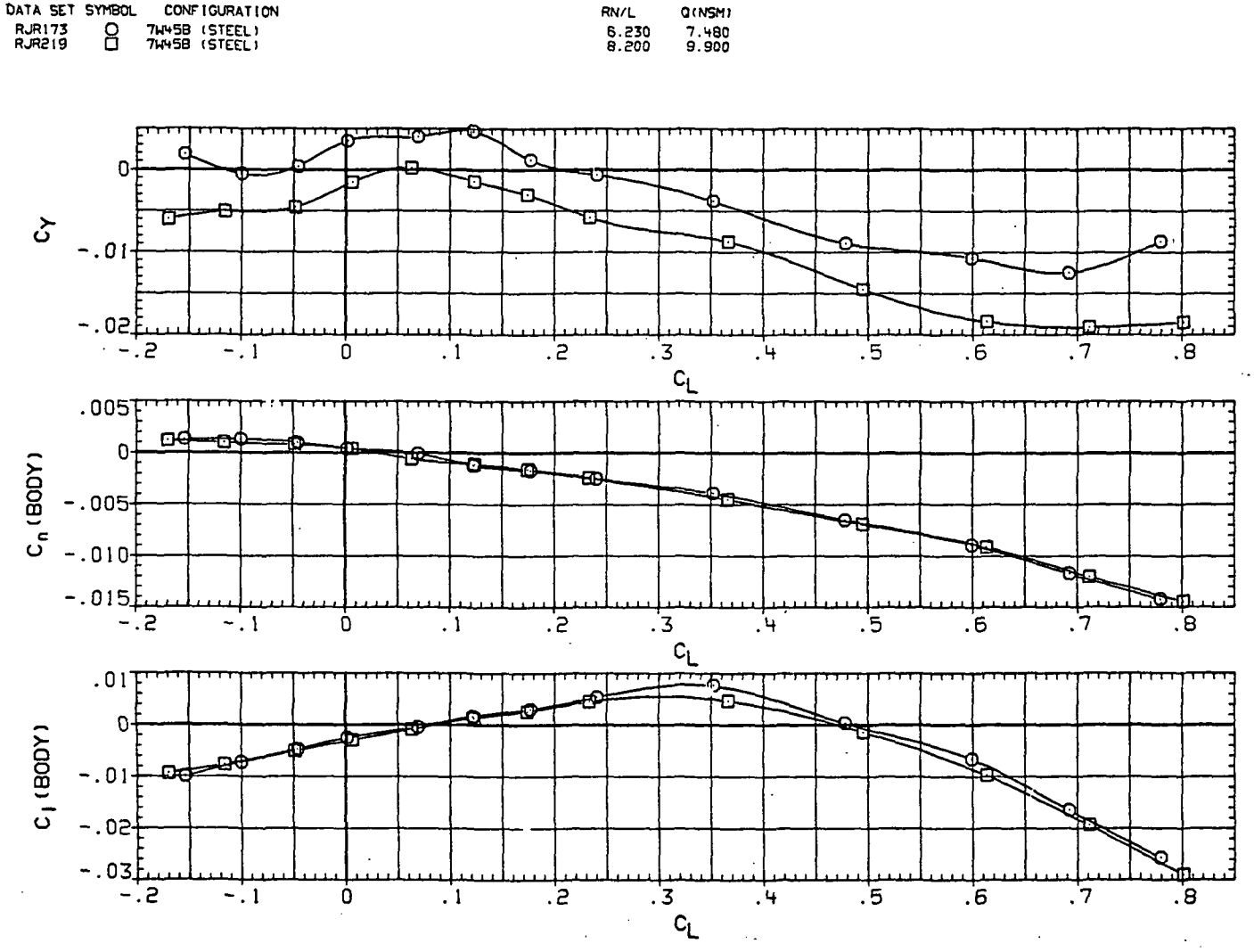

(e) C_Y, C_n and C_ℓ vs C_L.

Figure 49.– Concluded.

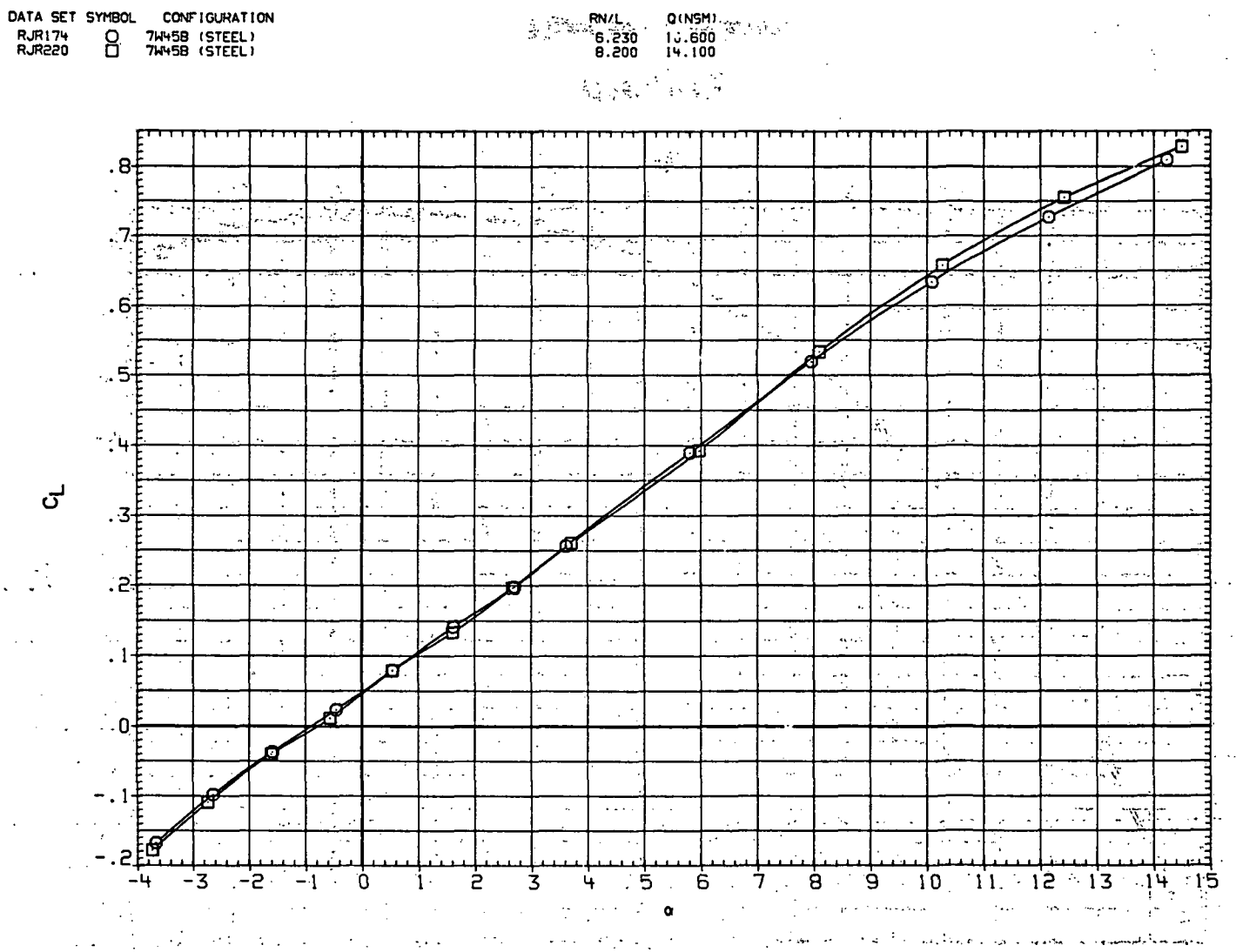

(a) C_L vs α.

Figure 50.– Dynamic-pressure effects on the aerodynamic characteristics of the steel trapezoidal oblique wing-body combination ($\Lambda = 45°$, $M = 0.6$ and the NACA 65A204 airfoil).

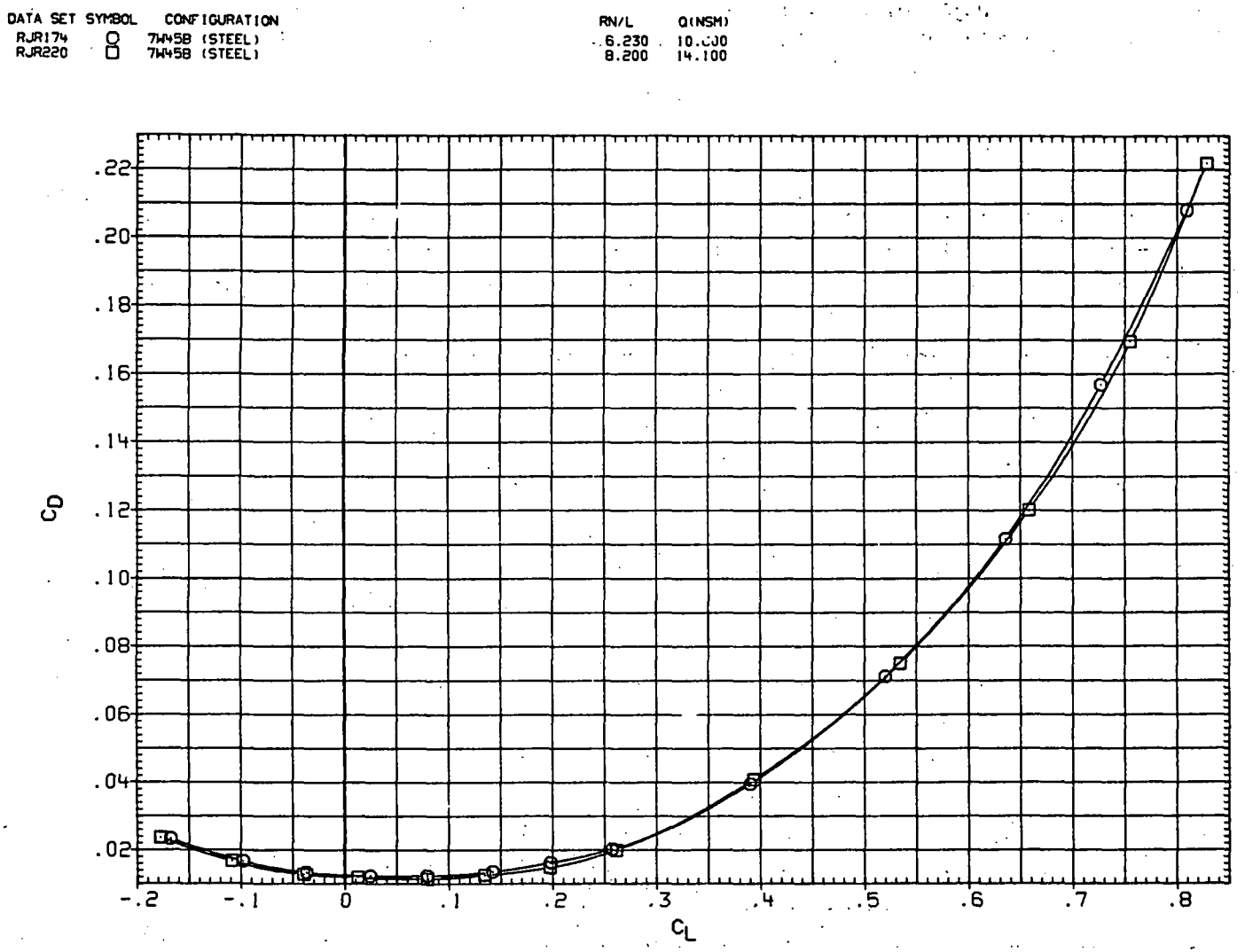

(b) C_D vs C_L.

Figure 50.– Continued.

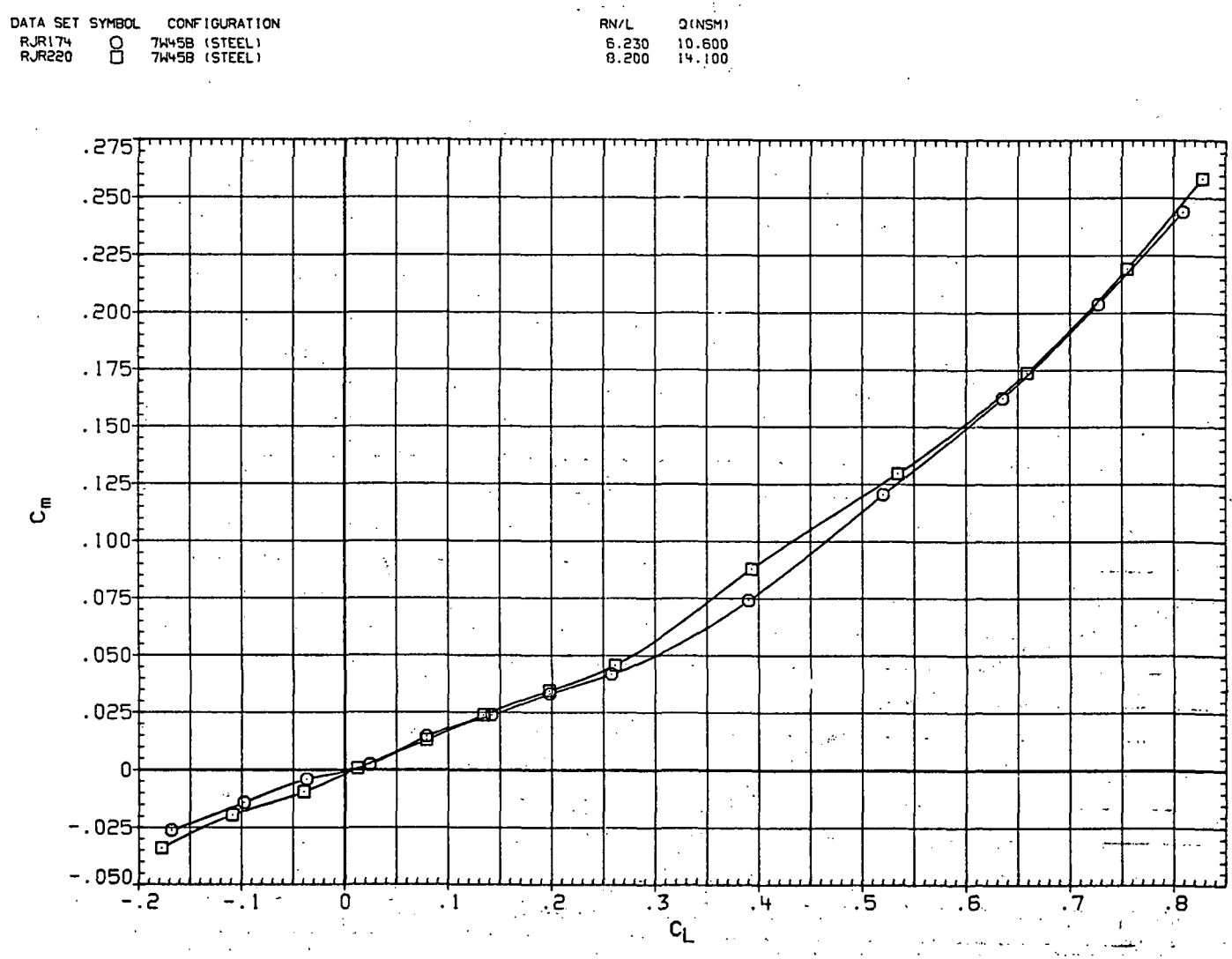

(c) C_m vs C_L.

Figure 50.– Continued.

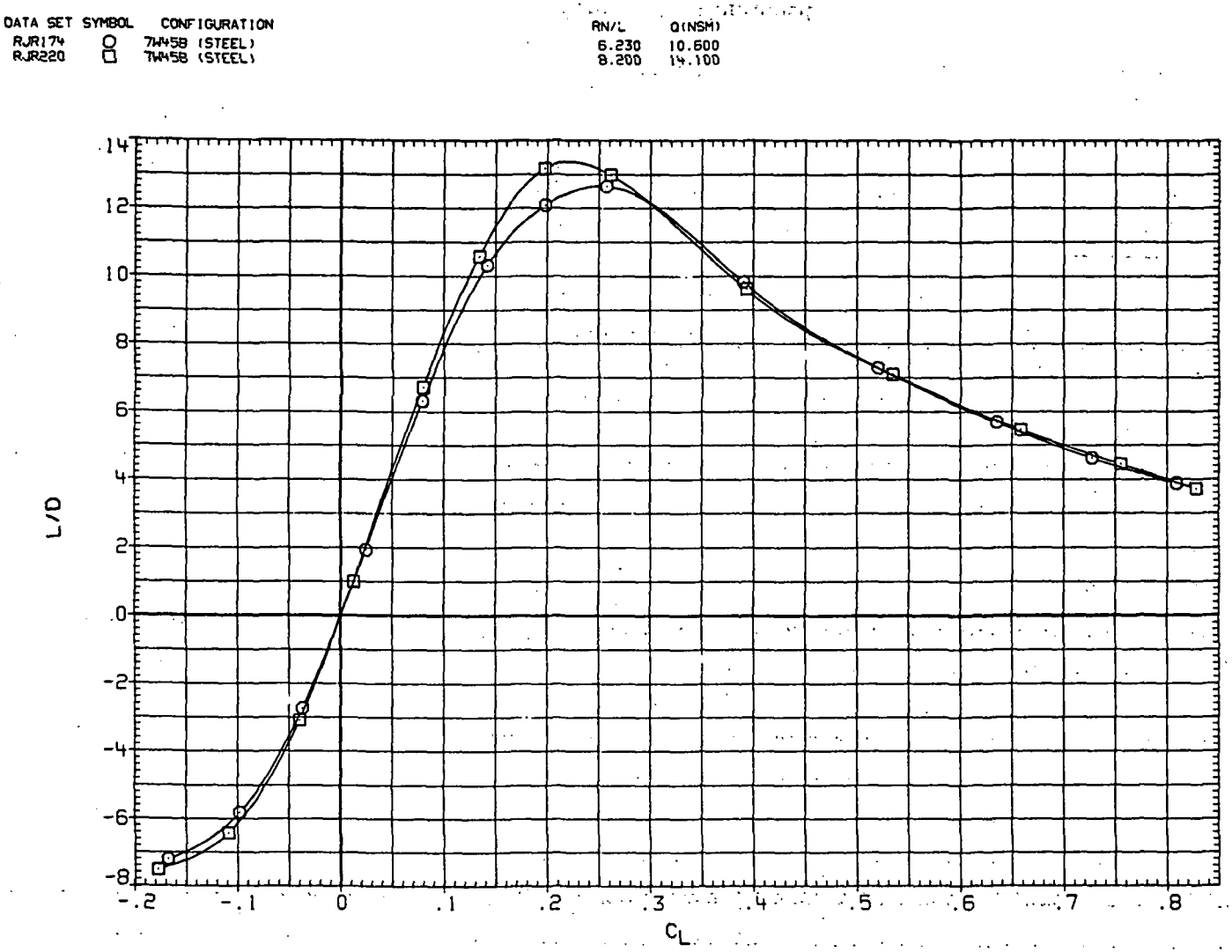

(d) L/D vs C_L.

Figure 50.– Continued.

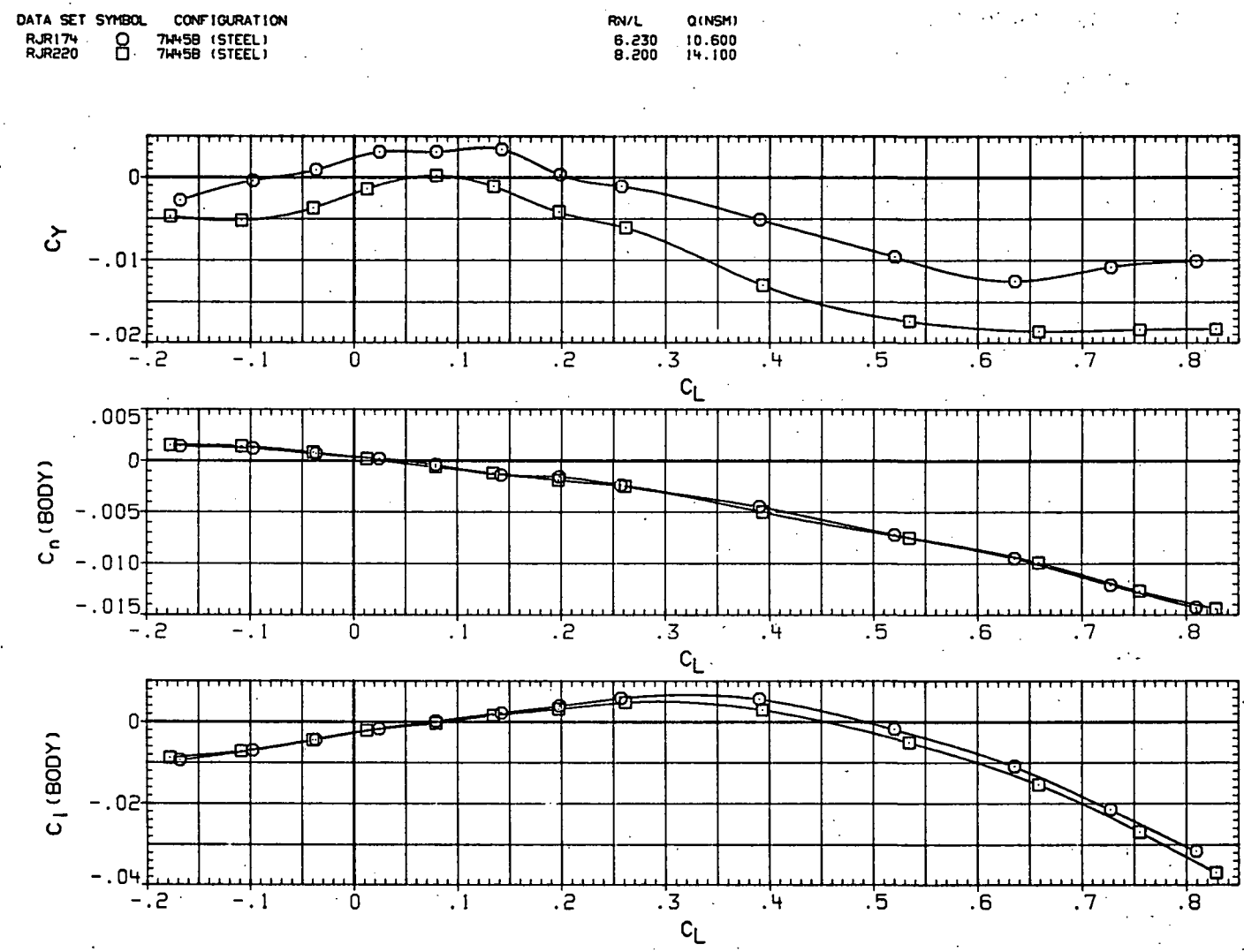

(e) C_Y, C_n and C_ℓ vs C_L.

Figure 50.– Concluded.

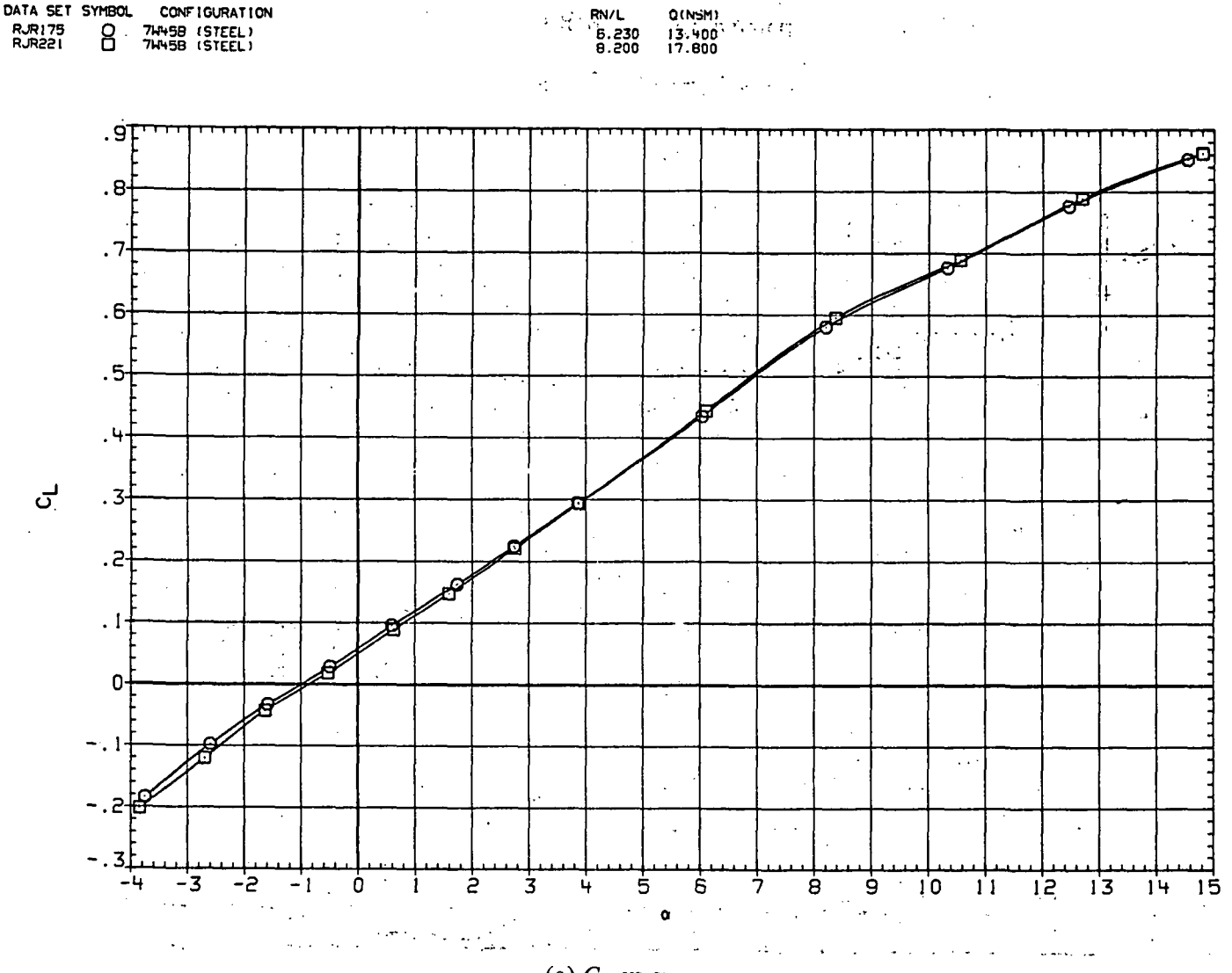

(a) C_L vs α.

Figure 51.– Dynamic-pressure effects on the aerodynamic characteristics of the steel trapezoidal oblique wing-body combination ($\Lambda = 45°$, $M = 0.8$ and the NACA 65A204 airfoil).

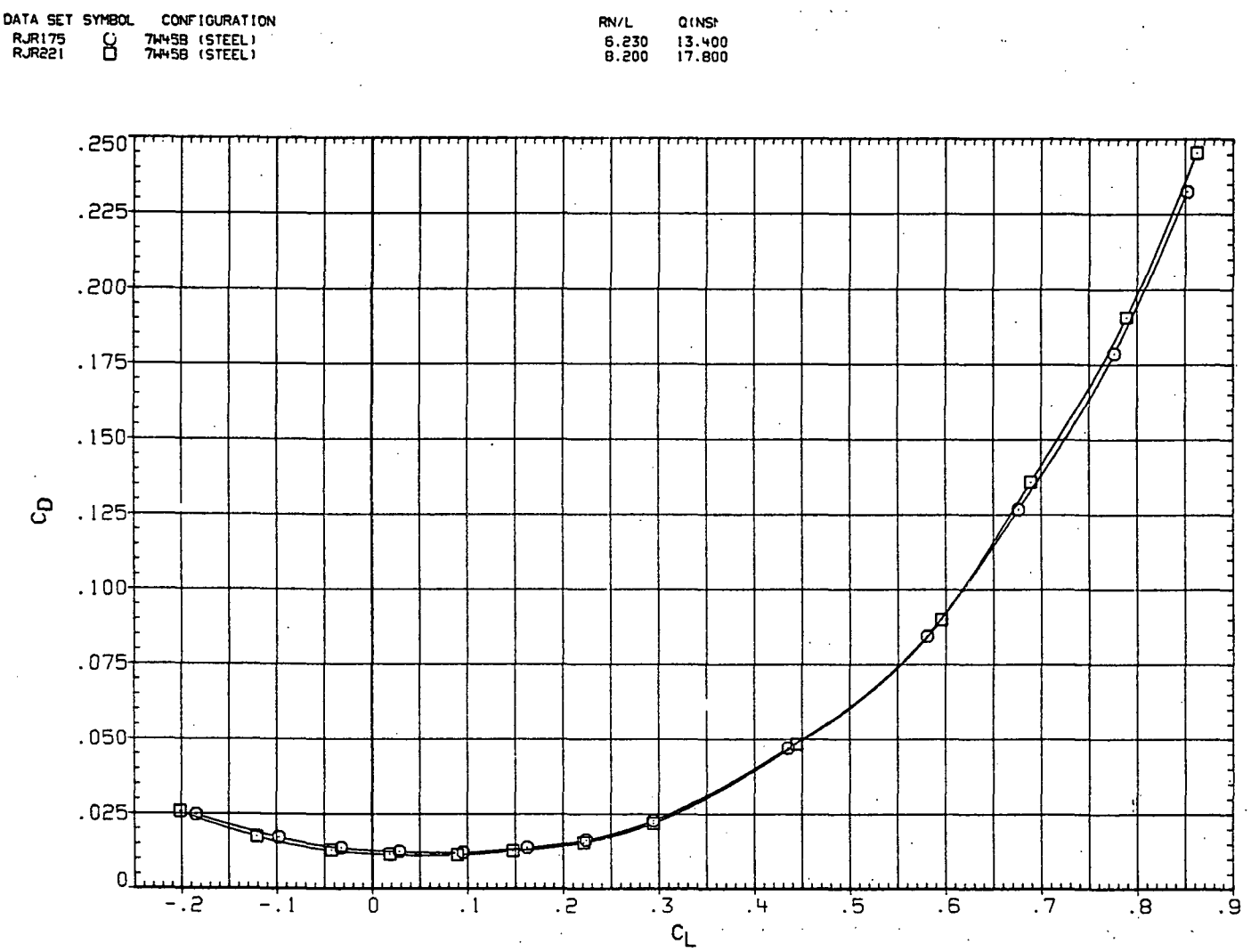

(b) C_D vs C_L.

Figure 51.– Continued.

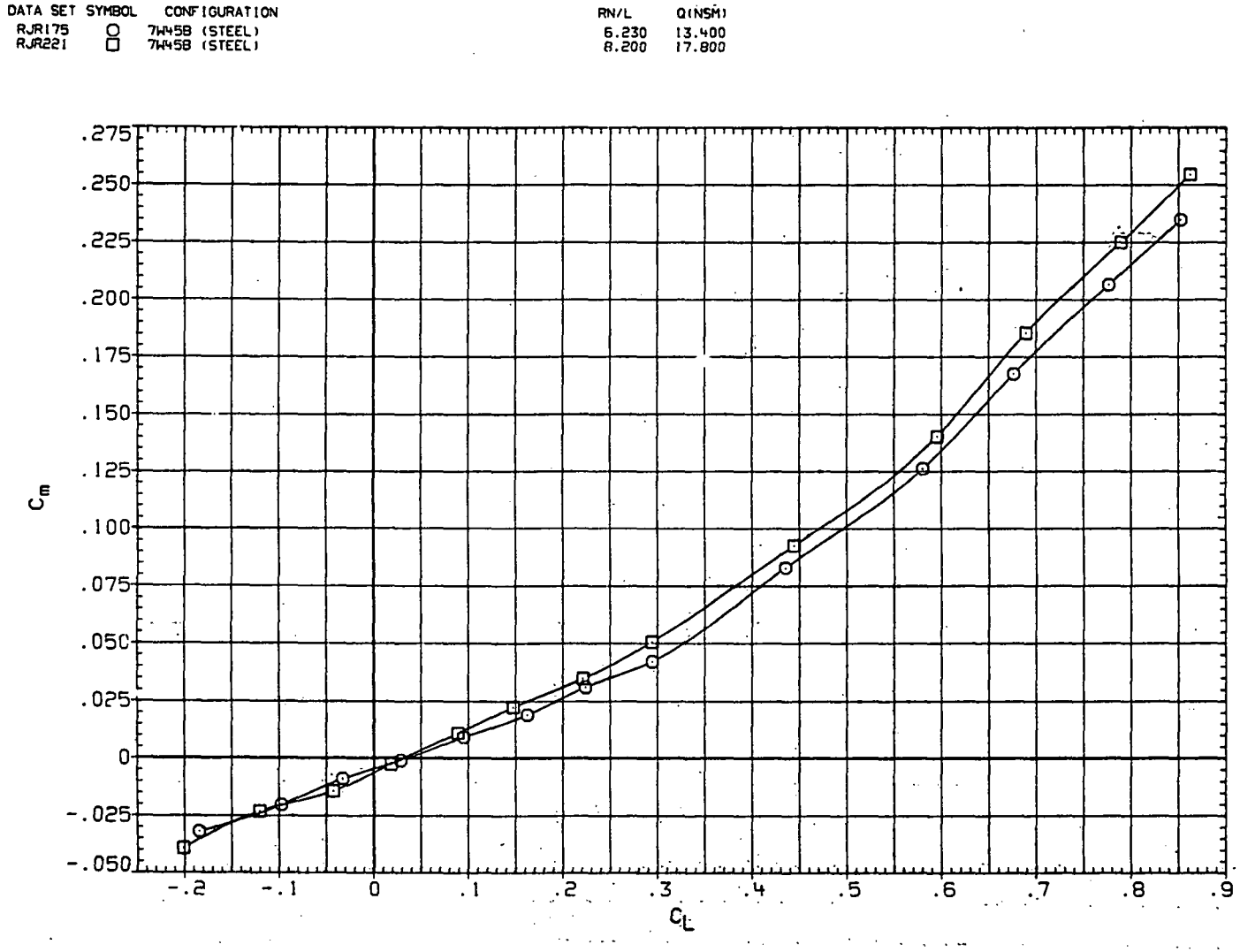

(c) C_m vs C_L.

Figure 51.– Continued.

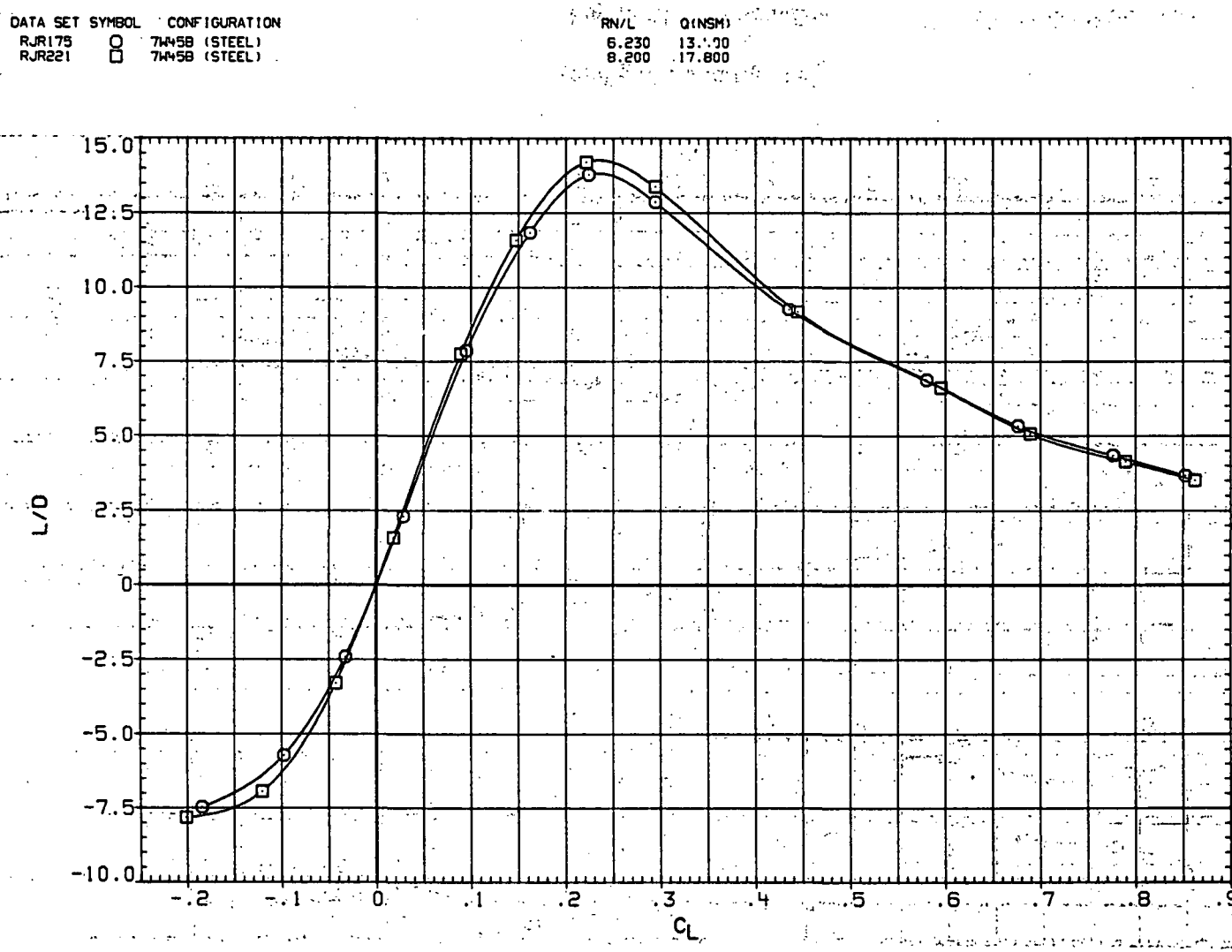

(d) L/D vs C_L.

Figure 51.– Continued.

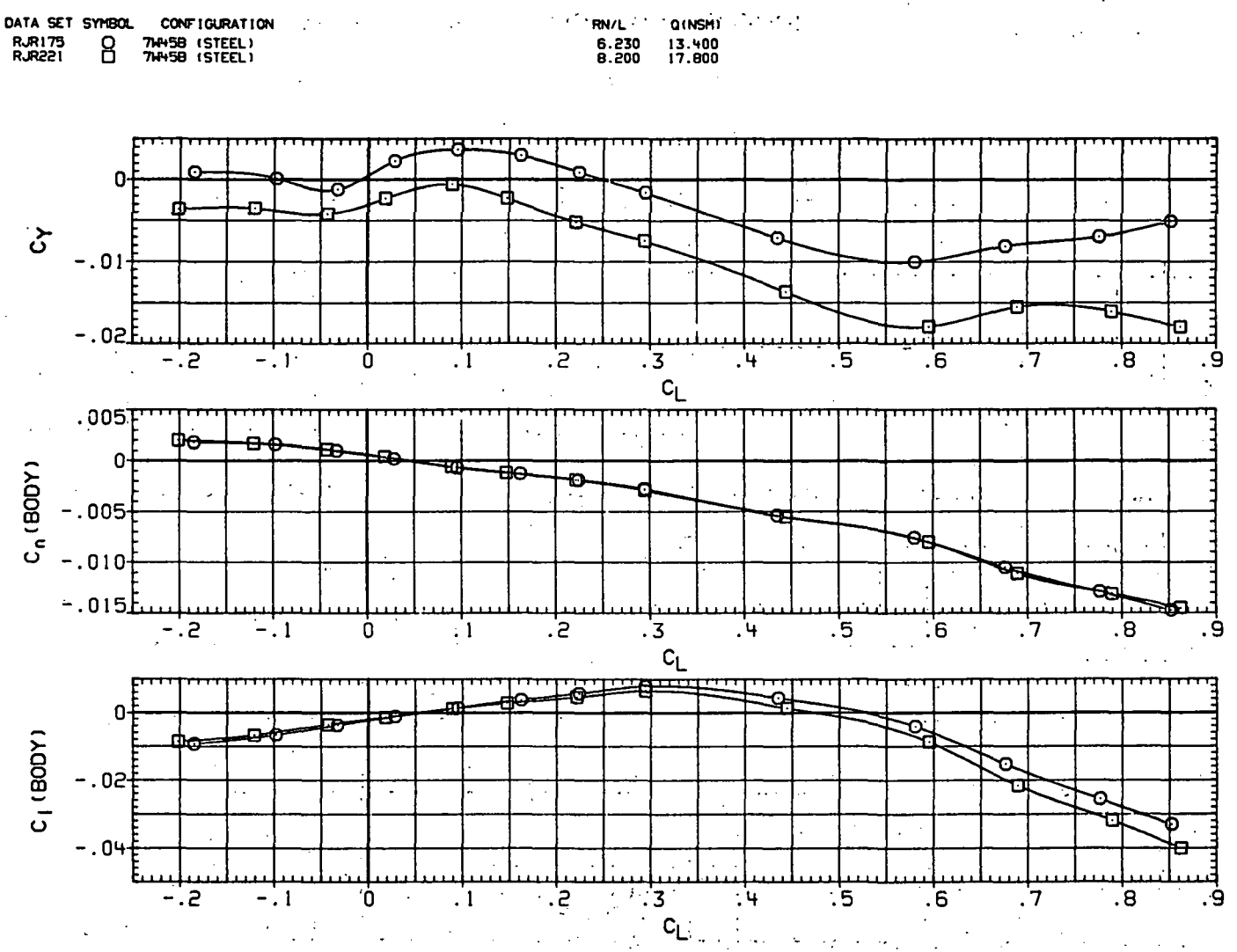

(e) C_Y, C_n and C_ℓ vs C_L.

Figure 51.– Concluded.

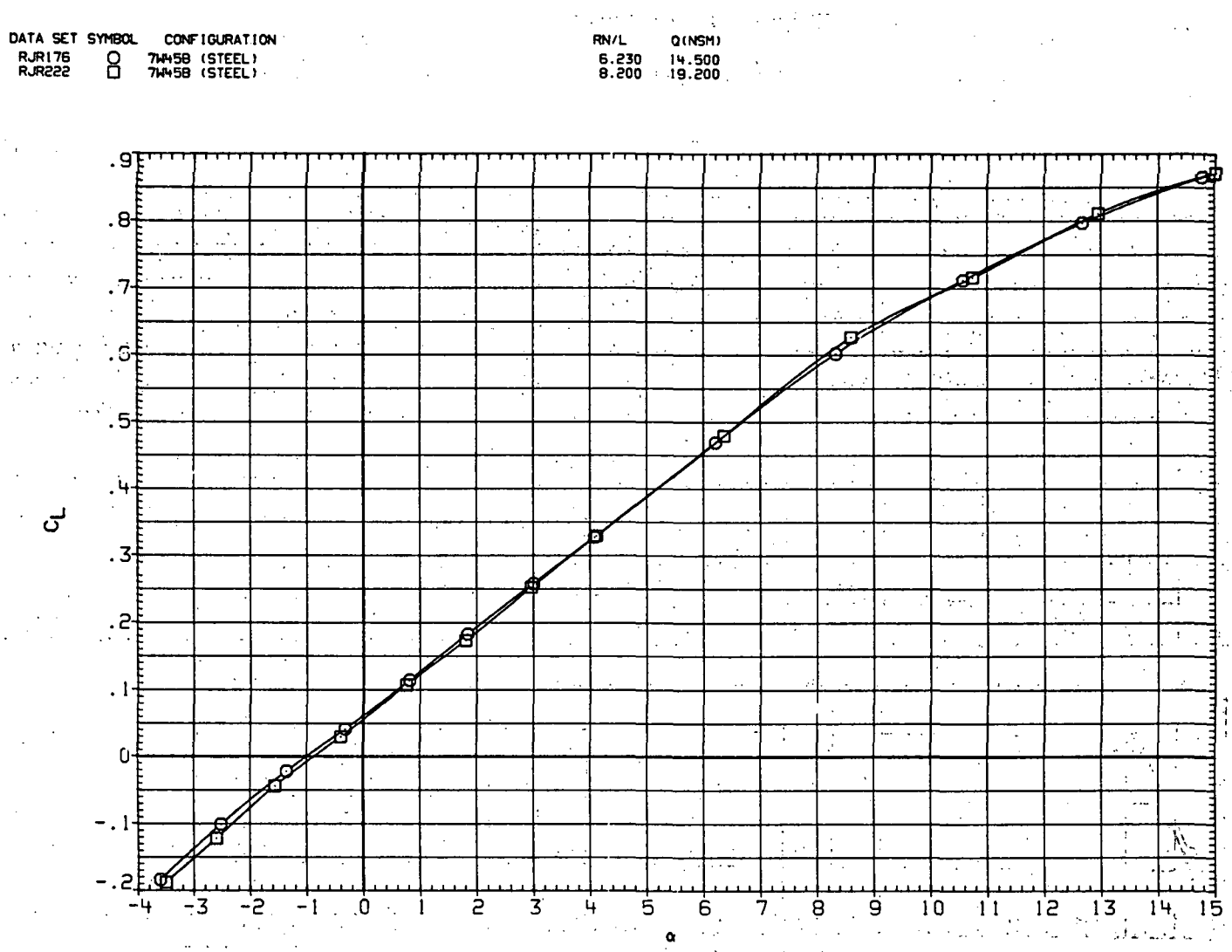

(a) C_L vs α.

Figure 52.– Dynamic-pressure effects on the aerodynamic characteristics of the steel trapezoidal oblique wing-body combination ($\Lambda = 45°, M = 0.9$ and the NACA 65A204 airfoil).

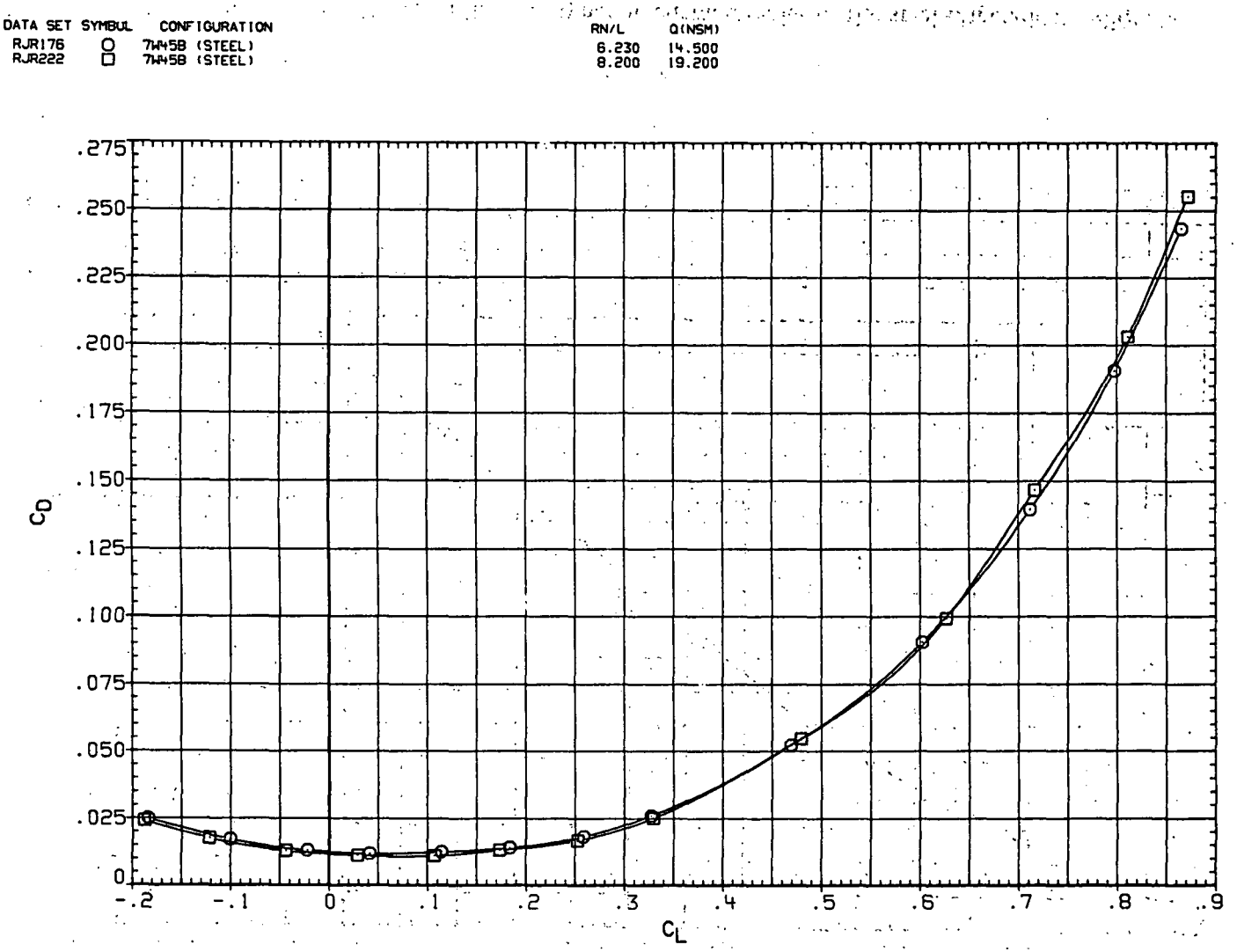

(b) C_D vs C_L.

Figure 52.– Continued.

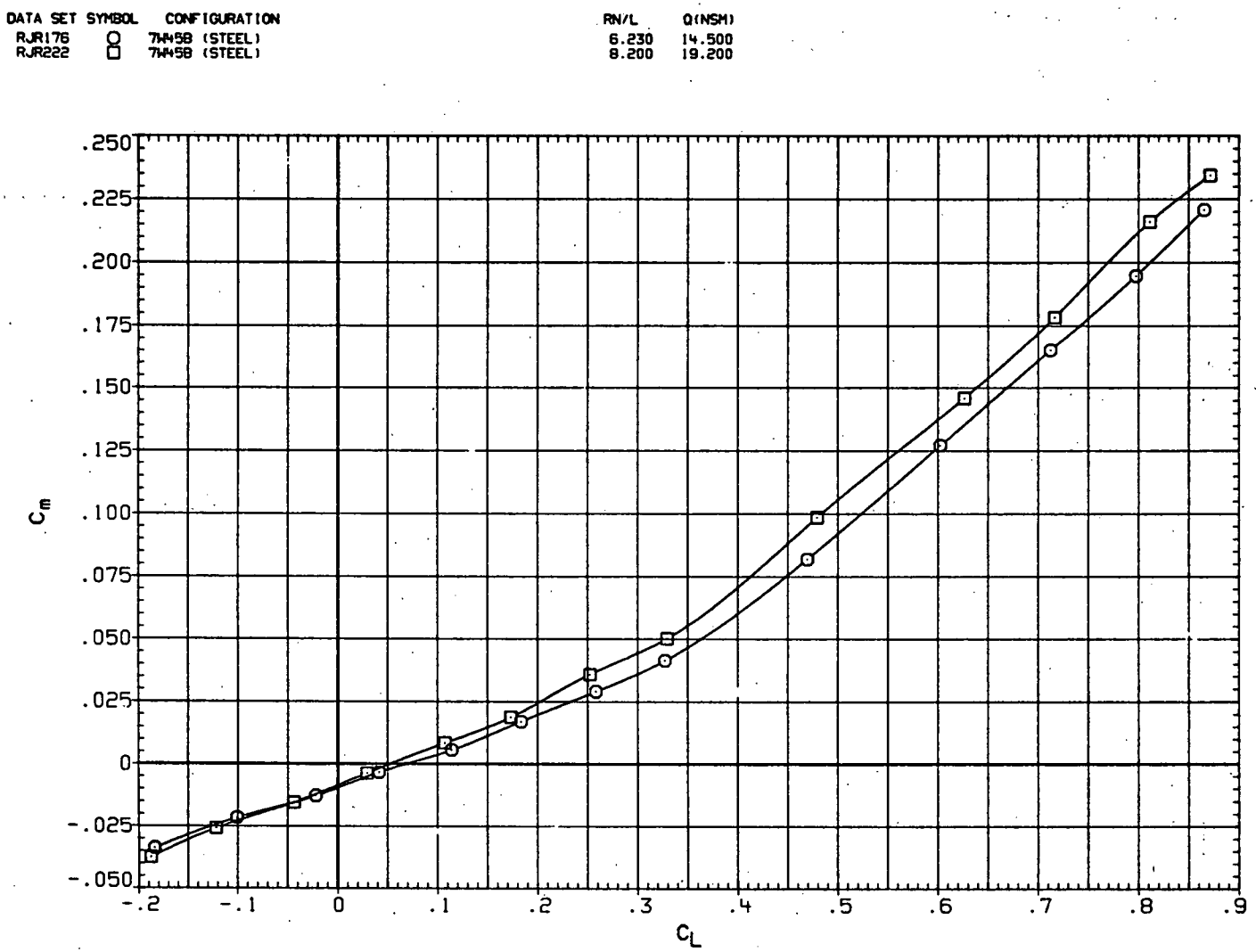

(c) C_m vs C_L.

Figure 52.– Continued.

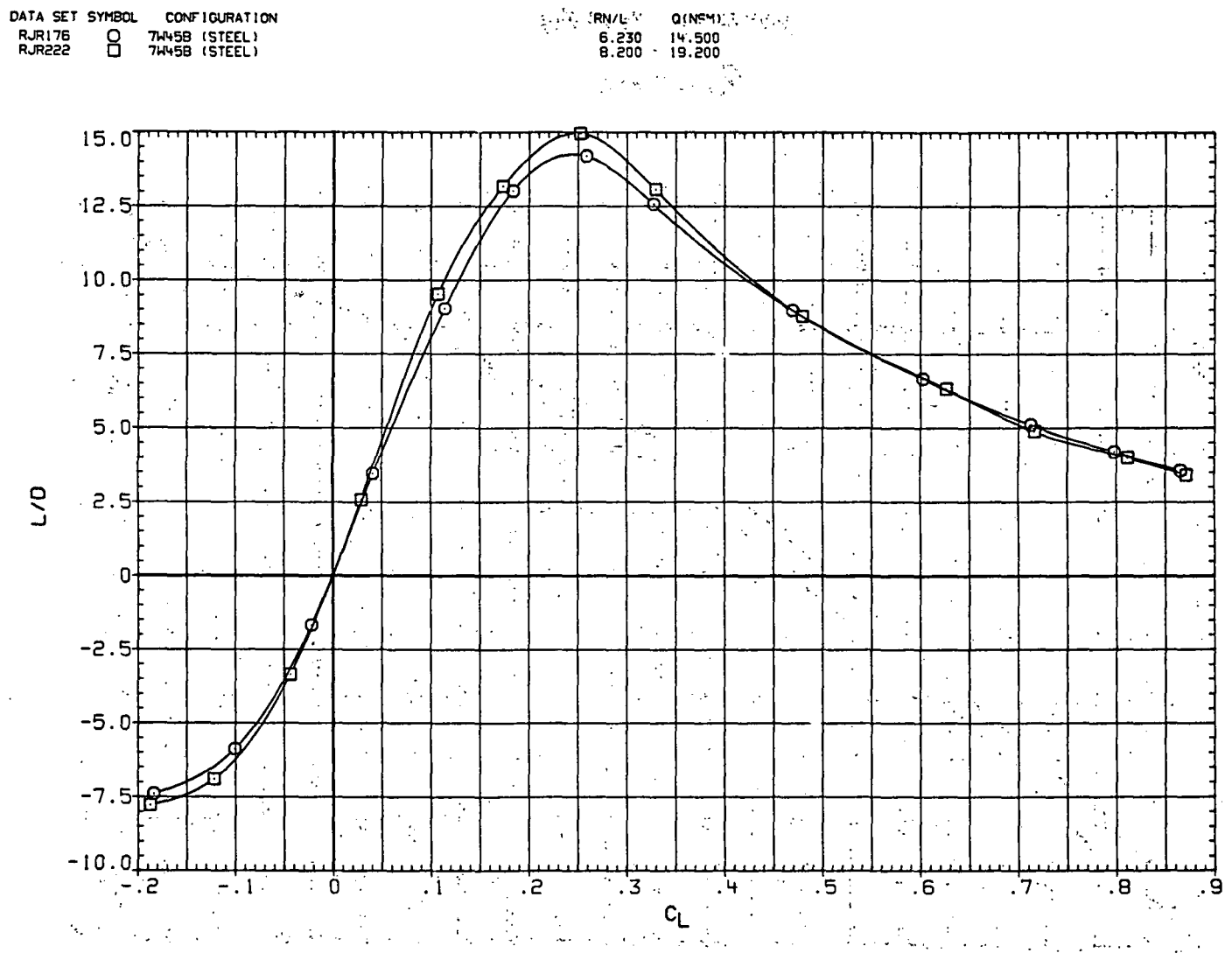

(d) L/D vs C_L.

Figure 52.– Continued.

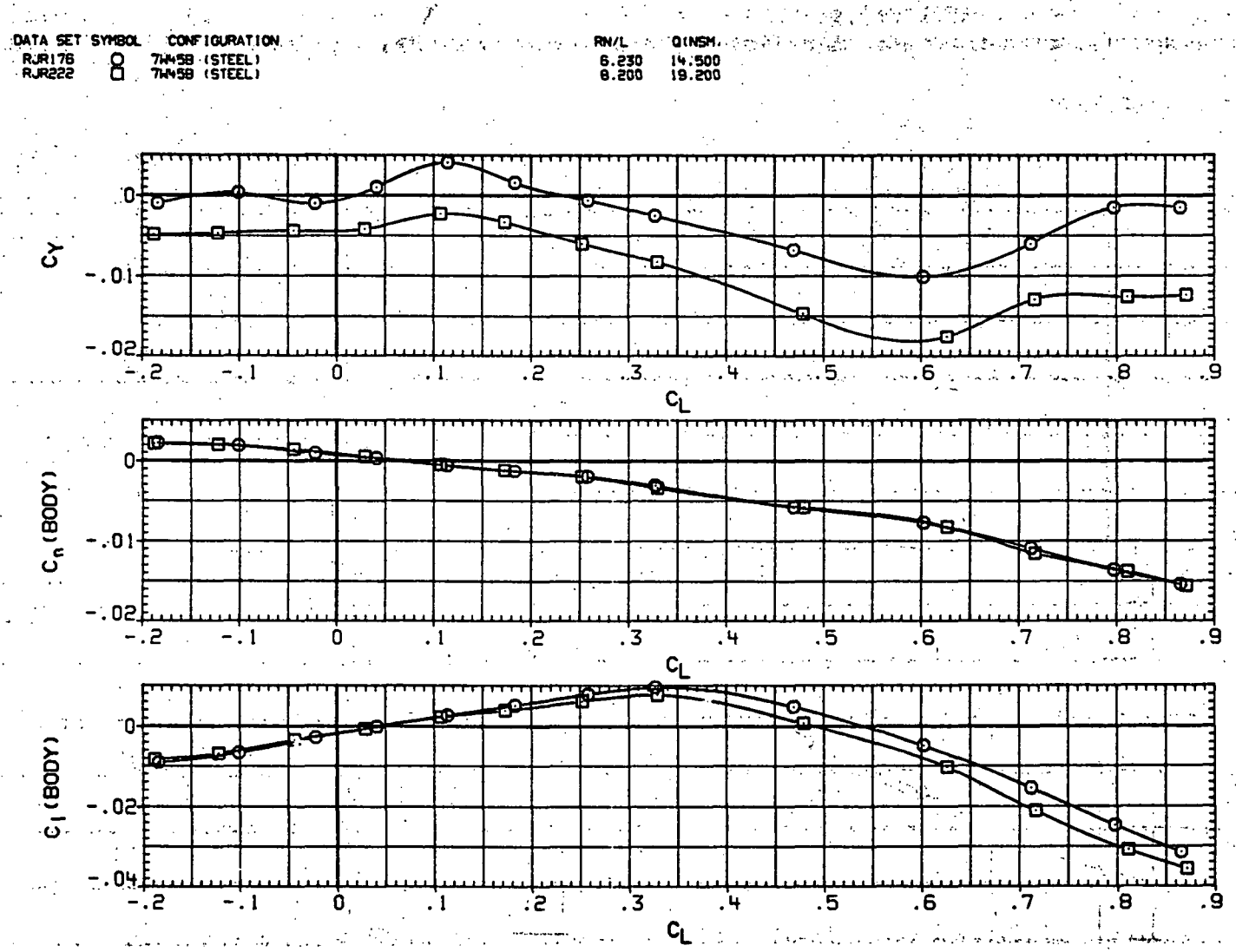

(e) C_Y, C_n and C_ℓ vs C_L.

Figure 52.– Concluded.

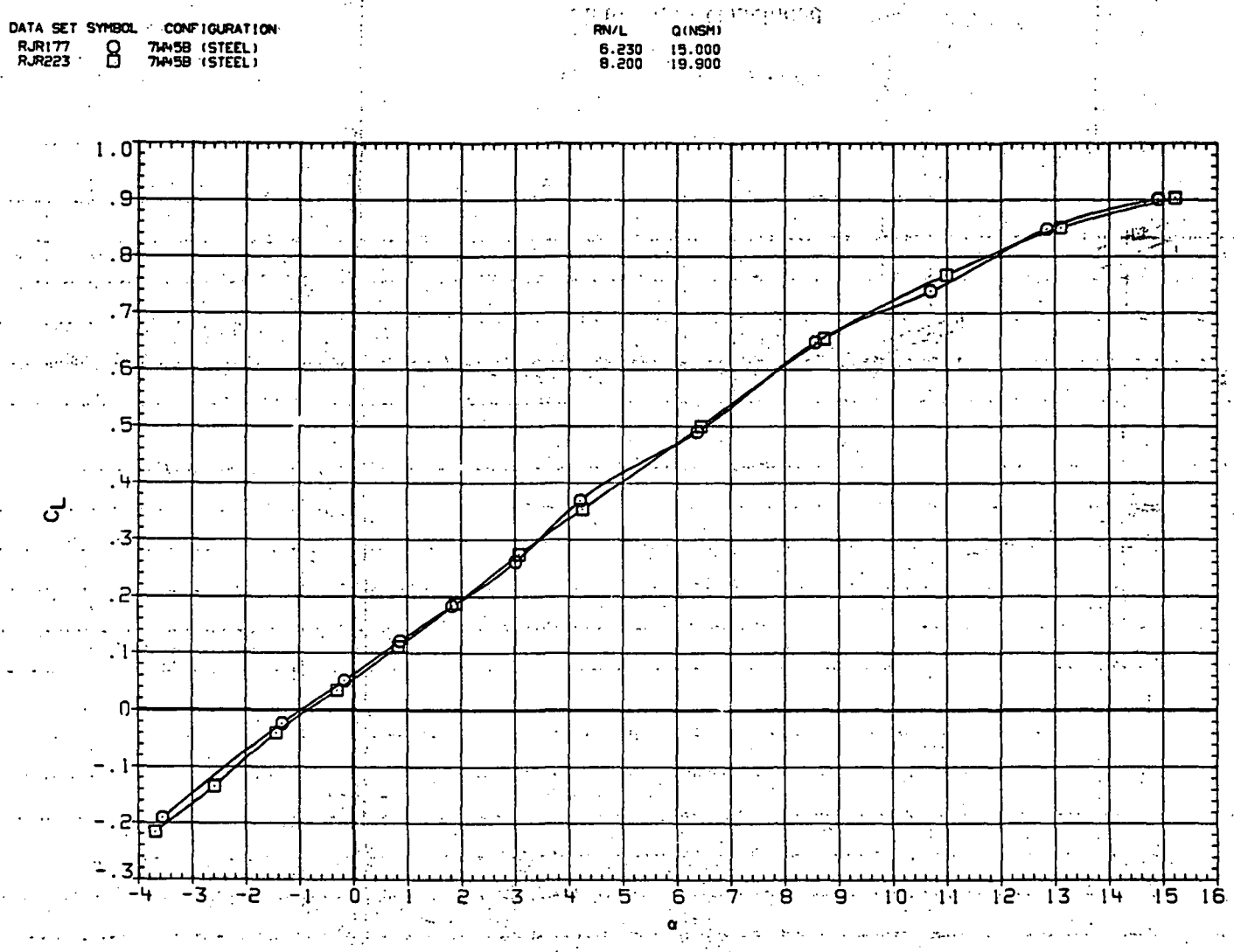

(a) C_L vs α.

Figure 53.– Dynamic-pressure effects on the aerodynamic characteristics of the steel trapezoidal oblique wing-body combination ($\Lambda = 45°$, M =0.95 and the NACA 65A204 airfoil).

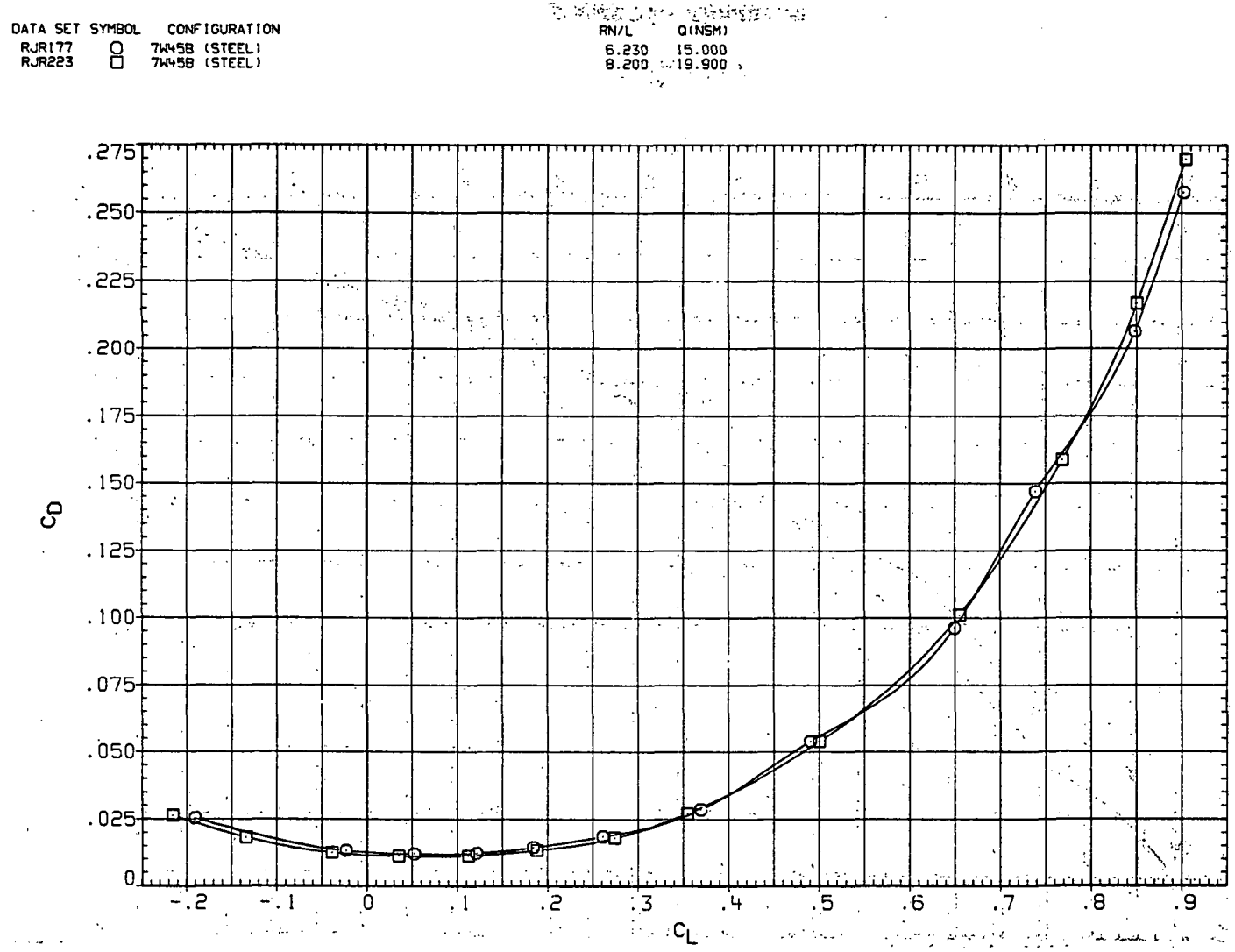

(b) C_D vs C_L.

Figure 53.– Continued.

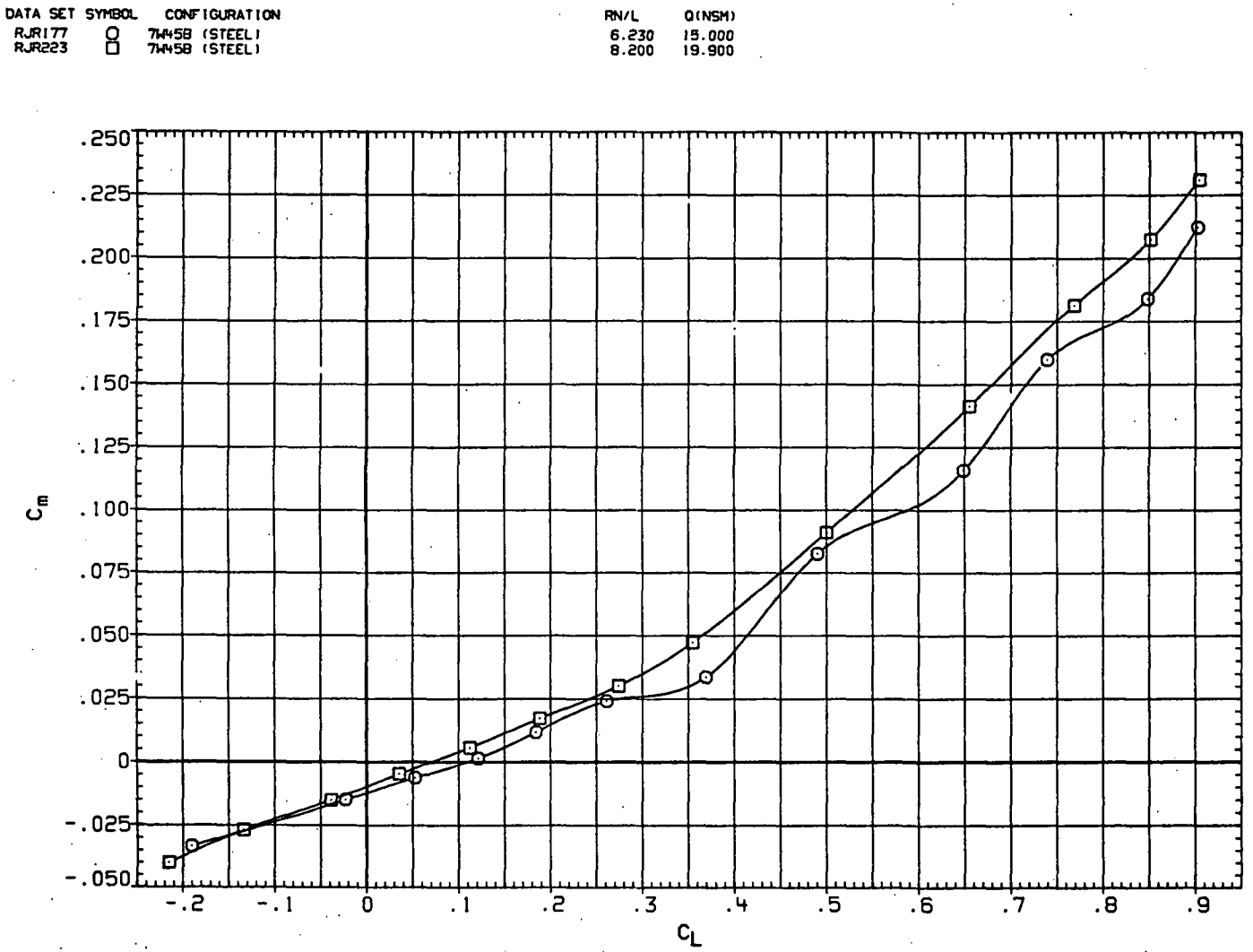

(c) C_m vs C_L.

Figure 53.– Continued.

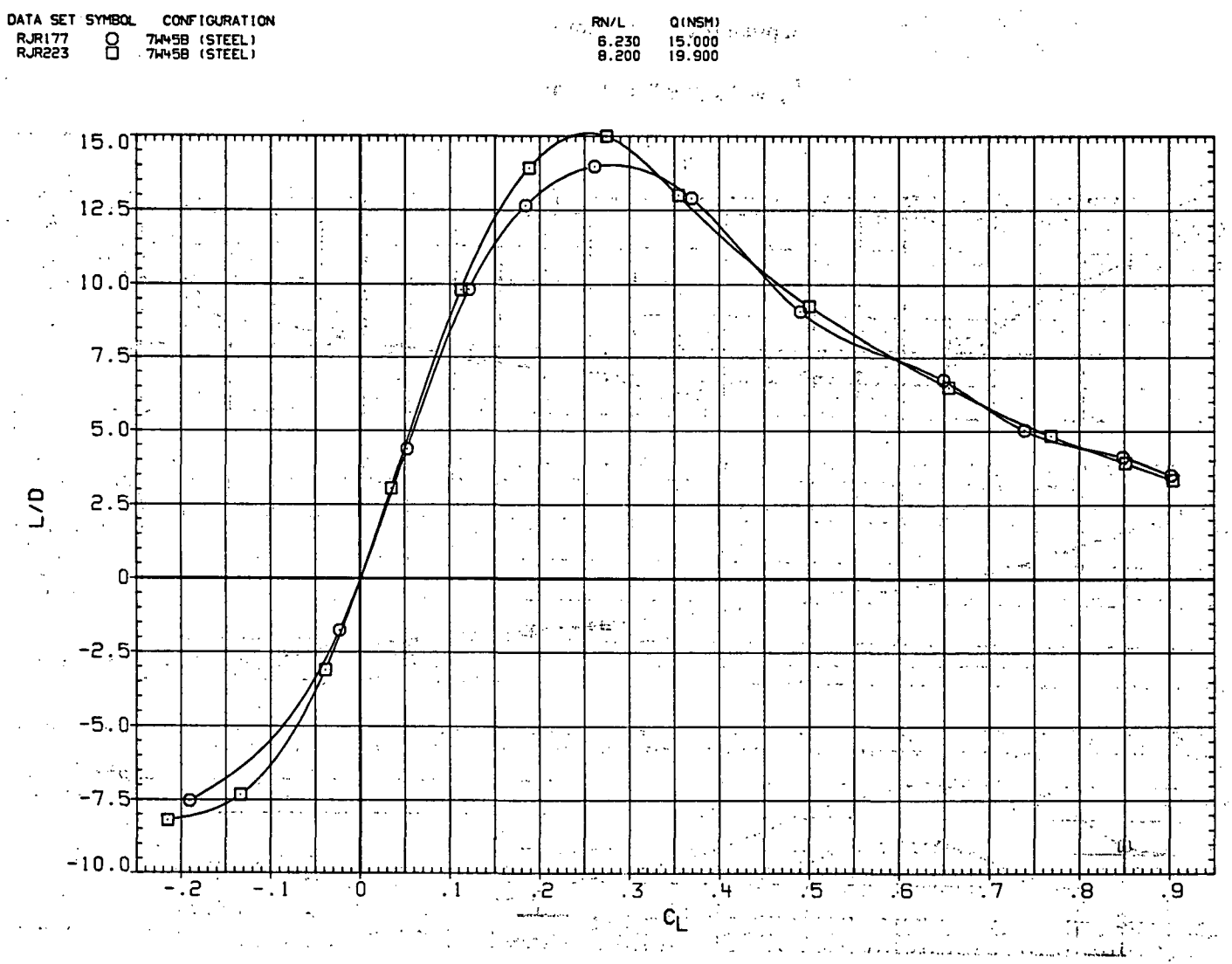

(d) L/D vs C_L.

Figure 53.—Continued.

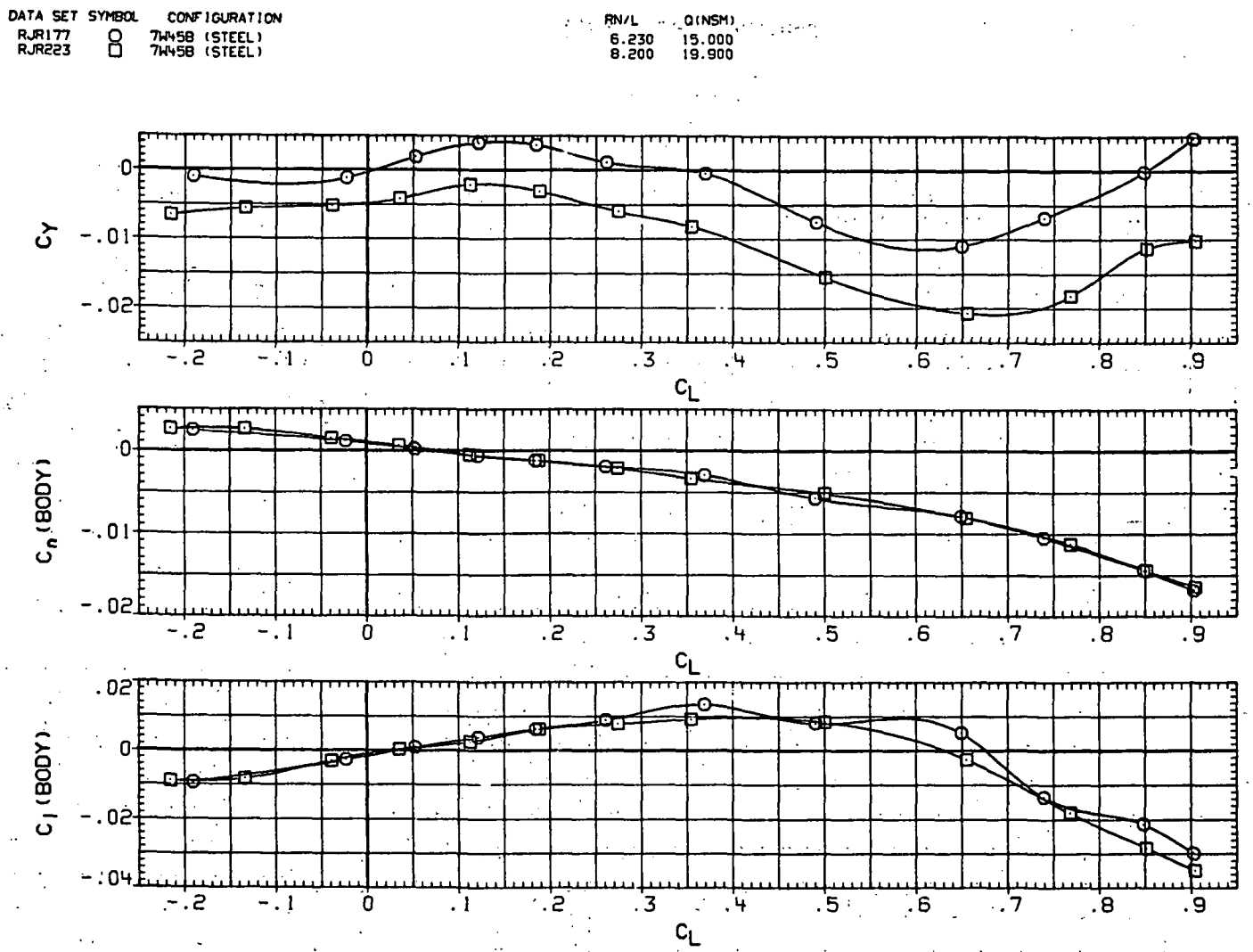

(e) C_Y, C_n and C_ℓ vs C_L.

Figure 53.– Concluded.

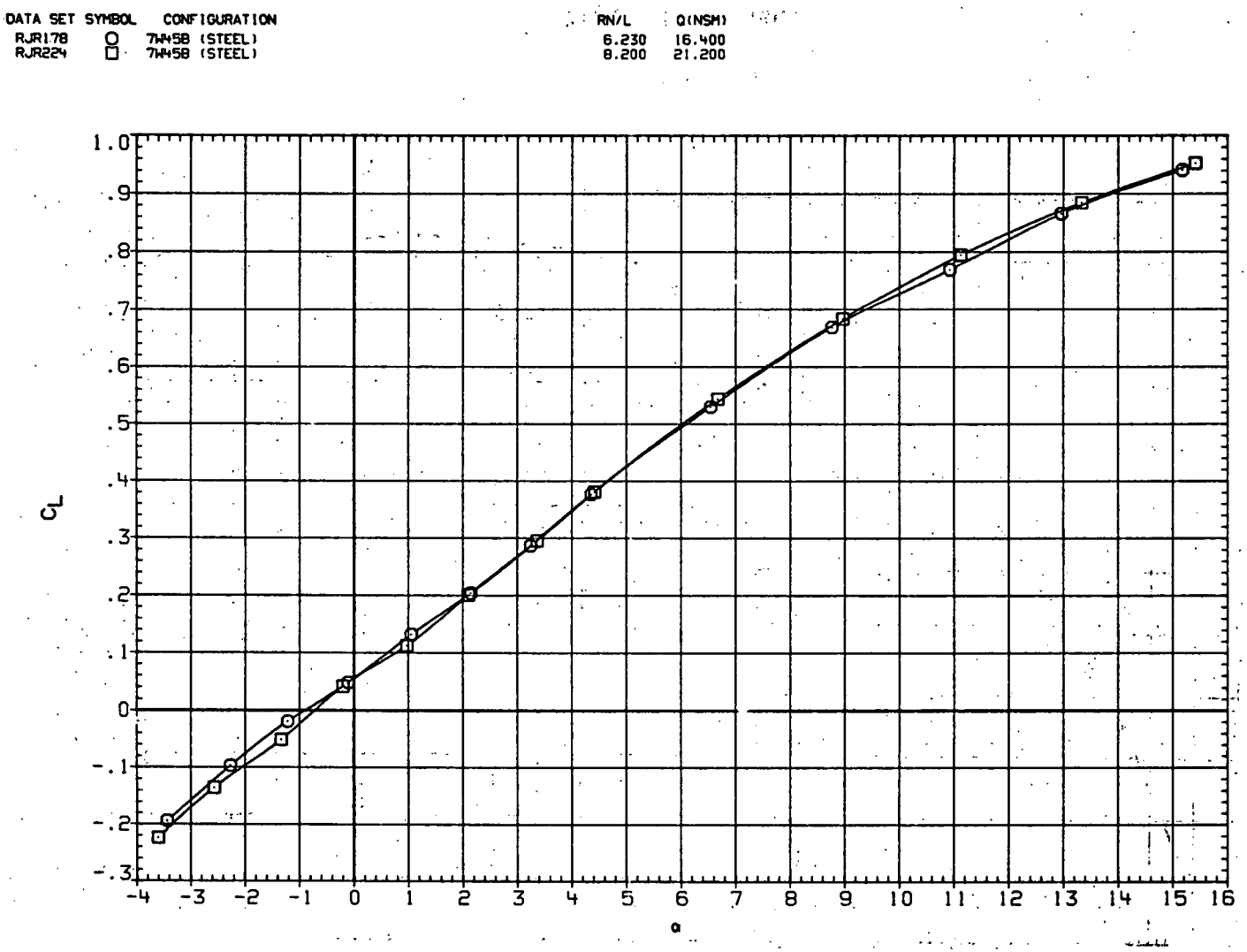

(a) C_L vs α.

Figure 54.– Dynamic-pressure effects on the aerodynamic characteristics of the steel trapezoidal oblique wing-body combination ($\Lambda = 45°, M = 1.1$ and the NACA 65A204 airfoil).

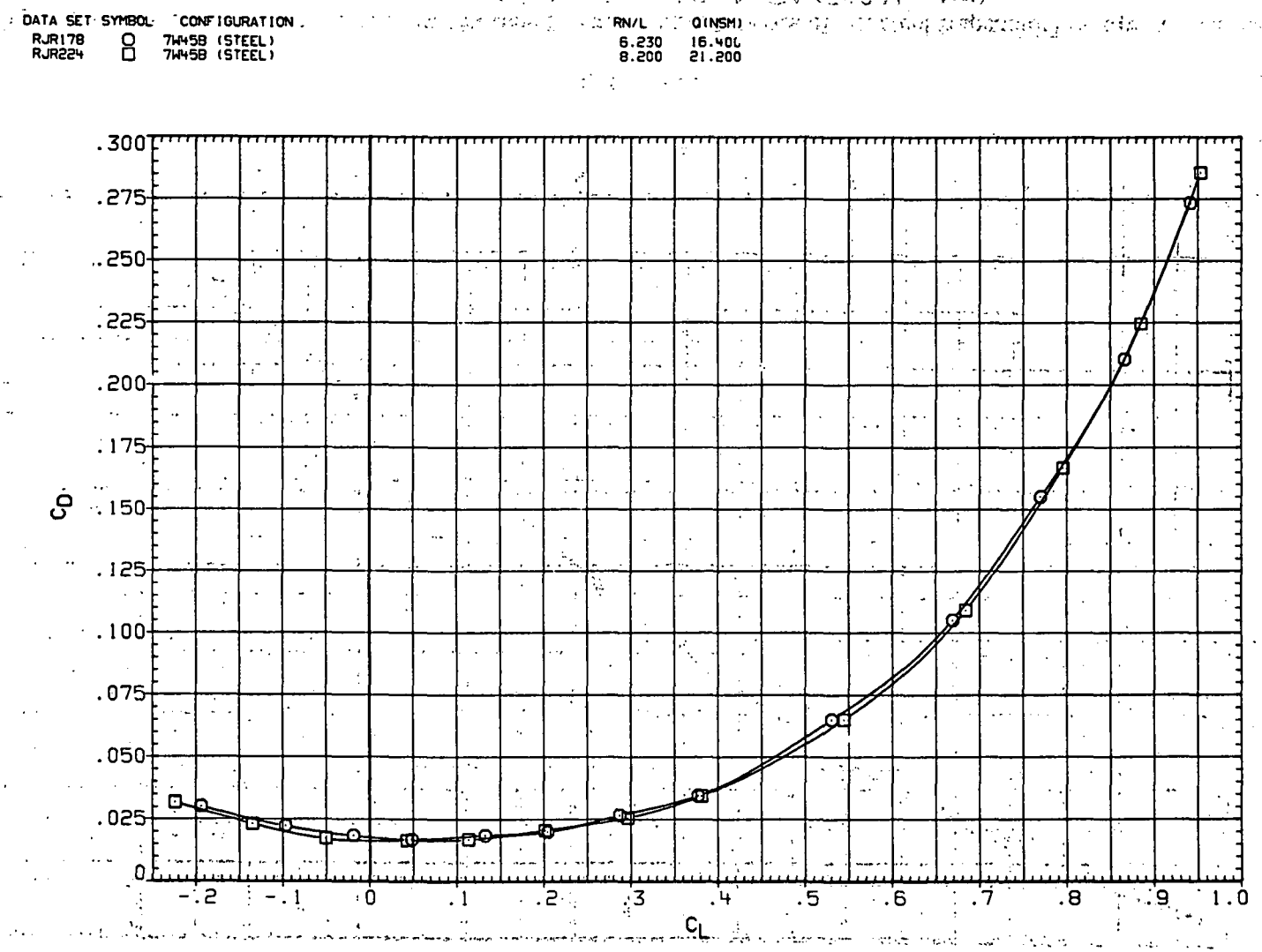

(b) C_D vs C_L.

Figure 54.– Continued.

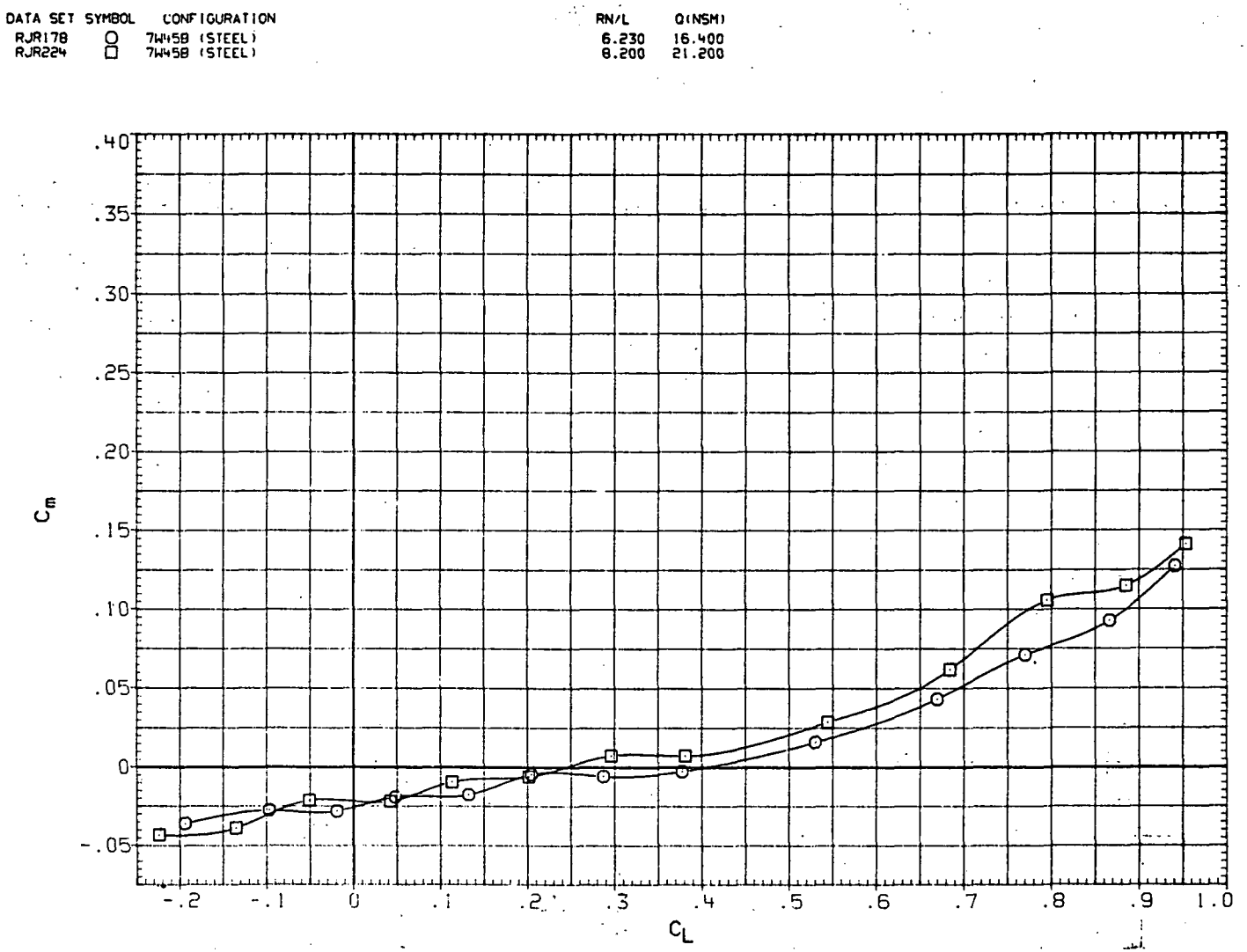

(c) C_m vs C_L.

Figure 54.– Continued.

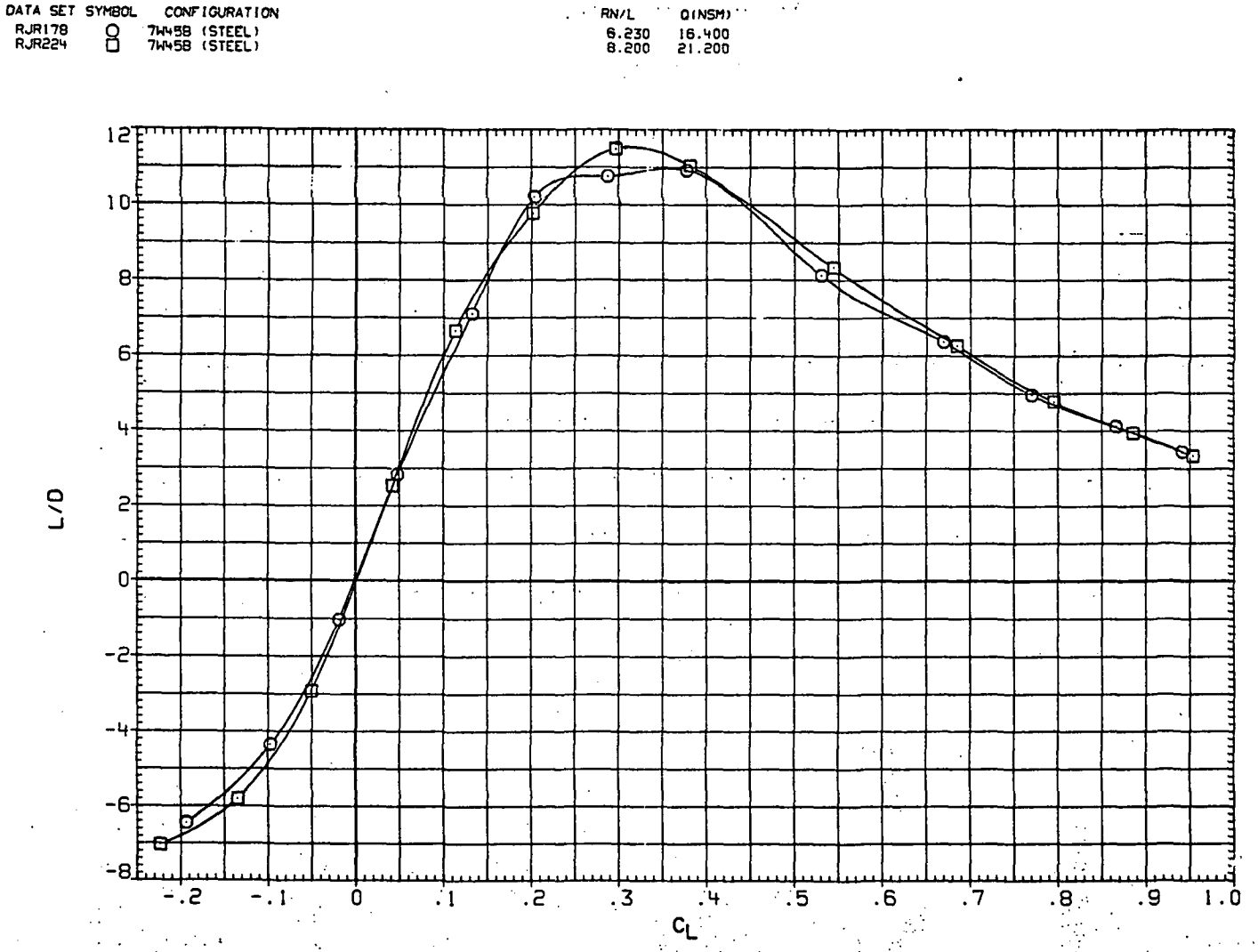

(d) L/D vs C_L.

Figure 54.— Continued.

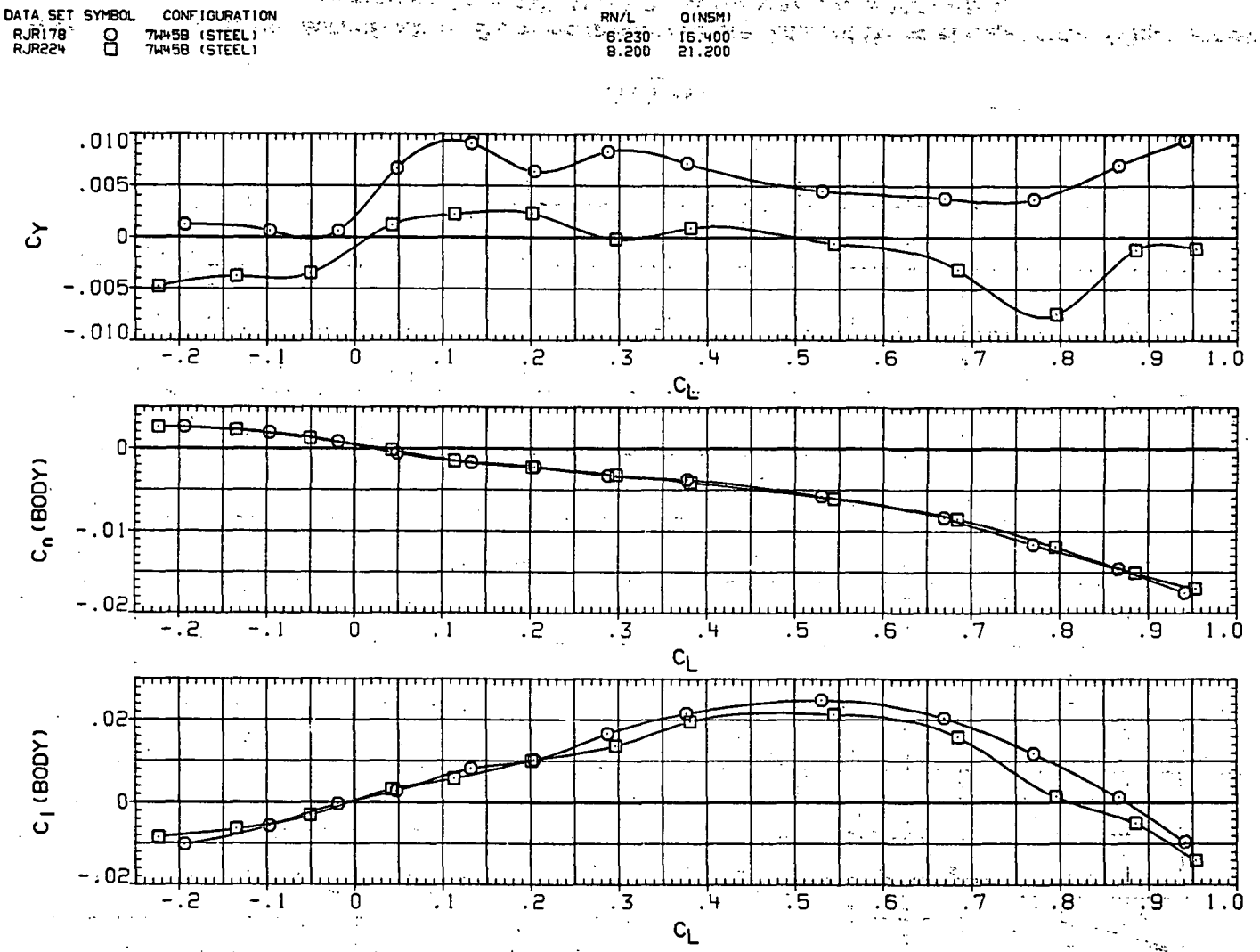

(e) C_Y, C_n and C_ℓ vs C_L.

Figure 54.—Concluded.

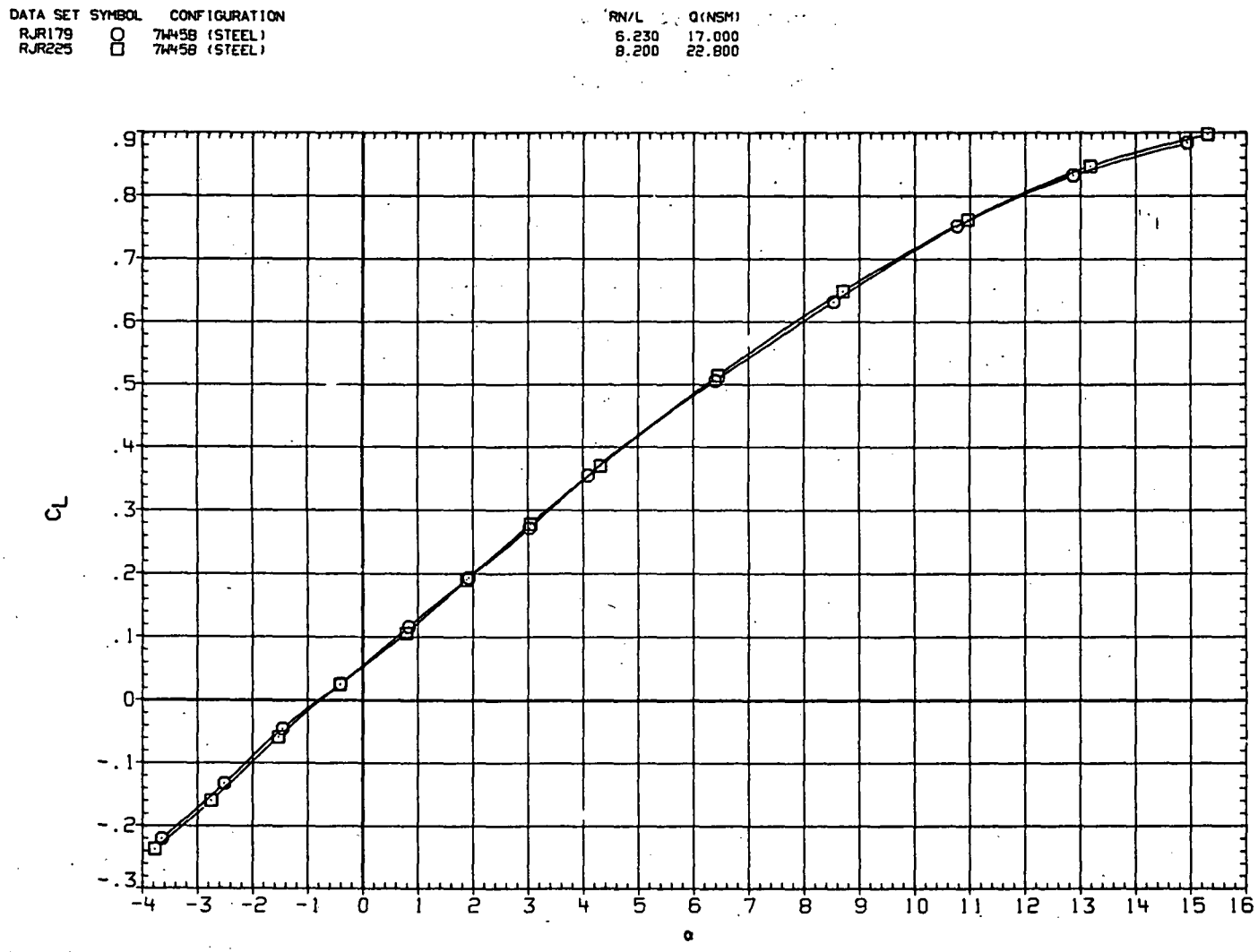

(a) C_L vs α.

Figure 55.– Dynamic-pressure effects on the aerodynamic characteristics of the steel trapezoidal oblique wing-body combination ($\Lambda = 45°, M = 1.2$ and the NACA 65A204 airfoil).

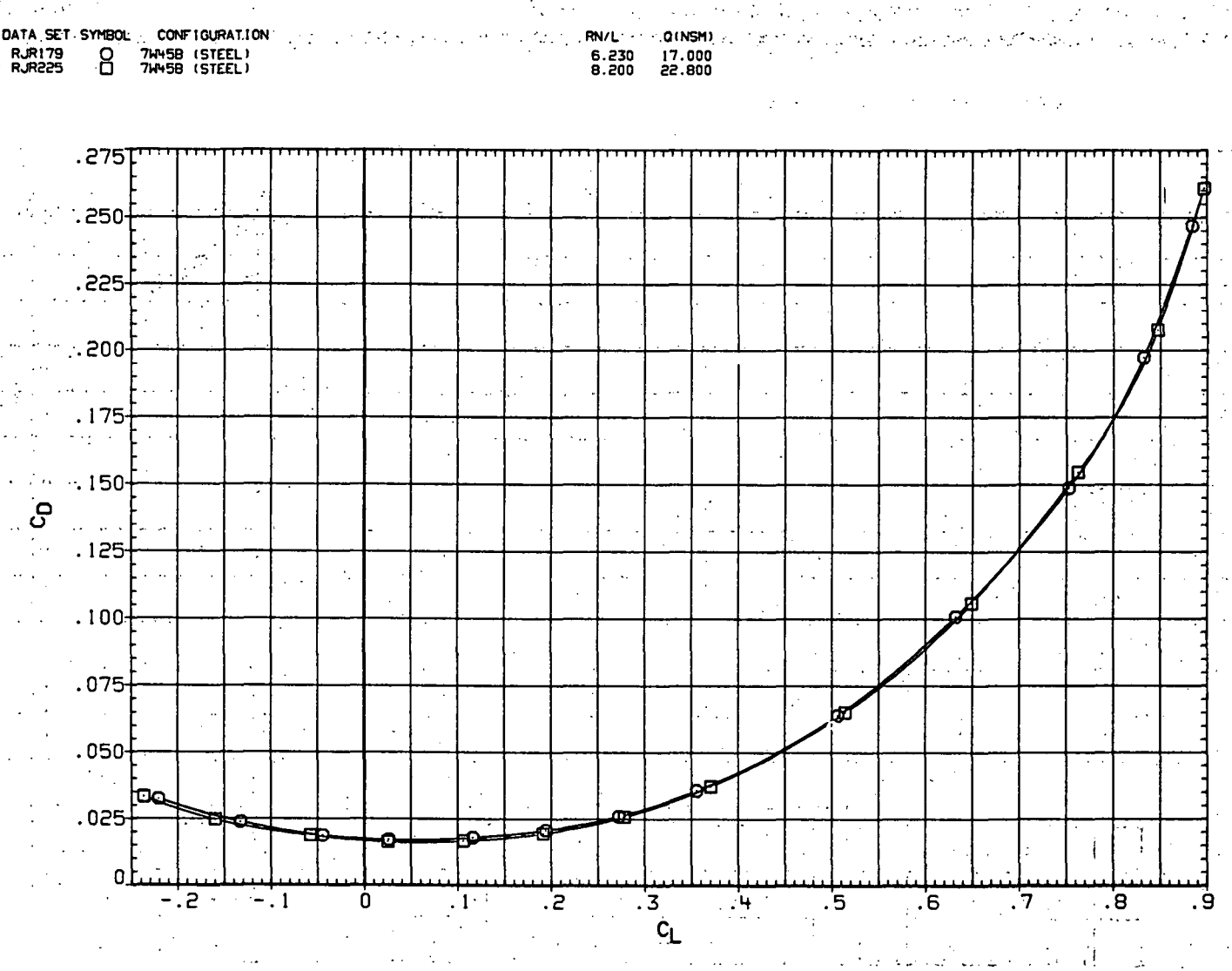

(b) C_D vs C_L.

Figure 55.– Continued.

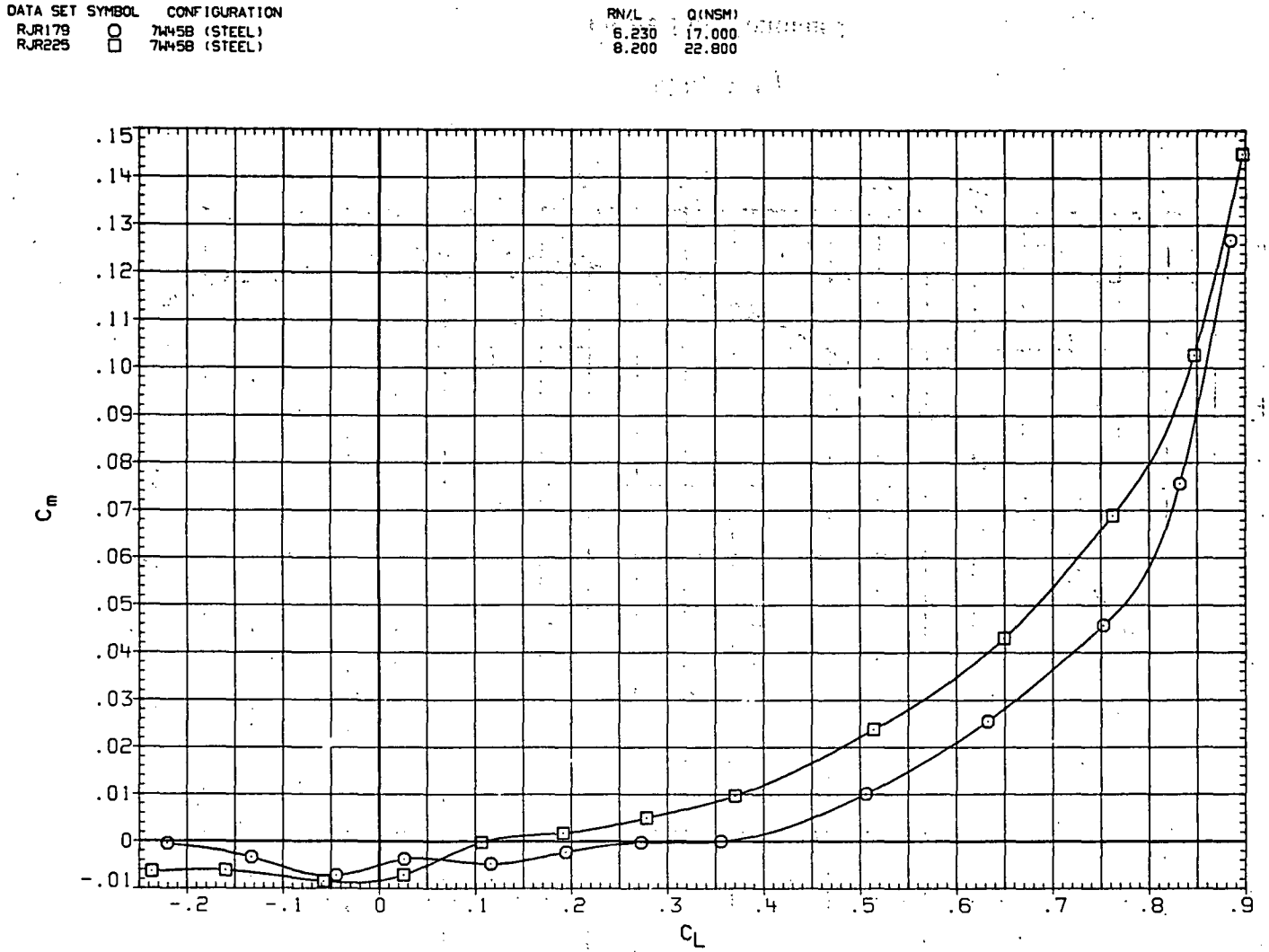

(c) C_m vs C_L.

Figure 55.– Continued.

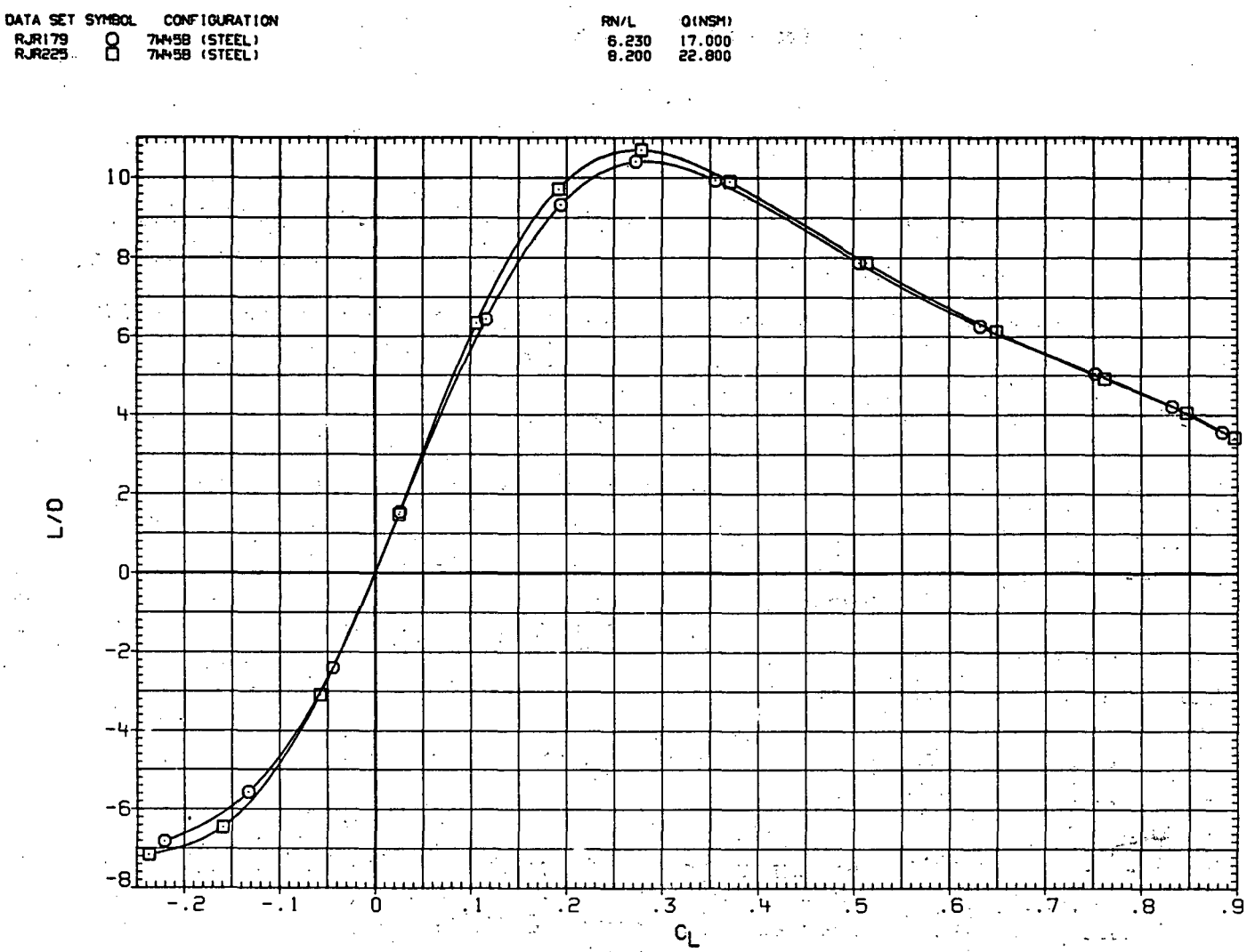

(d) L/D vs C_L.

Figure 55.– Continued.

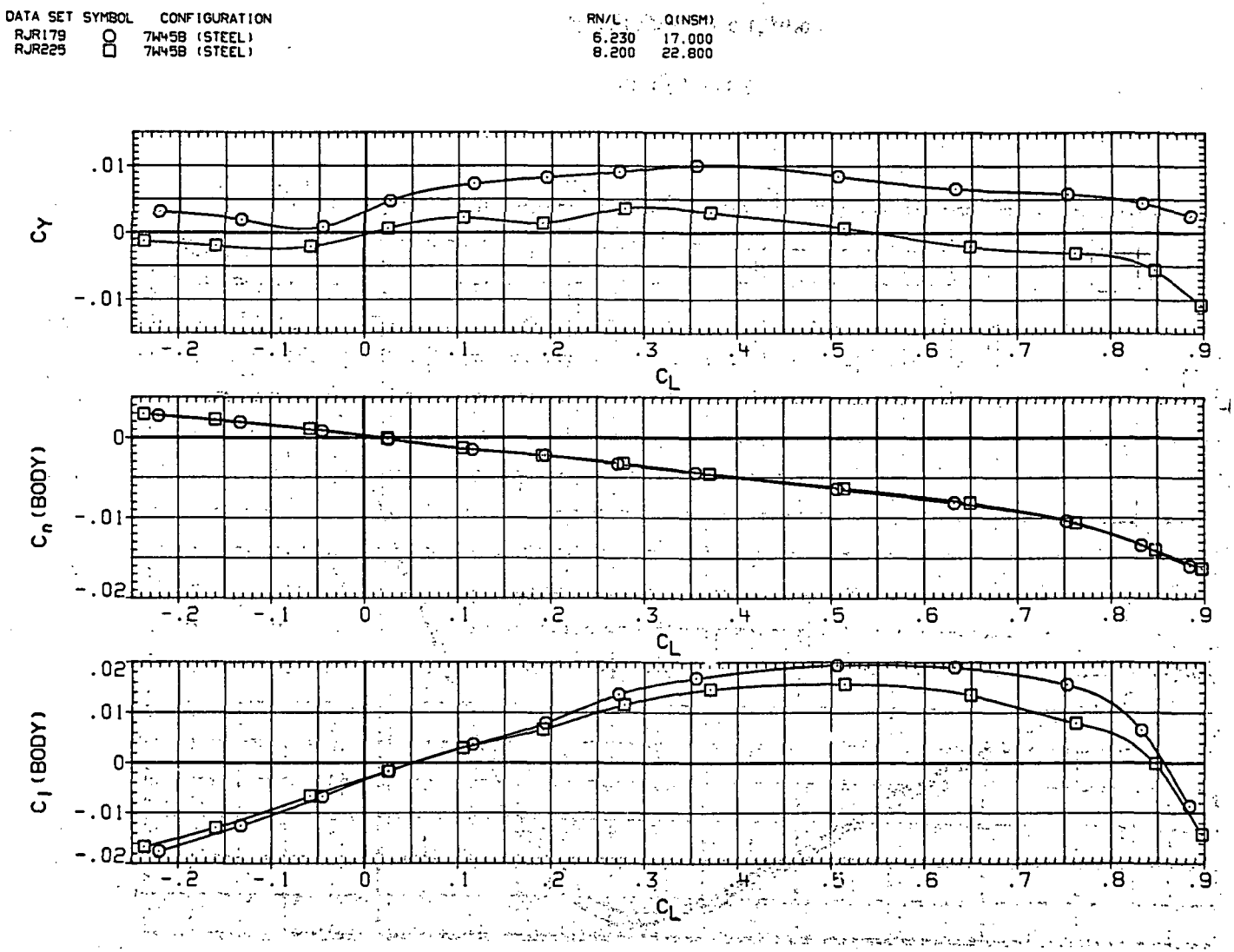

(e) C_Y, C_n and C_ℓ vs C_L.

Figure 55.– Concluded.

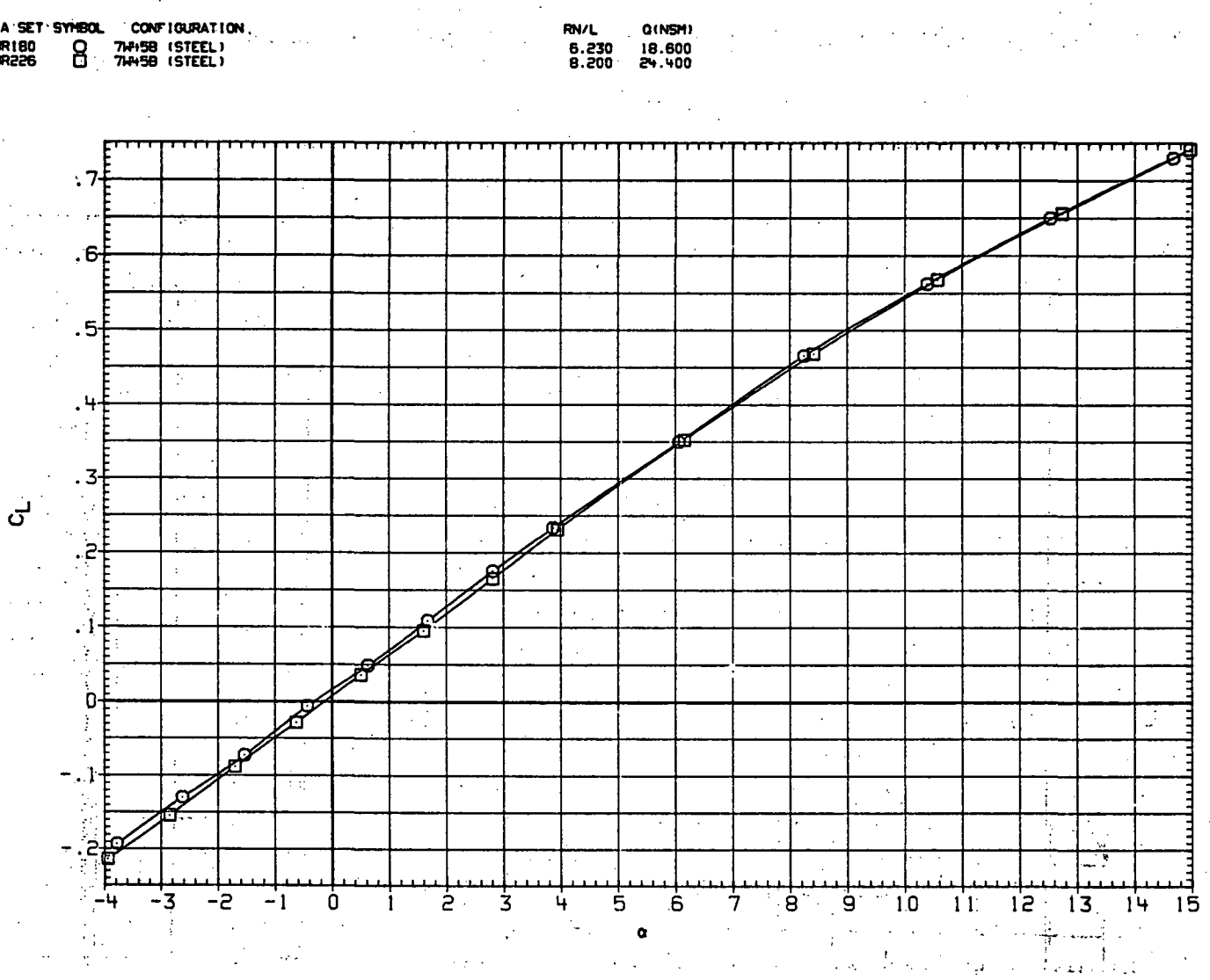

(a) C_L vs α.

Figure 56.– Dynamic-pressure effects on the aerodynamic characteristics of the steel trapezoidal oblique wing-body combination ($\Lambda = 45°$, $M = 1.6$ and the NACA 65A204 airfoil).

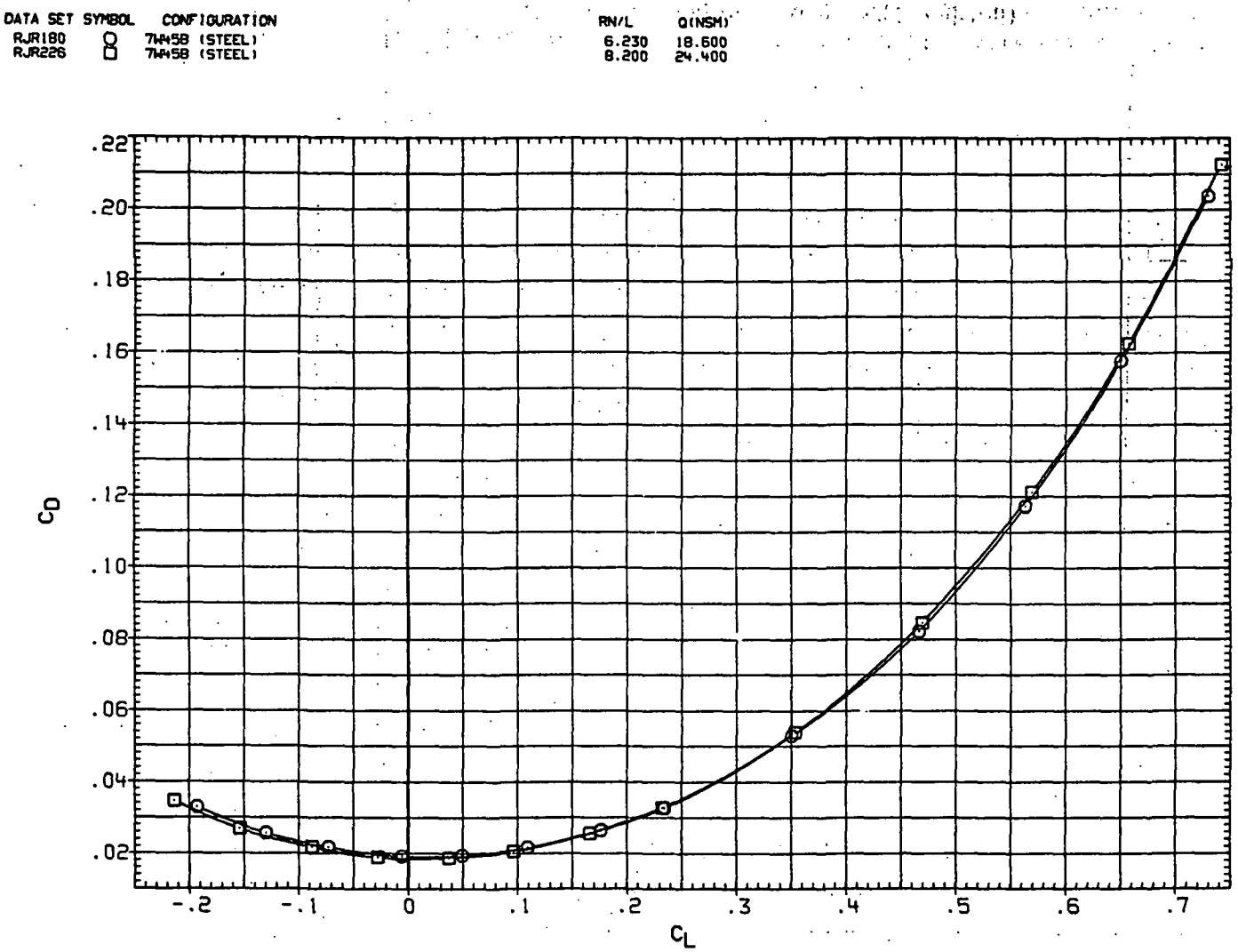

(b) C_D vs C_L.

Figure 56.– Continued.

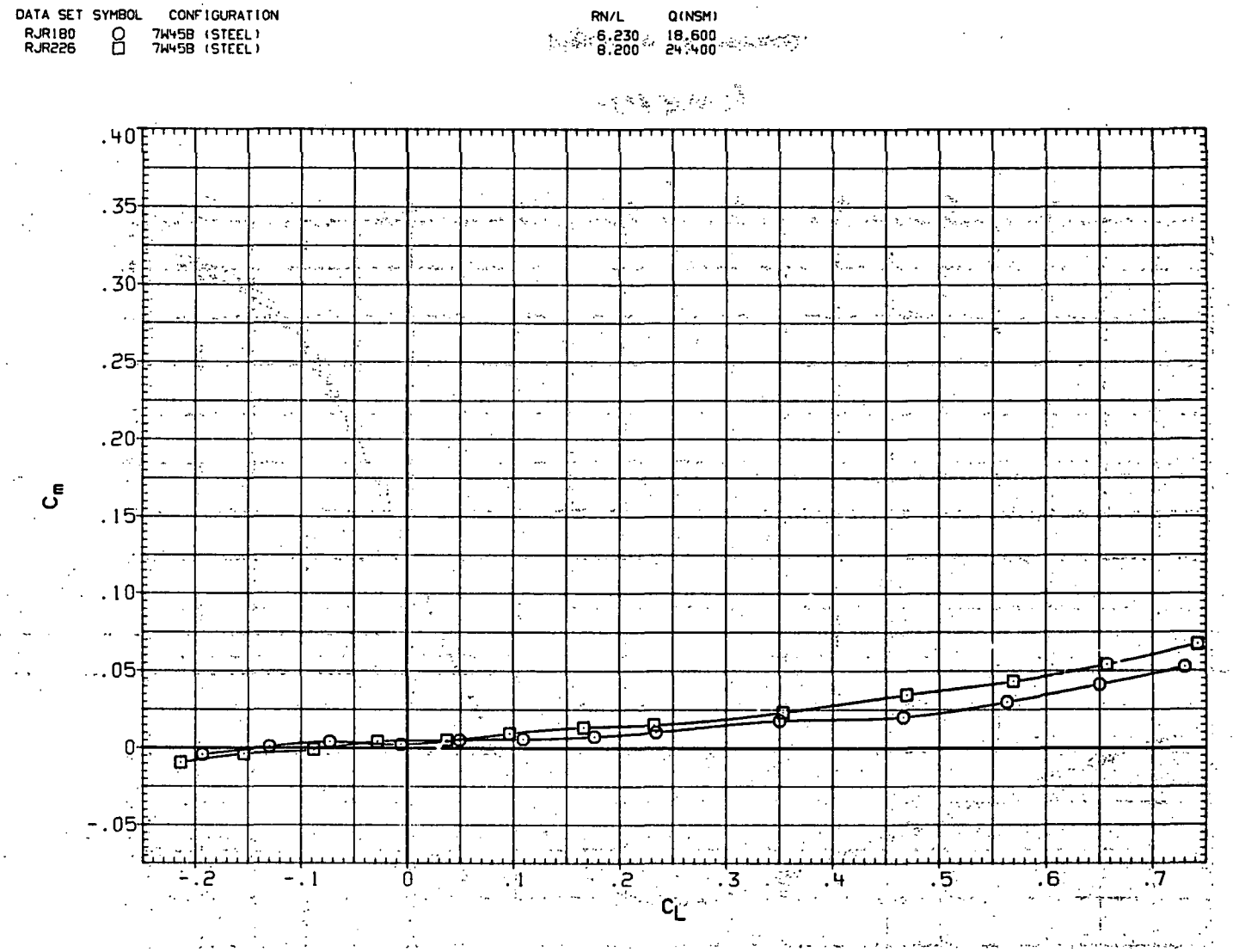

(c) C_m vs C_L.

Figure 56.– Continued.

(d) L/D vs C_L.

Figure 56.– Continued.

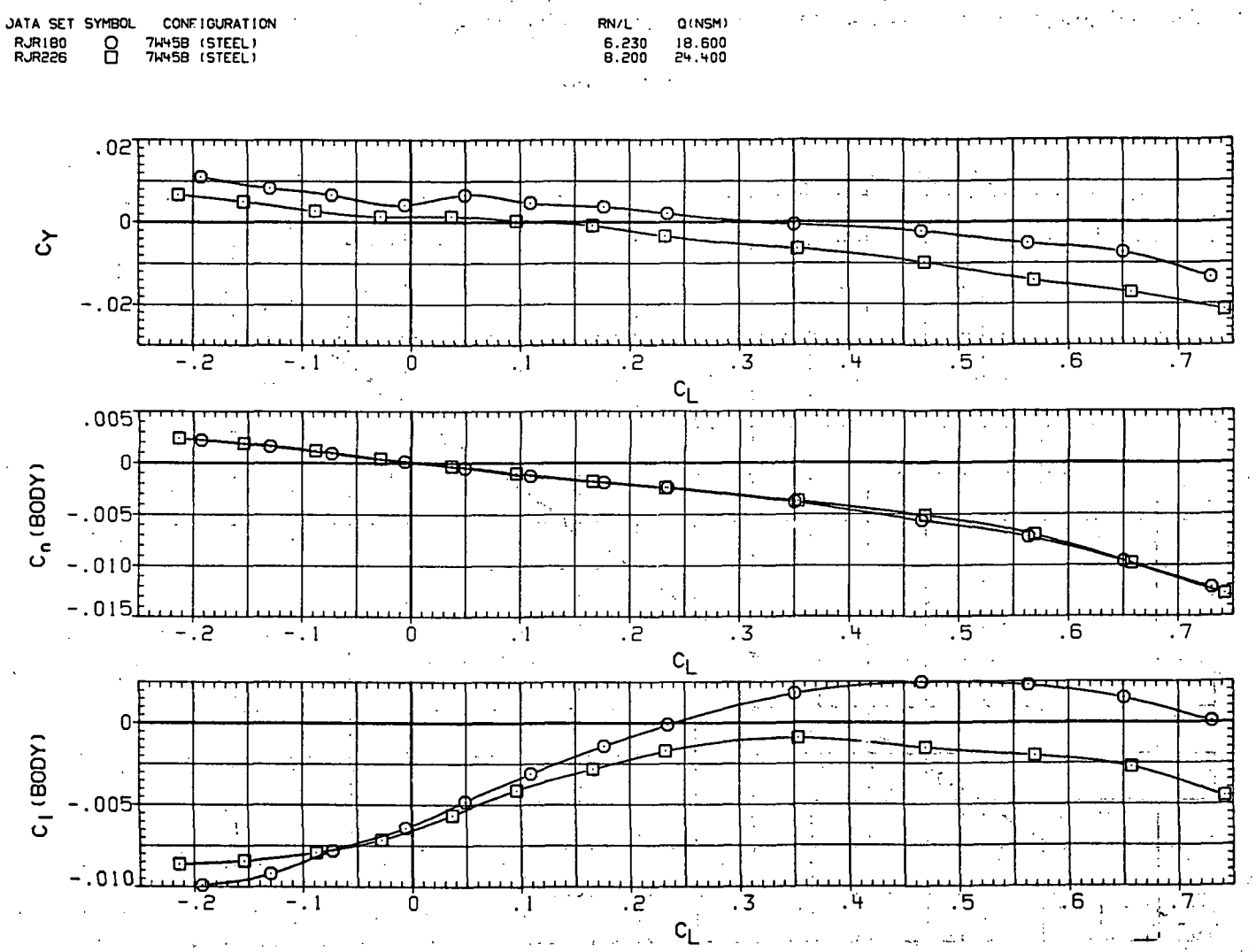

(e) C_Y, C_n and C_ℓ vs C_L.

Figure 56.– Concluded.

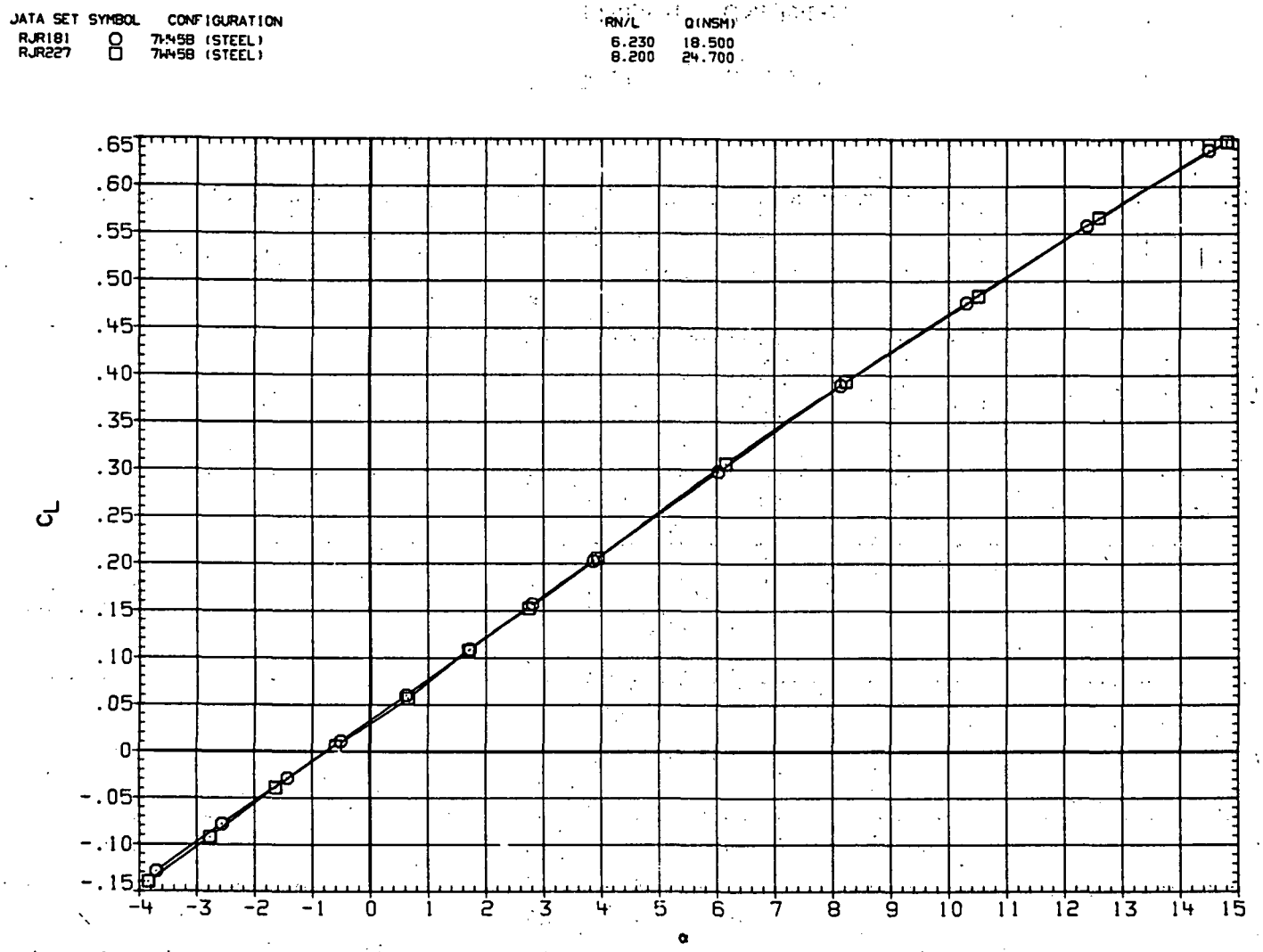

(a) C_L vs α.

Figure 57.– Dynamic-pressure effects on the aerodynamic characteristics of the steel trapezoidal oblique wing-body combination ($\Lambda = 45°$, $M = 2.0$ and the NACA 65A204 airfoil).

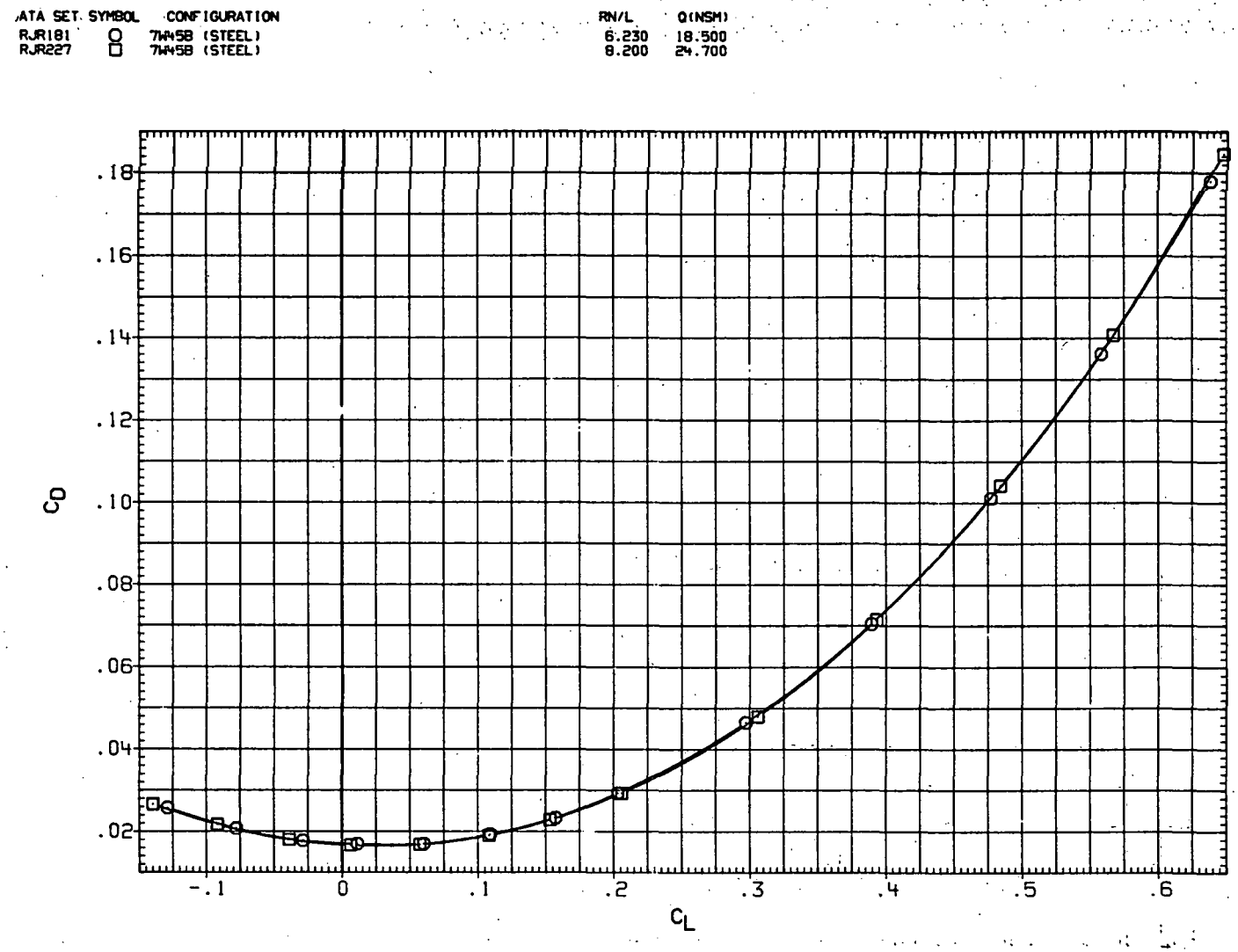

(b) C_D vs C_L.

Figure 57.– Continued.

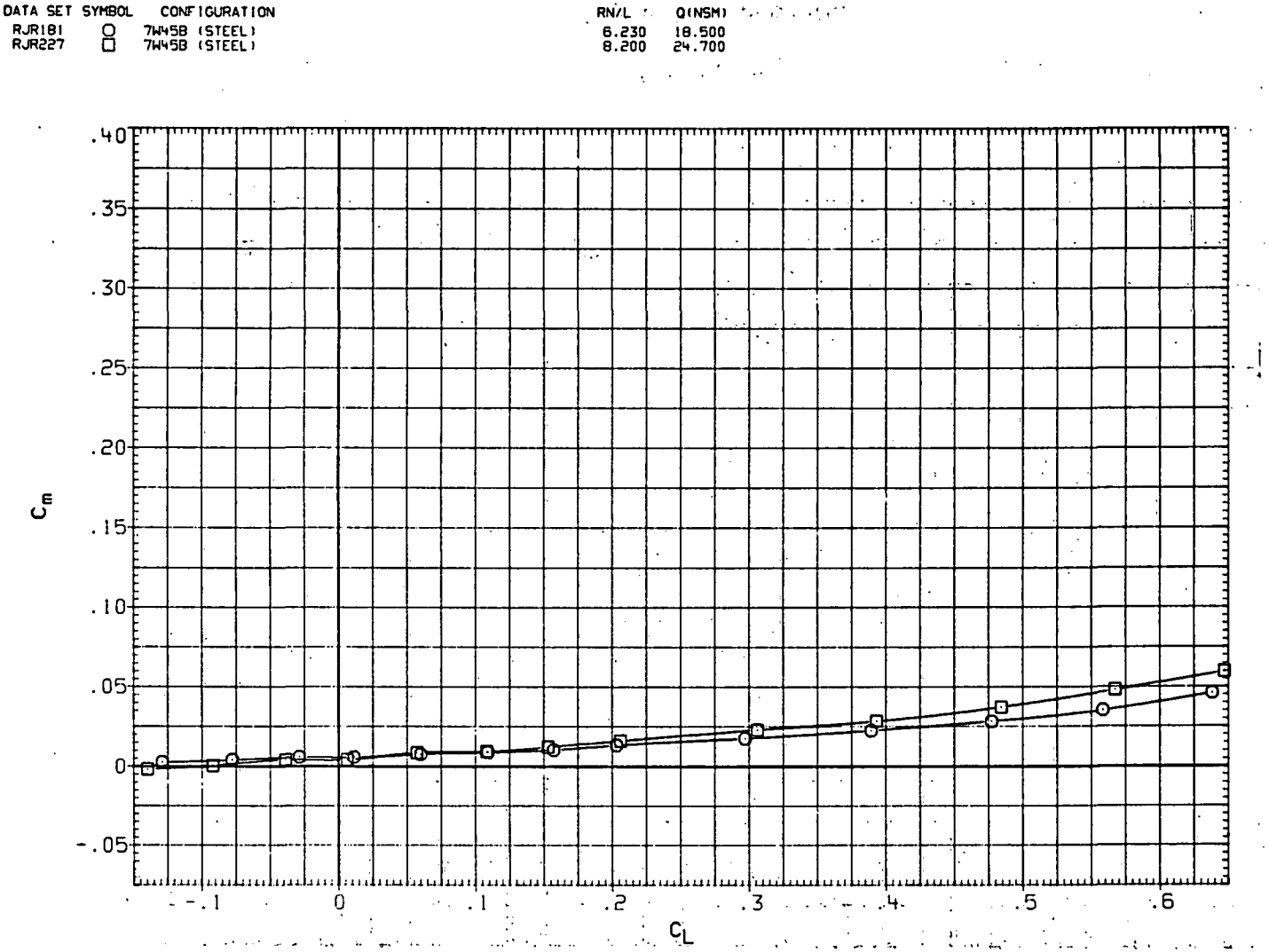

(c) C_m vs C_L.

Figure 57.– Continued.

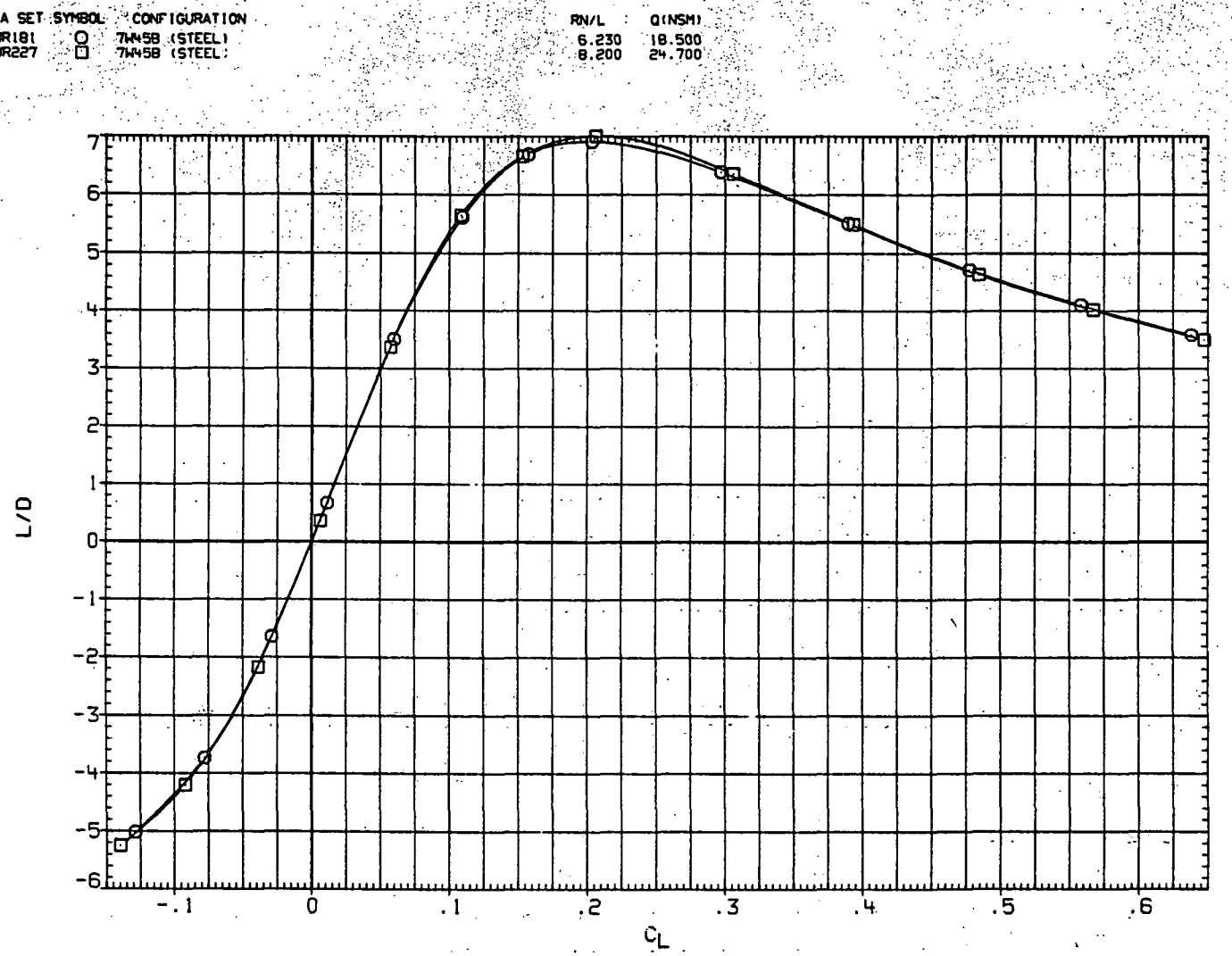

(d) L/D vs C_L.

Figure 57.– Continued.

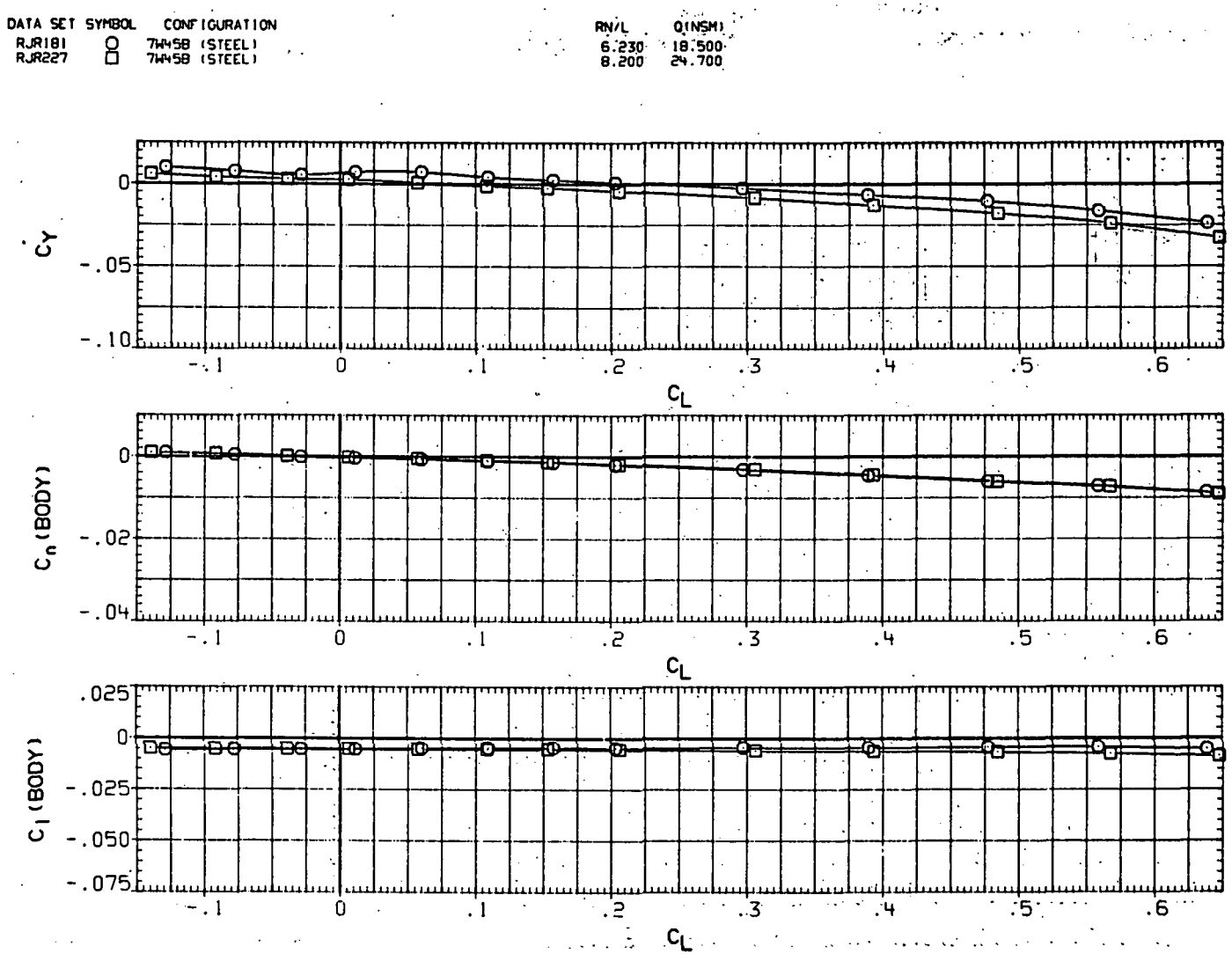

(e) C_Y, C_n and C_ℓ vs C_L.

Figure 57.– Concluded.

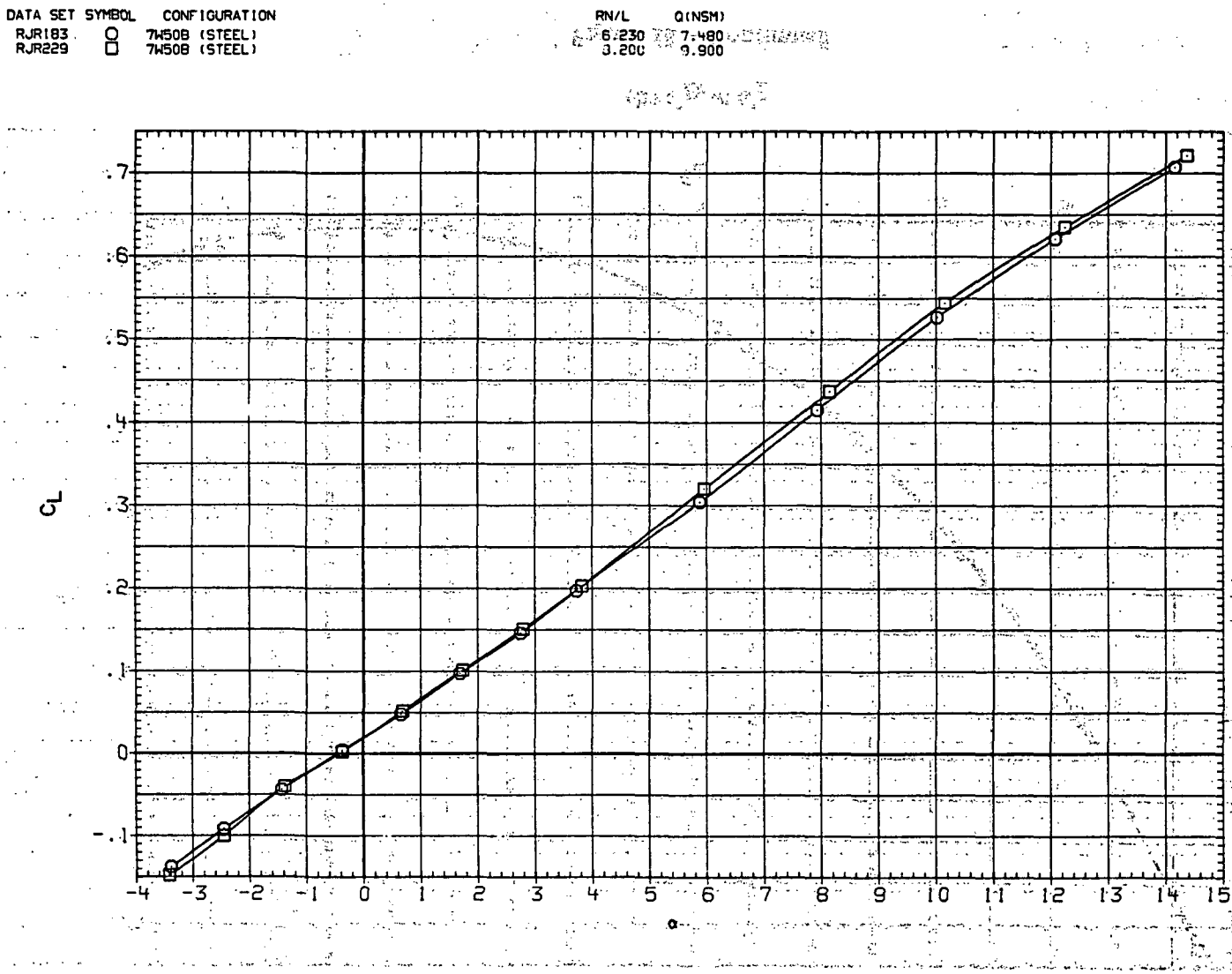

(a) C_L vs α.

Figure 58.– Dynamic-pressure effects on the aerodynamic characteristics of the steel trapezoidal oblique wing-body combination ($\Lambda = 50°$, $M = 0.4$ and the NACA 65A204 airfoil).

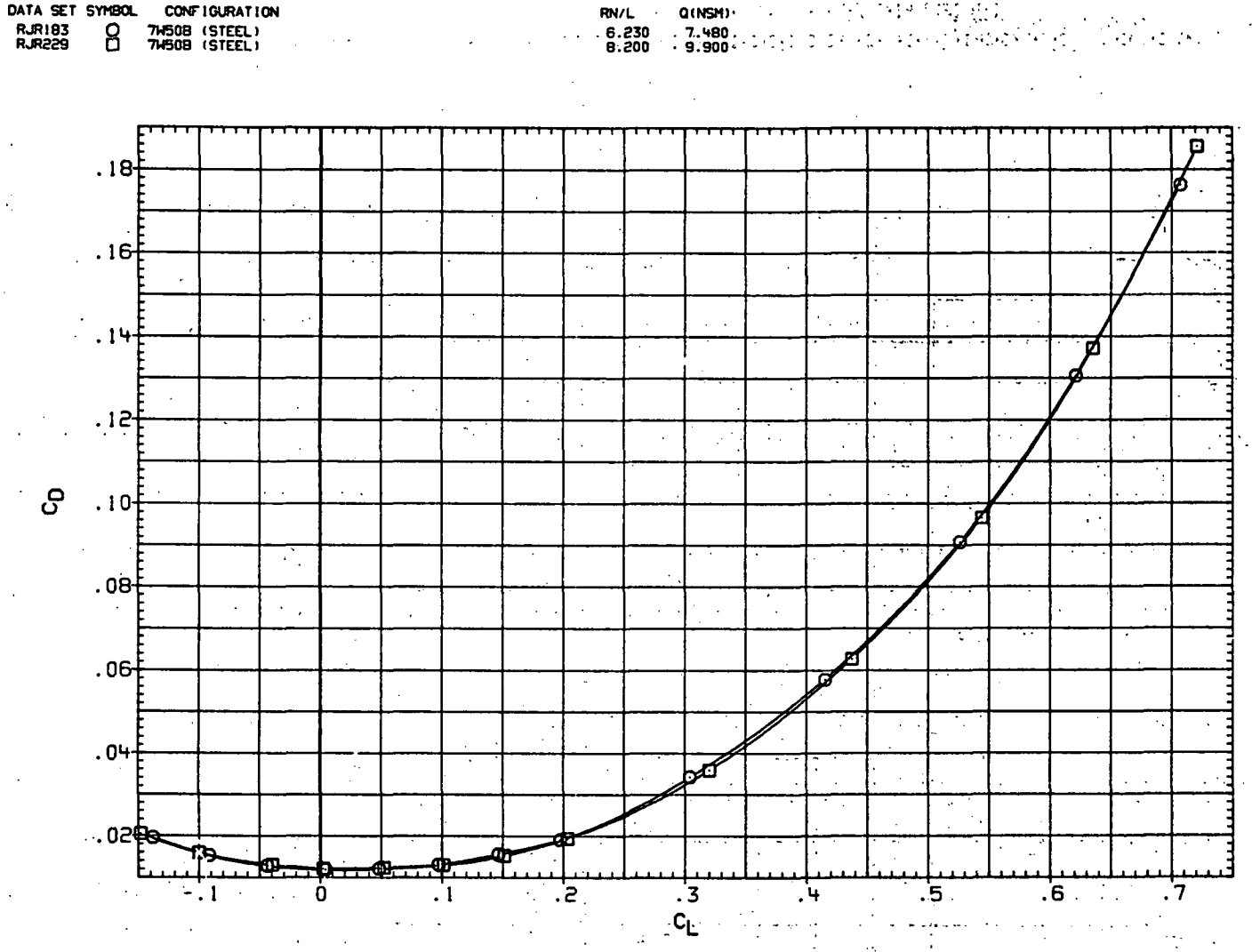

(b) C_D vs C_L.

Figure 58.– Continued.

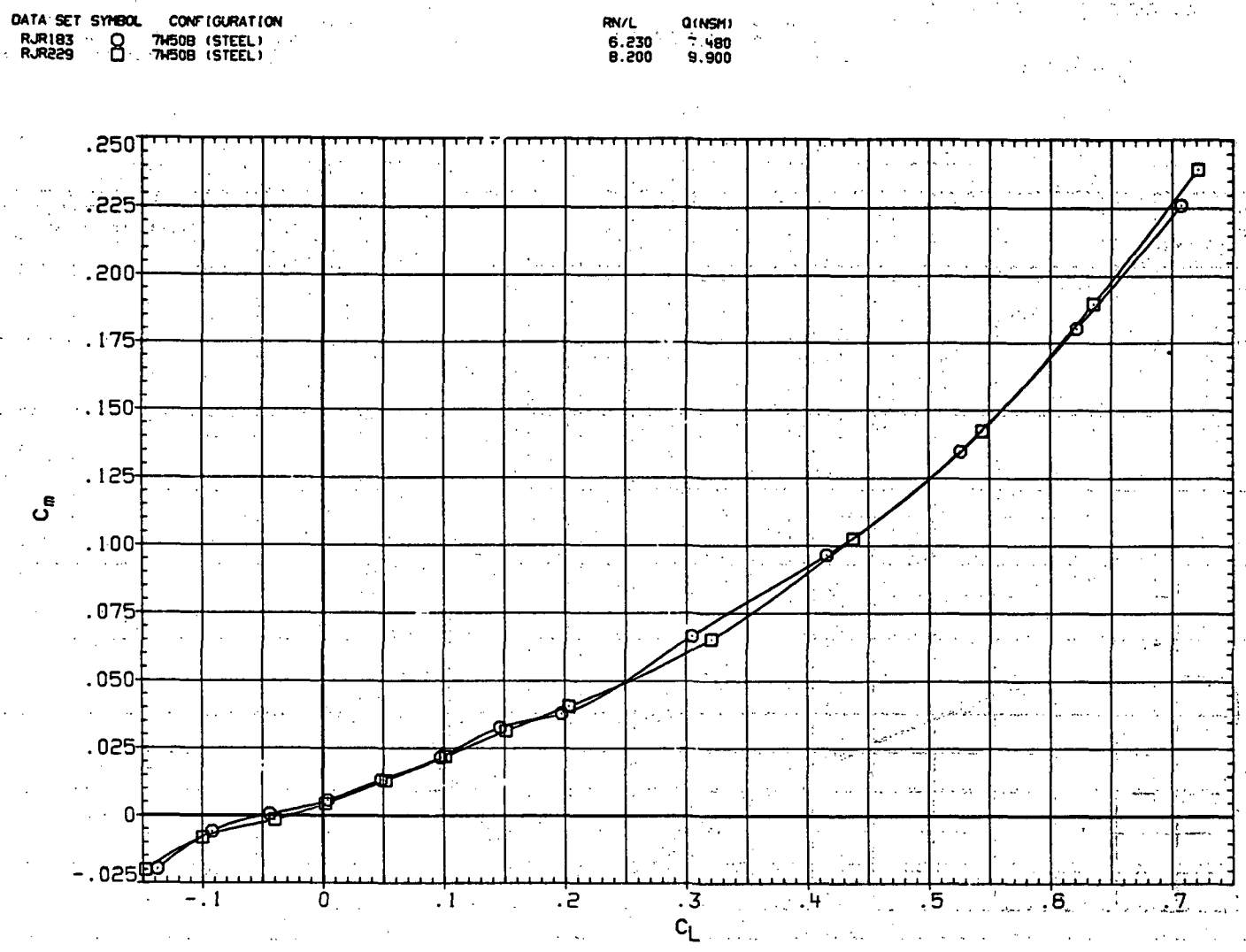

(c) C_m vs C_L.

Figure 58.– Continued.

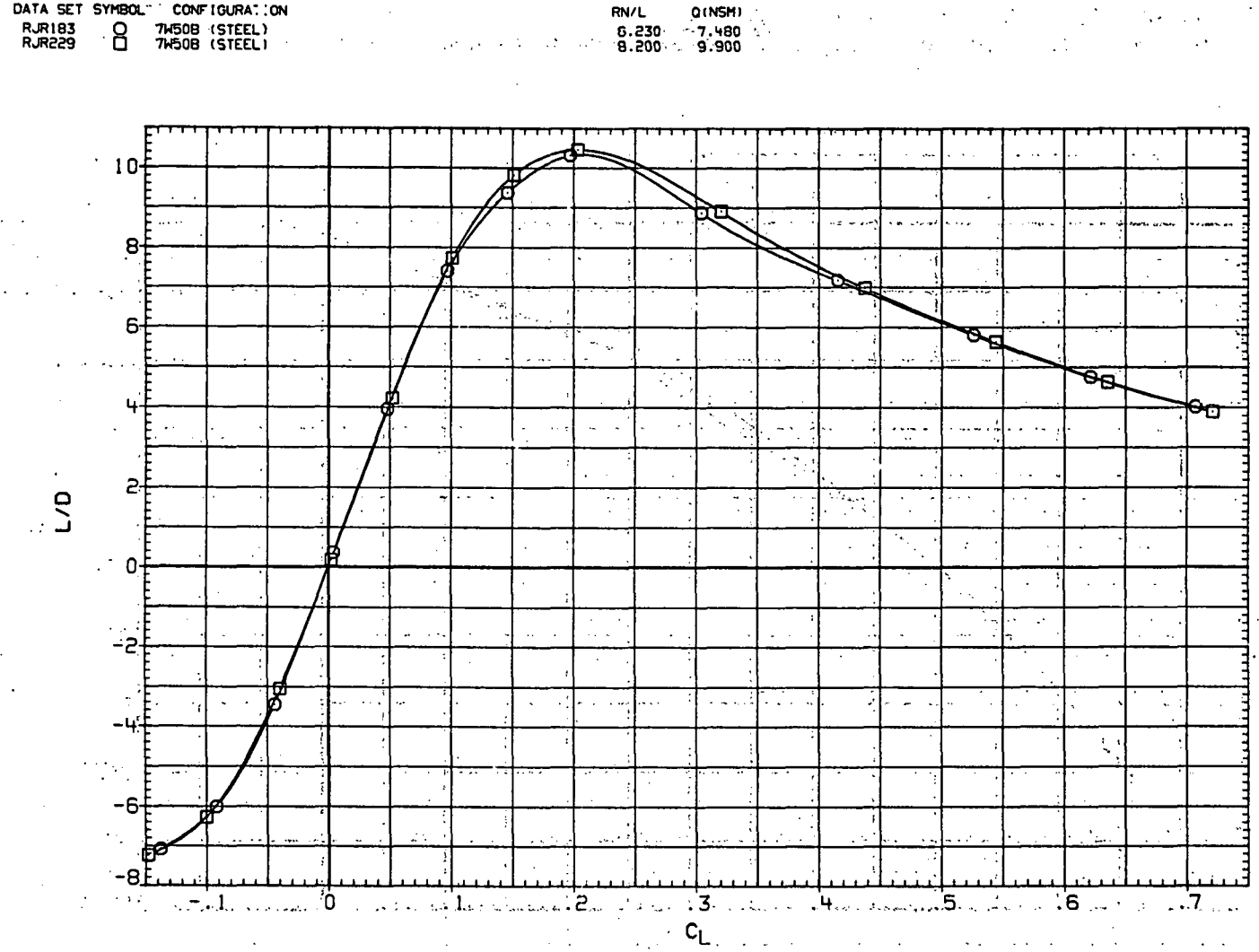

(d) L/D vs C_L.

Figure 58.– Continued.

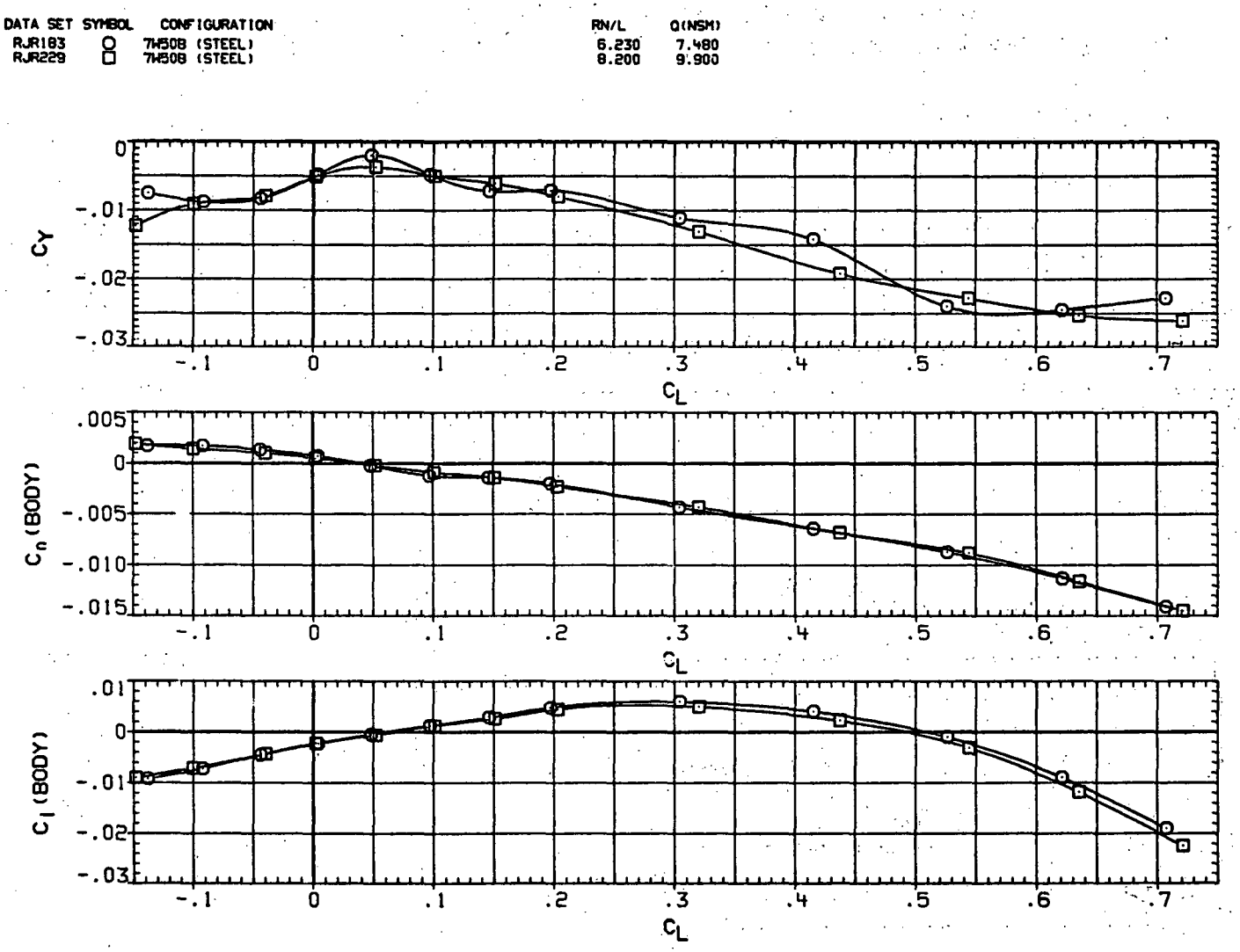

(e) C_Y, C_n and C_ℓ vs C_L.

Figure 58.– Concluded.

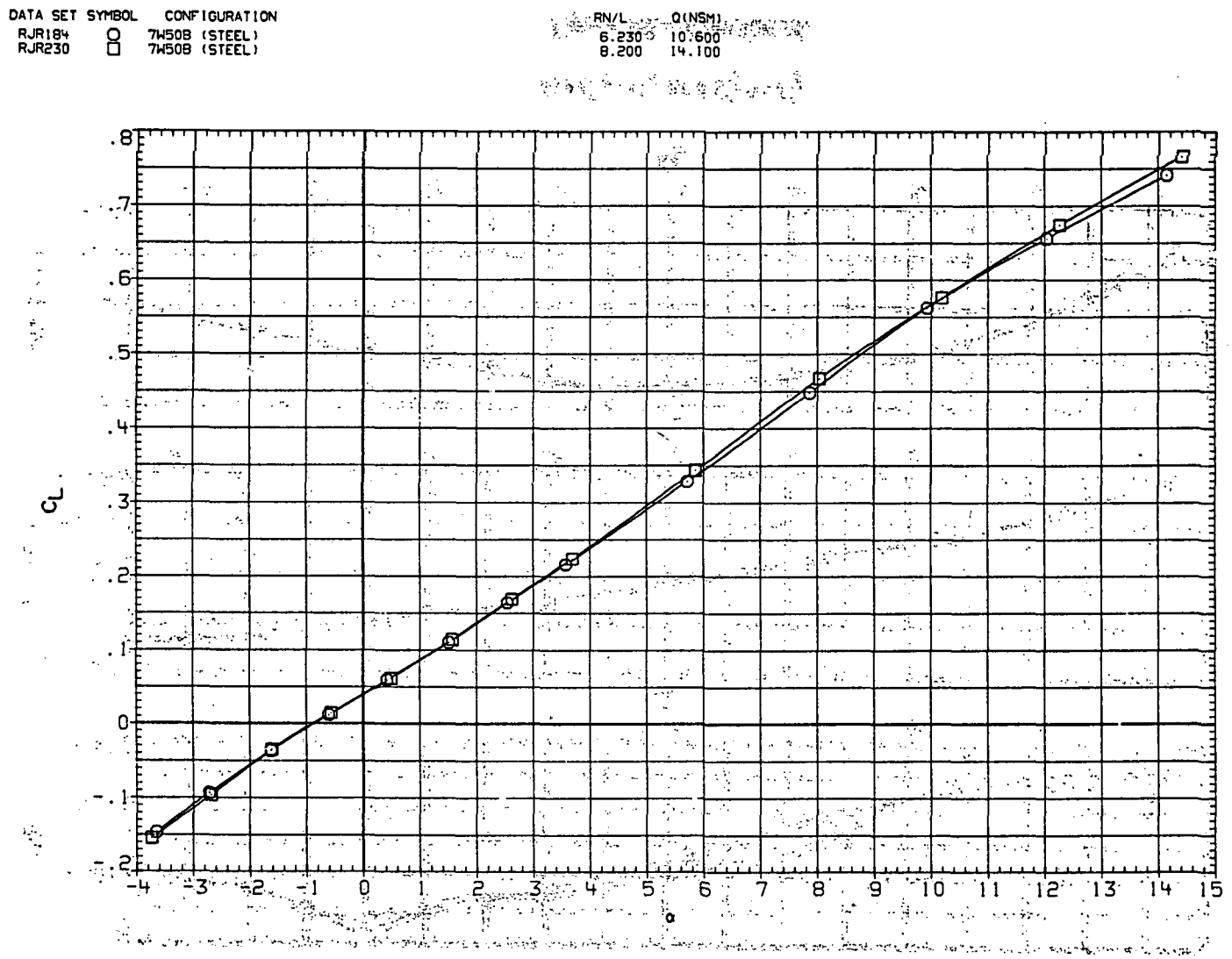

(a) C_L vs α.

Figure 59.– Dynamic-pressure effects on the aerodynamic characteristics of the steel trapezoidal oblique wing-body combination ($\Lambda = 50°$, $M = 0.6$ and the NACA 65A204 airfoil).

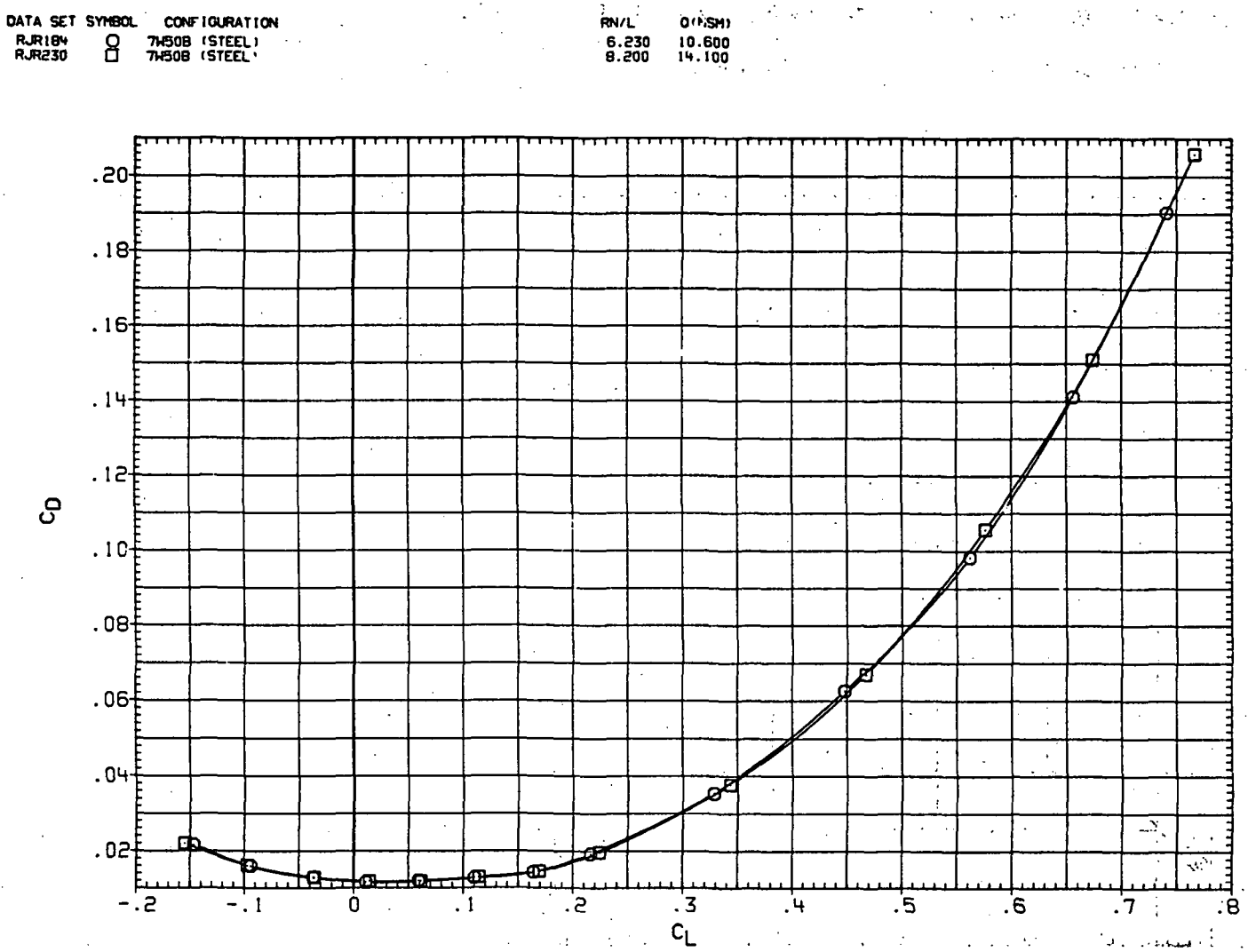

(b) C_D vs C_L.

Figure 59.– Continued.

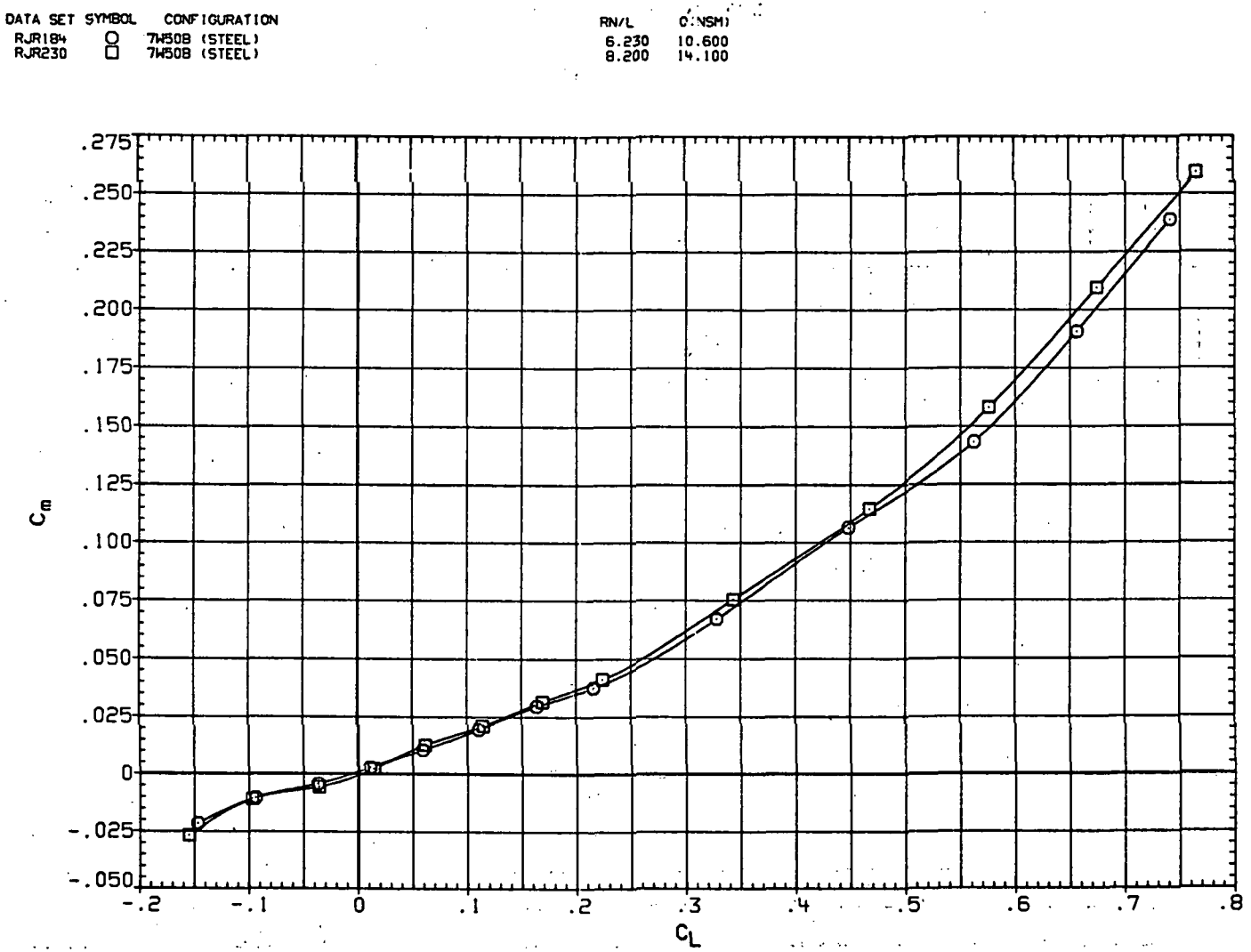

(c) C_m vs C_L.

Figure 59.– Continued.

(d) L/D vs C_L.

Figure 59.– Continued.

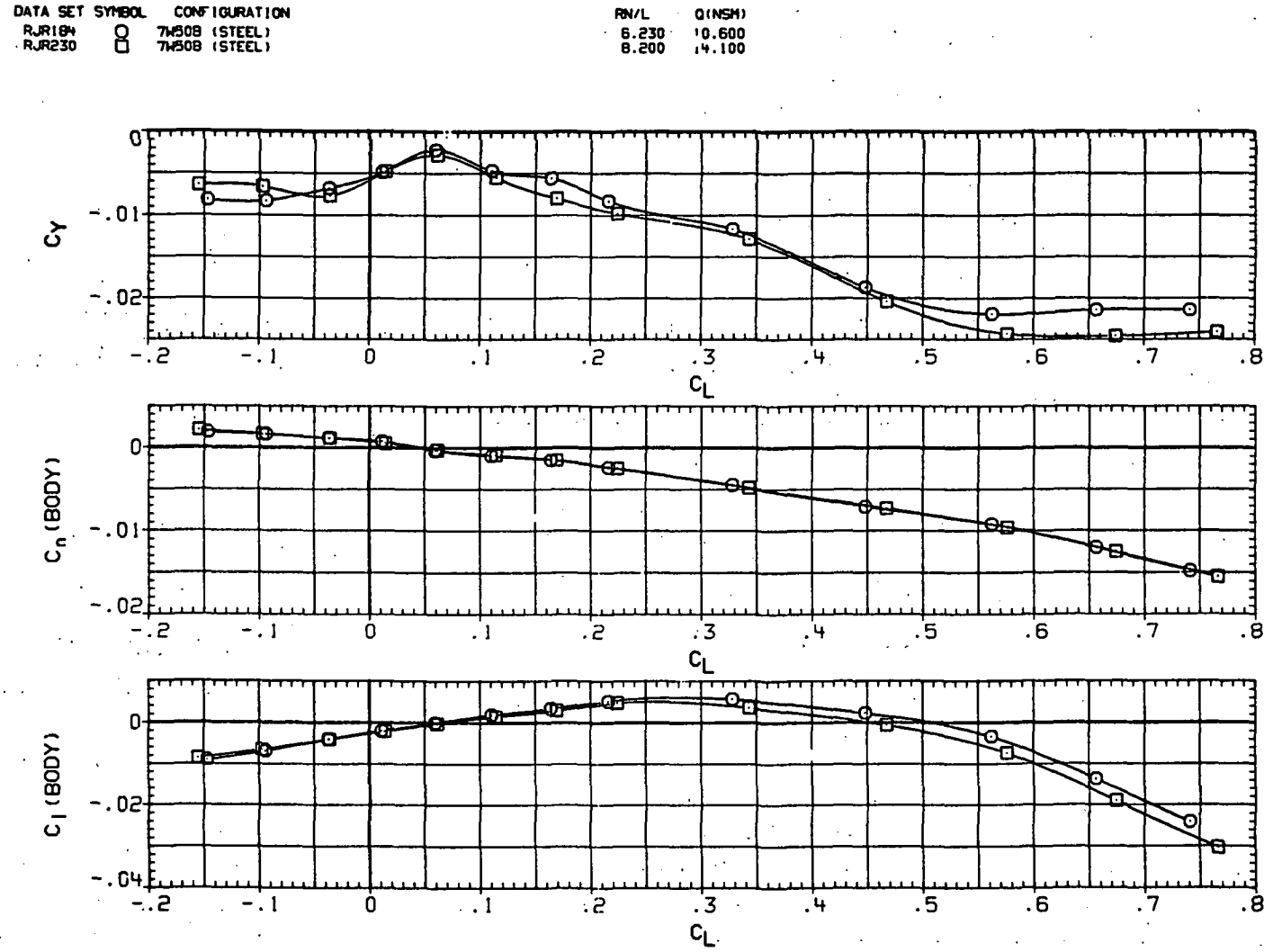

(e) C_Y, C_n and C_ℓ vs C_L.

Figure 59.– Concluded.

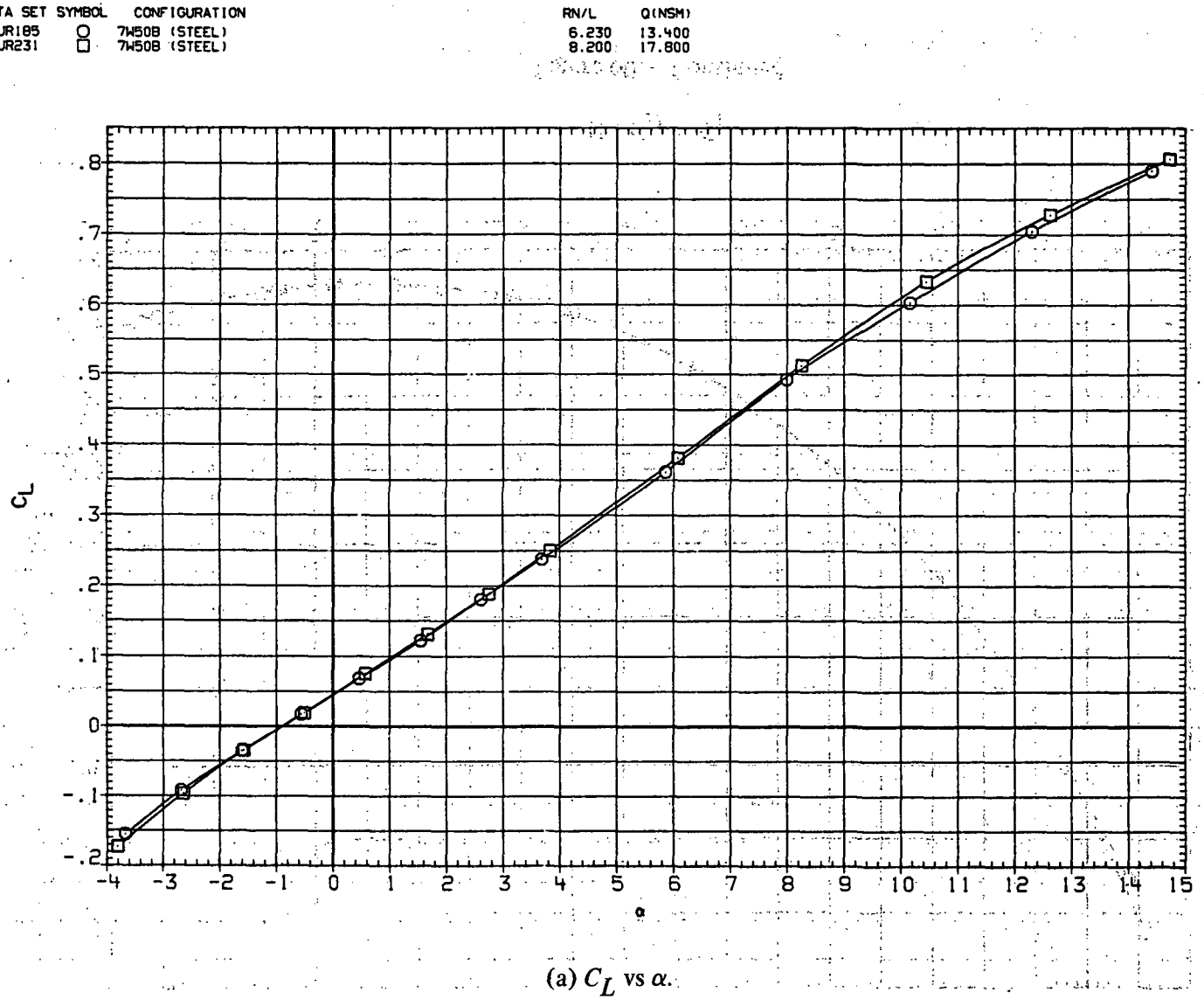

(a) C_L vs α.

Figure 60.– Dynamic-pressure effects on the aerodynamic characteristics of the steel trapezoidal oblique wing-body combination ($\Lambda = 50°$, $M = 0.8$ and the NACA 65A204 airfoil).

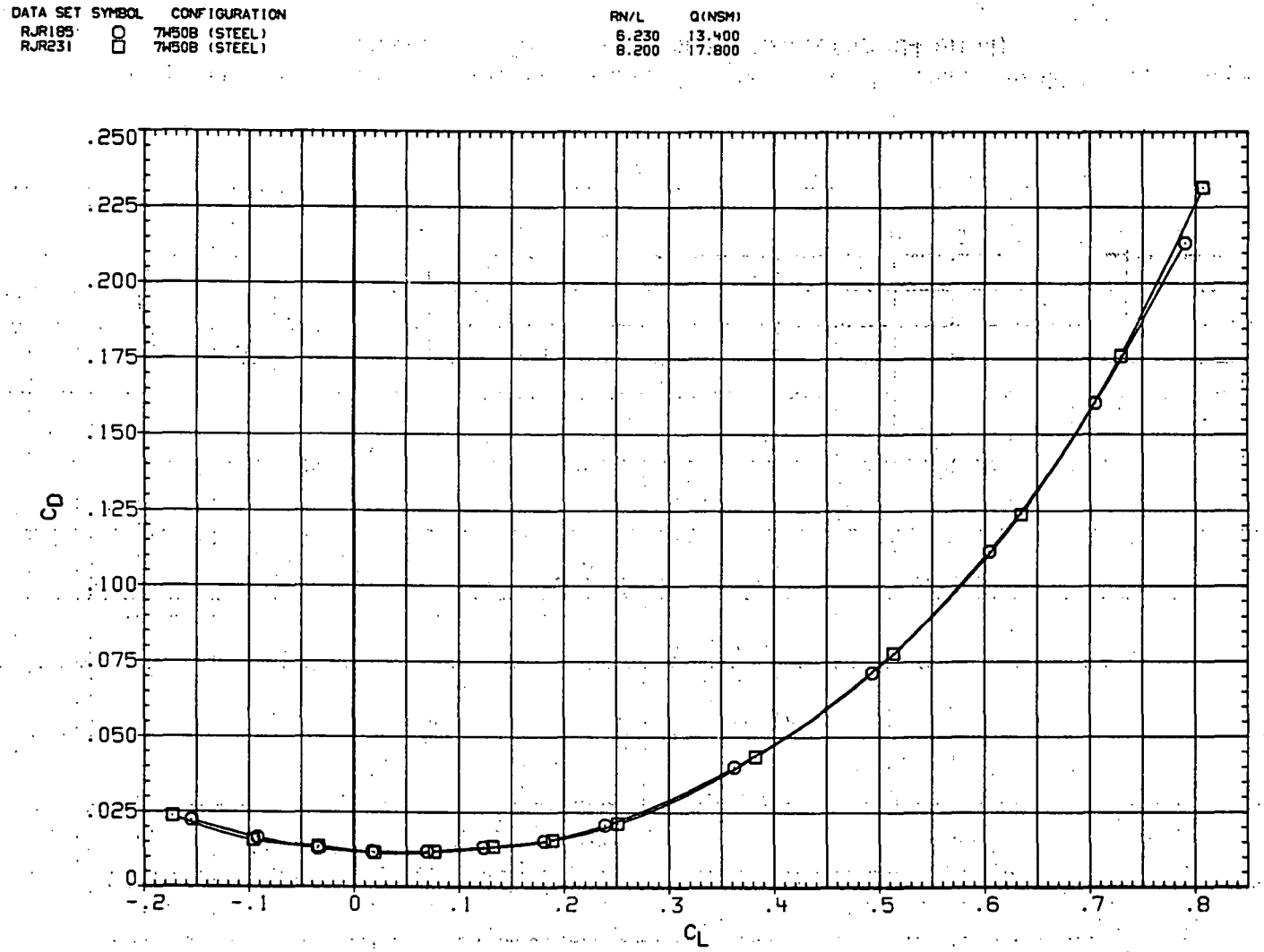

(b) C_D vs C_L.

Figure 60.– Continued.

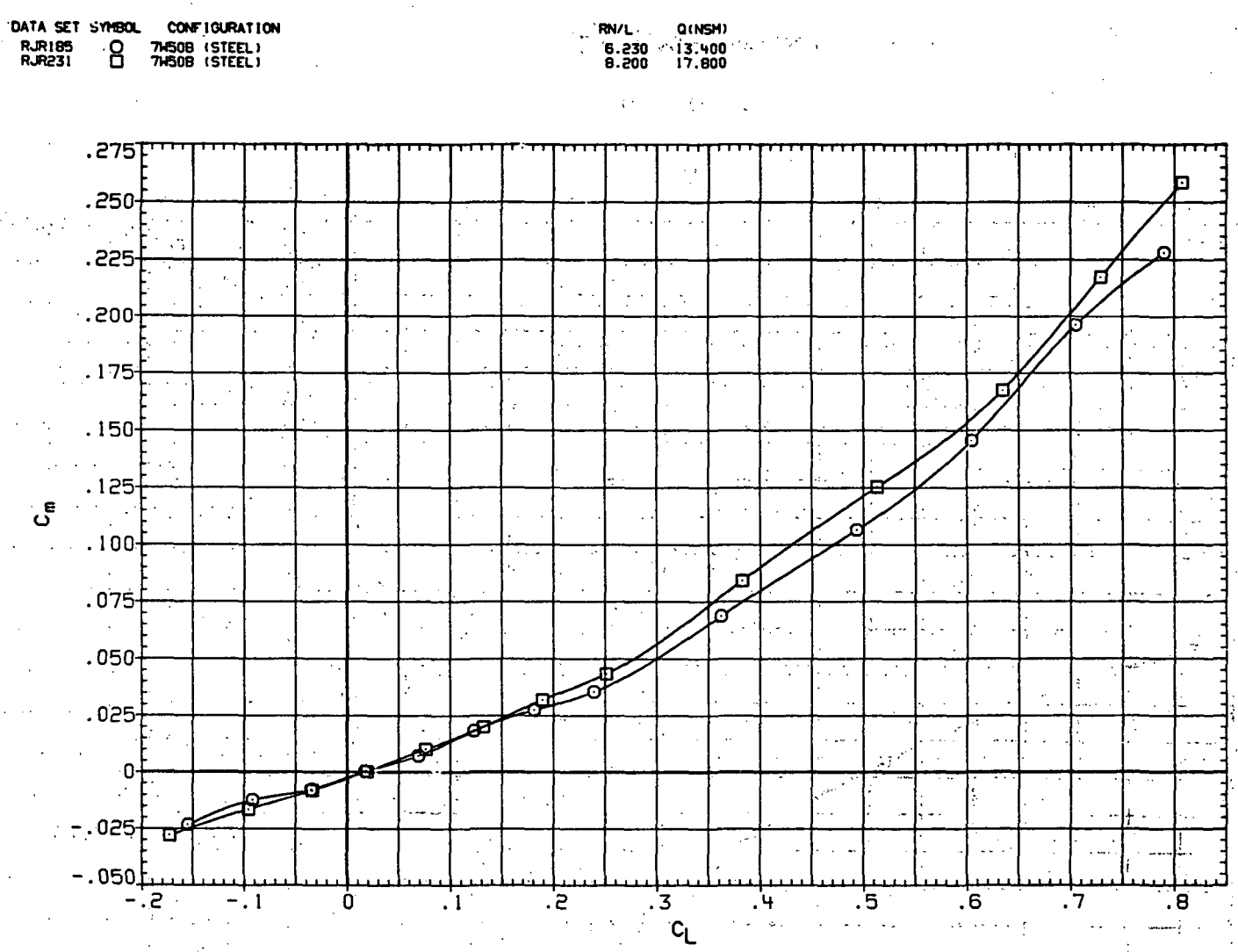

(c) C_m vs C_L.

Figure 60.- Continued.

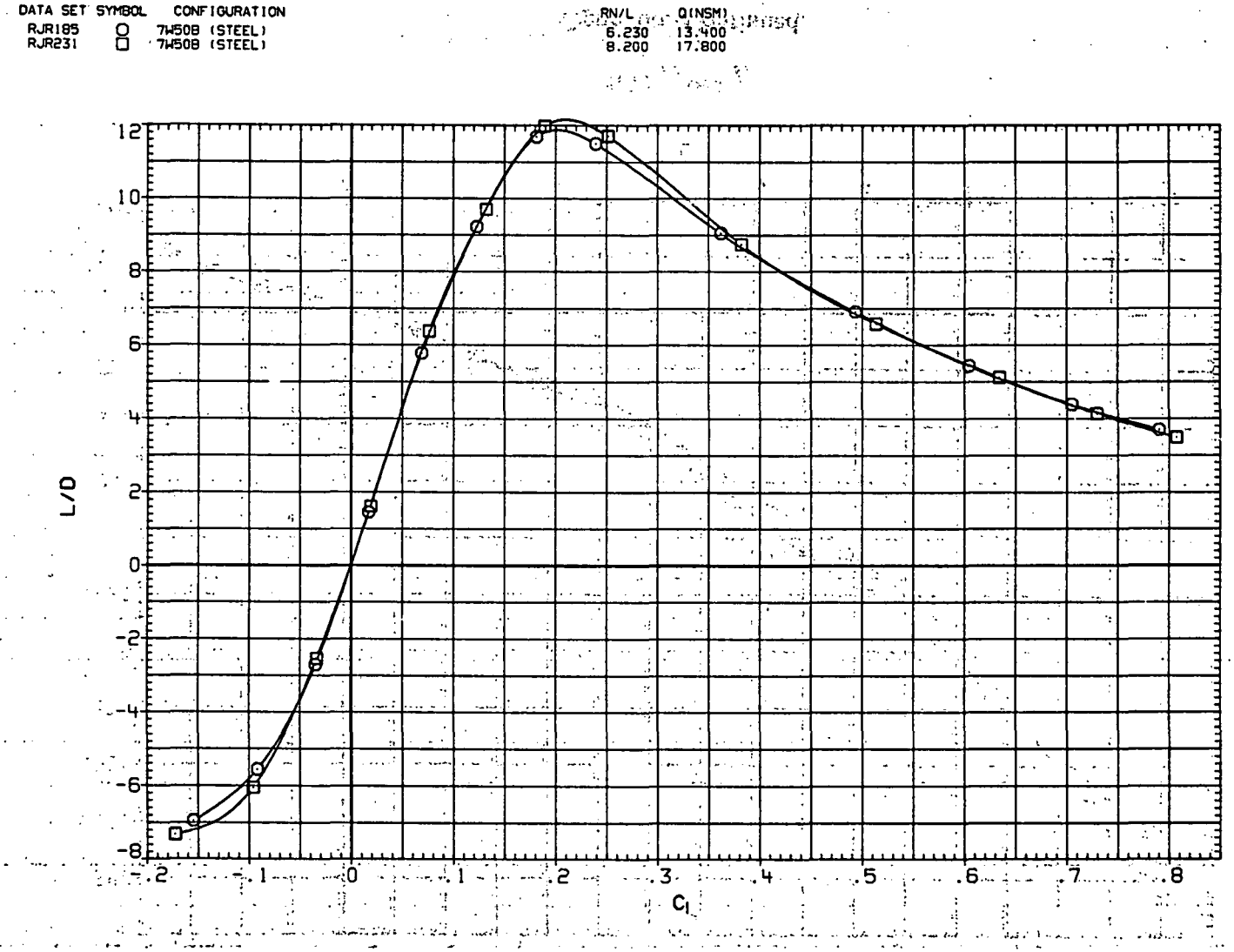

(d) L/D vs C_L.

Figure 60.- Continued.

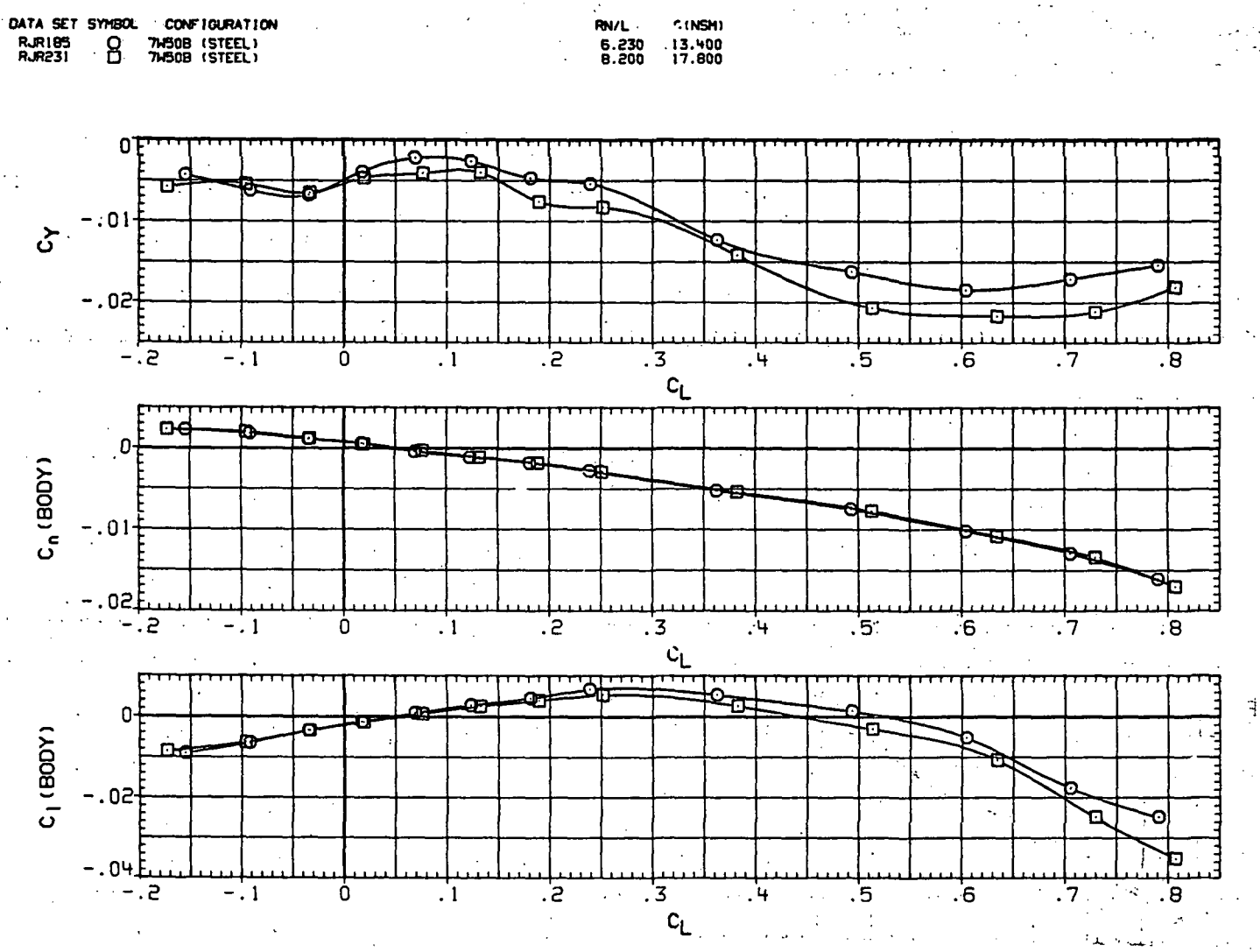

(e) C_Y, C_n and C_ℓ vs C_L.

Figure 60.– Concluded.

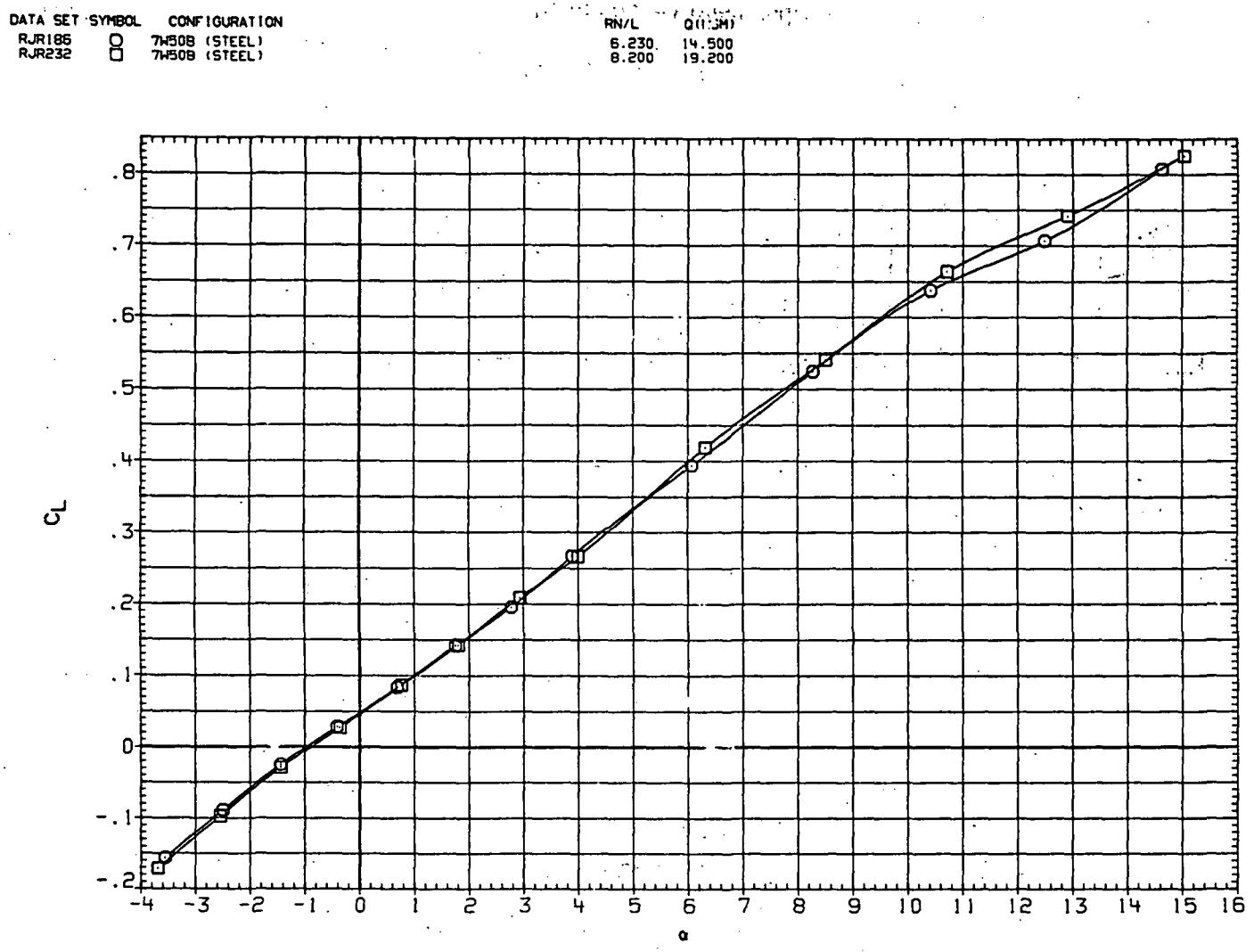

(a) C_L vs α.

Figure 61.– Dynamic-pressure effects on the aerodynamic characteristics of the steel trapezoidal oblique wing-body combination ($\Lambda = 50°$, $M = 0.9$ and the NACA 65A204 airfoil).

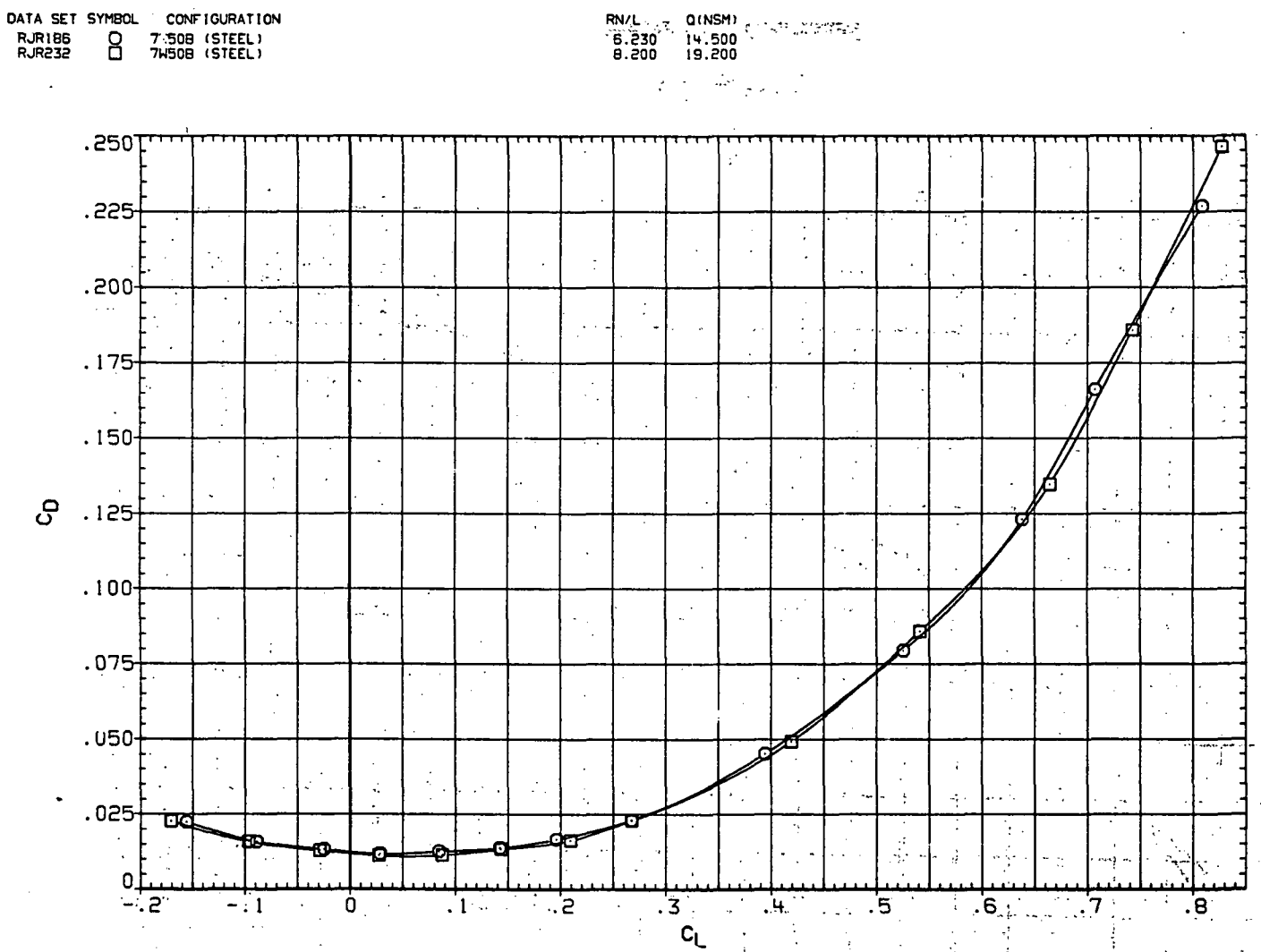

(b) C_D vs C_L.

Figure 61.– Continued.

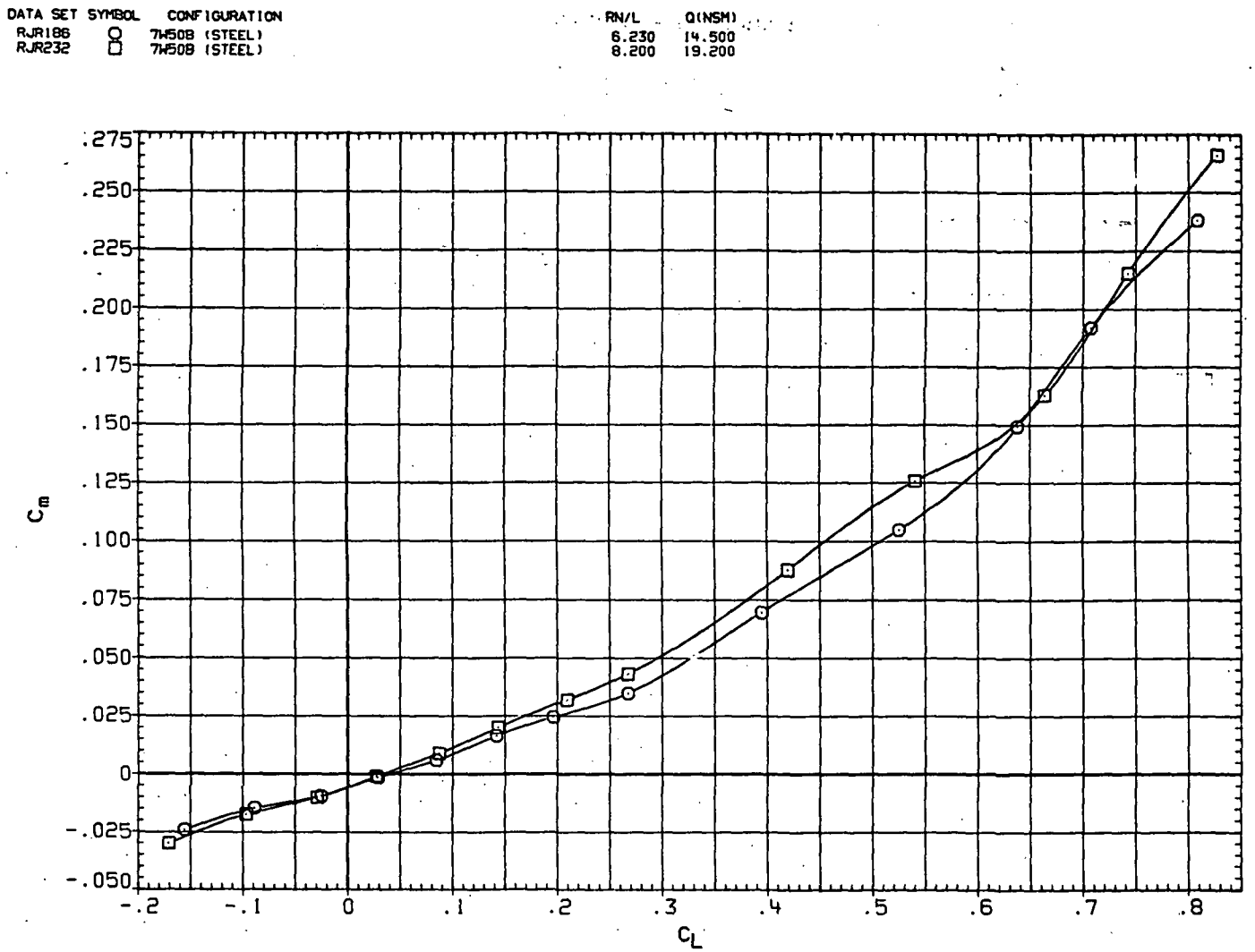

(c) C_m vs C_L.

Figure 61.– Continued.

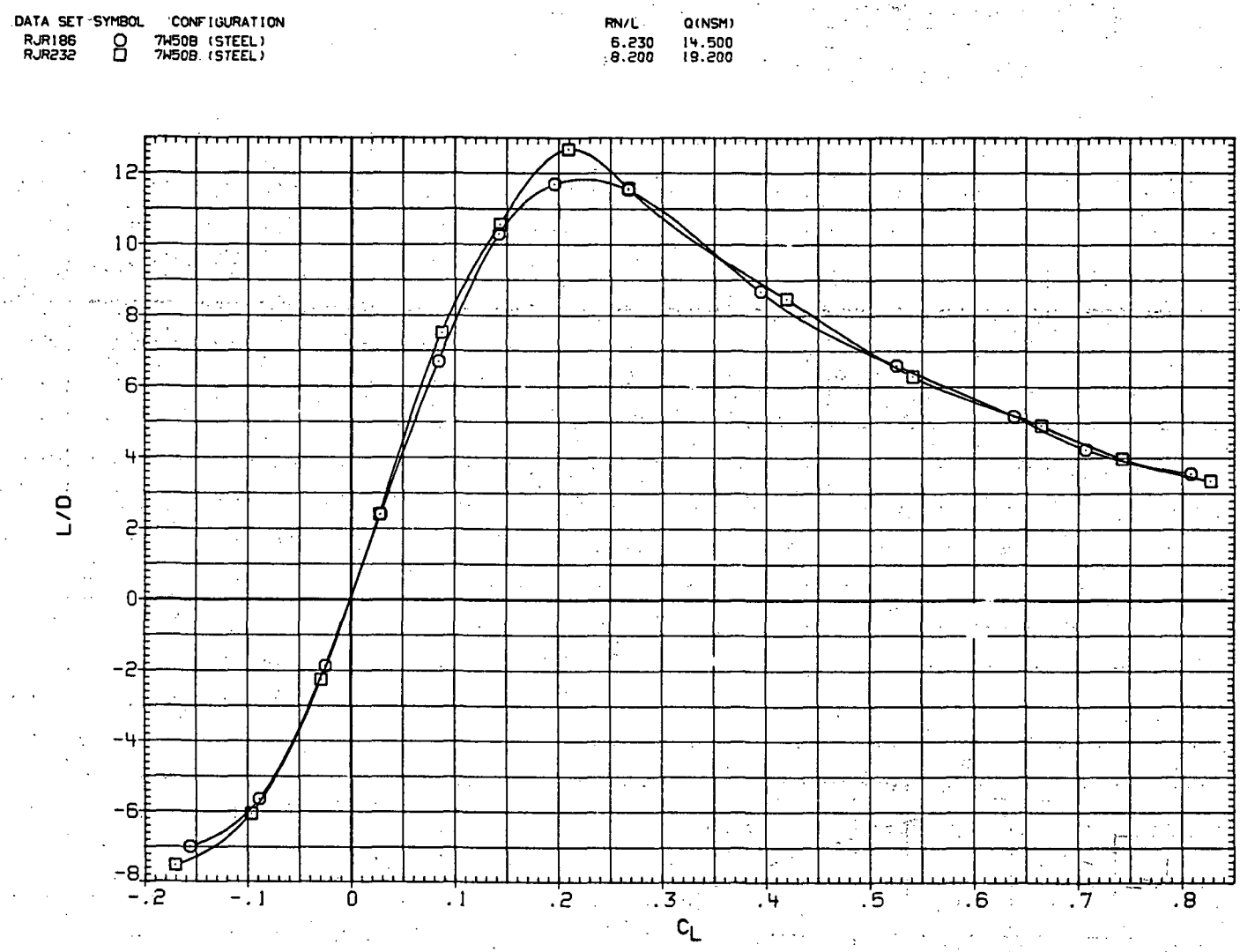

(d) L/D vs C_L.

Figure 61.– Continued.

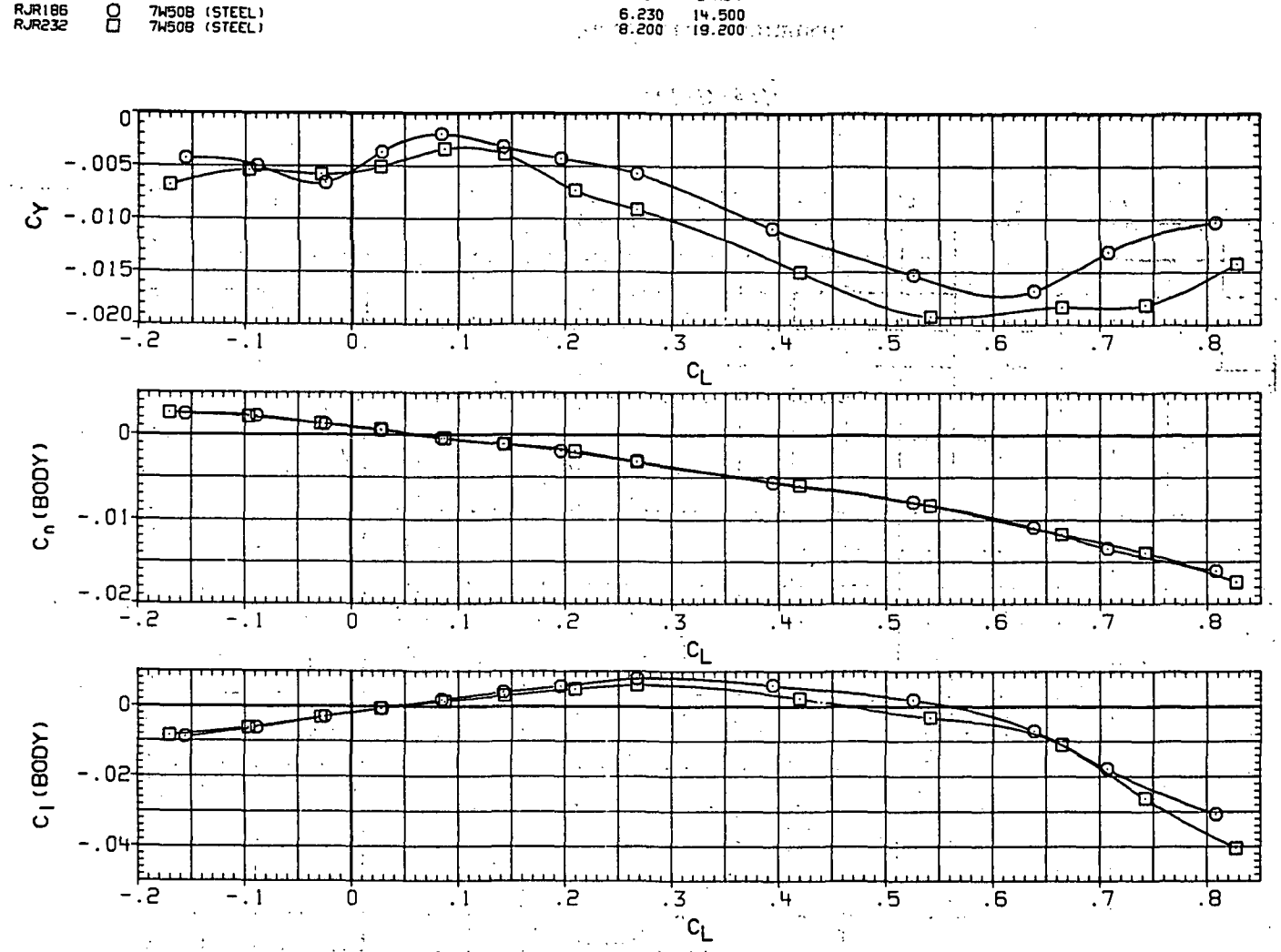

(e) C_Y, C_n and C_ℓ vs C_L.

Figure 61.— Concluded.

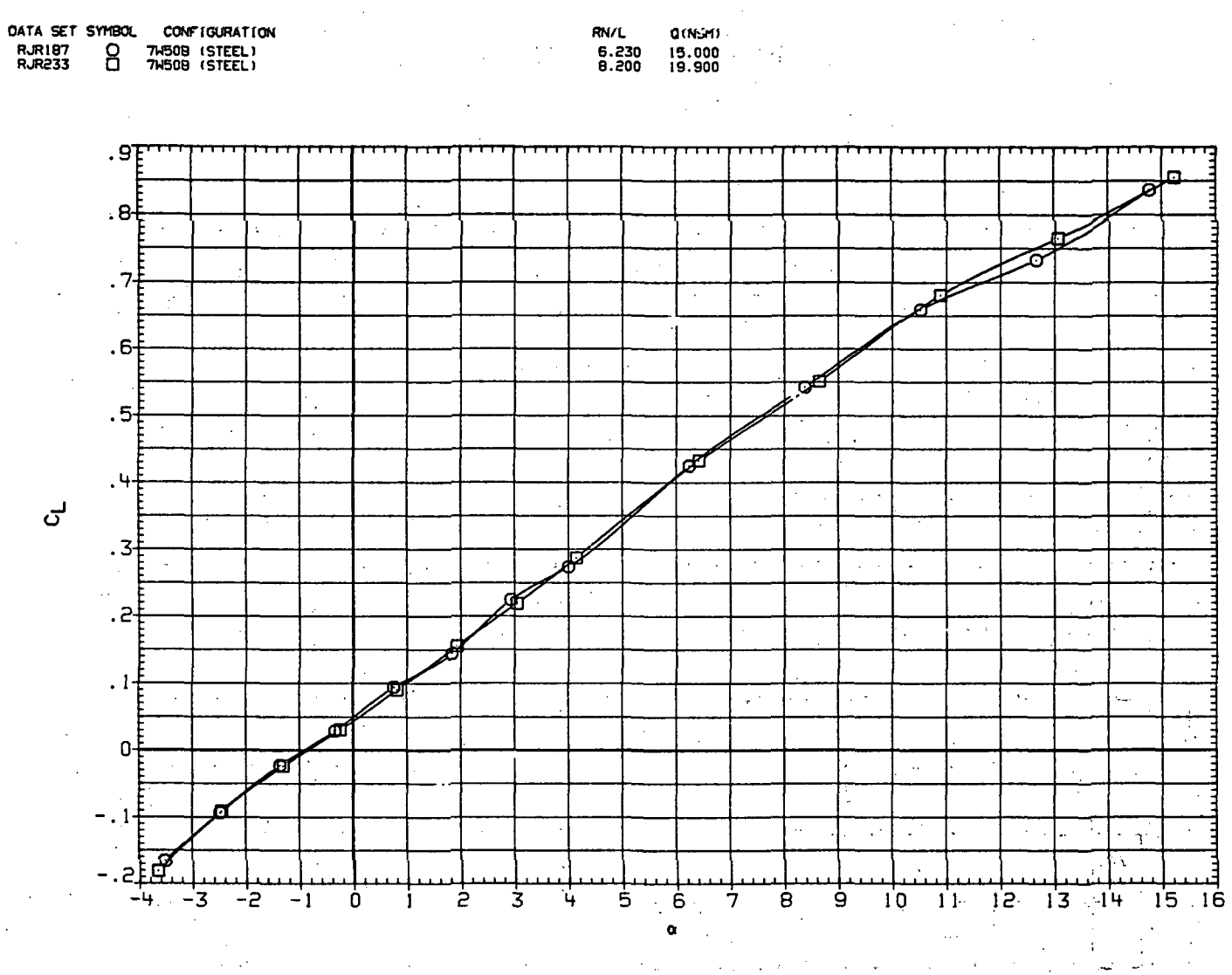

(a) C_L vs α.

Figure 62.– Dynamic-pressure effects on the aerodynamic characteristics of the steel trapezoidal oblique wing-body combination ($\Lambda = 50°$, $M = 0.95$ and the NACA 65A204 airfoil).

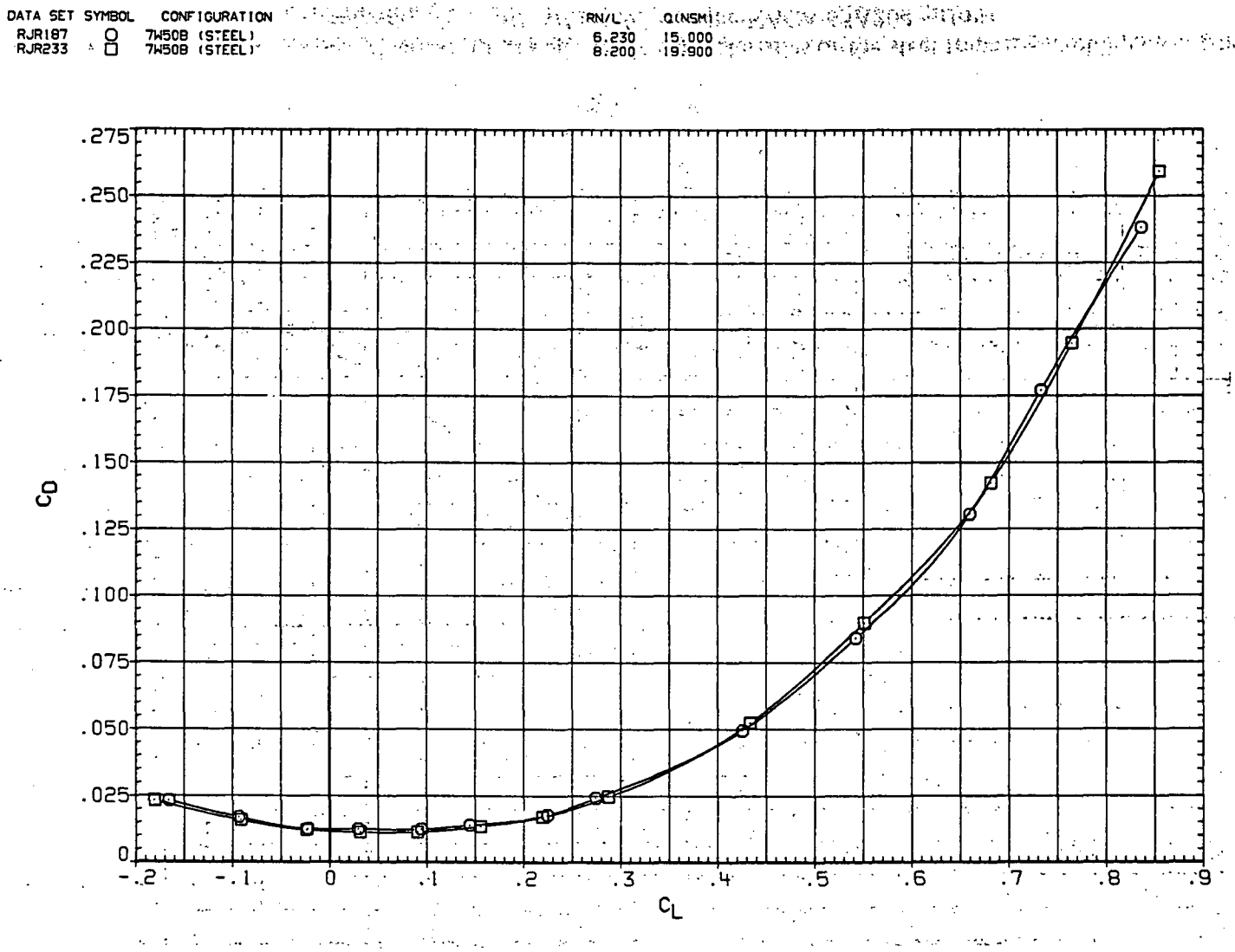

(b) C_D vs C_L.

Figure 62.– Continued.

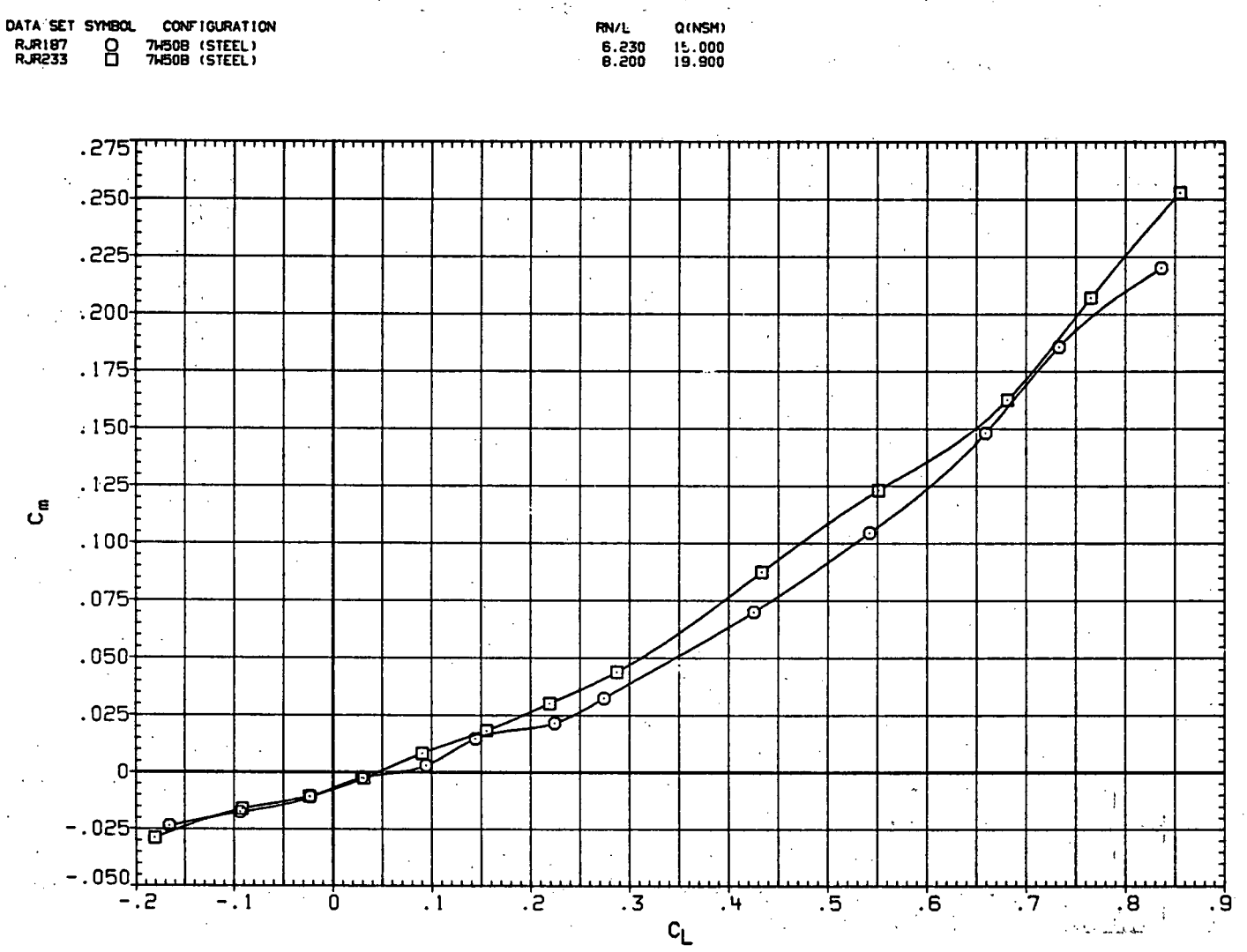

(c) C_m vs C_L.

Figure 62.– Continued.

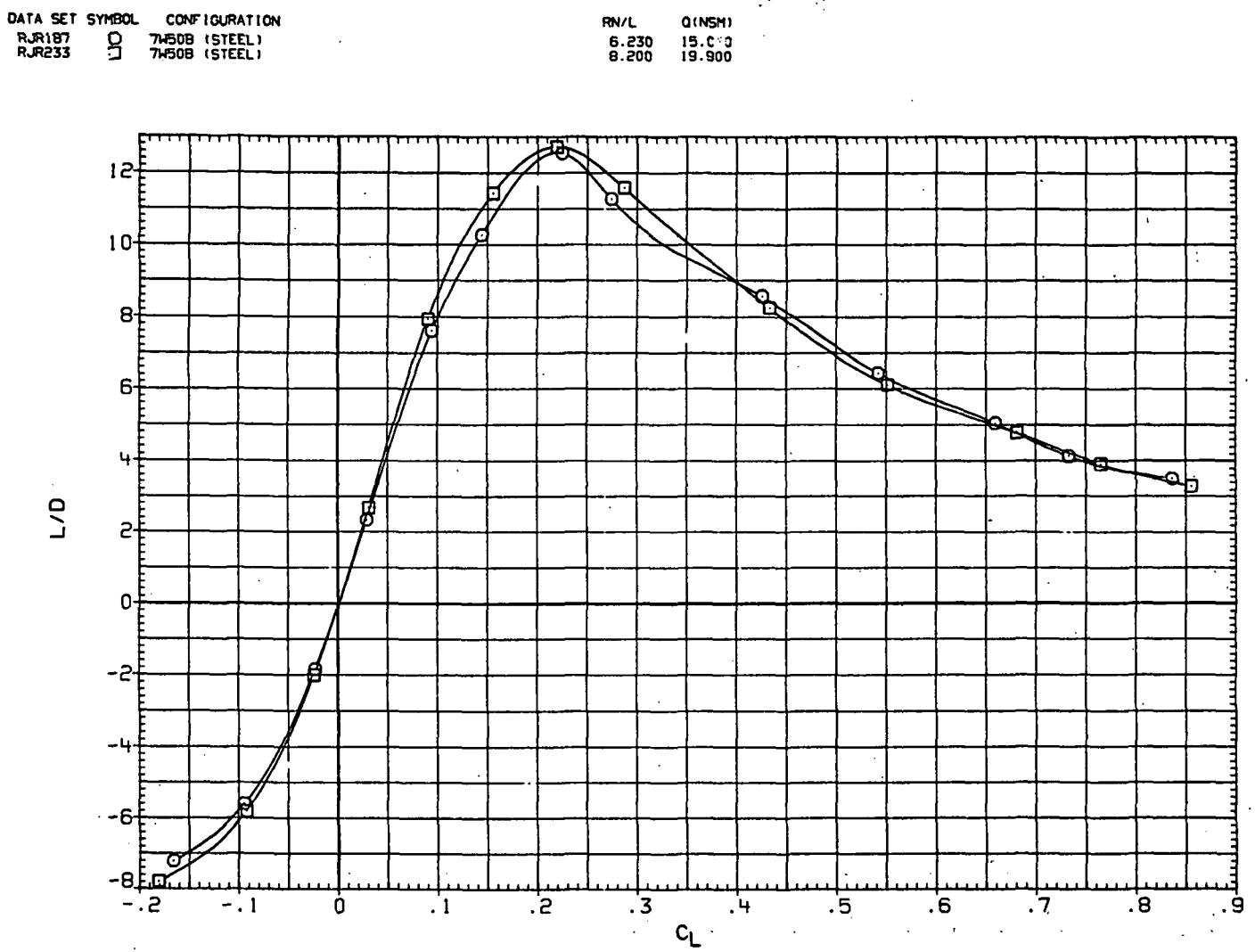

(d) L/D vs C_L.

Figure 62.– Continued.

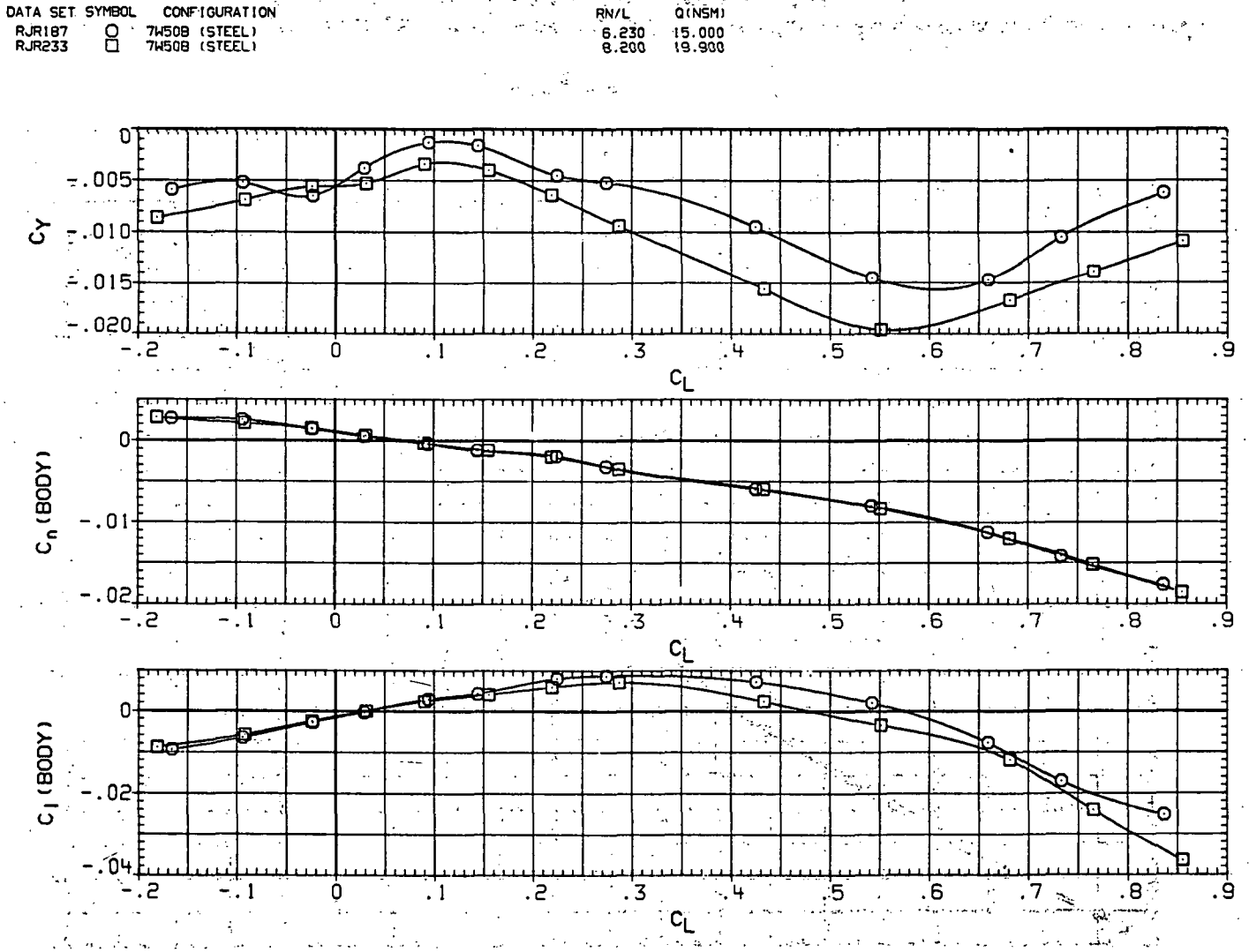

(e) C_Y, C_n and C_ℓ vs C_L.

Figure 62.– Concluded.

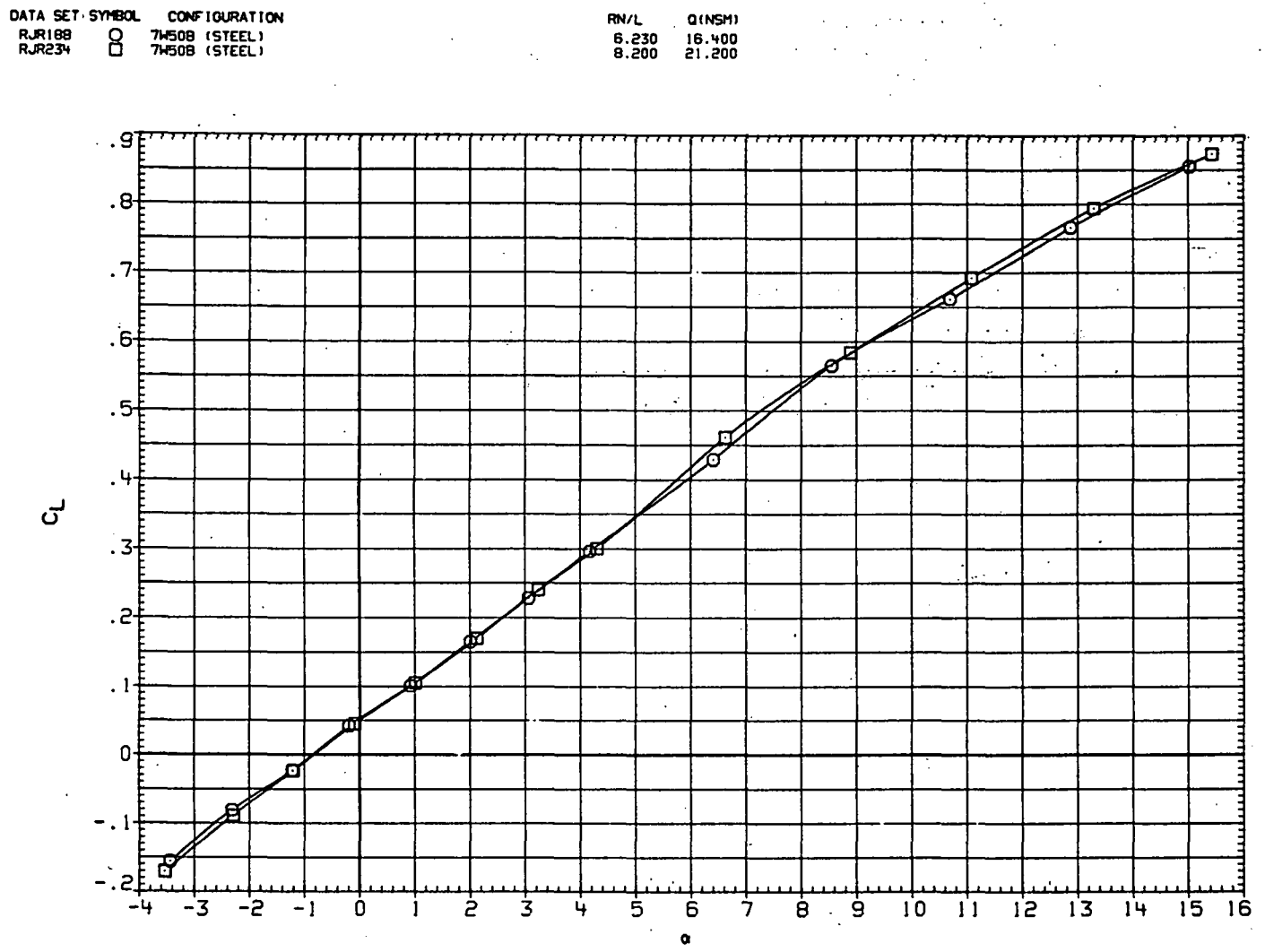

(a) C_L vs α.

Figure 63.– Dynamic-pressure effects on the aerodynamic characteristics of the steel trapezoidal oblique wing-body combination ($\Lambda = 50°$, $M = 1.1$ and the NACA 65A204 airfoil).

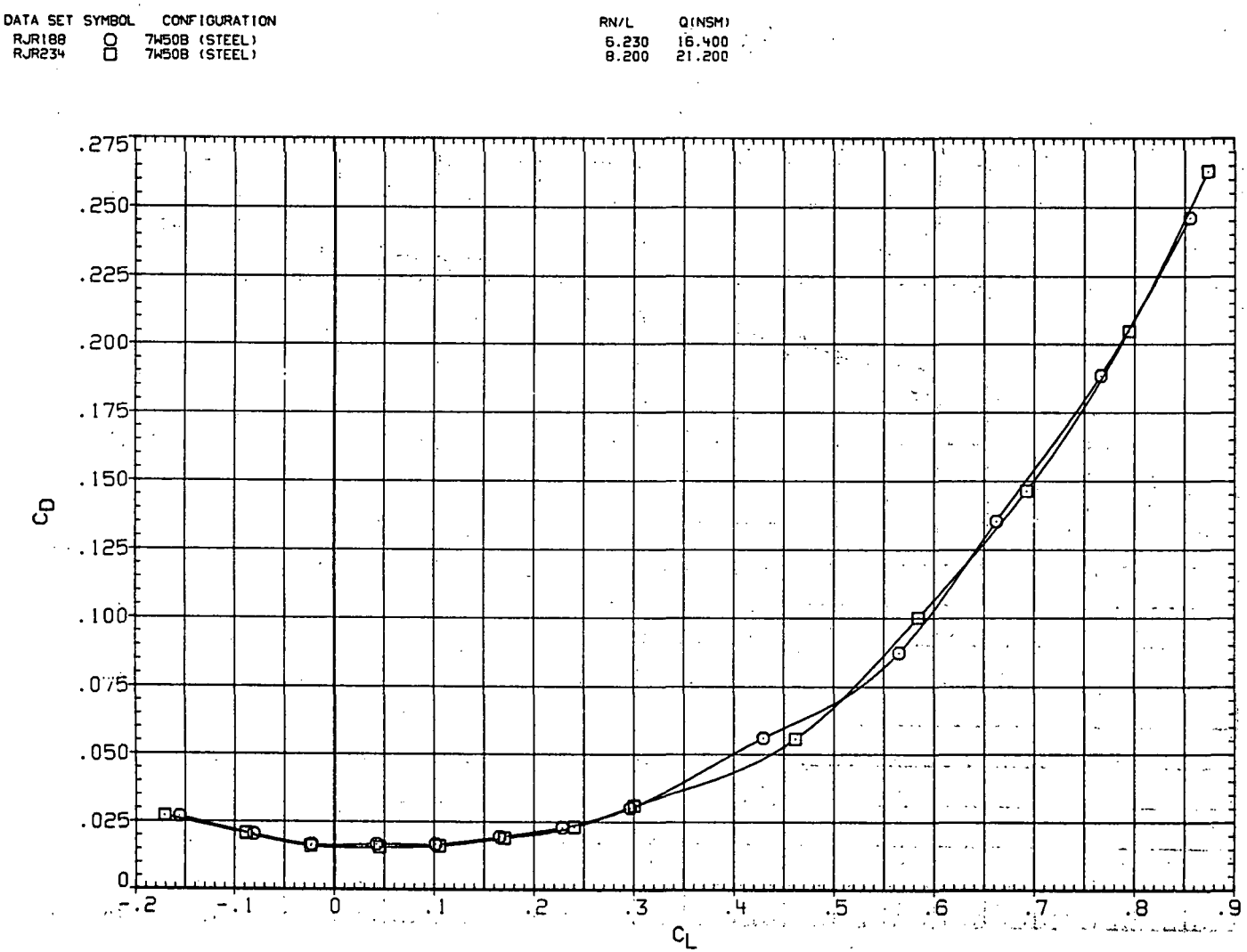

(b) C_D vs C_L.

Figure 63.– Continued.

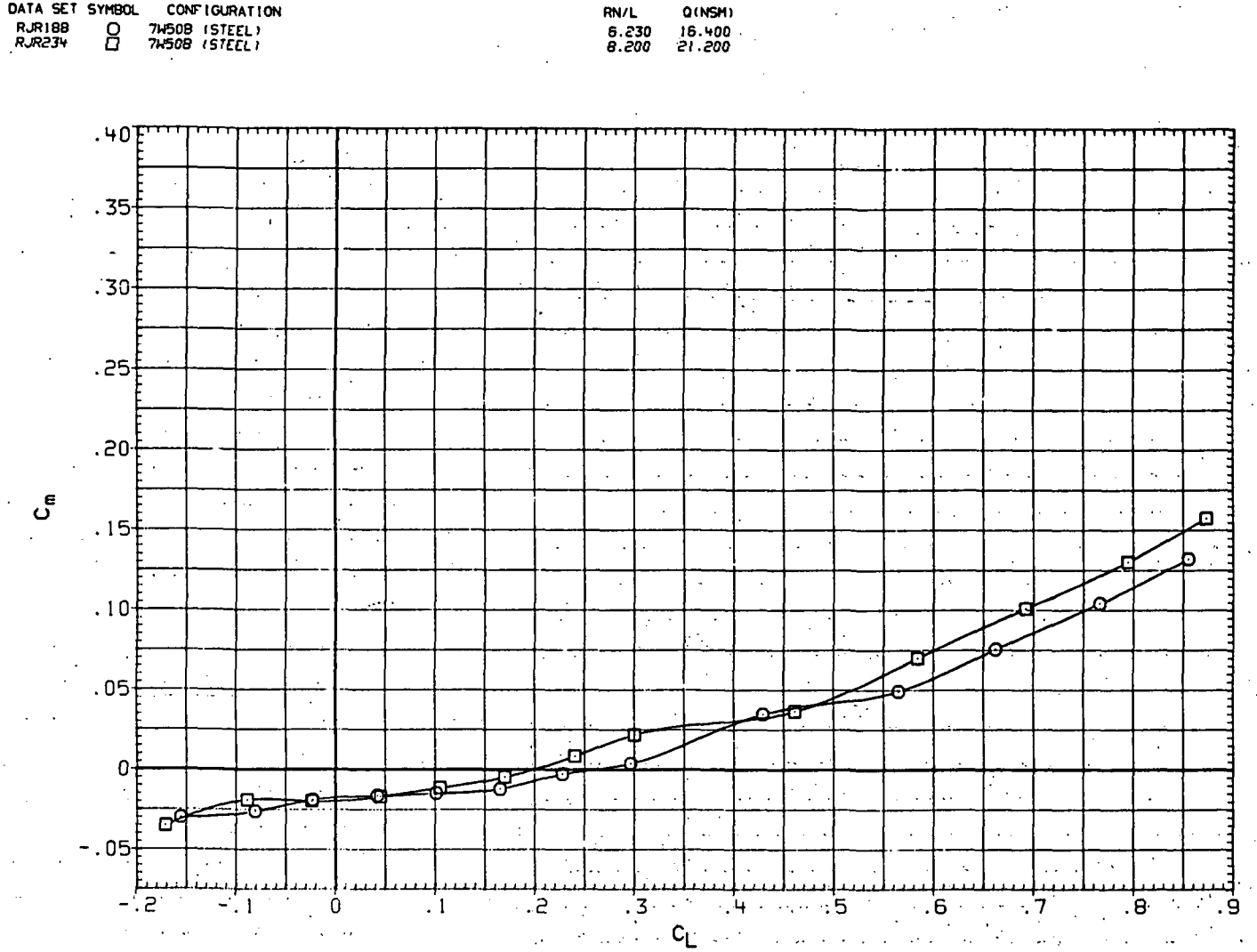

(c) C_m vs C_L.

Figure 63.– Continued.

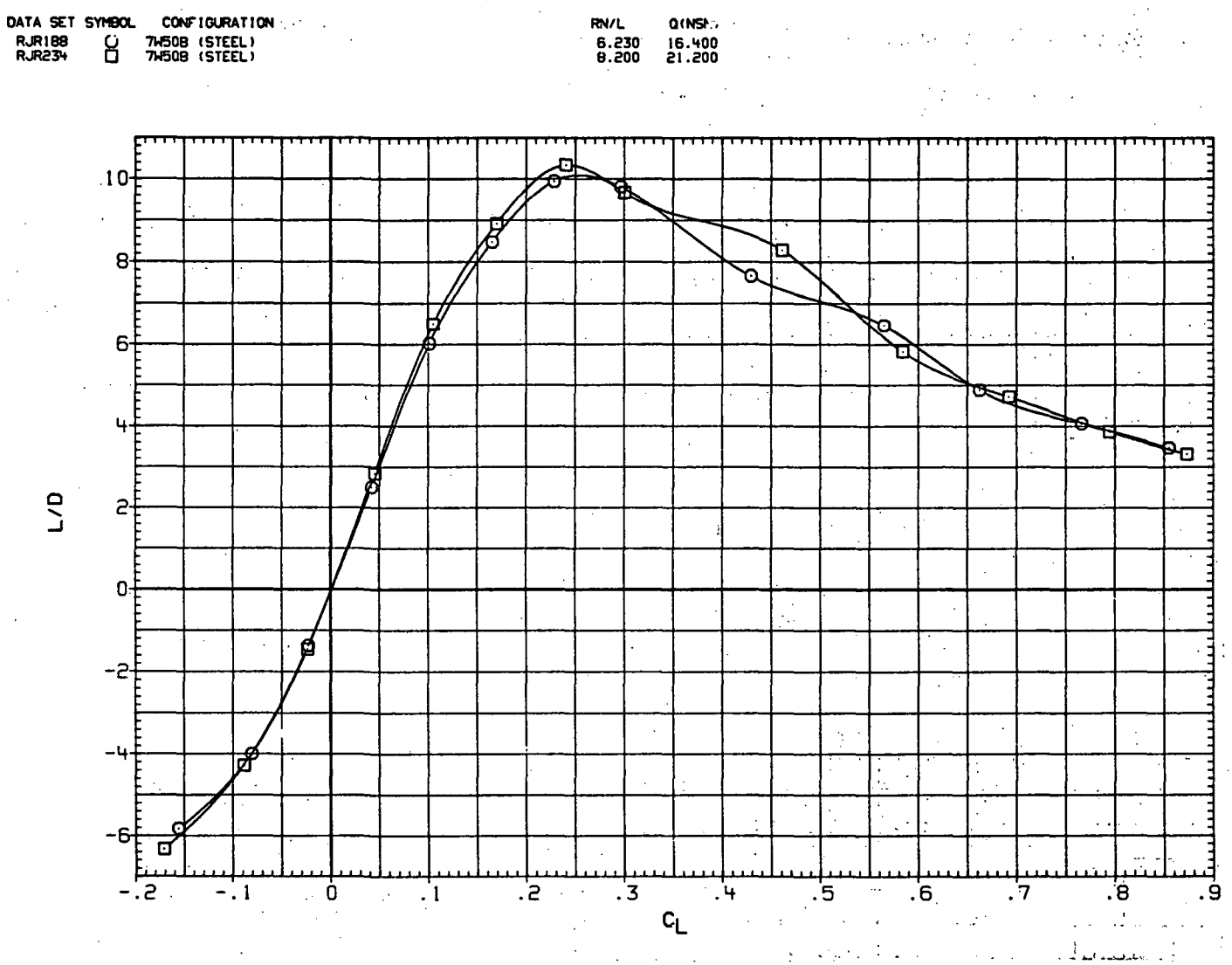

(d) L/D vs C_L.

Figure 63.– Continued.

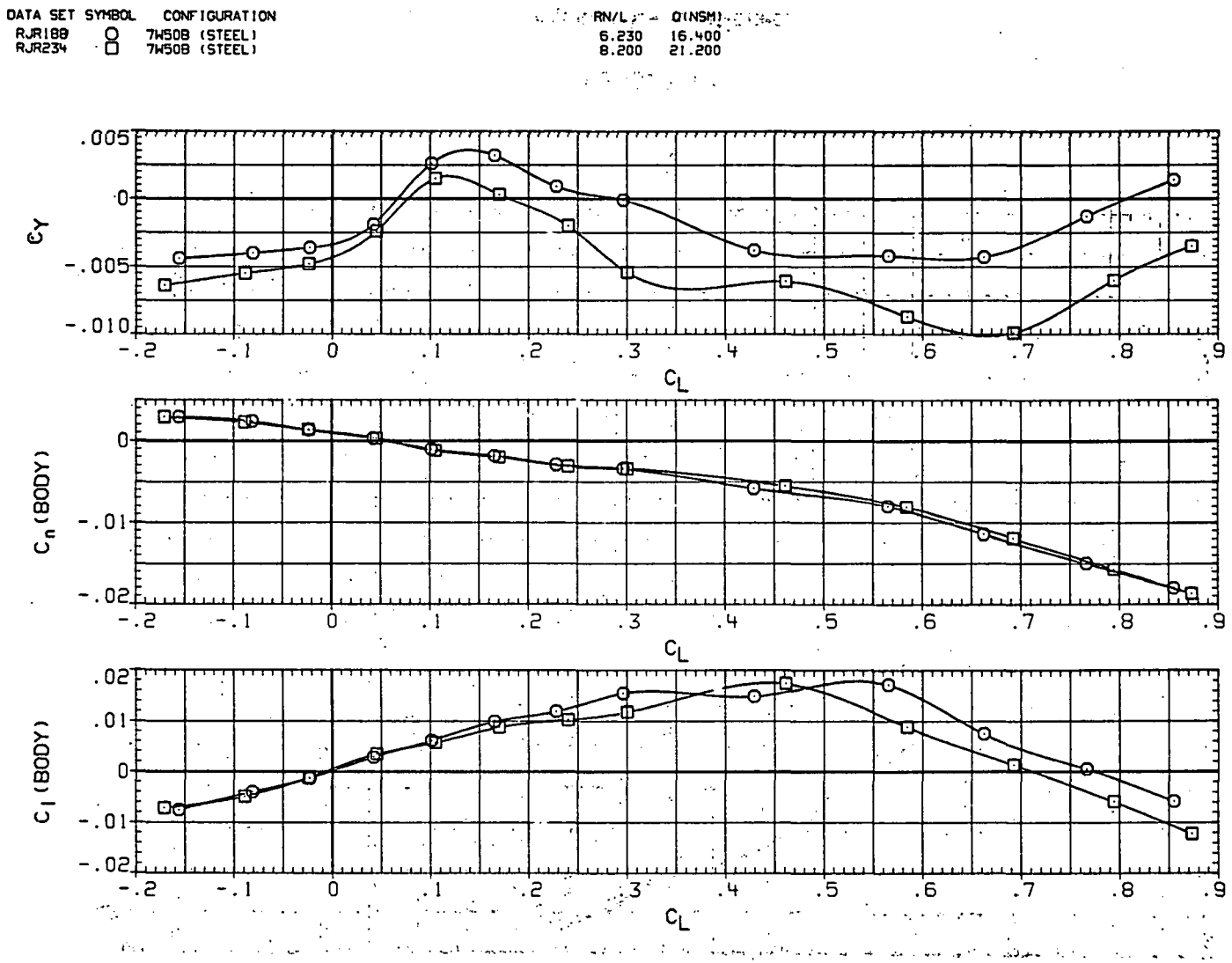

(e) C_Y, C_n and C_ℓ vs C_L.

Figure 63.– Concluded.

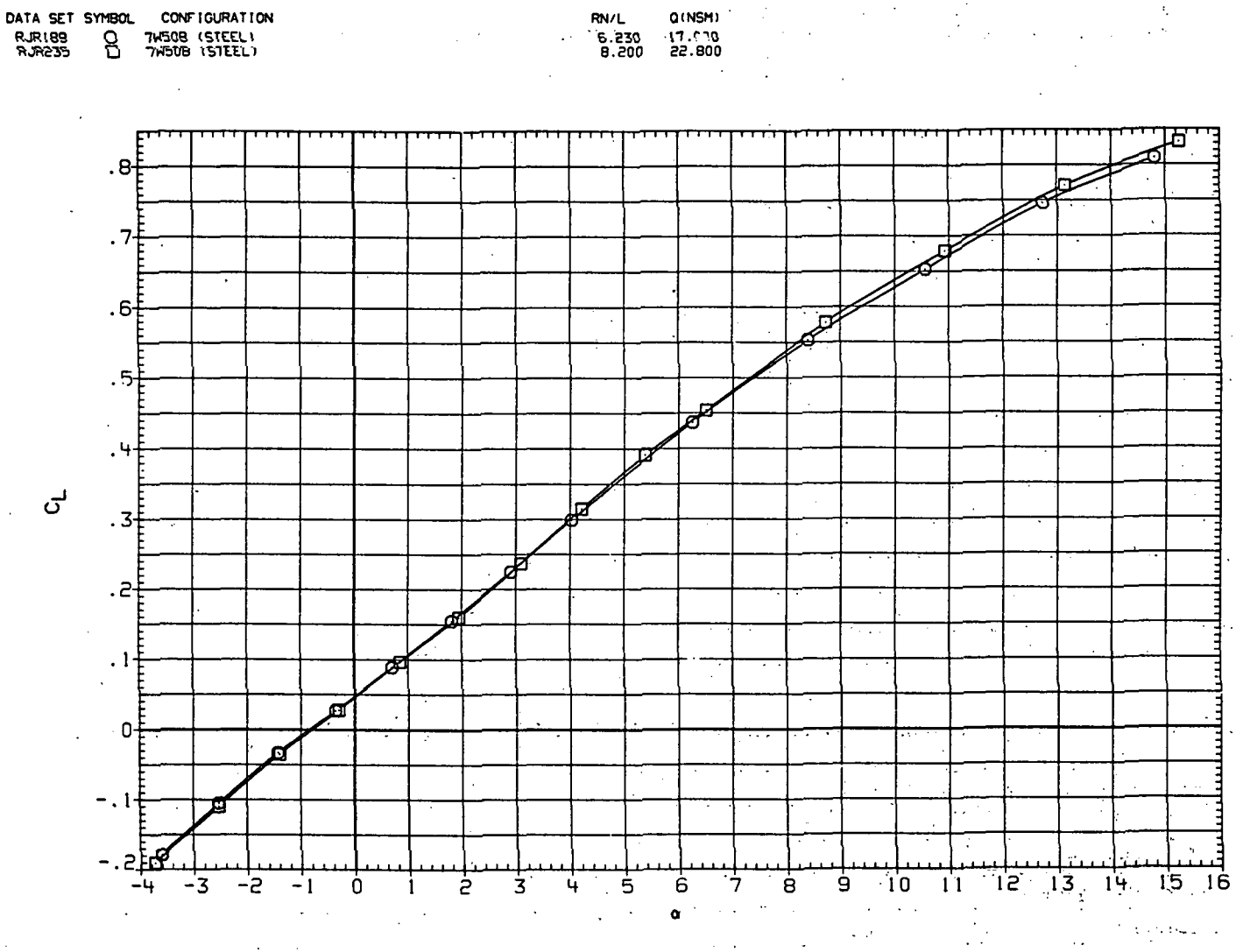

(a) C_L vs α.

Figure 64.– Dynamic-pressure effects on the aerodynamic characteristics of the steel trapezoidal oblique wing-body combination ($\Lambda = 50°$, $M = 1.2$ and the NACA 65A204 airfoil).

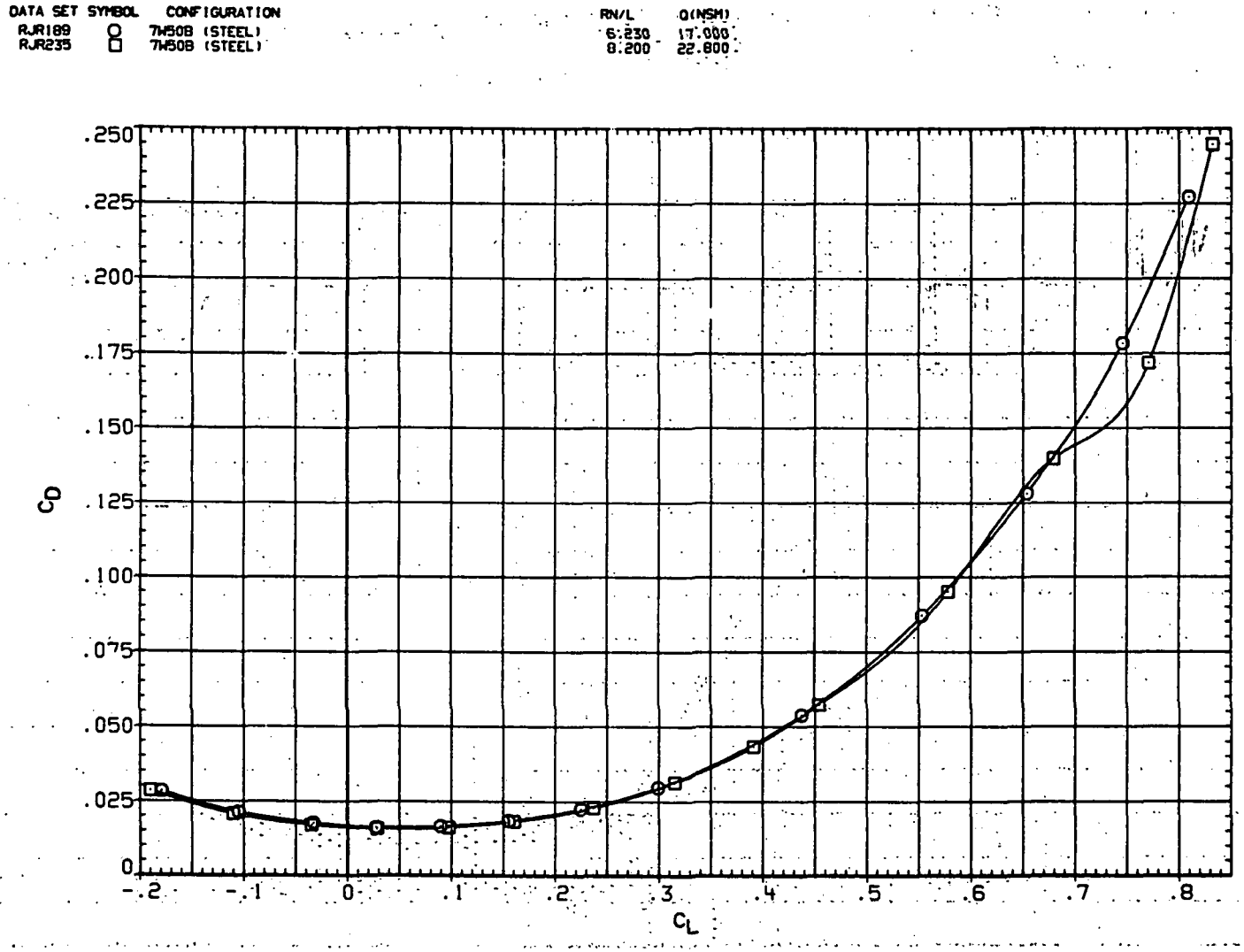

(b) C_D vs C_L.

Figure 64.– Continued.

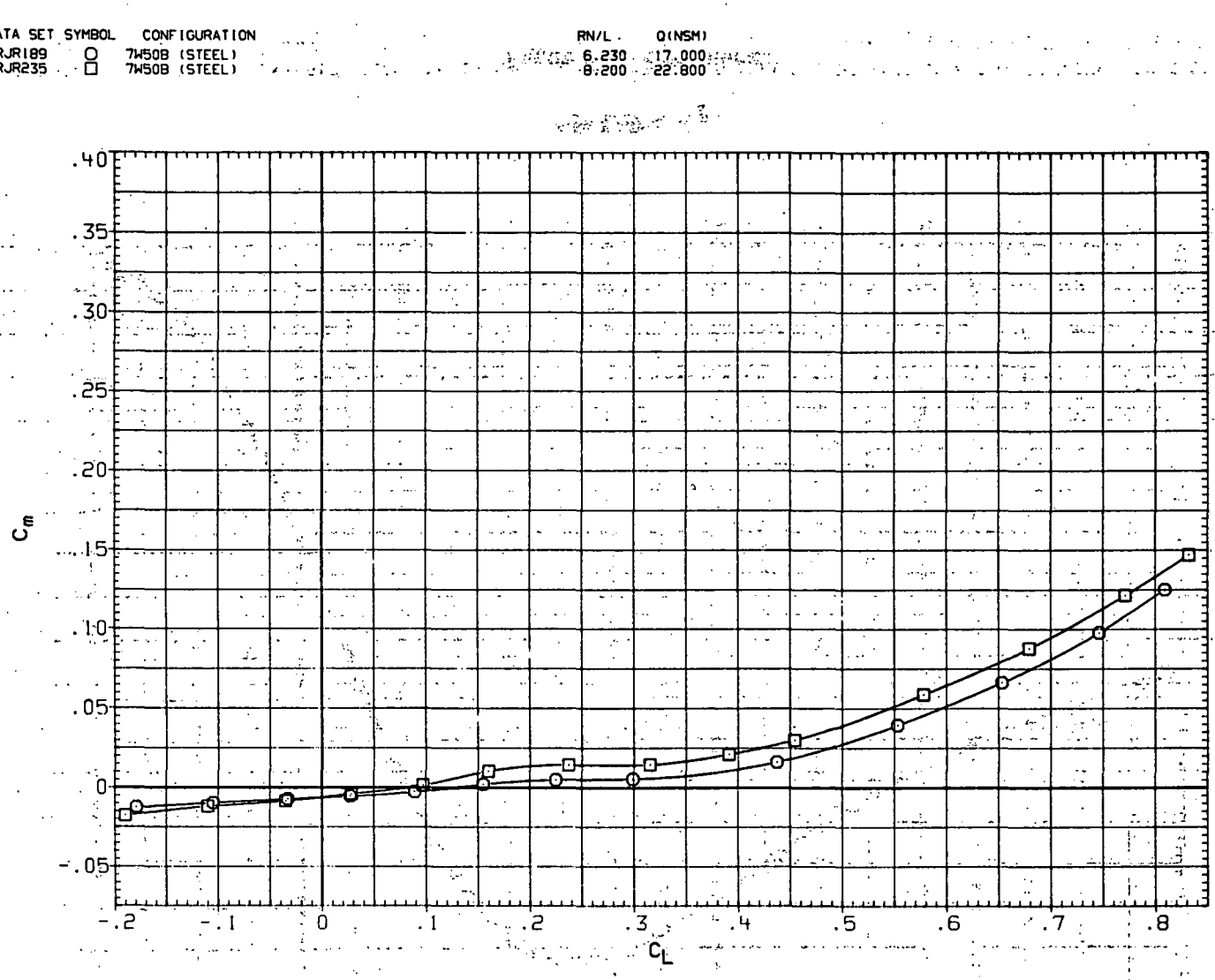

(c) C_m vs C_L.

Figure 64.– Continued.

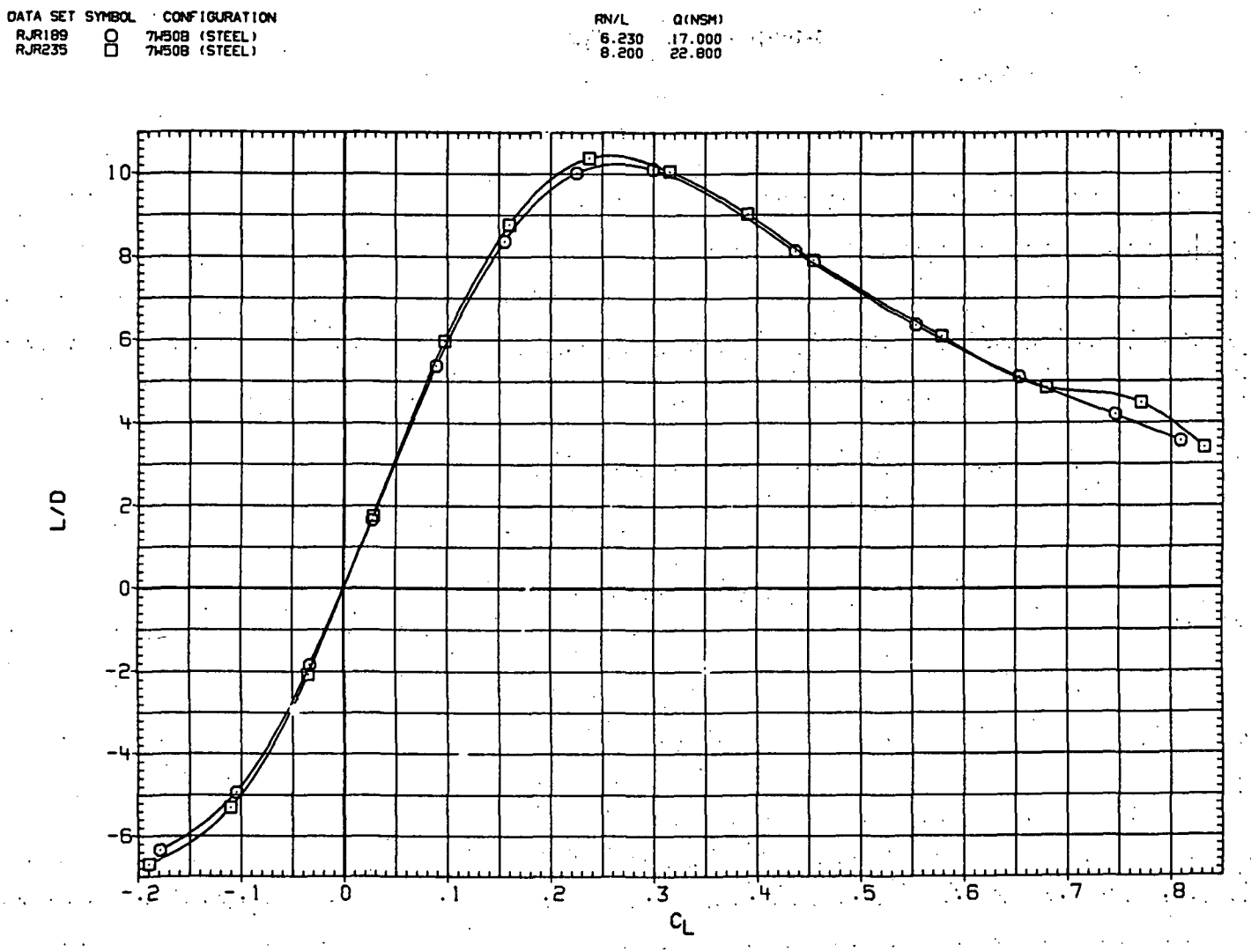

(d) L/D vs C_L.

Figure 64.– Continued.

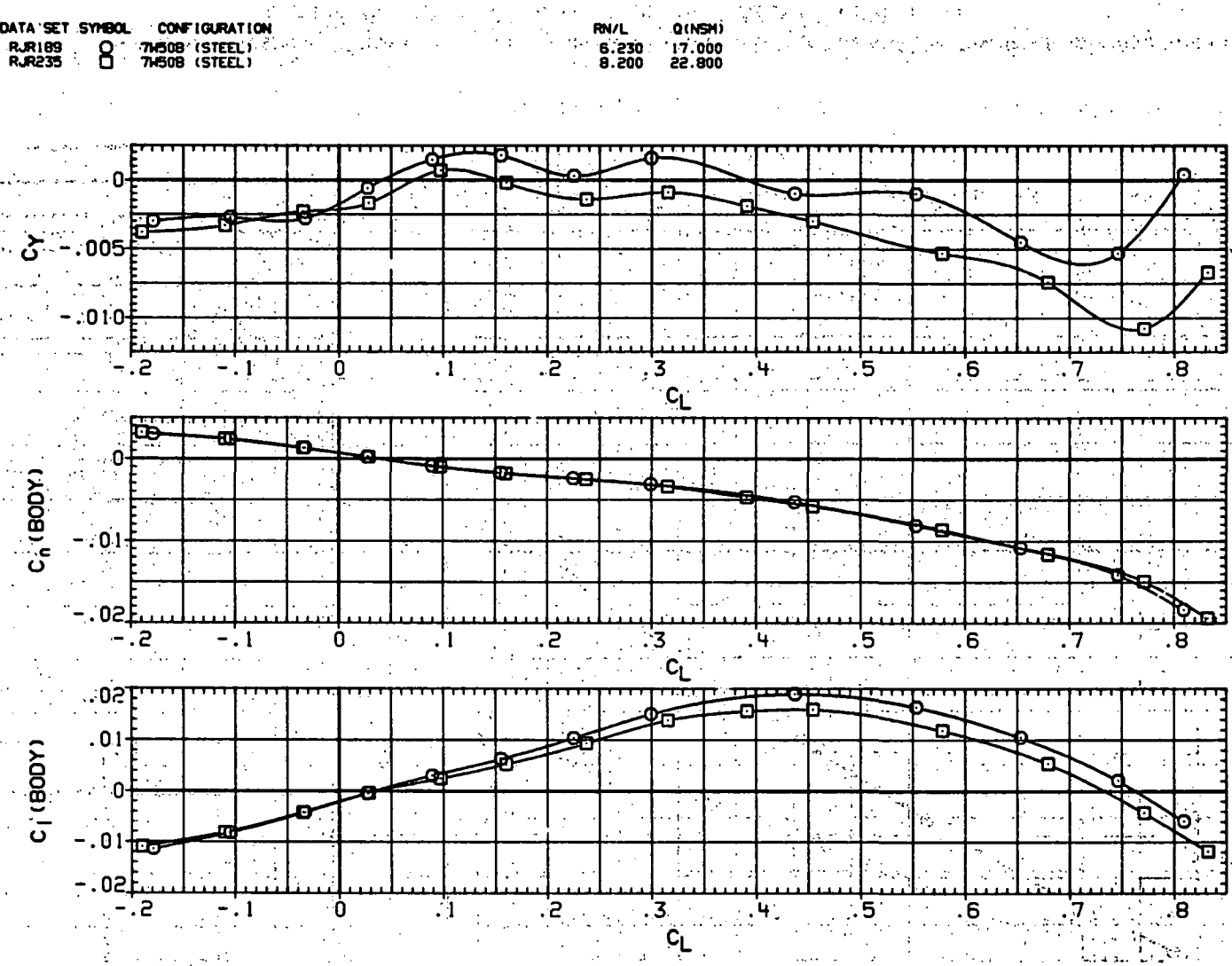

(e) C_Y, C_n and C_ℓ vs C_L.

Figure 64.– Concluded.

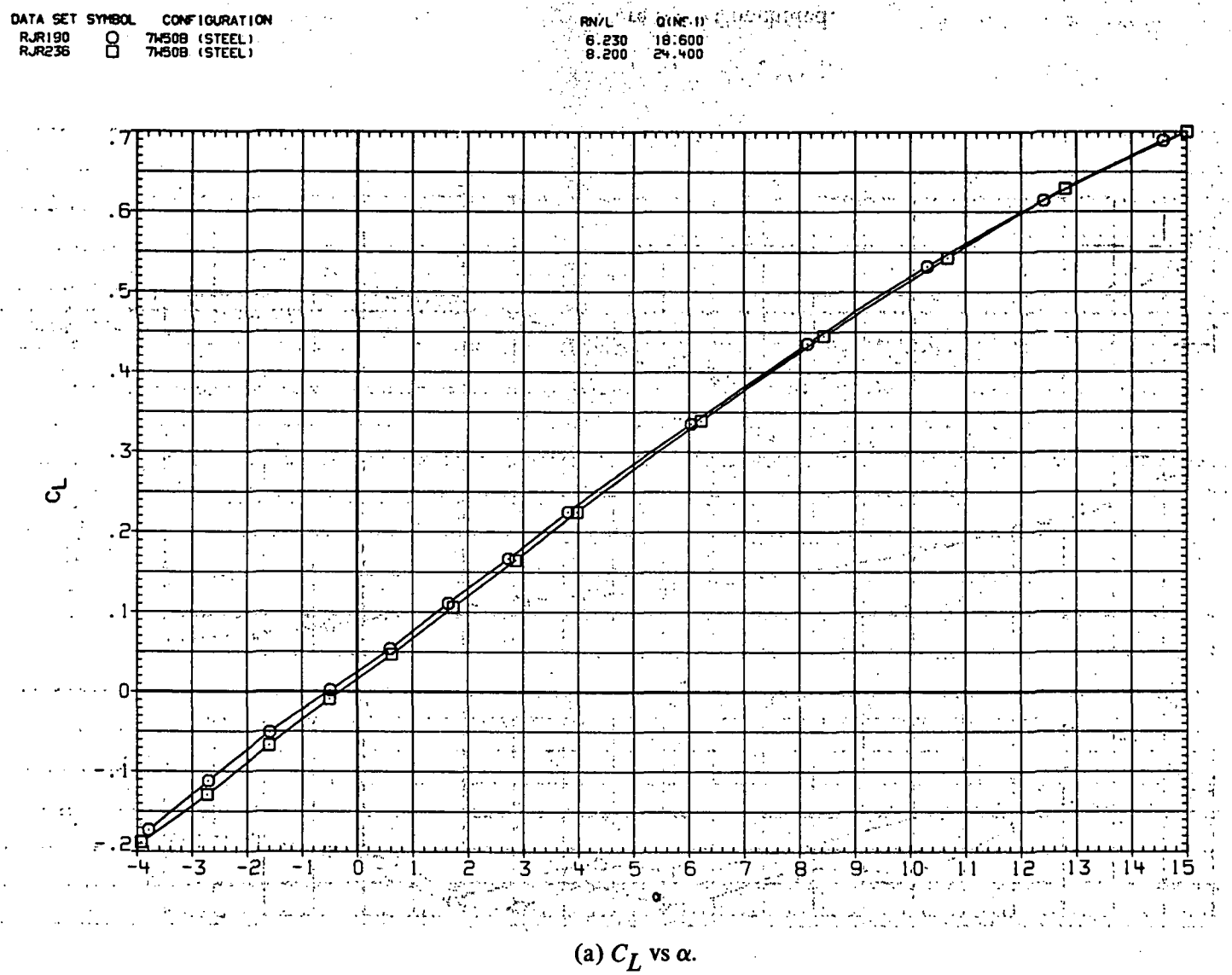

(a) C_L vs α.

Figure 65.– Dynamic-pressure effects on the aerodynamic characteristics of the steel trapezoidal oblique wing-body combination ($\Lambda = 50°$, $M = 1.6$ and the NACA 65A204 airfoil).

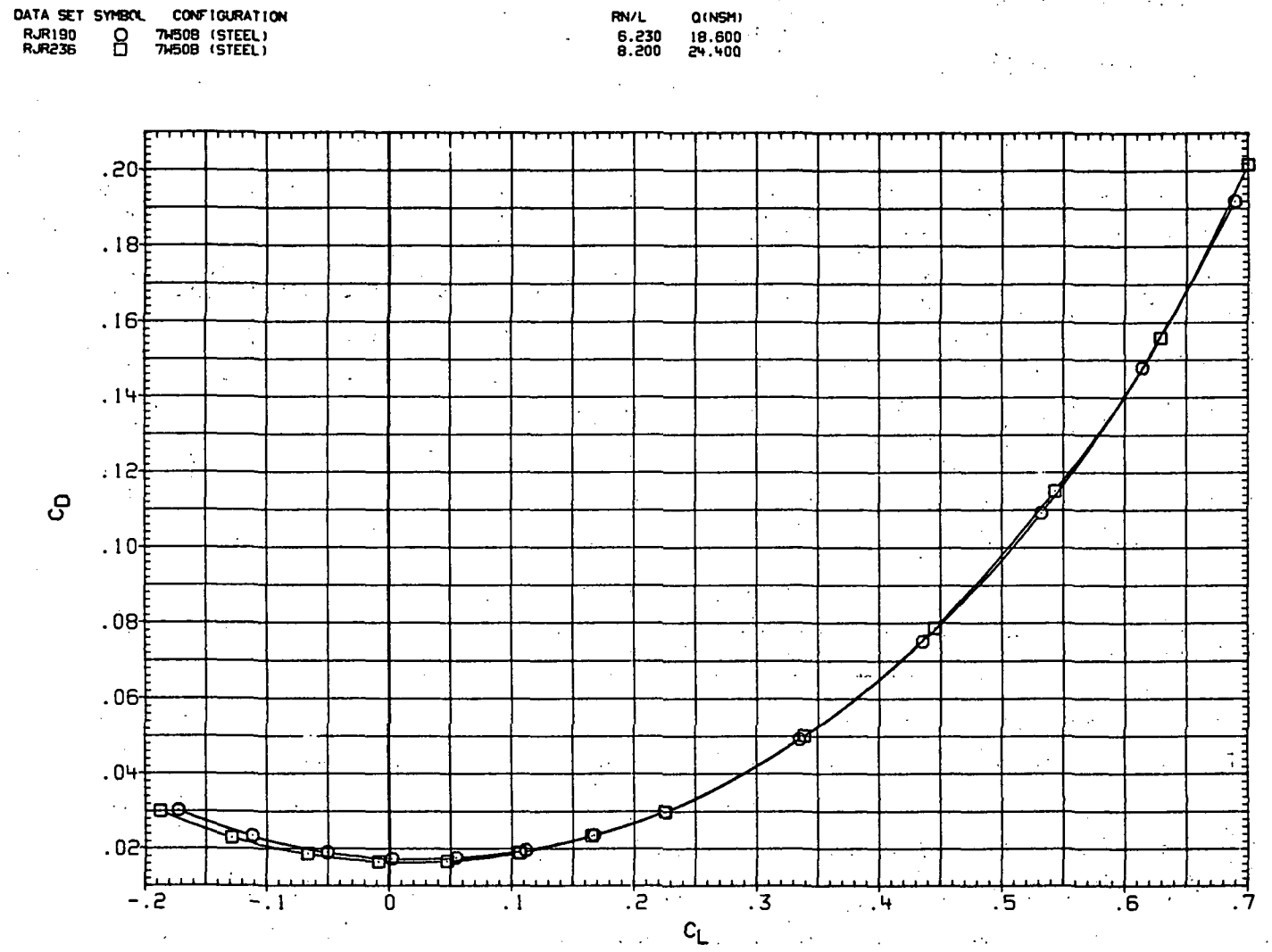

(b) C_D vs C_L.

Figure 65.– Continued.

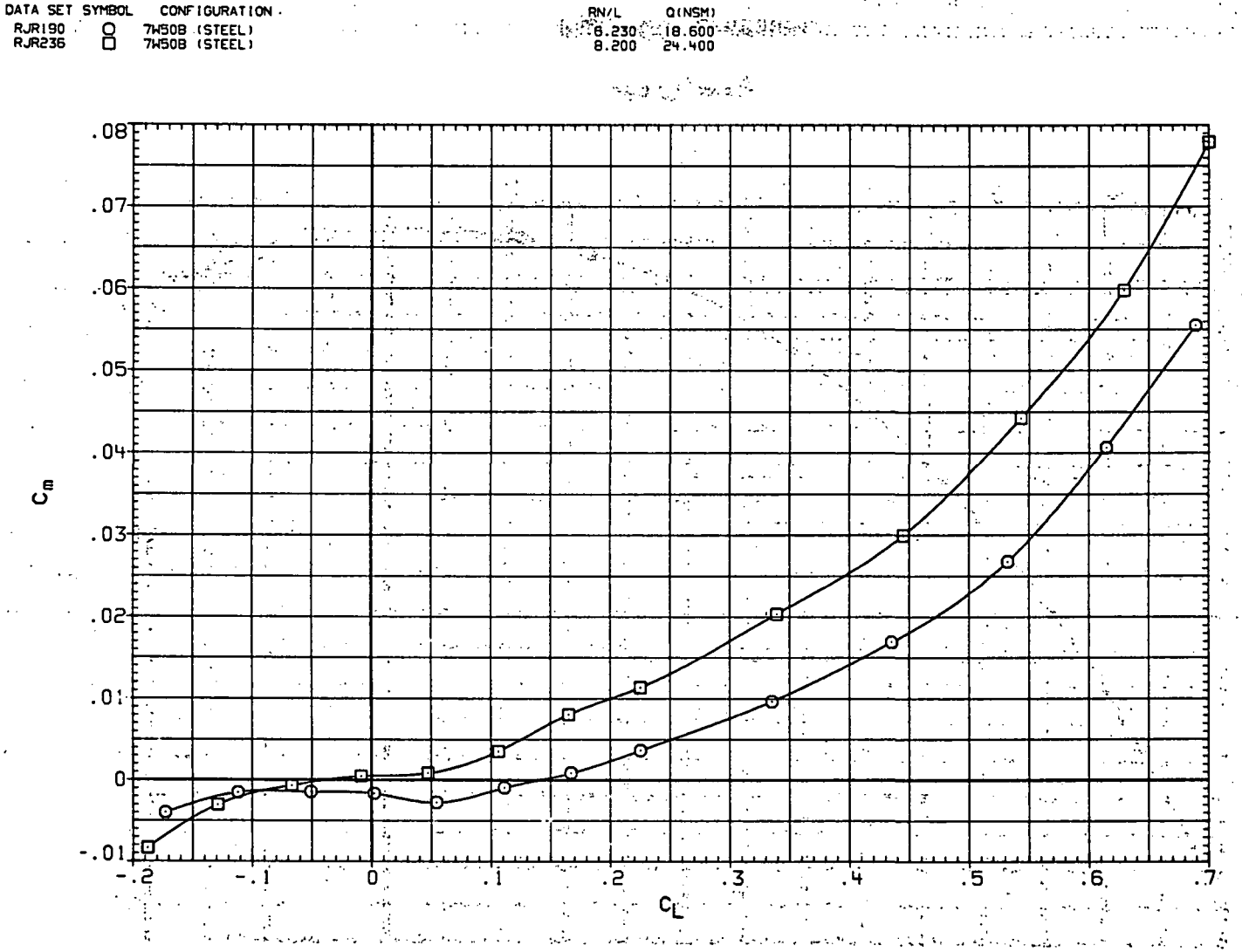

(c) C_m vs C_L.

Figure 65.– Continued.

(d) L/D vs C_L.

Figure 65.– Continued.

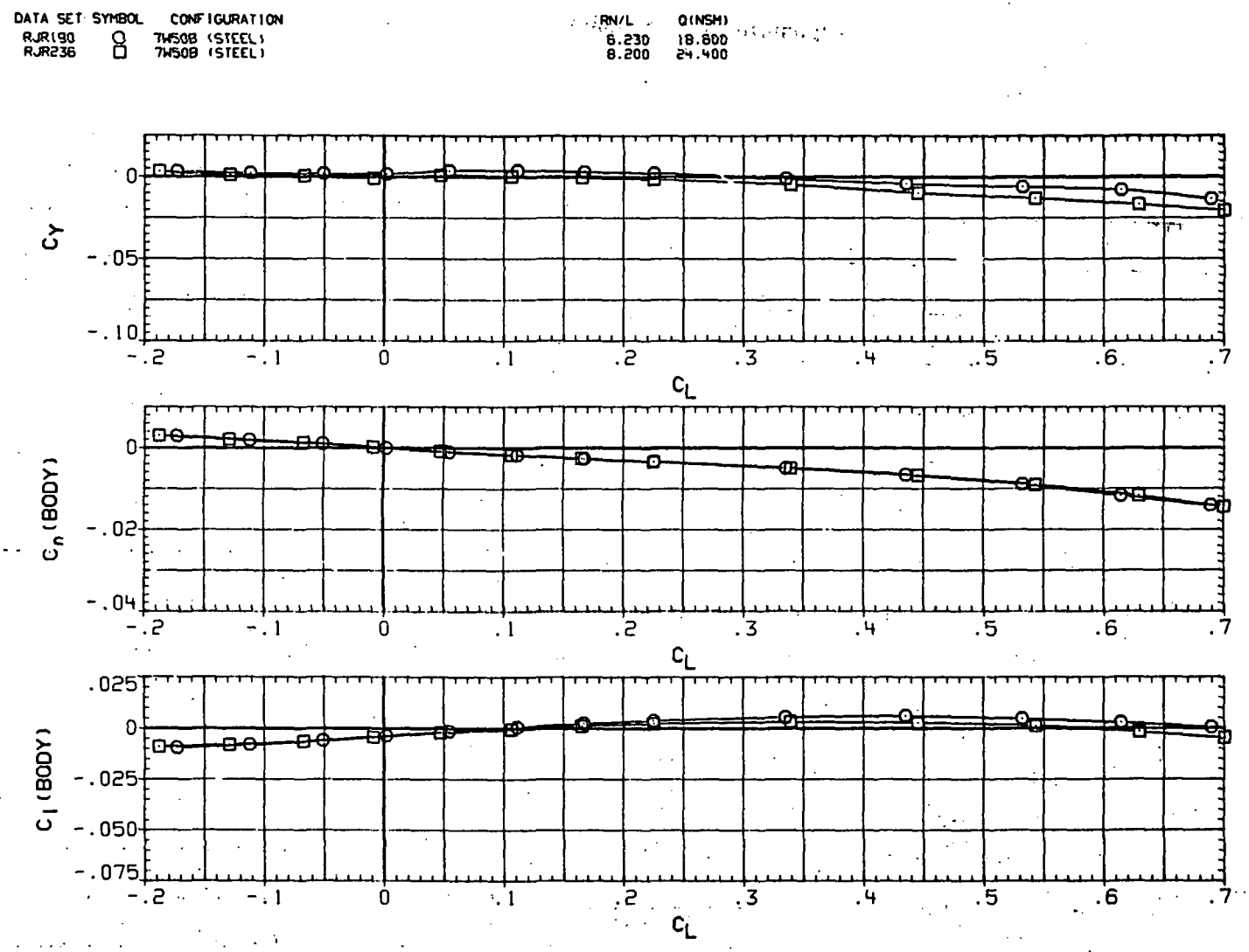

(e) C_Y, C_n and C_ℓ vs C_L.

Figure 65.– Concluded.

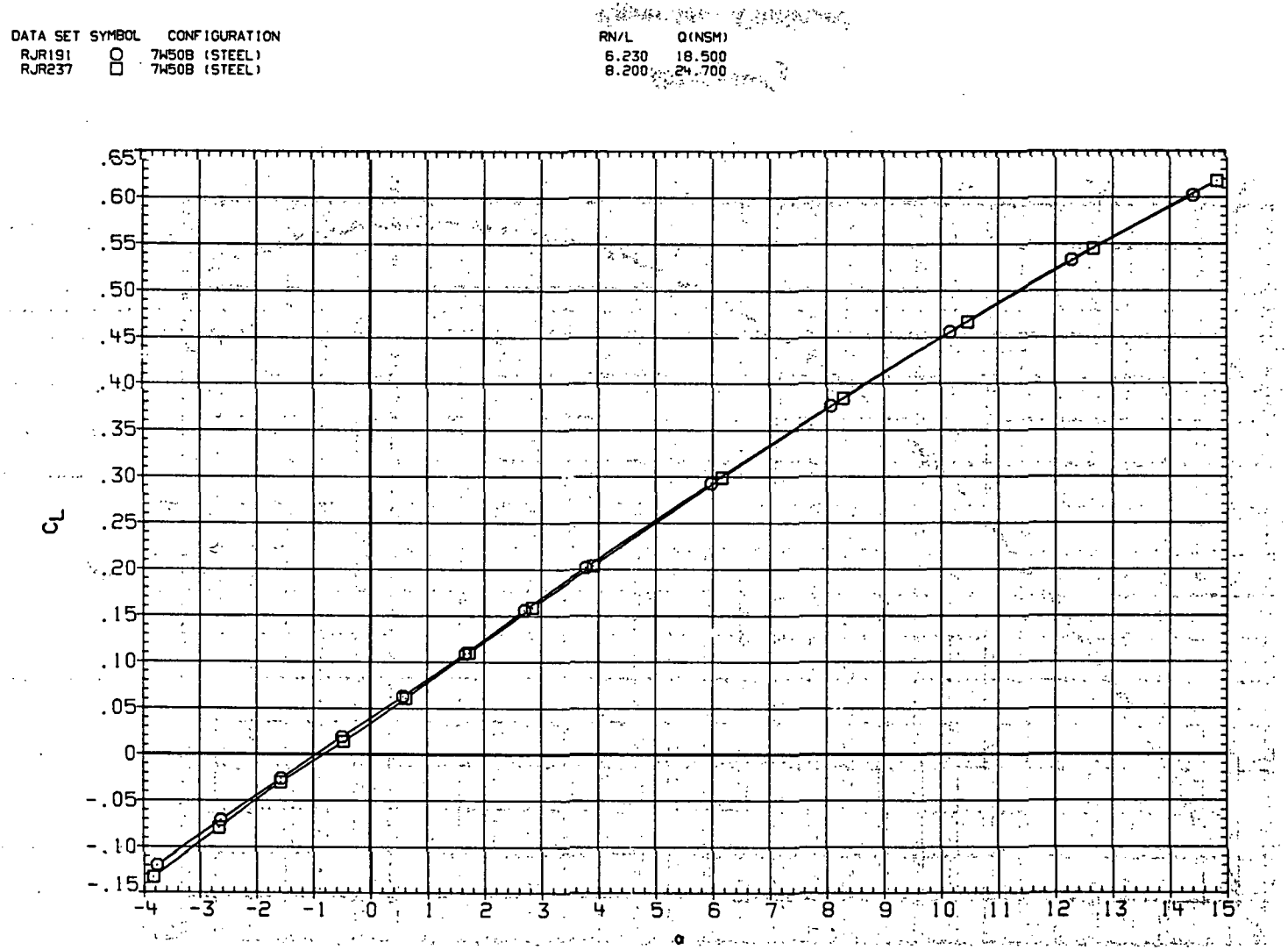

Figure 66.– Dynamic-pressure effects on the aerodynamic characteristics of the steel trapezoidal oblique wing-body combination ($\Lambda = 50°$, $M = 2.0$ and the NACA 65A204 airfoil).

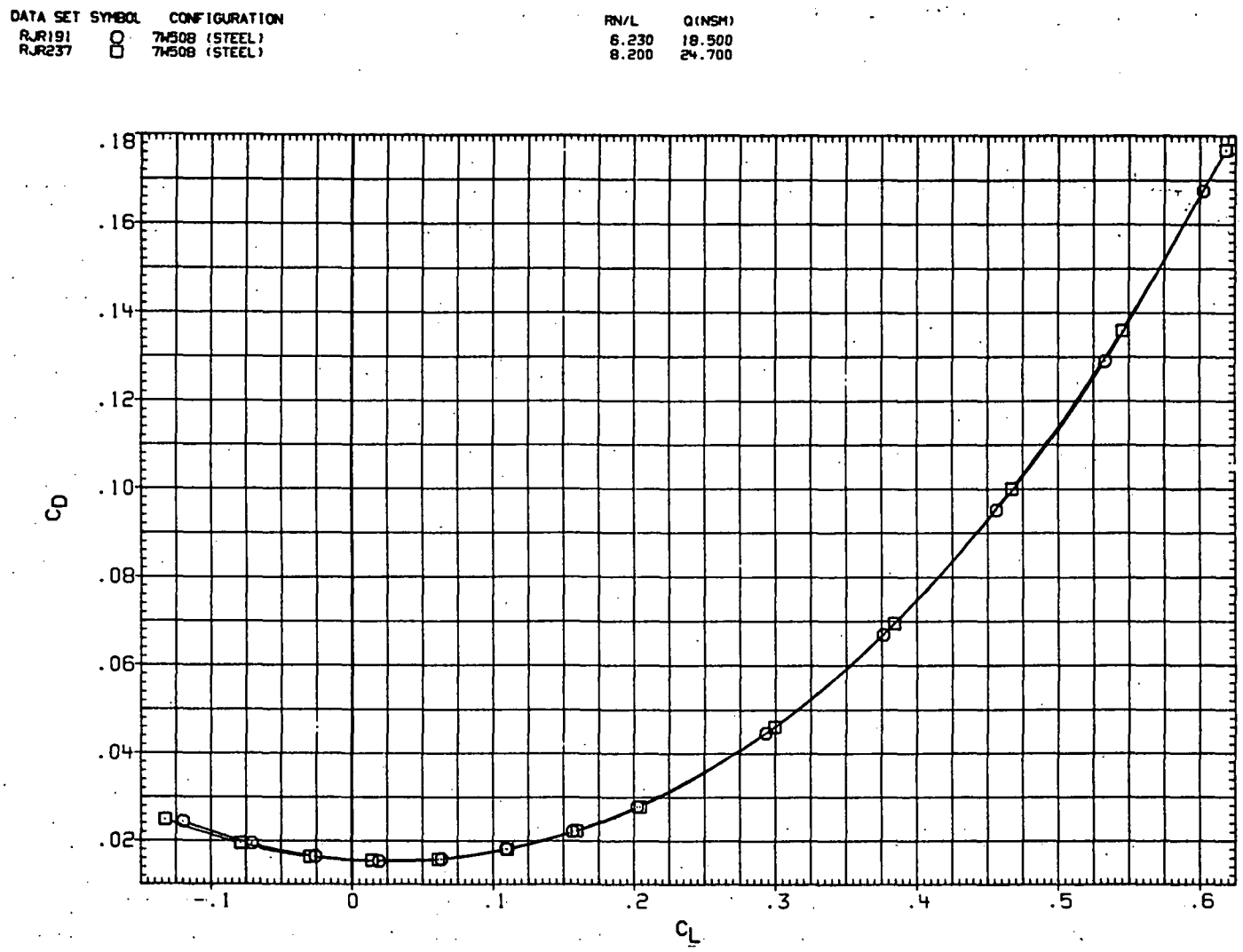

(b) C_D vs C_L.

Figure 66.– Continued.

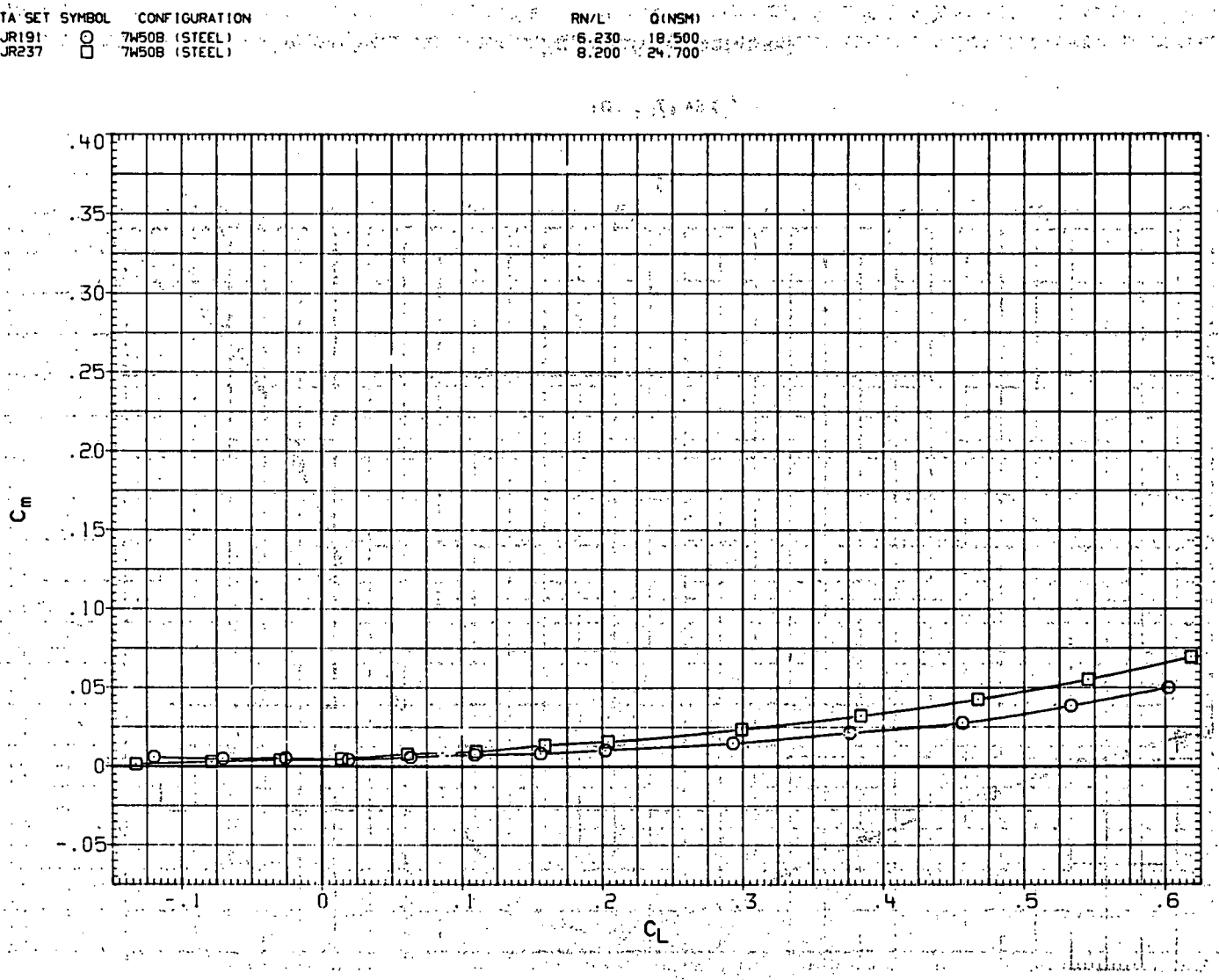

(c) C_m vs C_L.

Figure 66.– Continued.

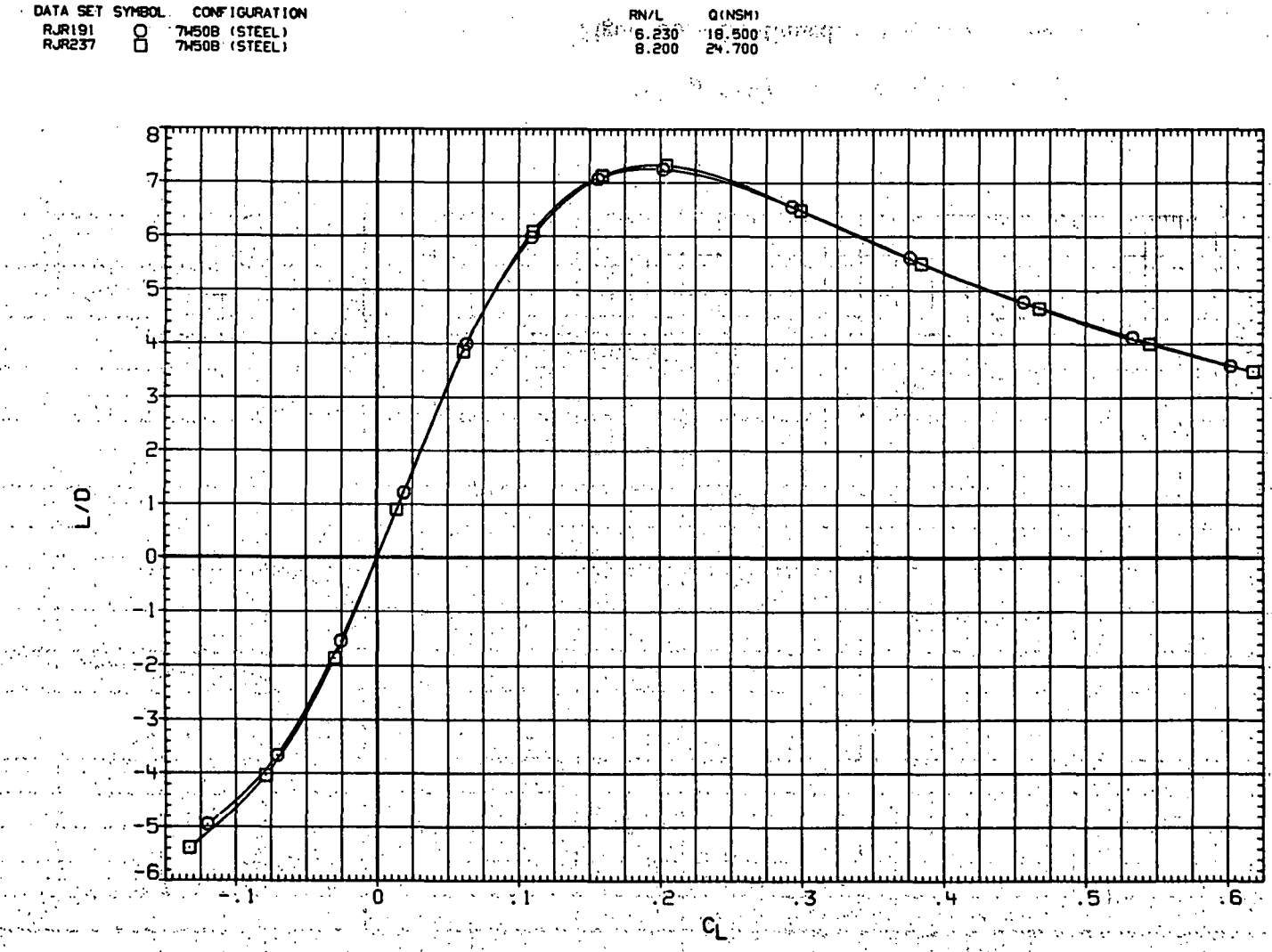

(d) L/D vs C_L.

Figure 66.– Continued.

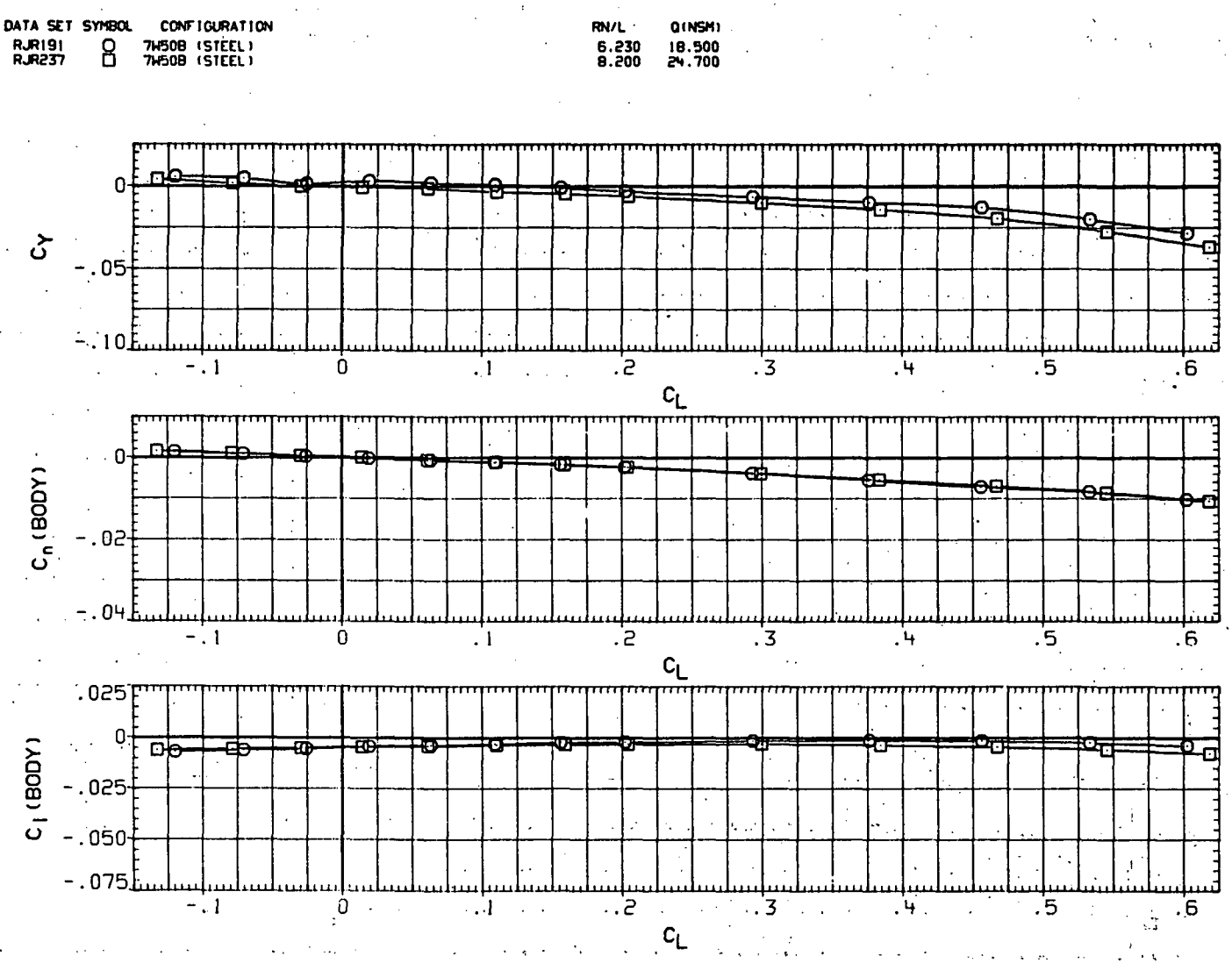

(e) C_Y, C_n and C_ℓ vs C_L.

Figure 66.– Concluded.

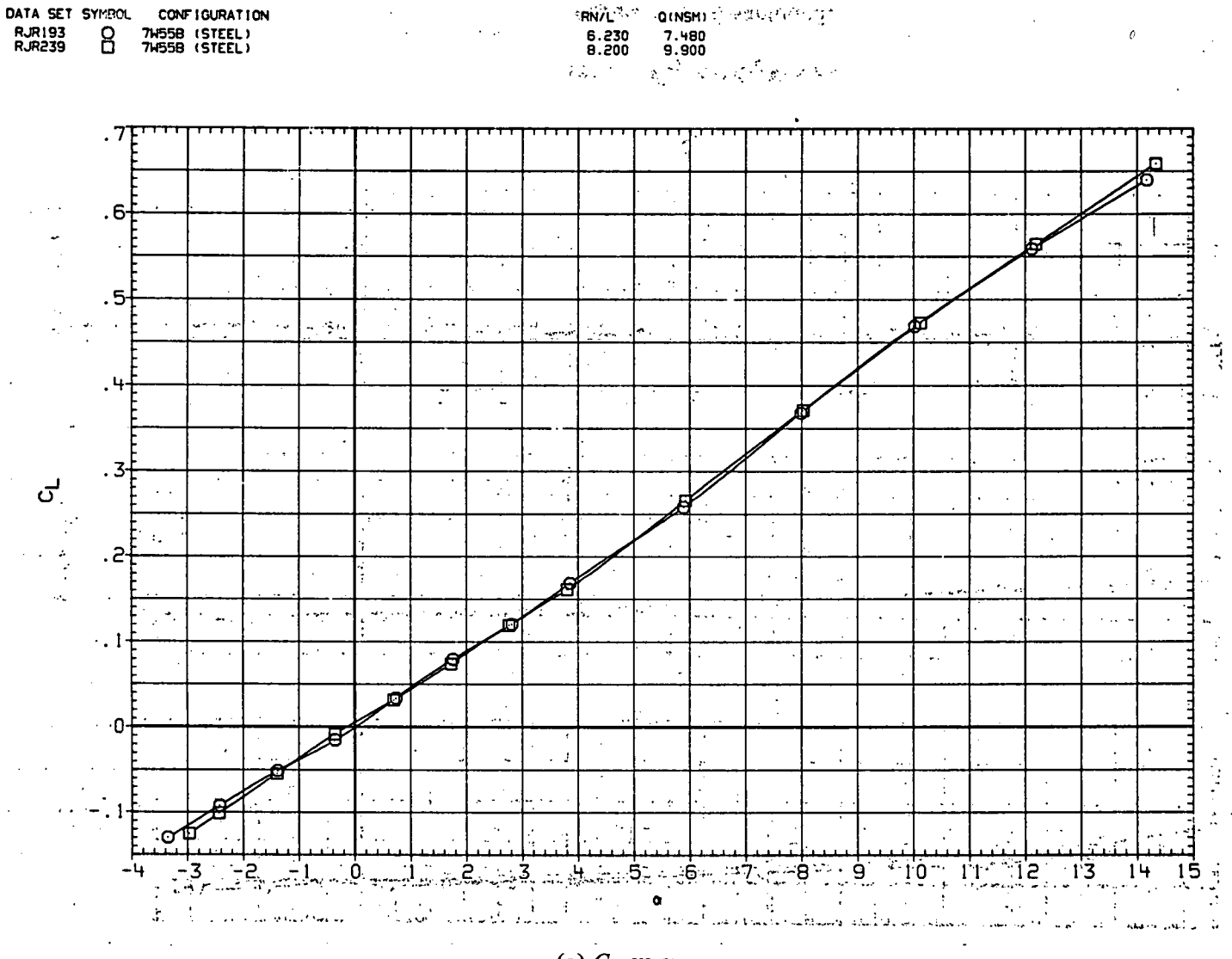

(a) C_L vs α.

Figure 67.– Dynamic-pressure effects on the aerodynamic characteristics of the steel trapezoidal oblique wing-body combination ($\Lambda = 55°$, $M = 0.4$ and the NACA 65A204 airfoil).

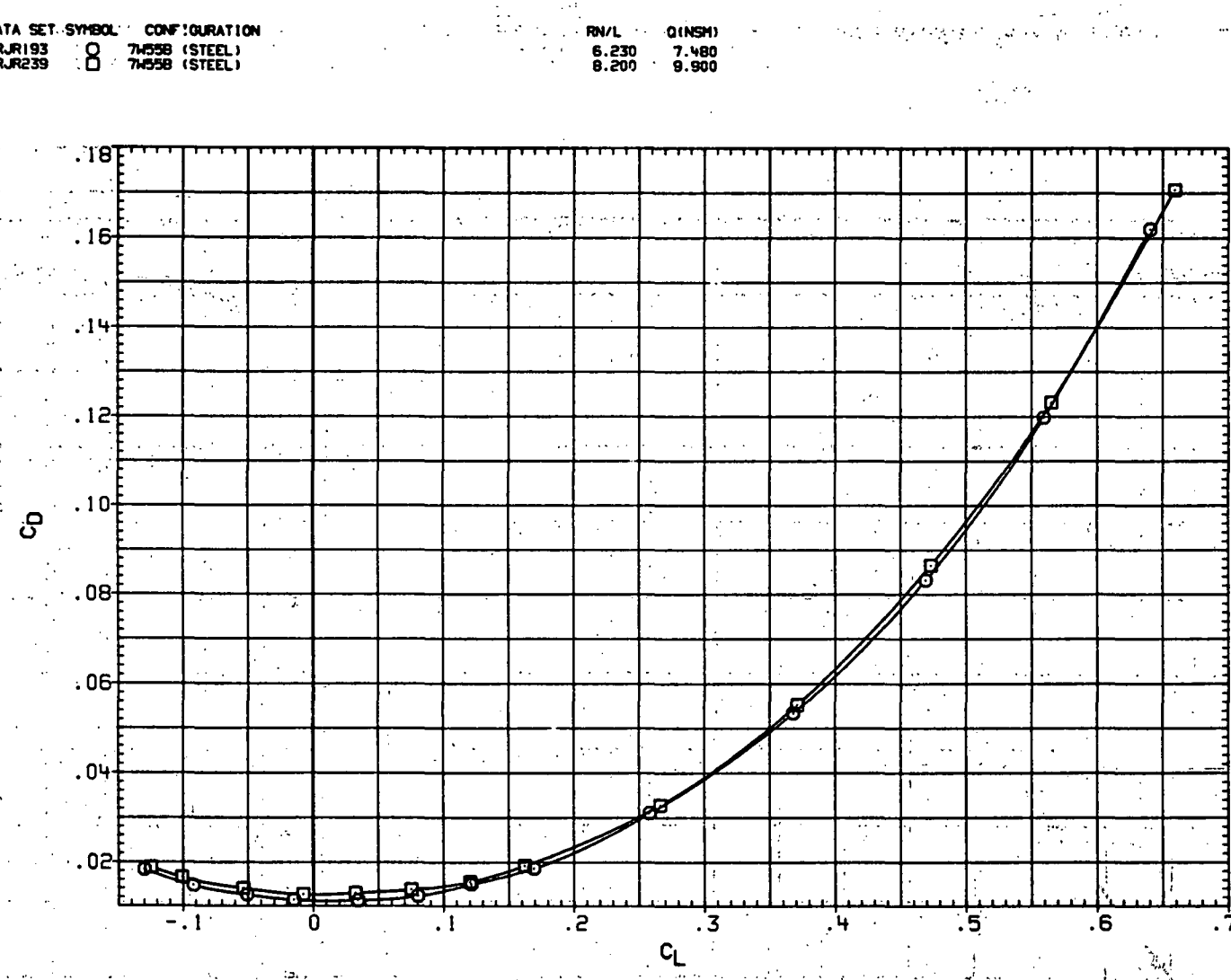

(b) C_D vs C_L.

Figure 67.– Continued.

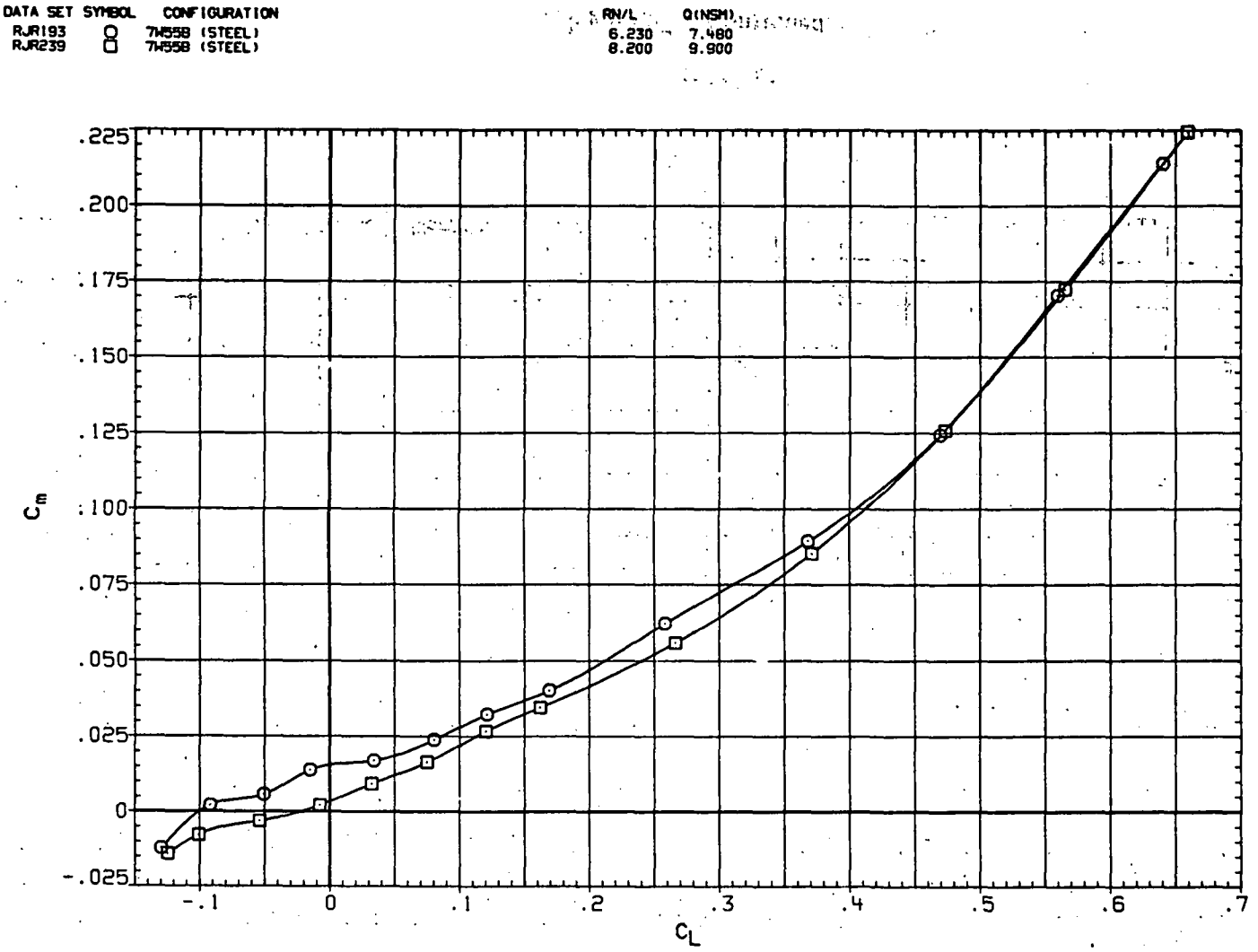

(c) C_m vs C_L.

Figure 67.– Continued.

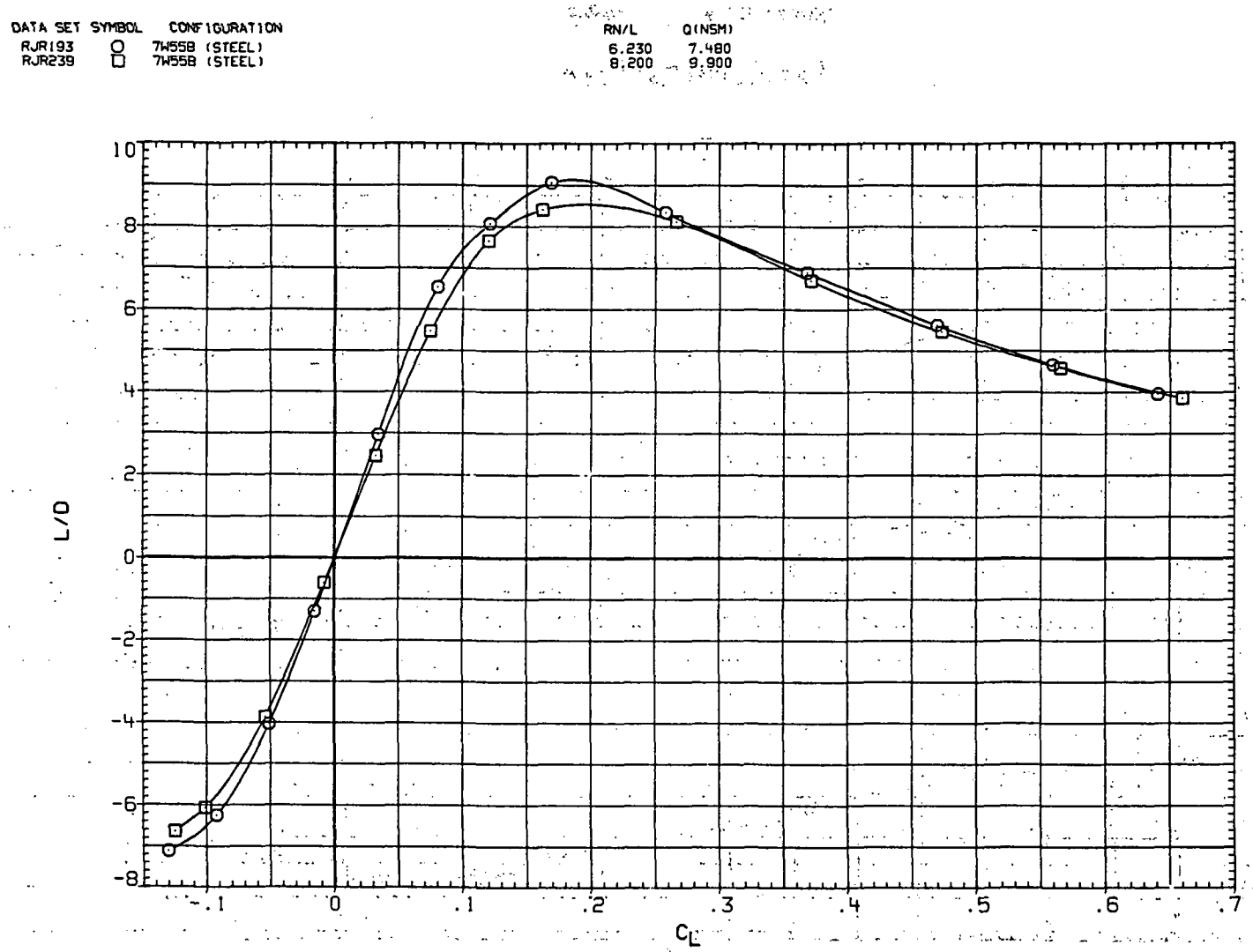

(d) L/D vs C_L.

Figure 67.– Continued.

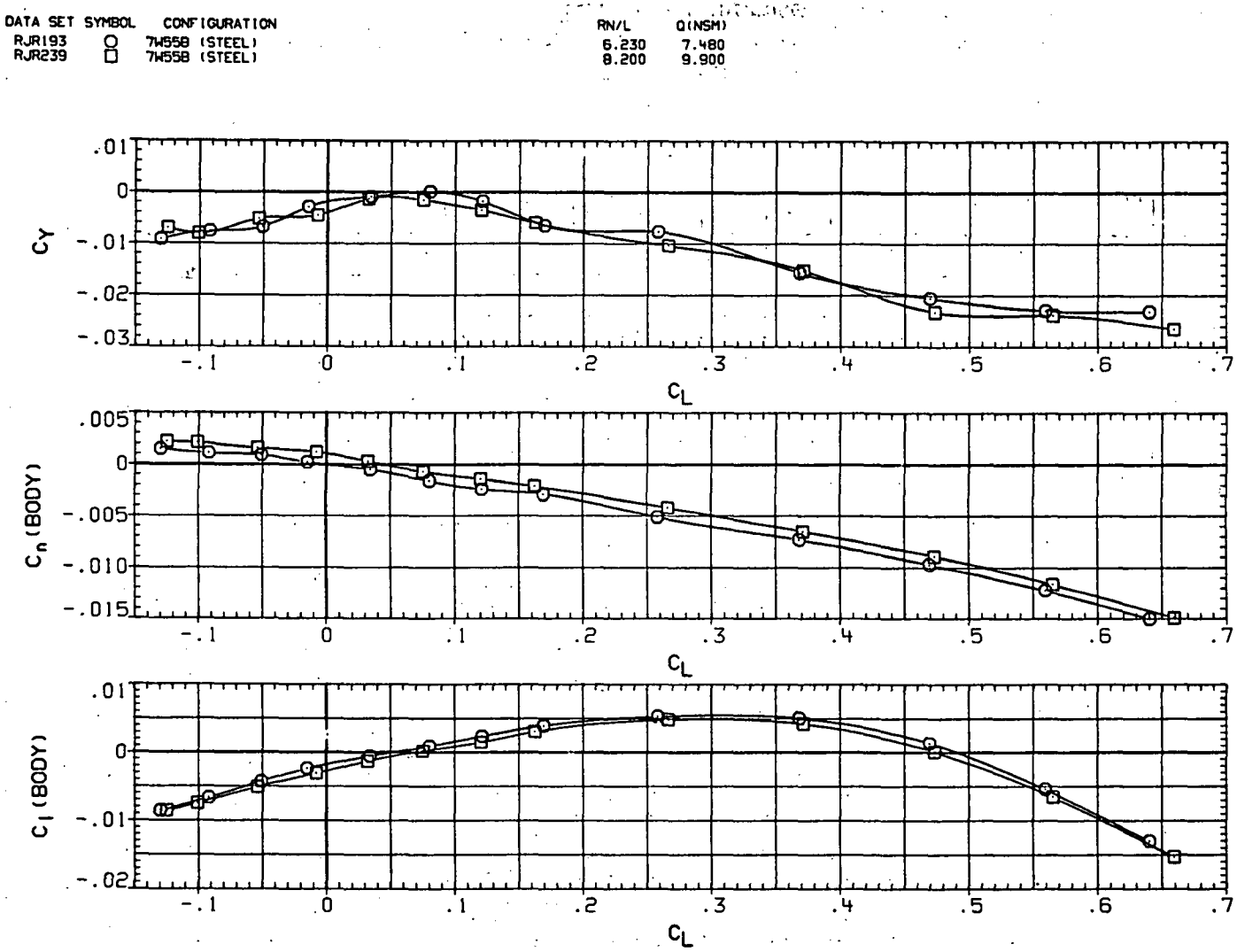

(e) C_Y, C_n and C_ℓ vs C_L.

Figure 67.– Concluded.

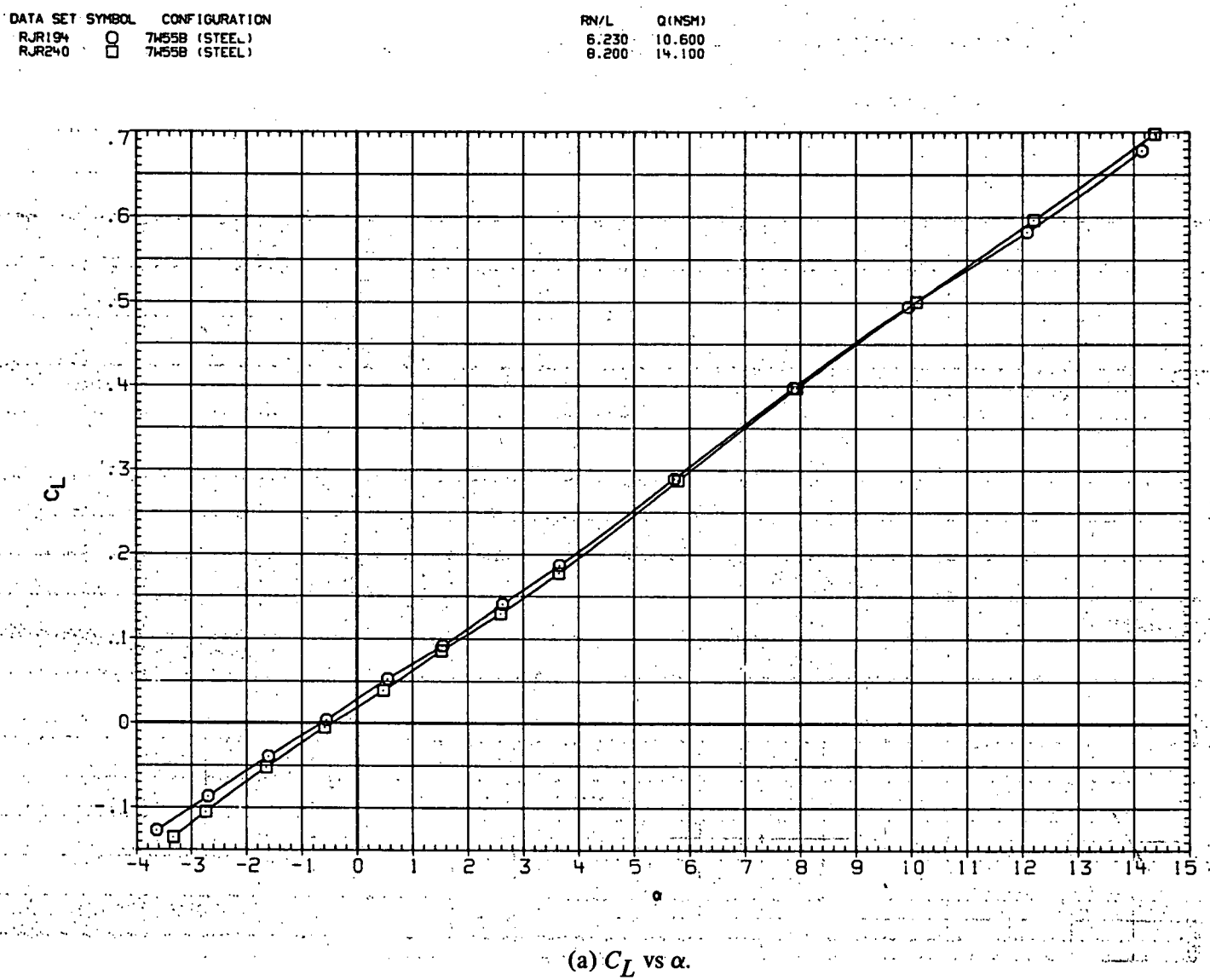

(a) C_L vs α.

Figure 68.– Dynamic-pressure effects on the aerodynamic characteristics of the steel trapezoidal oblique wing-body combination ($\Lambda = 55°$, $M = 0.6$ and the NACA 65A204 airfoil).

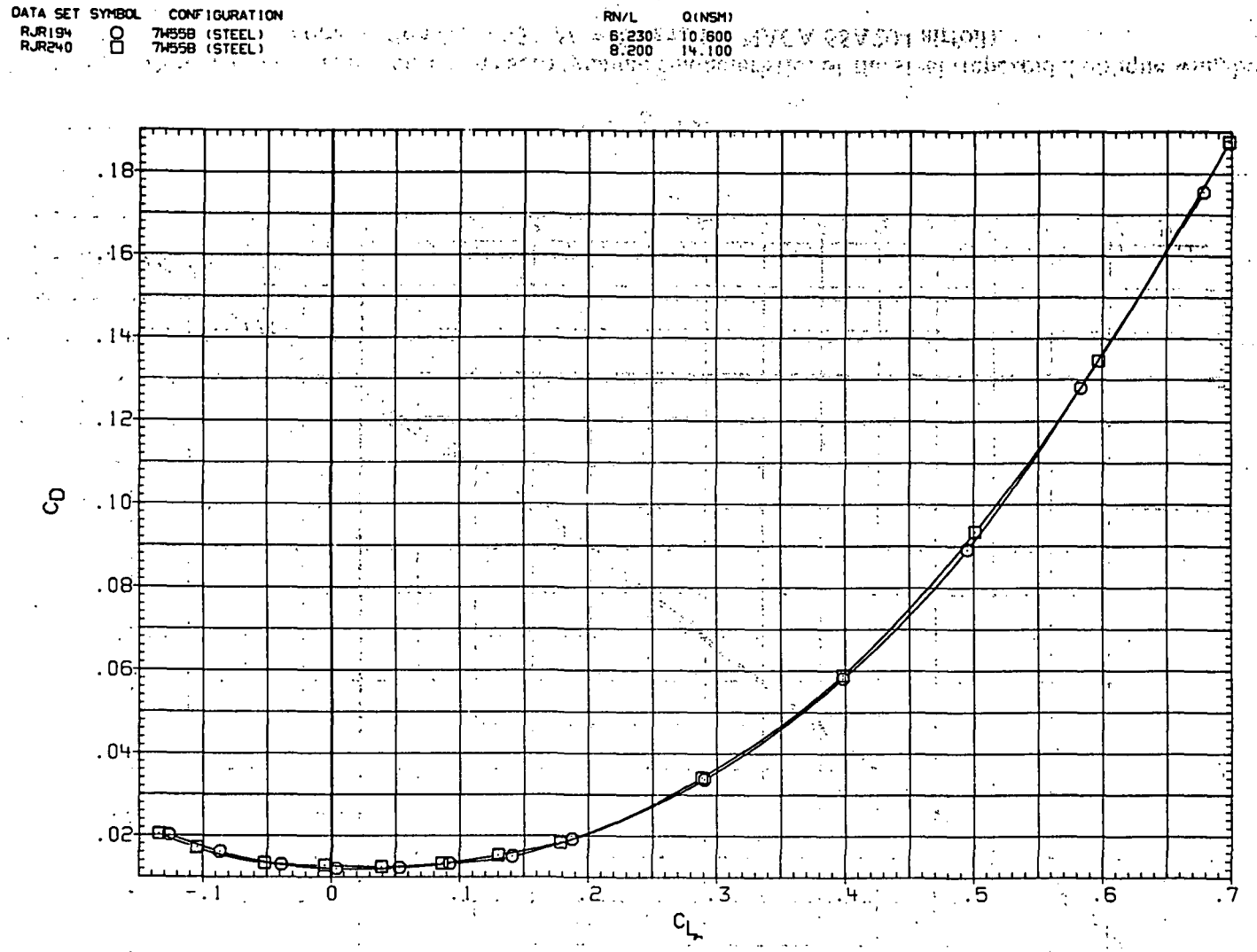

(b) C_D vs C_L.

Figure 68.—Continued.

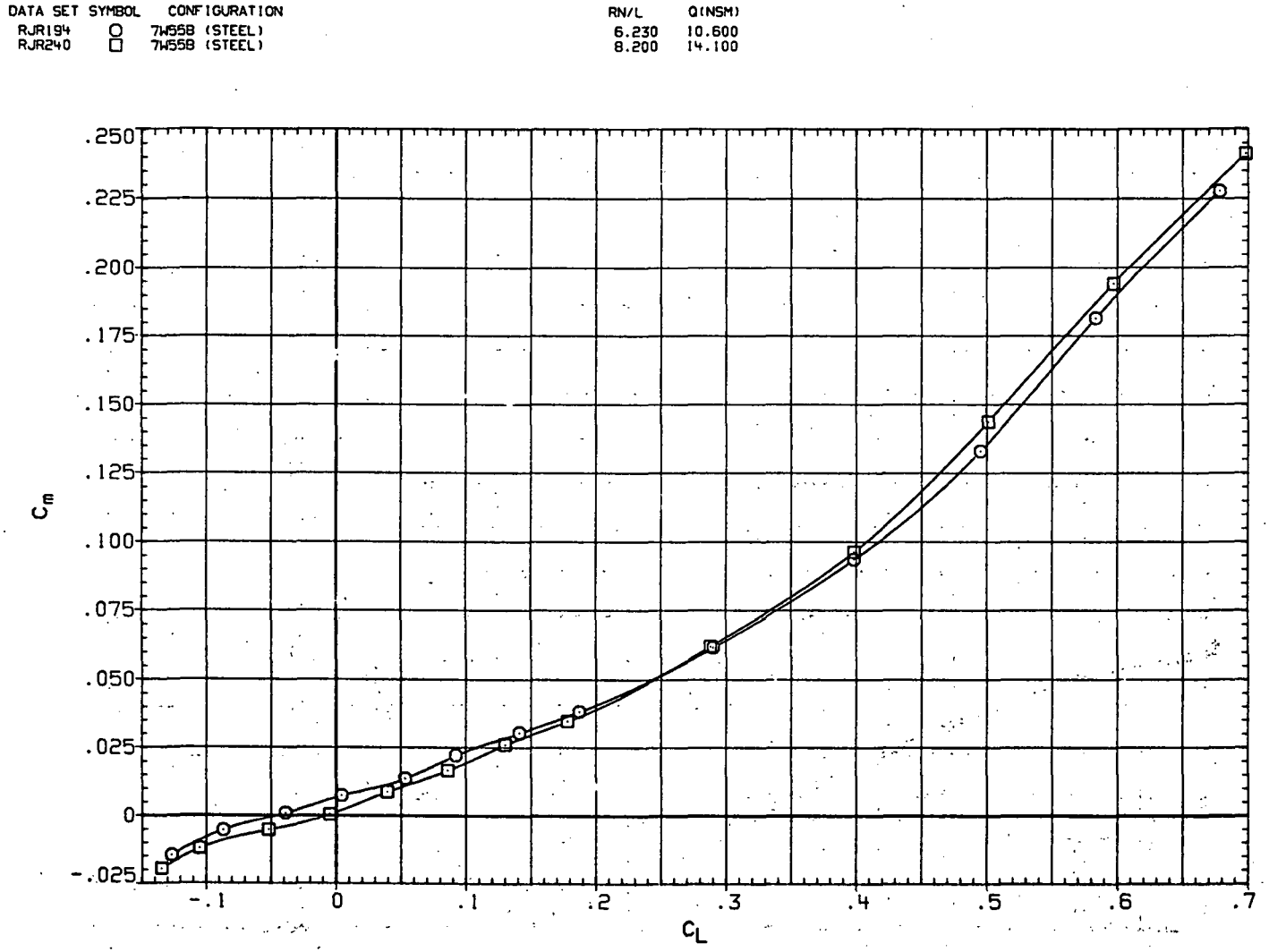

(c) C_m vs C_L.

Figure 68.– Continued.

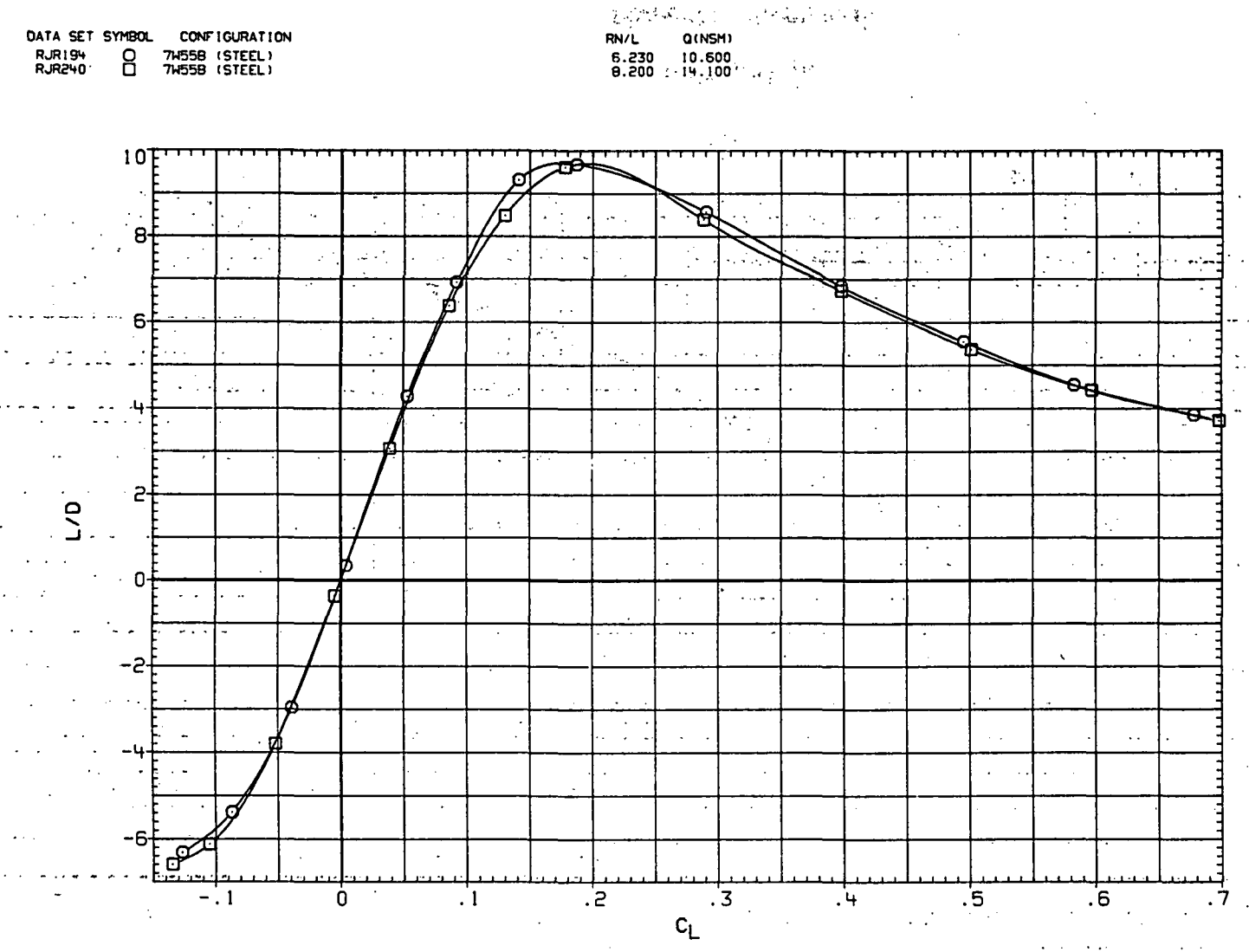

(d) L/D vs C_L.

Figure 68.– Continued.

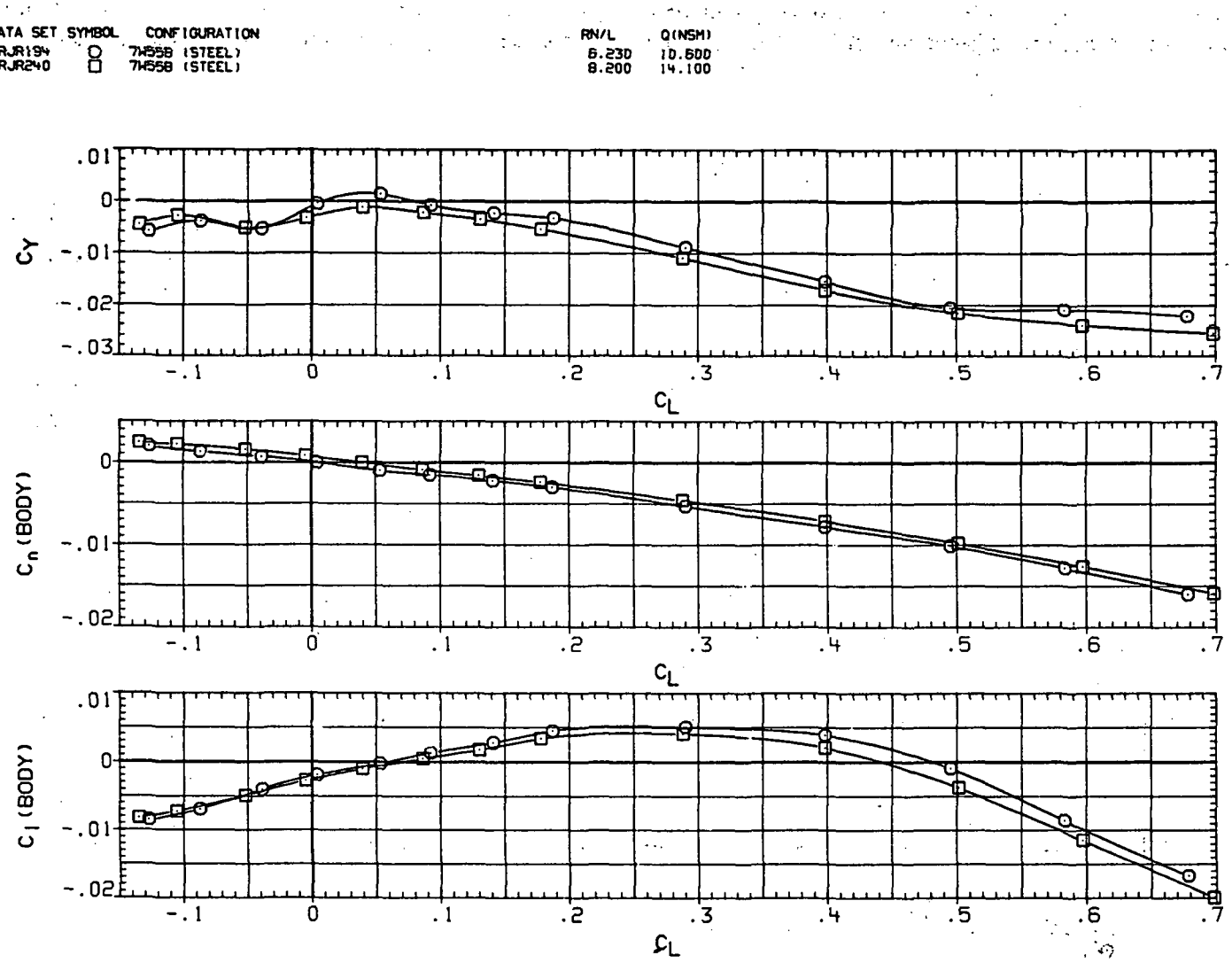

(e) C_Y, C_n and C_ℓ vs C_L.

Figure 68.– Concluded.

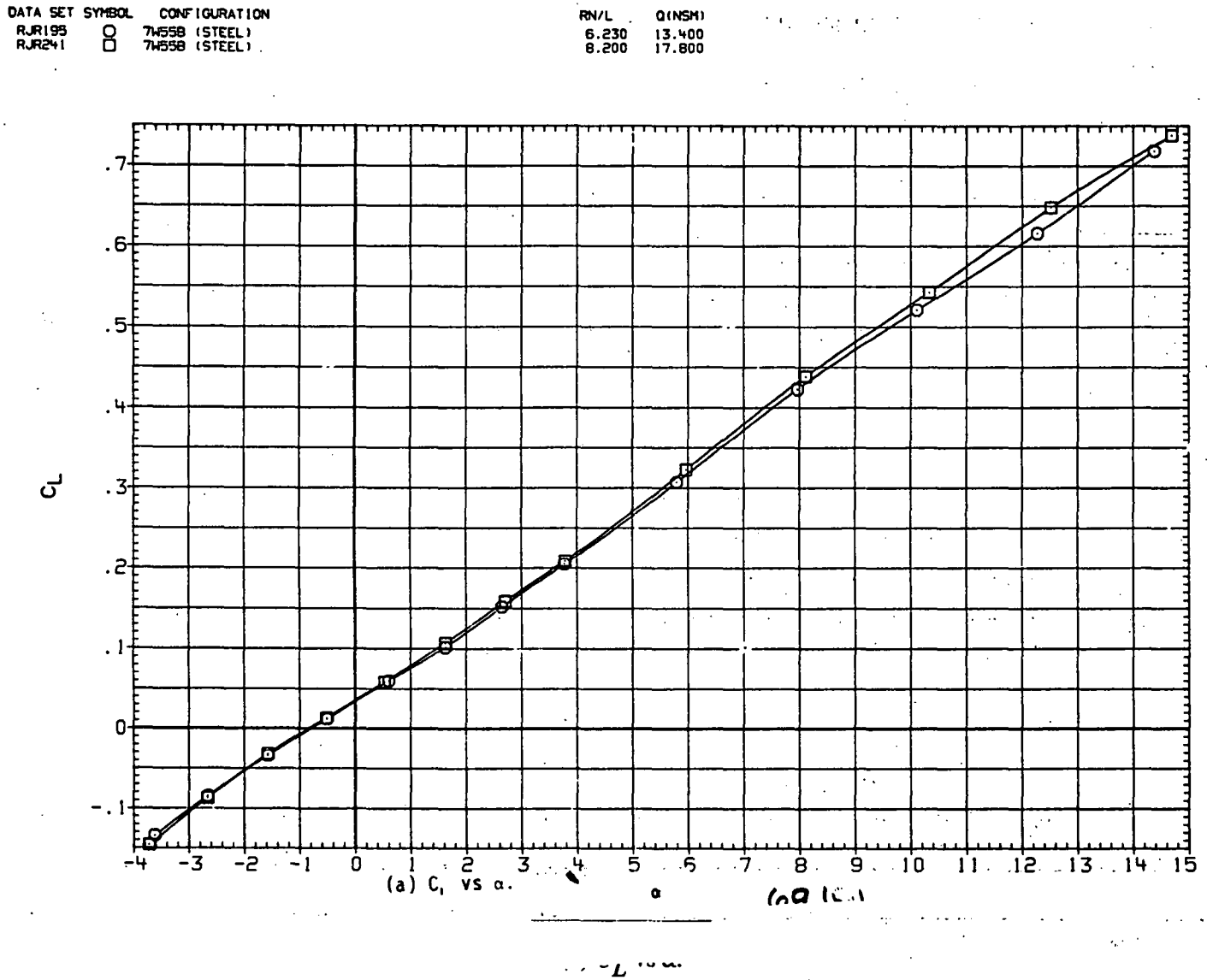

Figure 69.– Dynamic-pressure effects on the aerodynamic characteristics of the steel trapezoidal oblique wing-body combination ($\Lambda = 55°, M = 0.8$ and the NACA 65A204 airfoil).

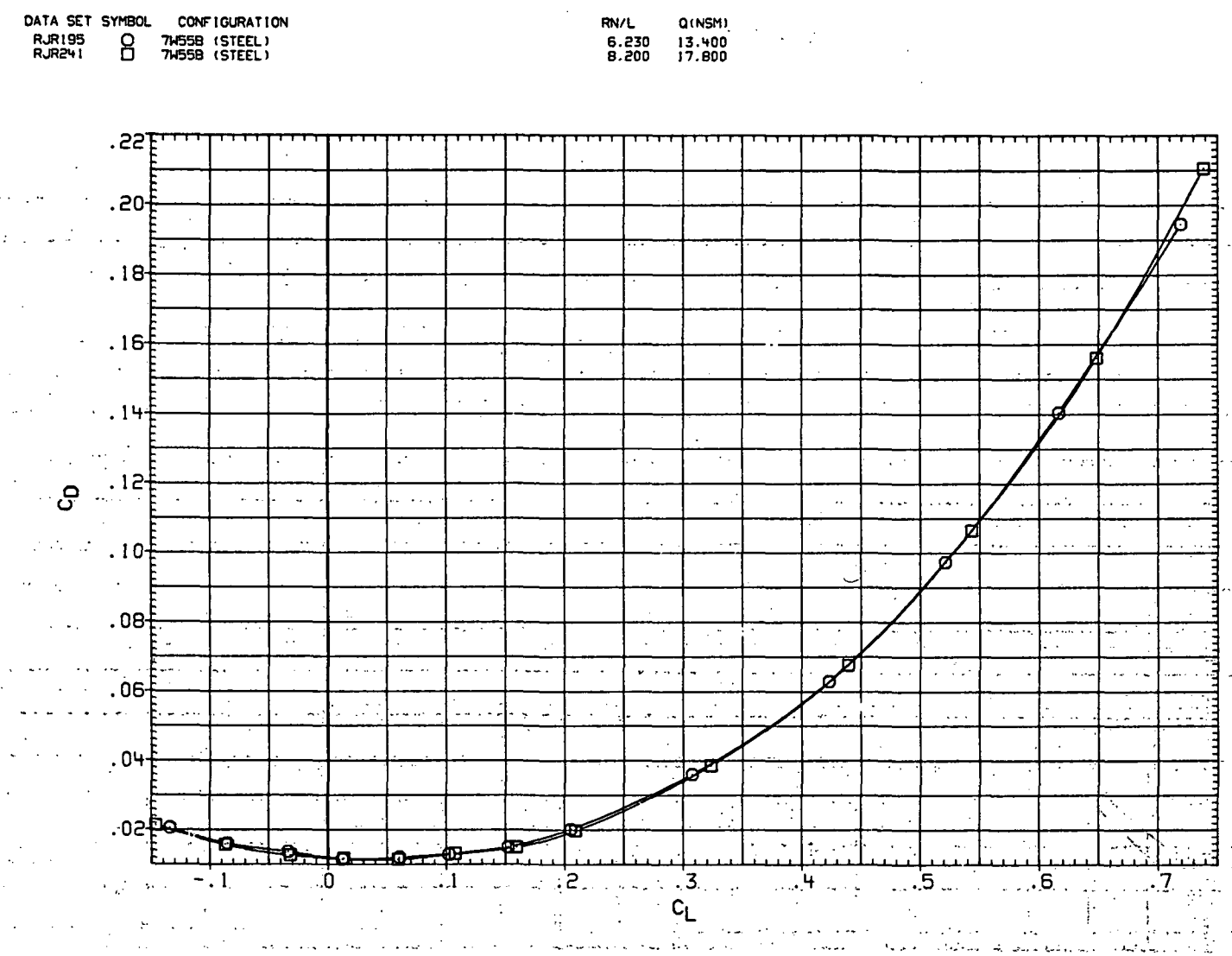

(b) C_D vs C_L.

Figure 69.– Continued.

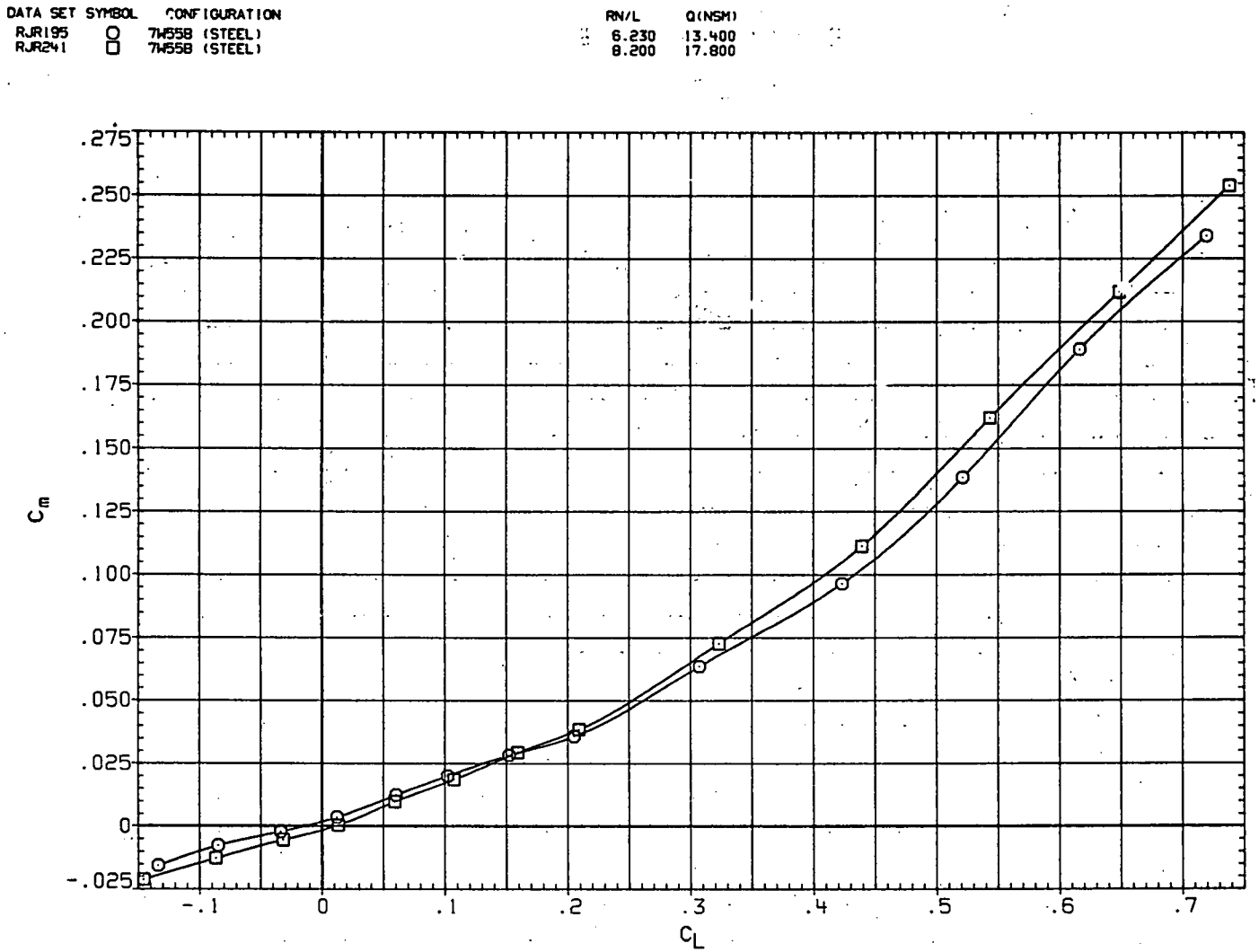

(c) C_m vs C_L.

Figure 69.– Continued.

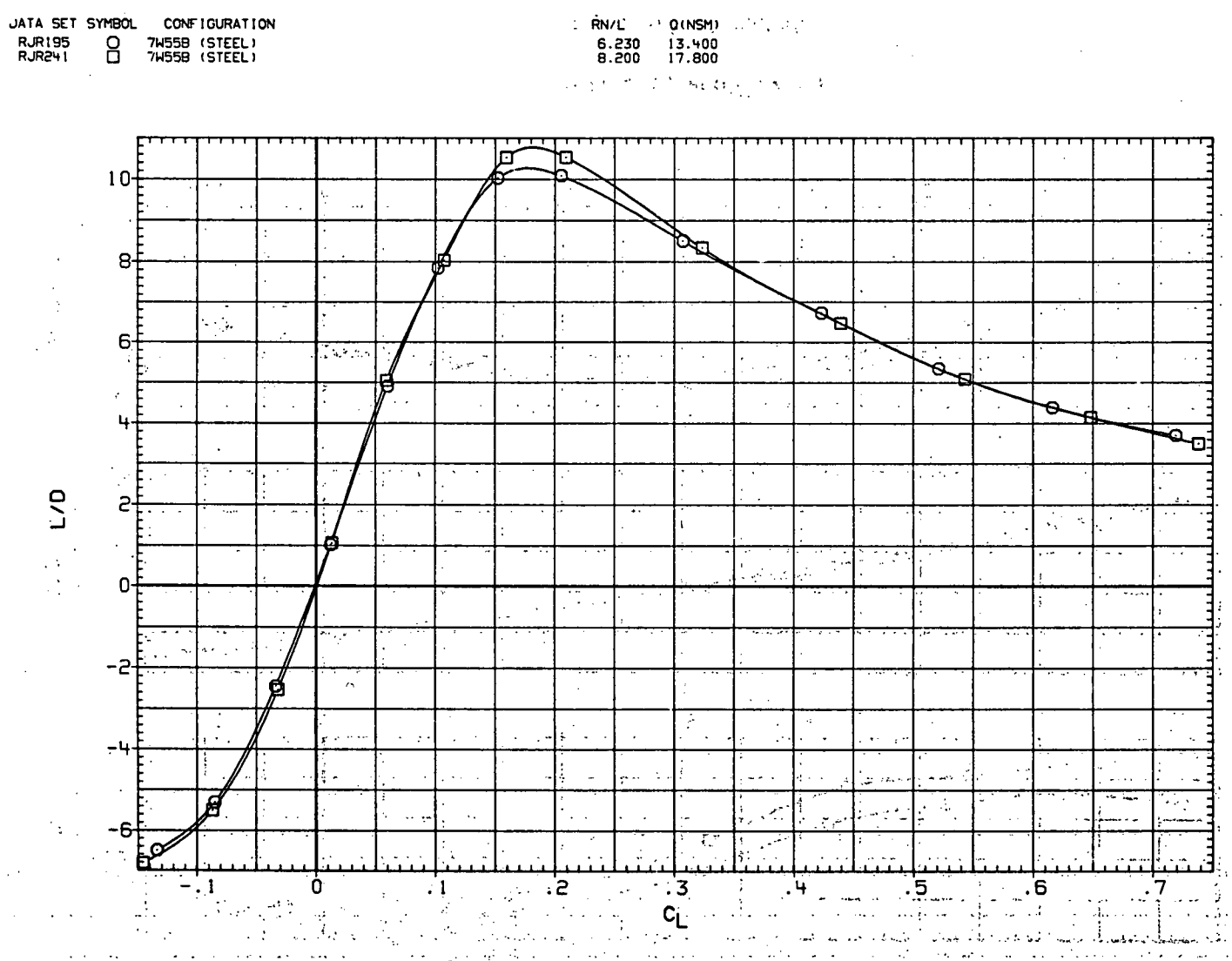

(d) L/D vs C_L.

Figure 69.— Continued.

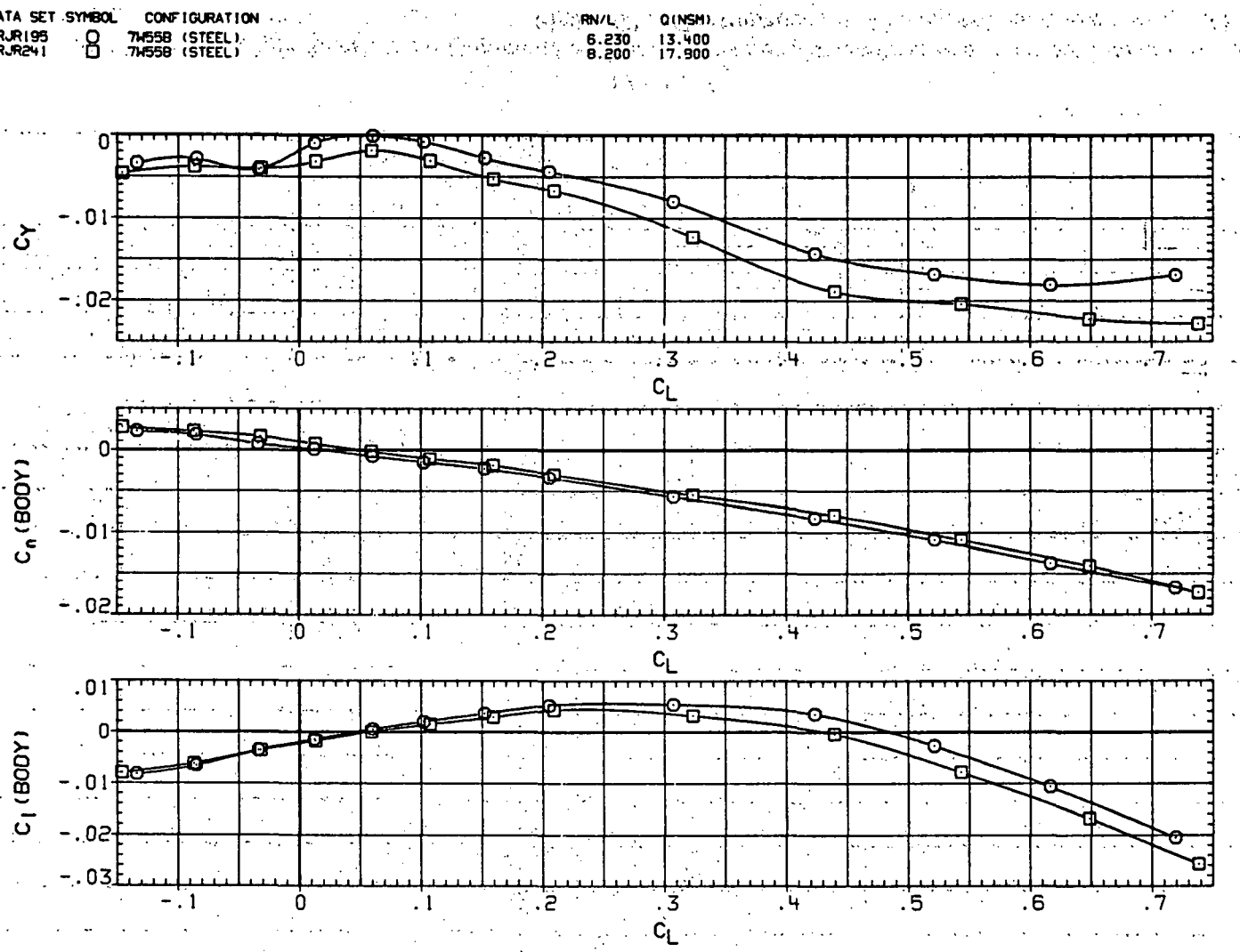

(e) C_Y, C_n and C_ℓ vs C_L.

Figure 69.—Concluded.

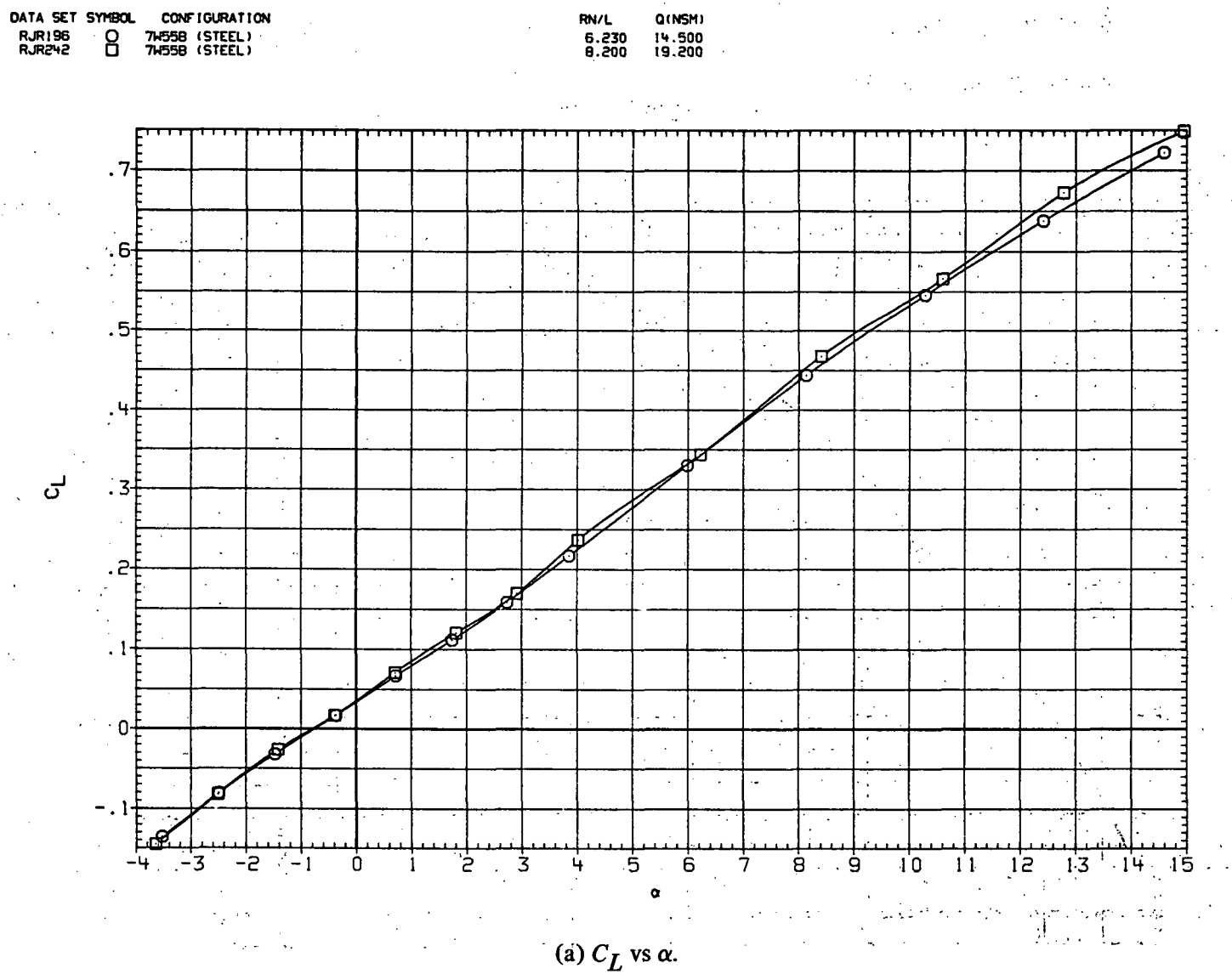

(a) C_L vs α.

Figure 70.– Dynamic-pressure effects on the aerodynamic characteristics of the steel trapezoidal oblique wing-body combination ($\Lambda = 55°$, $M = 0.9$ and the NACA 65A204 airfoil).

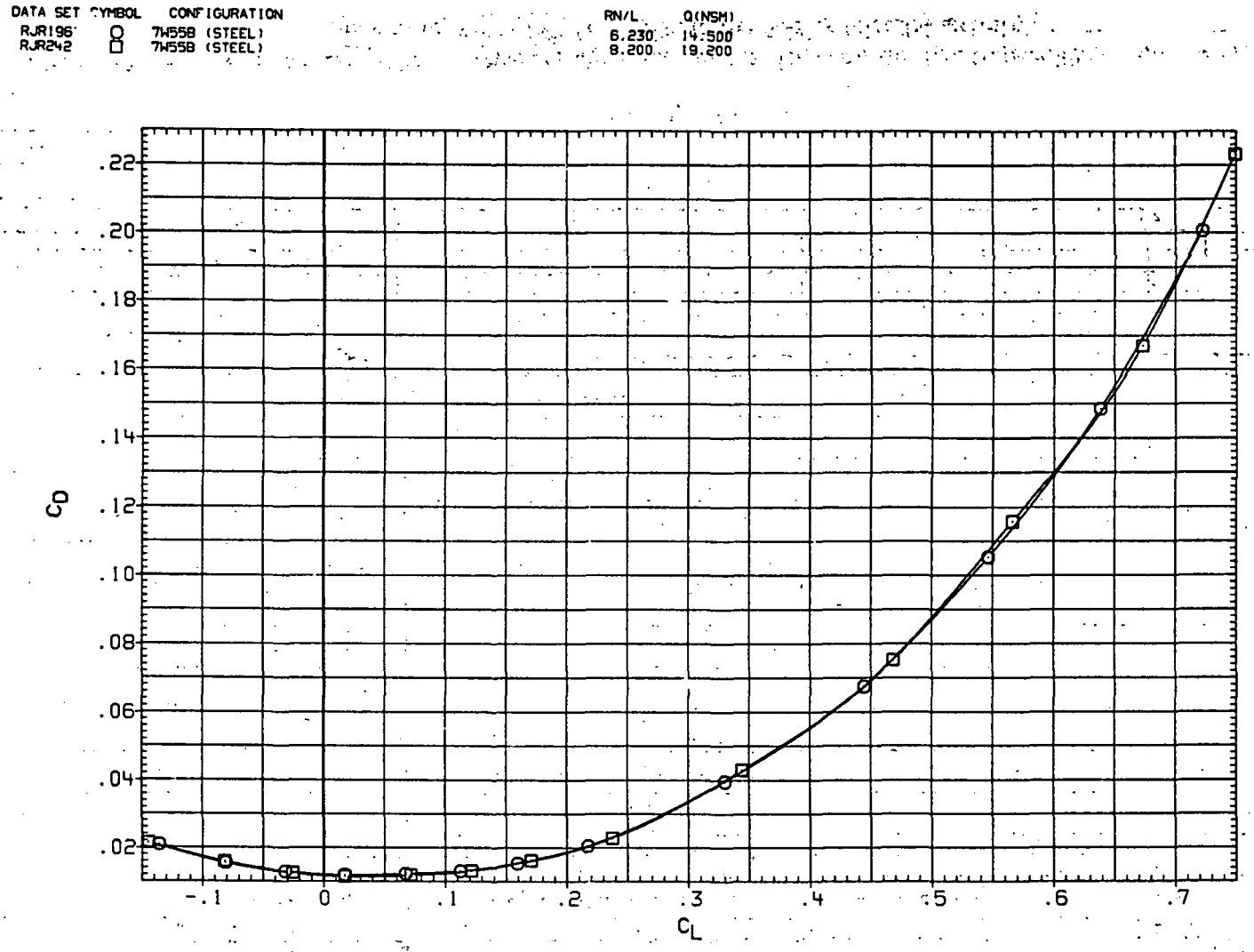

(b) C_D vs C_L.

Figure 70.– Continued.

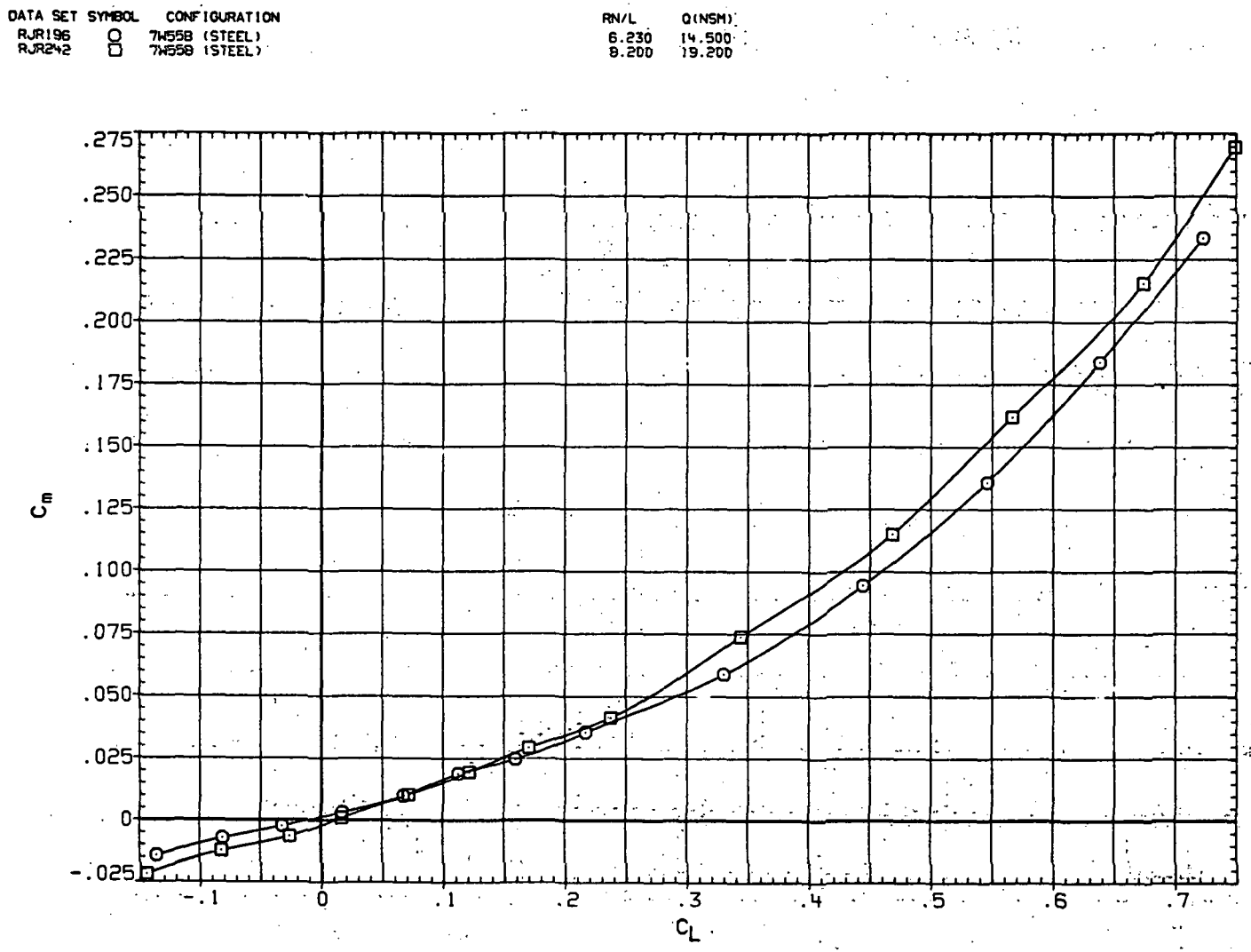

(c) C_m vs C_L.

Figure 70.– Continued.

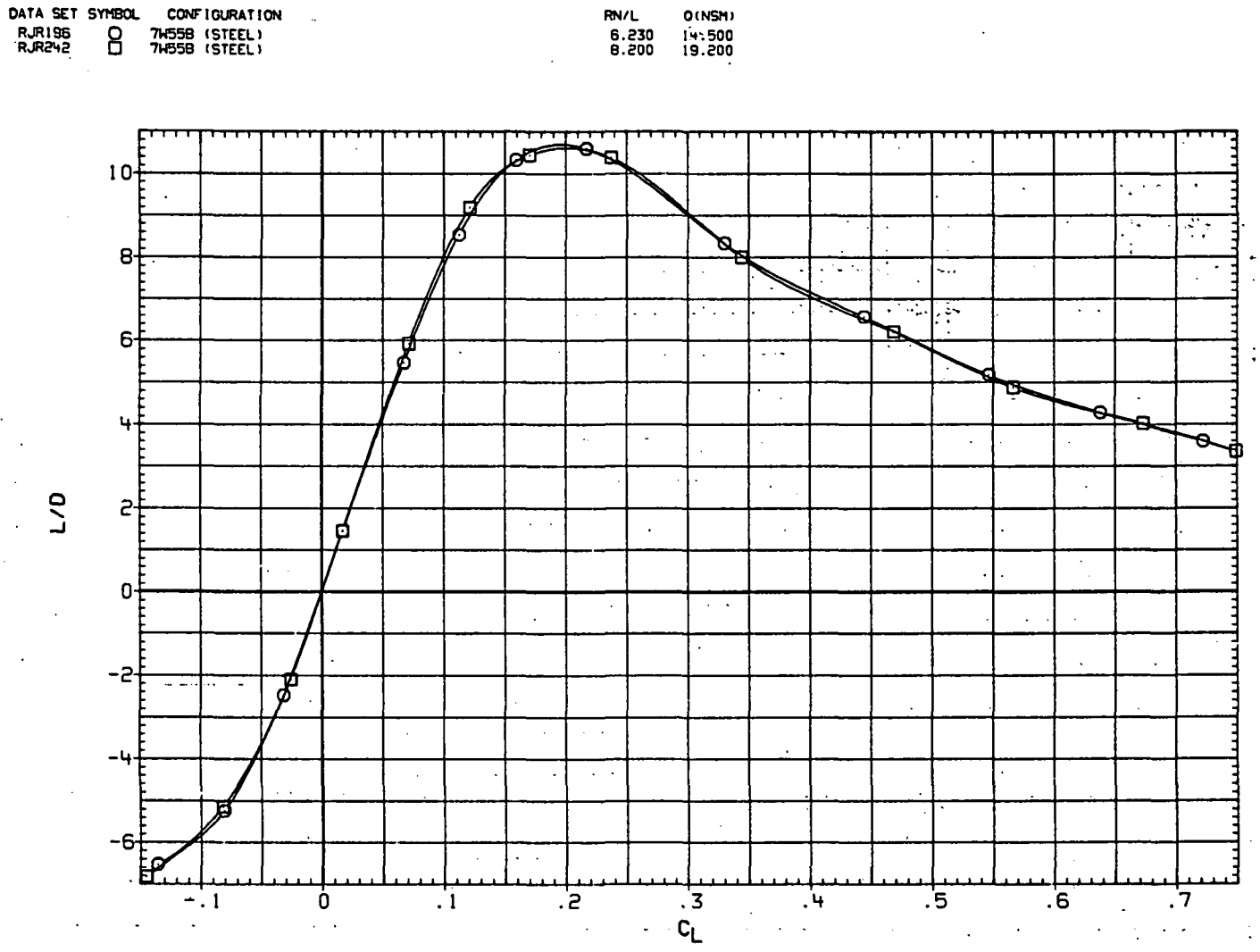

(d) L/D vs C_L.

Figure 70.– Continued.

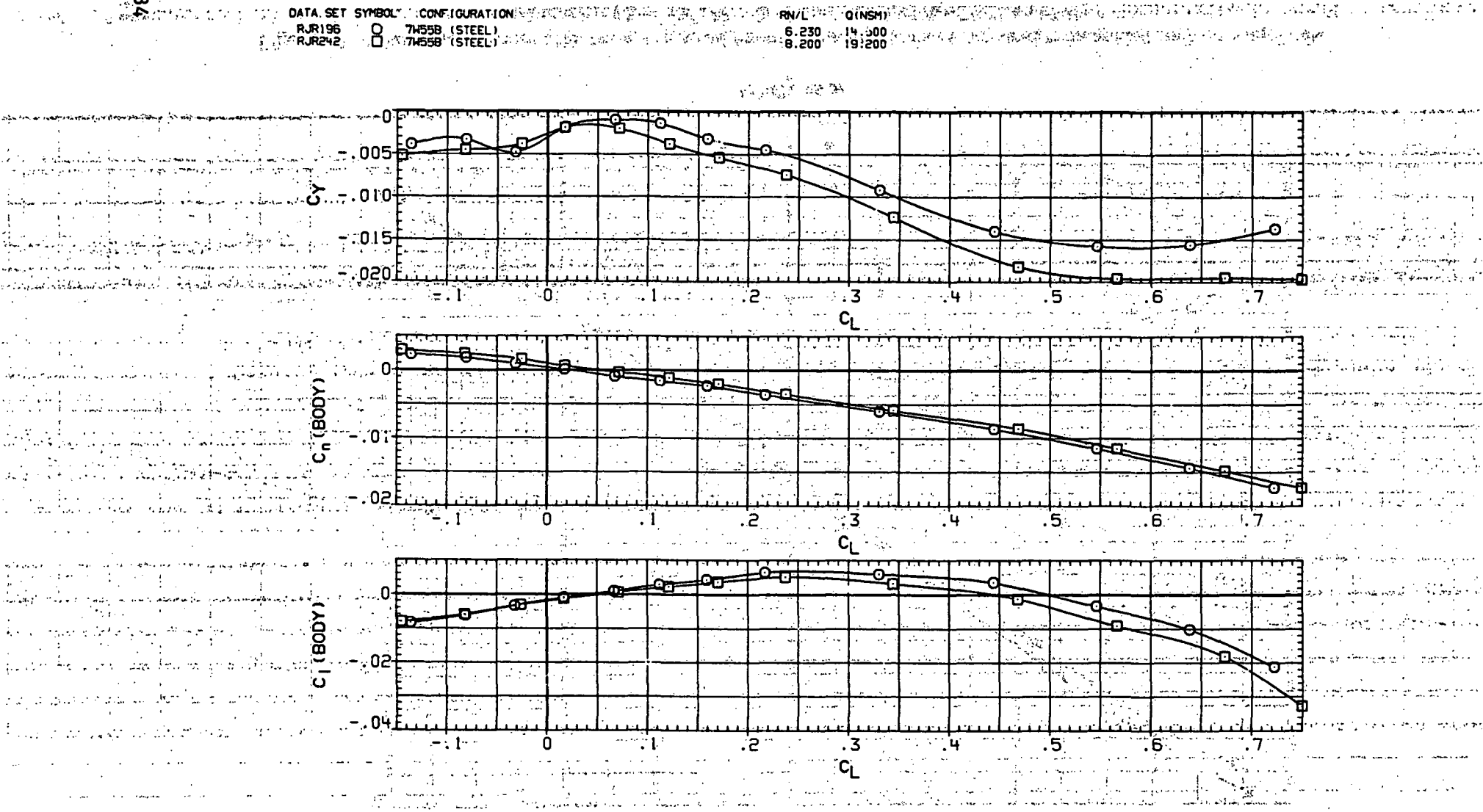

(e) C_Y, C_n and C_ℓ vs C_L.

Figure 70.– Concluded.

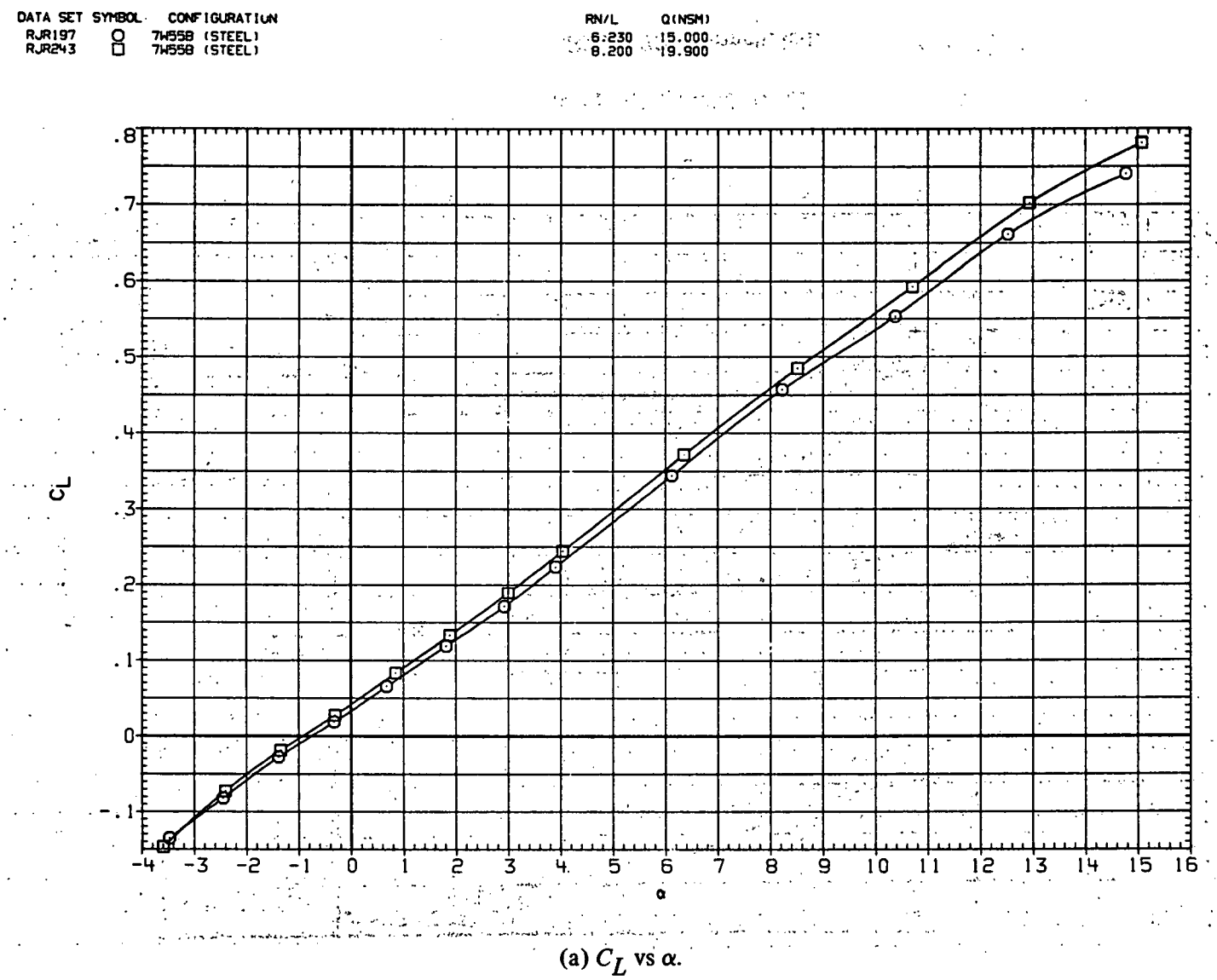

(a) C_L vs α.

Figure 71.– Dynamic-pressure effects on the aerodynamic characteristics of the steel trapezoidal oblique wing-body combination ($\Lambda = 55°$, $M = 0.95$ and the NACA 65A204 airfoil).

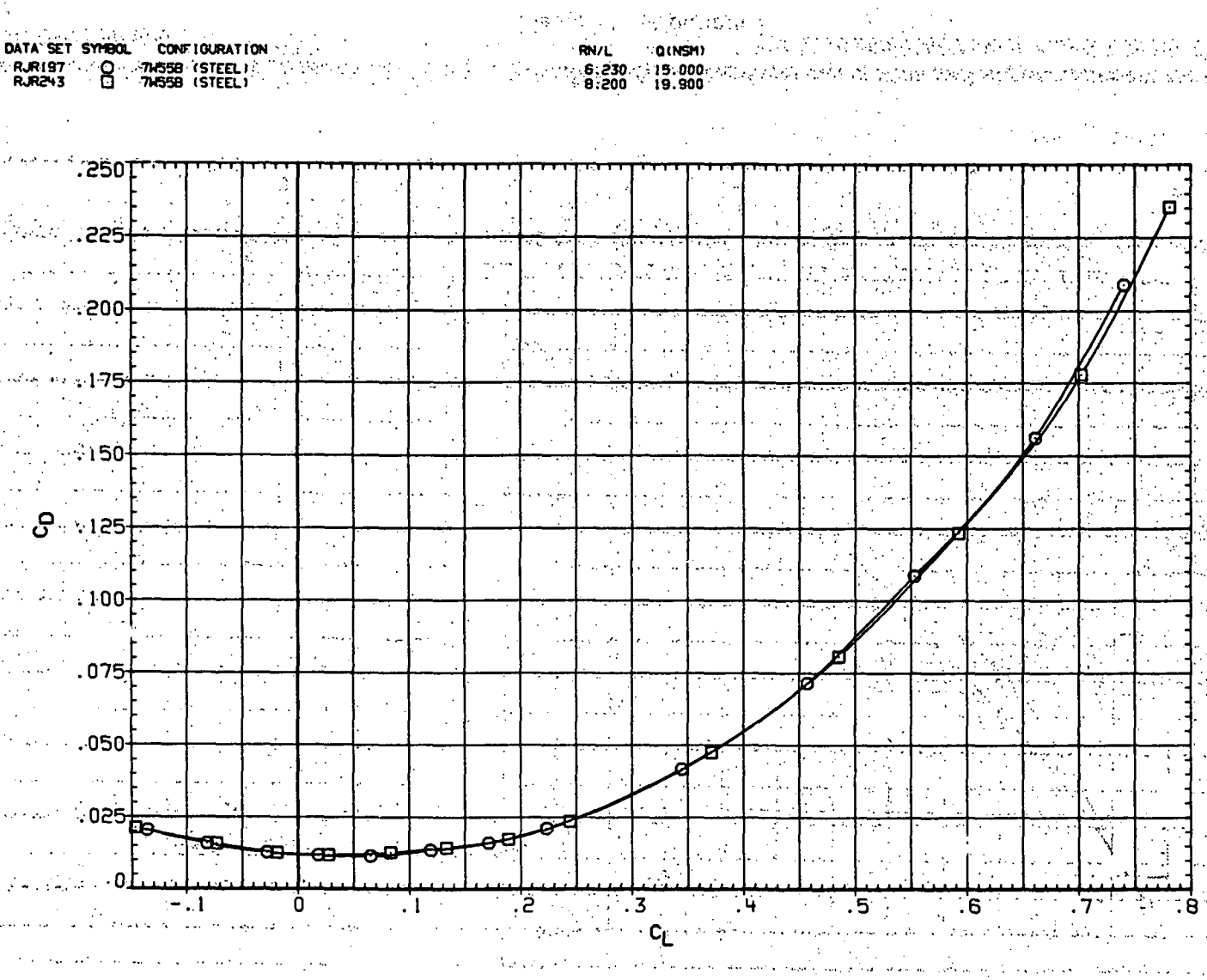

(b) C_D vs C_L.

Figure 7.1.– Continued.

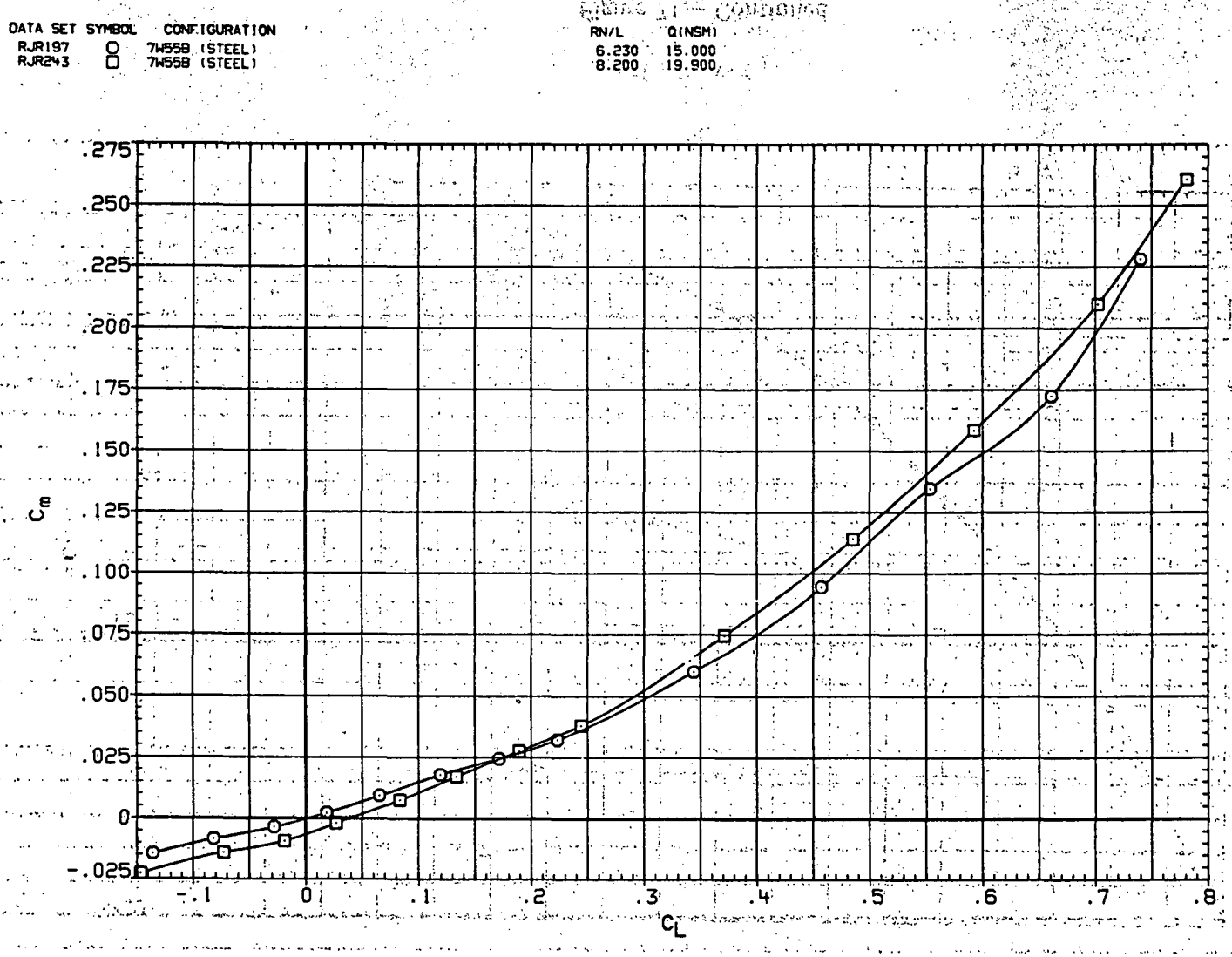

(c) C_m vs C_L.

Figure 71.– Continued.

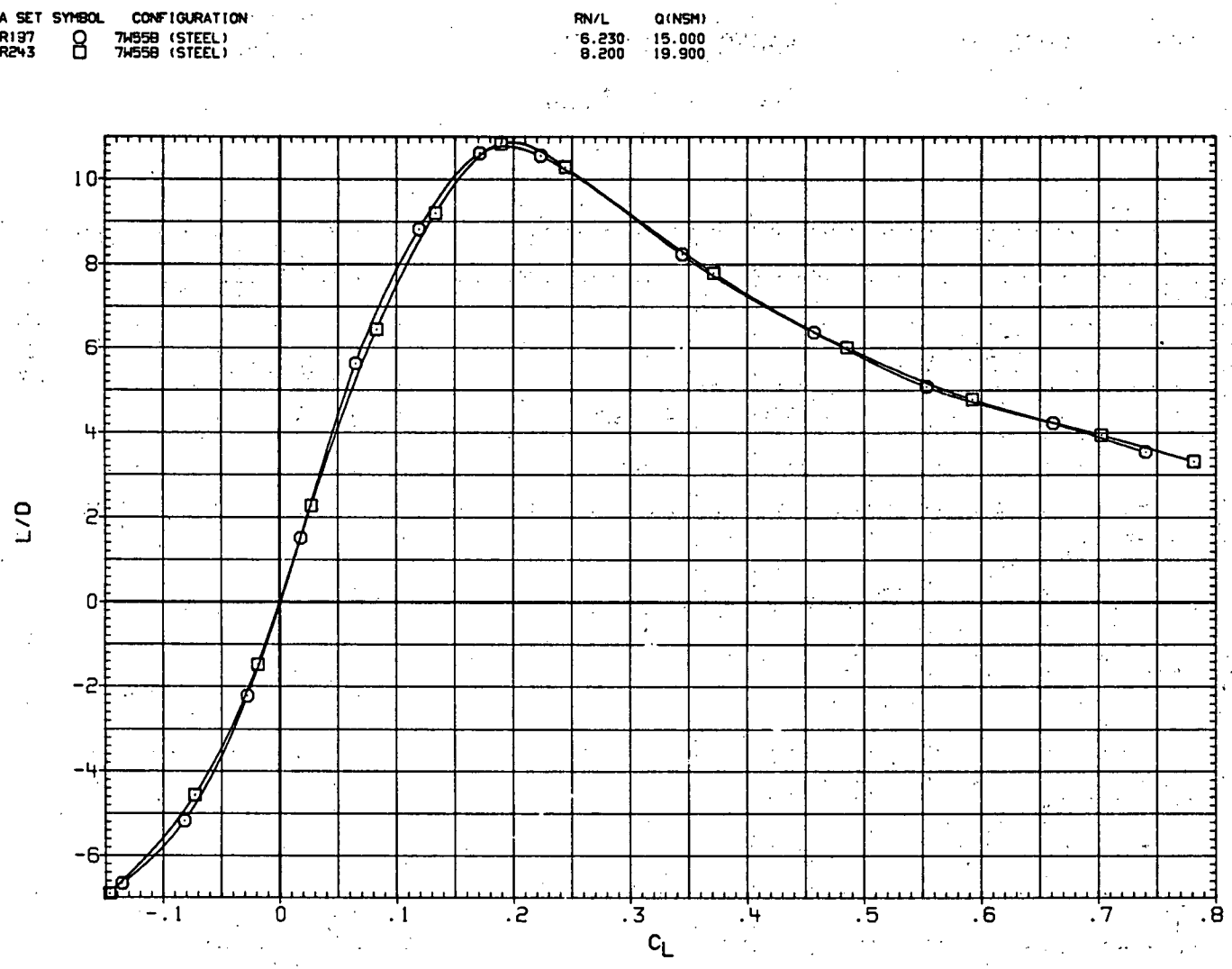

(d) L/D vs C_L.

Figure 71.– Continued.

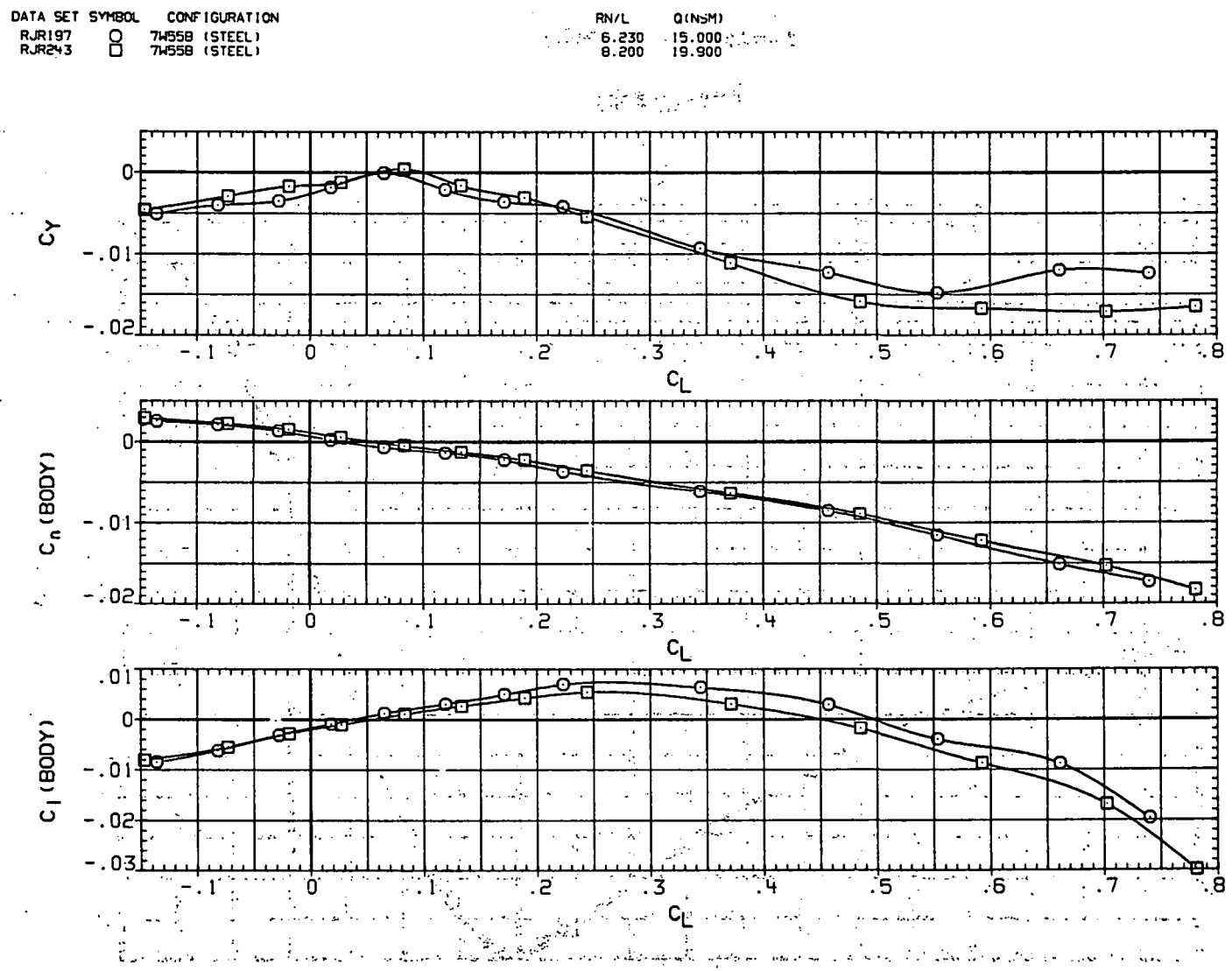

(e) C_Y, C_n and C_ℓ vs C_L.

Figure 71.– Concluded.

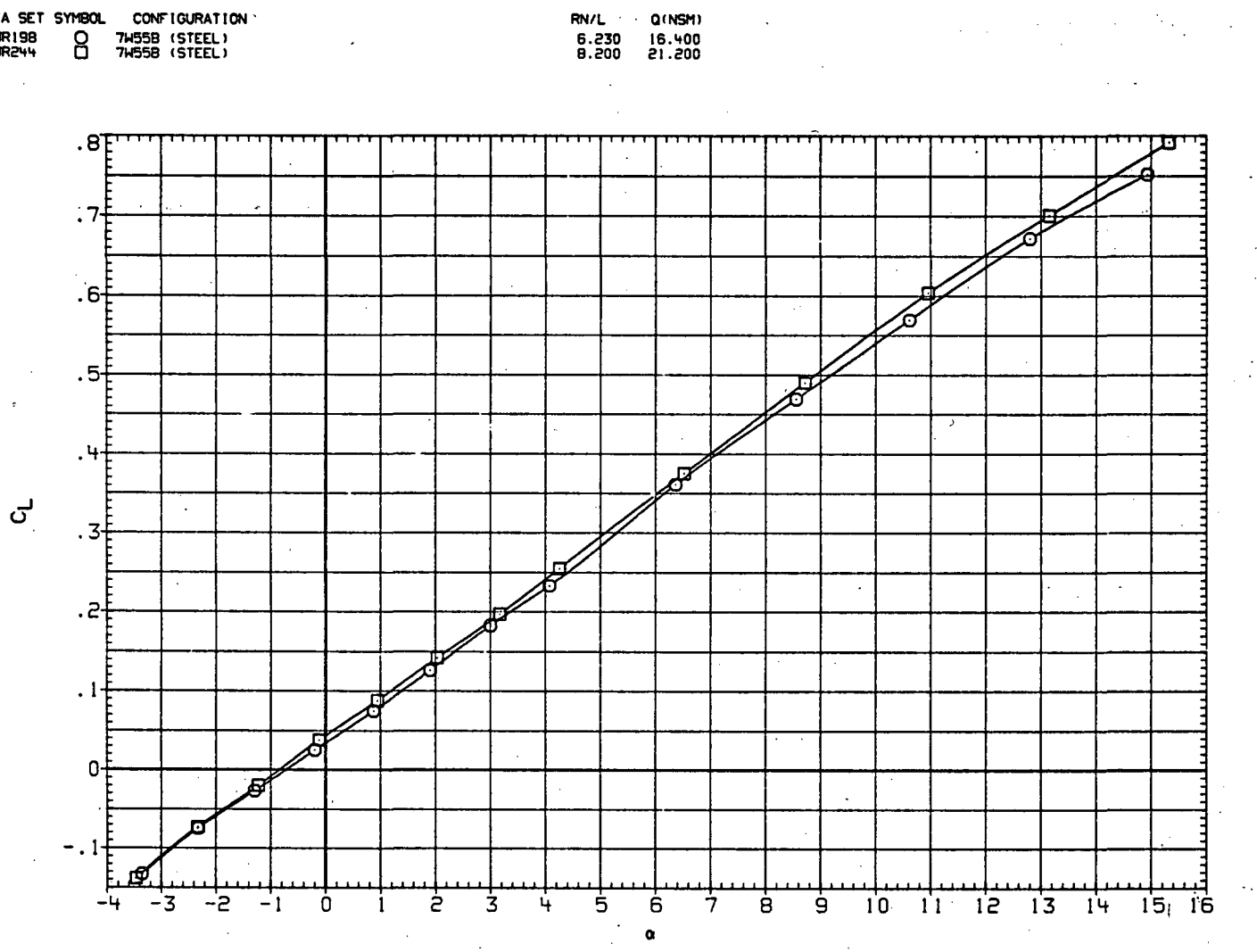

(a) C_L vs α.

Figure 72.– Dynamic-pressure effects on the aerodynamic characteristics of the steel trapezoidal oblique wing-body combination ($\Lambda = 55°, M = 1.1$ and the NACA 65A204 airfoil).

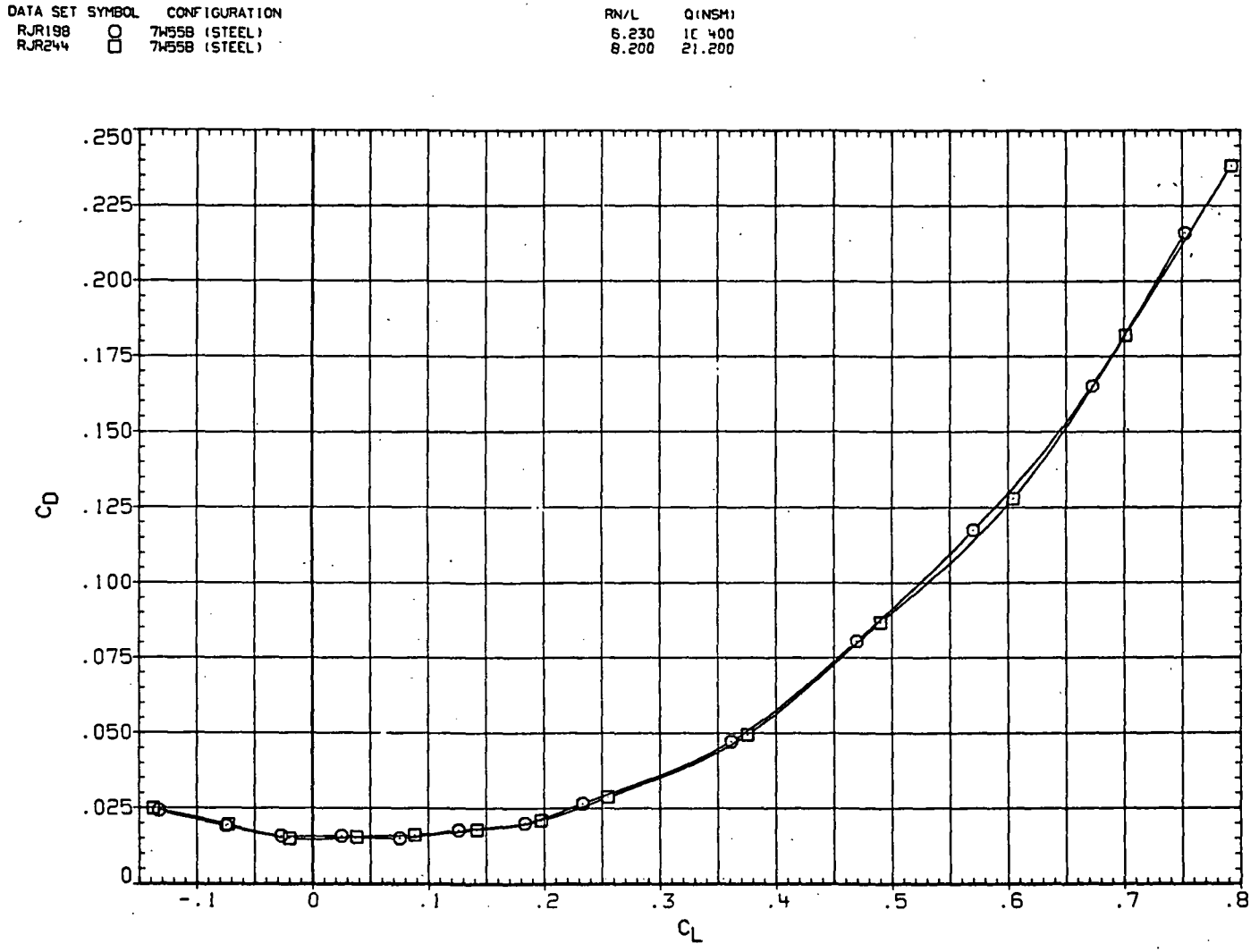

(b) C_D vs C_L.

Figure 72.– Continued.

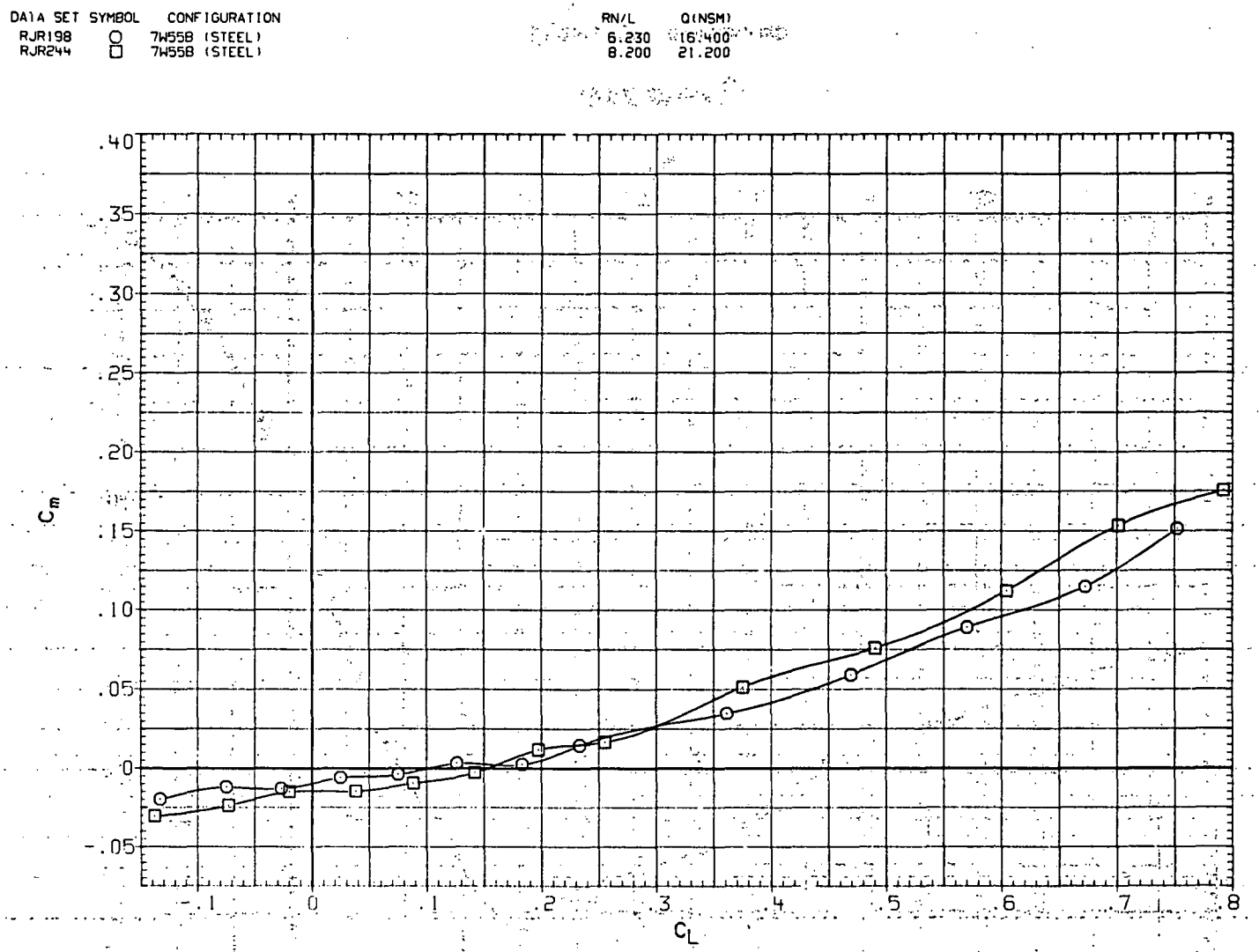

(c) C_m vs C_L.

Figure 72.– Continued.

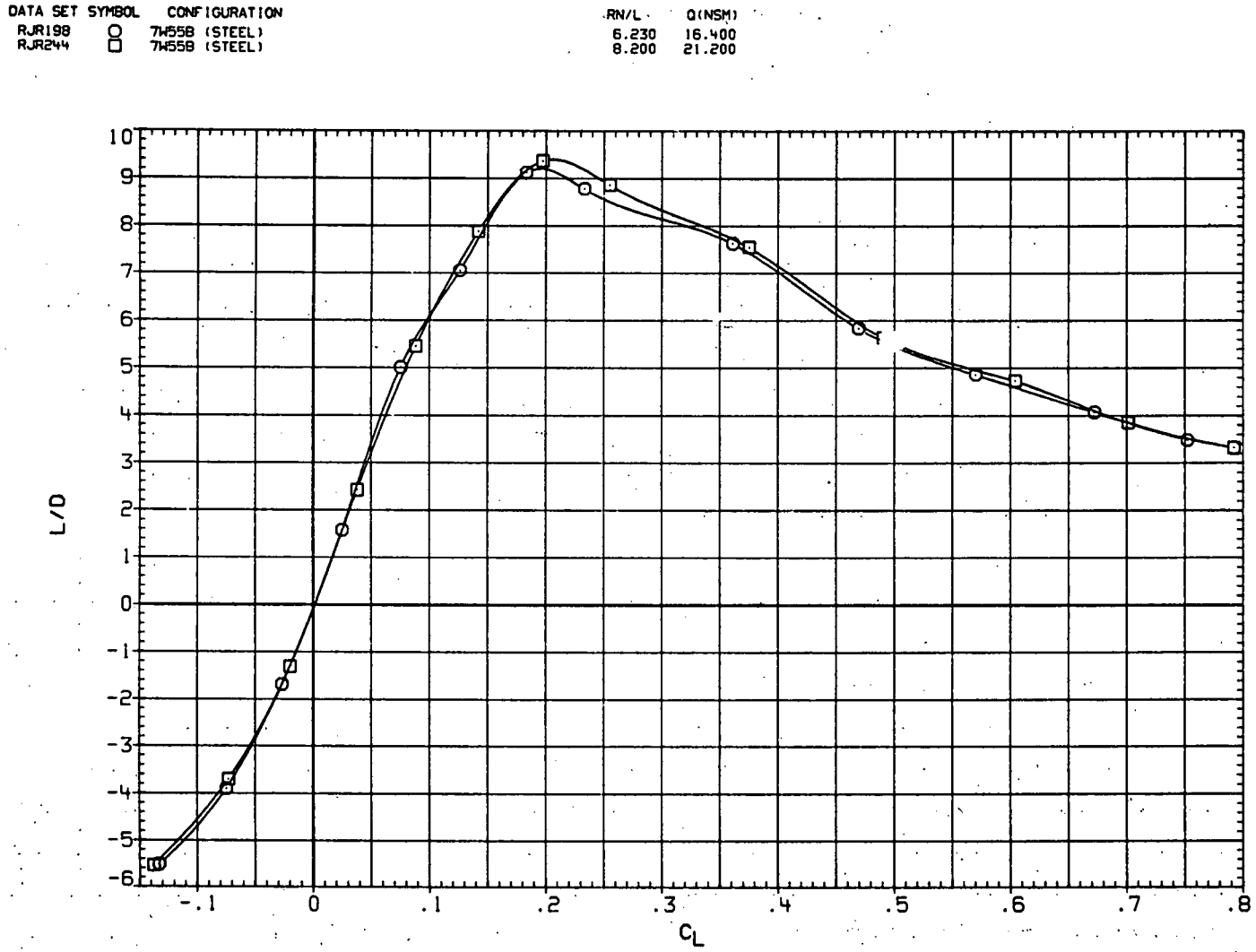

(d) L/D vs C_L.

Figure 72.– Continued.

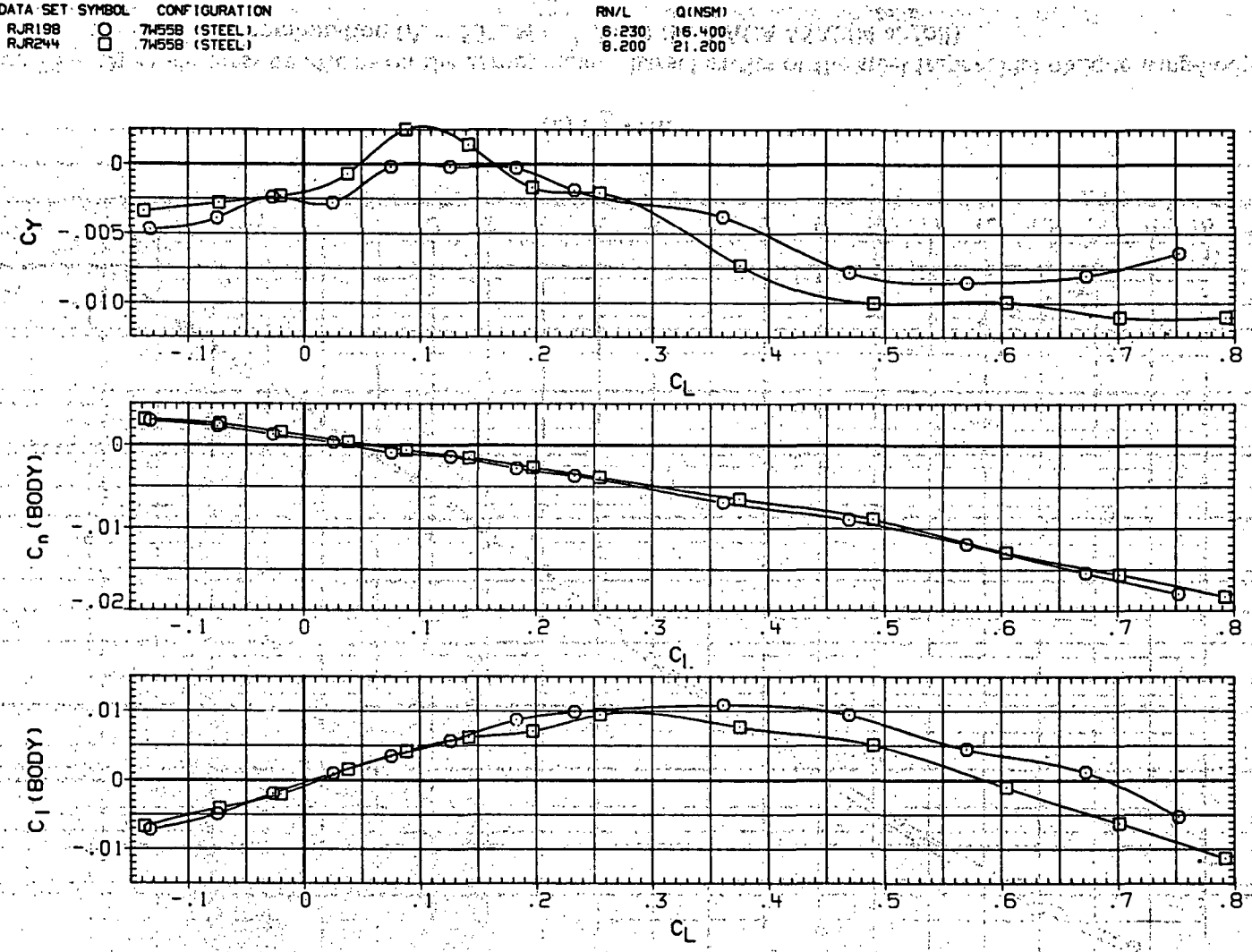

(e) C_Y, C_n and C_ℓ vs C_L.

Figure 72.– Concluded.

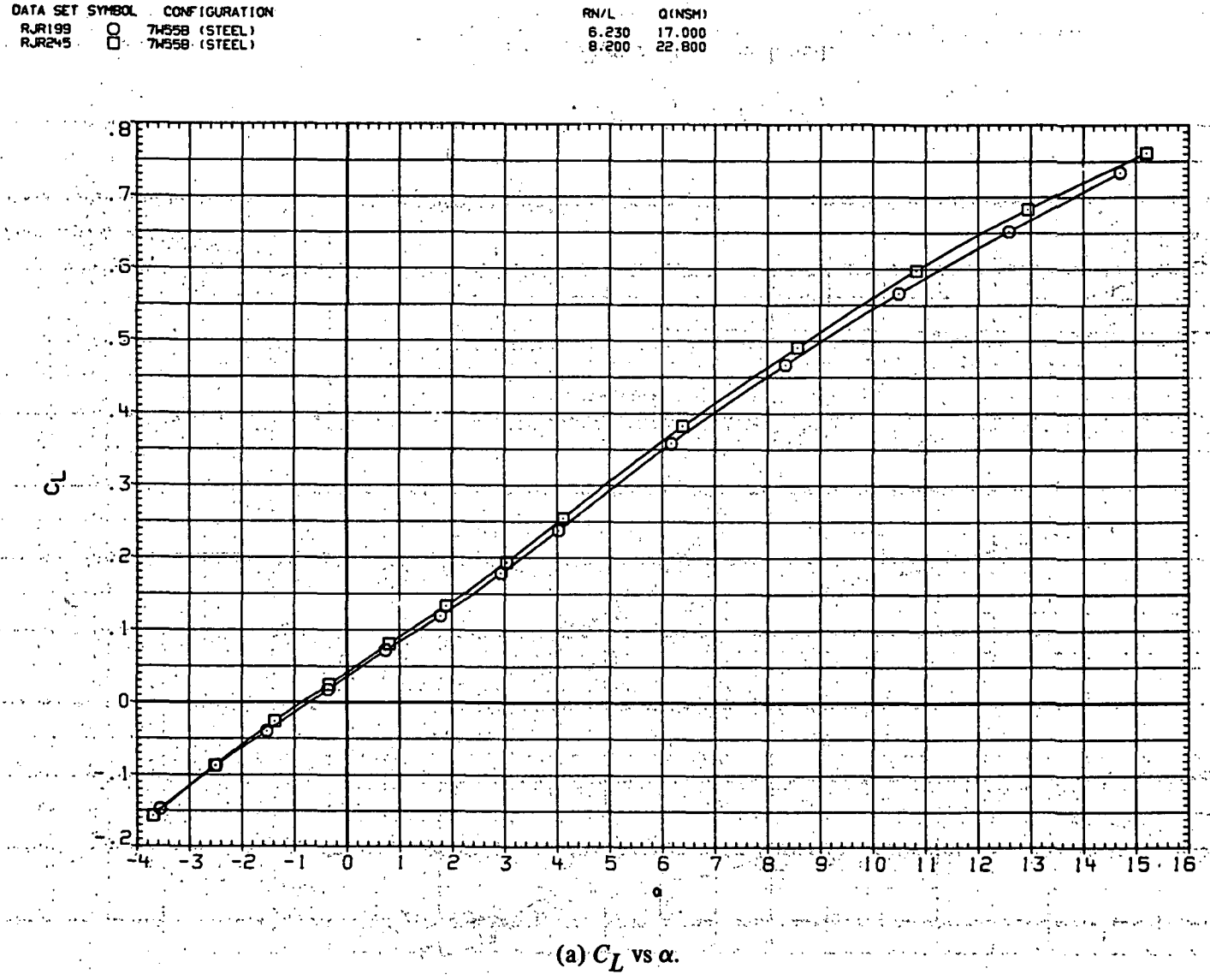

(a) C_L vs α.

Figure 73.– Dynamic-pressure effects on the aerodynamic characteristics of the steel trapezoidal oblique wing-body combination ($\Lambda = 55°$, $M = 1.2$ and the NACA 65A204 airfoil).

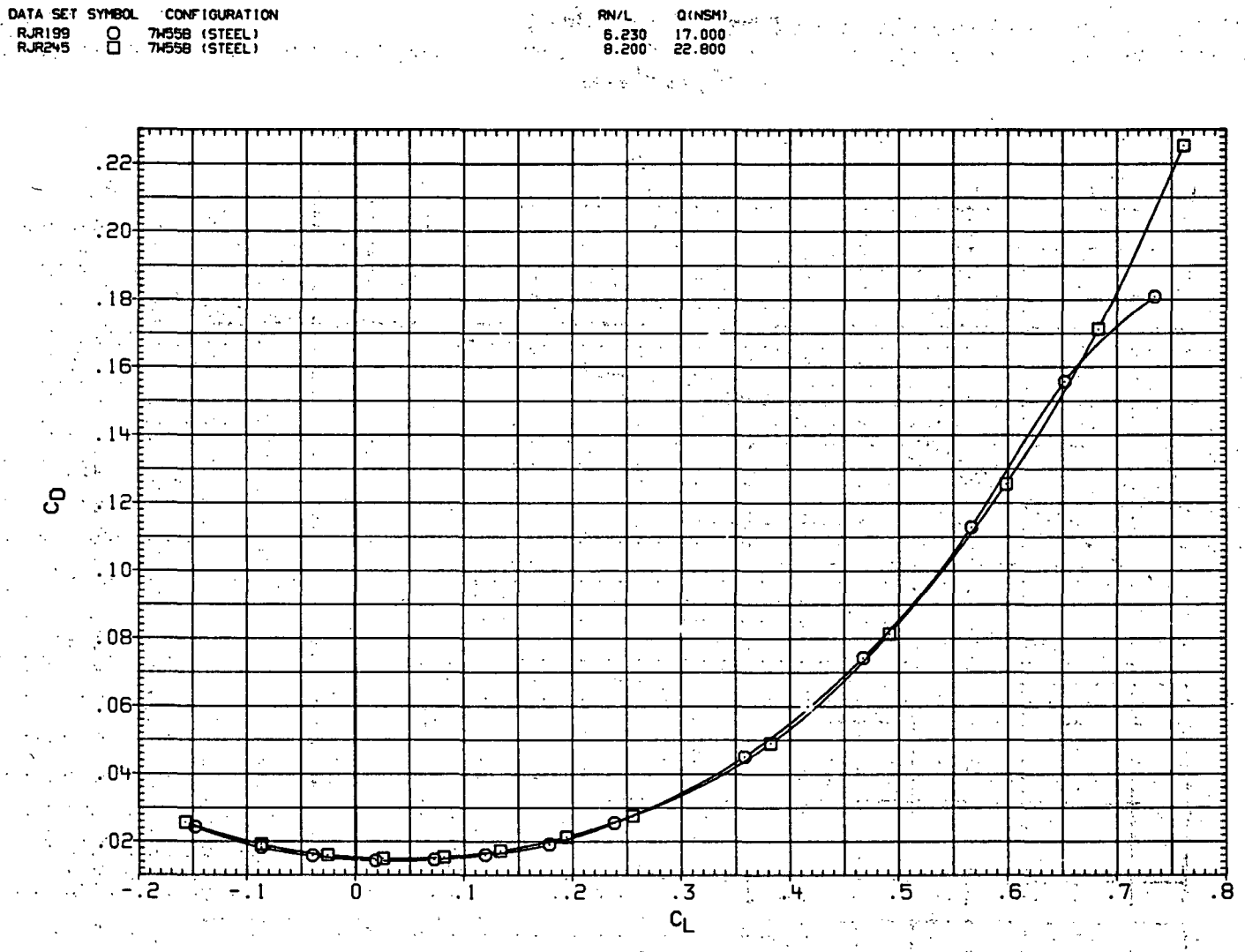

(b) C_D vs C_L.

Figure 73.– Continued.

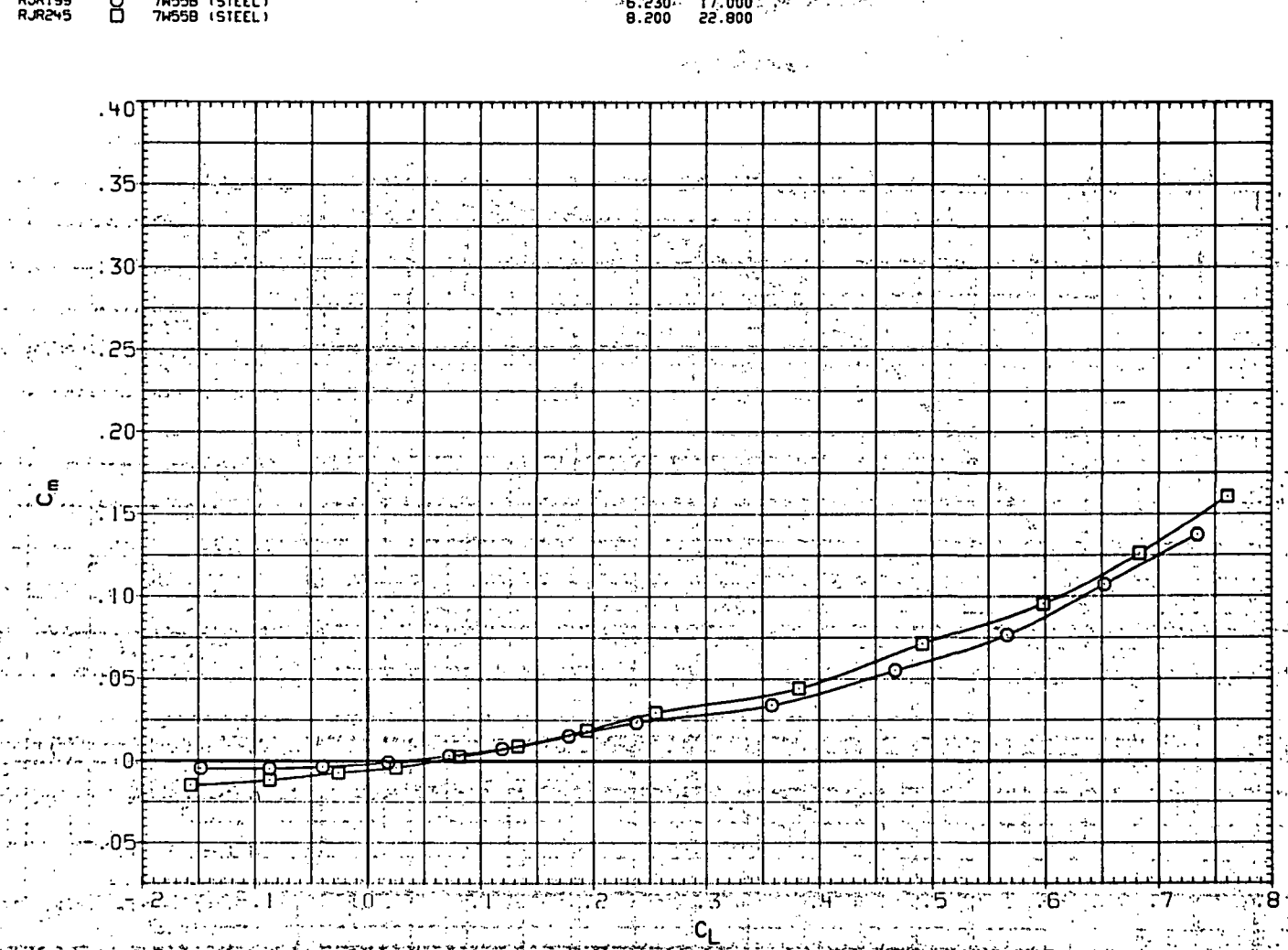

(c) C_m vs C_L.

Figure 73.– Continued.

(d) L/D vs C_L.

Figure 73.– Continued.

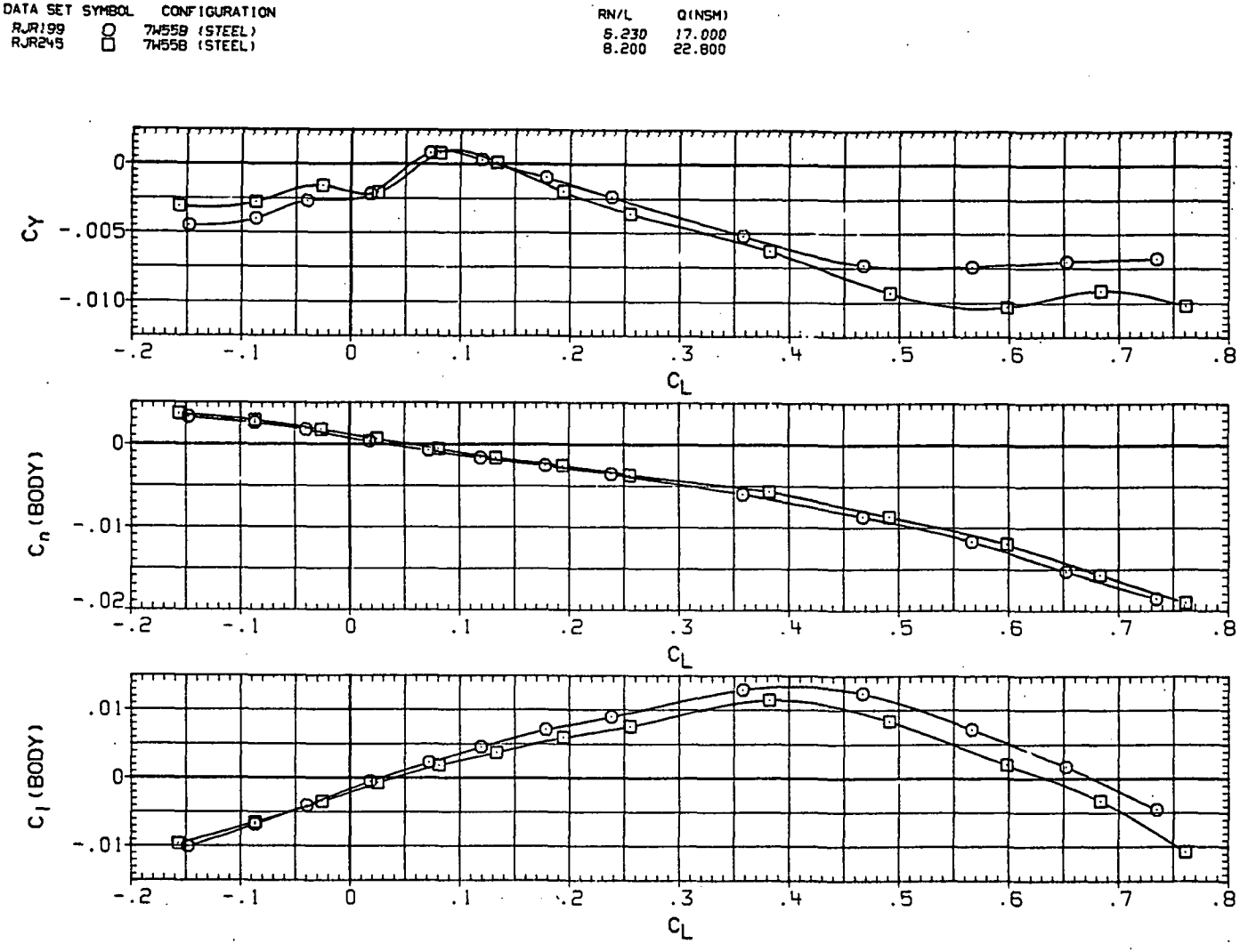

(e) C_Y, C_n and C_ℓ vs C_L.

Figure 73.– Concluded.

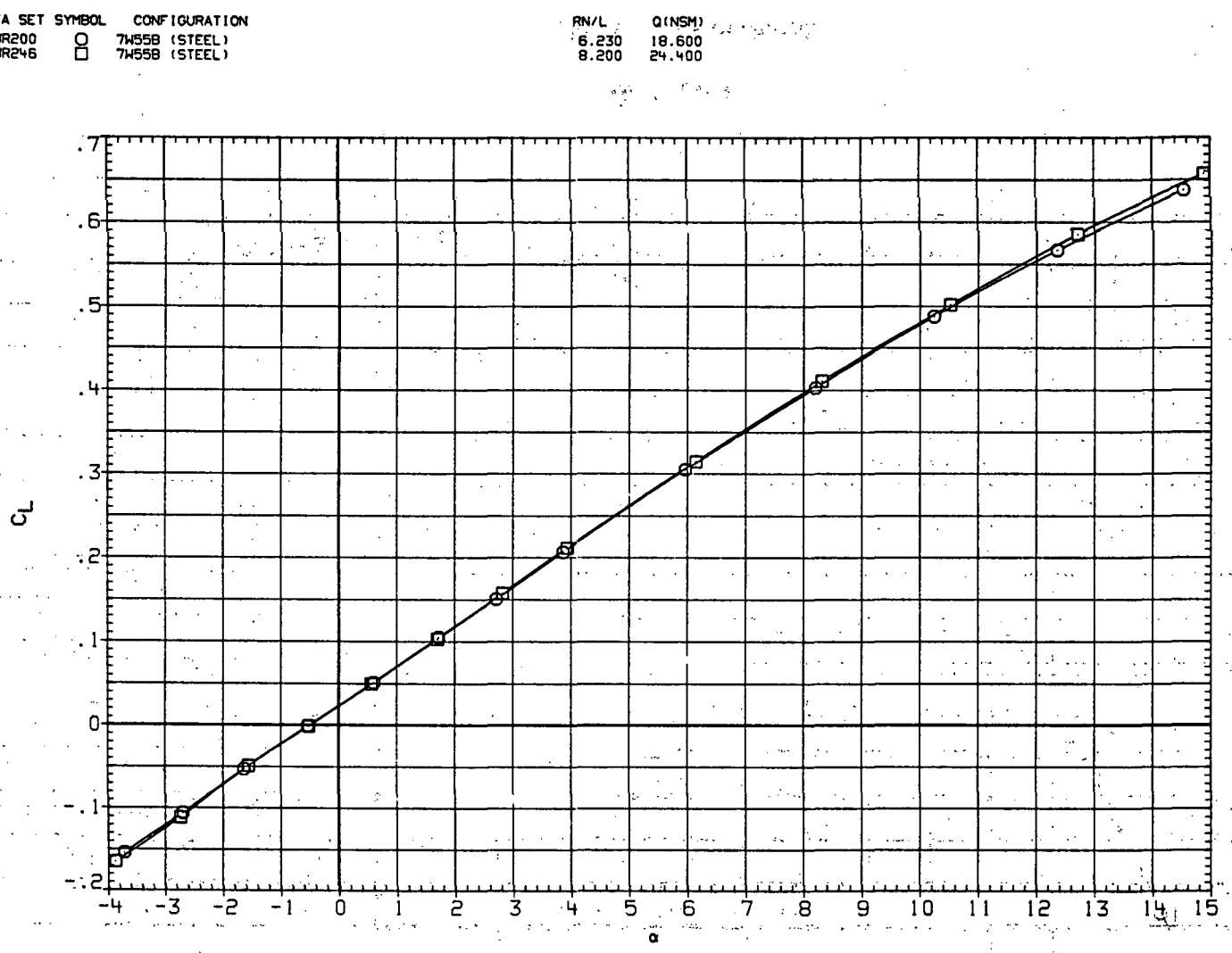

(a) C_L vs α.

Figure 74.– Dynamic-pressure effects on the aerodynamic characteristics of the steel trapezoidal oblique wing-body combination ($\Lambda = 55°, M = 1.6$ and the NACA 65A204 airfoil).

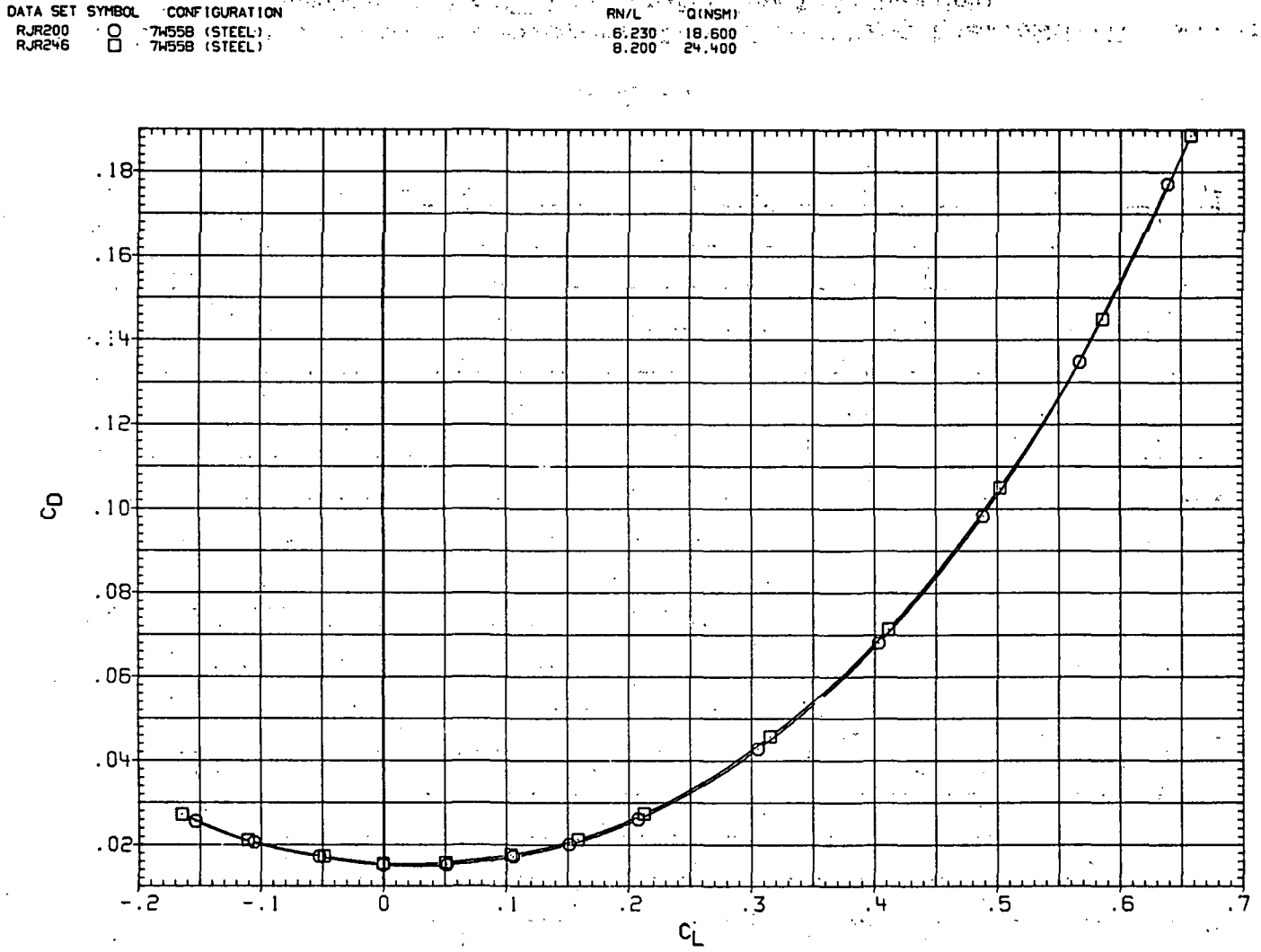

(b) C_D vs C_L.

Figure 74.– Continued.

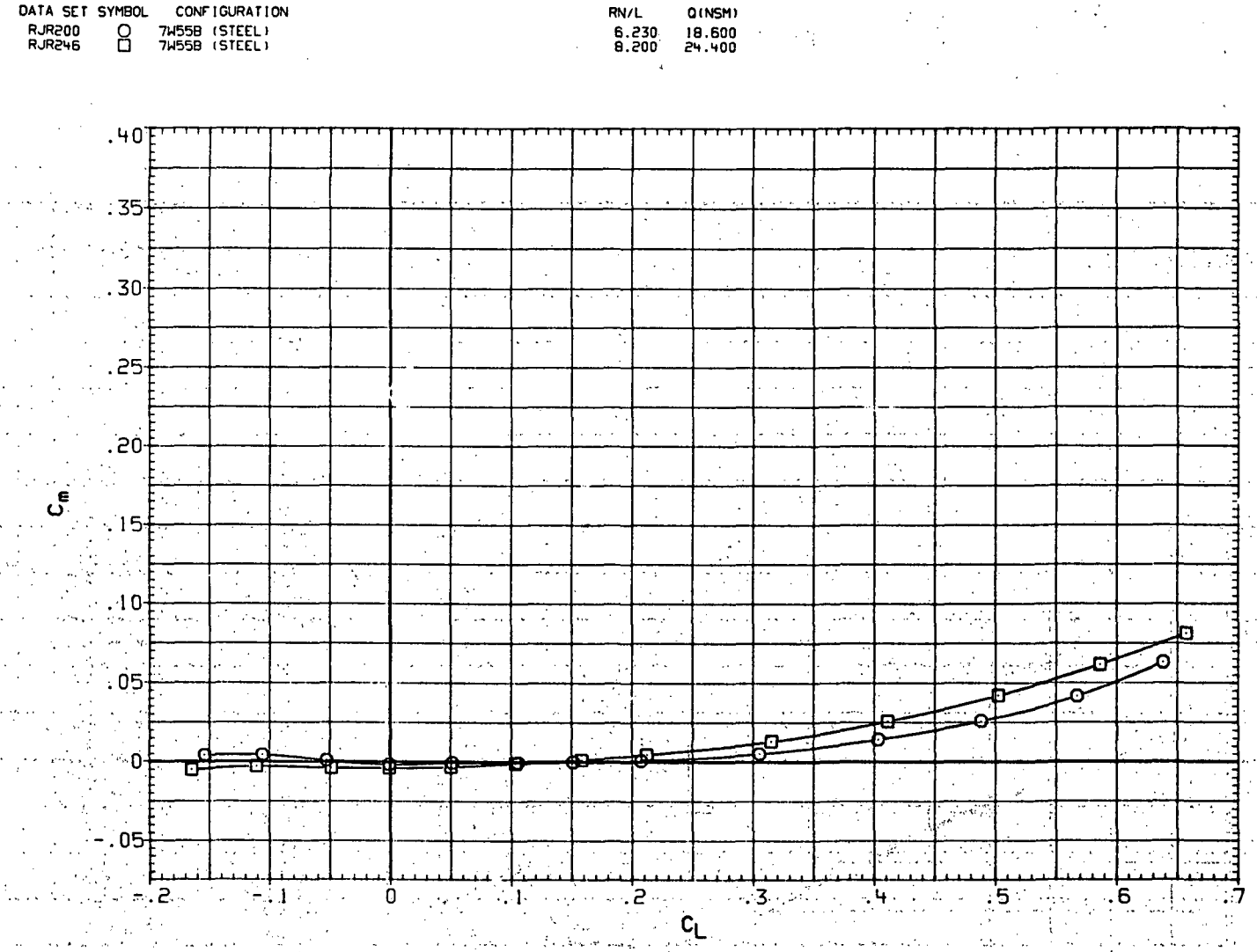

(c) C_m vs C_L.

Figure 74.– Continued.

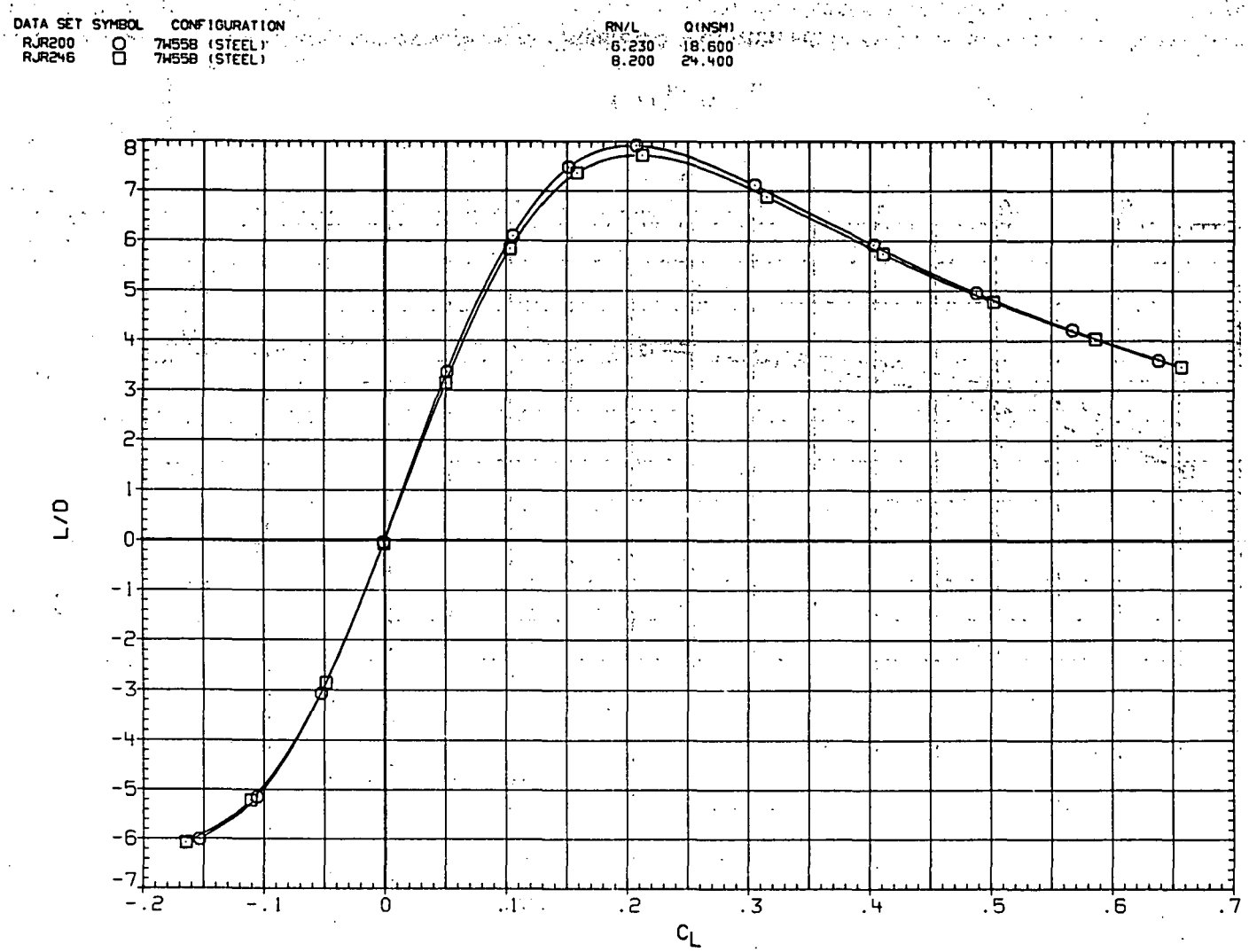

(d) L/D vs C_L.

Figure 74.– Continued.

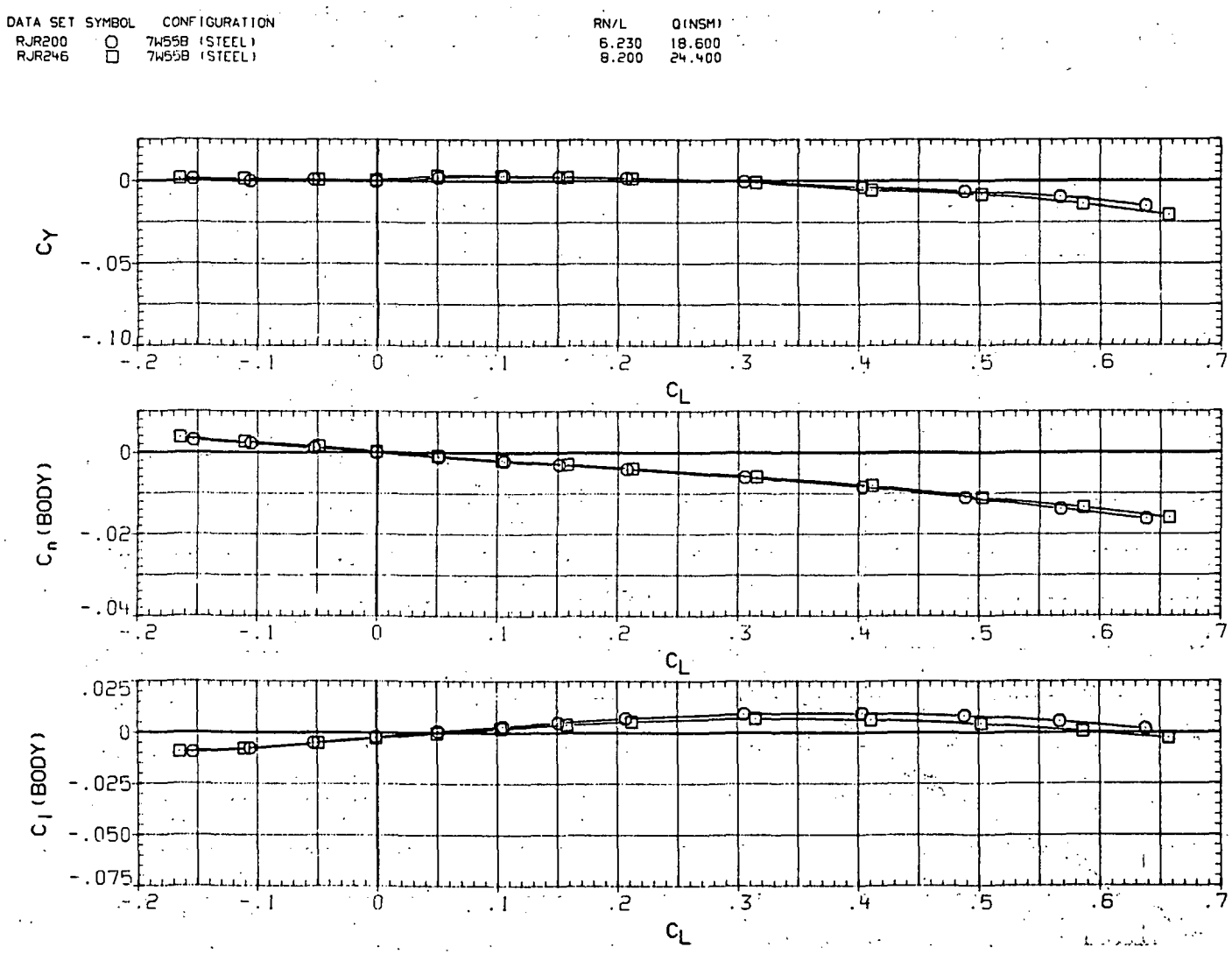

(e) C_Y, C_n and C_ℓ vs C_L.

Figure 74.– Concluded.

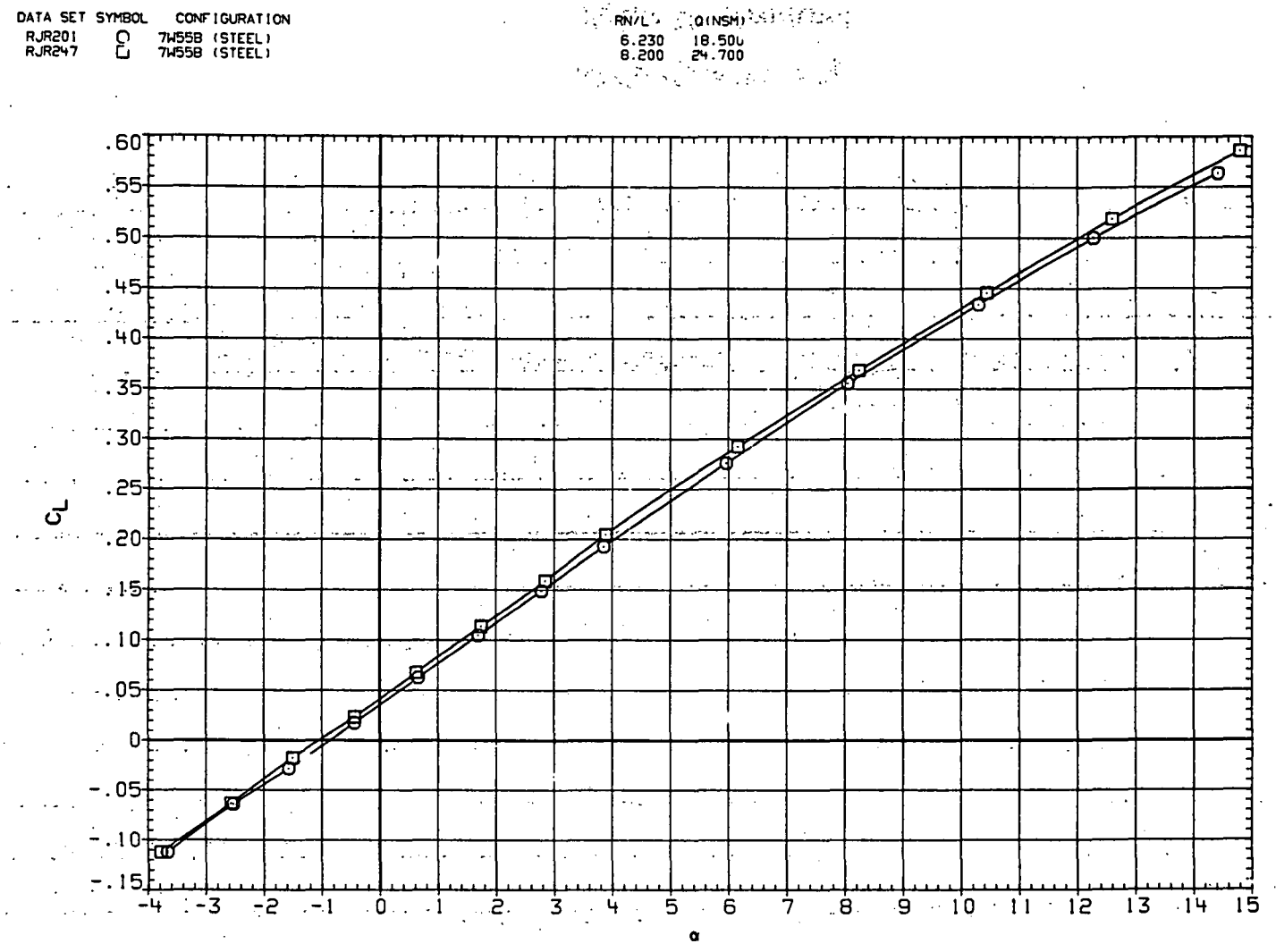

(a) C_L vs α.

Figure 75.– Dynamic-pressure effects on the aerodynamic characteristics of the steel trapezoidal oblique wing-body combination ($\Lambda = 55°, M = 2.0$ and the NACA 65A204 airfoil).

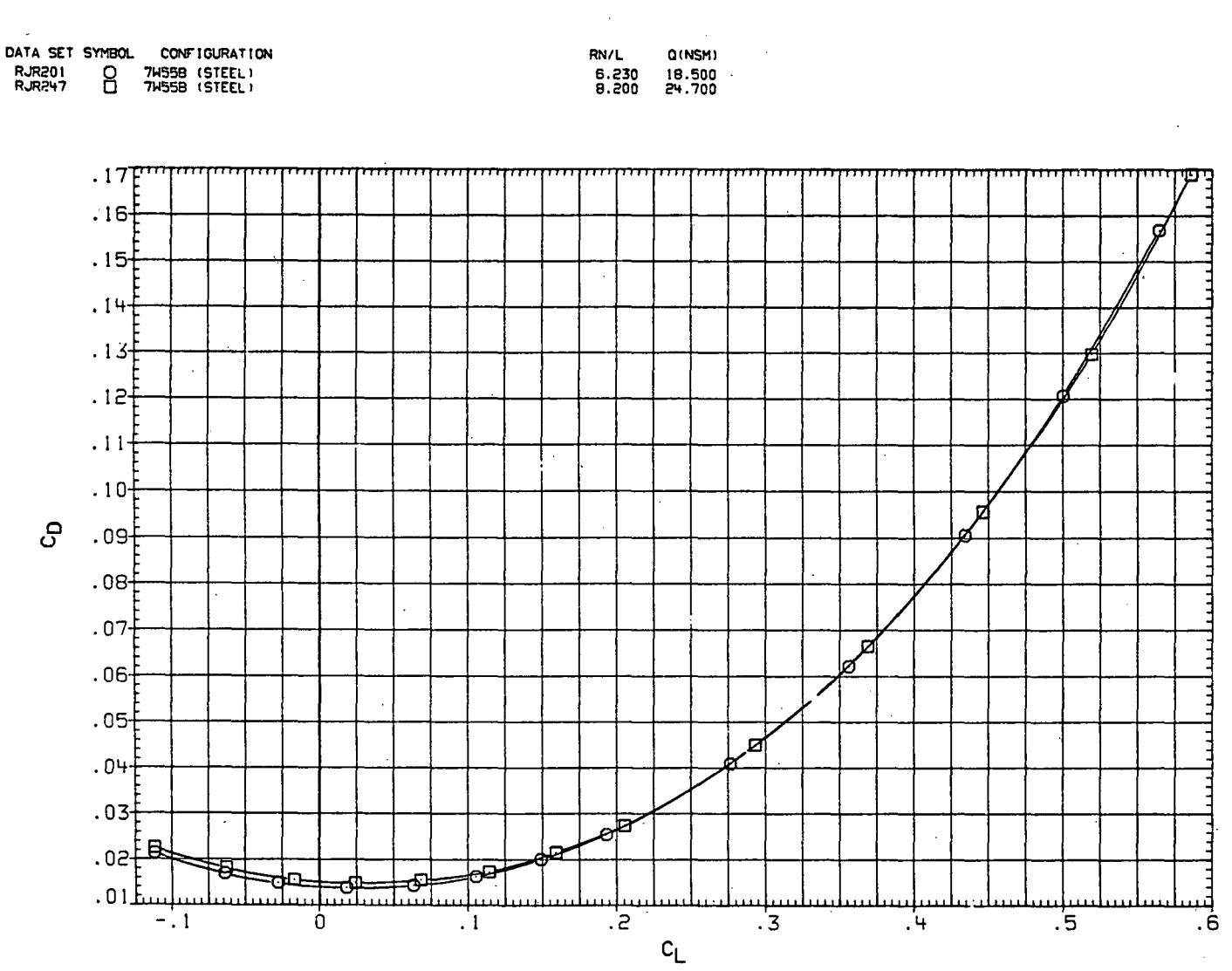

(b) C_D vs C_L.

Figure 75.– Continued.

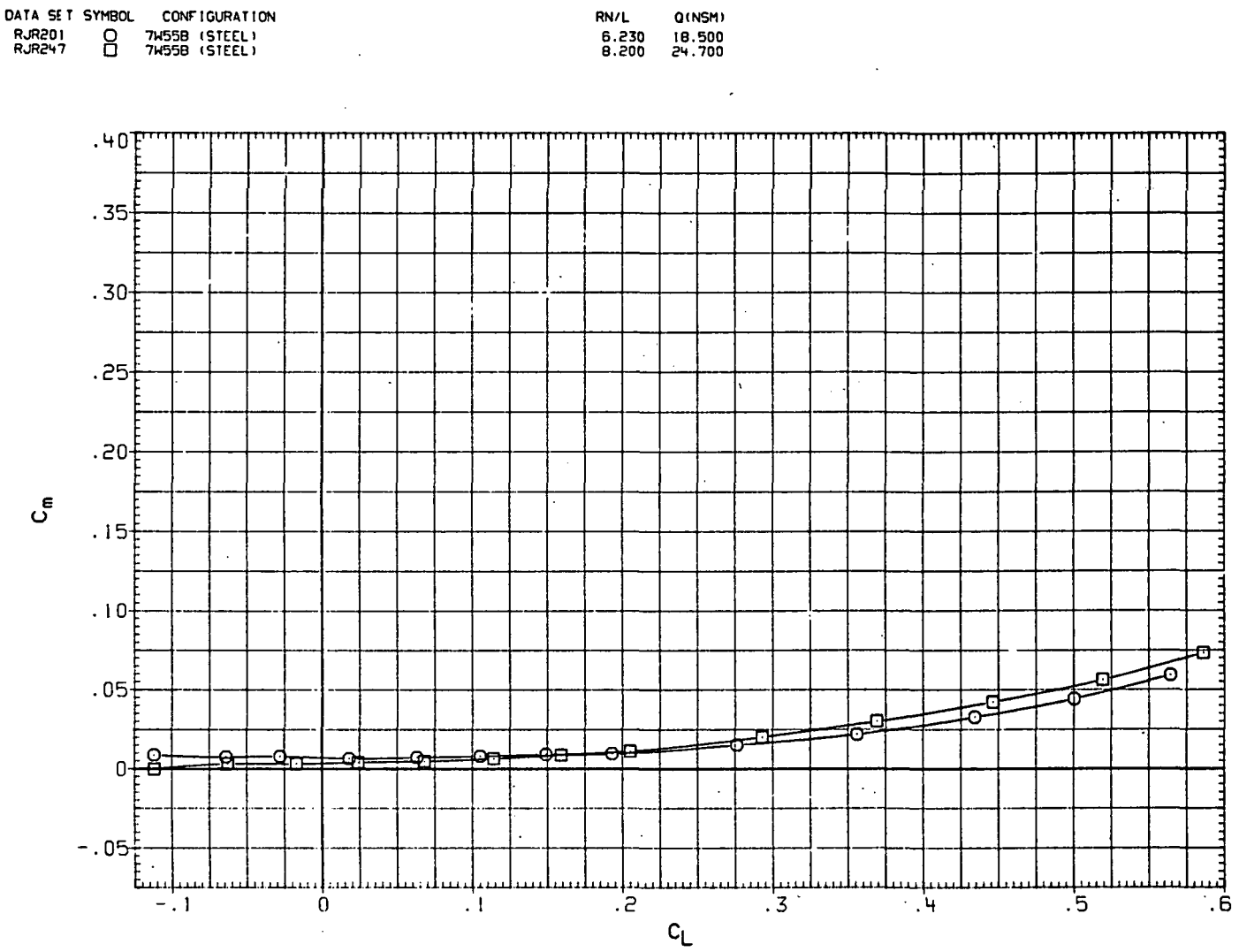

(c) C_m vs C_L.

Figure 75.– Continued.

(d) L/D vs C_L.

Figure 75.– Continued.

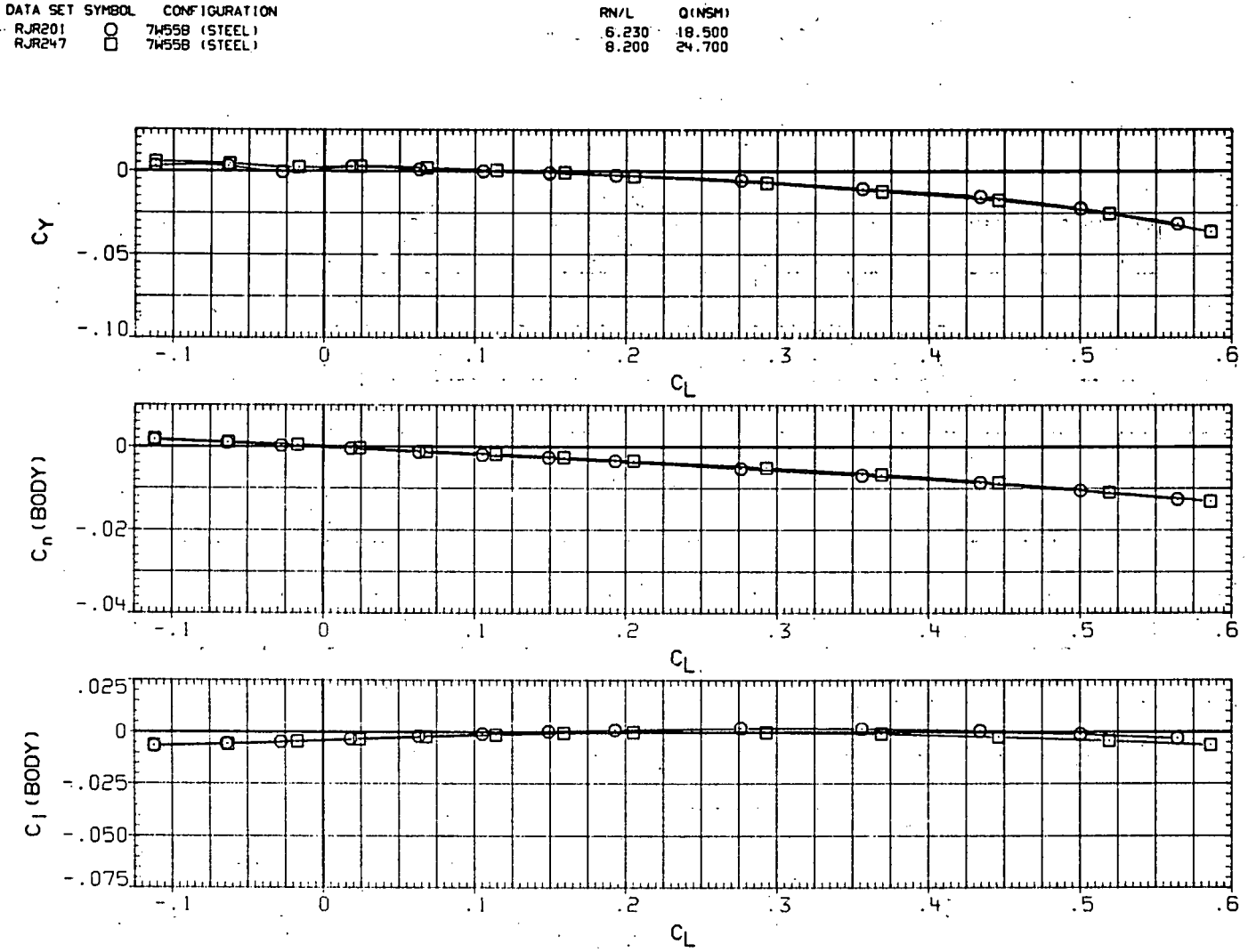

(e) C_Y, C_n and C_ℓ vs C_L.

Figure 75.– Concluded.

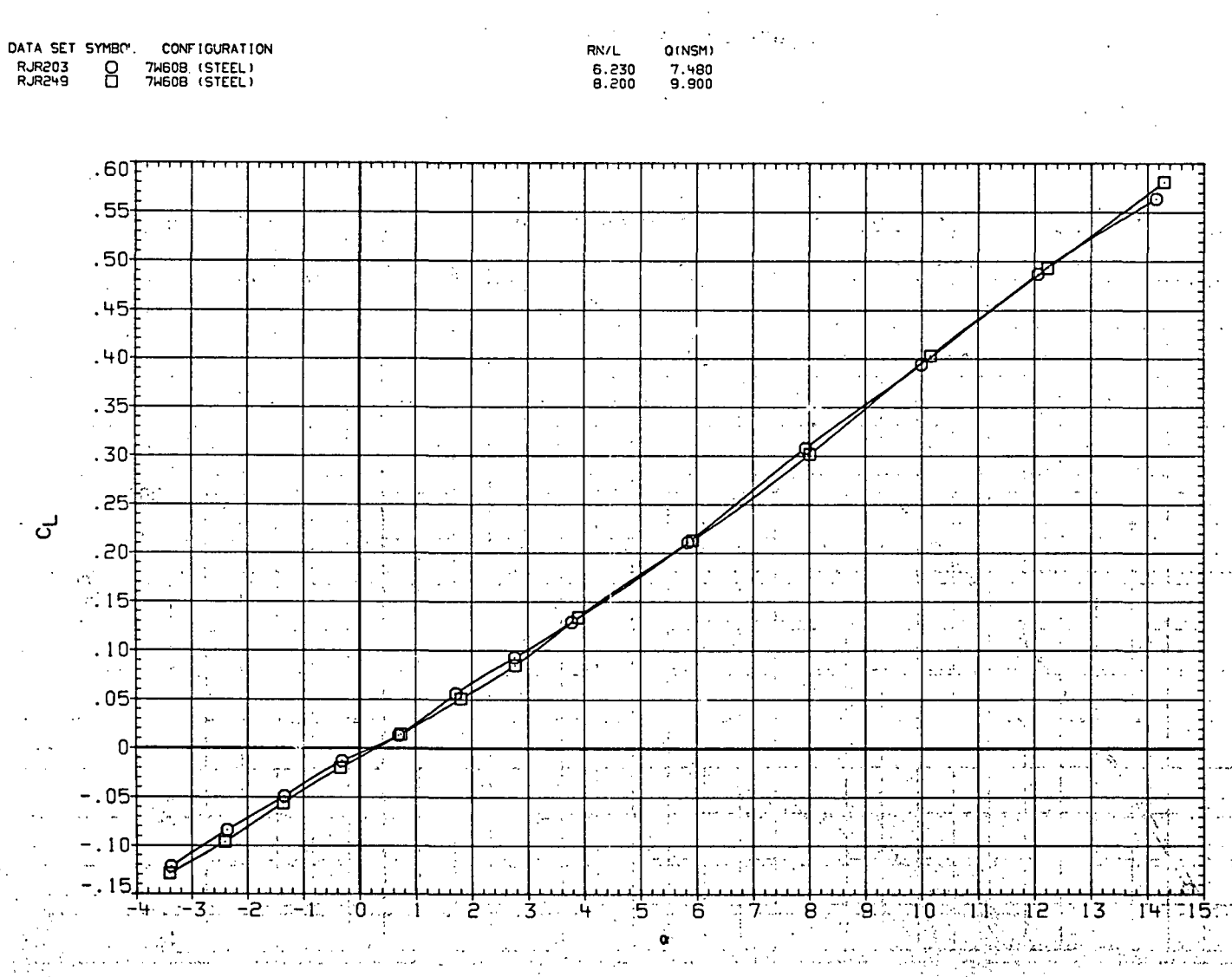

(a) C_L vs α.

Figure 76.– Dynamic-pressure effects on the aerodynamic characteristics of the steel trapezoidal oblique wing-body combination ($\Lambda = 60°$, $M = 0.4$ and the NACA 65A204 airfoil).

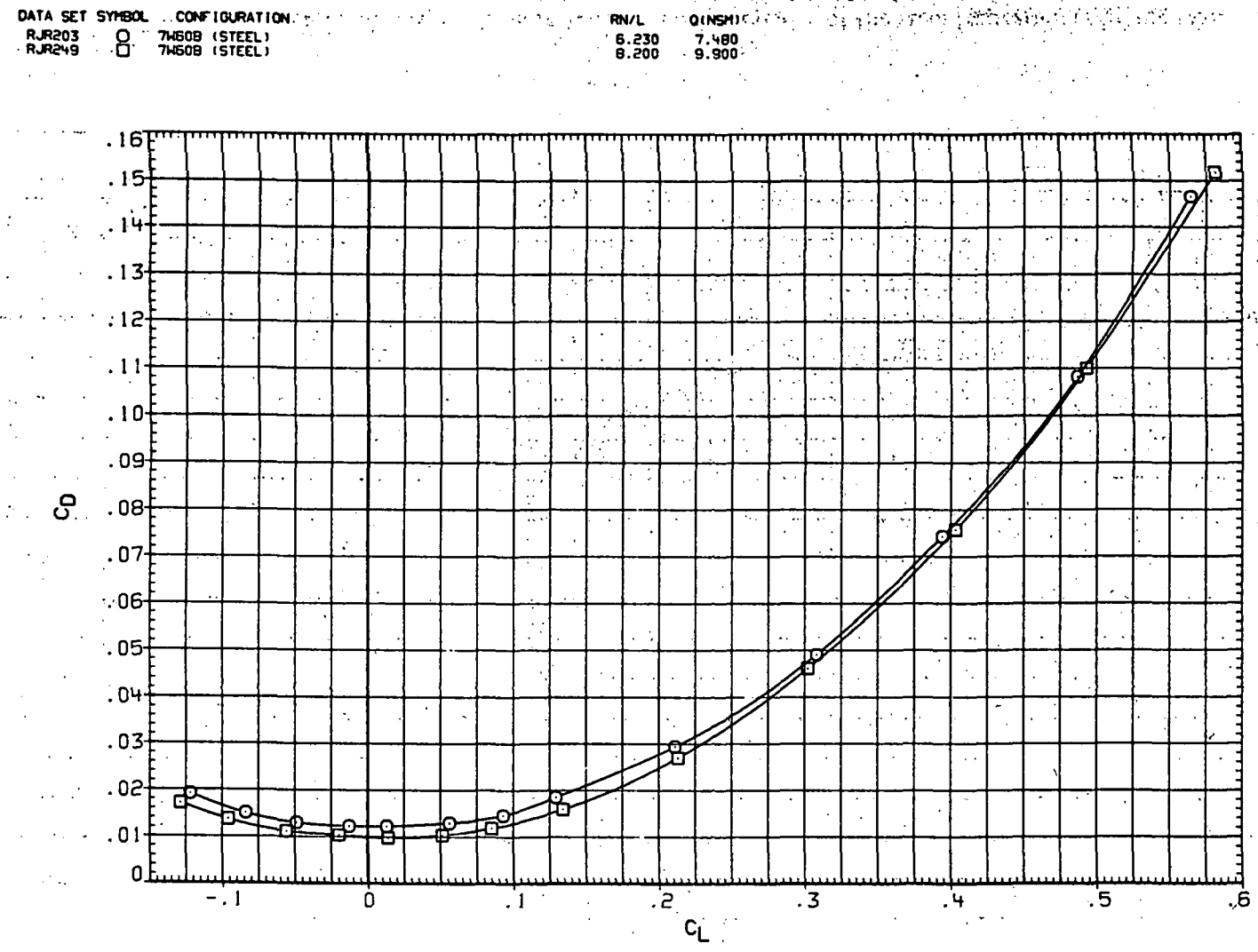

(b) C_D vs C_L.

Figure 76.– Continued.

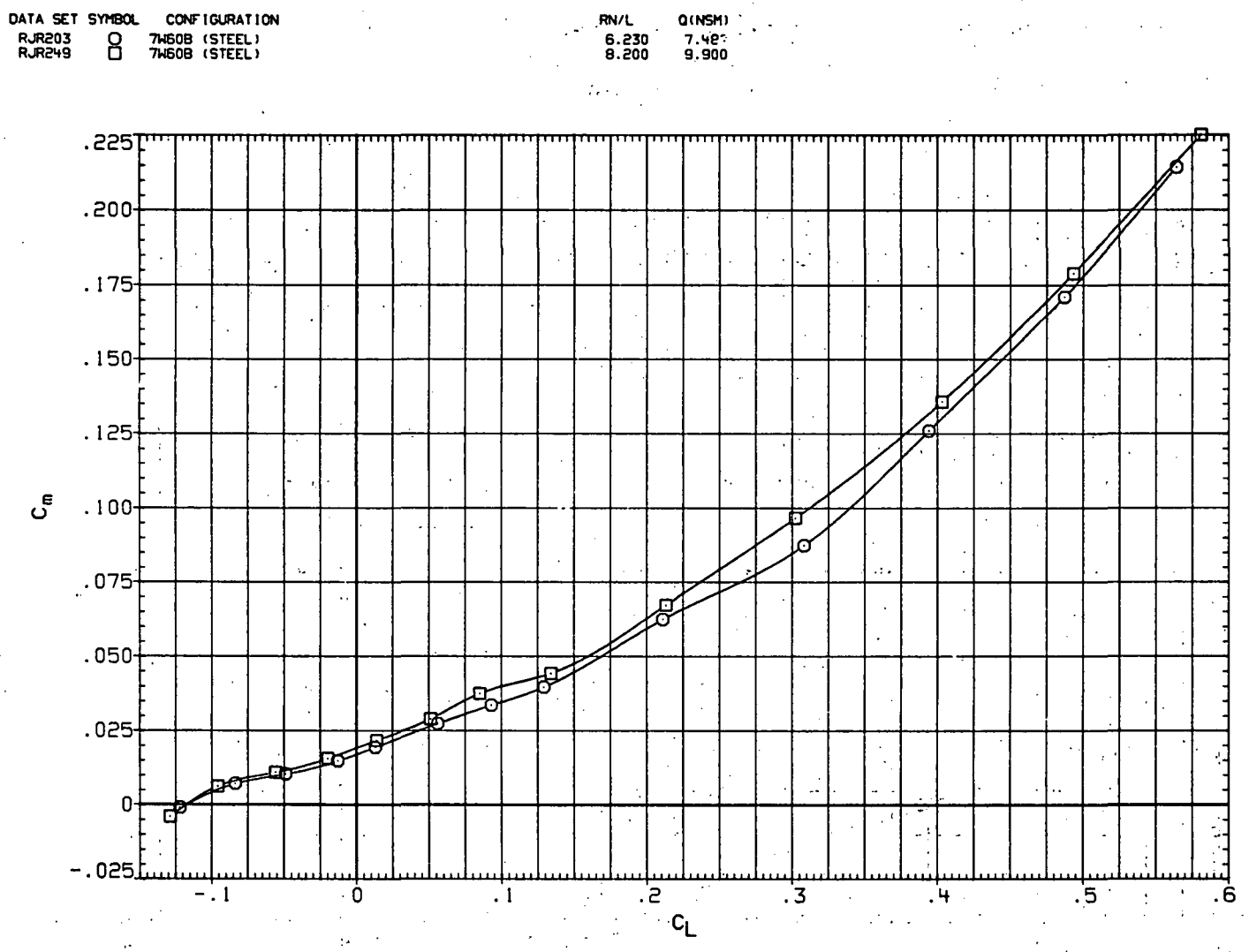

(c) C_m vs C_L.

Figure 76.– Continued.

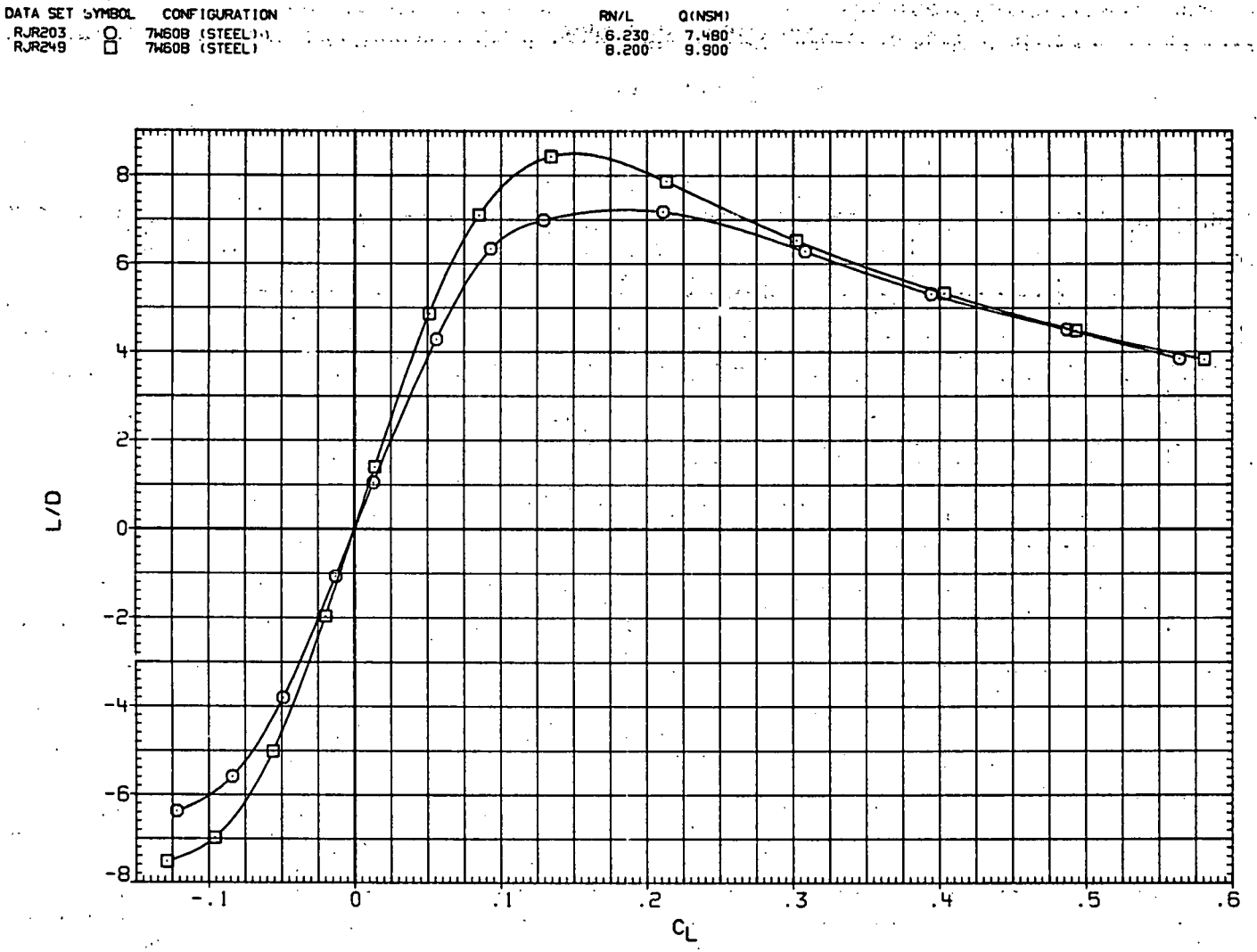

(d) L/D vs C_L.

Figure 76.– Continued.

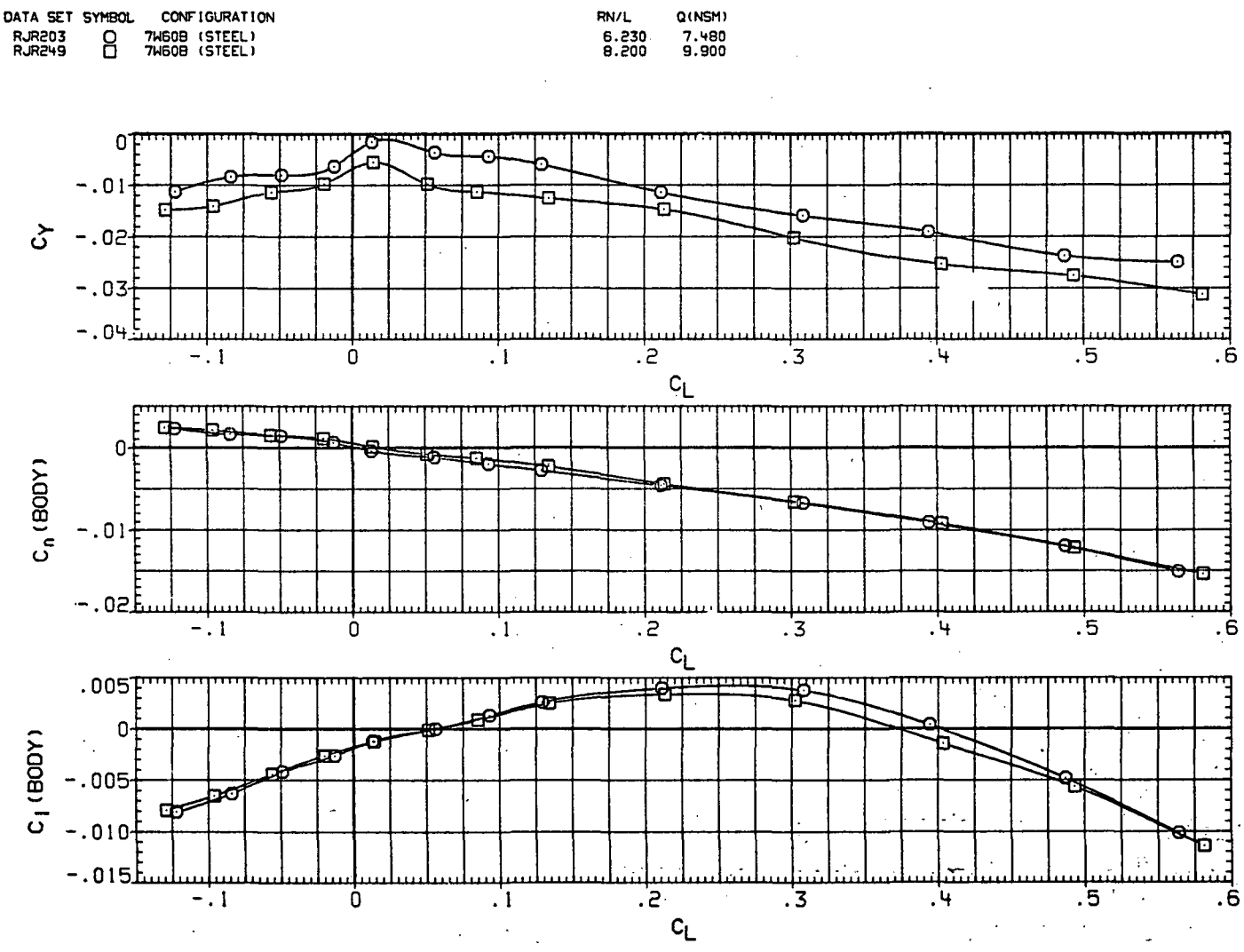

(e) C_Y, C_n and C_ℓ vs C_L.

Figure 76.– Concluded.

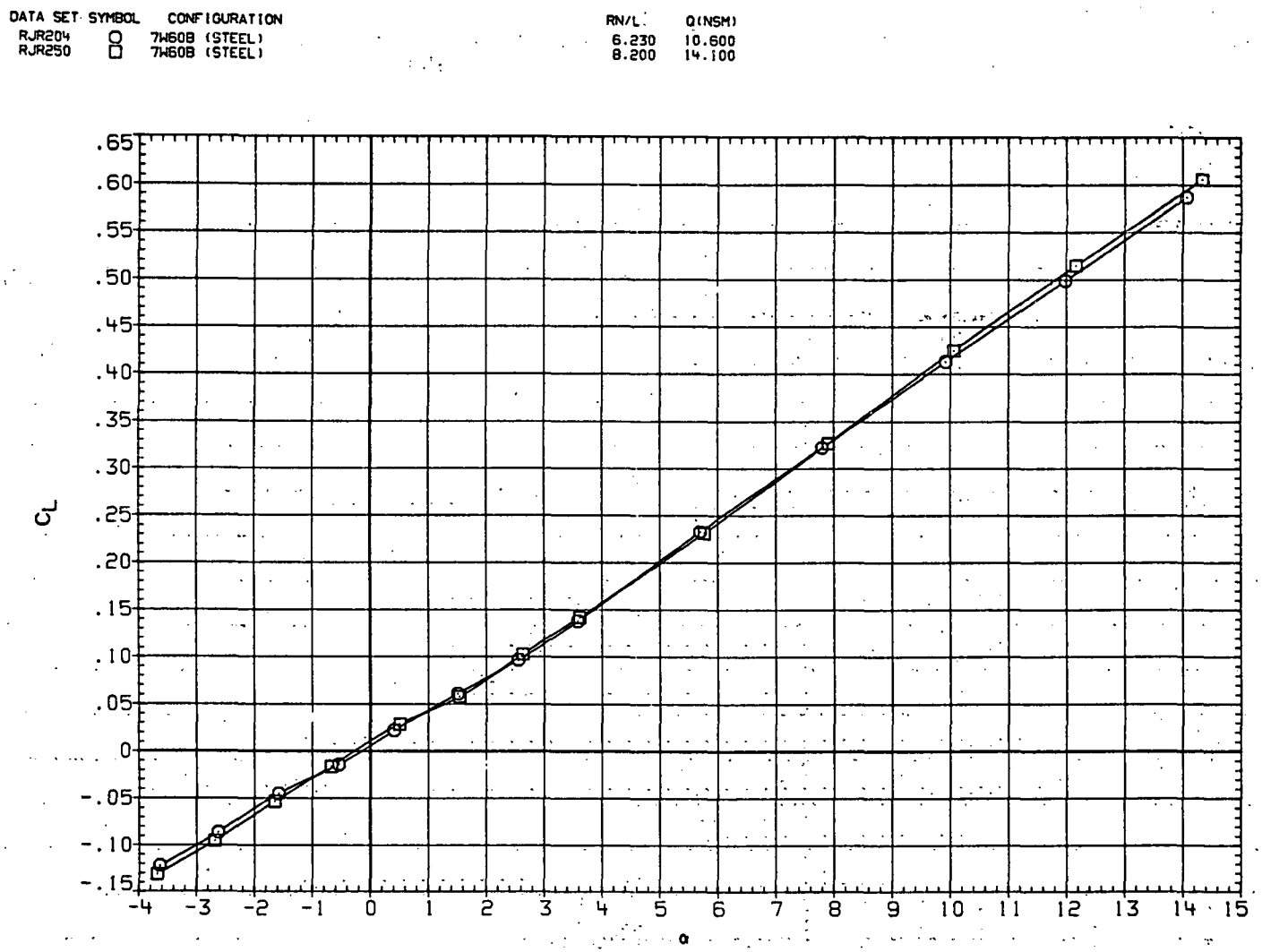

(a) C_L vs α.

Figure 77.– Dynamic-pressure effects on the aerodynamic characteristics of the steel trapezoidal oblique wing-body combination ($\Lambda = 60°$, $M = 0.6$ and the NACA 65A204 airfoil).

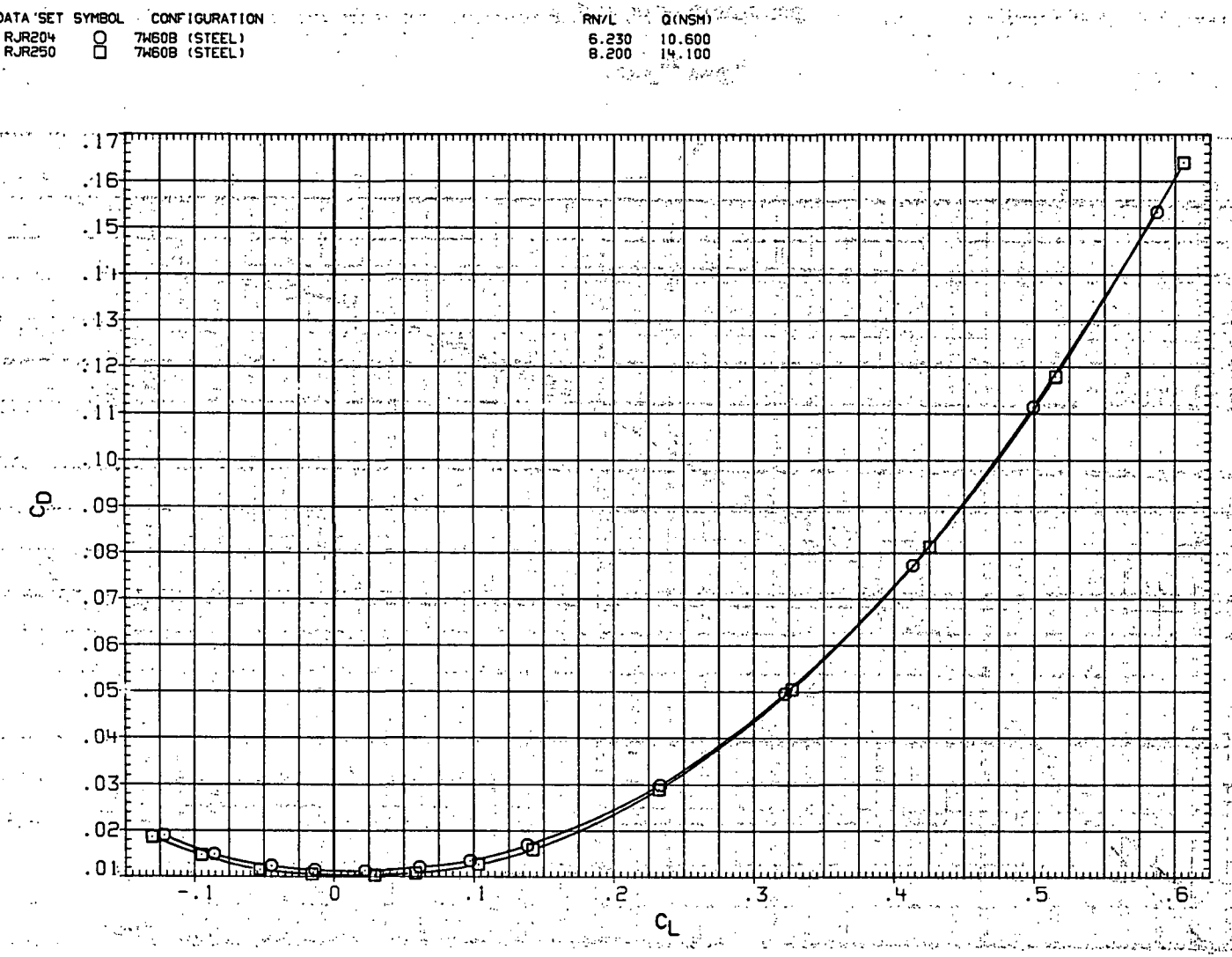

(b) C_D vs C_L.

Figure 77.– Continued.

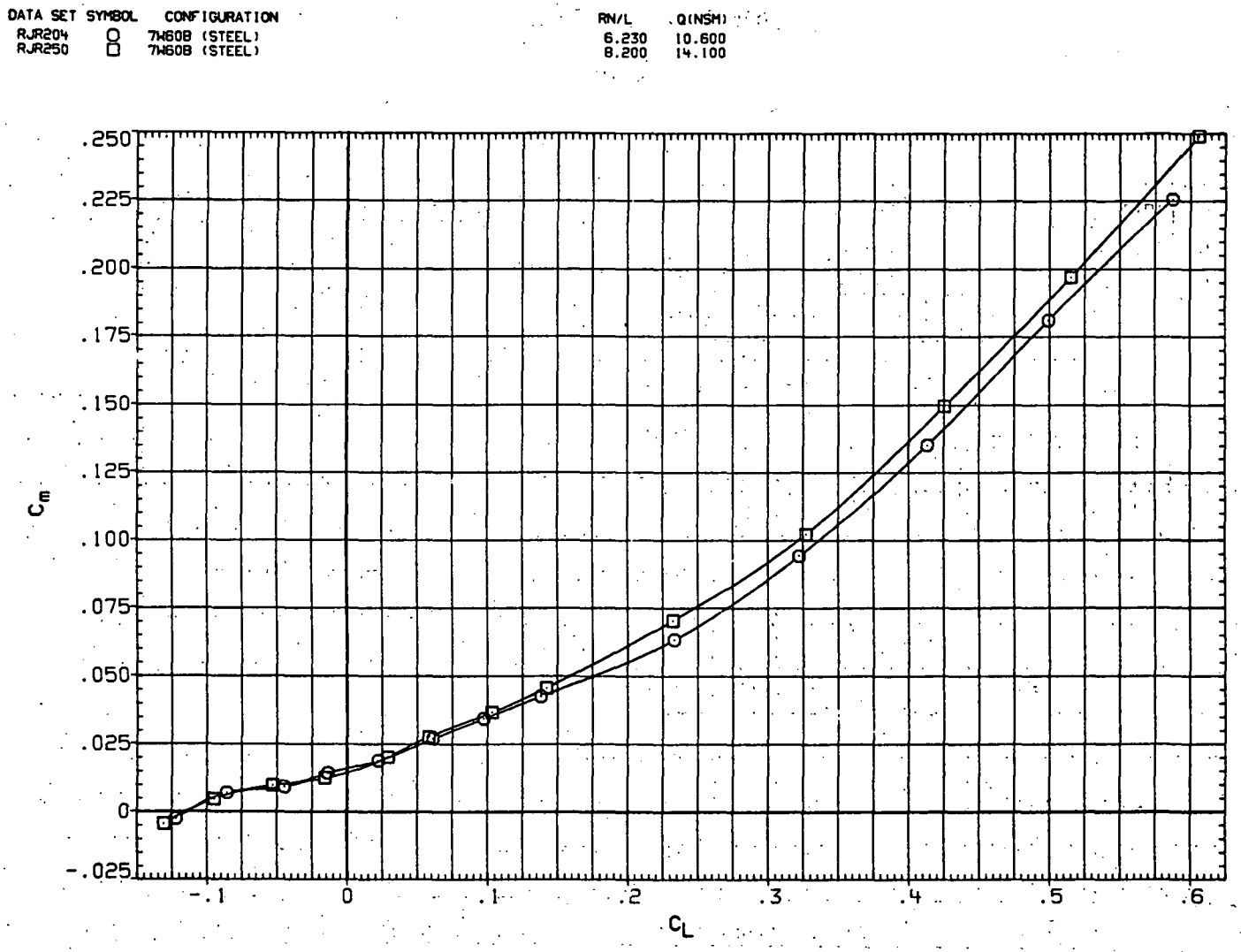

(c) C_m vs C_L.

Figure 77.– Continued.

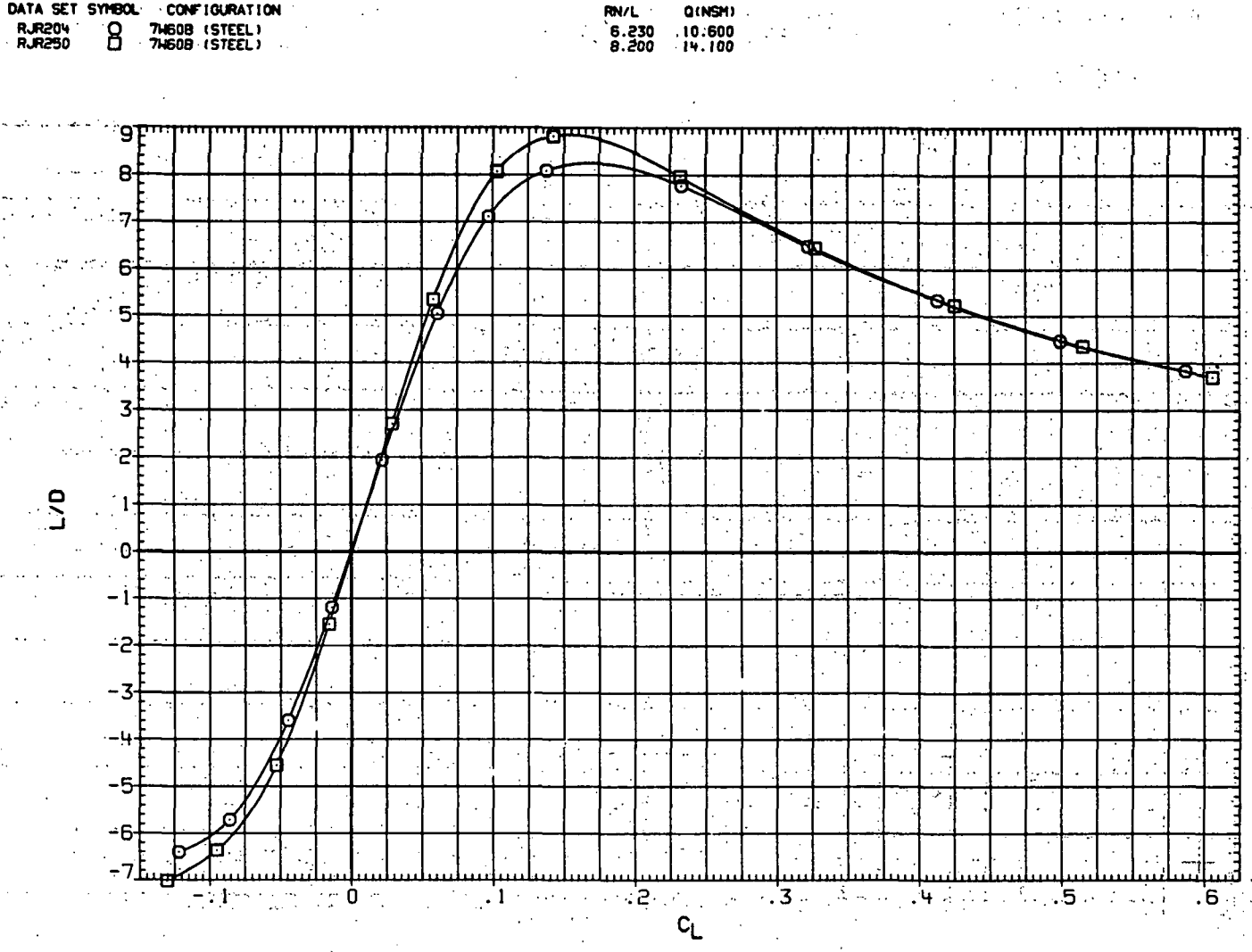

(d) L/D vs C_L.

Figure 77.– Continued.

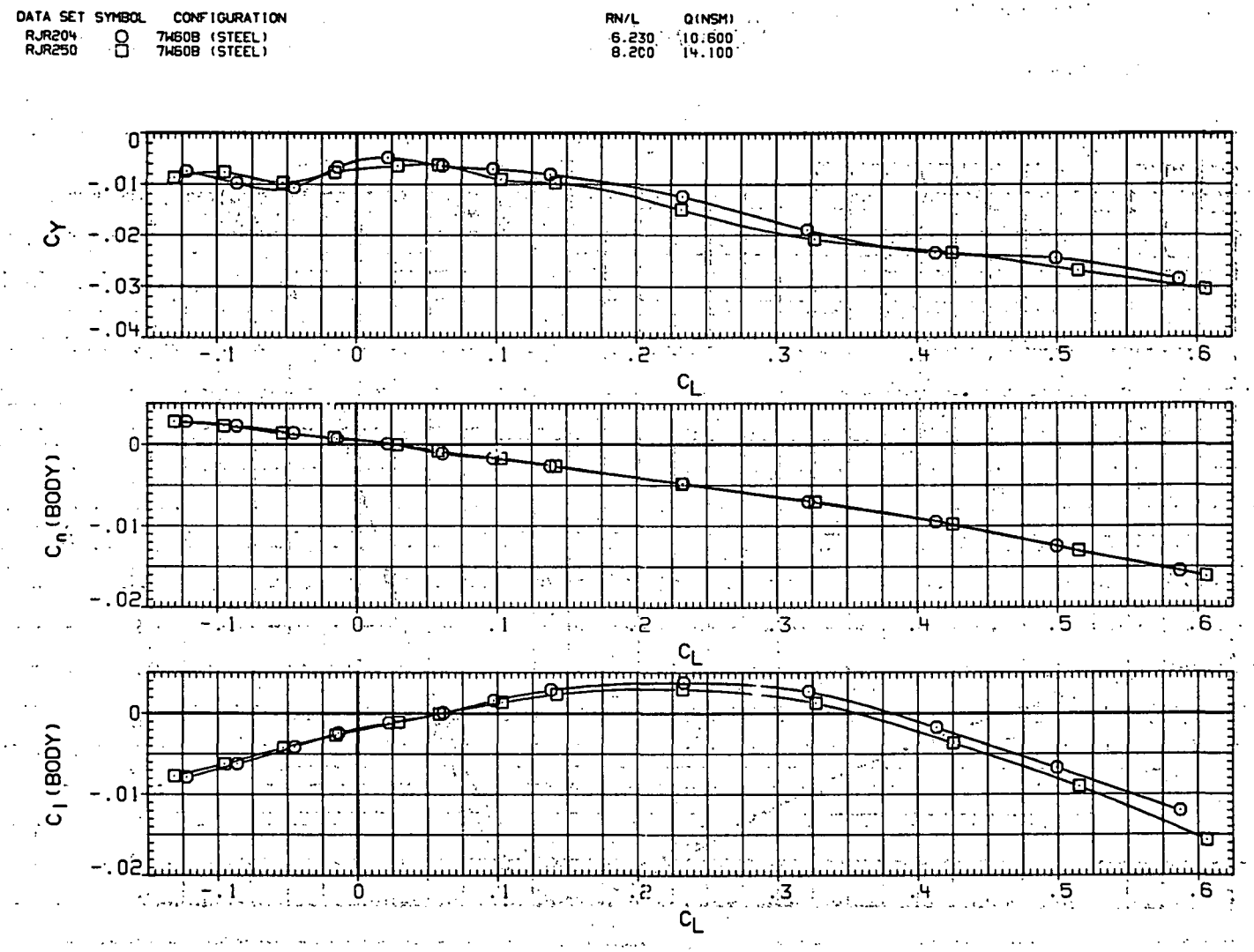

(e) C_Y, C_n and C_ℓ vs C_L.

Figure 77.– Concluded.

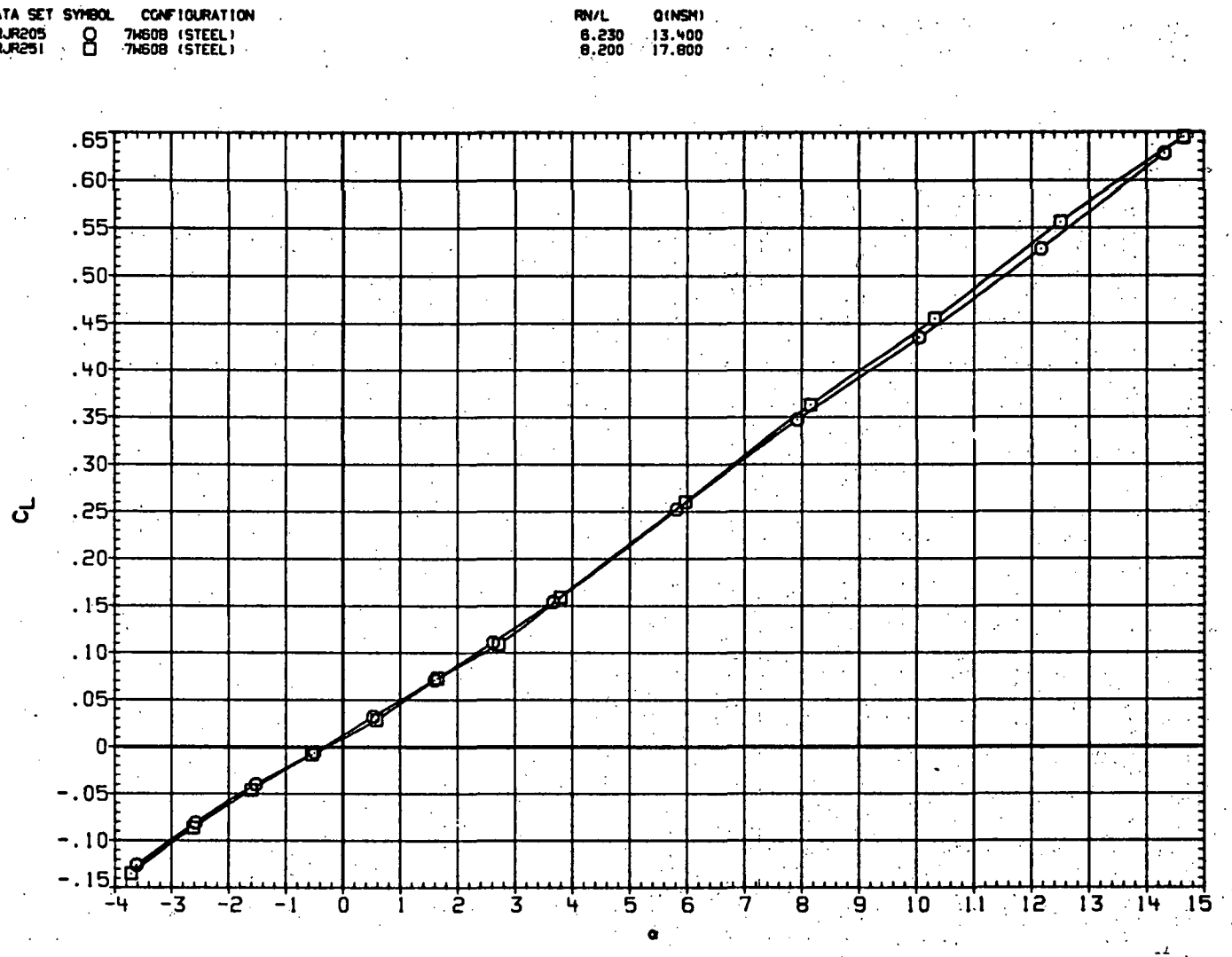

(a) C_L vs α.

Figure 78.– Dynamic-pressure effects on the aerodynamic characteristics of the steel trapezoidal oblique wing-body combination ($\Lambda = 60°, M = 0.8$ and the NACA 65A204 airfoil).

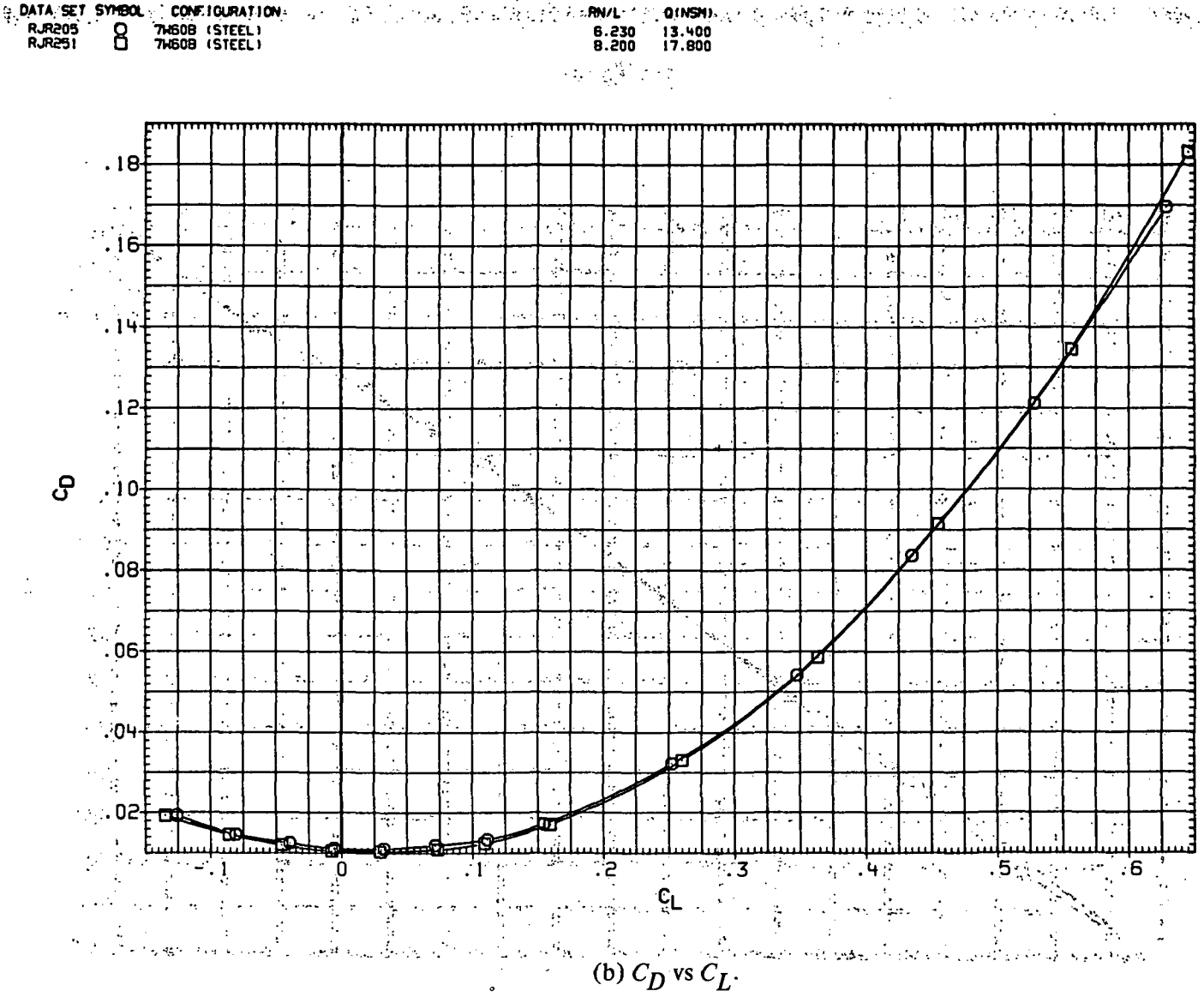

(b) C_D vs C_L.

Figure 78.— Continued.

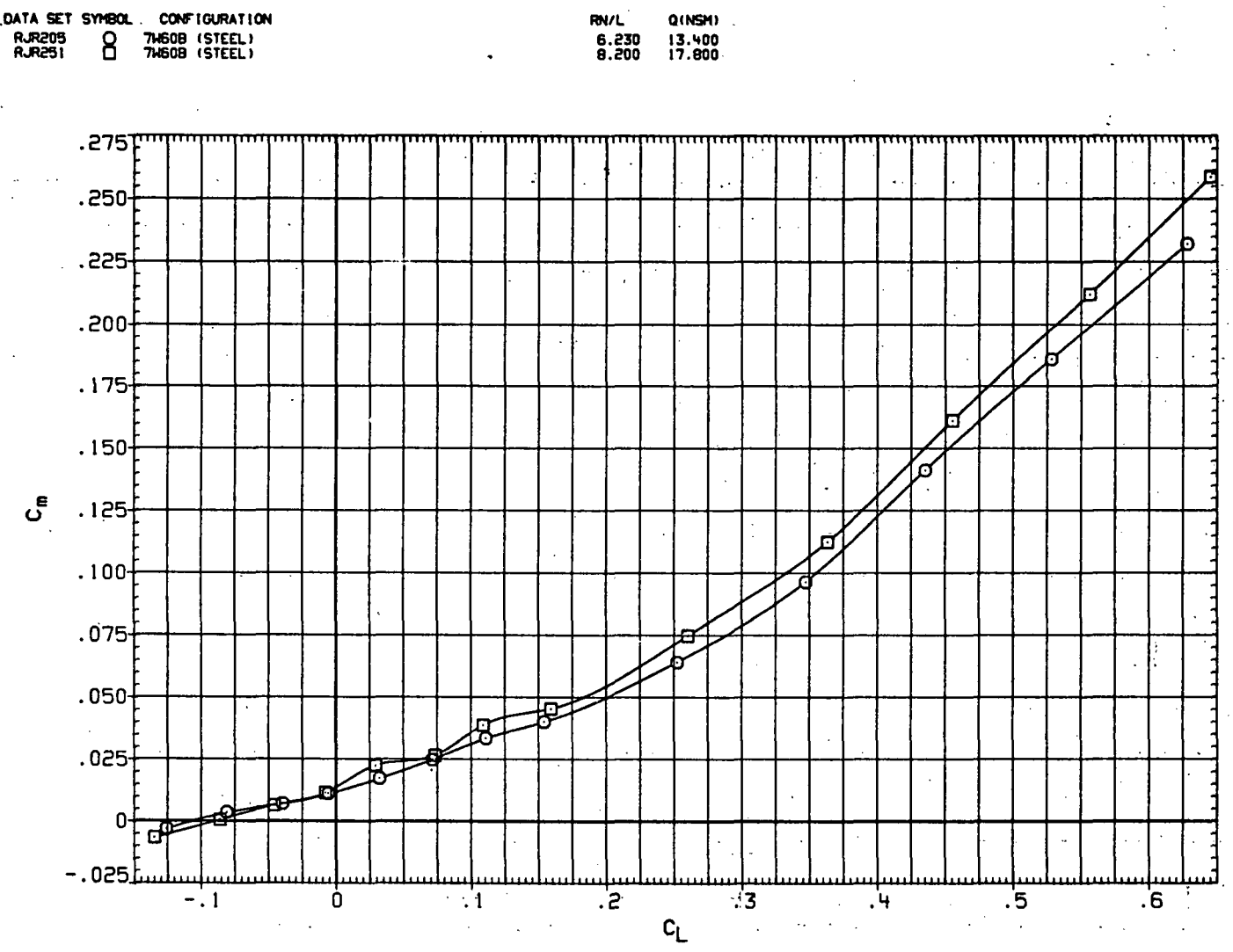

(c) C_m vs C_L.

Figure 78.– Continued.

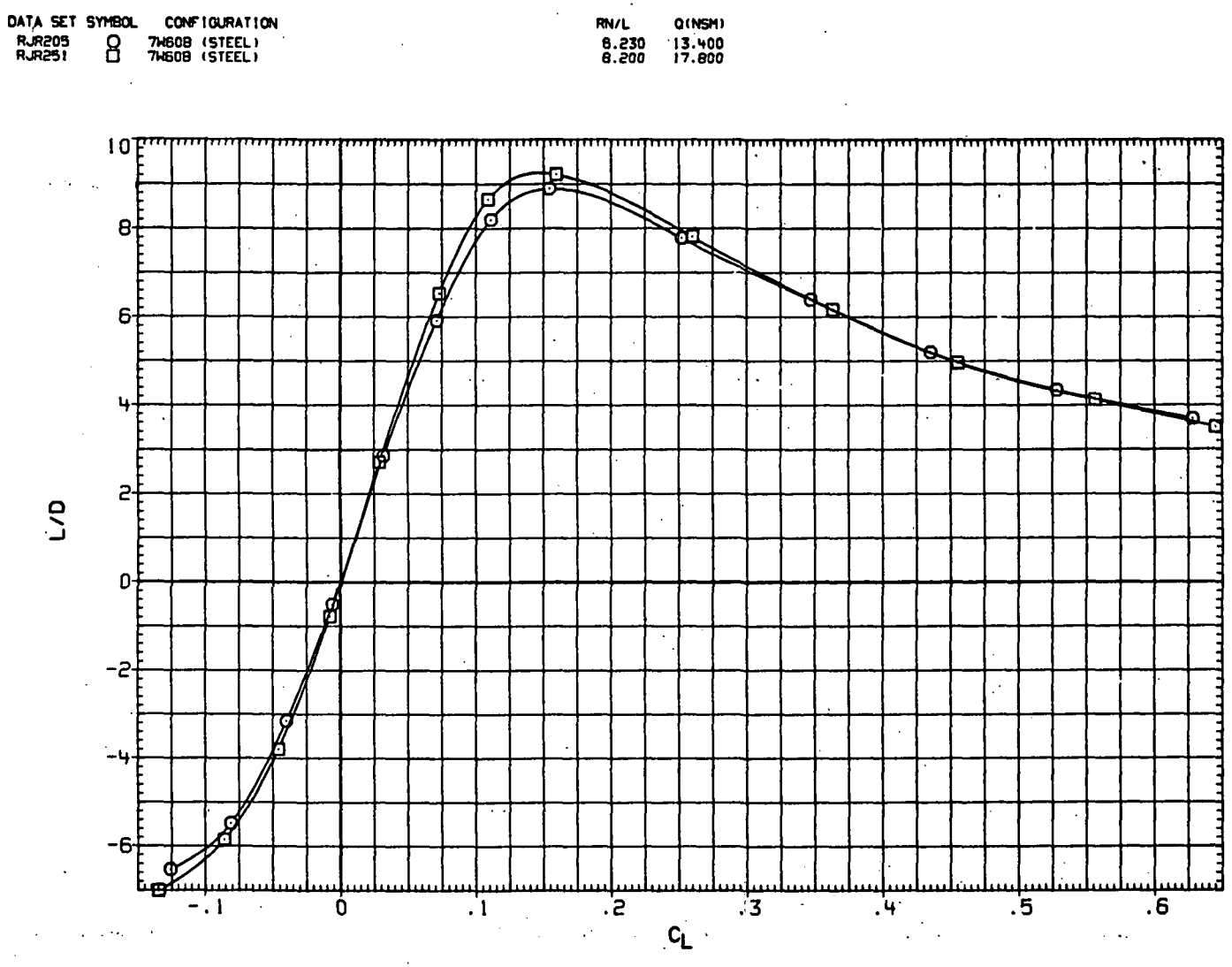

(d) L/D vs C_L.

Figure 78.– Continued.

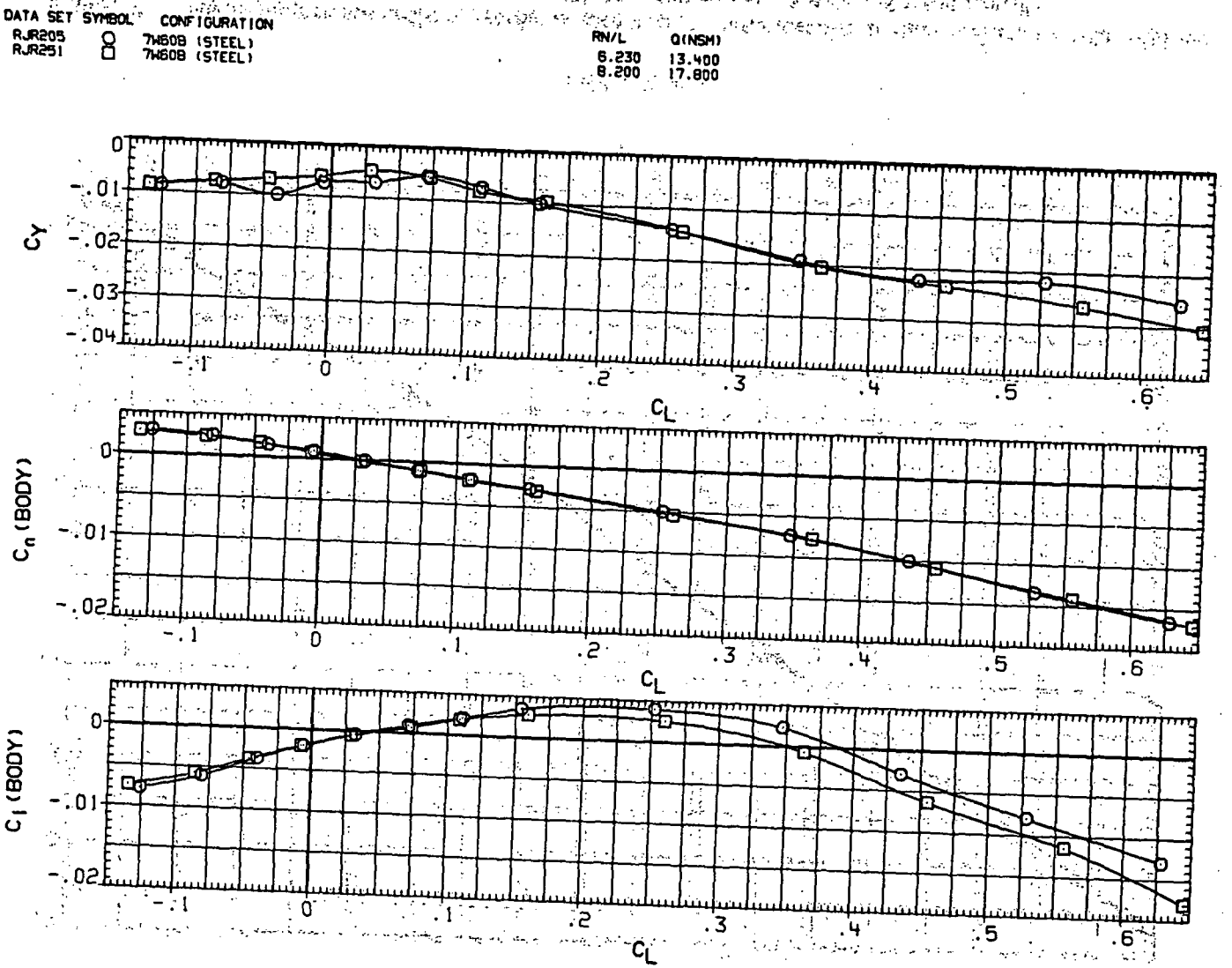

(e) C_Y, C_n and C_ℓ vs C_L.

Figure 78.– Concluded.

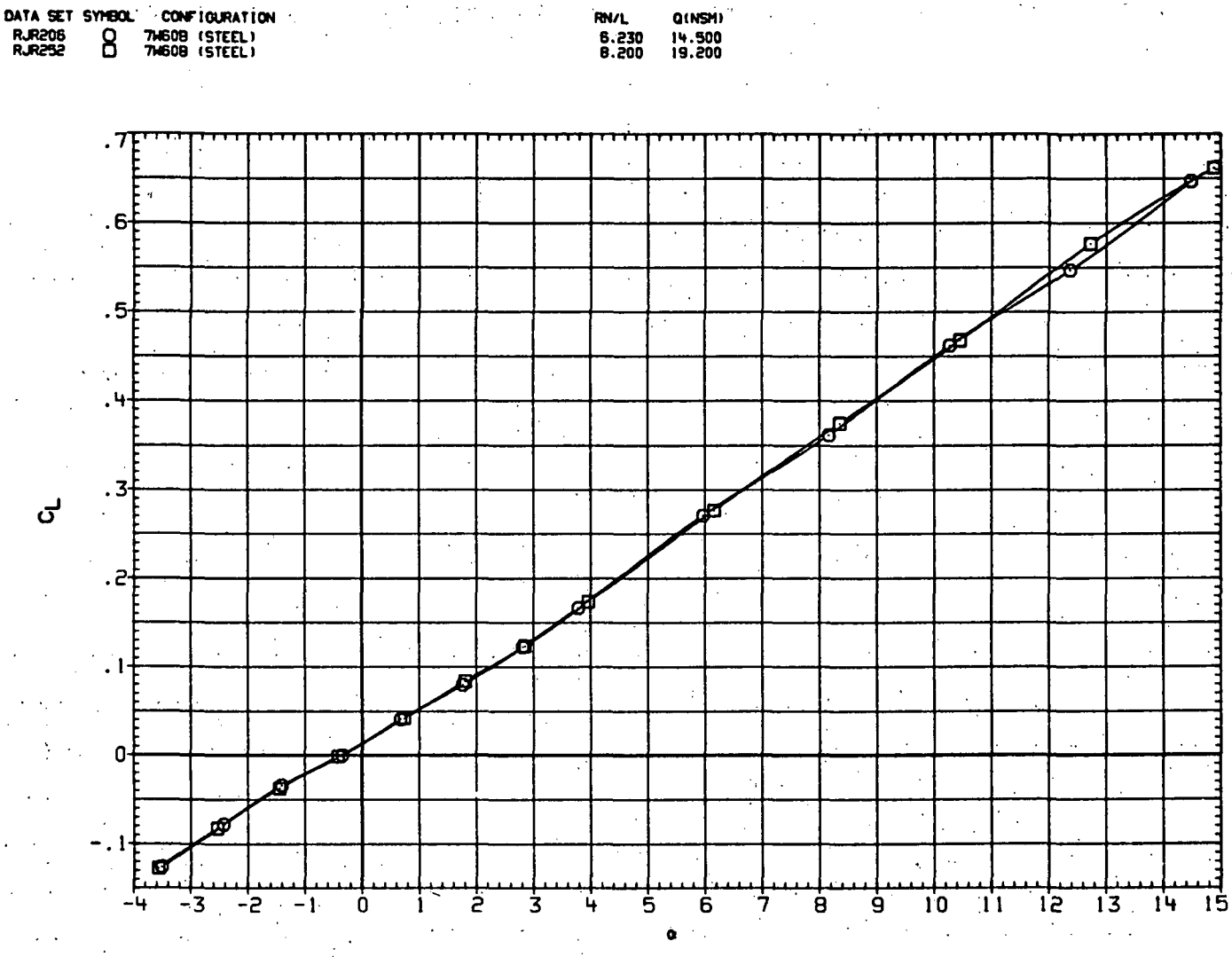

(a) C_L vs α.

Figure 79.– Dynamic-pressure effects on the aerodynamic characteristics of the steel trapezoidal oblique wing-body combination ($\Lambda = 60°$, $M = 0.9$ and the NACA 65A204 airfoil).

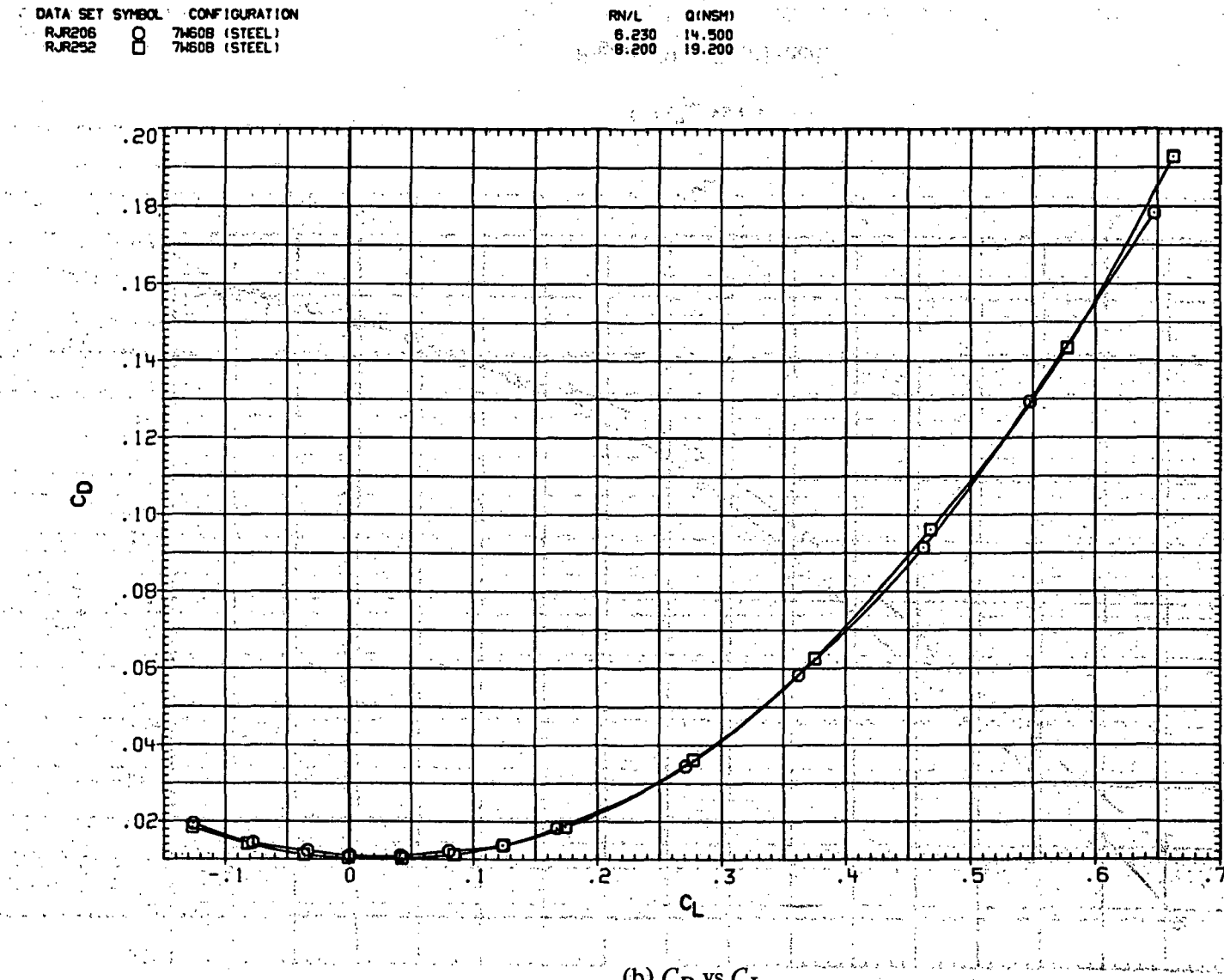

(b) C_D vs C_L.

Figure 79.– Continued.

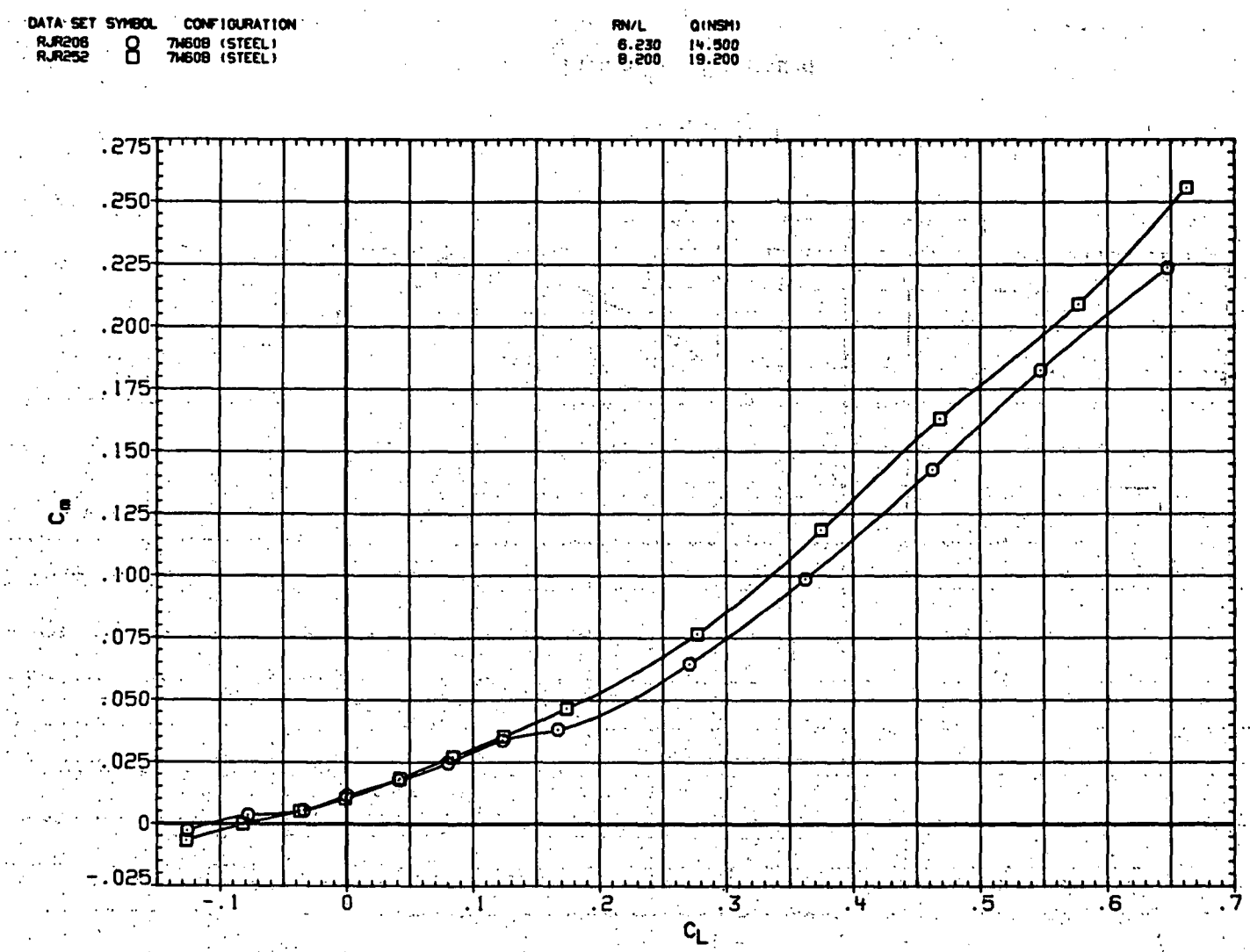

(c) C_m vs C_L.

Figure 79.– Continued.

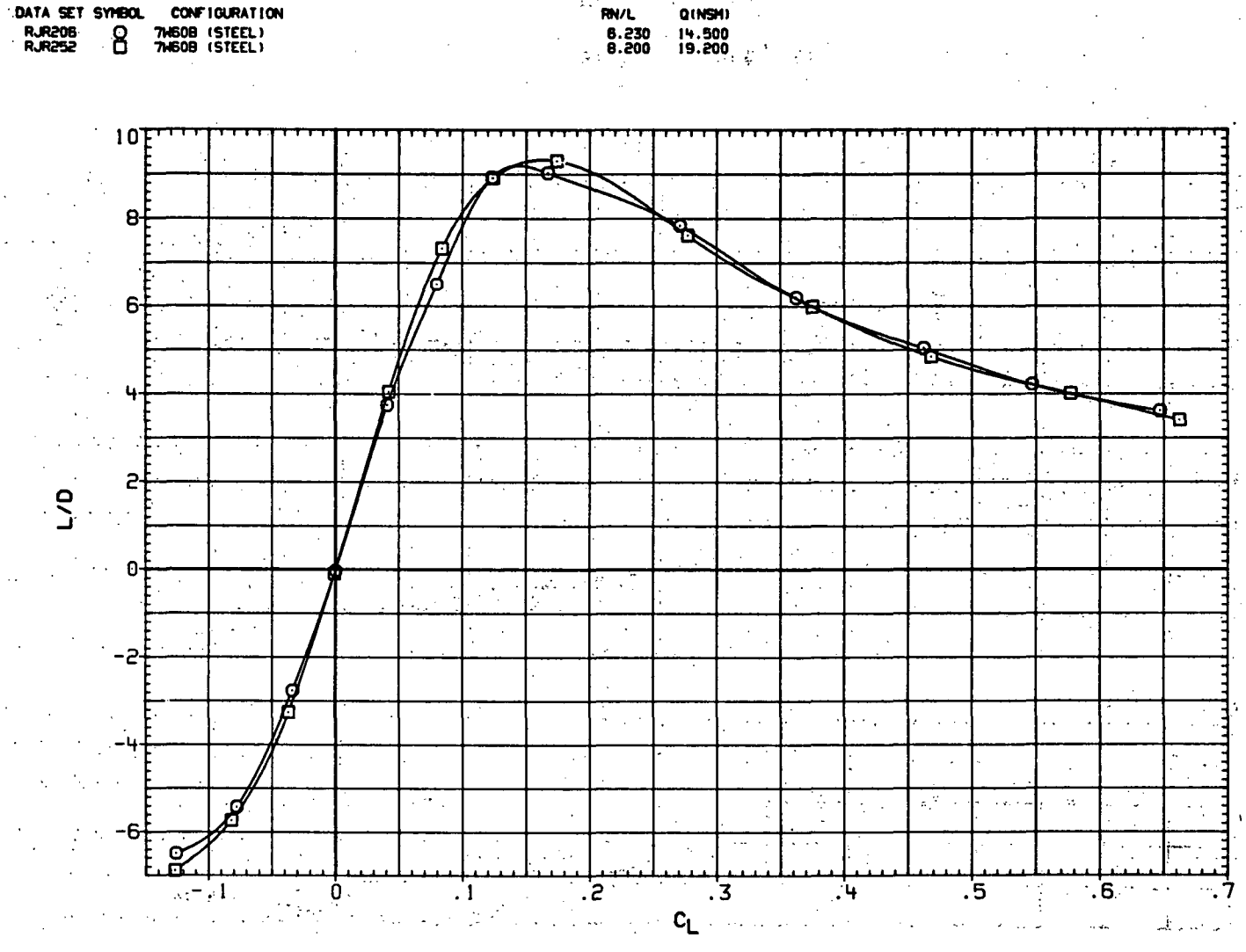

(d) L/D vs C_L.

Figure 79.– Continued.

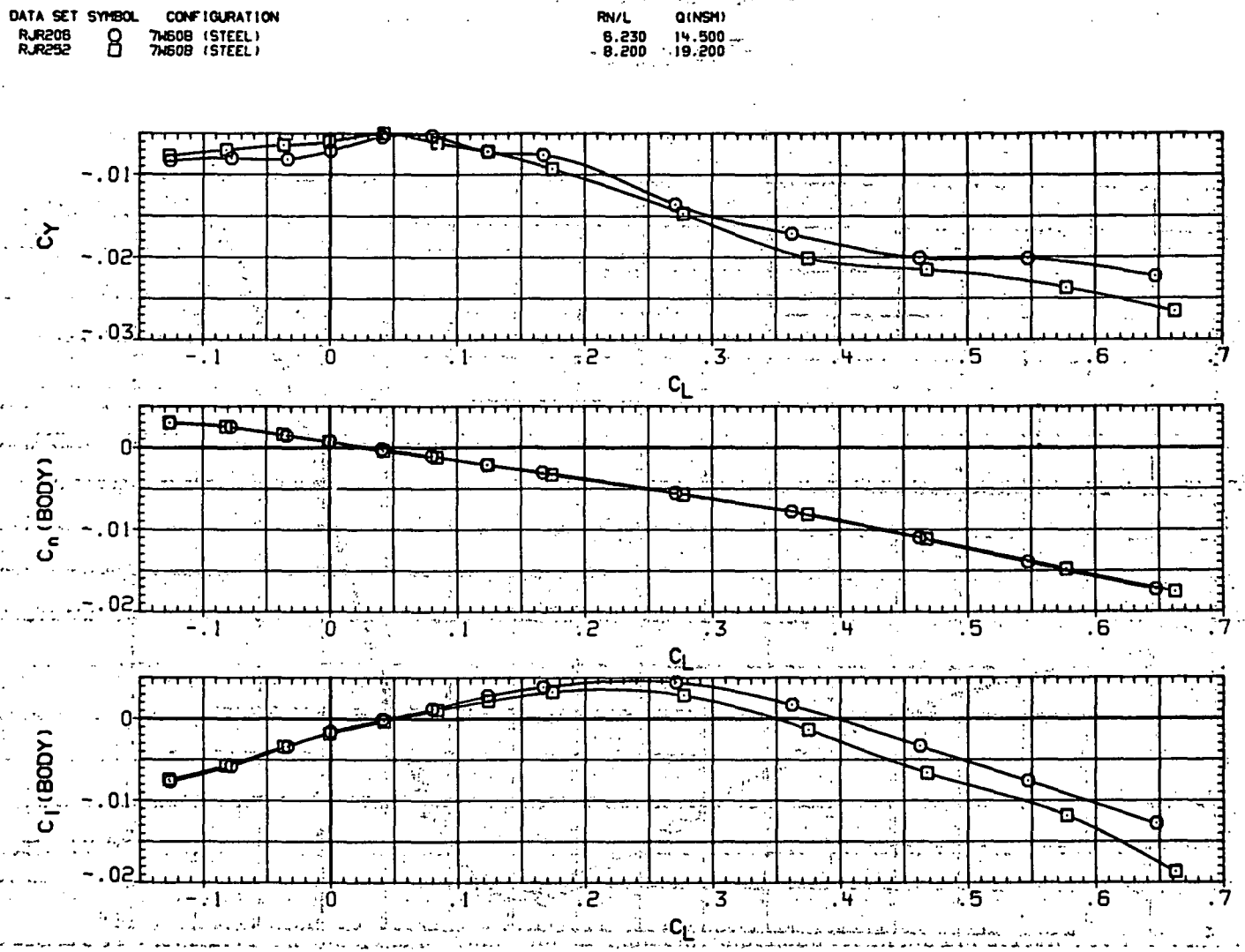

(e) C_Y, C_n and C_ℓ vs C_L.

Figure 79.– Concluded.

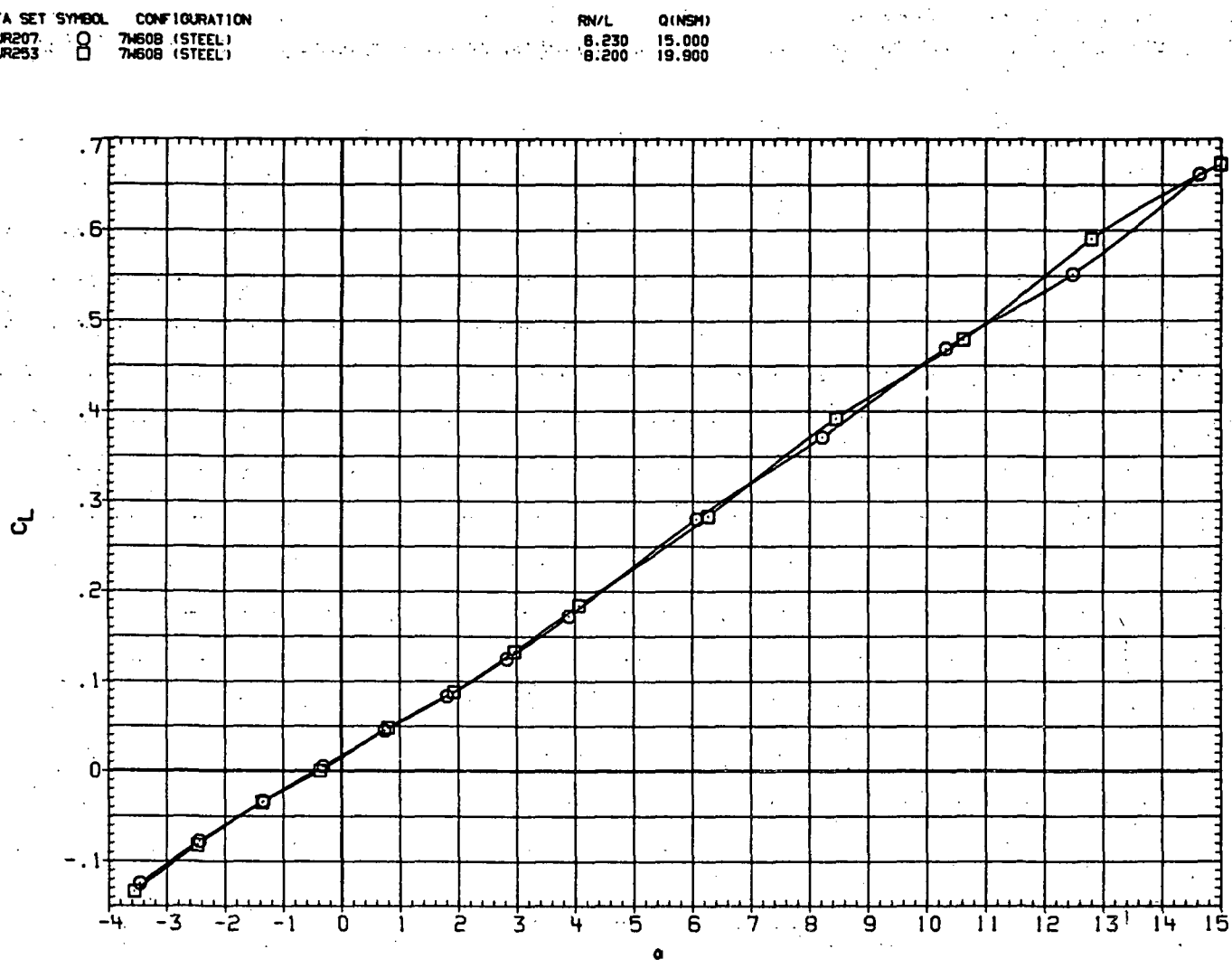

(a) C_L vs α.

Figure 80.– Dynamic-pressure effects on the aerodynamic characteristics of the steel trapezoidal oblique wing-body combination ($\Lambda = 60°$, $M = 0.95$ and the NACA 65A204 airfoil).

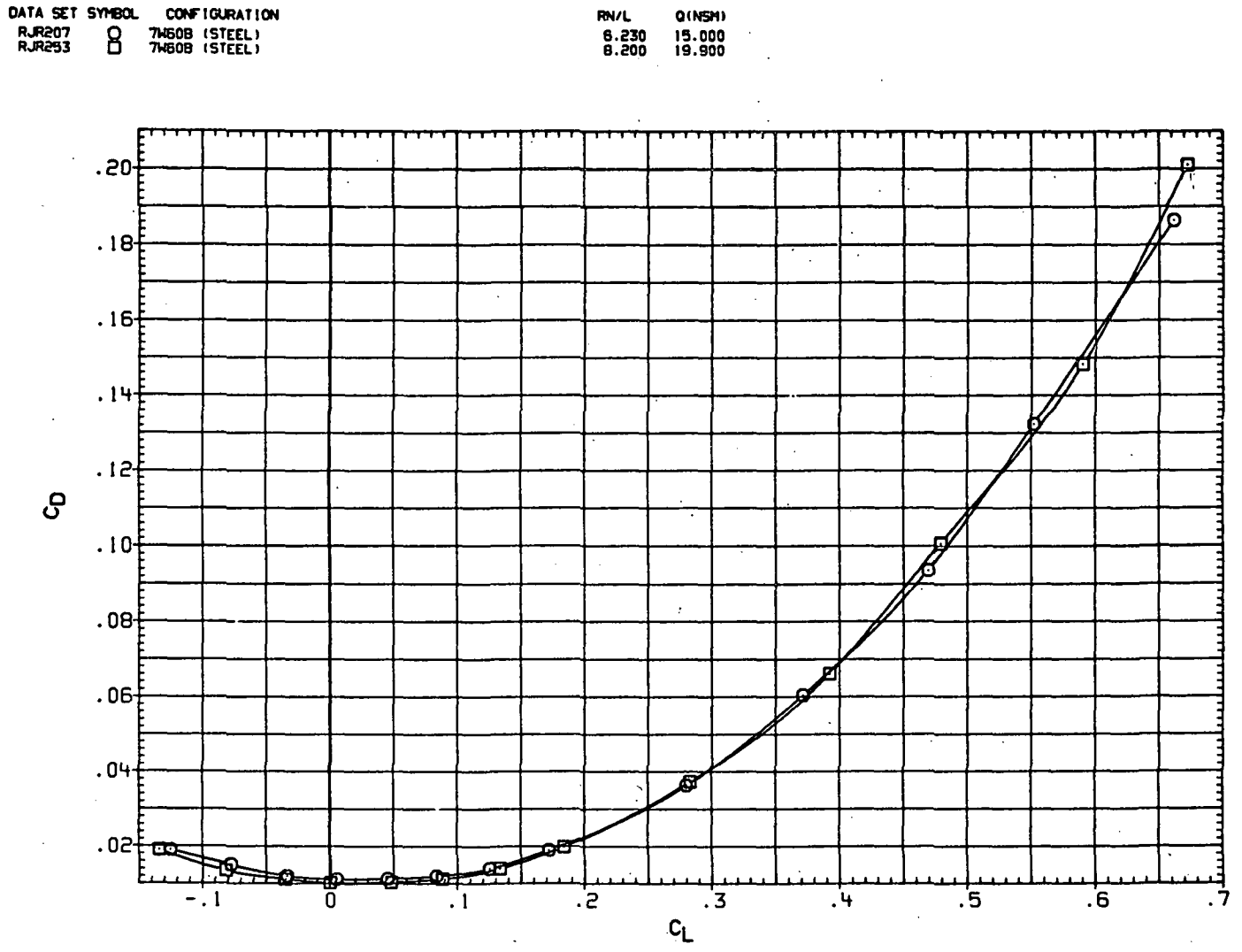

(b) C_D vs C_L.

Figure 80.– Continued.

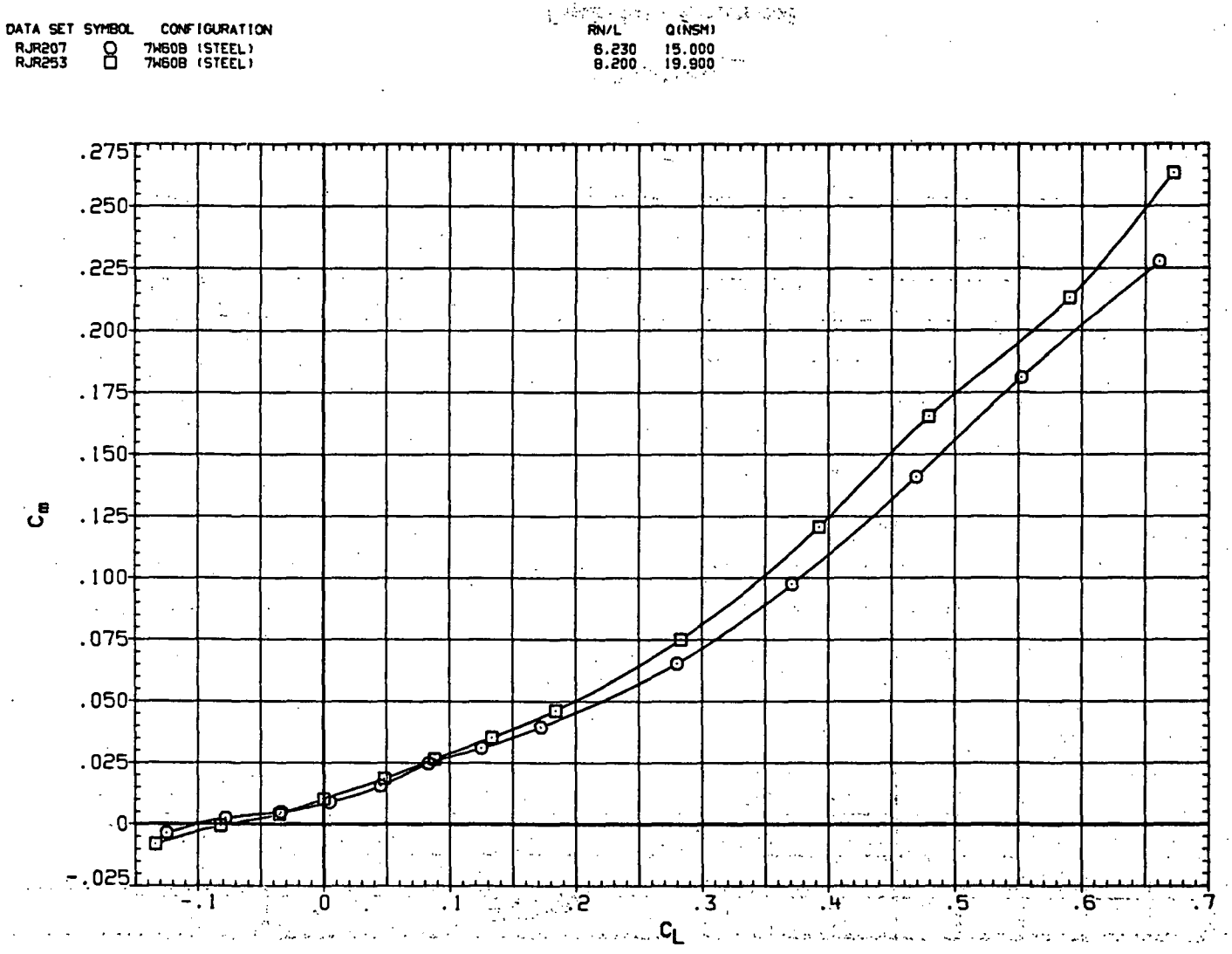

(c) C_m vs C_L.

Figure 80.– Continued.

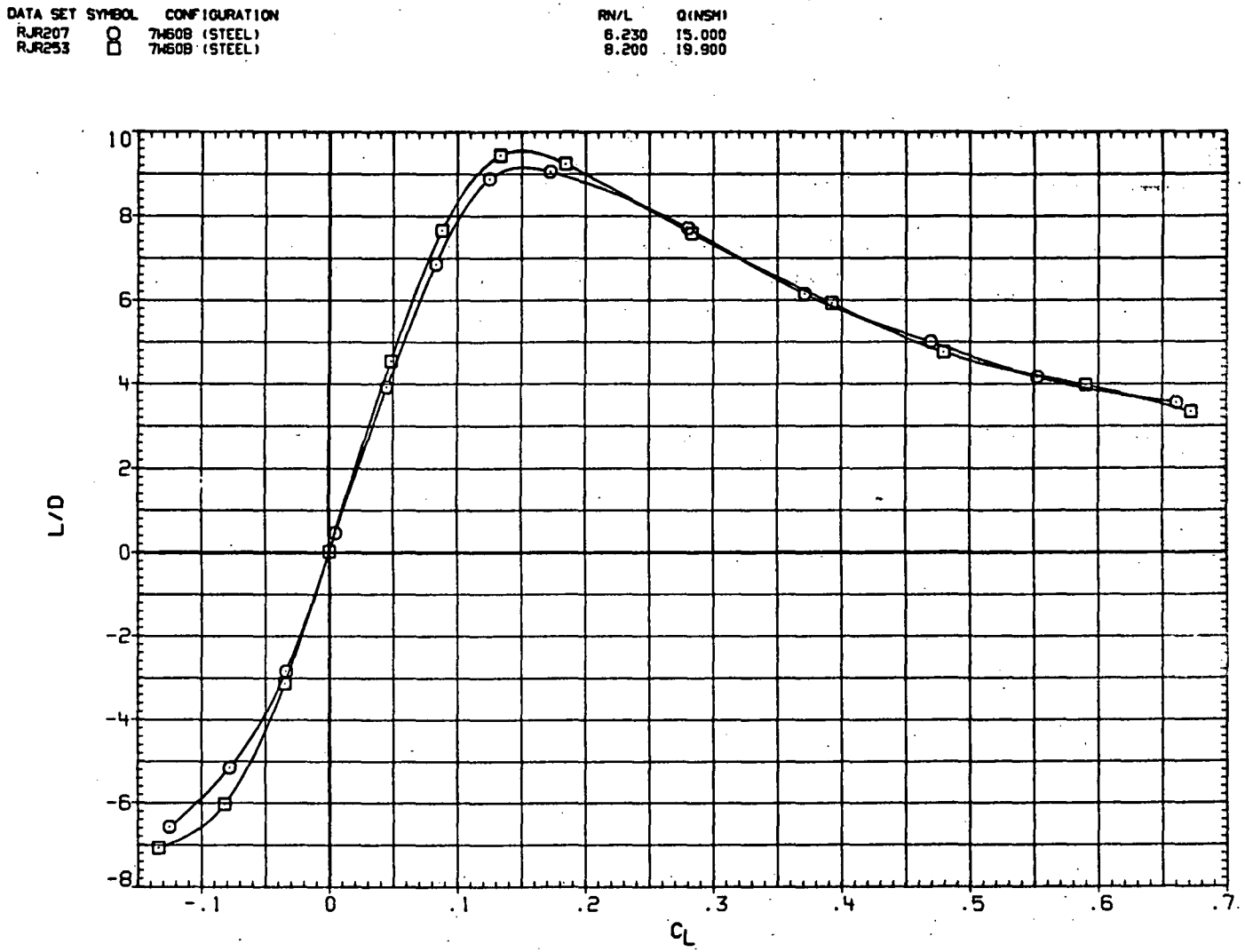

(d) L/D vs C_L.

Figure 80.– Continued.

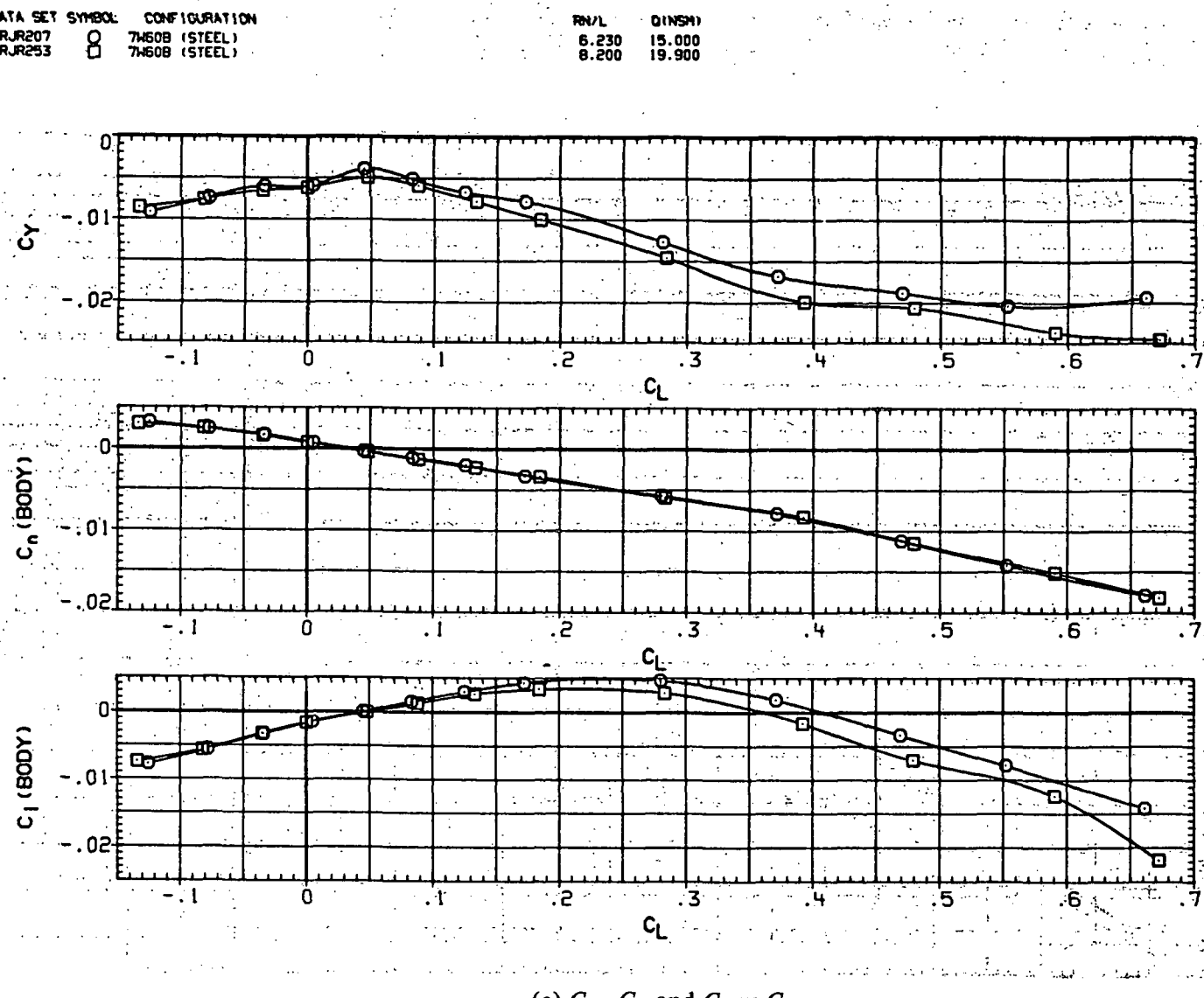

(e) C_Y, C_n and C_ℓ vs C_L.

Figure 80.– Concluded.

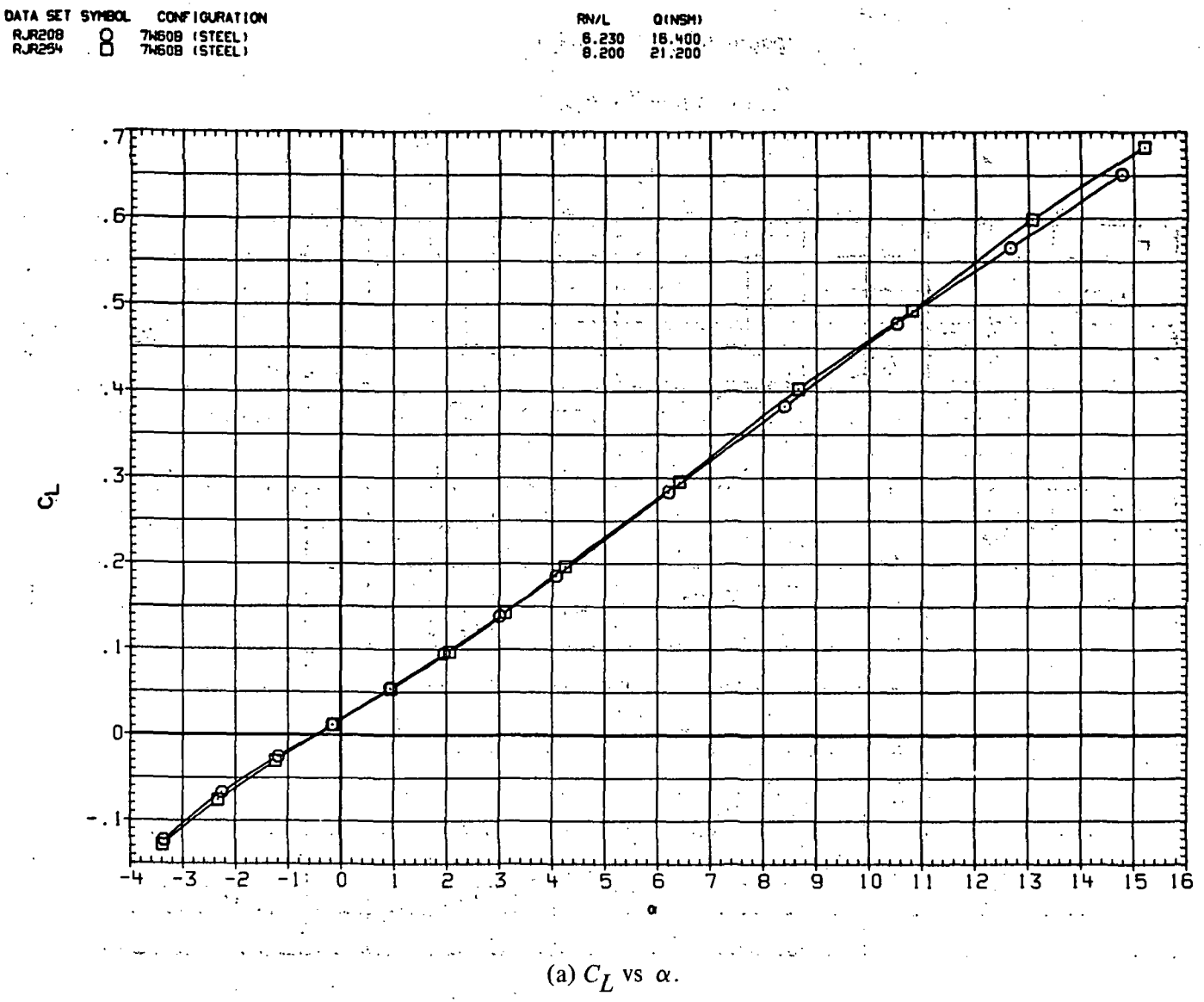

(a) C_L vs α.

Figure 81.– Dynamic-pressure effects on the aerodynamic characteristics of the steel trapezoidal oblique wing-body combination ($\Lambda = 60°, M = 1.1$ and the NACA 65A204 airfoil).

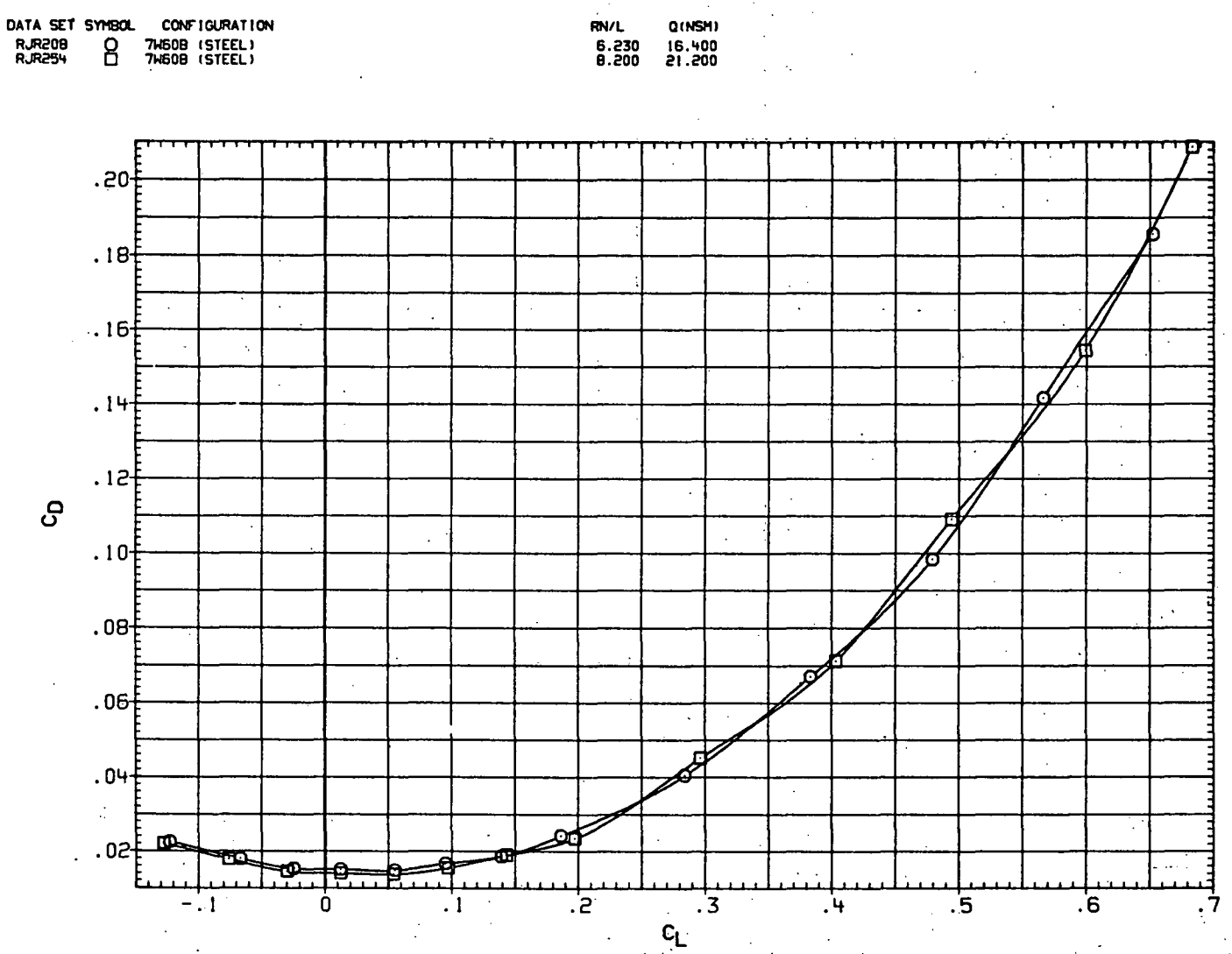

(b) C_D vs C_L.

Figure 81.– Continued.

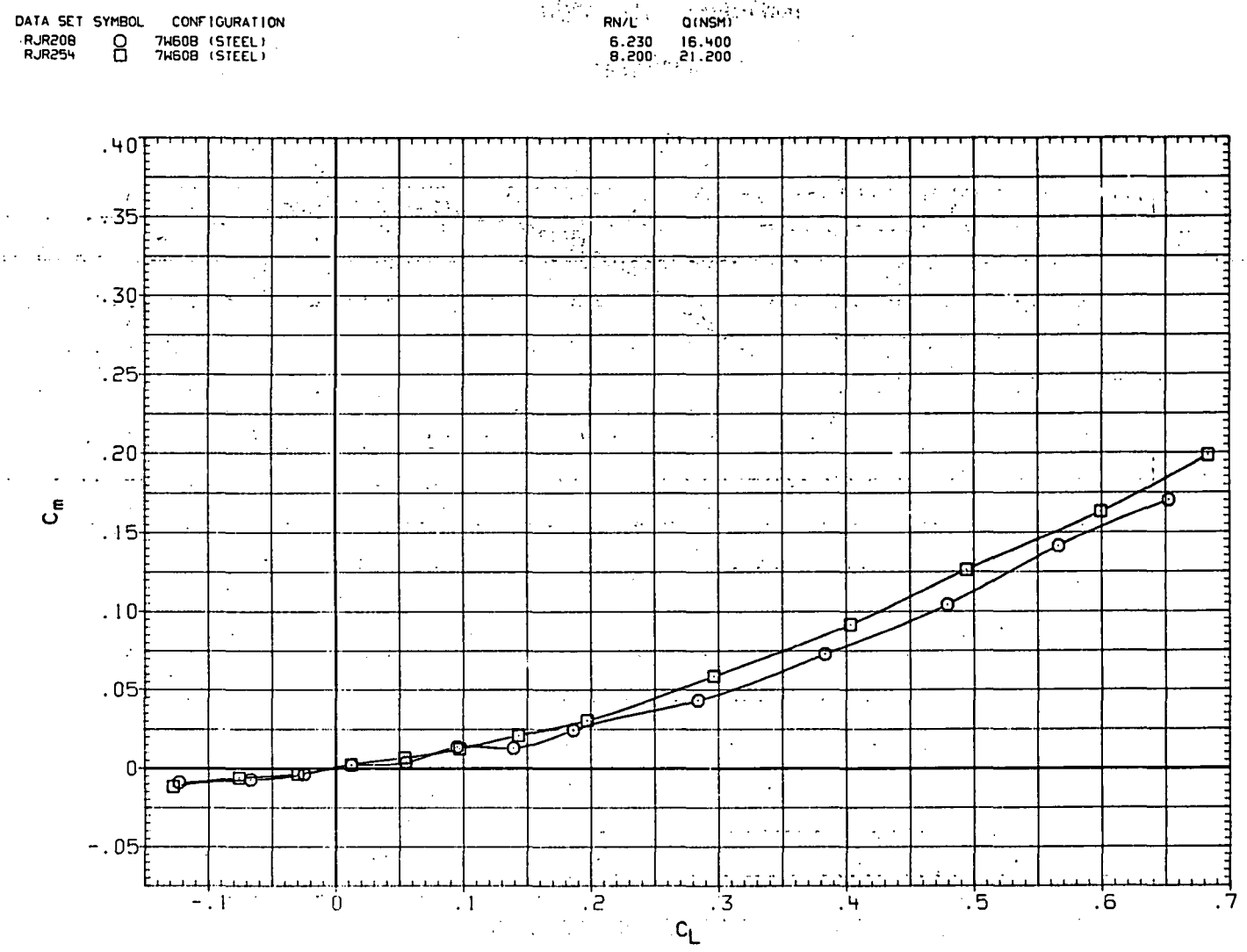

(c) C_m vs C_L.

Figure 81.– Continued.

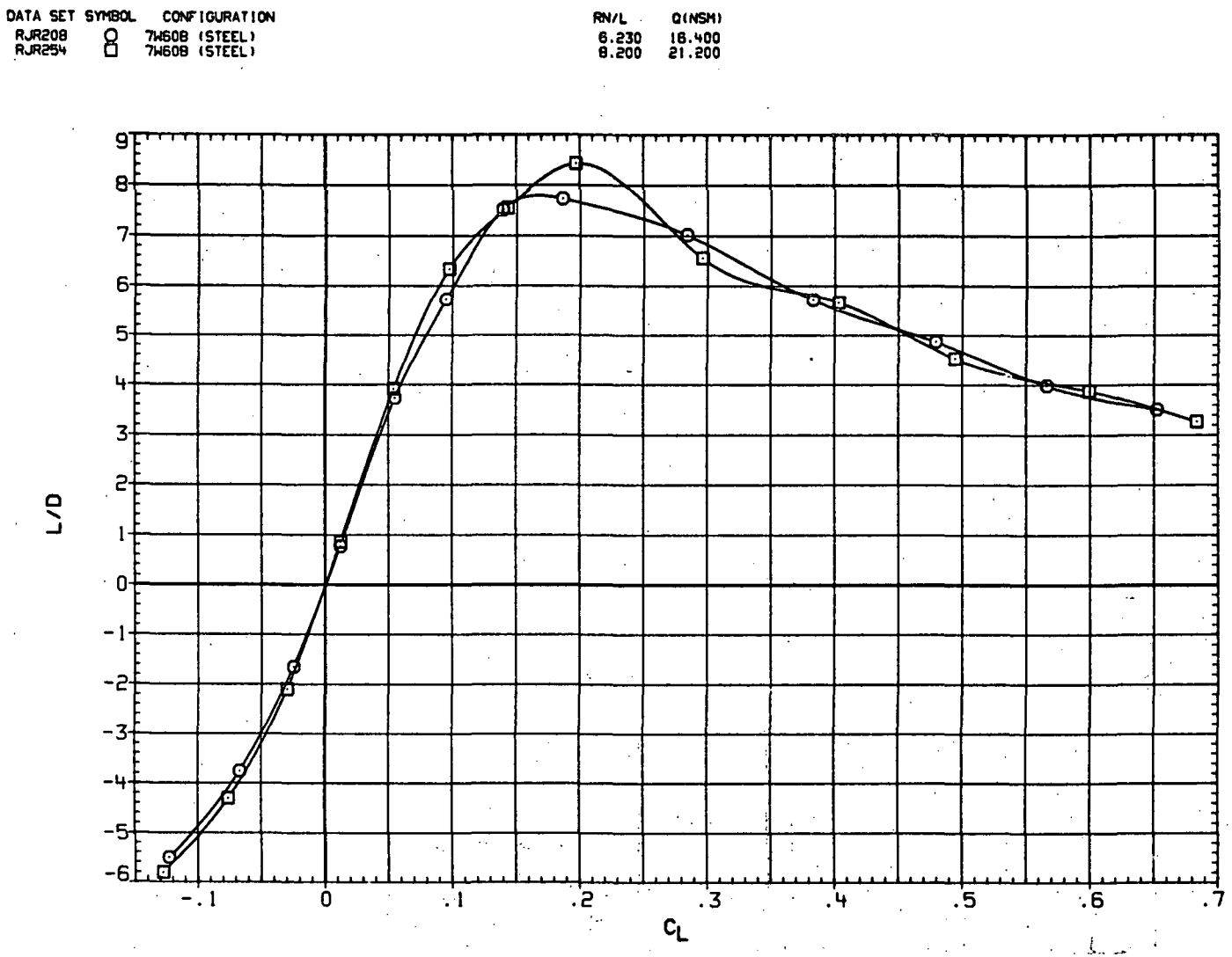

(d) L/D vs C_L.

Figure 81.– Continued.

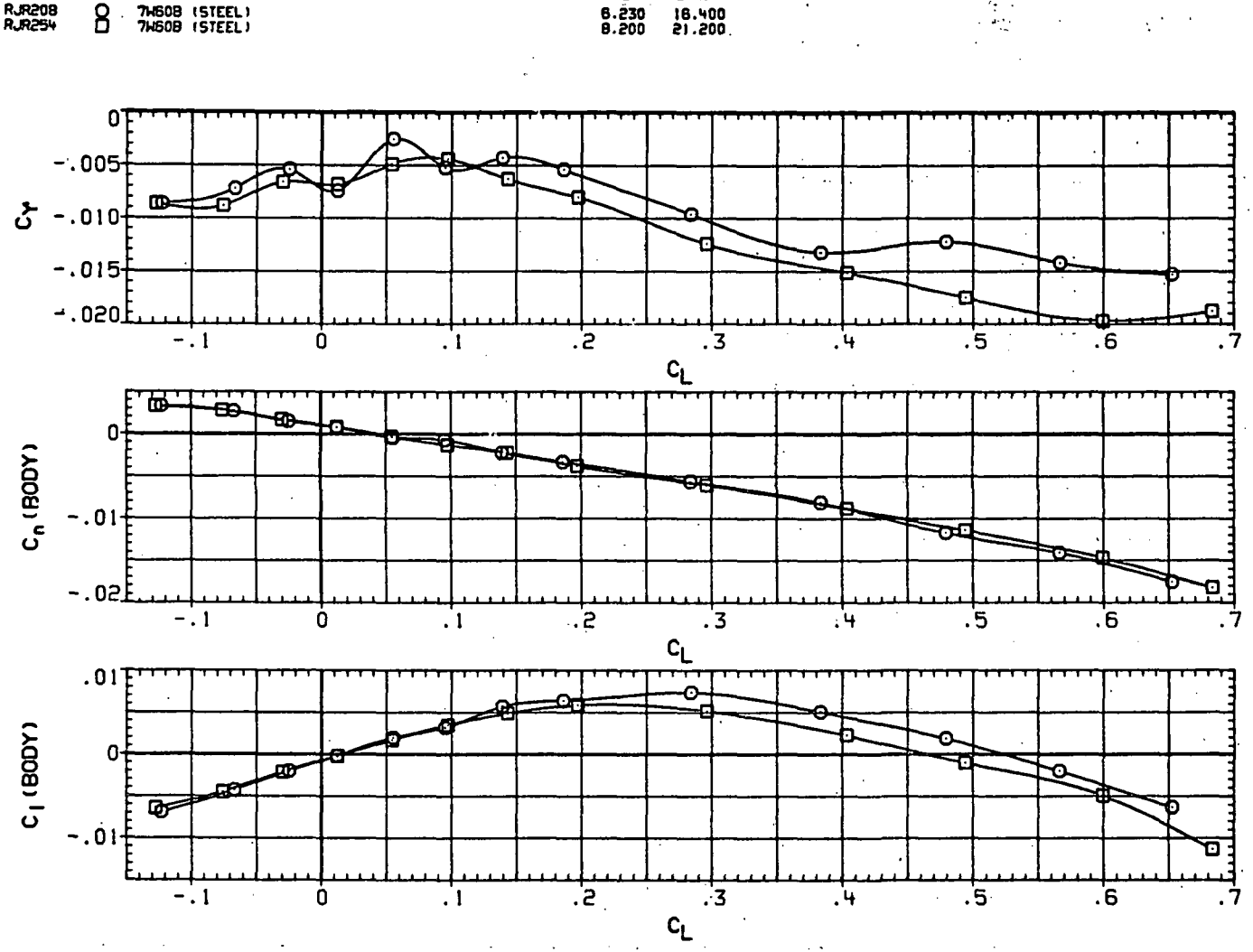

(e) C_Y, C_n and C_ℓ vs C_L.

Figure 81.– Concluded.

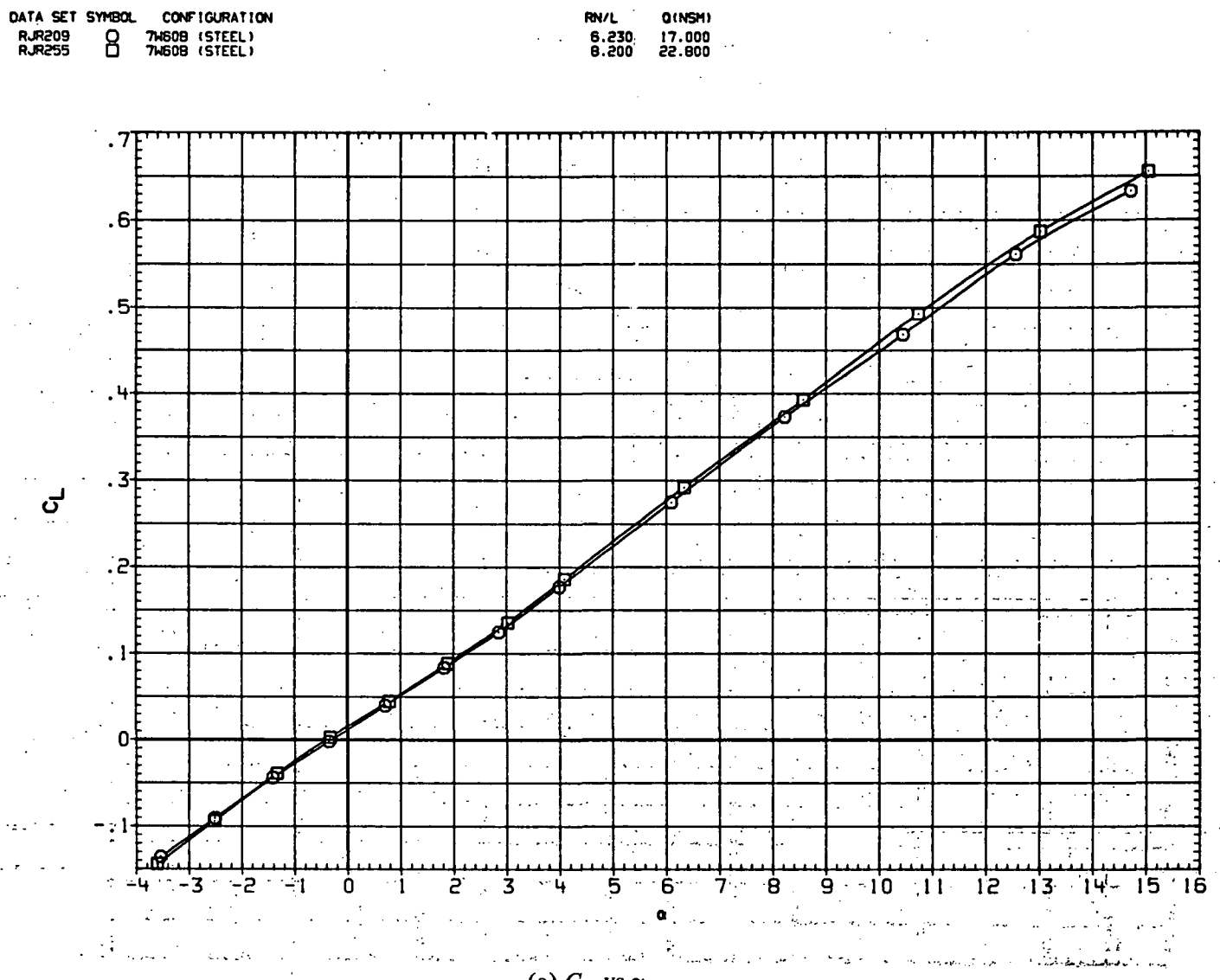

(a) C_L vs α.

Figure 82.– Dynamic-pressure effects on the aerodynamic characteristics of the steel trapezoidal oblique wing-body combination ($\Lambda = 60°, M = 1.2$ and the NACA 65A204 airfoil).

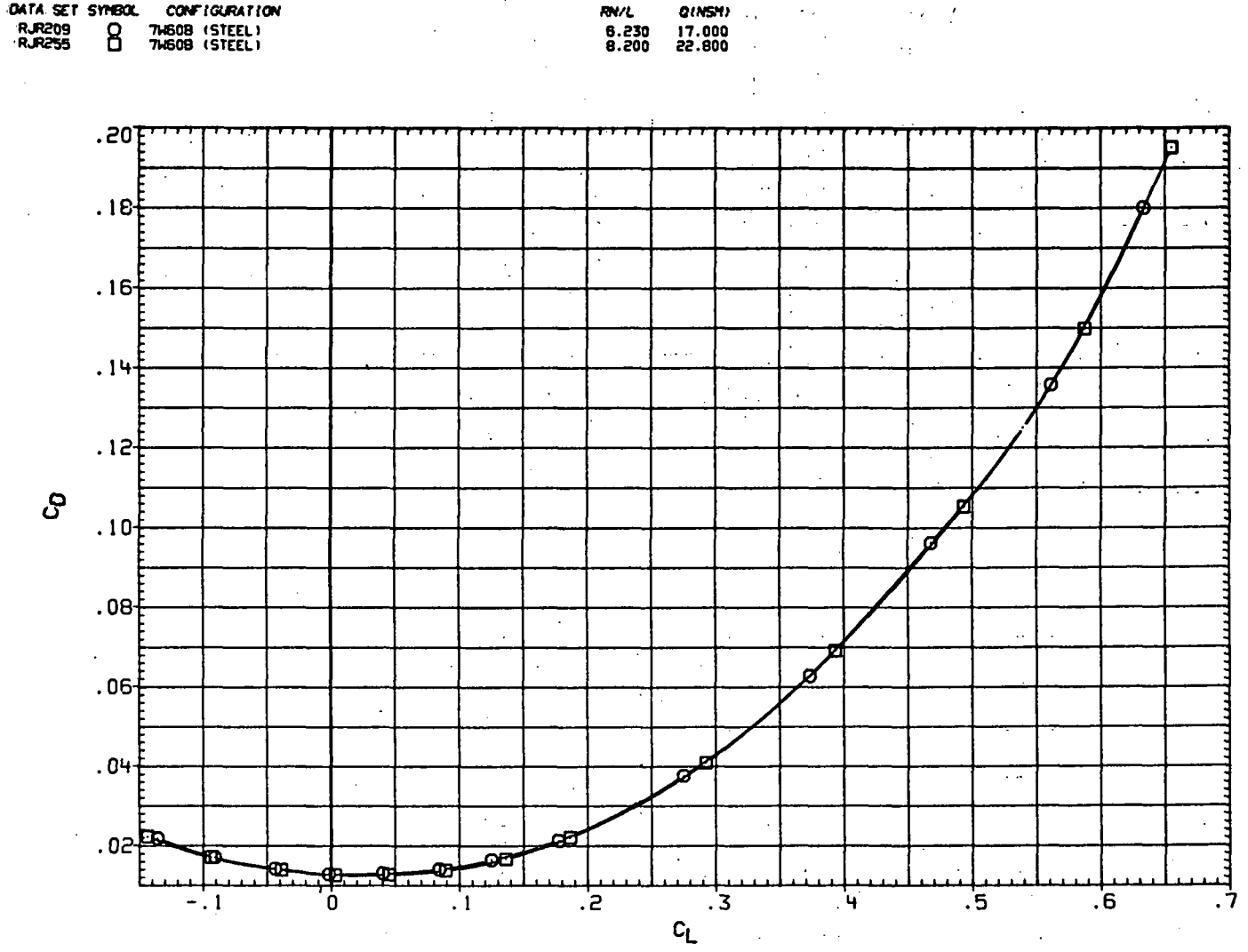

(b) C_D vs C_L.

Figure 82.– Continued.

DATA SET	SYMBOL	CONFIGURATION	RN/L	Q(NSM)
RJR209	○	7W60B (STEEL)	6.230	17.000
RJR255	□	7W60B (STEEL)	8.200	22.800

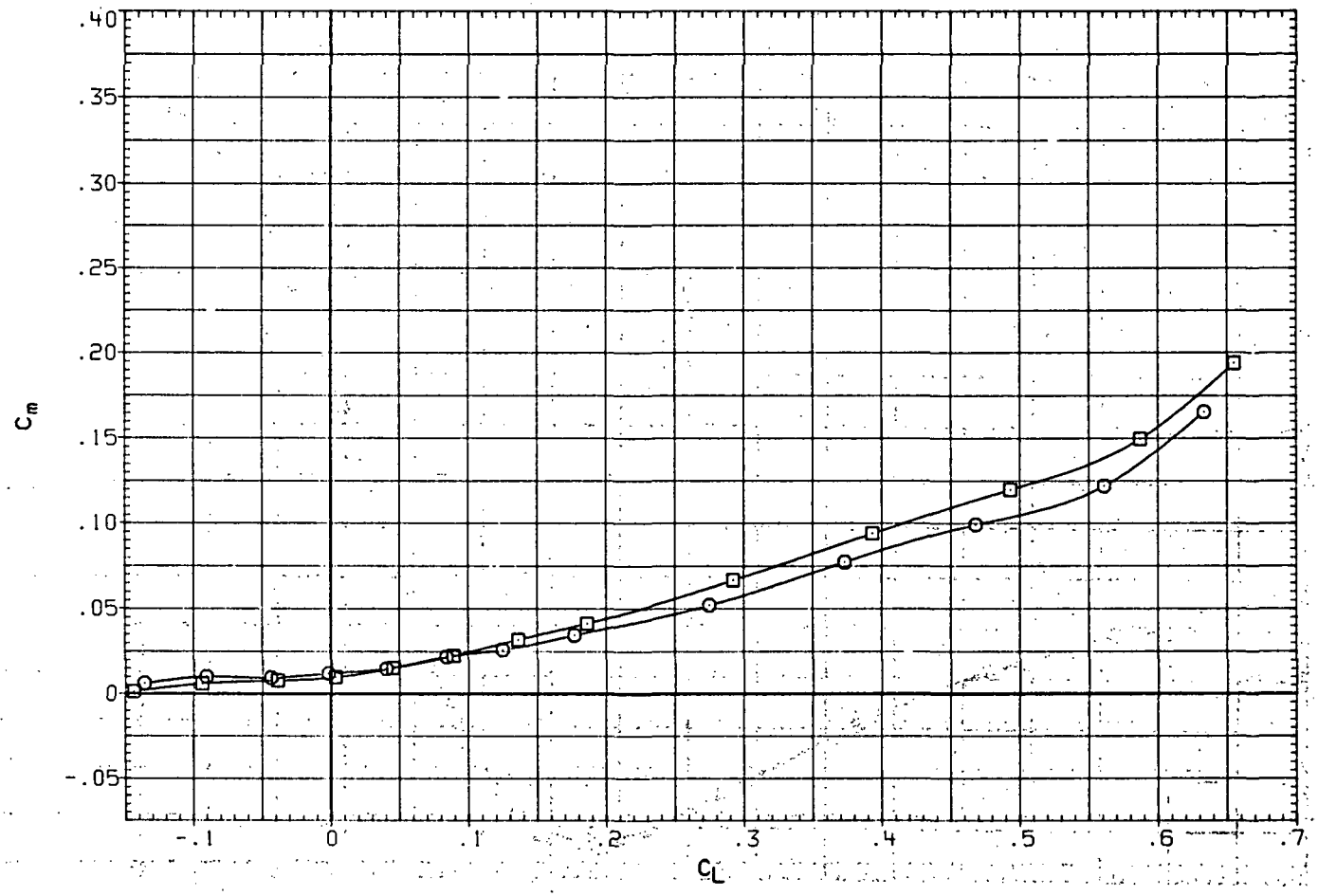

(c) C_m vs C_L.

Figure 82.– Continued.

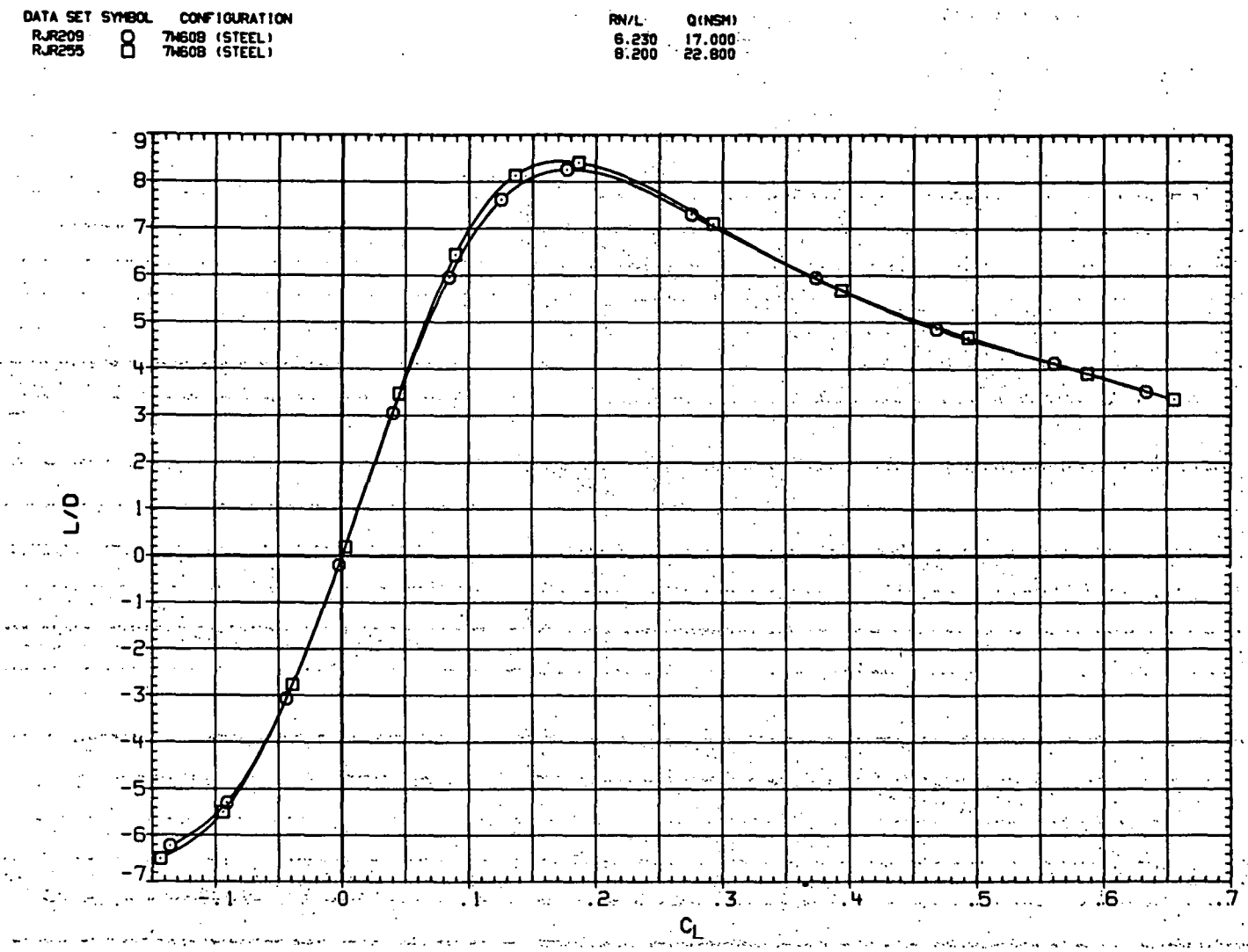

(d) L/D vs C_L.

Figure 82.– Continued.

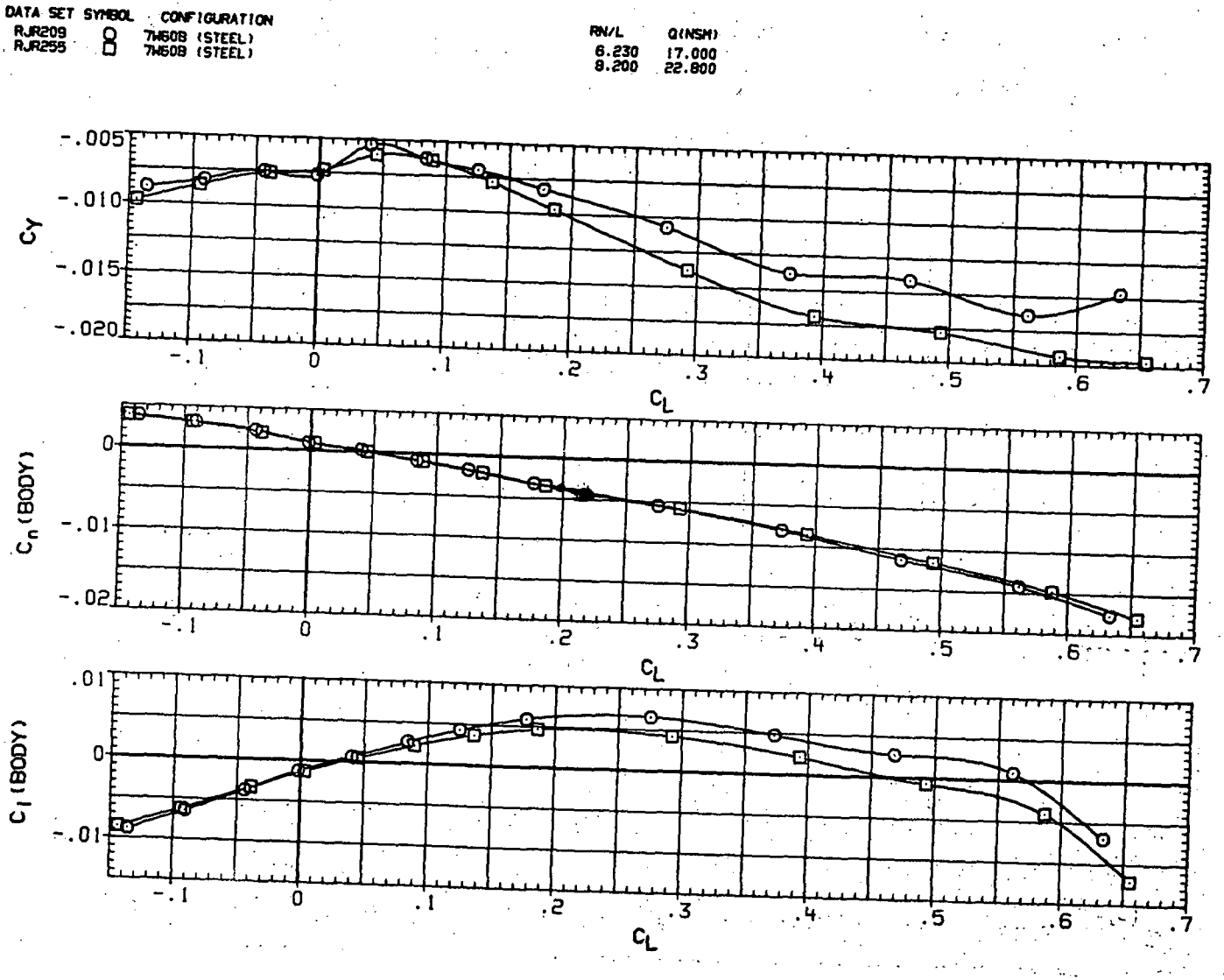

(e) C_Y, C_n and C_ℓ vs C_L.

Figure 82.– Concluded.

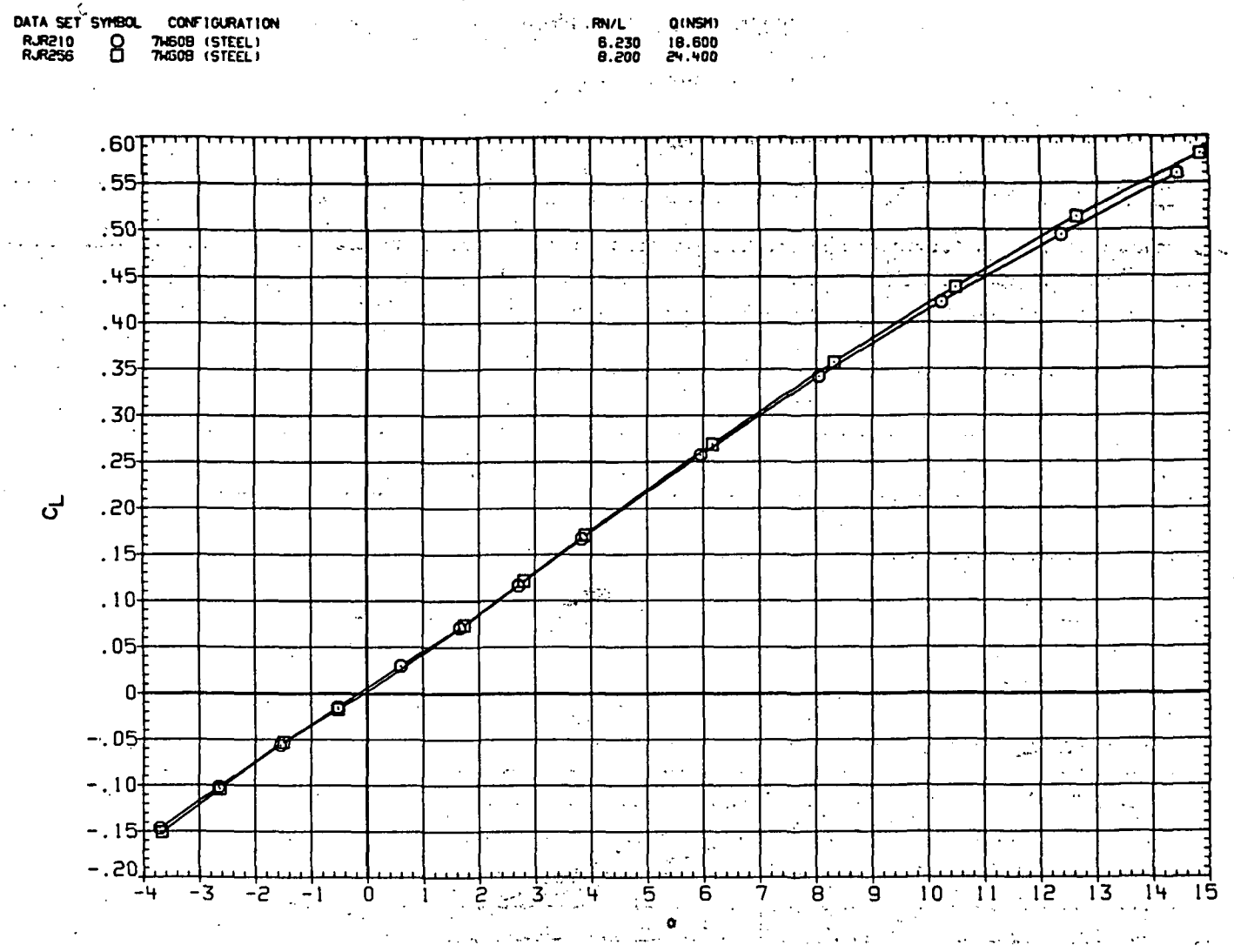

(a) C_L vs α.

Figure 83.– Dynamic-pressure effects on the aerodynamic characteristics of the steel trapezoidal oblique wing-body combination ($\Lambda = 60°$, $M = 1.6$ and the NACA 65A204 airfoil).

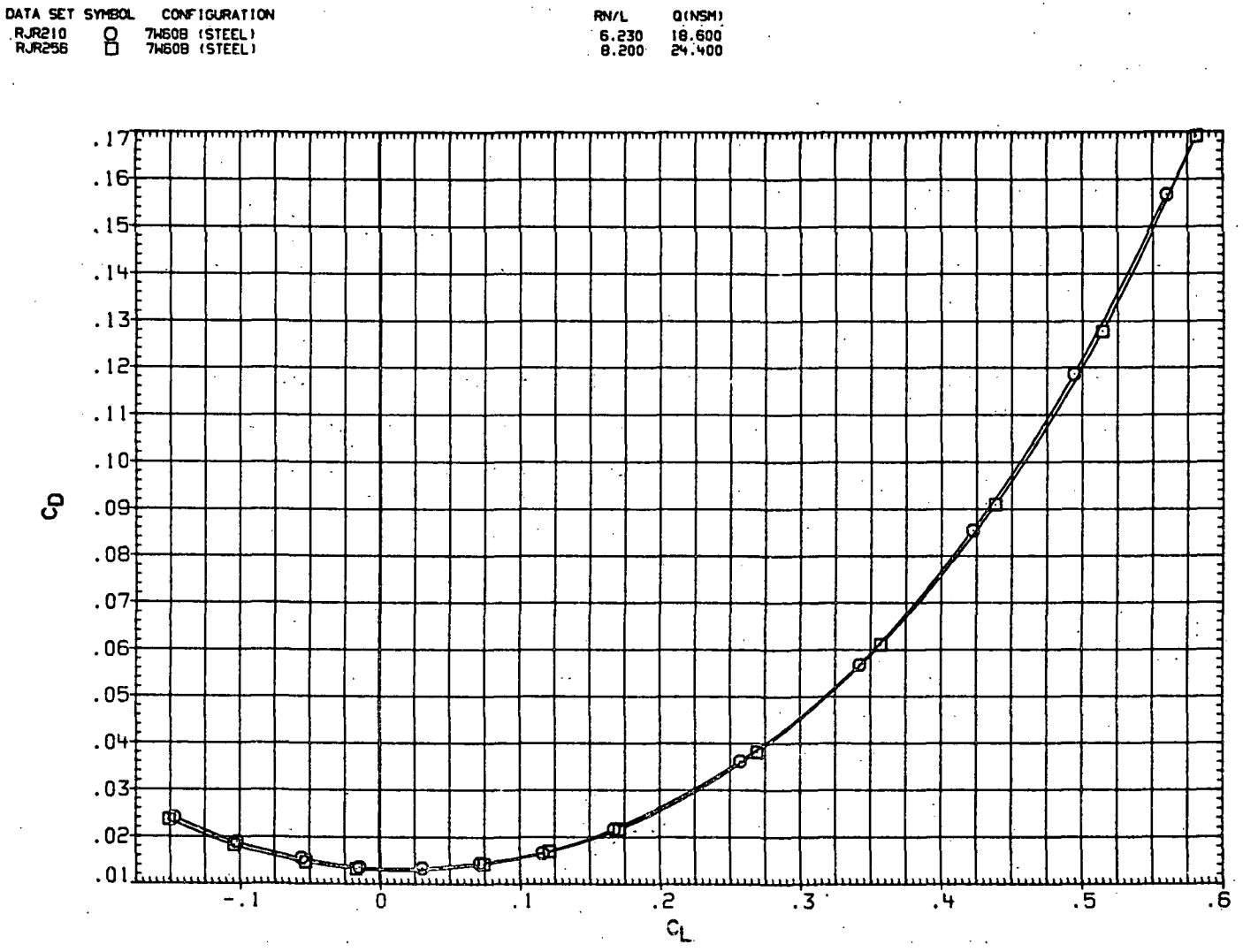

(b) C_D vs C_L.

Figure 83.– Continued.

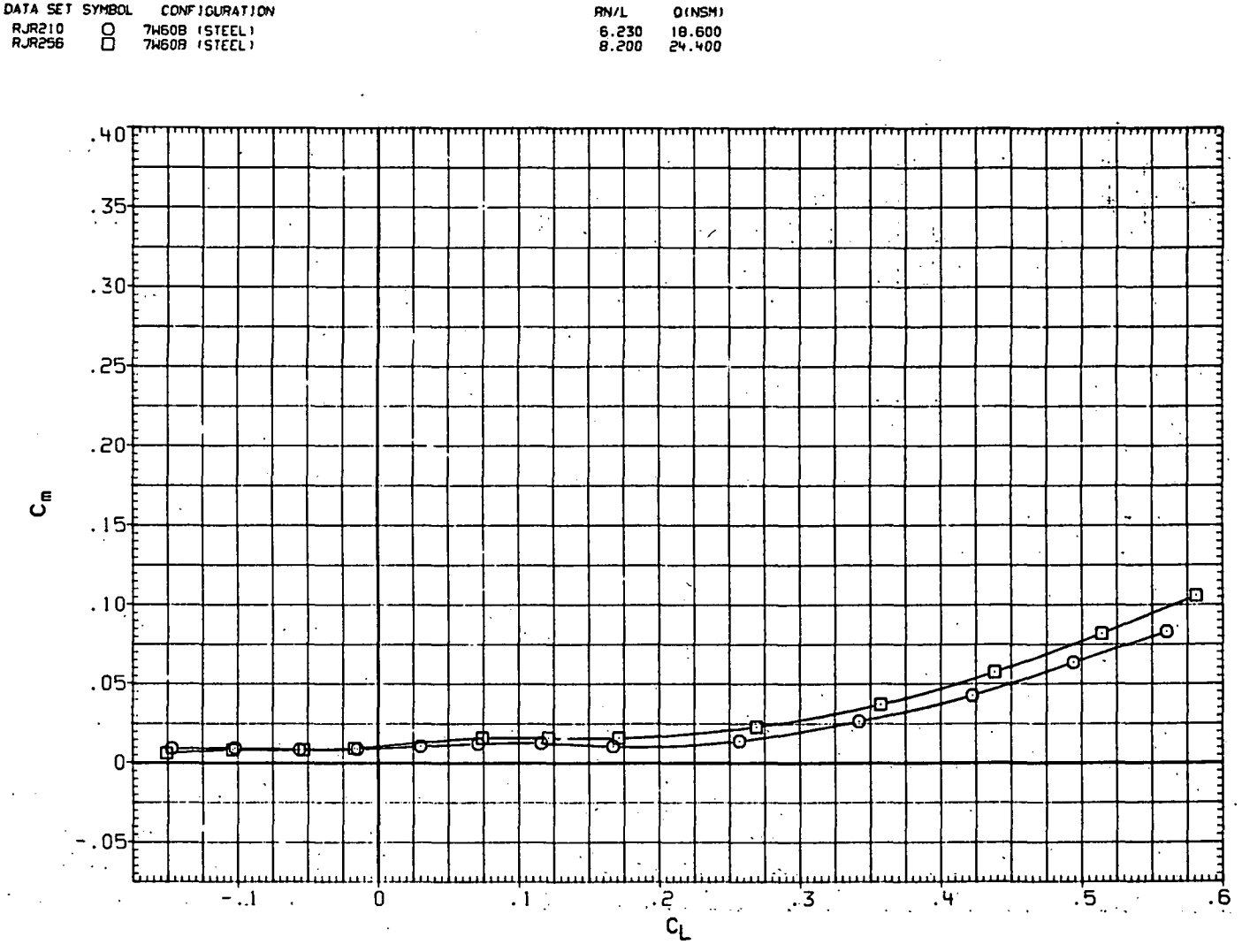

(c) C_m vs C_L.

Figure 83.– Continued.

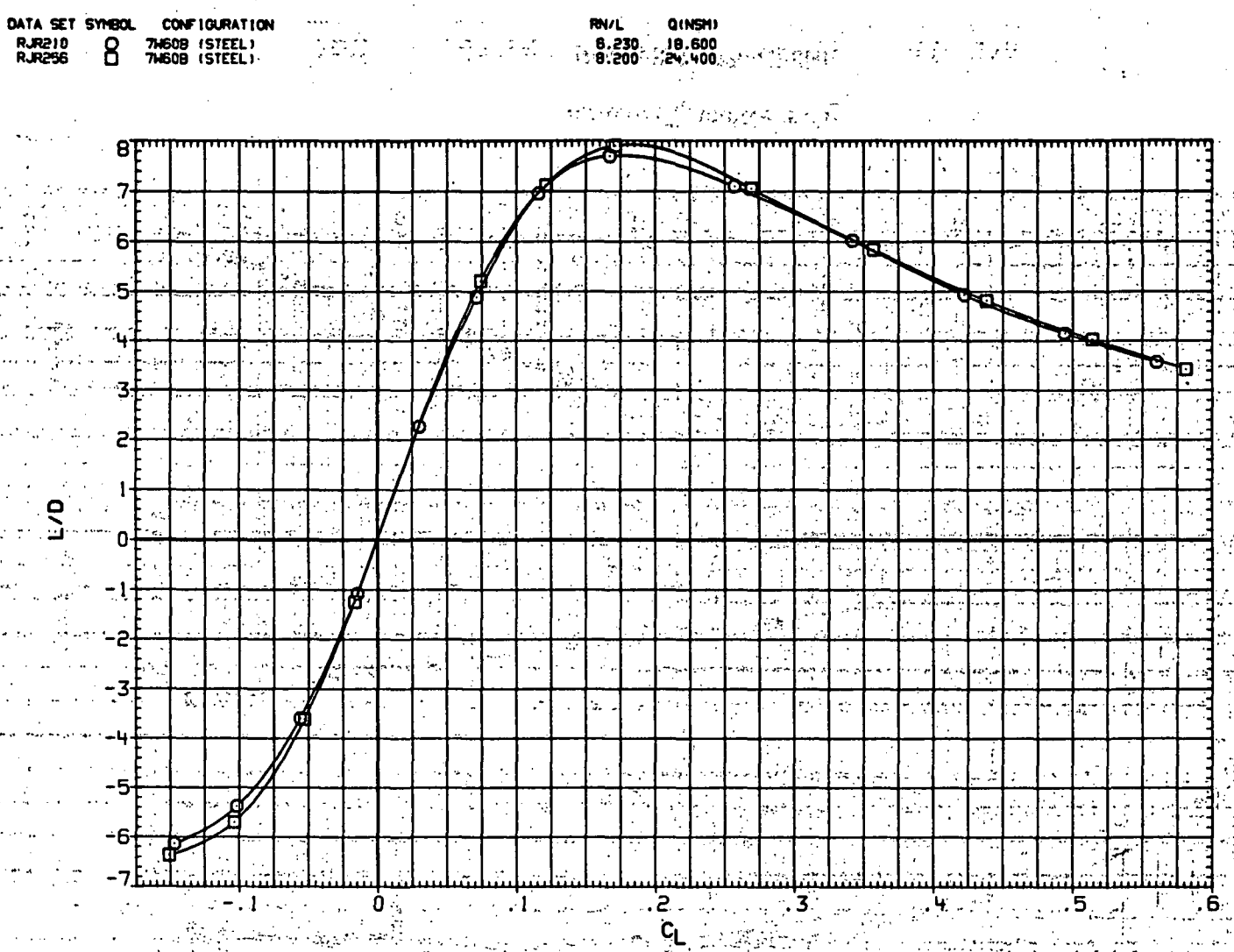

(d) L/D vs C_L.

Figure 83.– Continued.

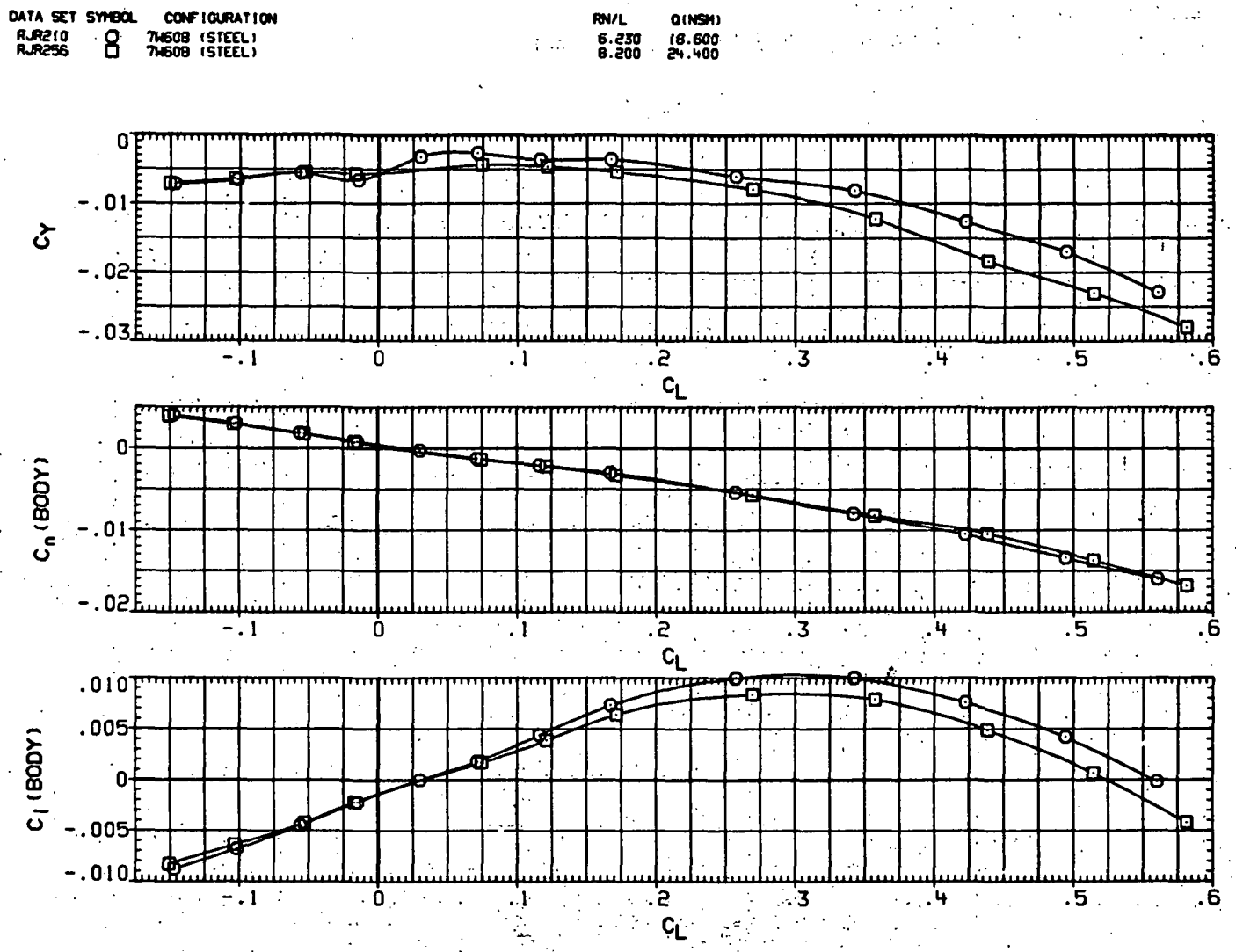

(e) C_Y, C_n and C_ℓ vs C_L.

Figure 83.– Concluded.

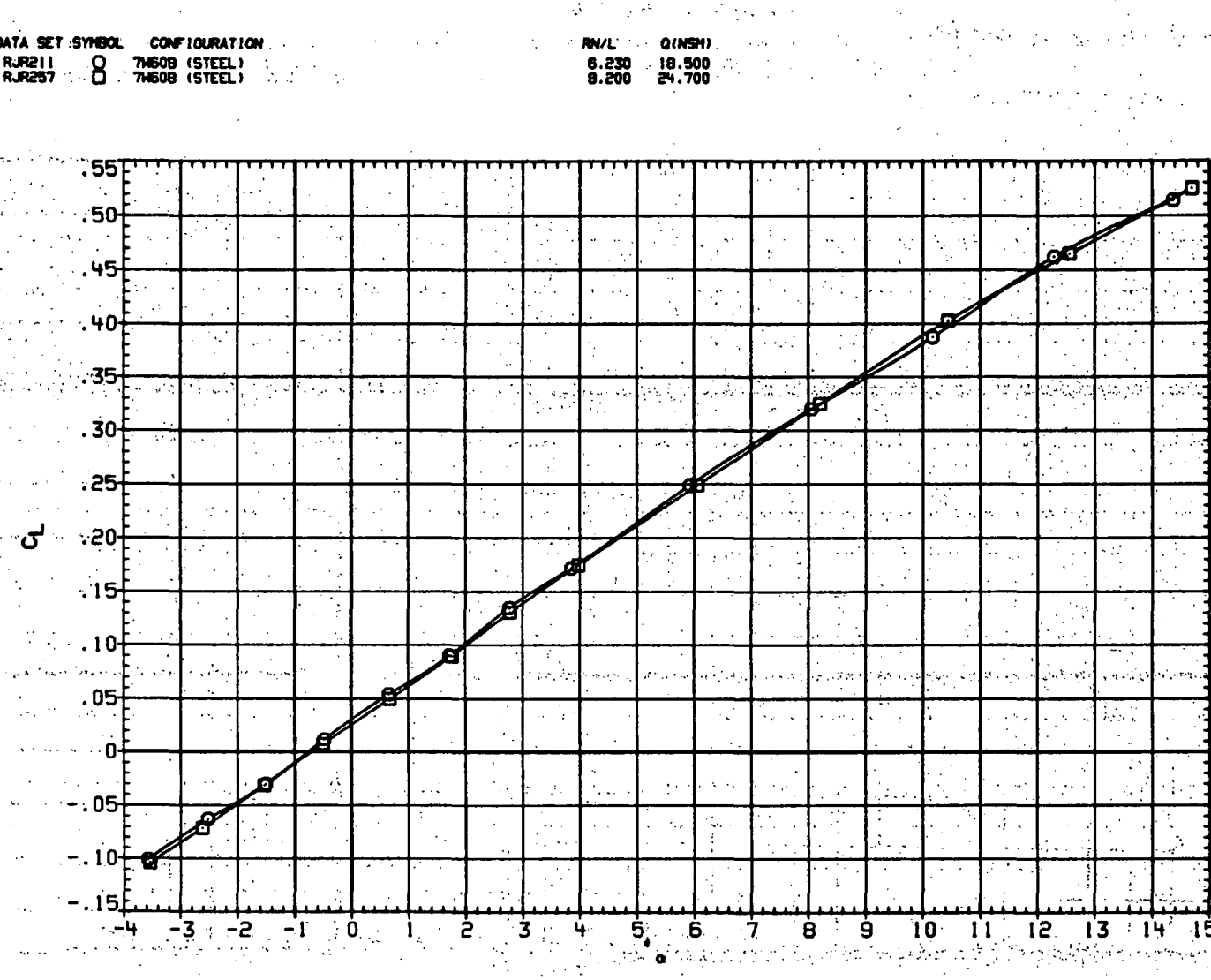

(a) C_L vs α.

Figure 84.– Dynamic-pressure effects on the aerodynamic characteristics of the steel trapezoidal oblique wing-body combination ($\Lambda = 60°$, $M = 2.0$ and the NACA 65A204 airfoil).

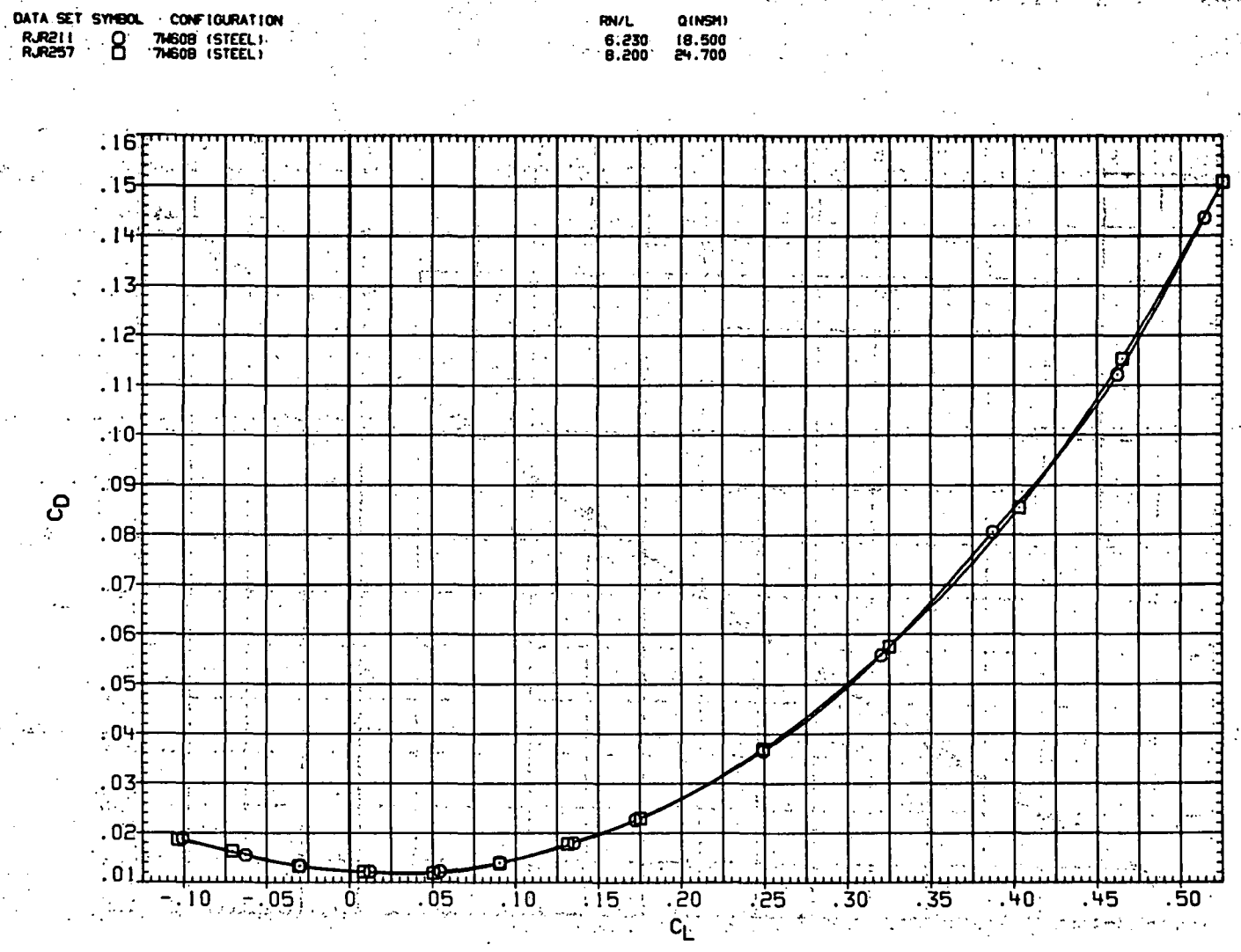

(b) C_D vs C_L.

Figure 84.– Continued.

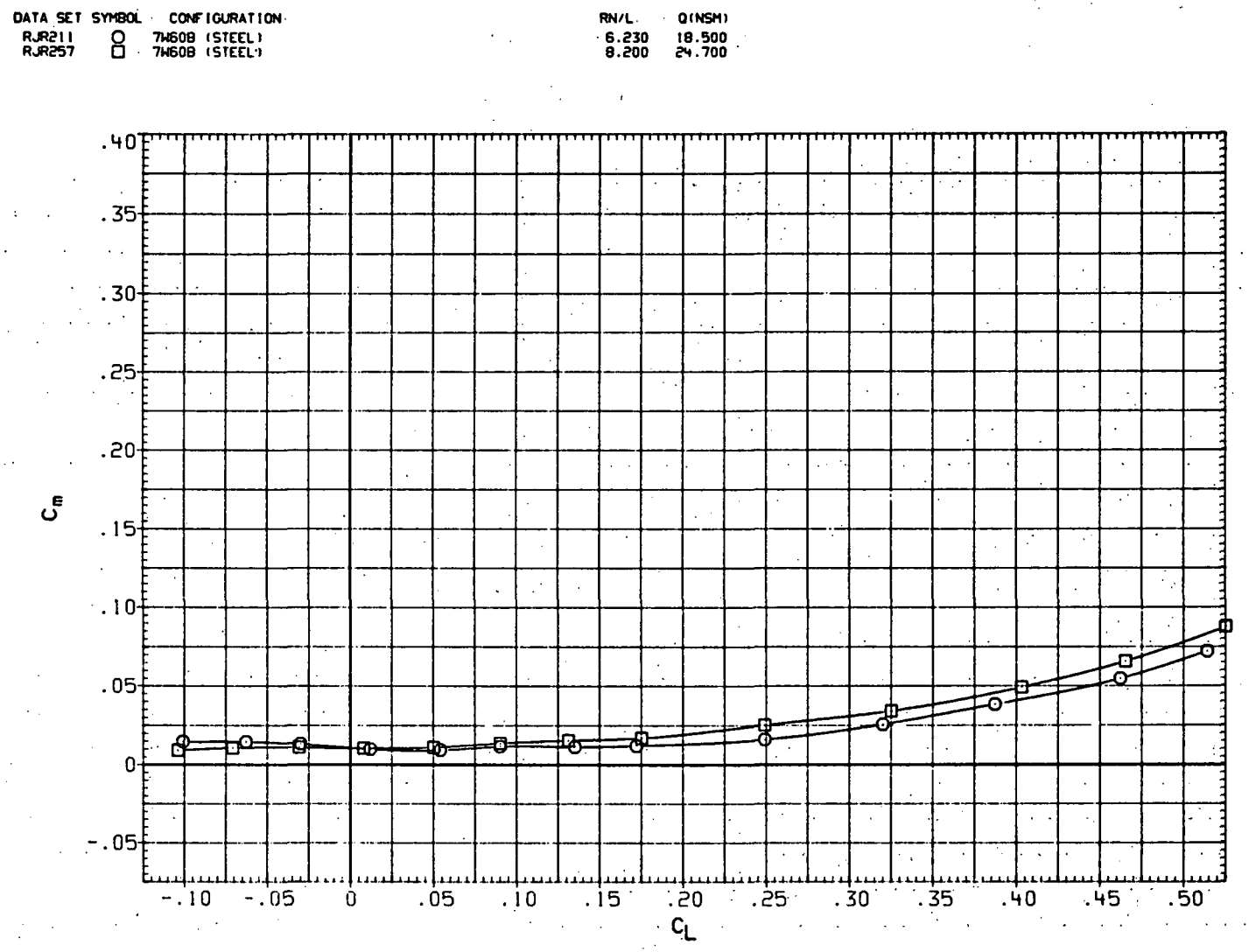

(c) C_m vs C_L.

Figure 84.– Continued.

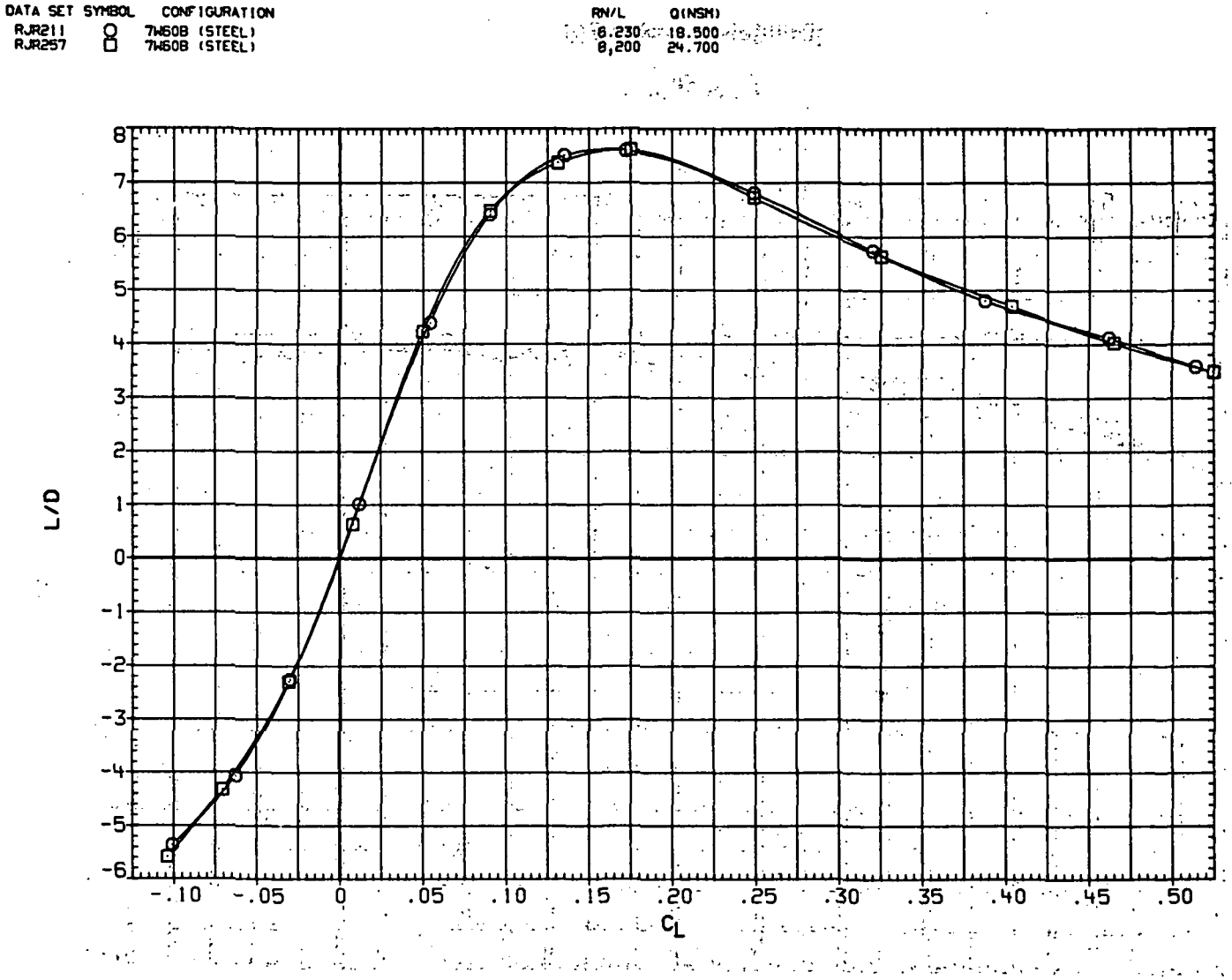

(d) L/D vs C_L.

Figure 84.—Continued.

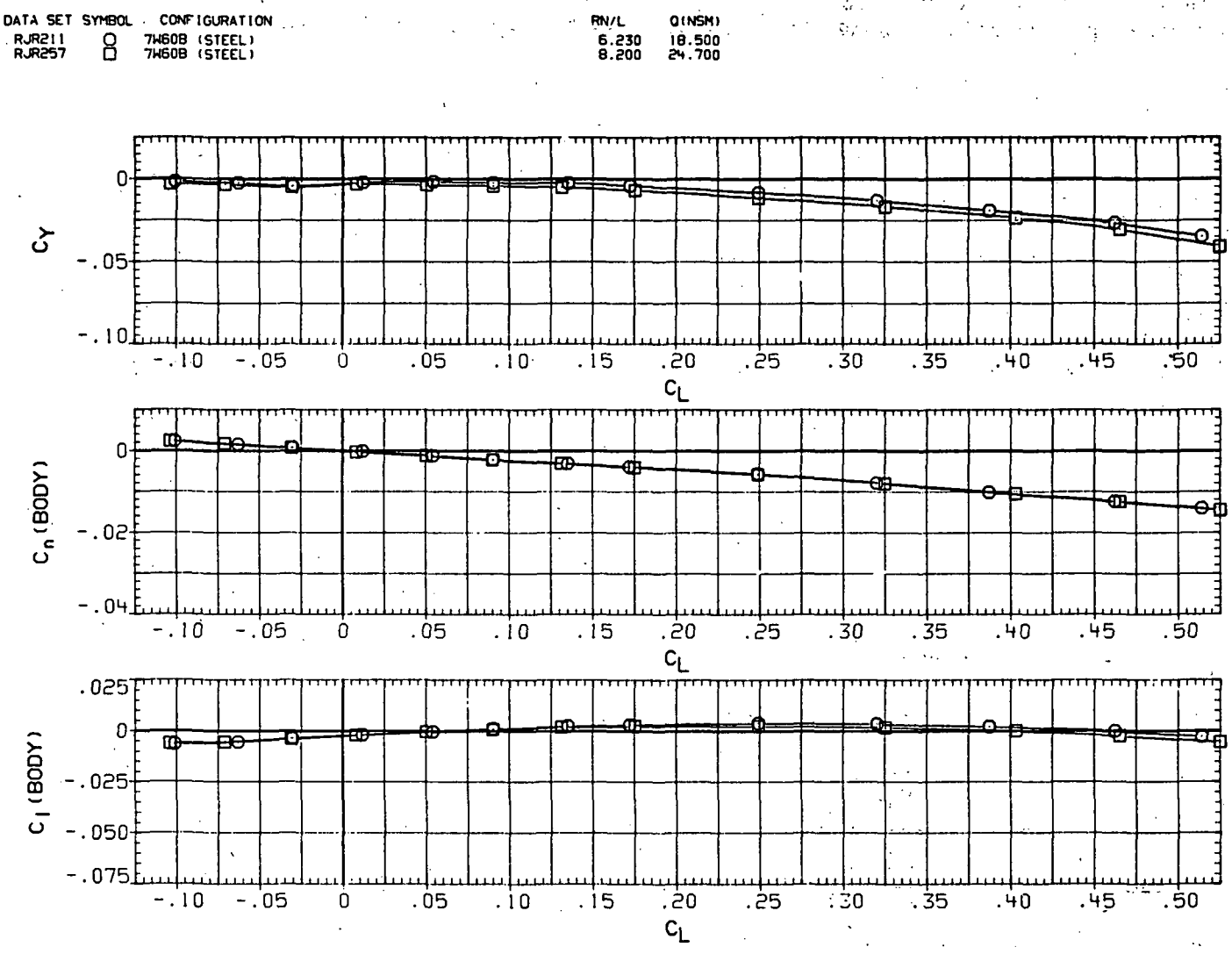

(e) C_Y, C_n and C_ℓ vs C_L.

Figure 84.– Concluded.

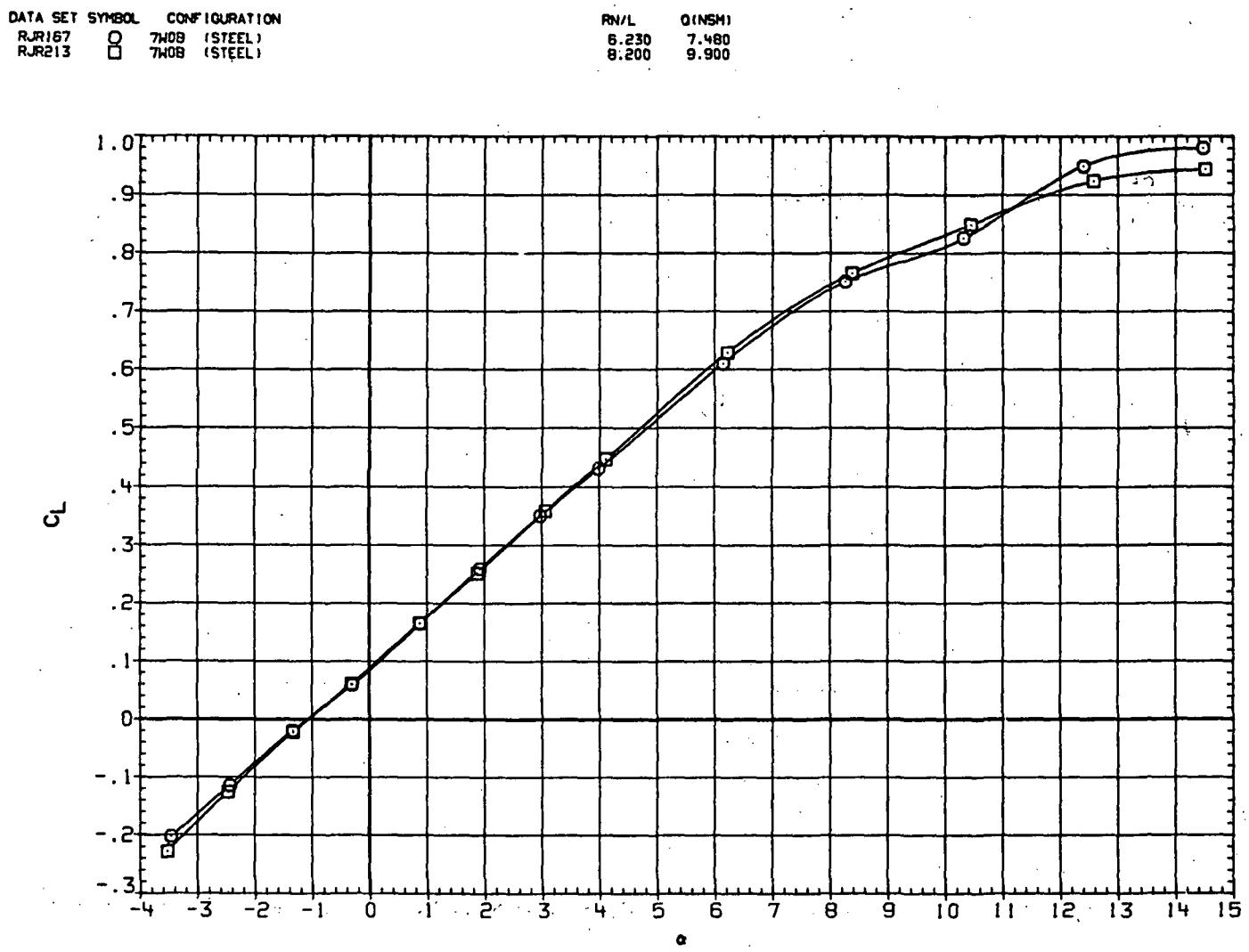

(a) C_L vs α.

Figure 85.– Dynamic-pressure effects on the aerodynamic characteristics of the steel trapezoidal oblique wing-body combination ($\Lambda = 0, M = 0.4$ and the NACA 65A204 airfoil).

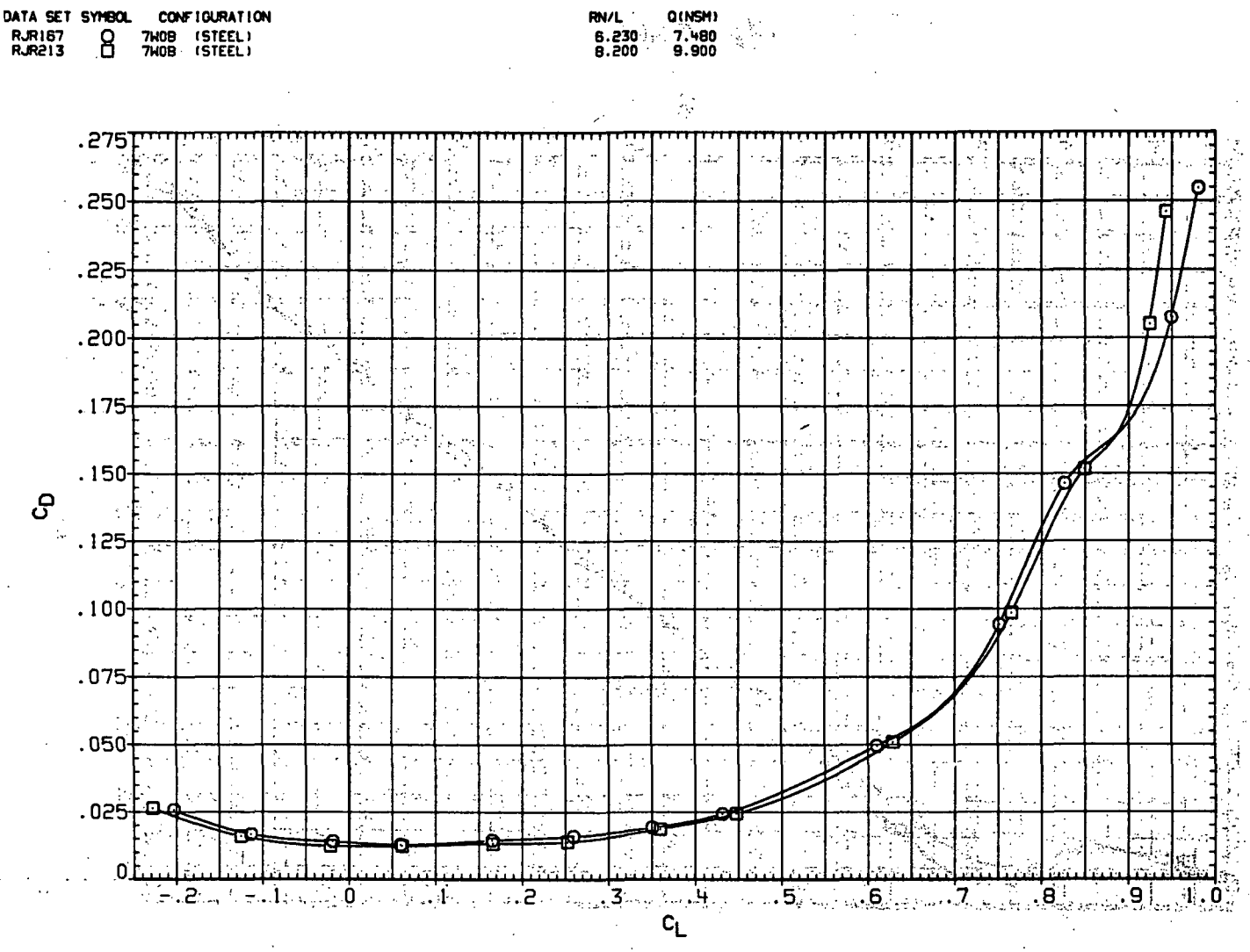

(b) C_D vs C_L.

Figure 85.– Continued.

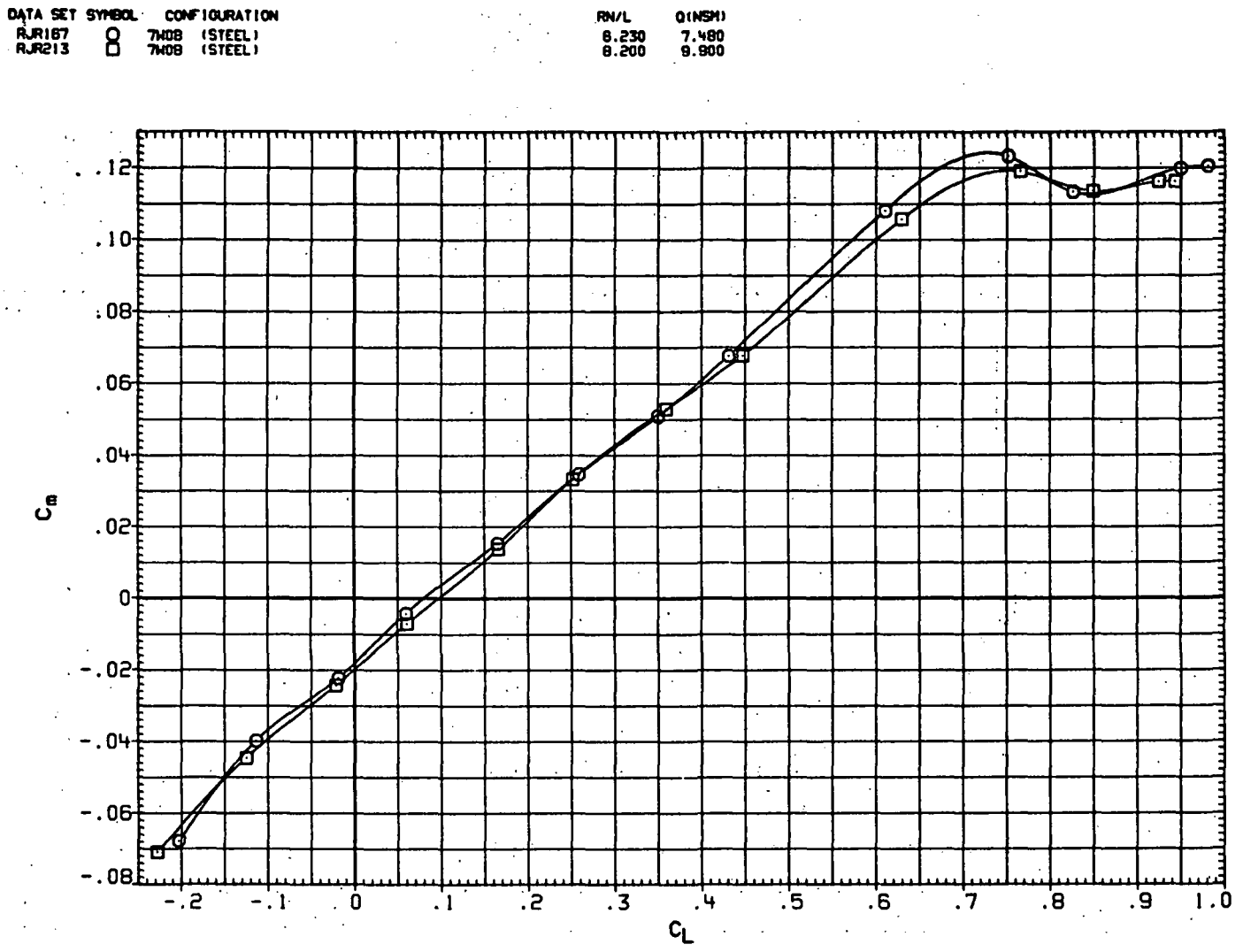

(c) C_m vs C_L.

Figure 85.– Continued.

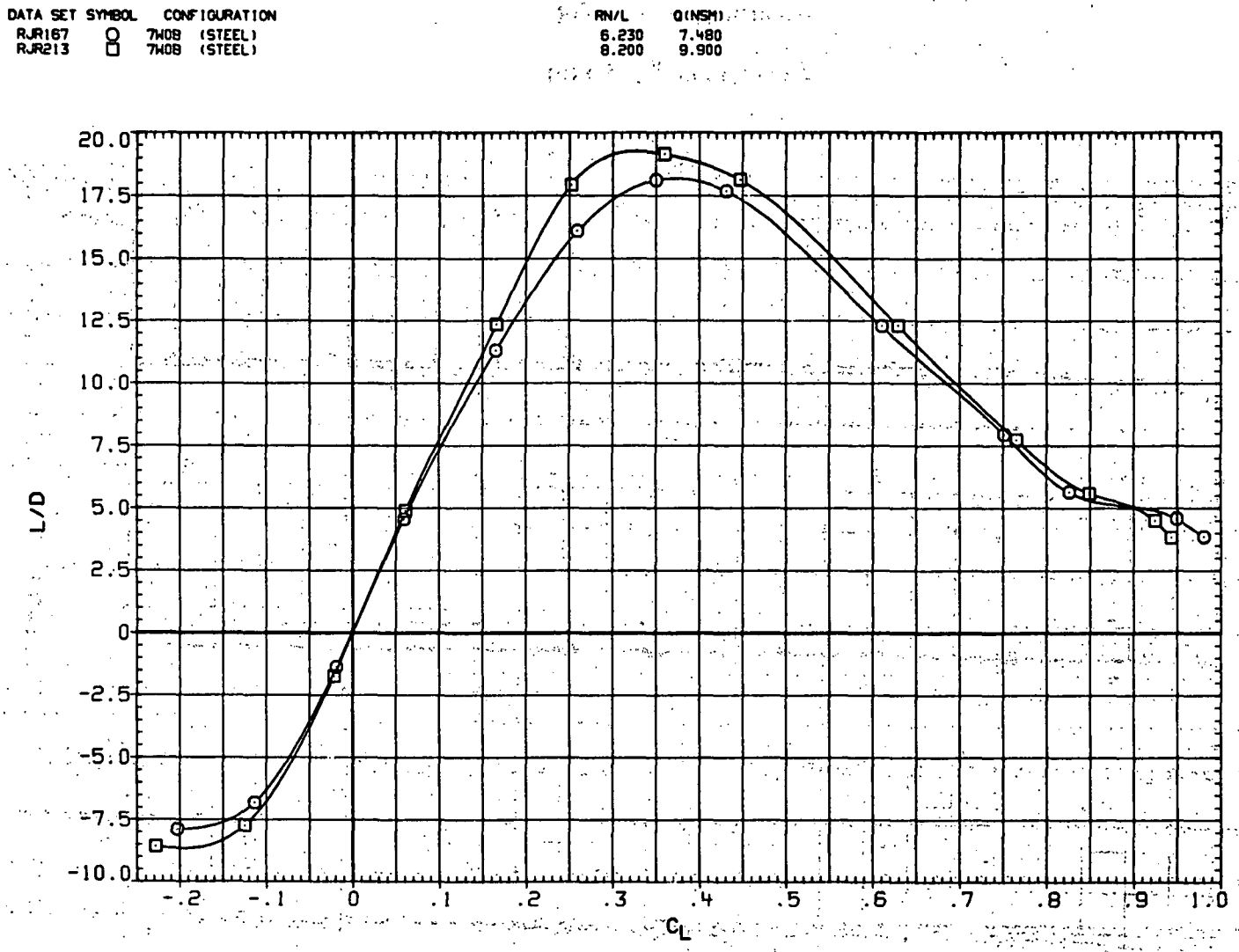

(d) L/D vs C_L.

Figure 85.– Continued.

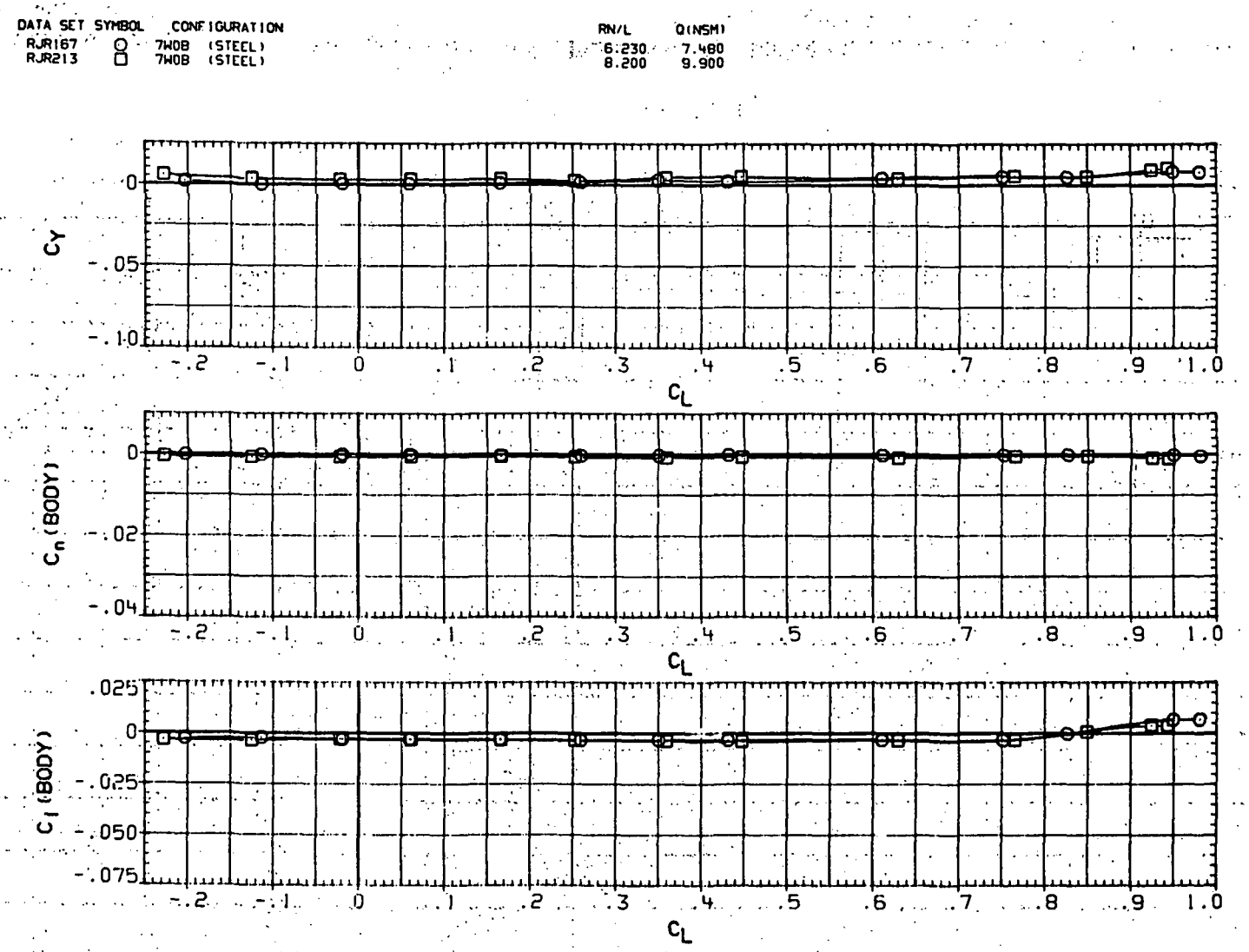

(e) C_Y, C_n and C_ℓ vs C_L.

Figure 85.– Concluded.

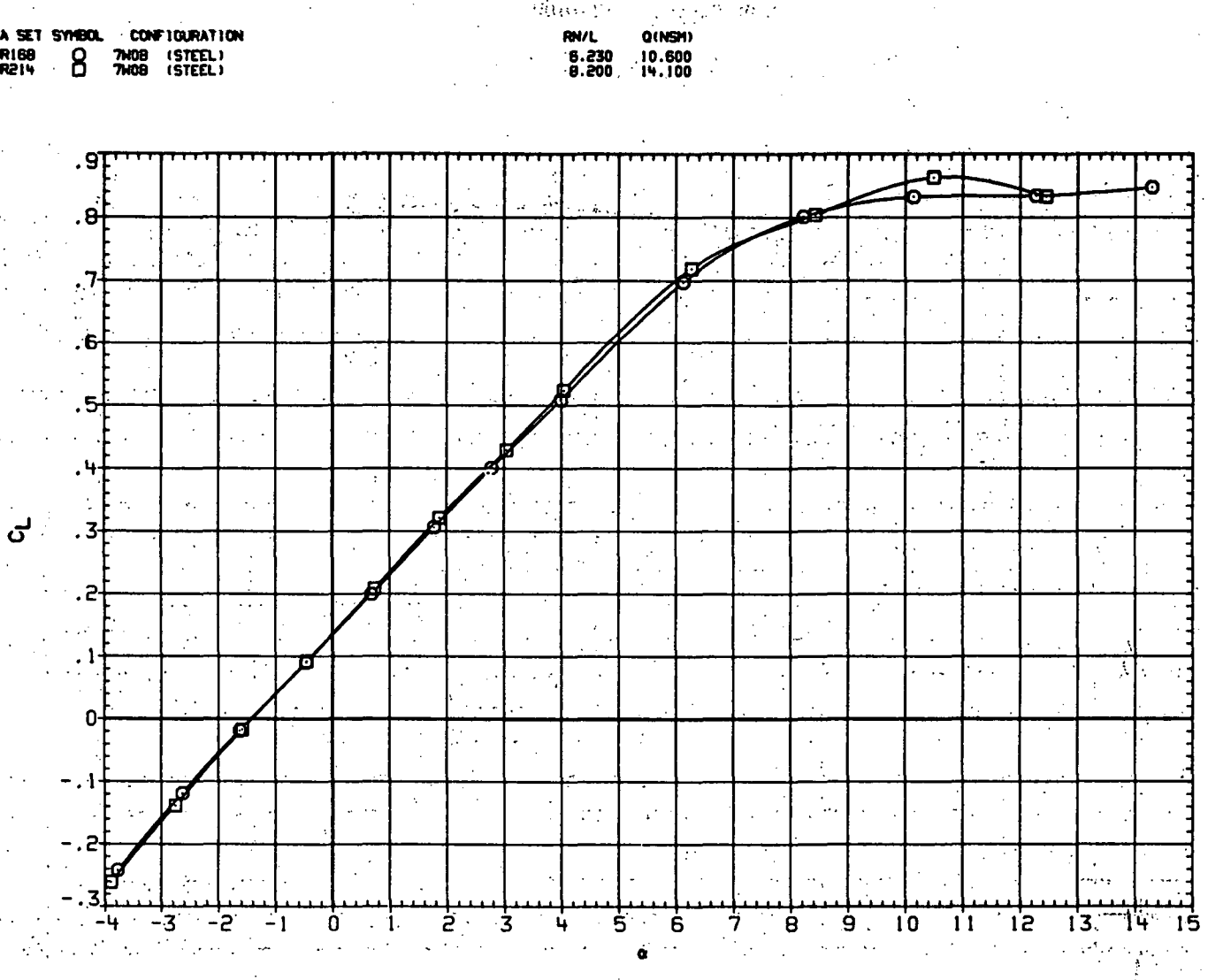

(a) C_L vs α.

Figure 86.– Dynamic-pressure effects on the aerodynamic characteristics of the steel trapezoidal oblique wing-body combination ($\Lambda = 0, M = 0.6$ and the NACA 65A204 airfoil).

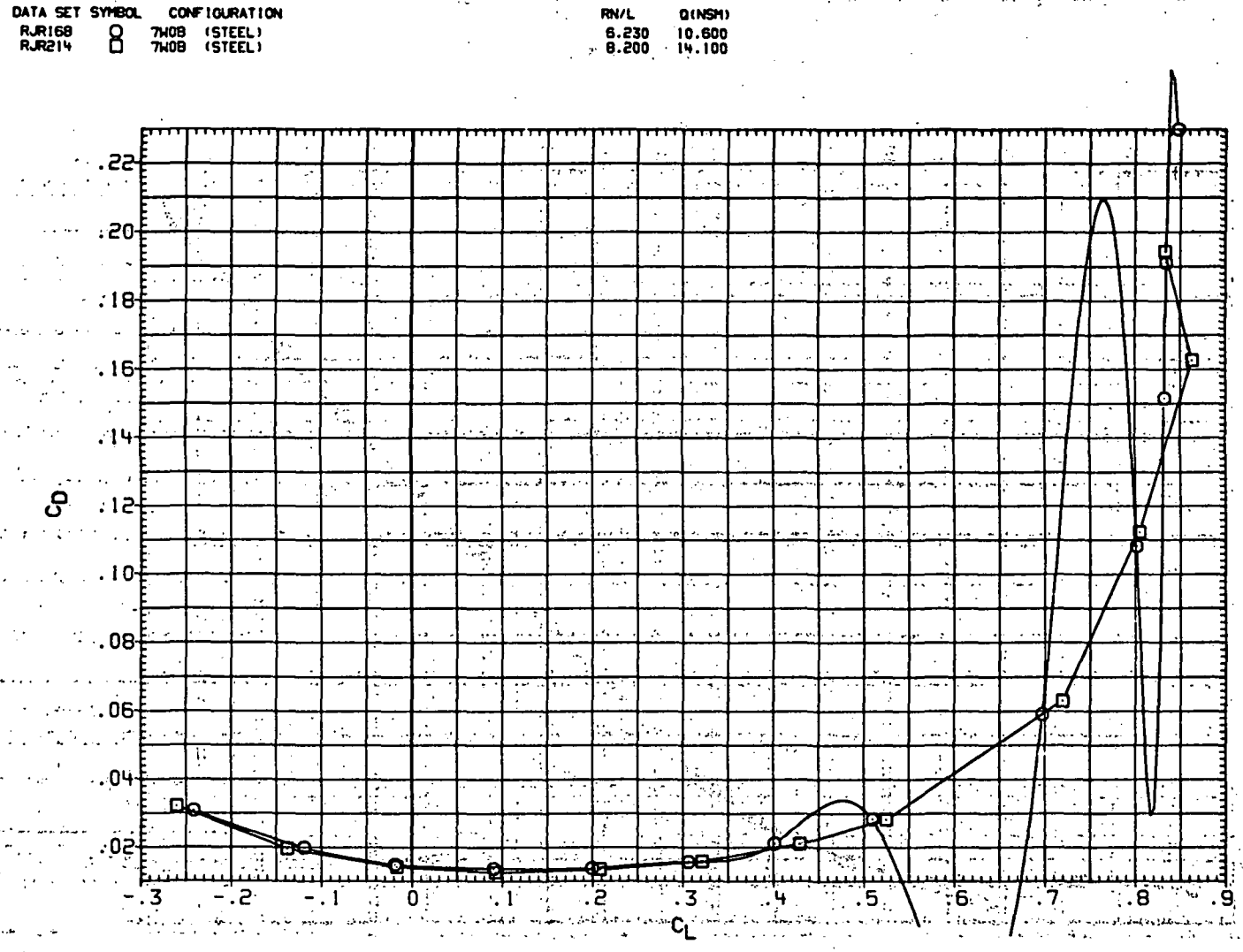

(b) C_D vs C_L.

Figure 86.– Continued.

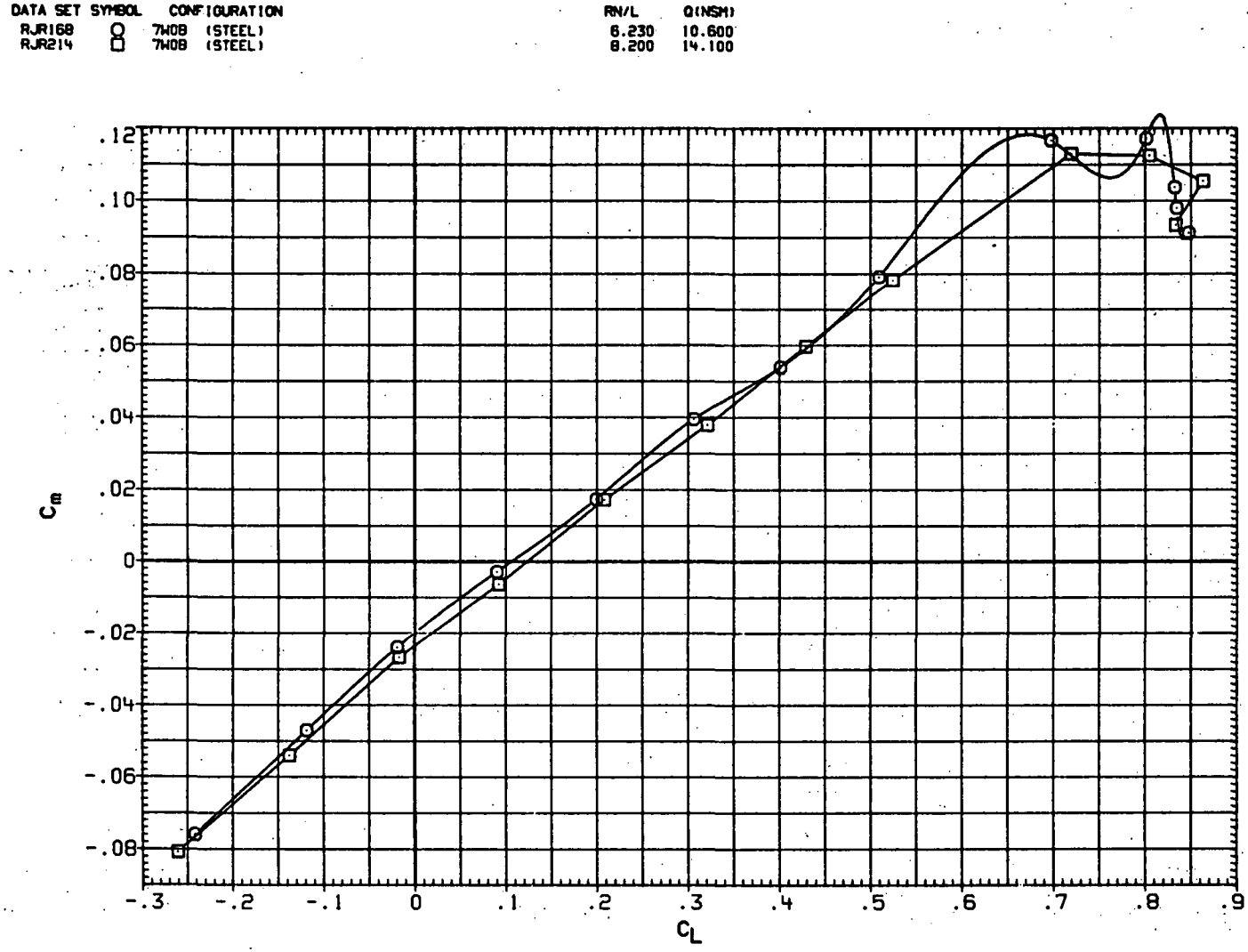

(c) C_m vs C_L.

Figure 86.– Continued.

(d) L/D vs C_L.

Figure 86.– Continued.

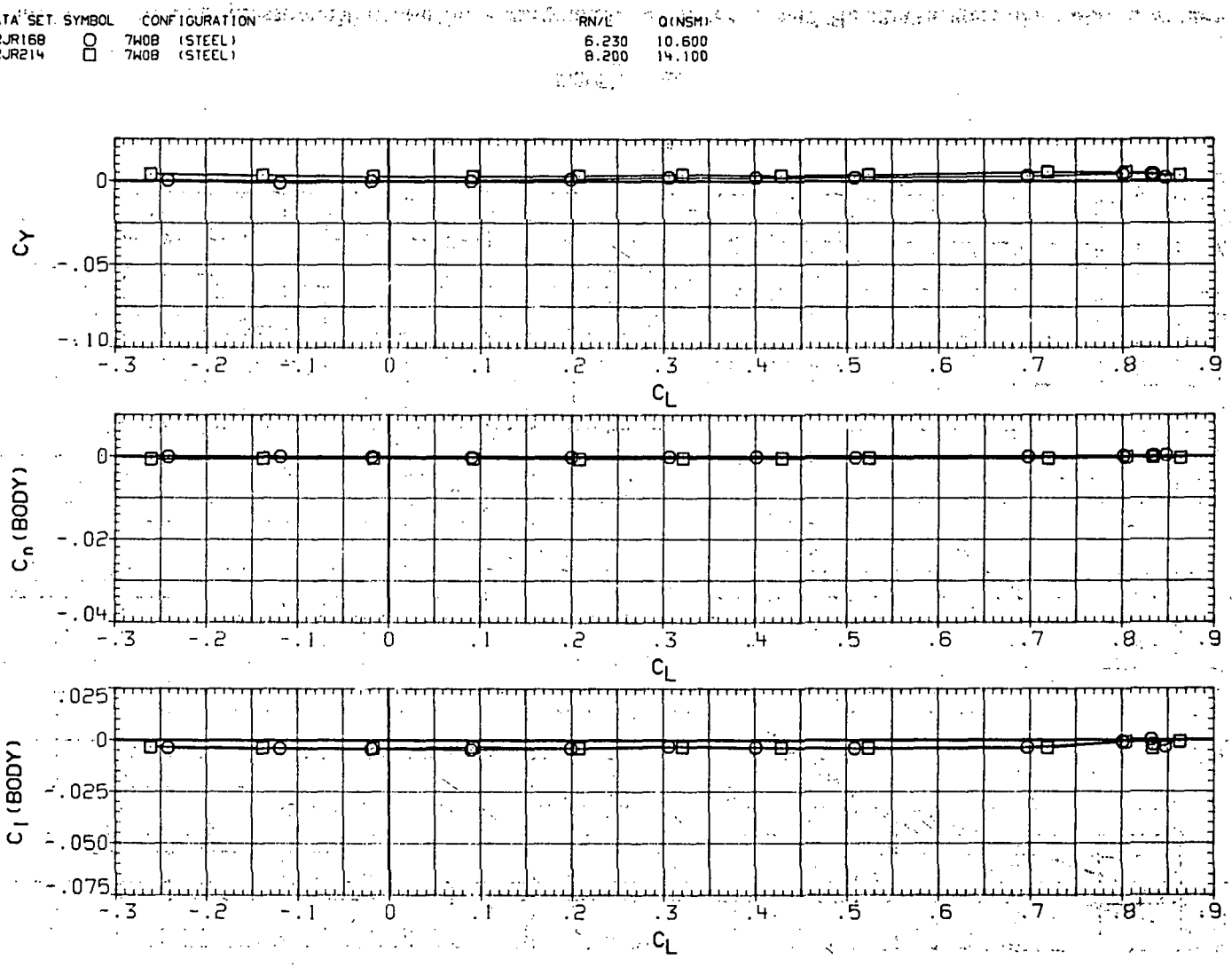

(e) C_Y, C_n and C_ℓ vs C_L.

Figure 86.– Concluded.

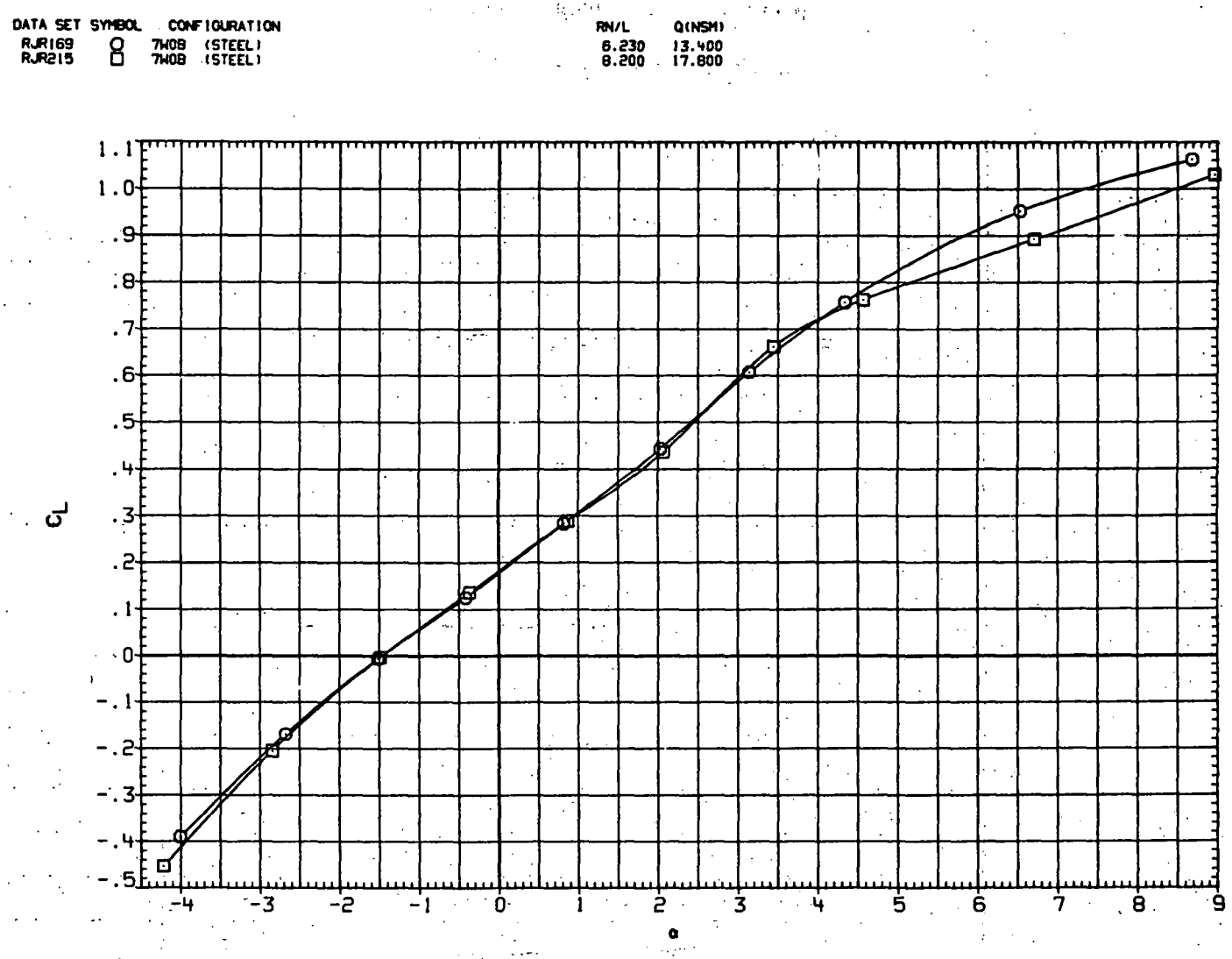

(a) C_L vs α.

Figure 87.– Dynamic-pressure effects on the aerodynamic characteristics of the steel trapezoidal oblique wing-body combination ($\Lambda = 0, M = 0.8$ and the NACA 65A204 airfoil).

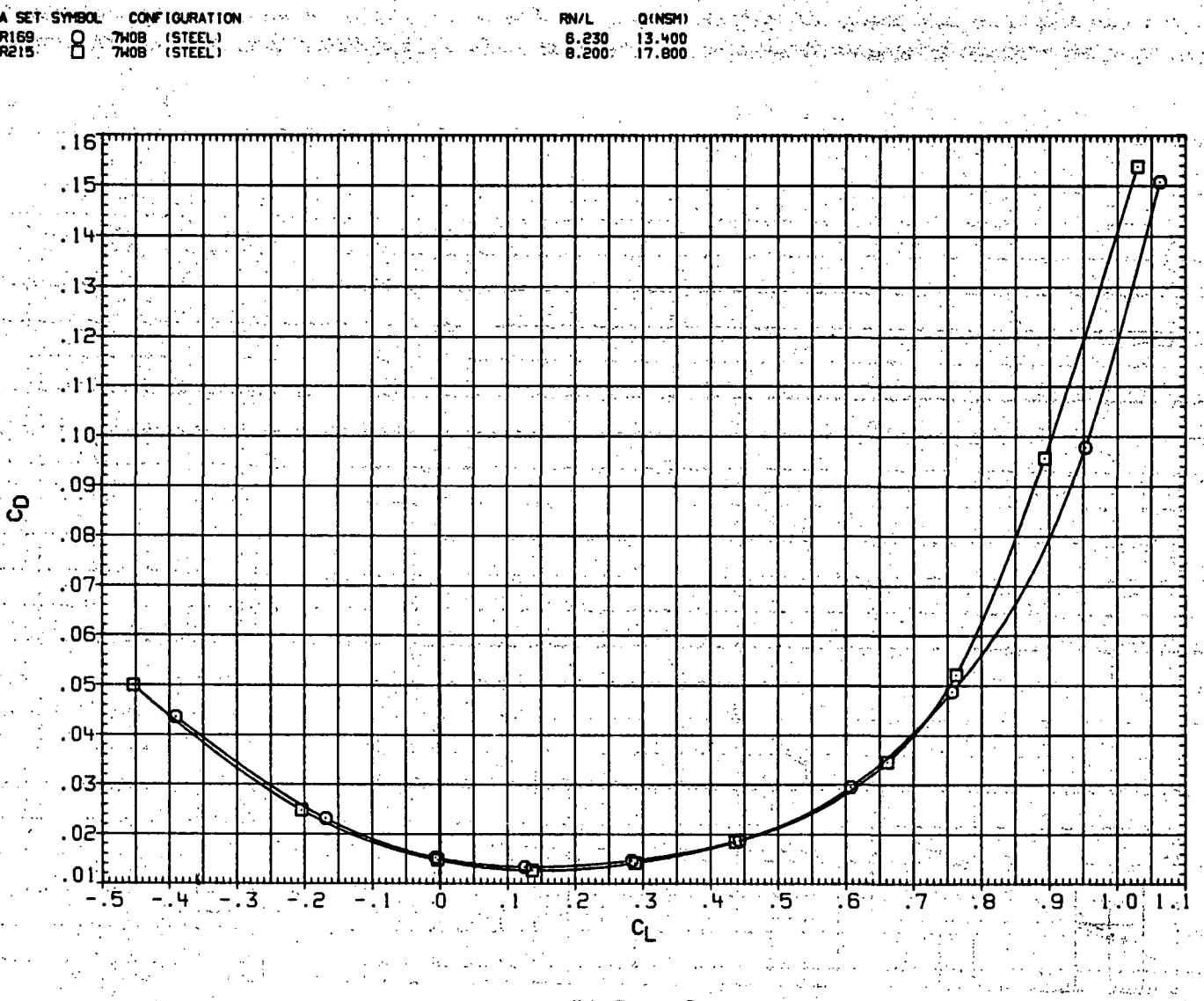

(b) C_D vs C_L.

Figure 87.– Continued.

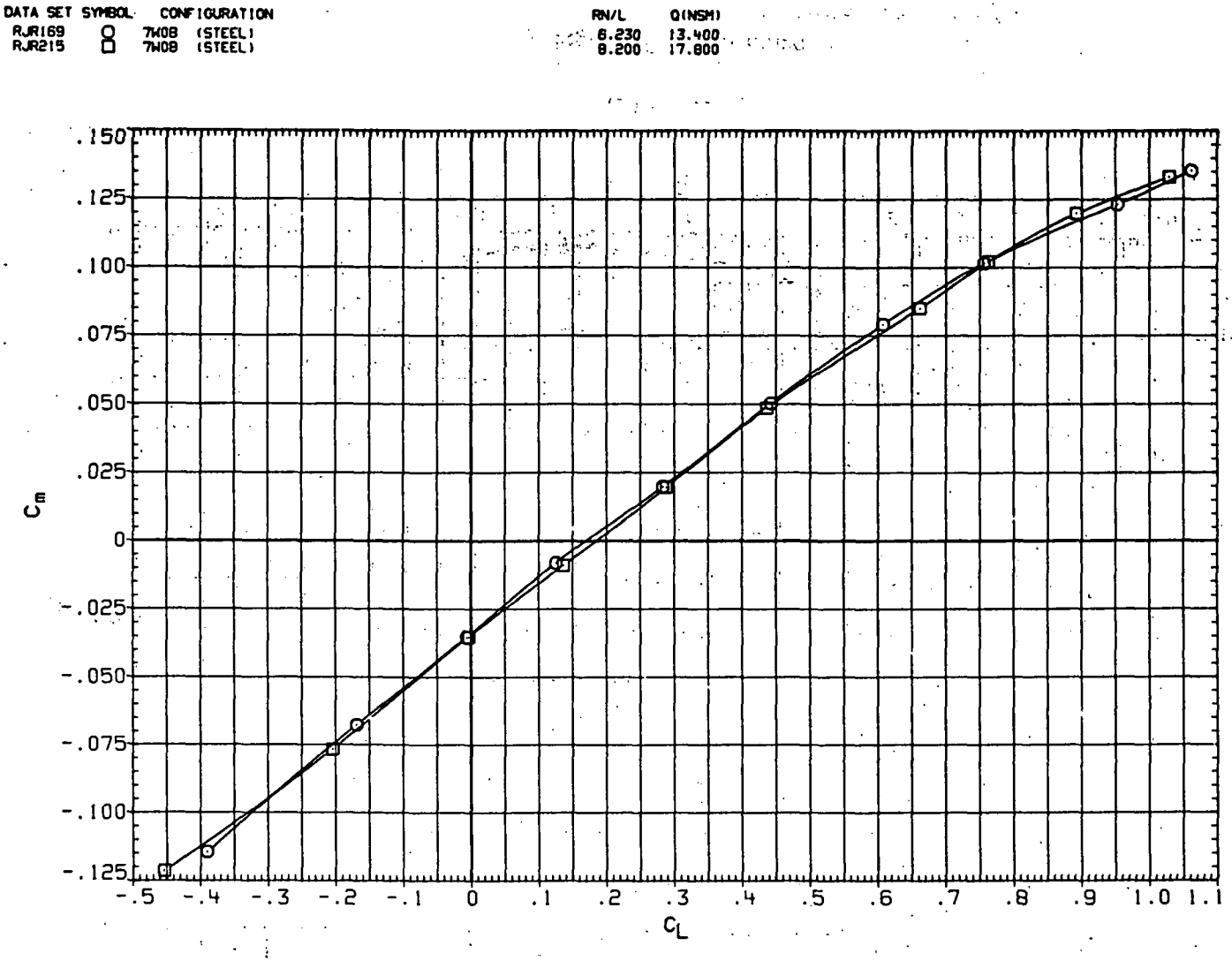

(c) C_m vs C_L.

Figure 87.– Continued.

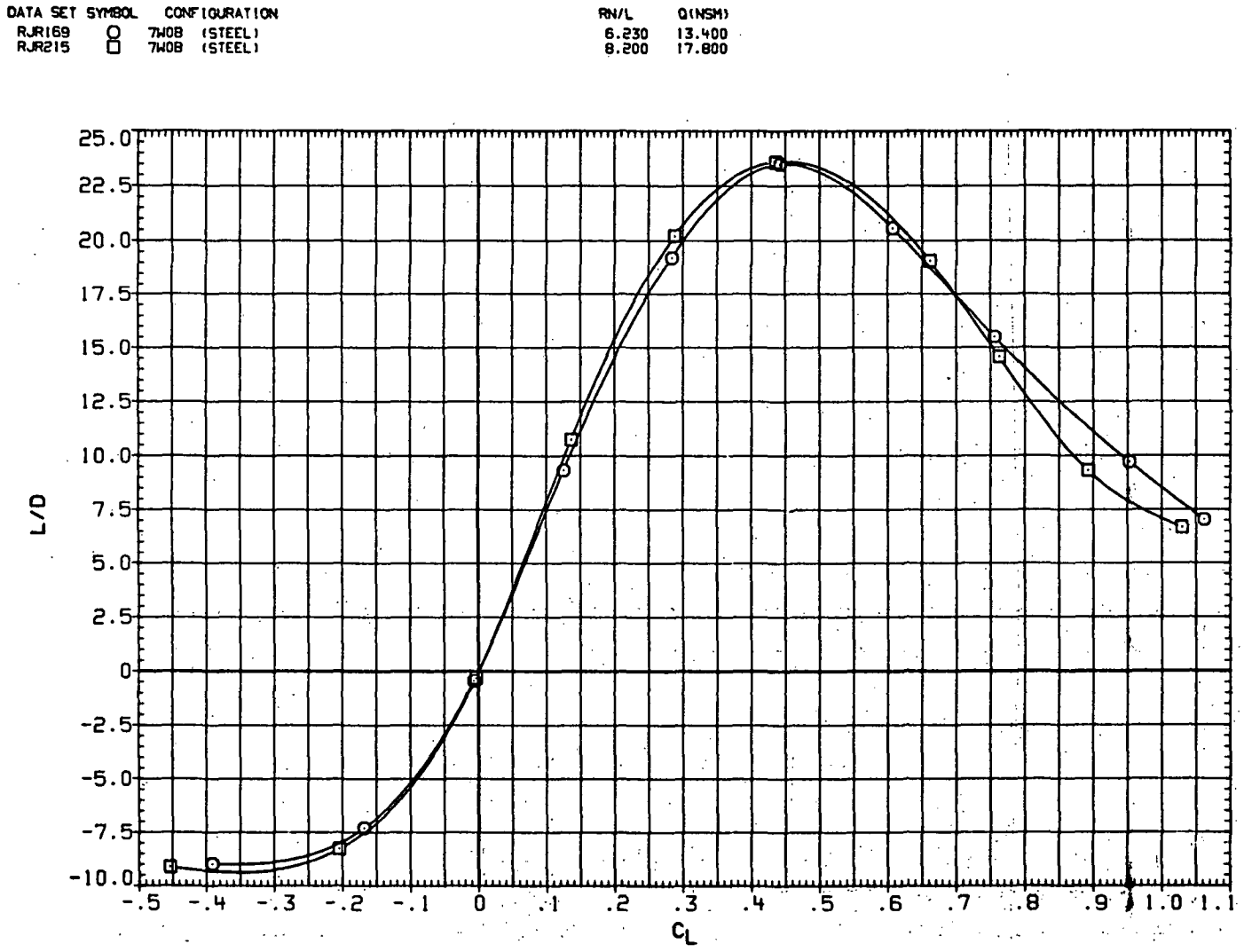

(d) L/D vs C_L.

Figure 87.– Continued.

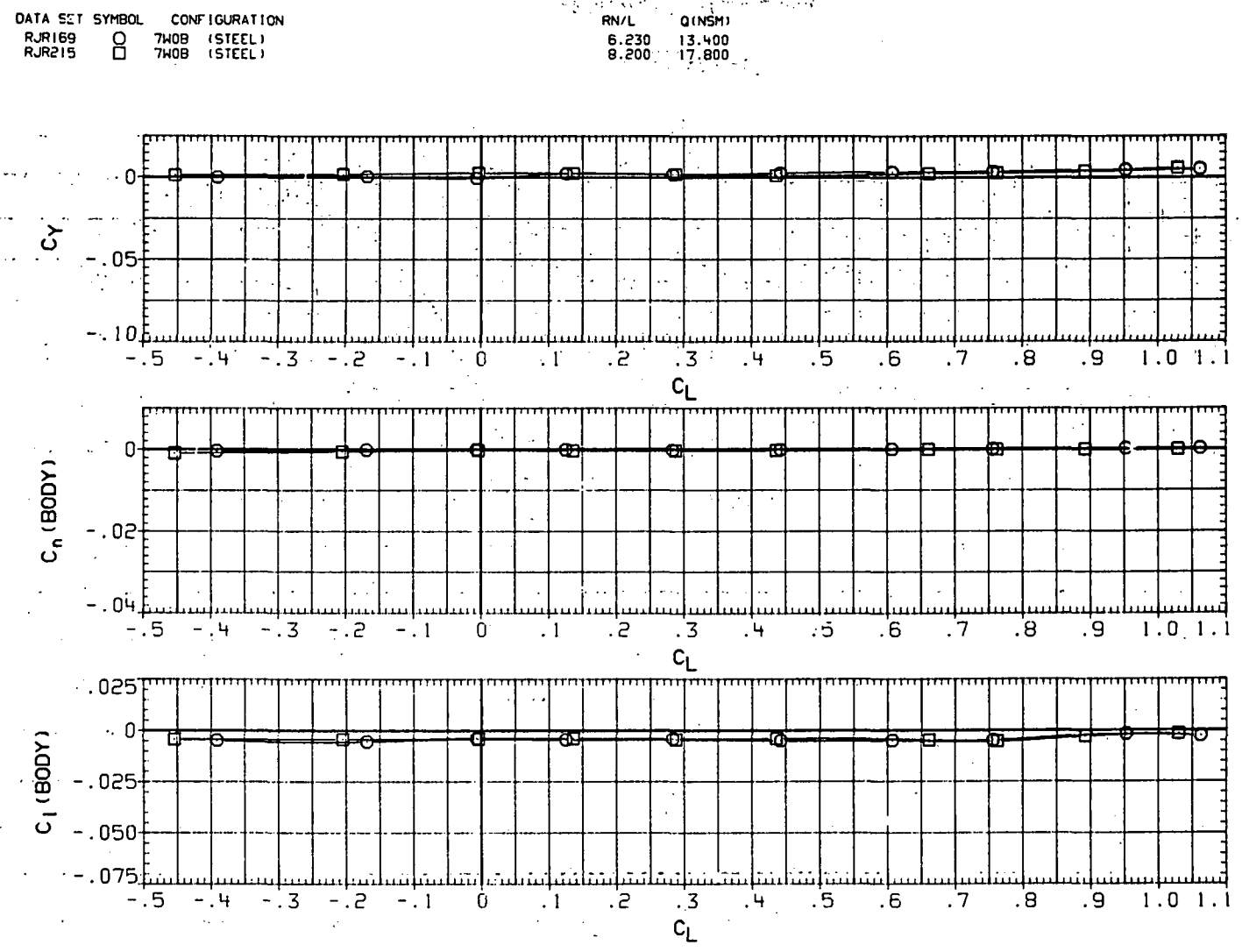

(e) C_Y, C_n and C_ℓ vs C_L.

Figure 87.– Concluded.

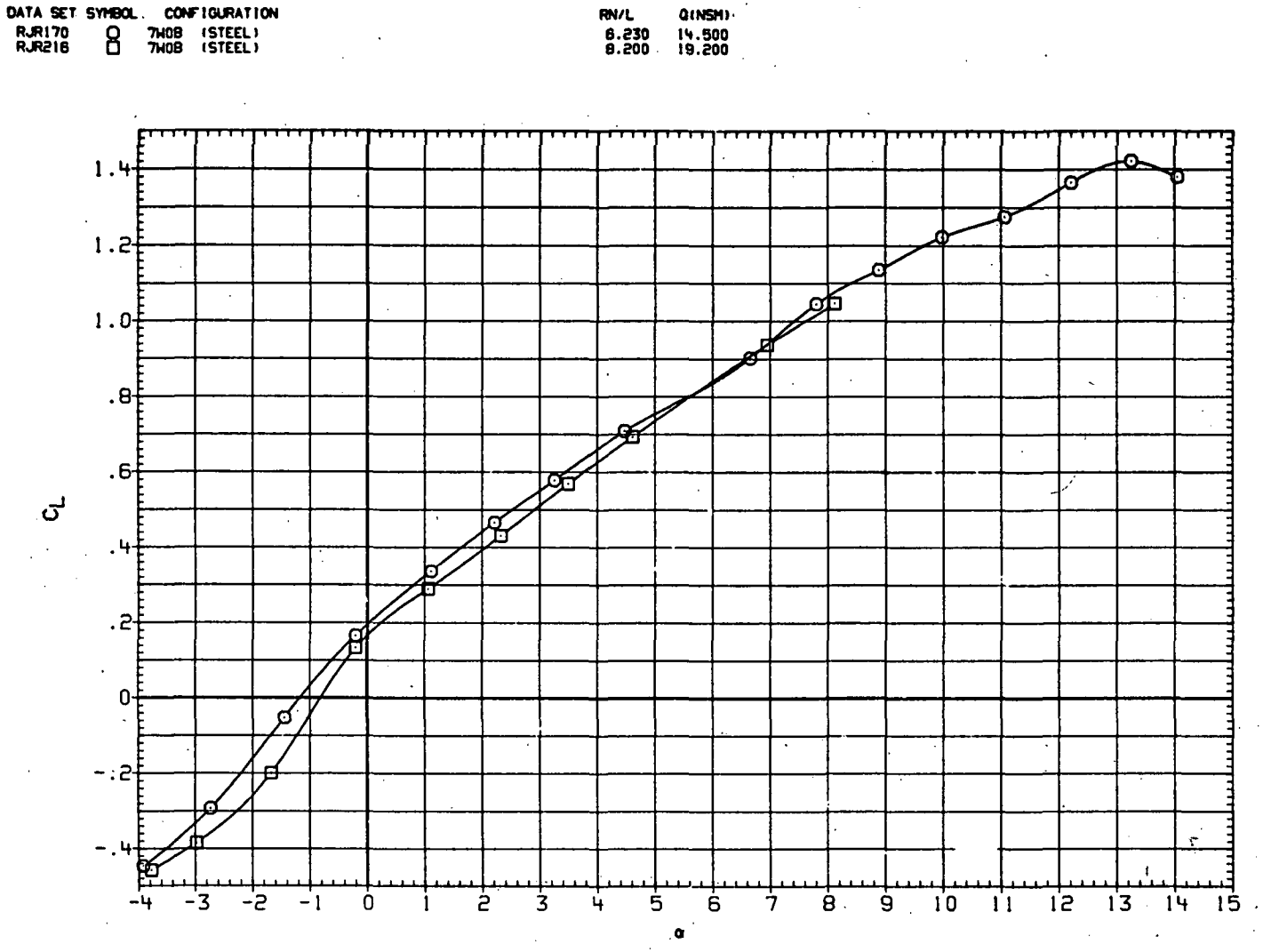

(a) C_L vs α.

Figure 88.– Dynamic-pressure effects on the aerodynamic characteristics of the steel trapezoidal oblique wing-body combination ($\Lambda = 0, M = 0.9$ and the NACA 65A204 airfoil).

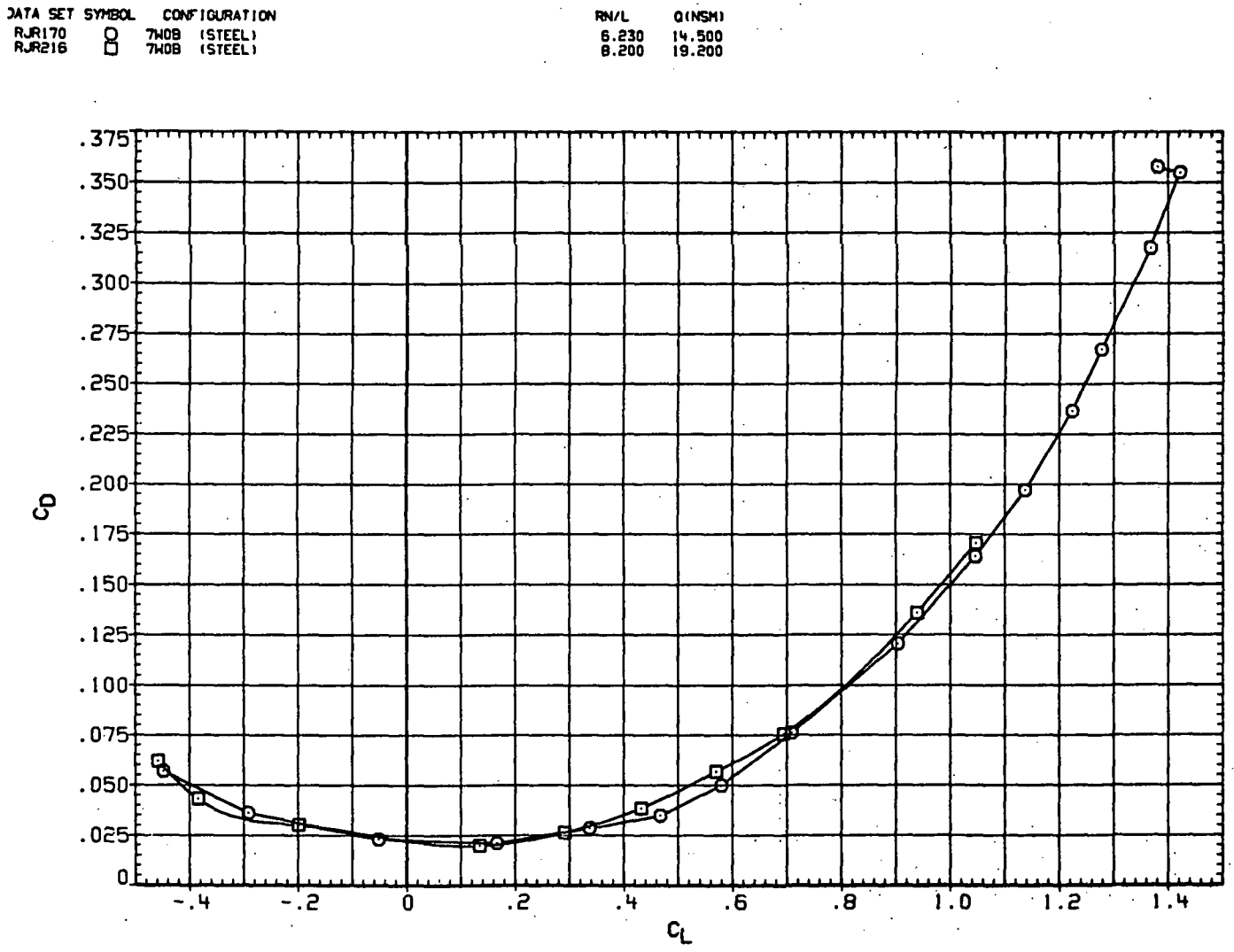

(b) C_D vs C_L.

Figure 88.– Continued.

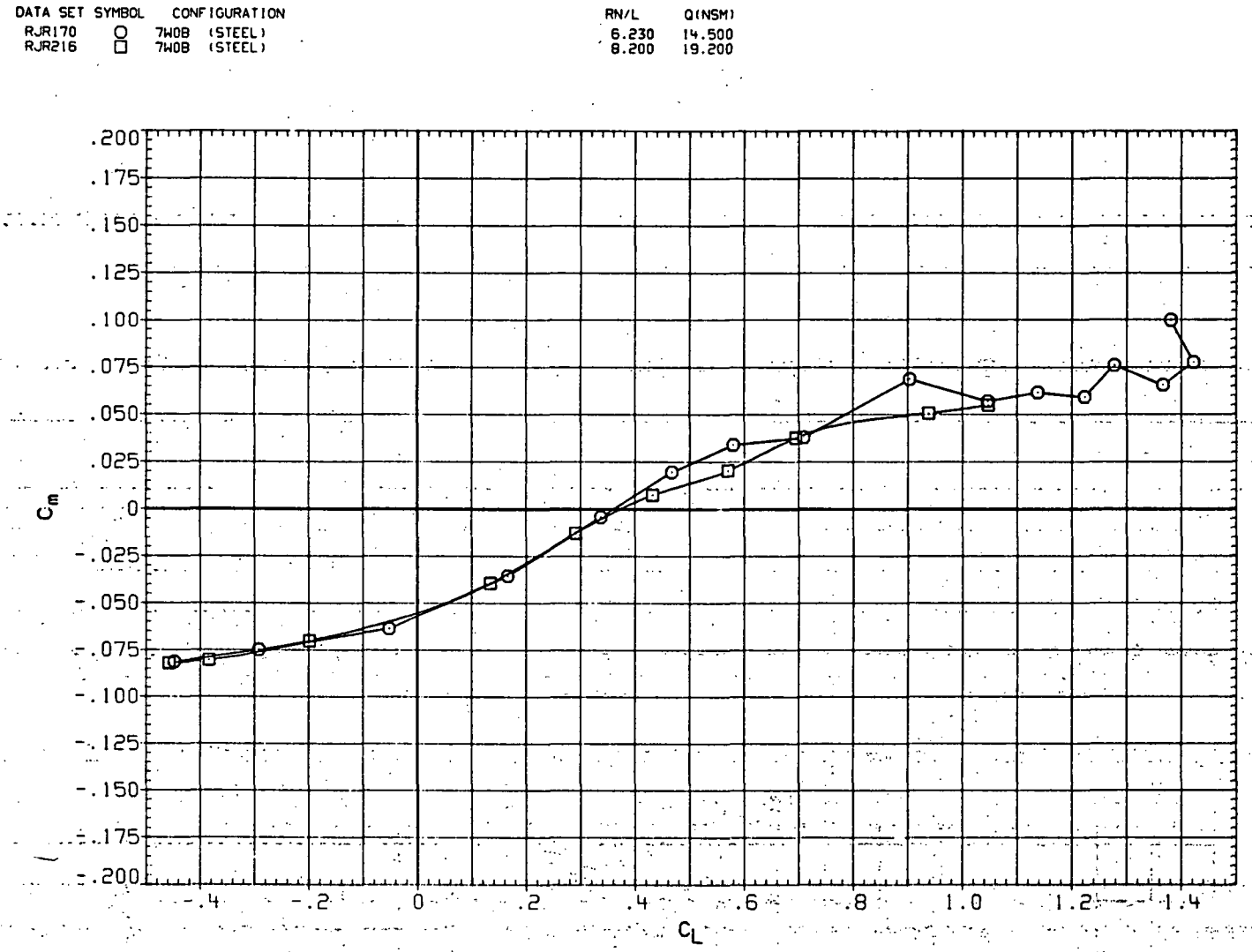

(c) C_m vs C_L.

Figure 88.– Continued.

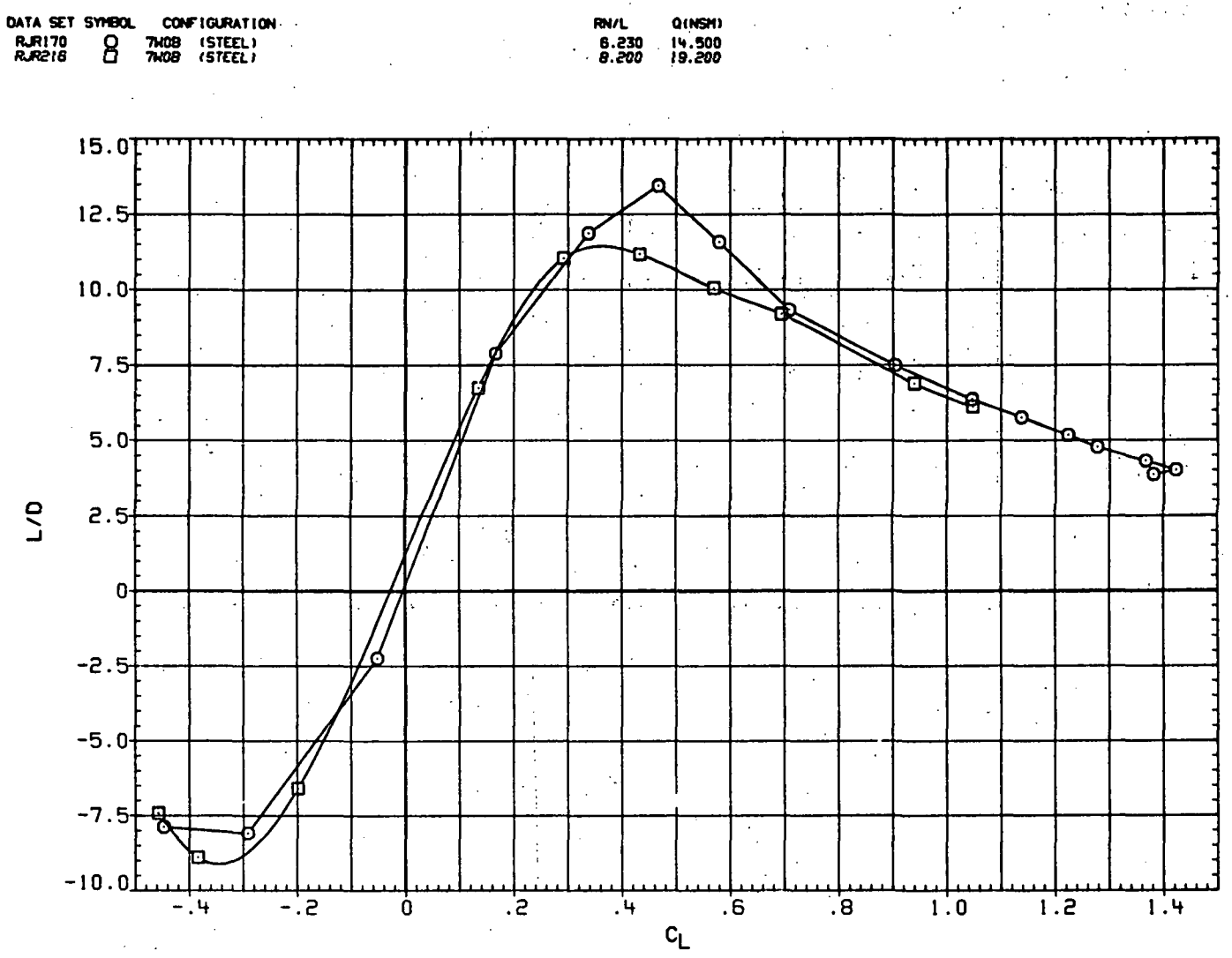

(d) L/D vs C_L.

Figure 88.– Continued.

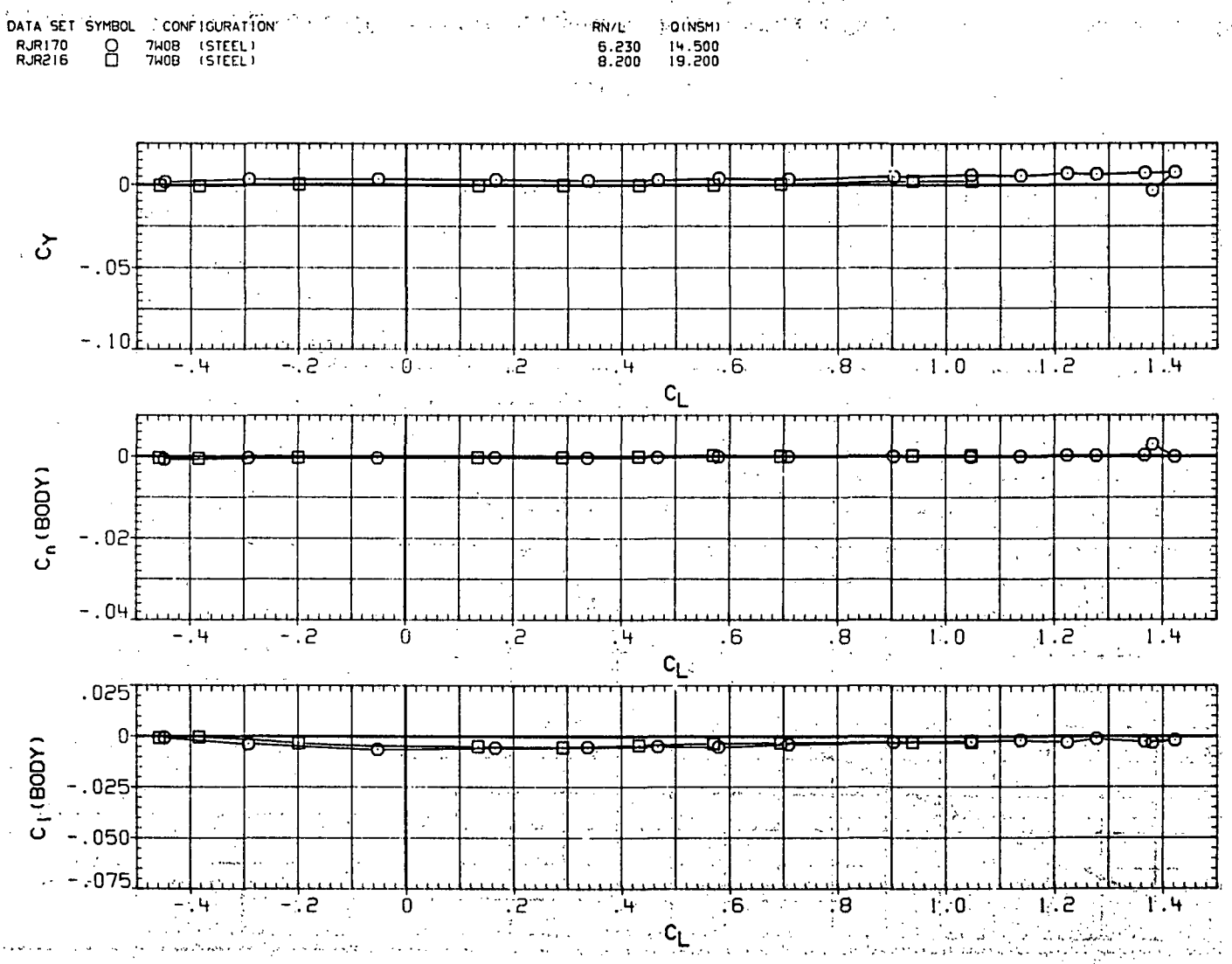

(e) C_Y, C_n and C_ℓ vs C_L.

Figure 88.– Concluded.

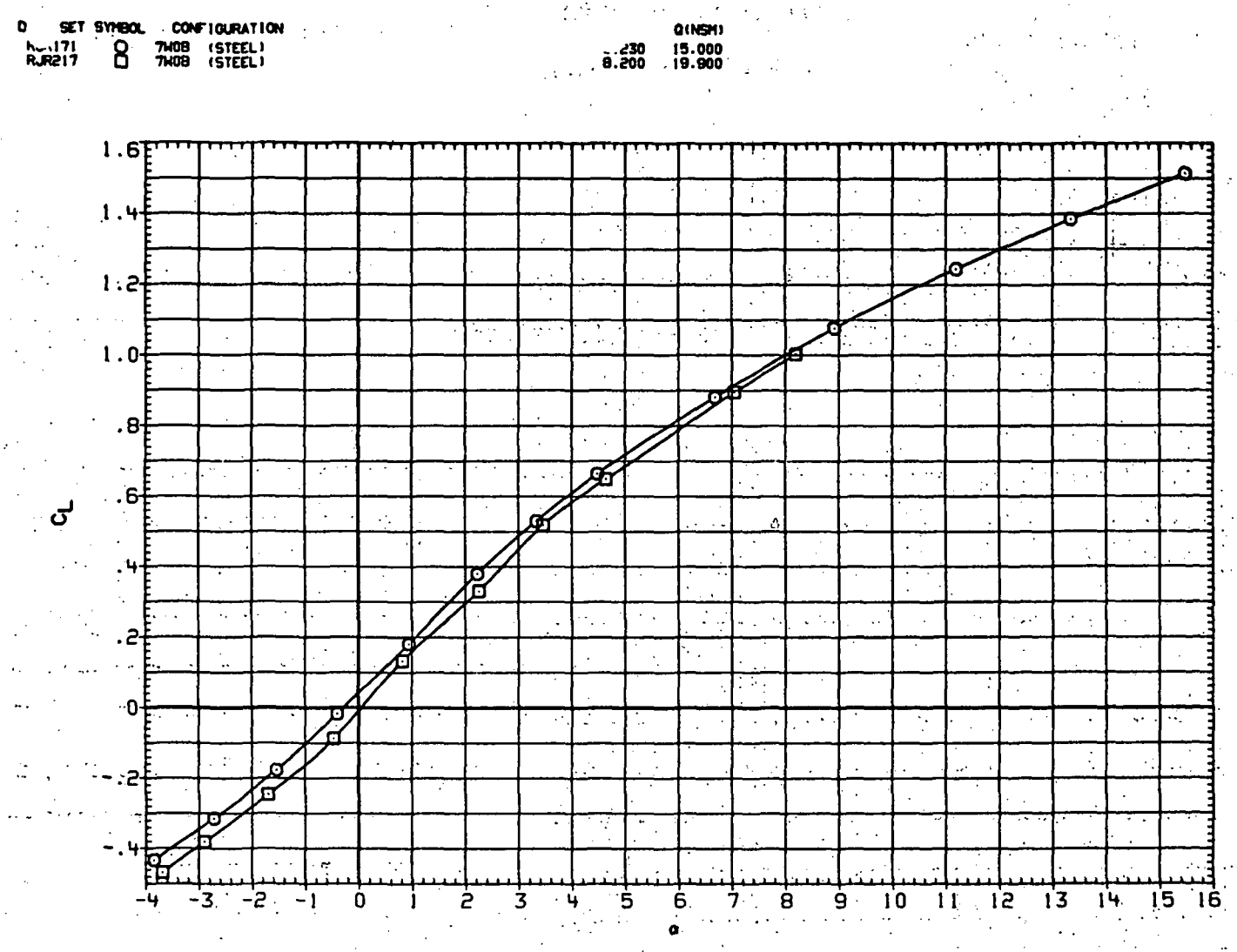

(a) C_L vs α

Figure 89.– Dynamic-pressure effects on the aerodynamic characteristics of the steel trapezoidal oblique wing-body combination ($\Lambda = 0, M = 0.95$ and the NACA 65A204 airfoil).

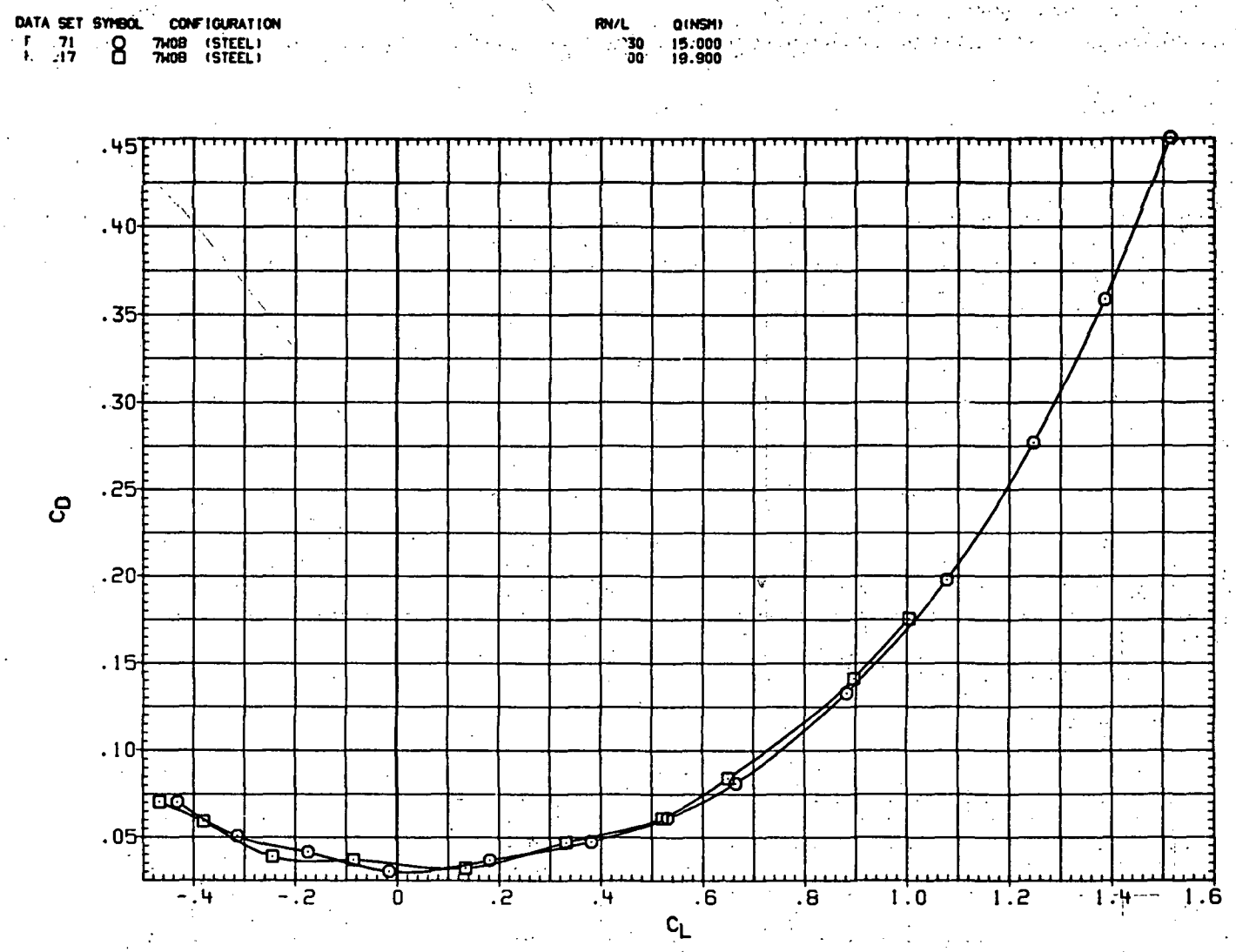

(b) C_D vs C_L.

Figure 89.– Continued.

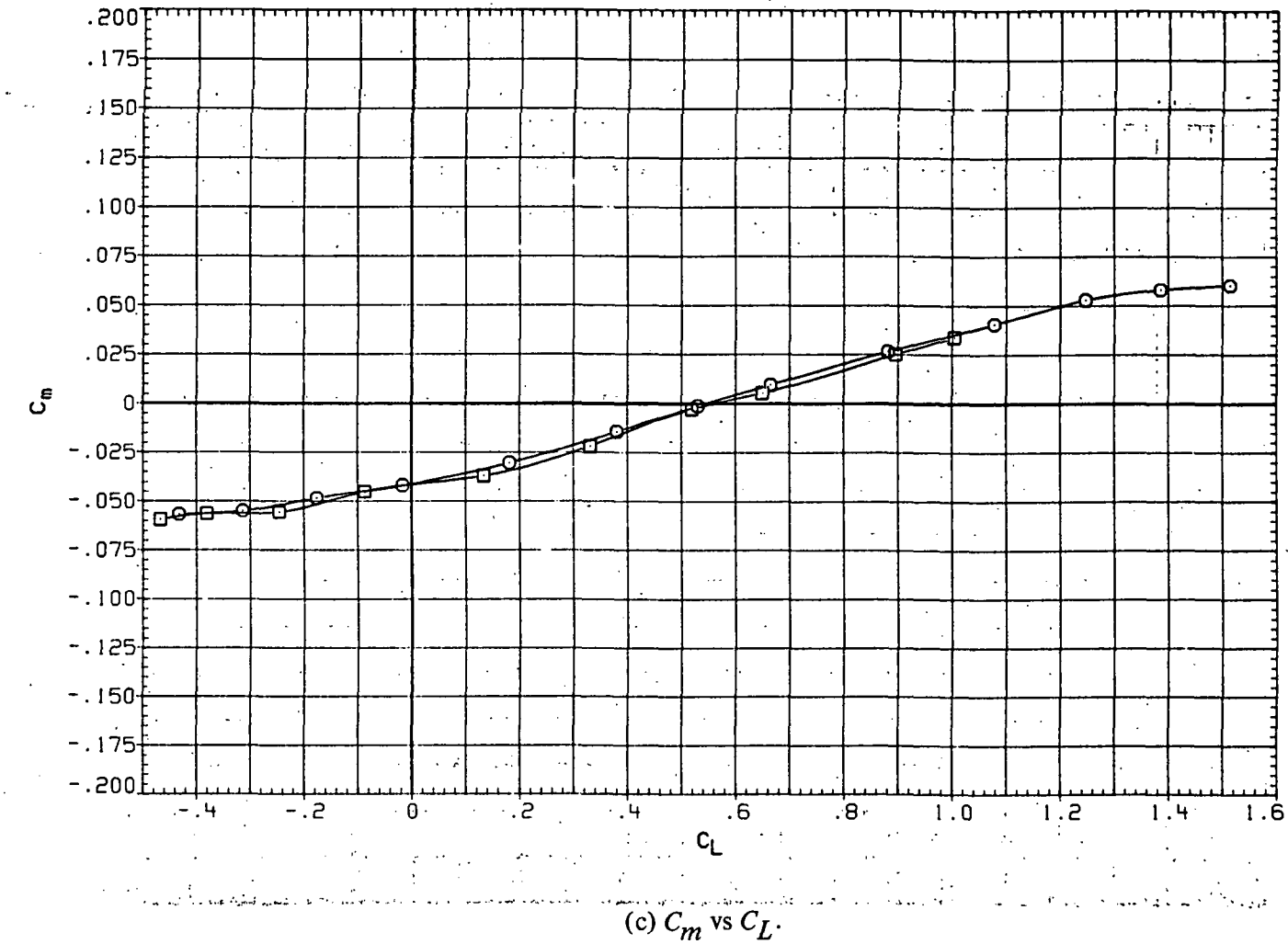

(c) C_m vs C_L.

Figure 89.—Continued.

(d) L/D vs C_L.

Figure 89.– Continued.

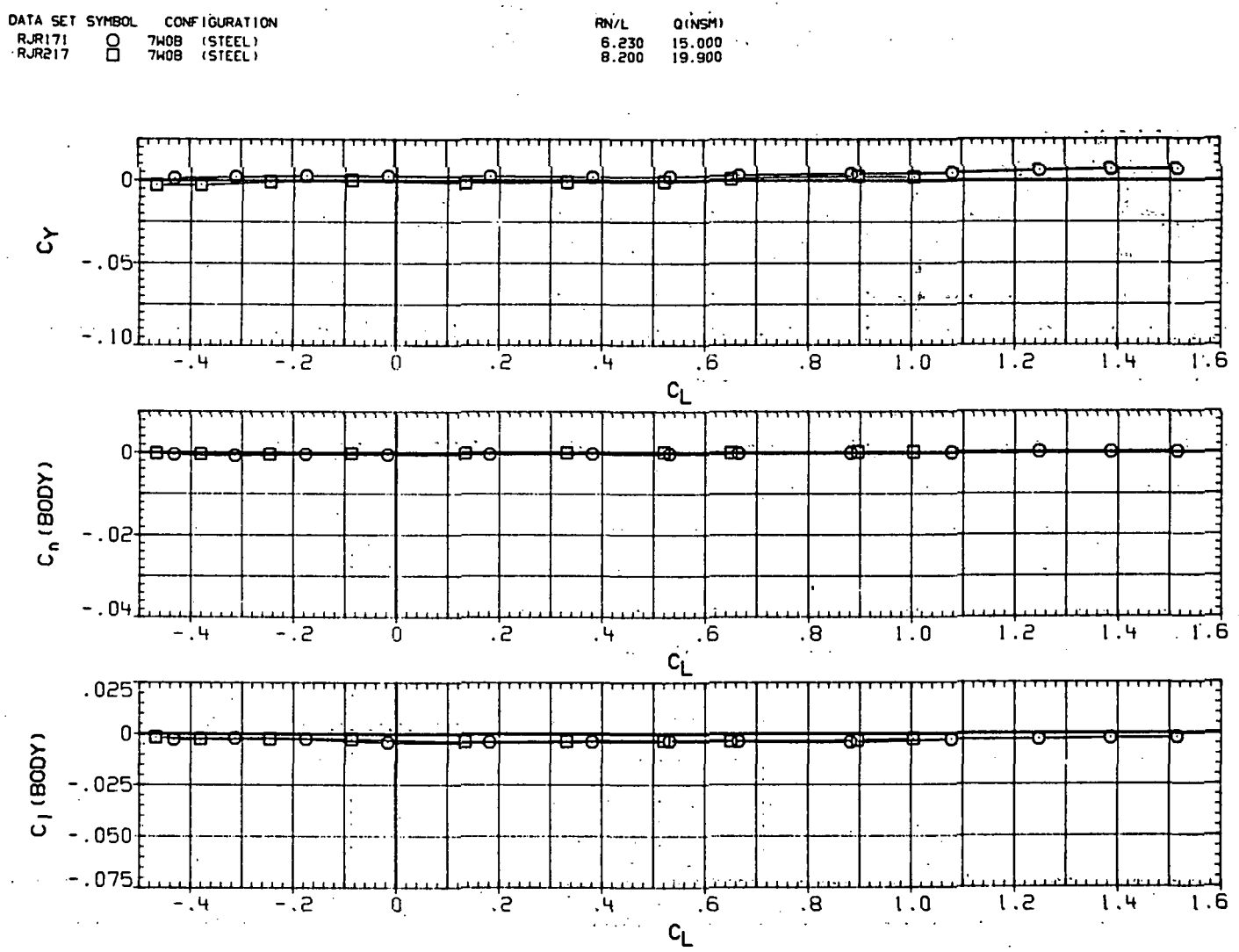

(e) C_Y, C_n and C_ℓ vs C_L.

Figure 89.– Concluded.

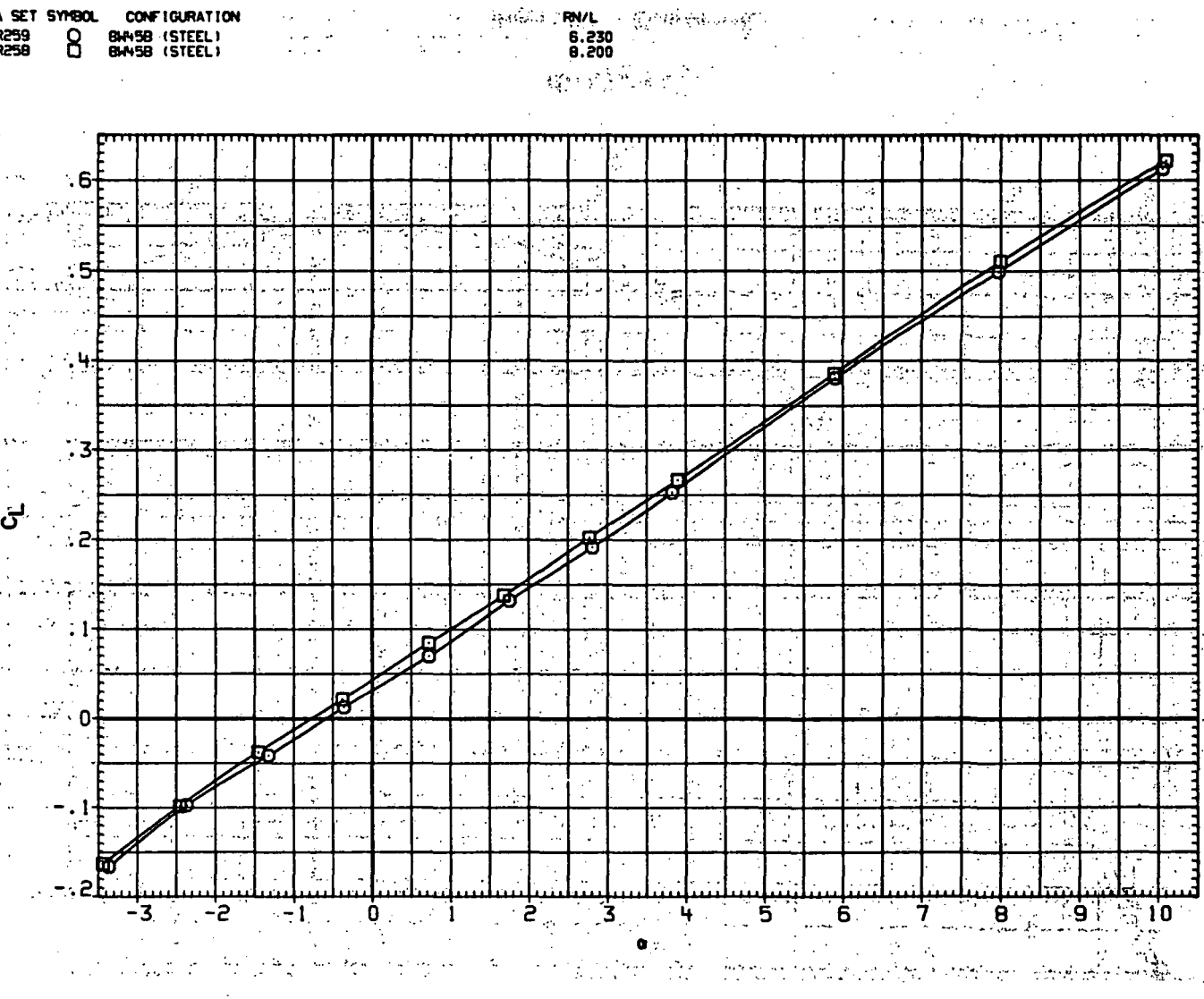

(a) C_L vs α.

gure 90.– Reynolds-number effects on the aerodynamic characteristics of the steel swept wing-body combination ($M = 0.4$ and the NACA 65A204 airfoil).

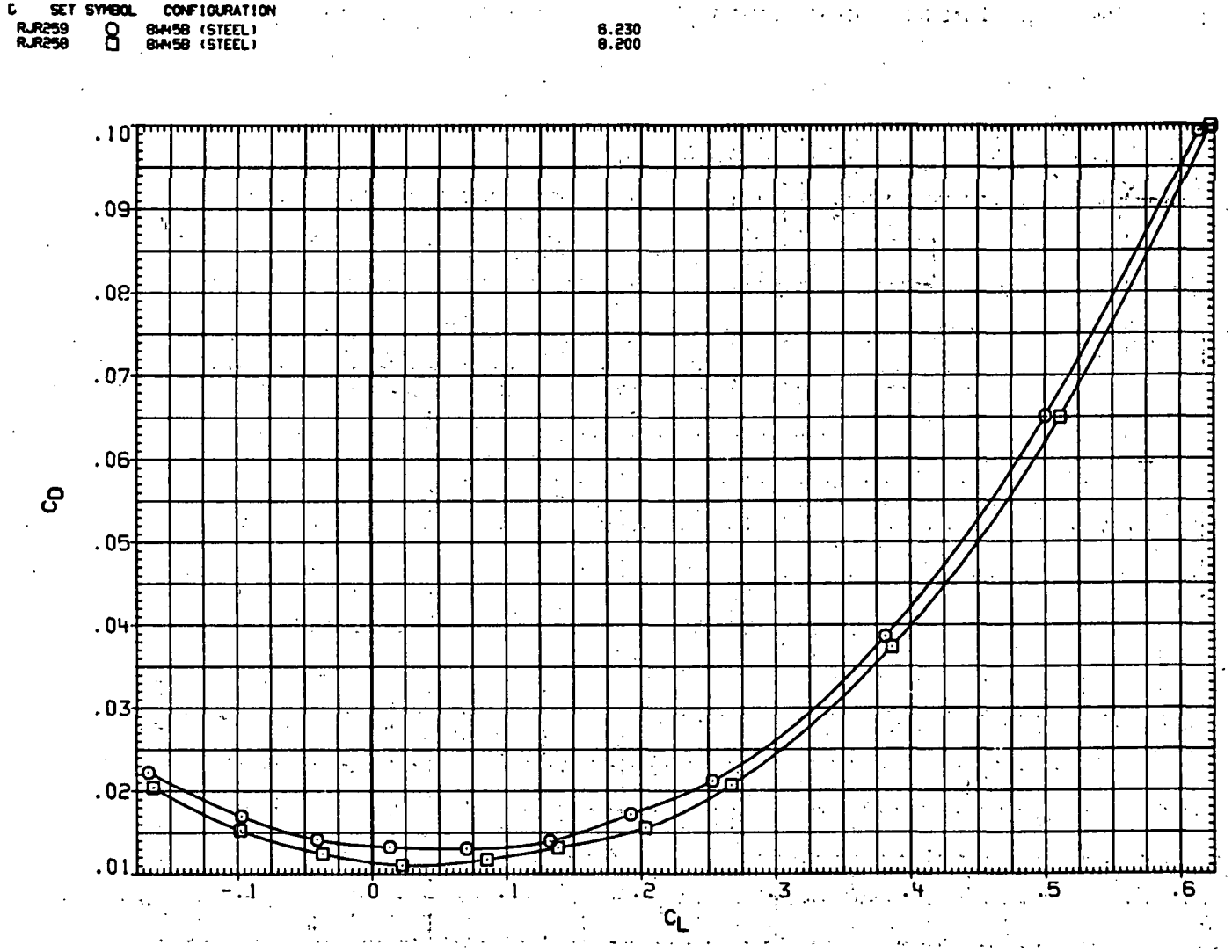

(b) C_D vs C_L.

Figure 90.– Continued.

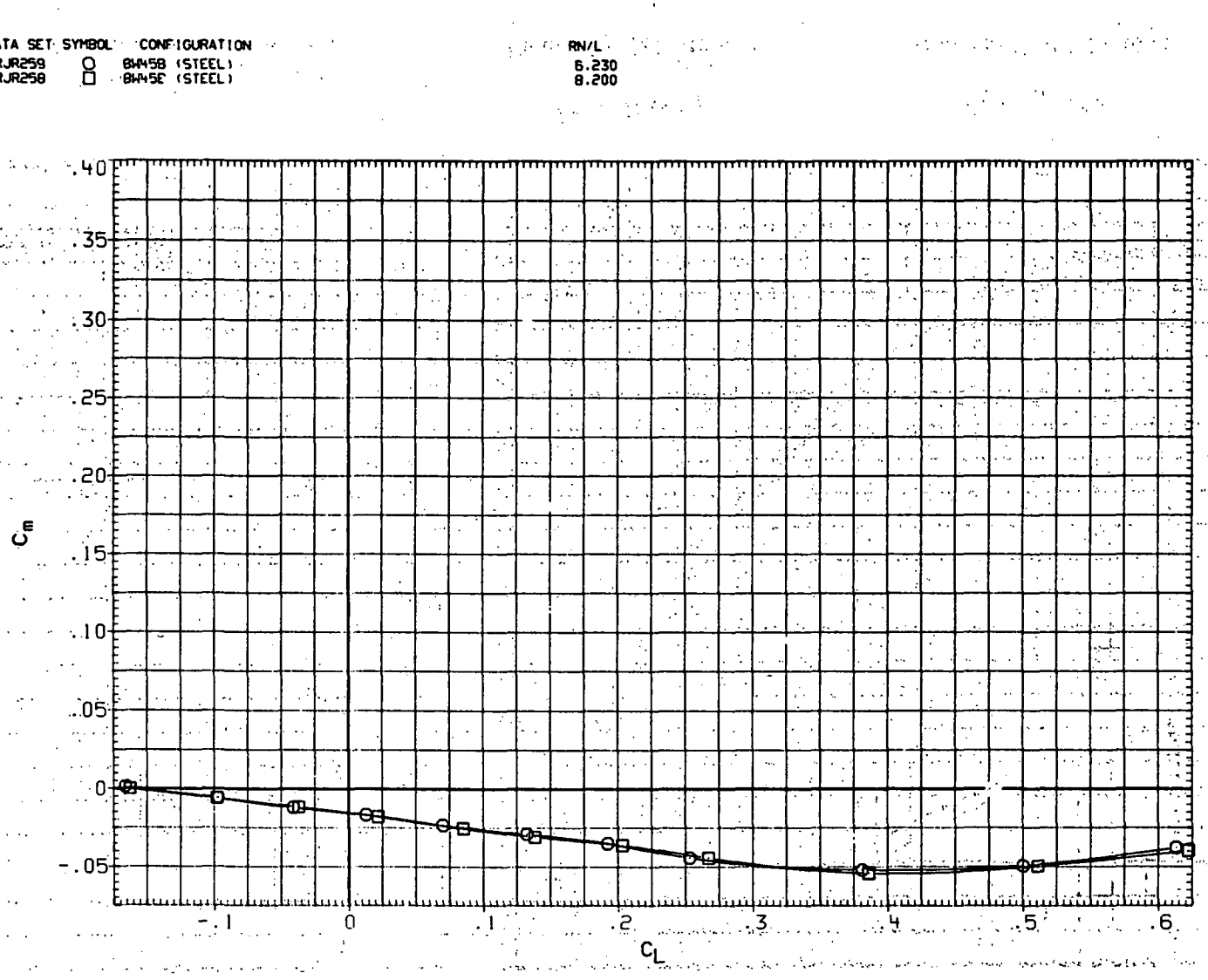

(c) C_m vs C_L.

Figure 90.– Continued.

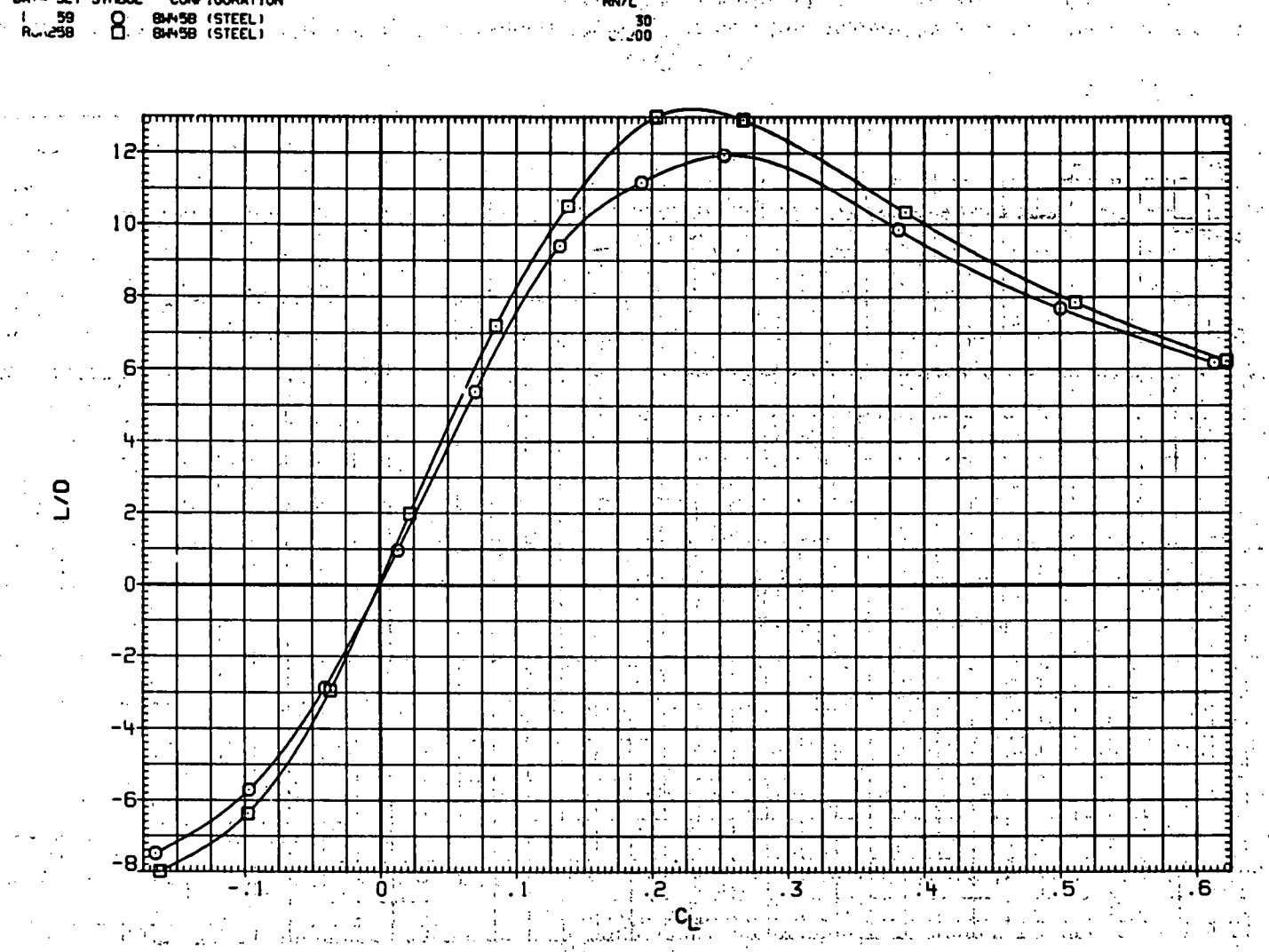

(d) L/D vs C_L.

Figure 90.– Continued.

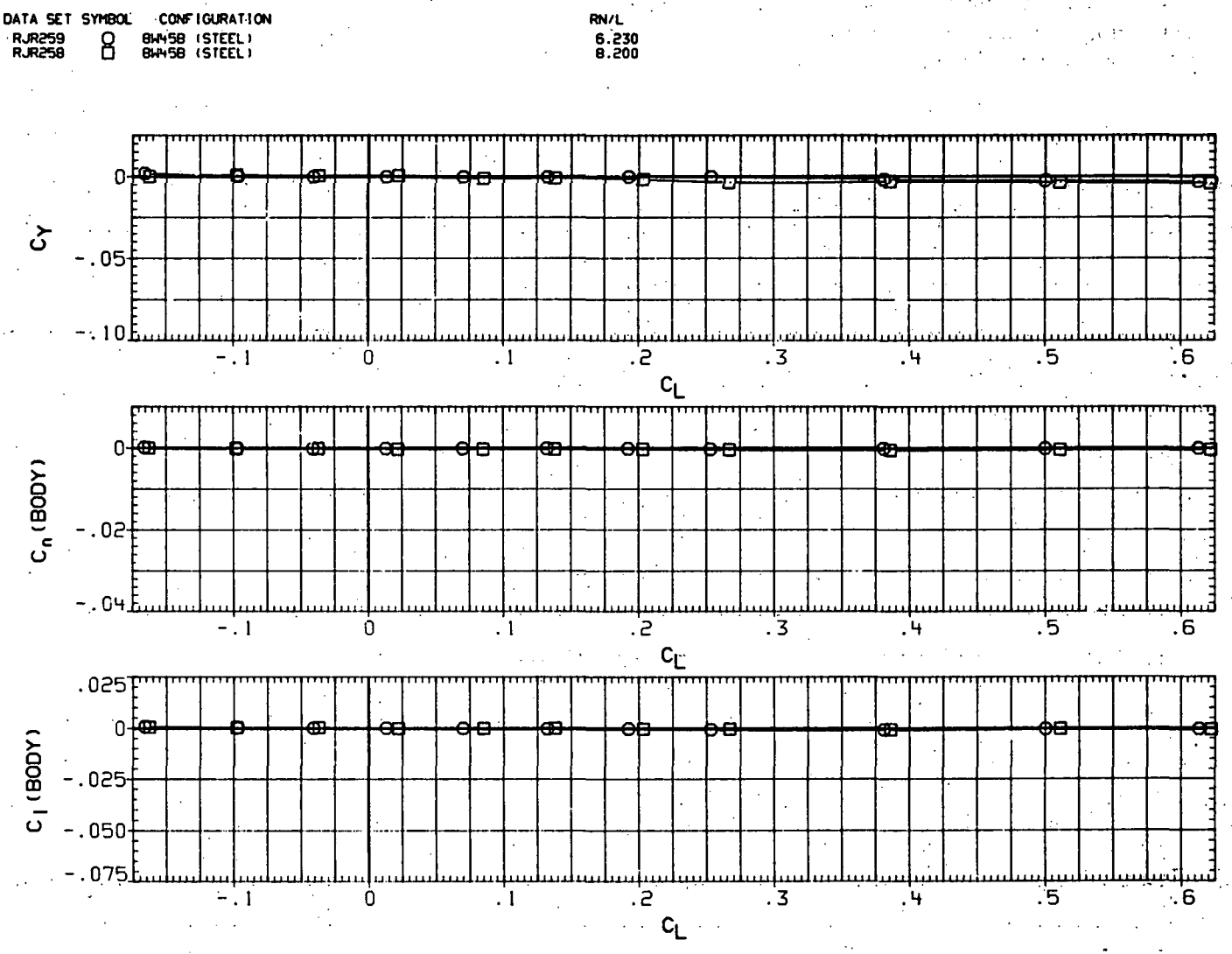

(e) C_Y, C_n and C_ℓ vs C_L.

Figure 90.– Concluded.

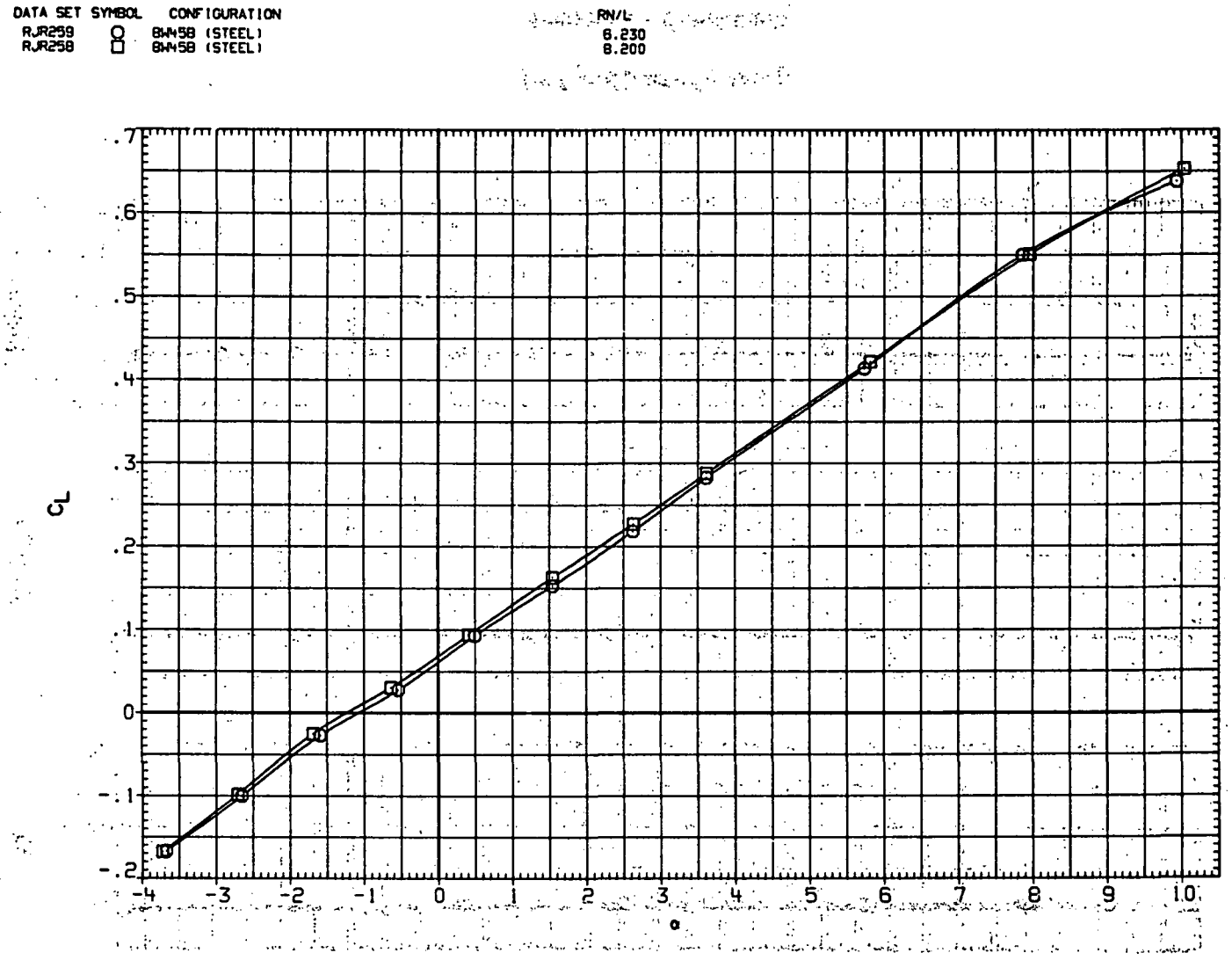

(a) C_L vs α.

Figure 91.– Reynolds-number effects on the aerodynamic characteristics of the steel swept wing-body combination (M = 0.6 and the NACA 65A204 airfoil).

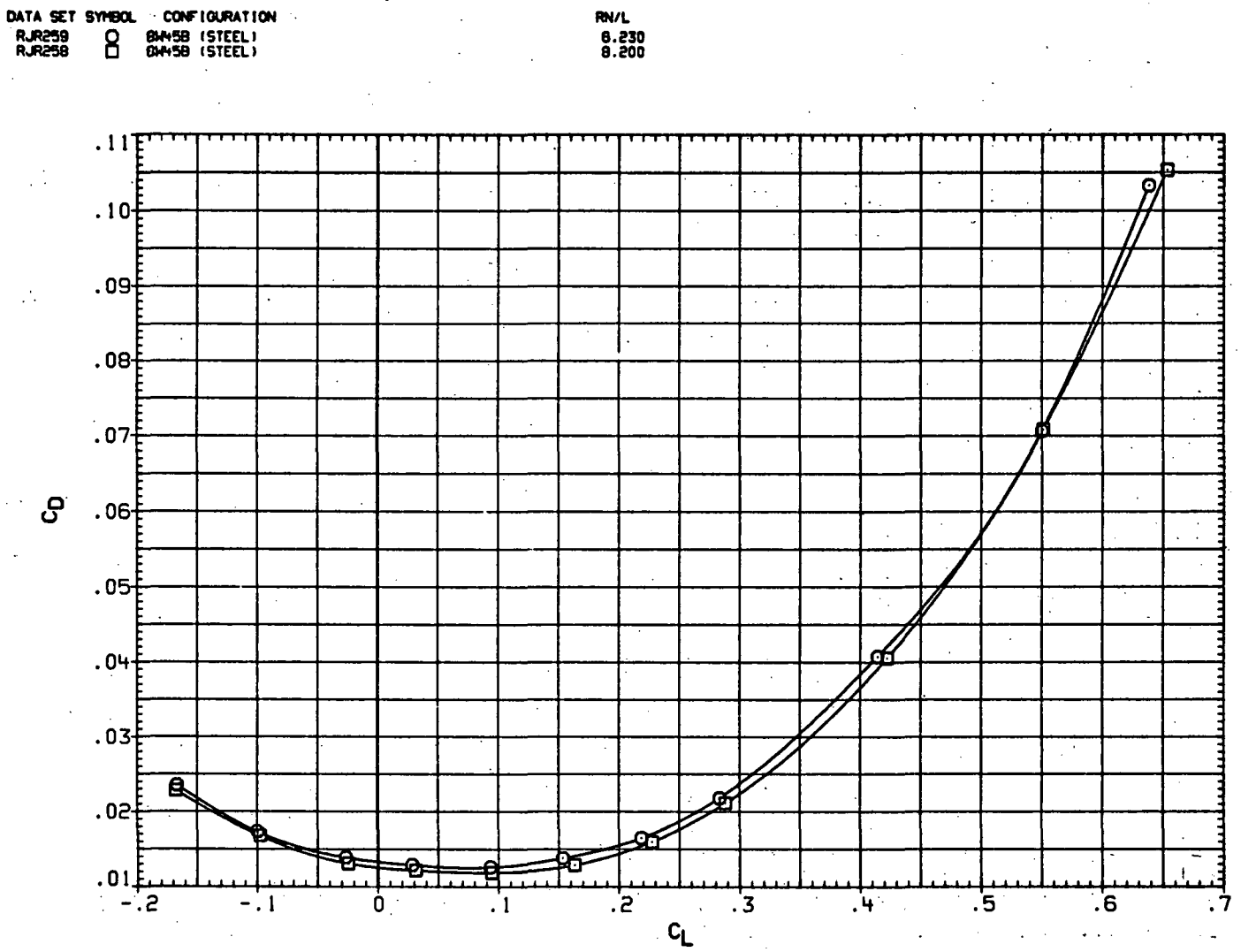

(b) C_D vs C_L.

Figure 91.– Continued.

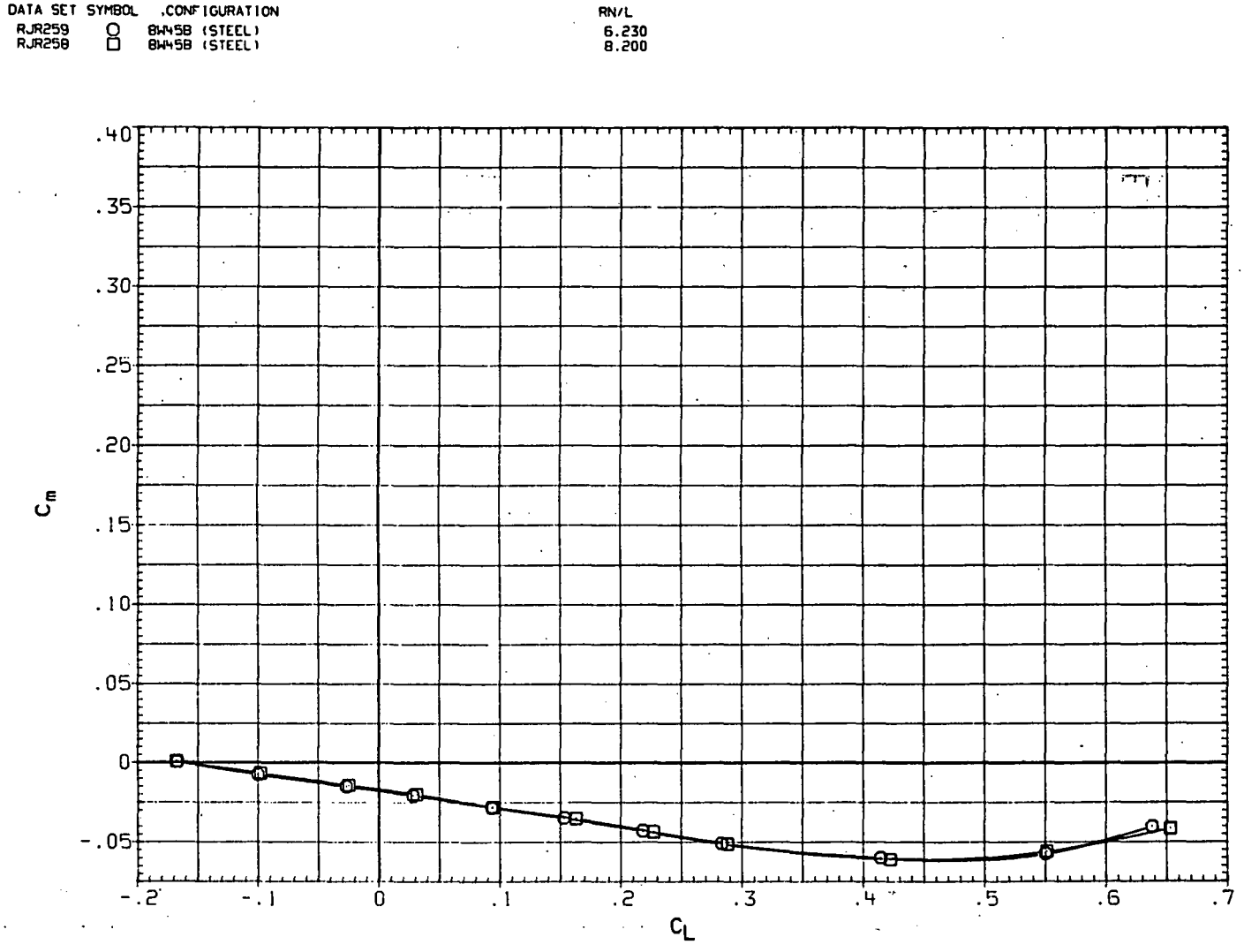

(c) C_m vs C_L.

Figure 91.– Continued.

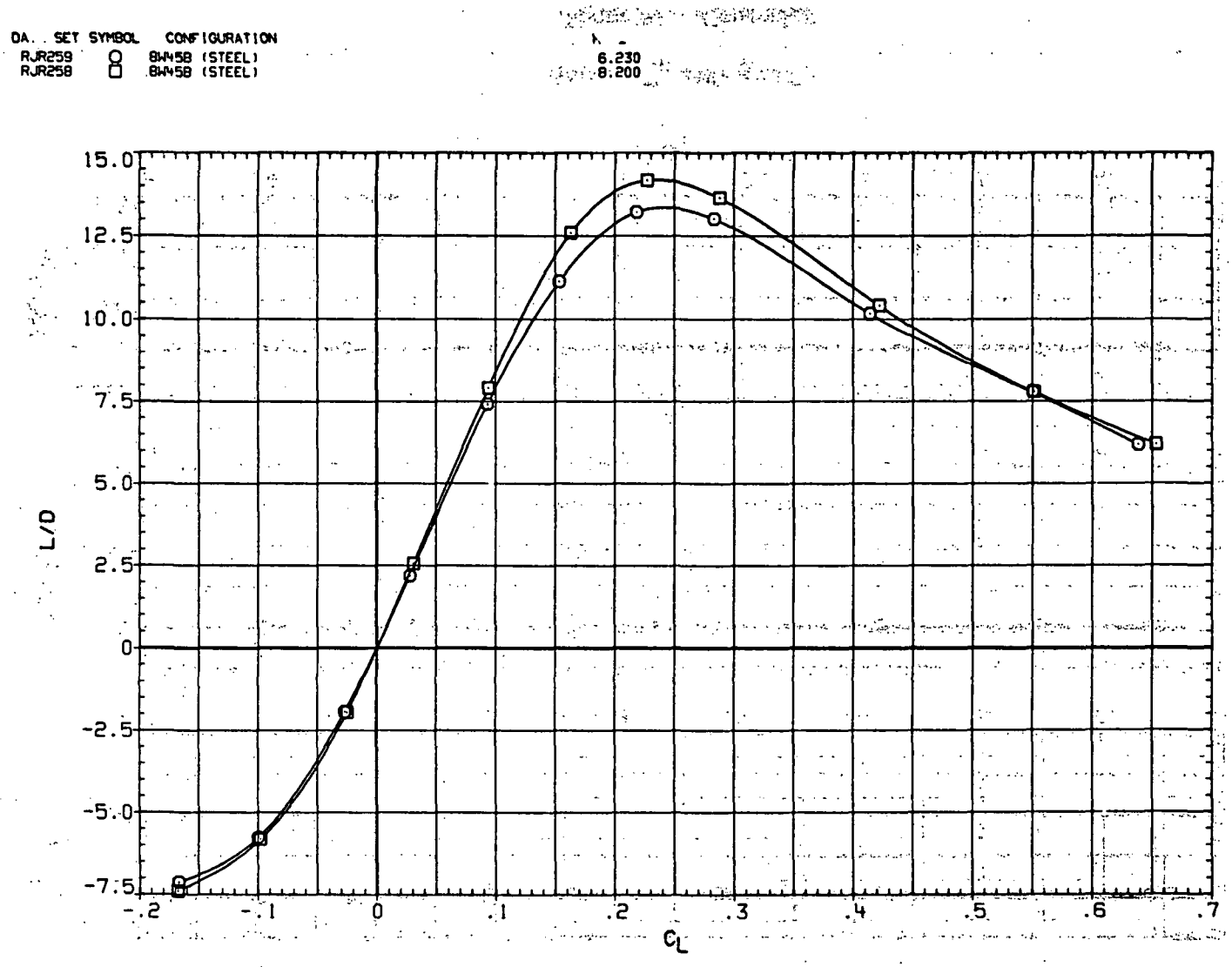

(d) L/D vs C_L.

Figure 91.– Continued.

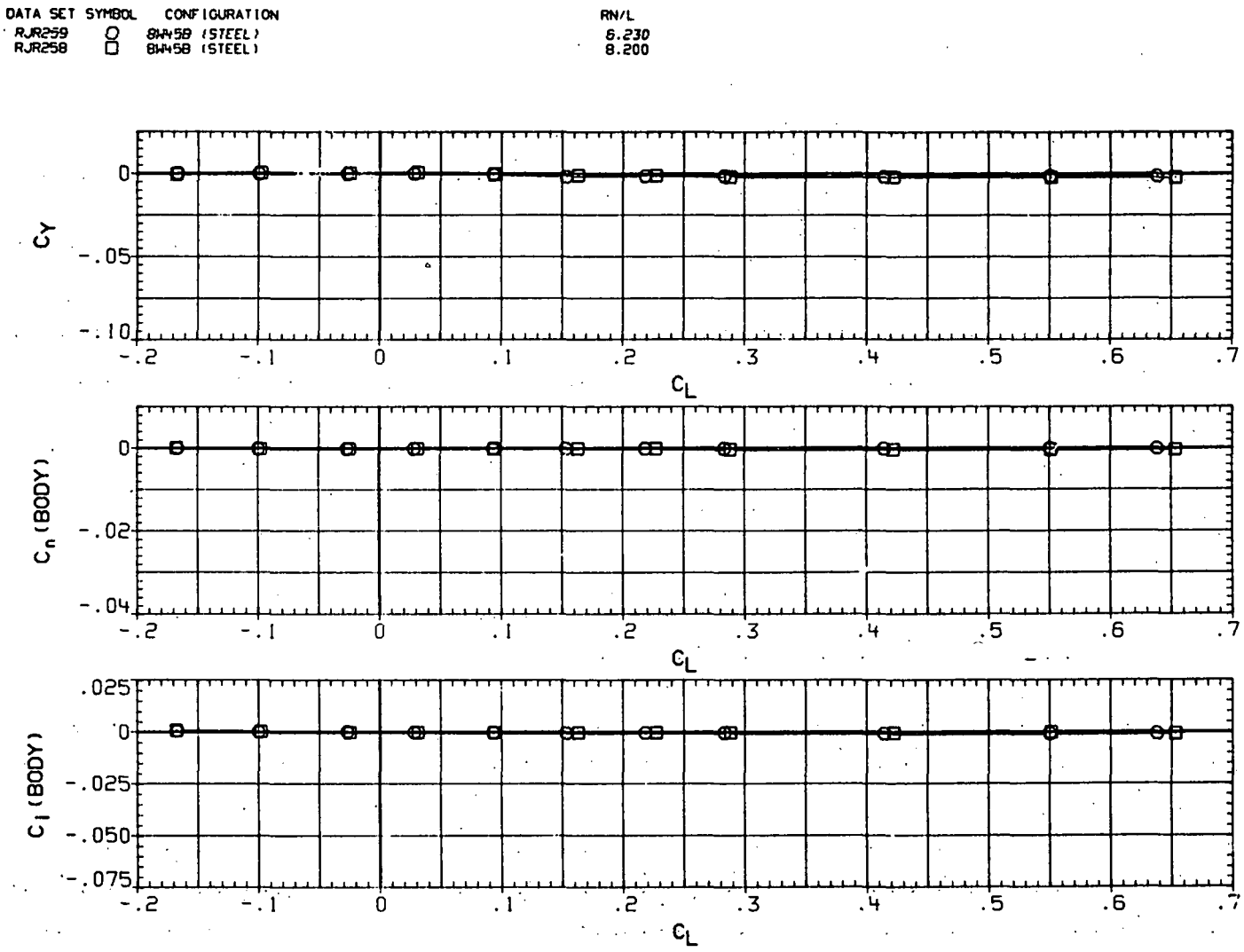

(e) C_Y, C_n and C_ℓ vs C_L.

Figure 91.– Concluded.

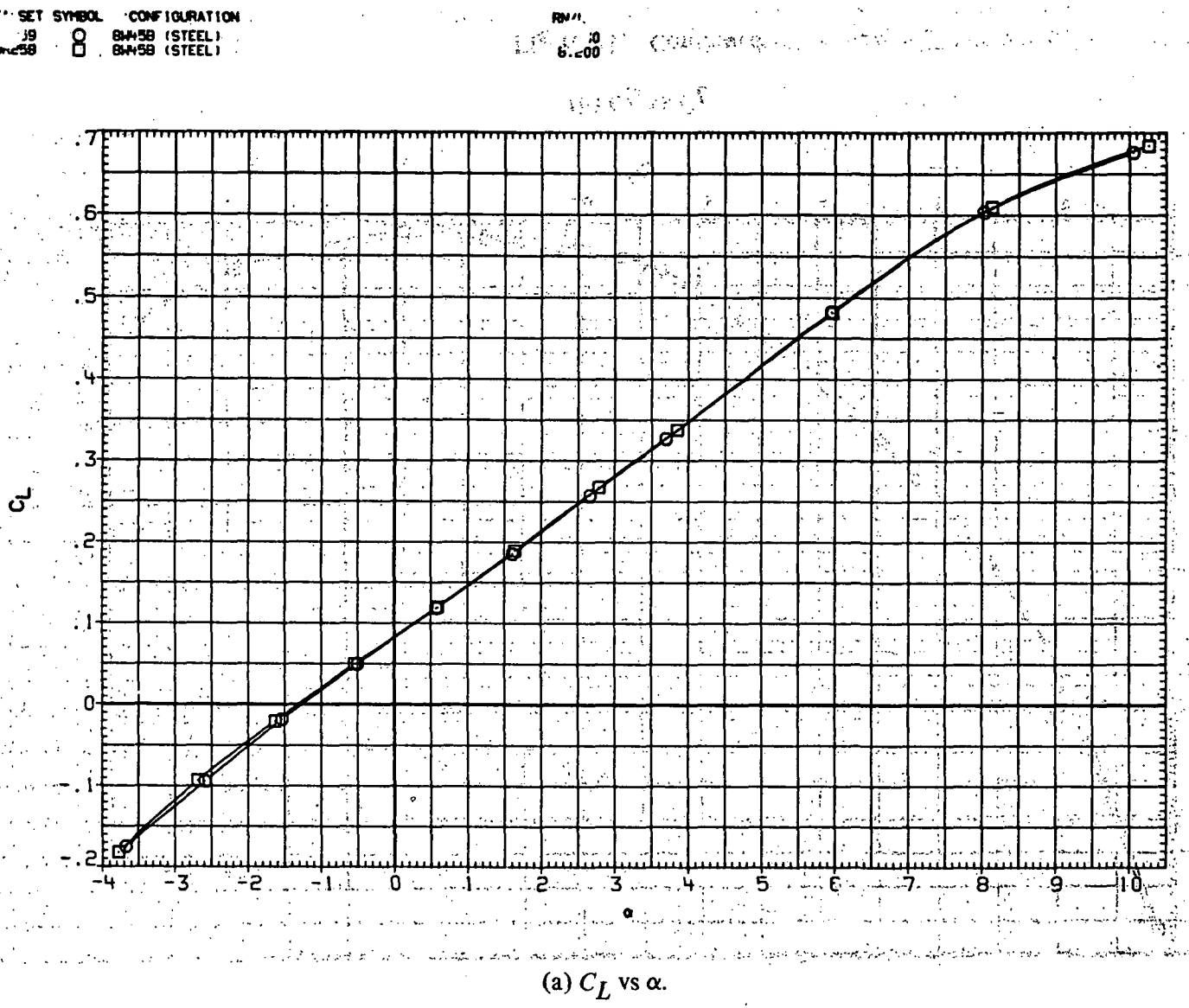

(a) C_L vs α.

Figure 92.– Reynolds-number effects on the aerodynamic characteristics of the steel swept wing-body combination ($M = 0.8$ and the NACA 65A204 airfoil).

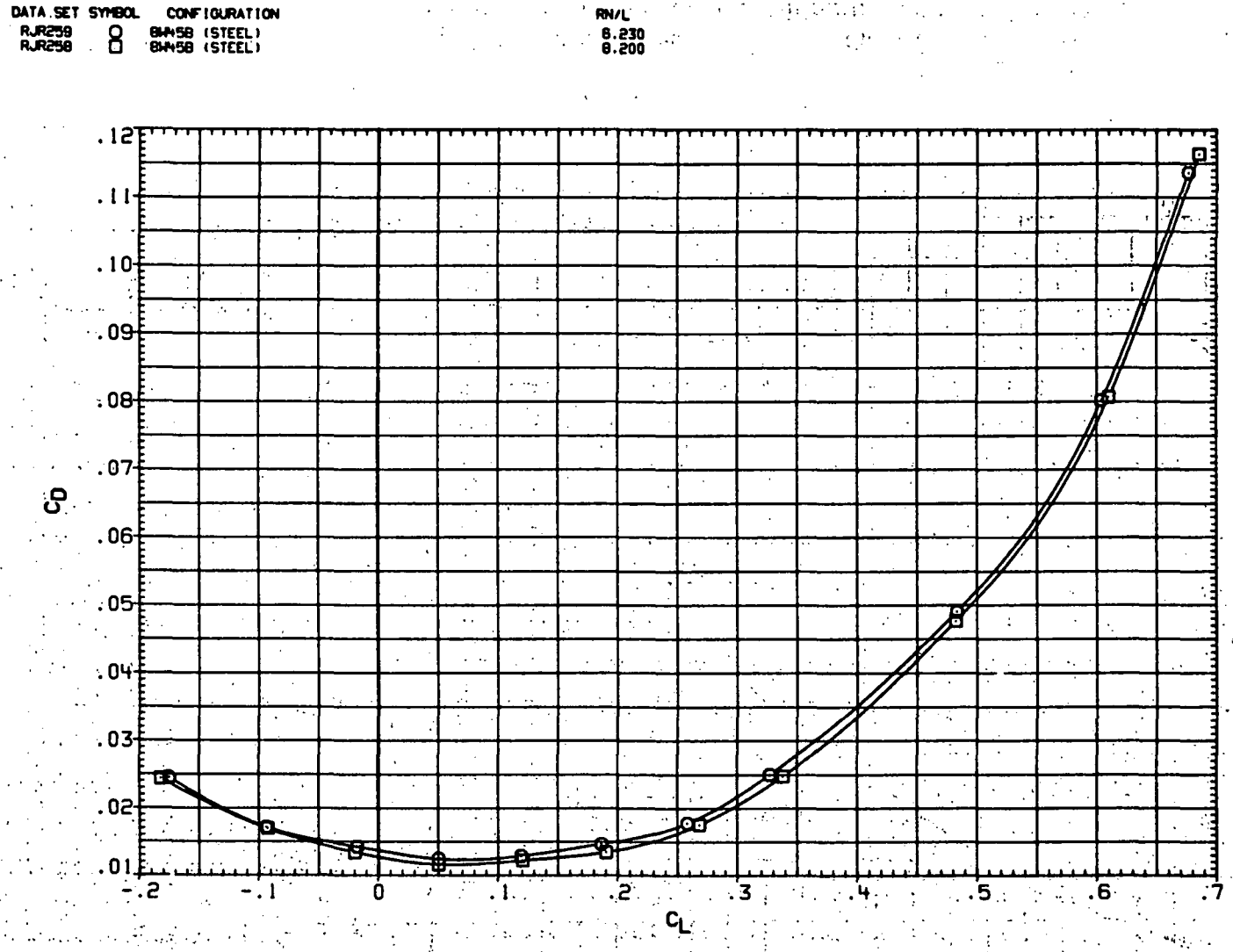

(b) C_D vs C_L.

Figure 92.– Continued.

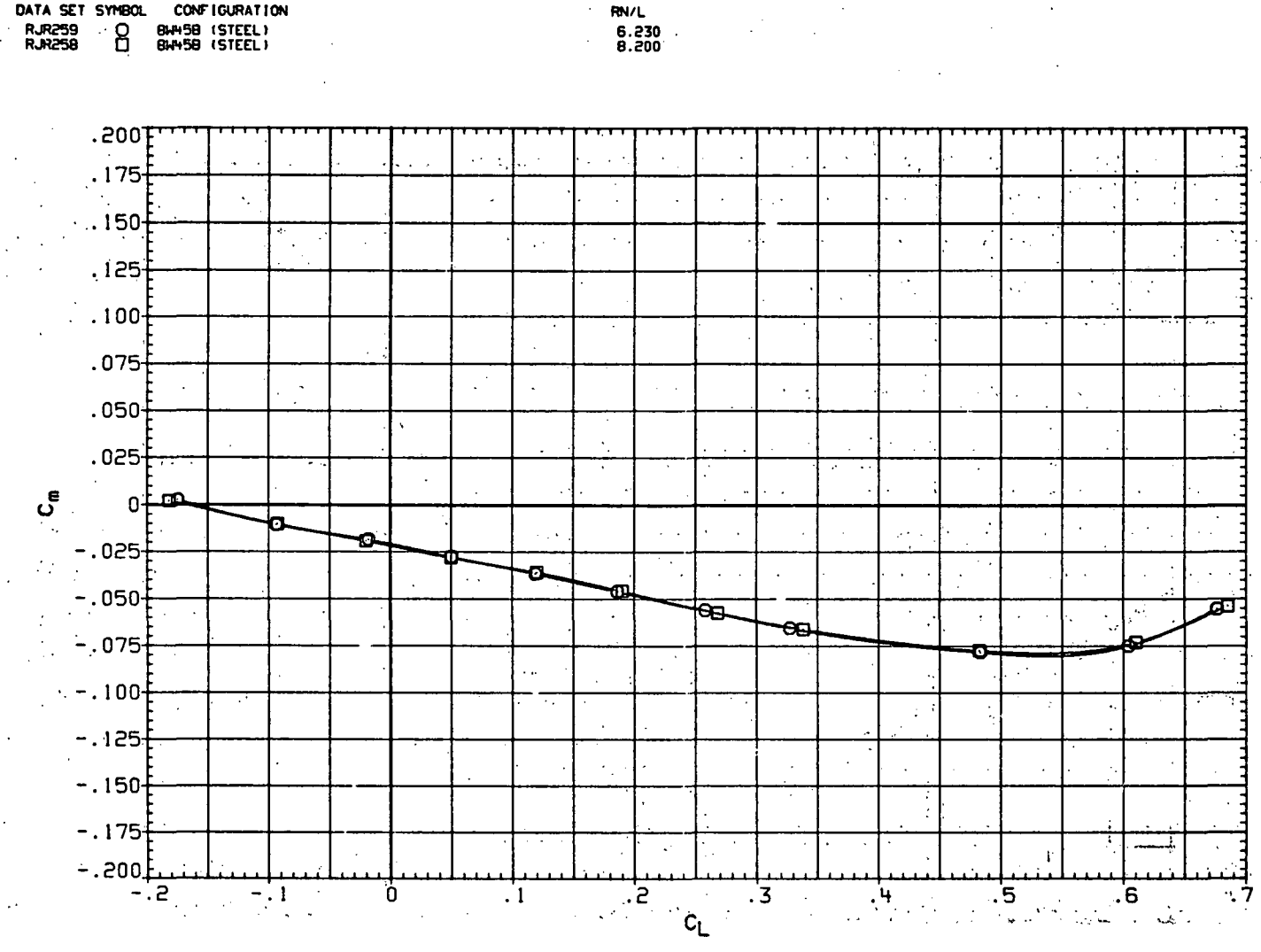

(c) C_m vs C_L.

Figure 92.– Continued.

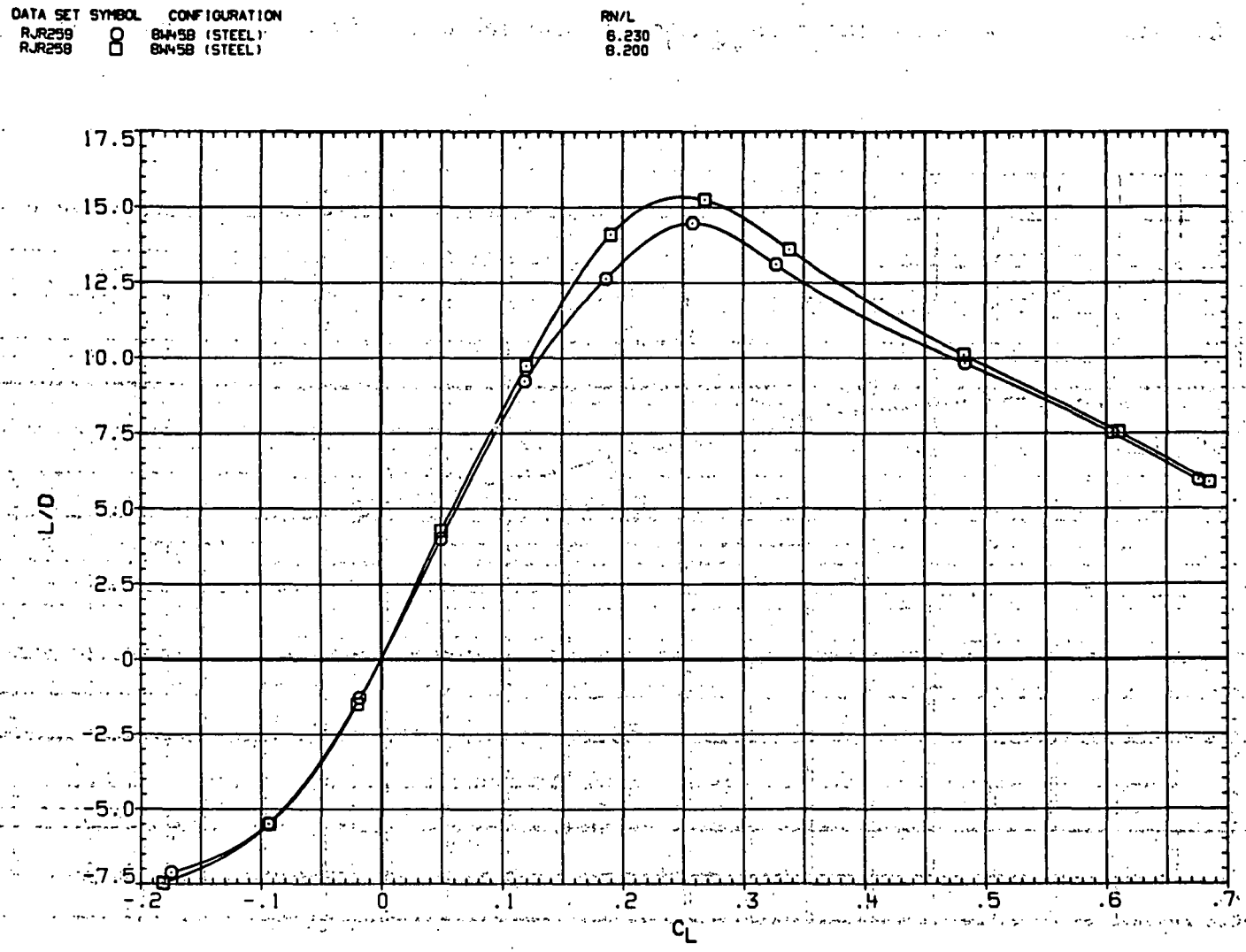

(d) L/D vs C_L.

Figure 92.– Continued.

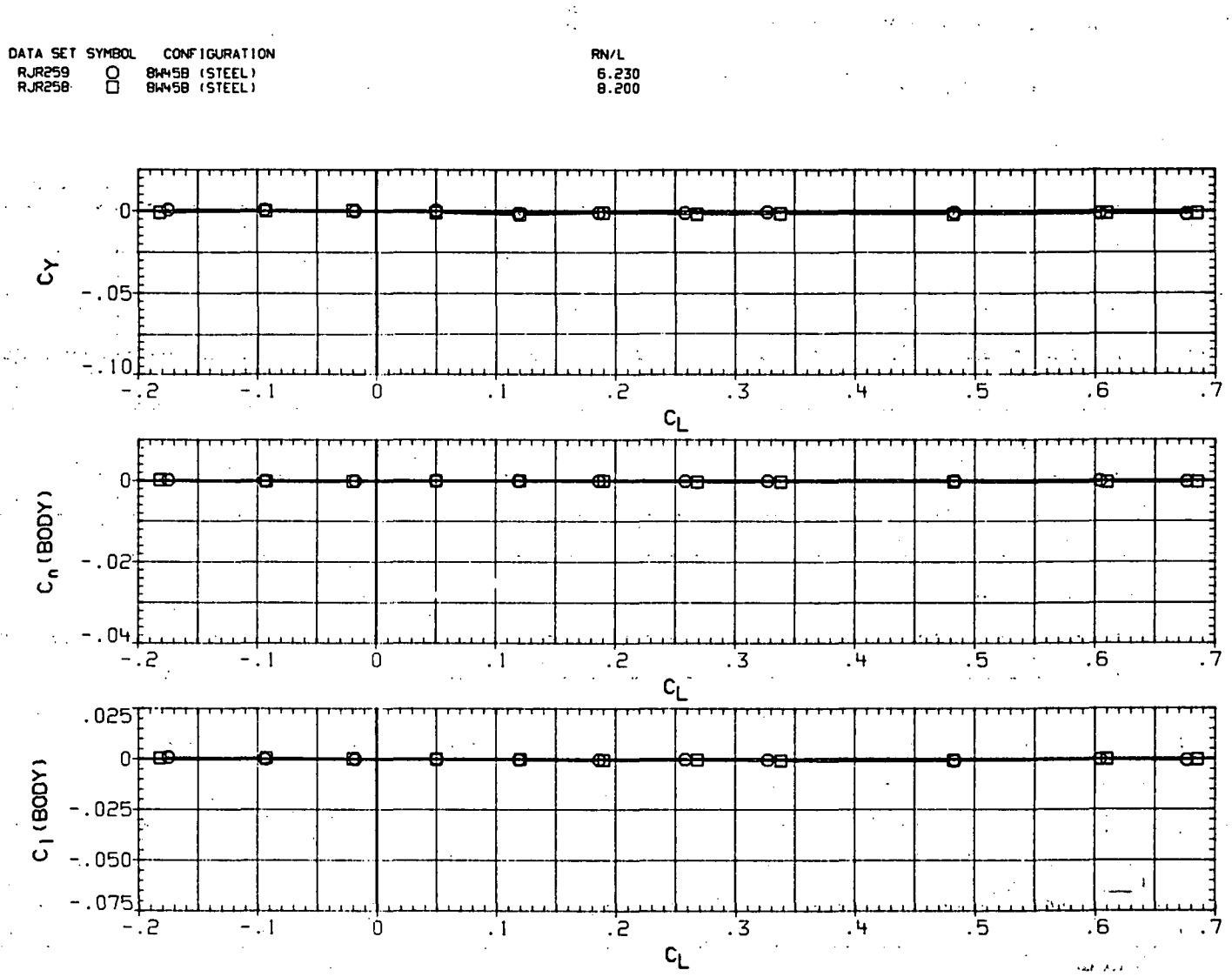

(e) C_Y, C_n and C_ℓ vs C_L.

Figure 92.– Concluded.

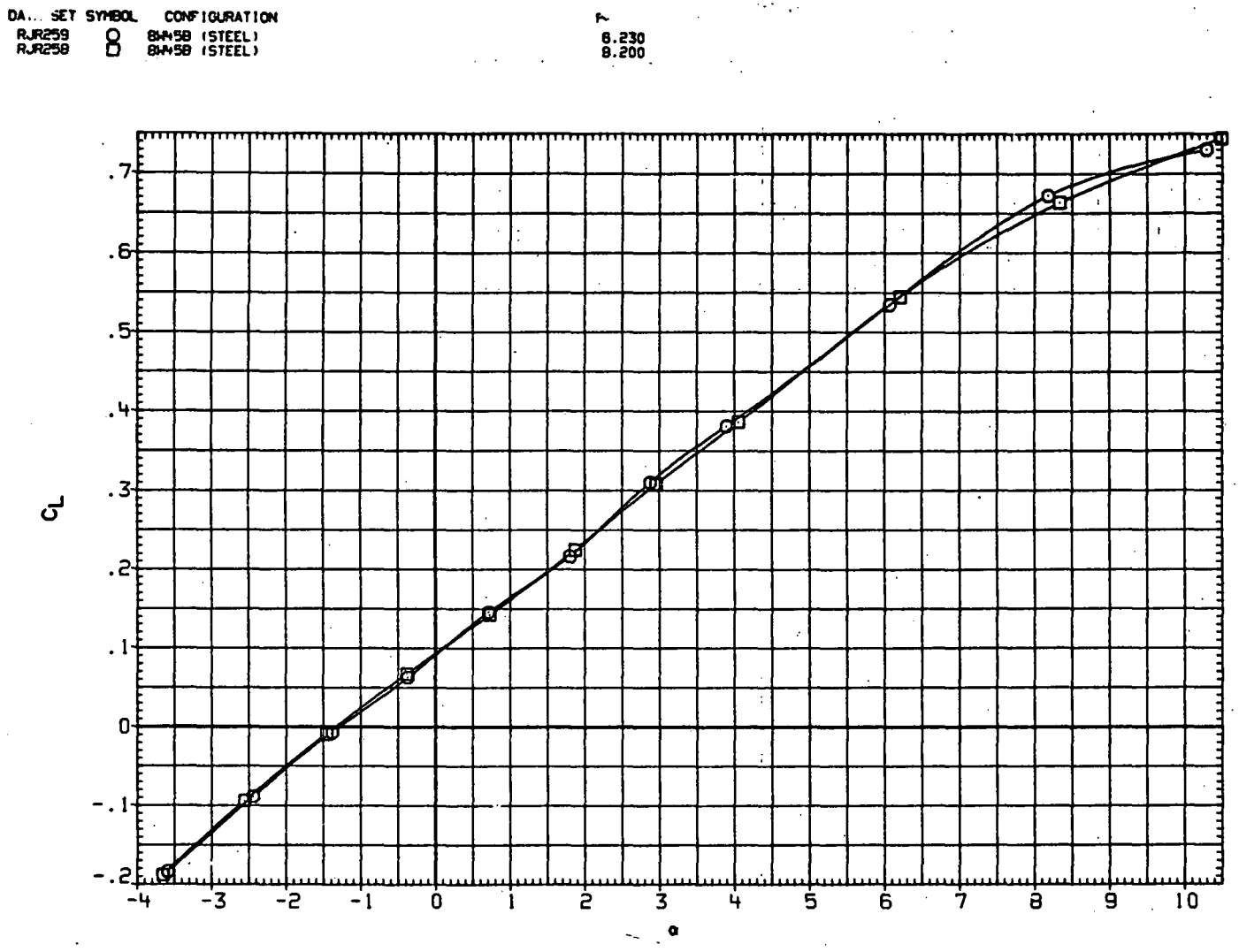

(a) C_L vs α.

Figure 93.– Reynolds-number effects on the aerodynamic characteristics of the steel swept wing-body combination ($M = 0.9$ and the NACA 65A204 airfoil).

DA	ST	SYMBOL	CONFIGURATION	R
RJR259		○	BW-5B (STEEL)	6.230
RJR258		□	BW-5B (STEEL)	8.200

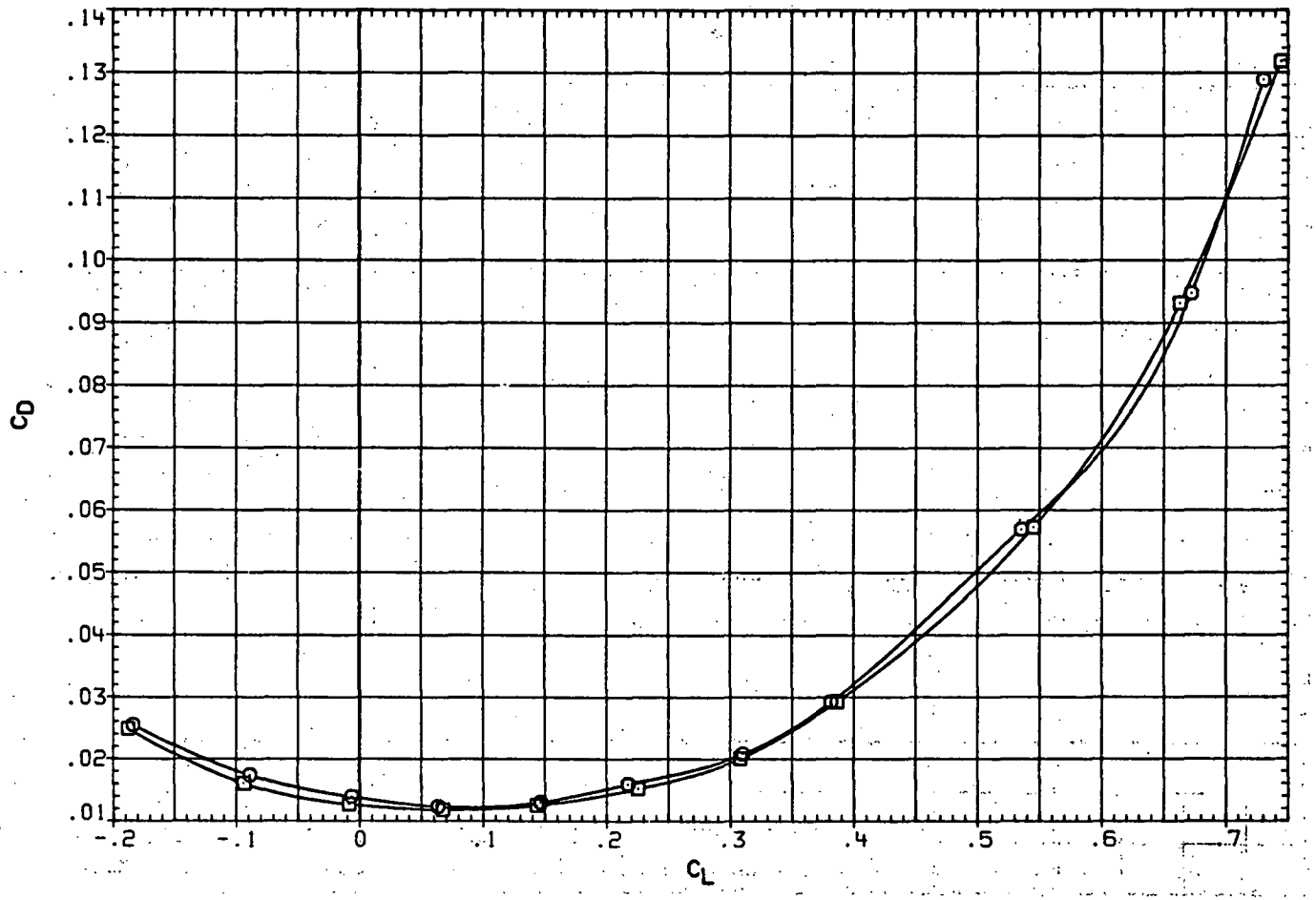

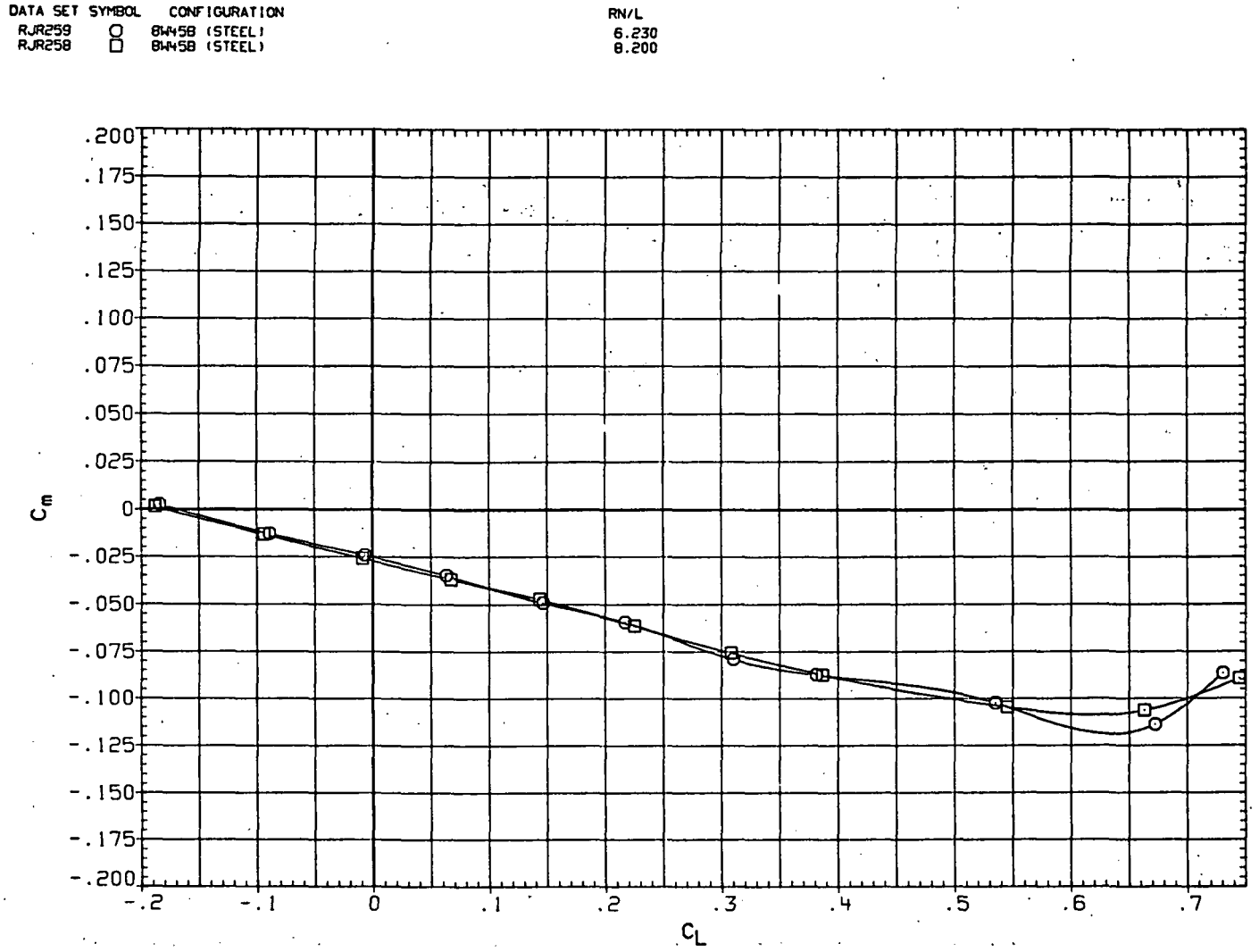

(c) C_m vs C_L.

Figure 93.– Continued.

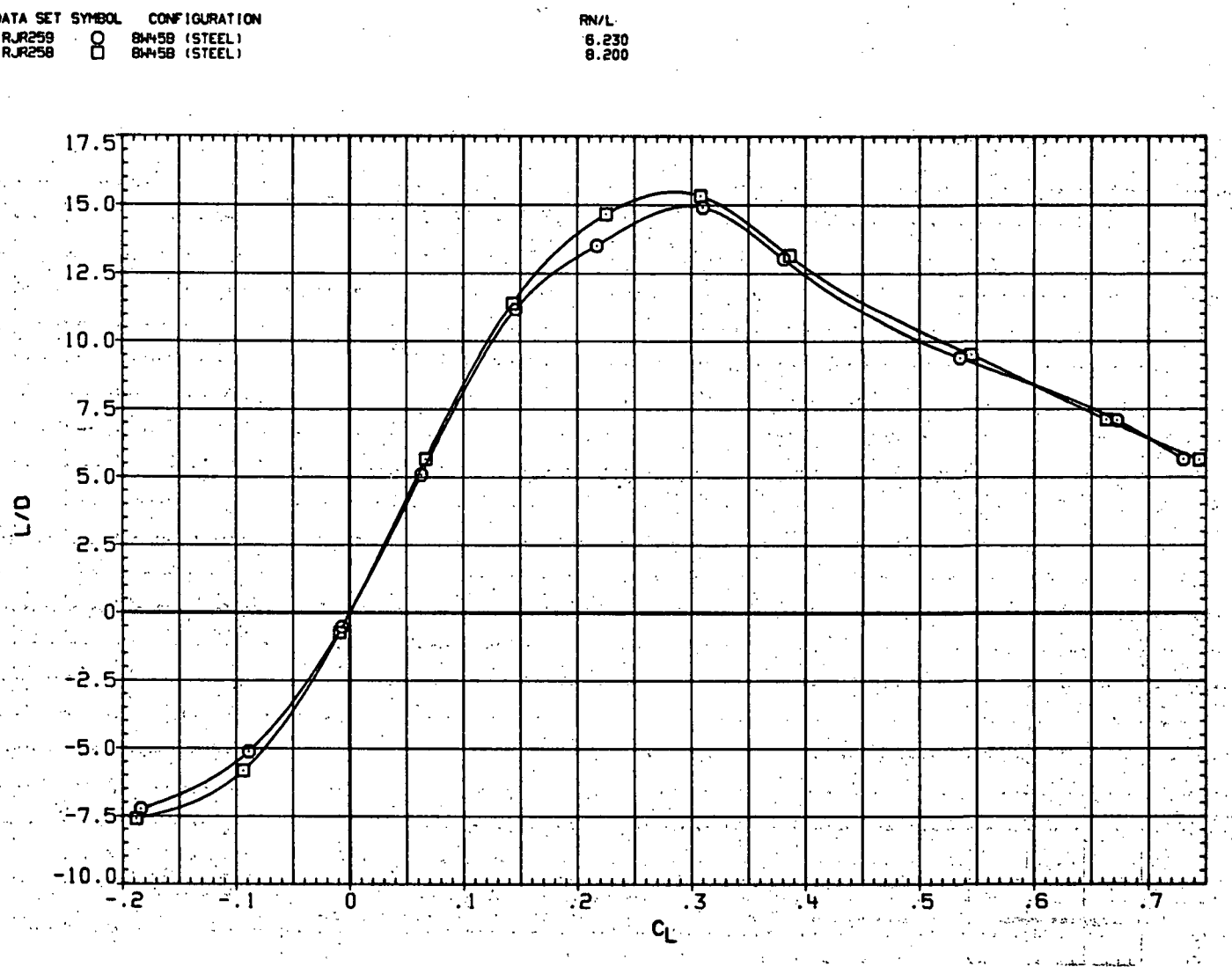

(d) L/D vs C_L.

Figure 93.– Continued.

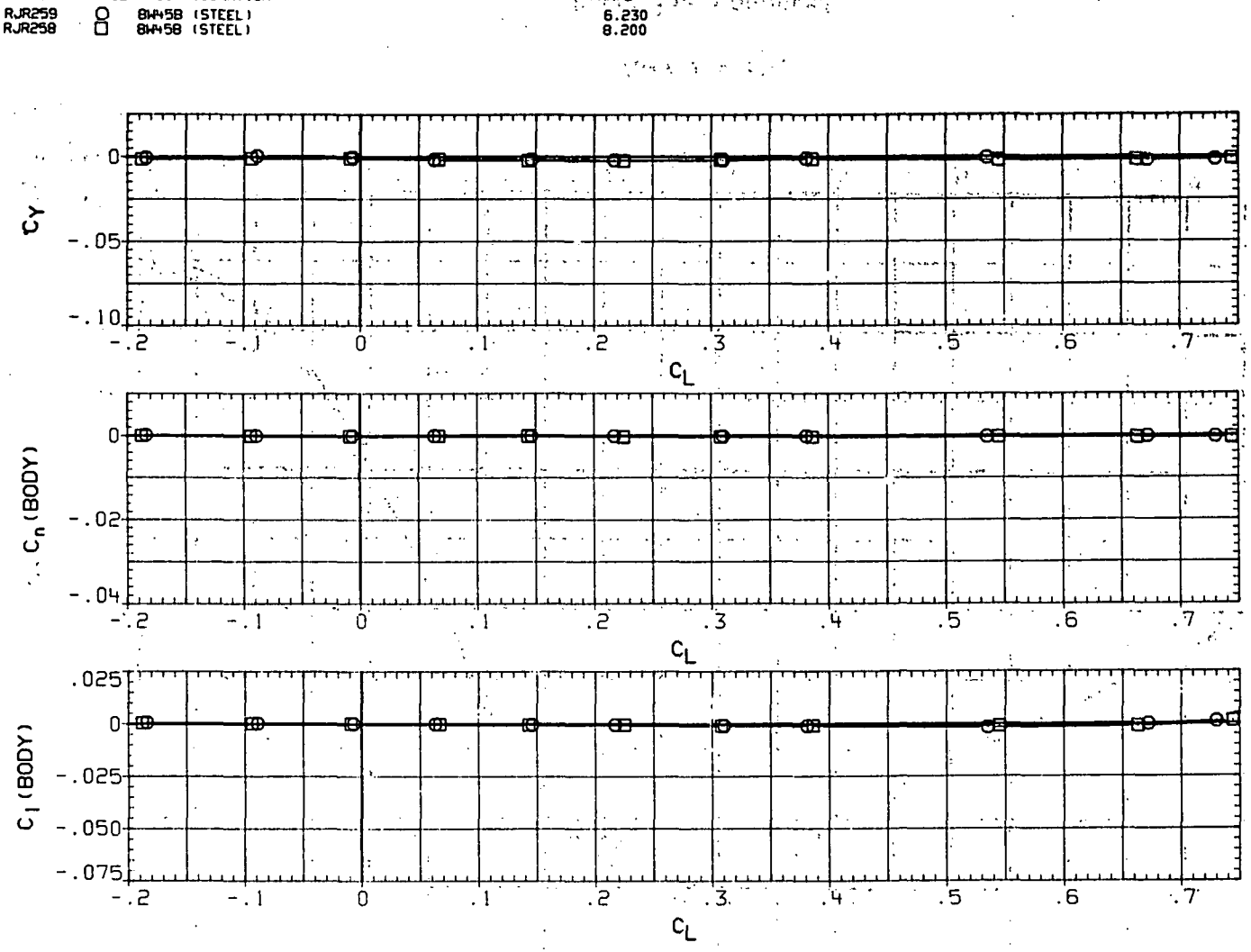

(e) C_Y, C_n and C_ℓ vs C_L.

Figure 93.– Concluded.

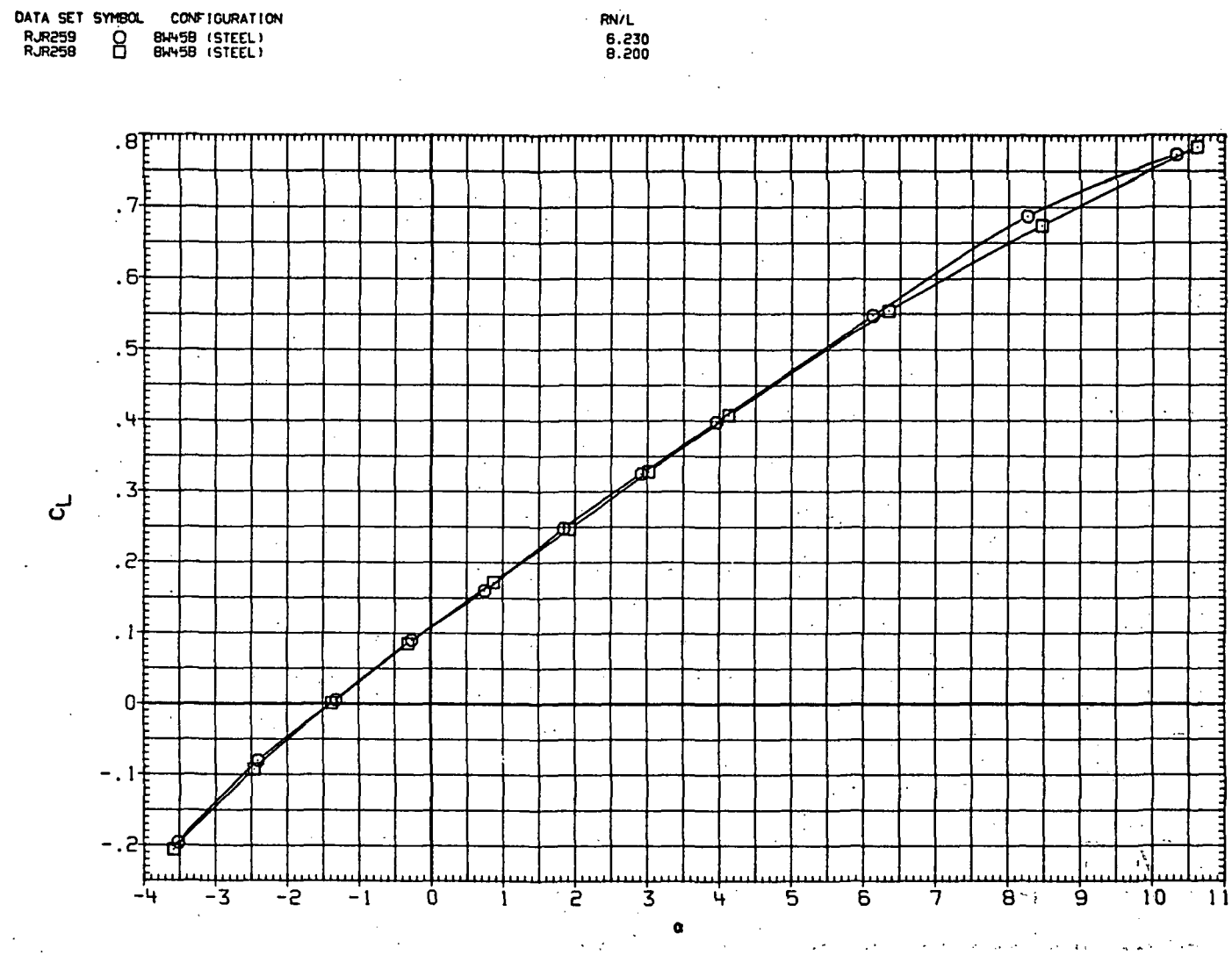

(a) C_L vs α.

Figure 94.– Reynolds-number effects on the aerodynamic characteristics of the steel swept wing-body combination ($M = 0.95$ and the NACA 65A204 airfoil).

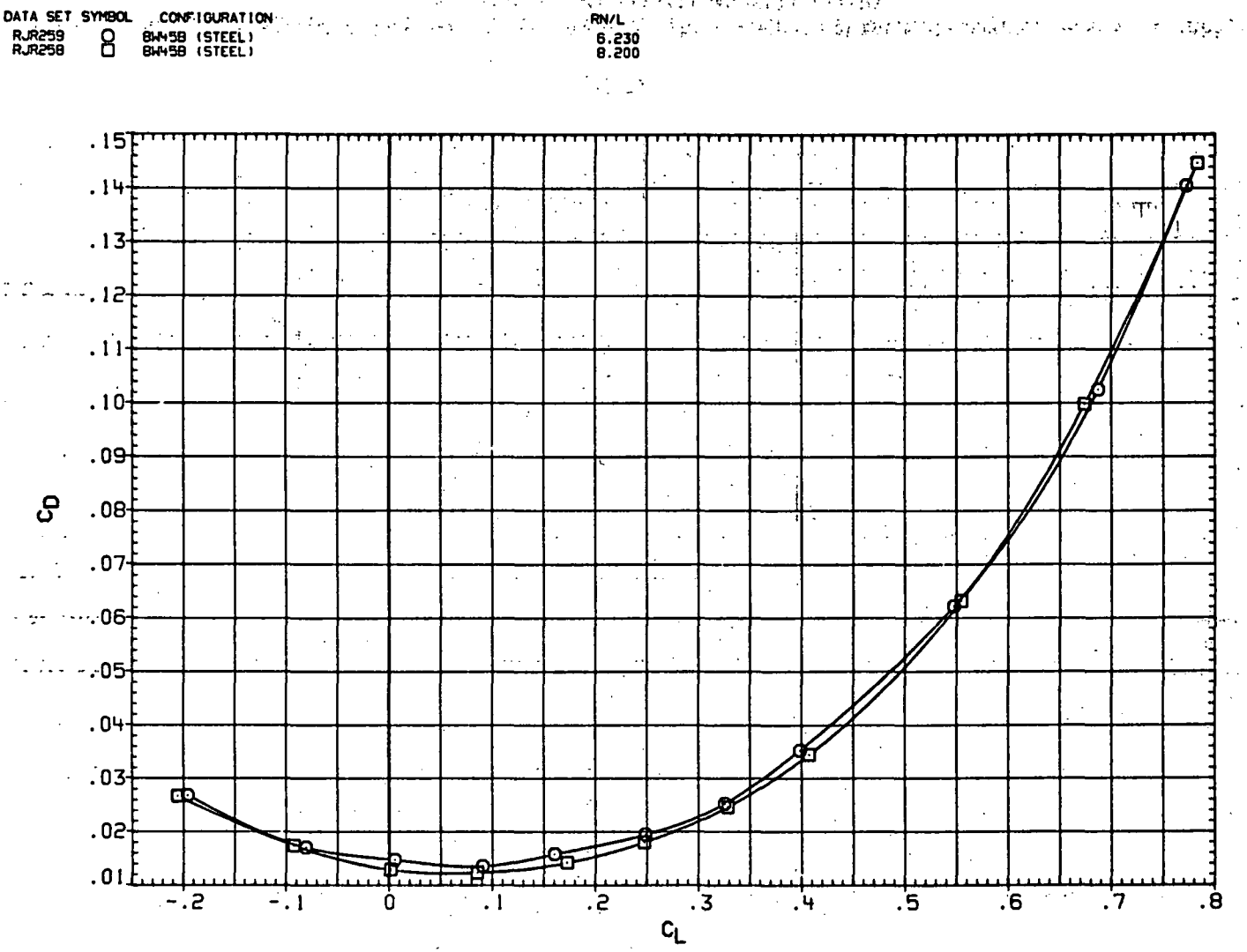

(b) C_D vs C_L.

Figure 94.– Continued.

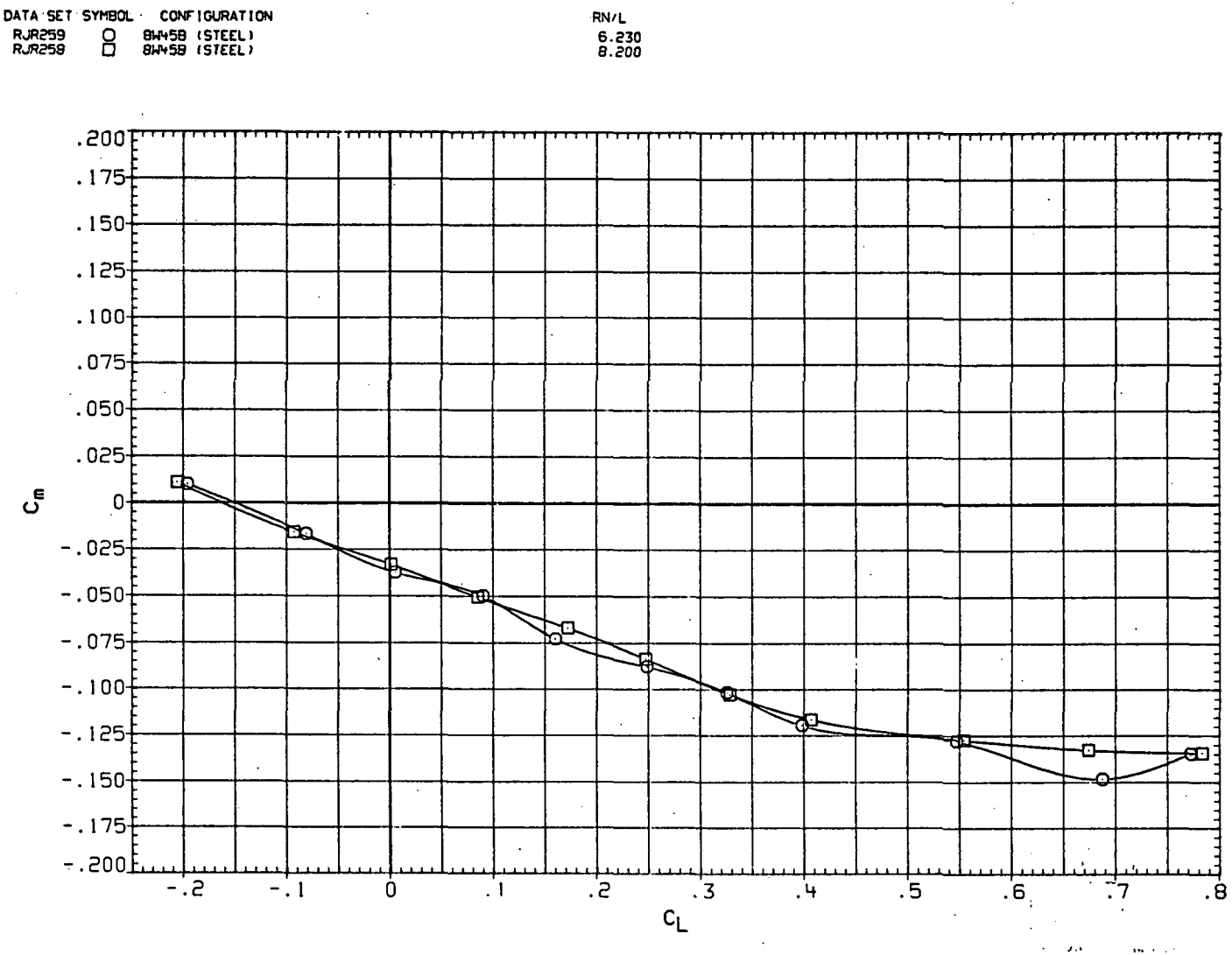

(c) C_m vs C_L.

Figure 94.– Continued.

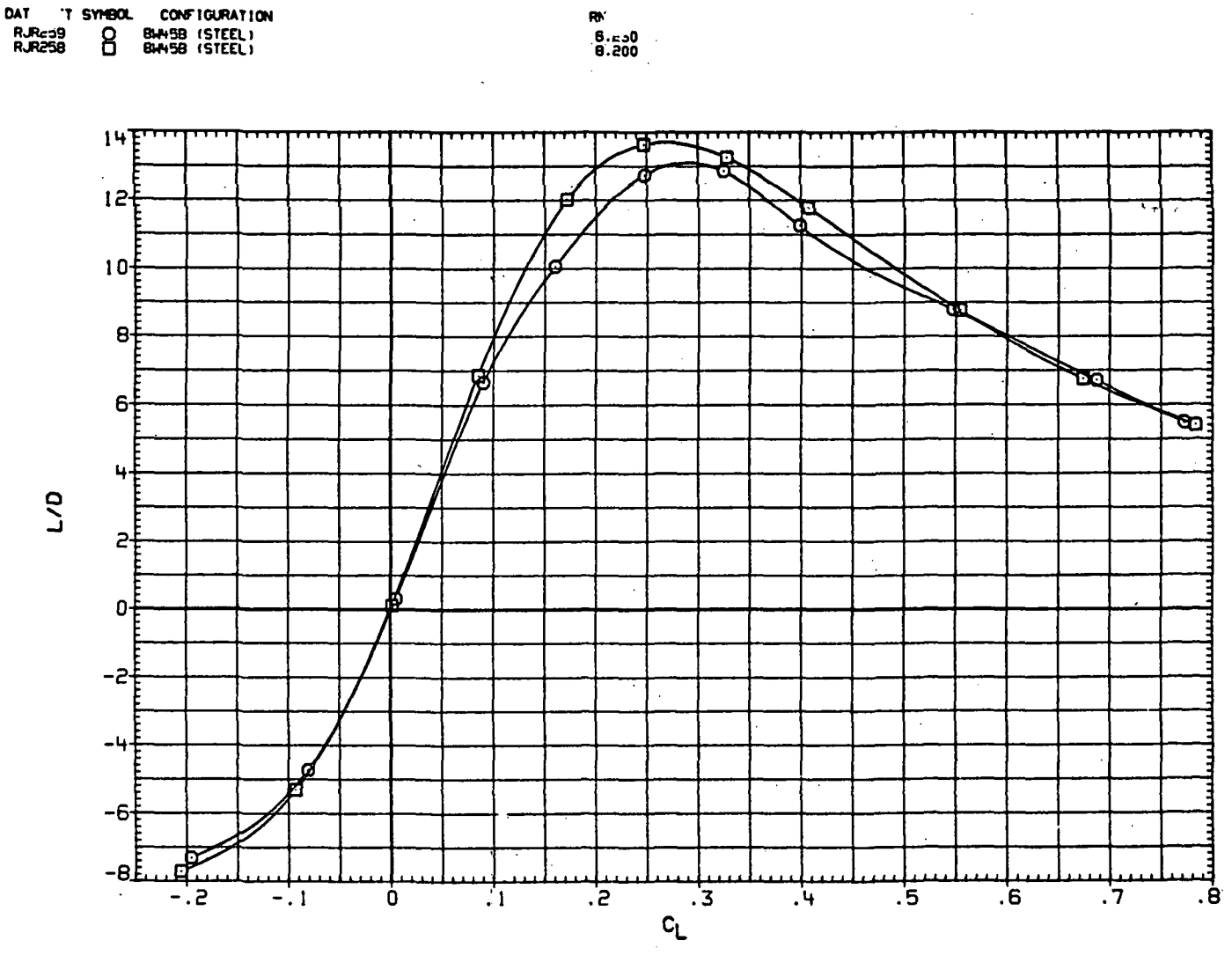

(d) L/D vs C_L.

Figure 94.– Continued.

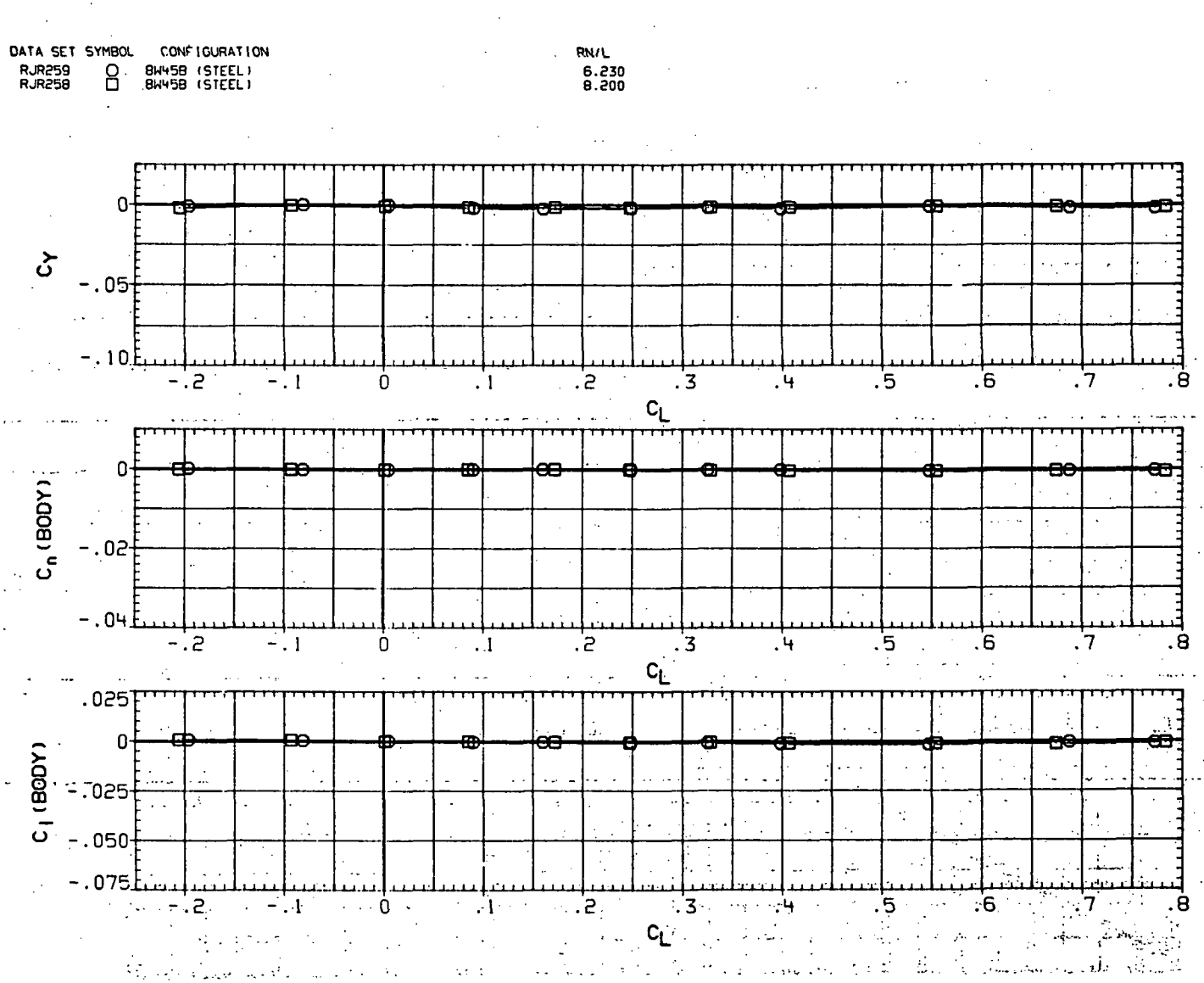

(e) C_Y, C_n and C_ℓ vs C_L.

Figure 94.– Concluded.

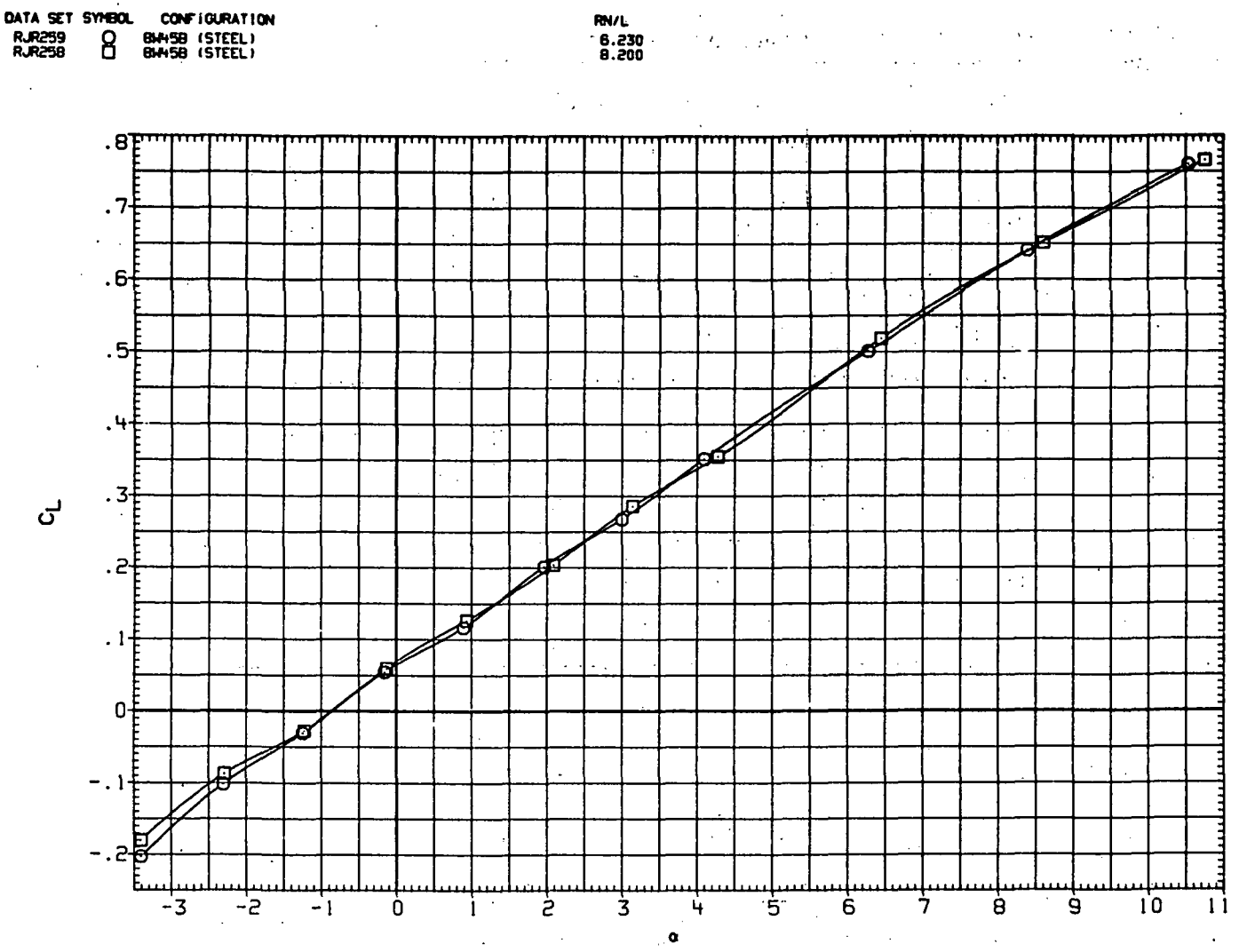

(a) C_L vs α.

Figure 95.– Reynolds-number effects on the aerodynamic characteristics of the steel swept wing-body combination (M = 1.1 and the NACA 65A204 airfoil).

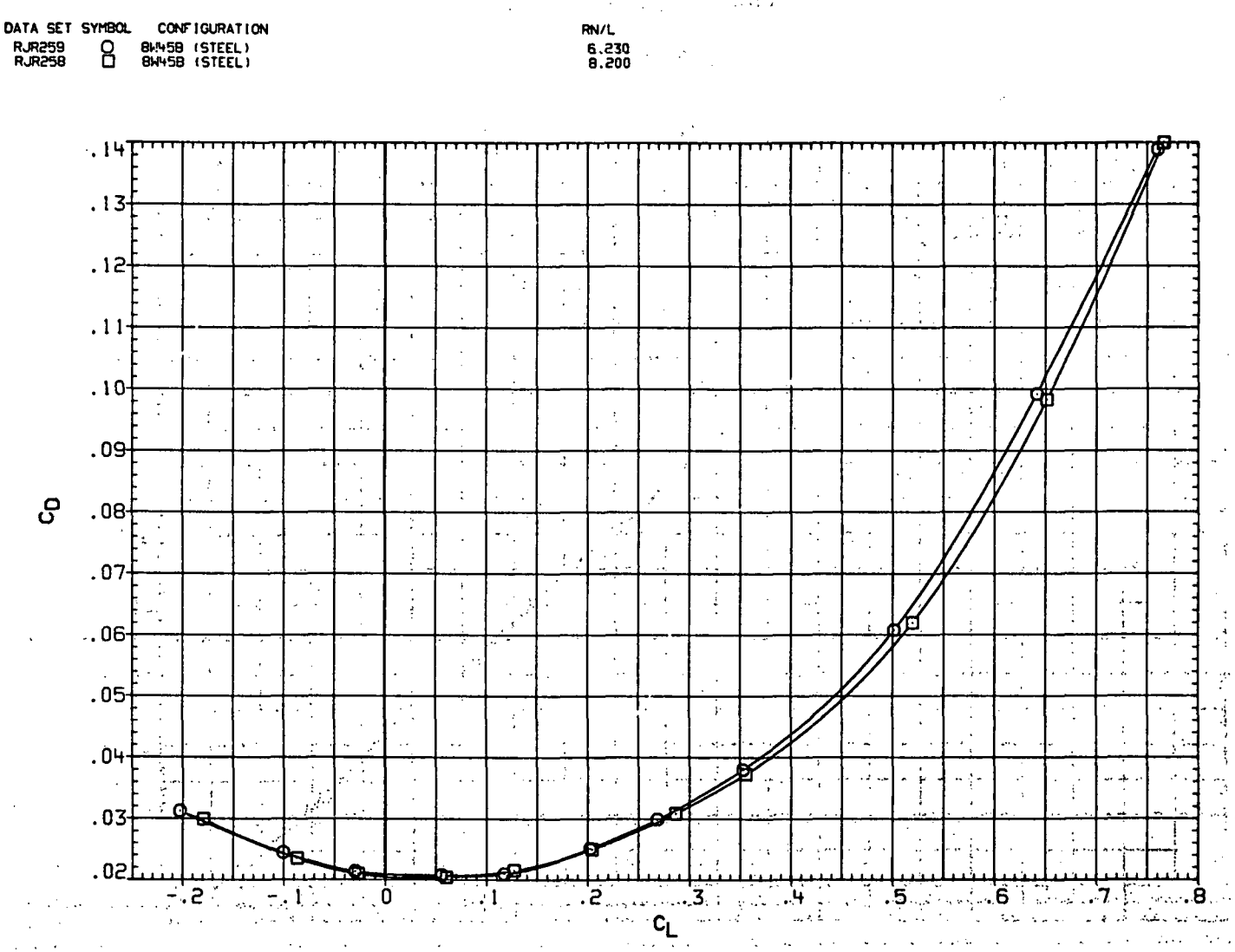

(b) C_D vs C_L.

Figure 95.– Continued.

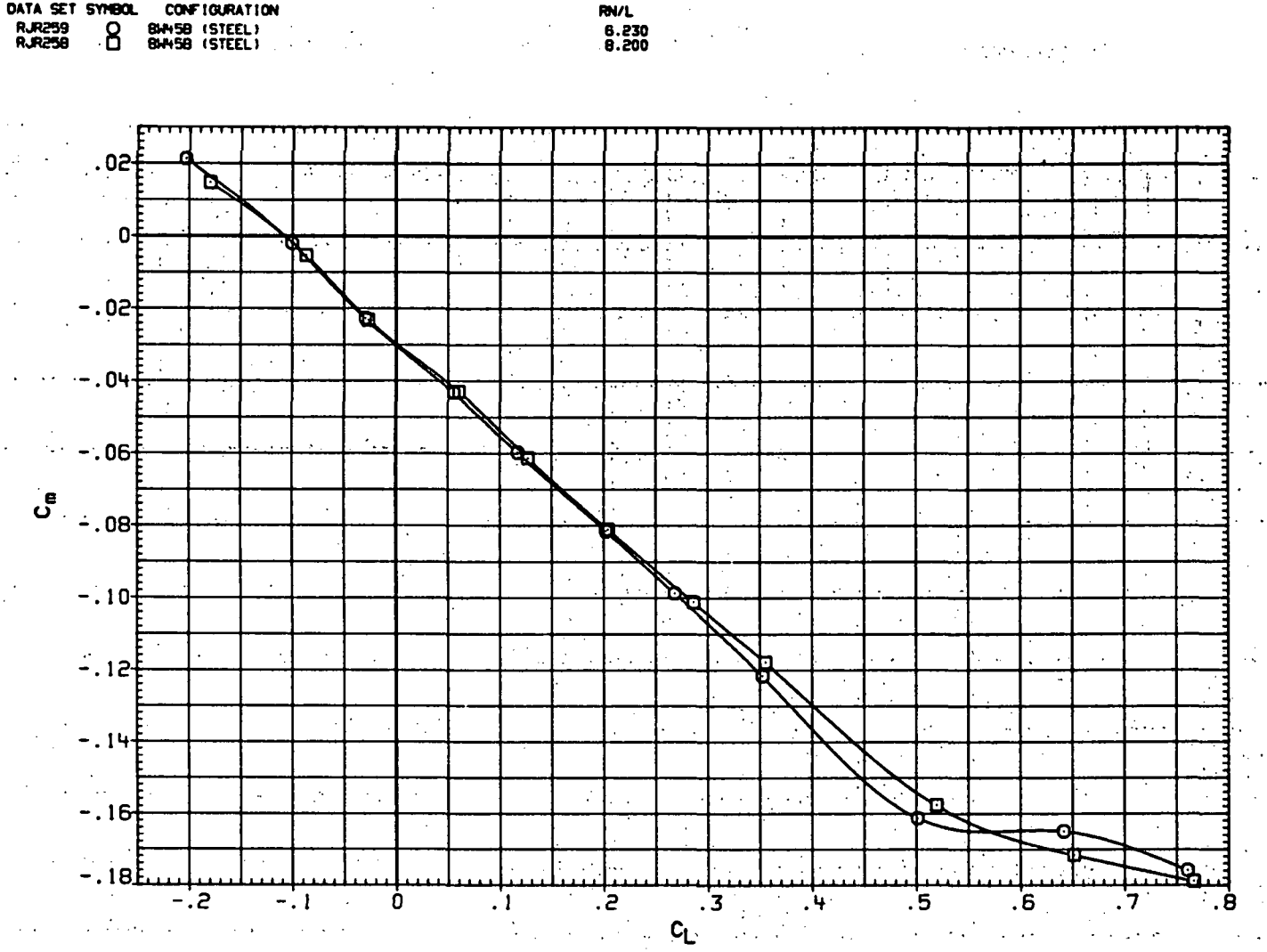

(c) C_m vs C_L.

Figure 95.– Continued.

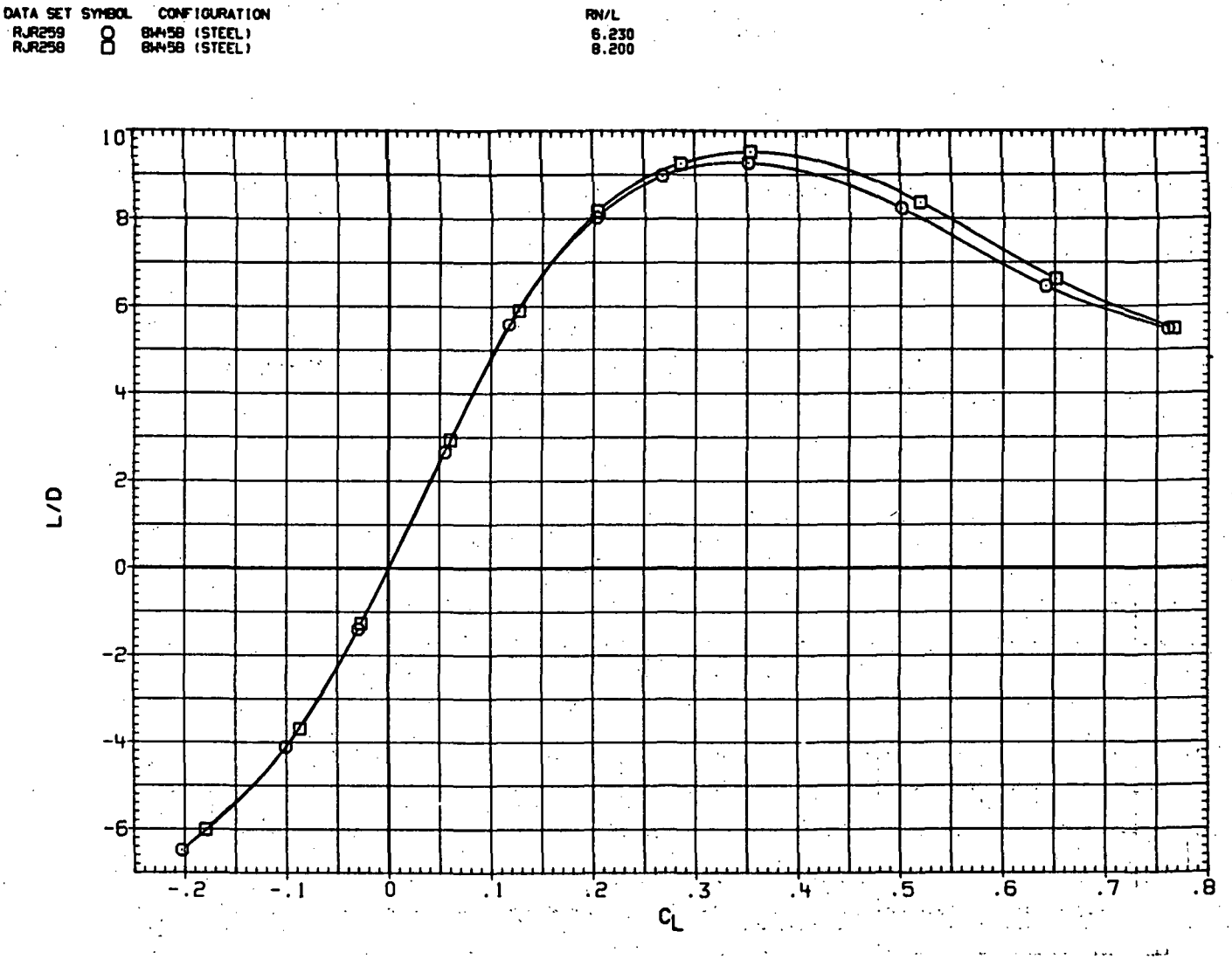

(d) L/D vs C_L.

Figure 95.– Continued.

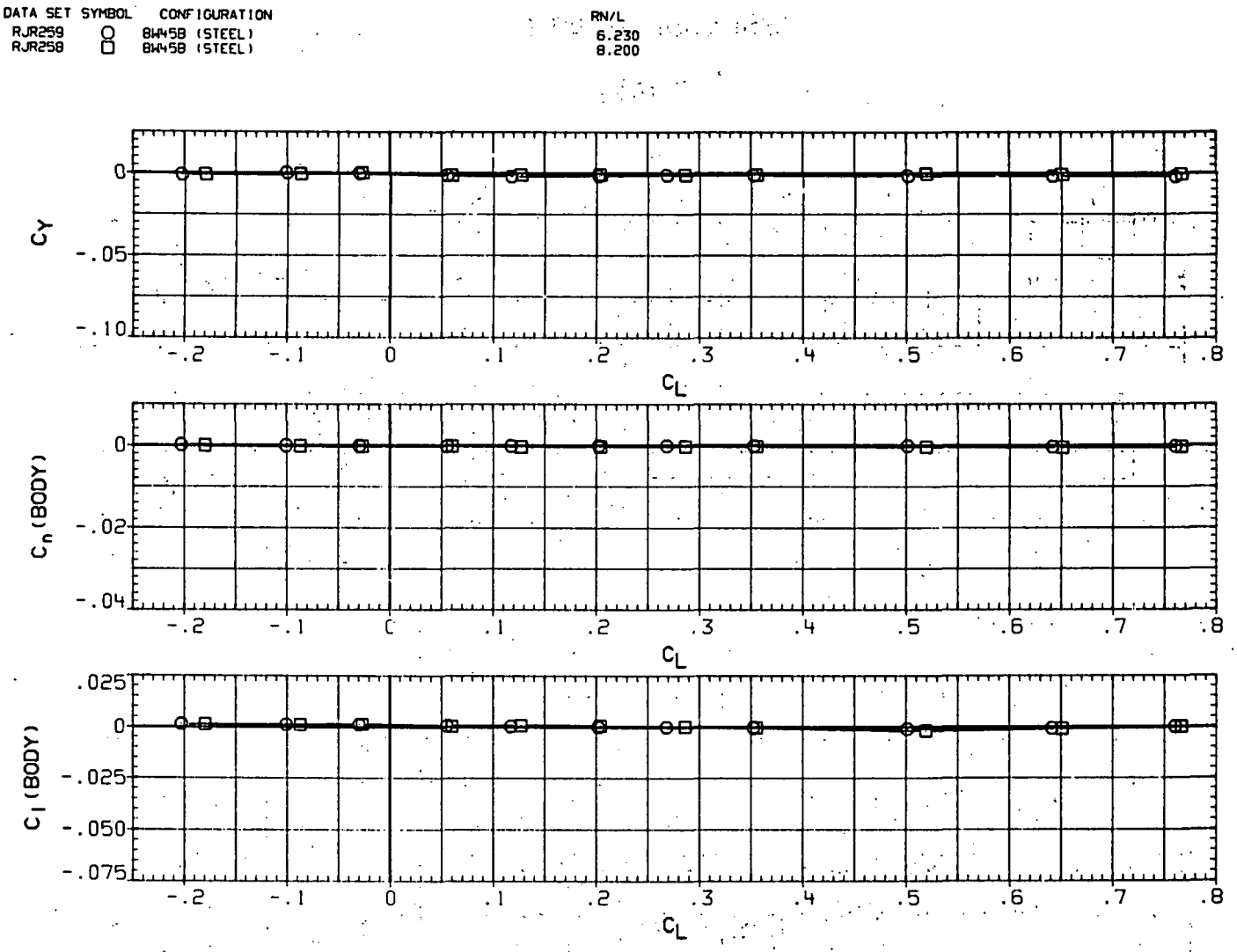

(e) C_Y, C_n and C_ℓ vs C_L.

Figure 95.– Concluded.

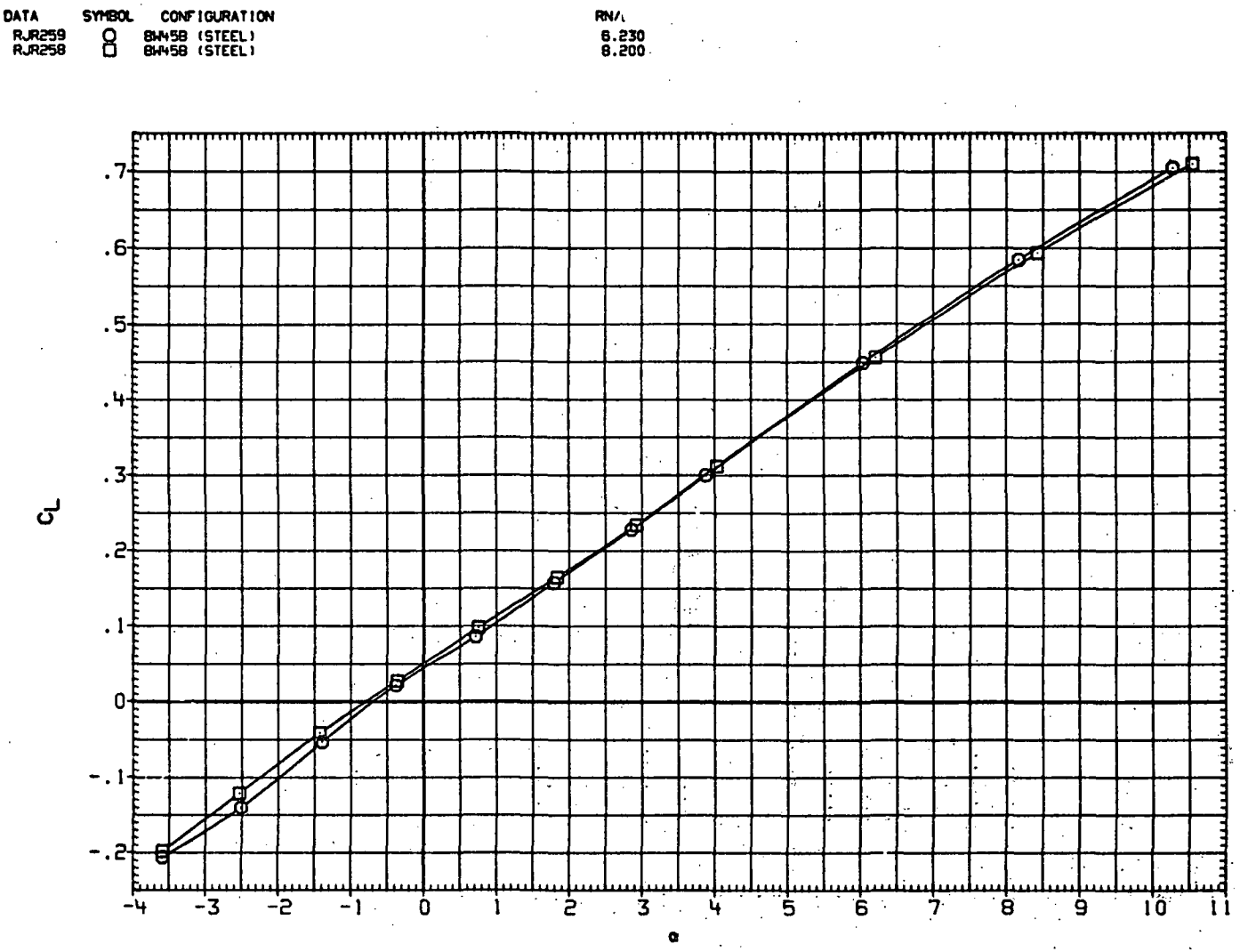

(a) C_L vs α.

Figure 96.– Reynolds-number effects on the aerodynamic characteristics of the steel swept wing-body combination ($M = 1.2$ and the NACA 65A204 airfoil).

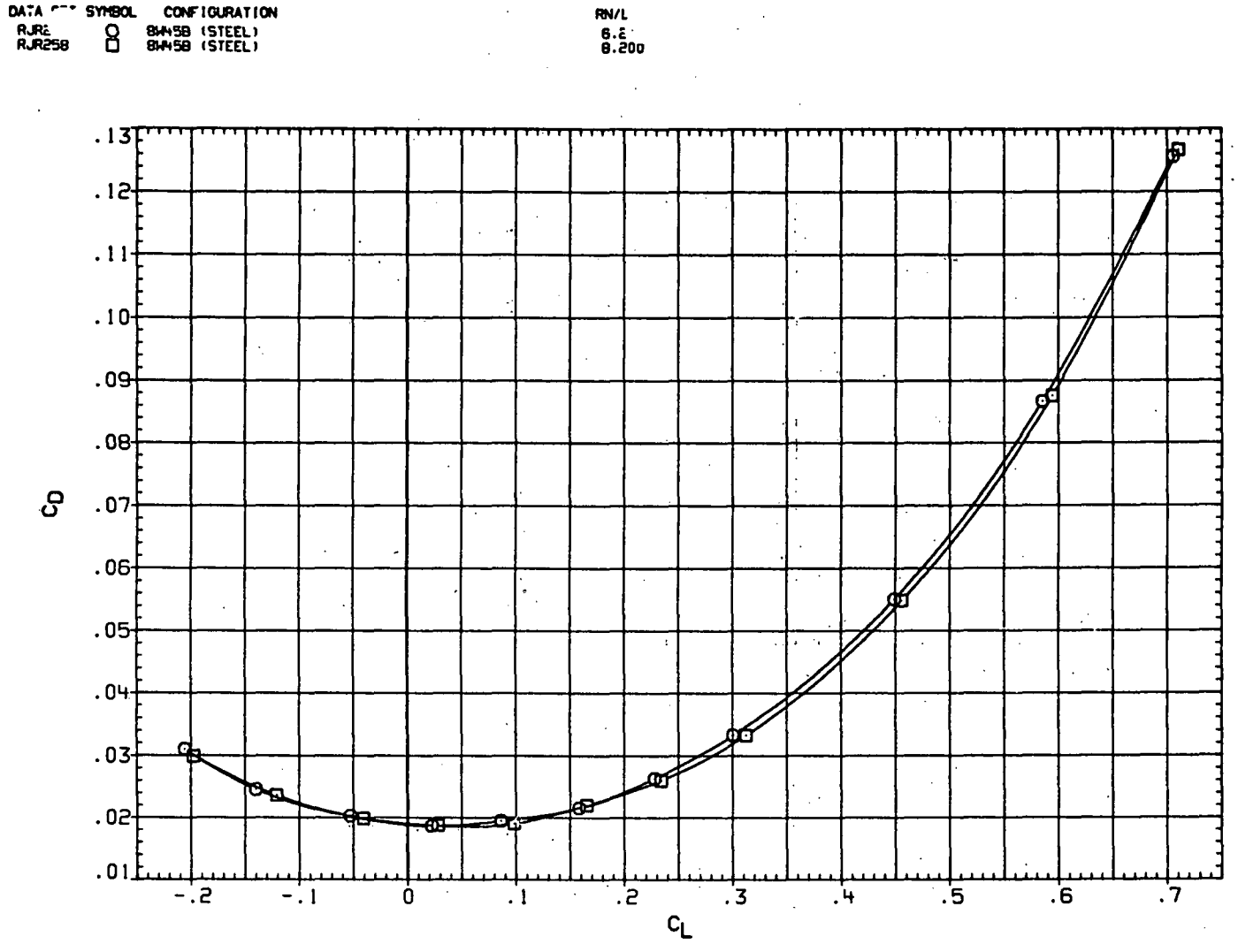

(b) C_D vs C_L.

Figure 96.– Continued.

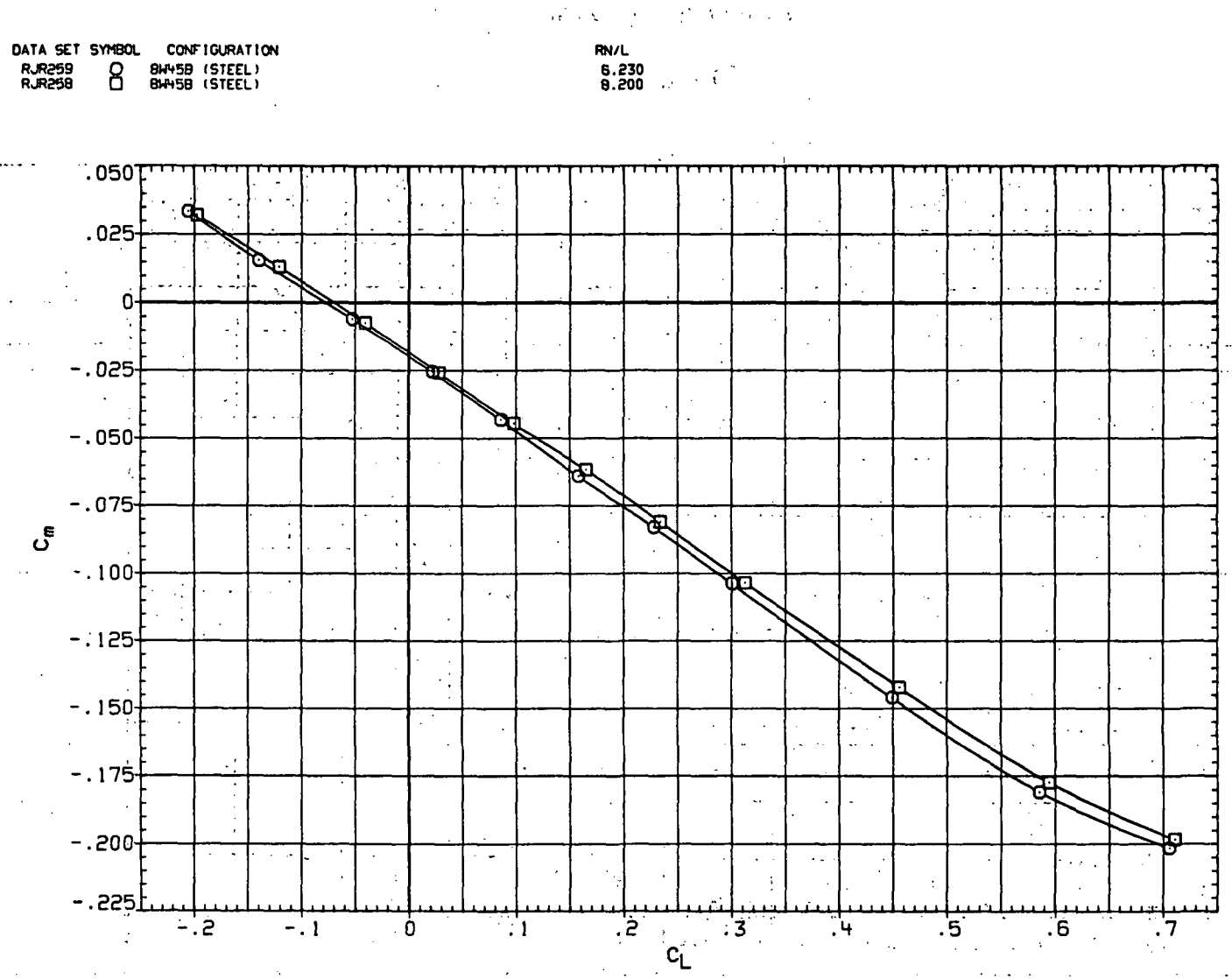

(c) C_m vs C_L.

Figure 96.– Continued.

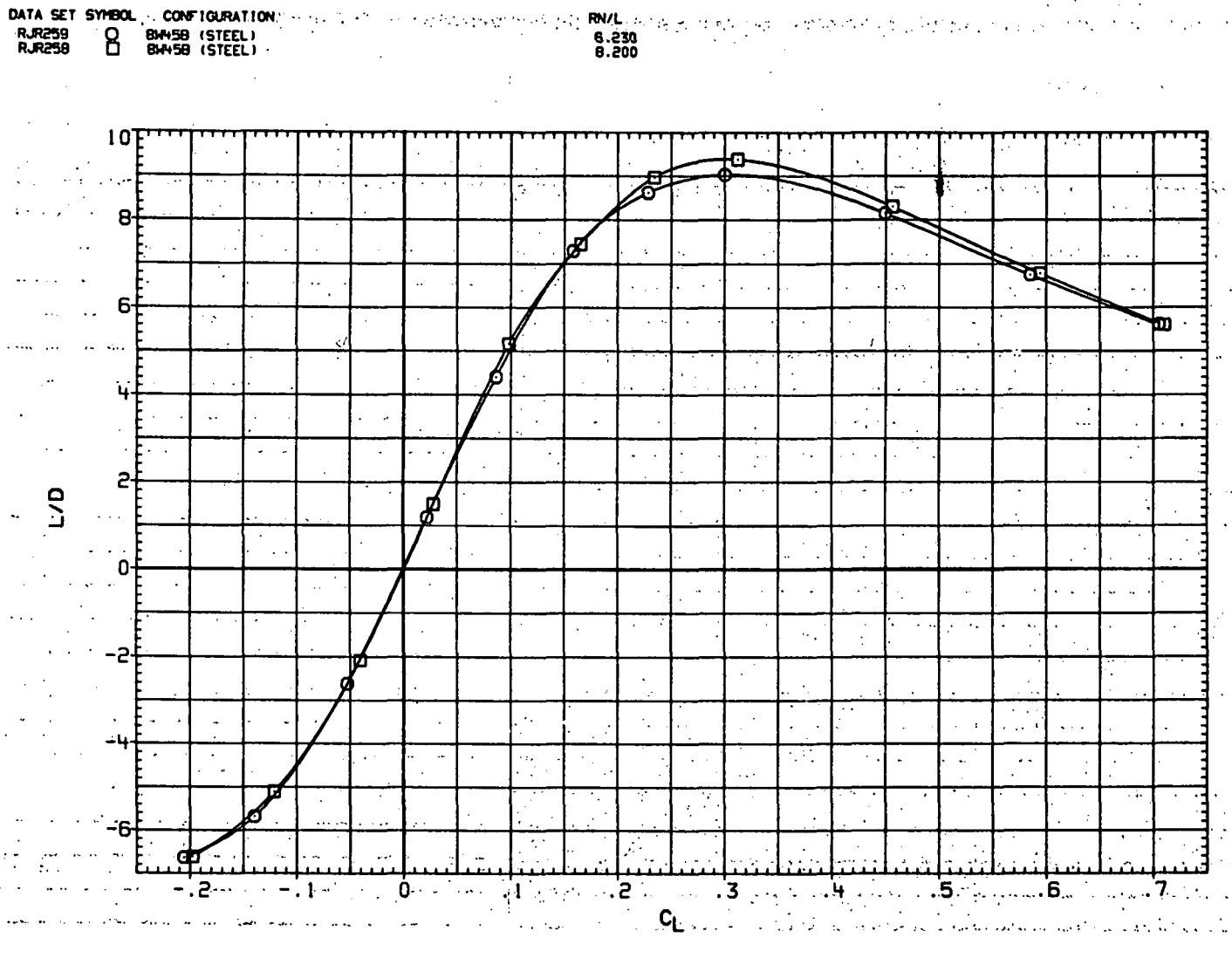

(d) L/D vs C_L.

Figure 96.– Continued.

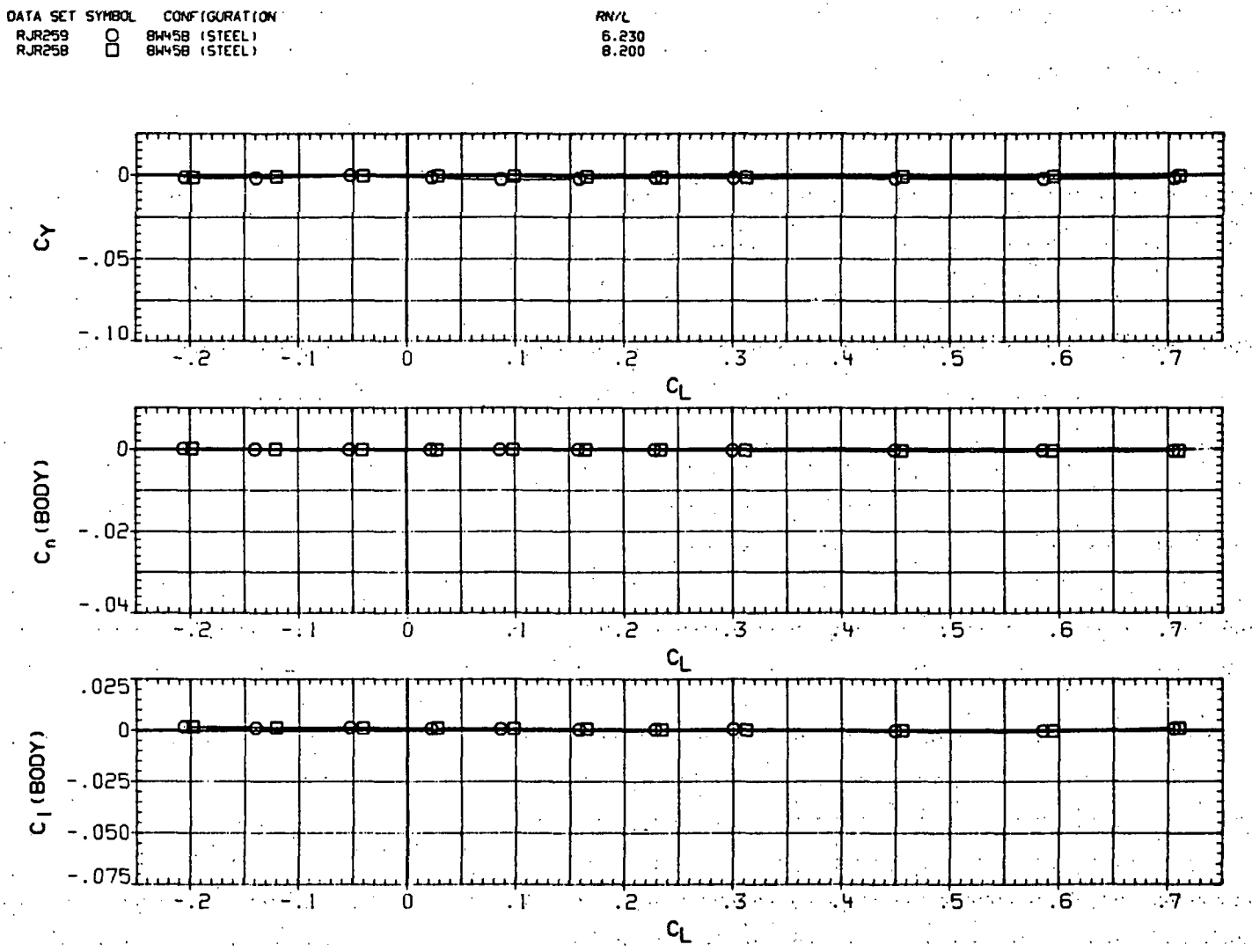

(e) C_Y, C_n and C_ℓ vs C_L.

Figure 96.– Concluded.

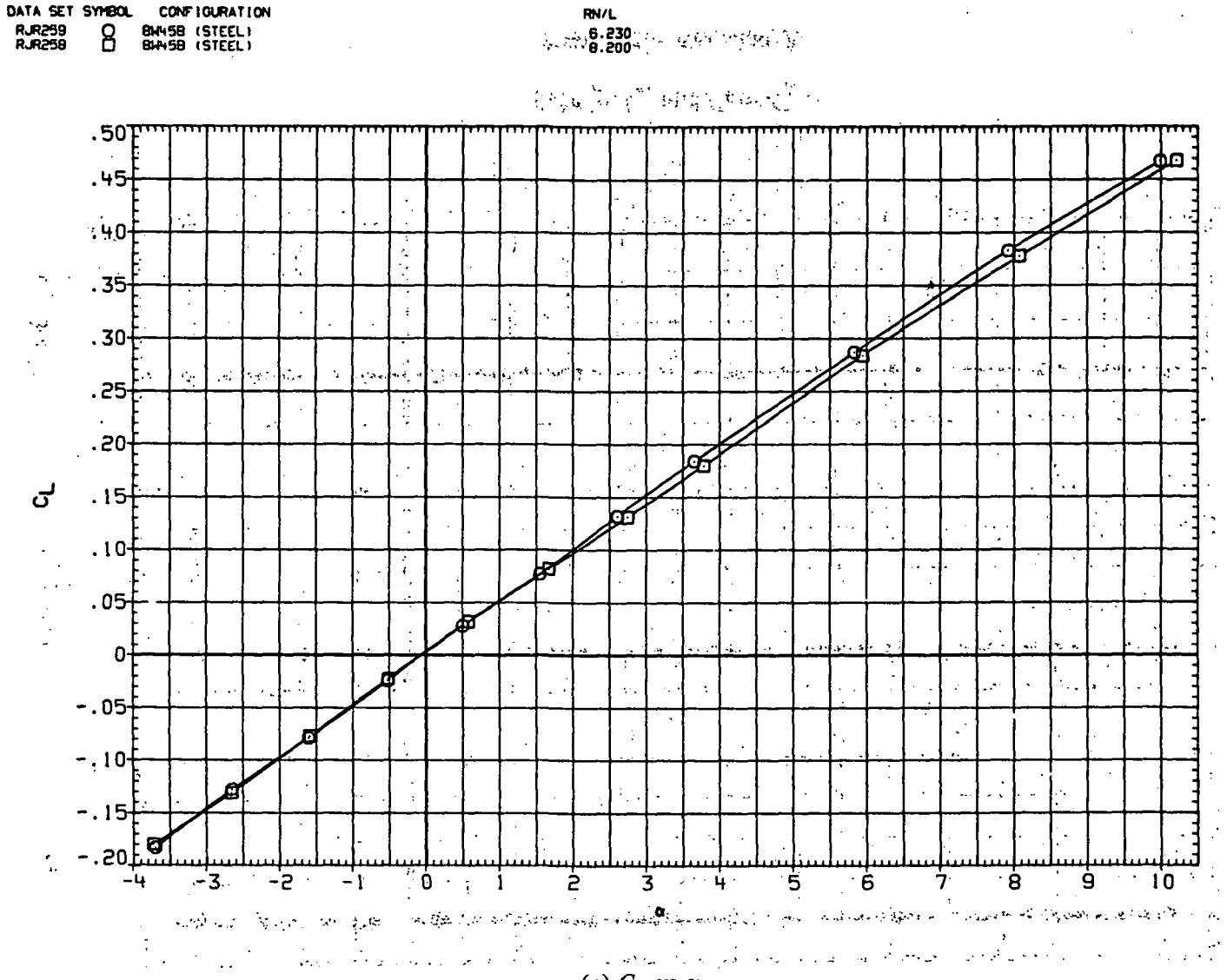

(a) C_L vs α.

Figure 97.– Reynolds-number effects on the aerodynamic characteristics of the steel swept wing-body combination (M = 1.6 and the NACA 65A204 airfoil).

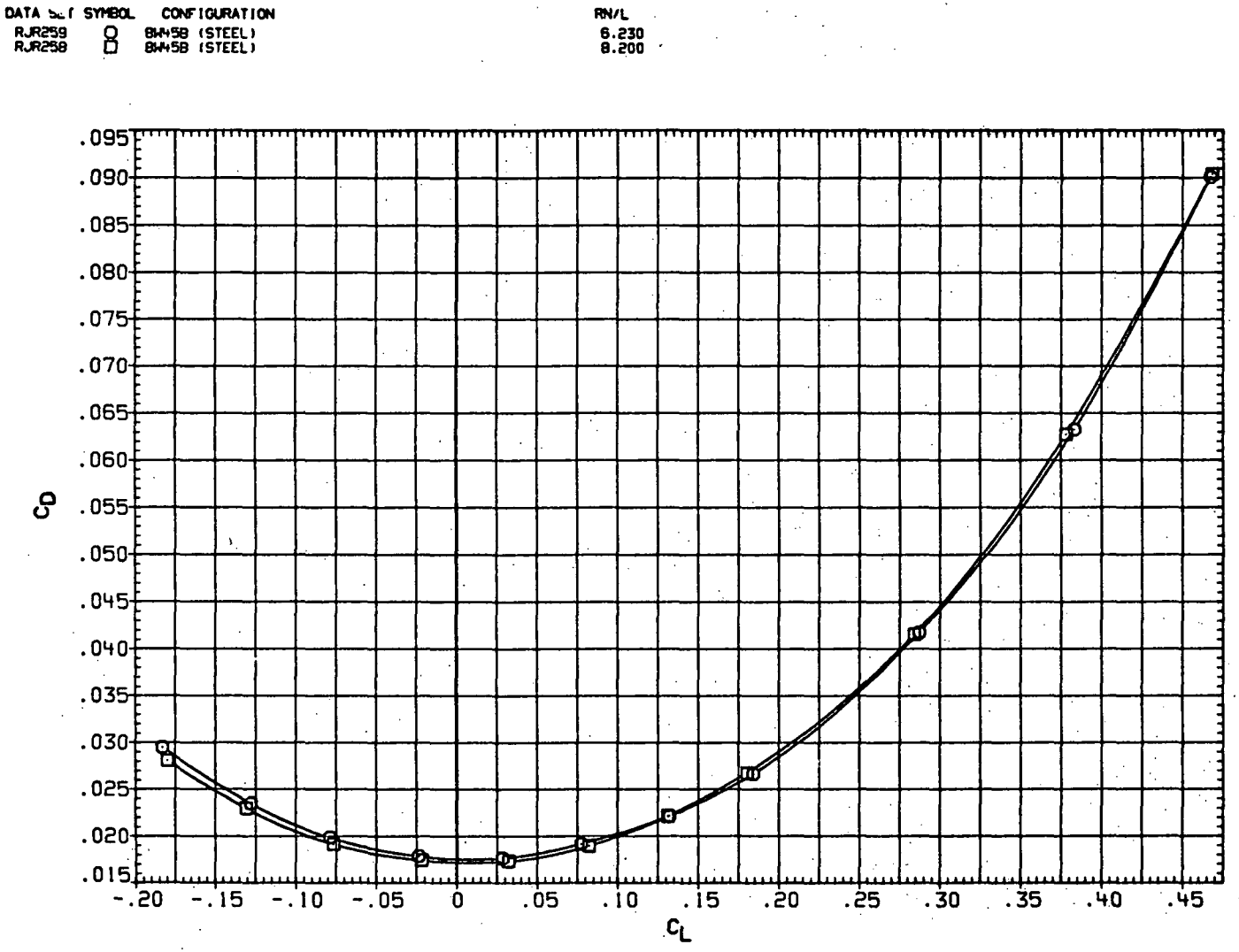

(b) C_D vs C_L.

Figure 97.– Continued.

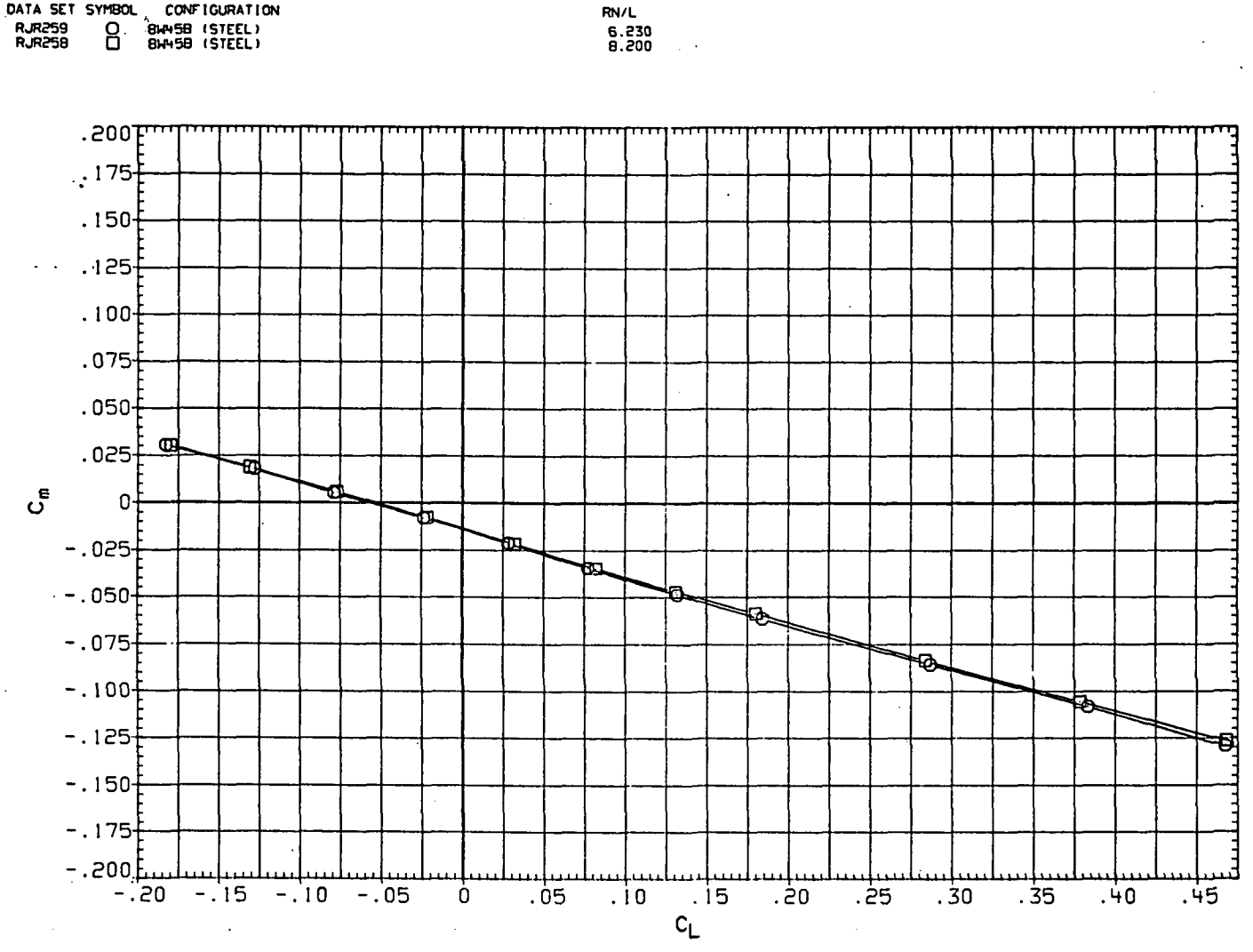

(c) C_m vs C_L.

Figure 97.– Continued.

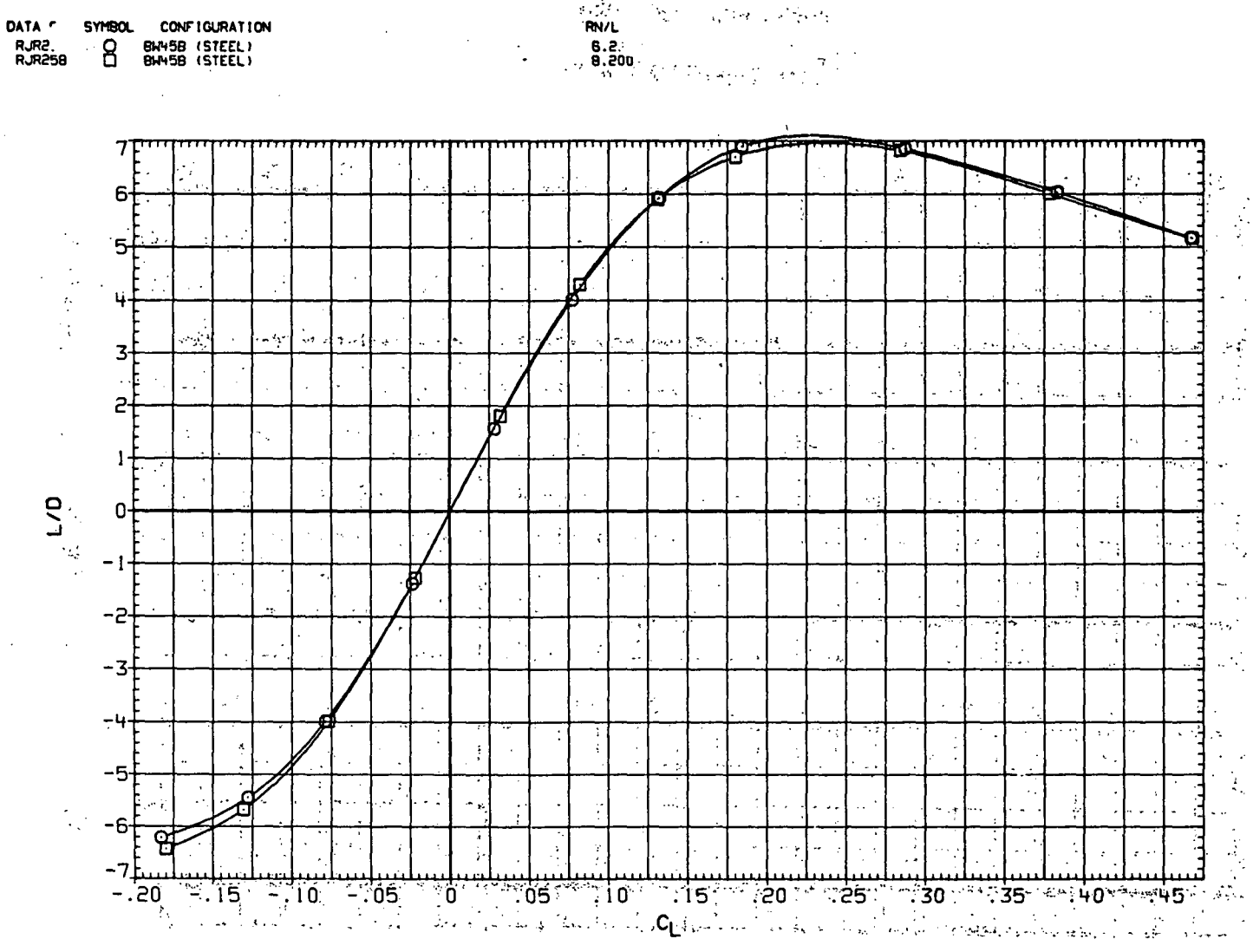

(d) L/D vs C_L.

Figure 97.– Continued.

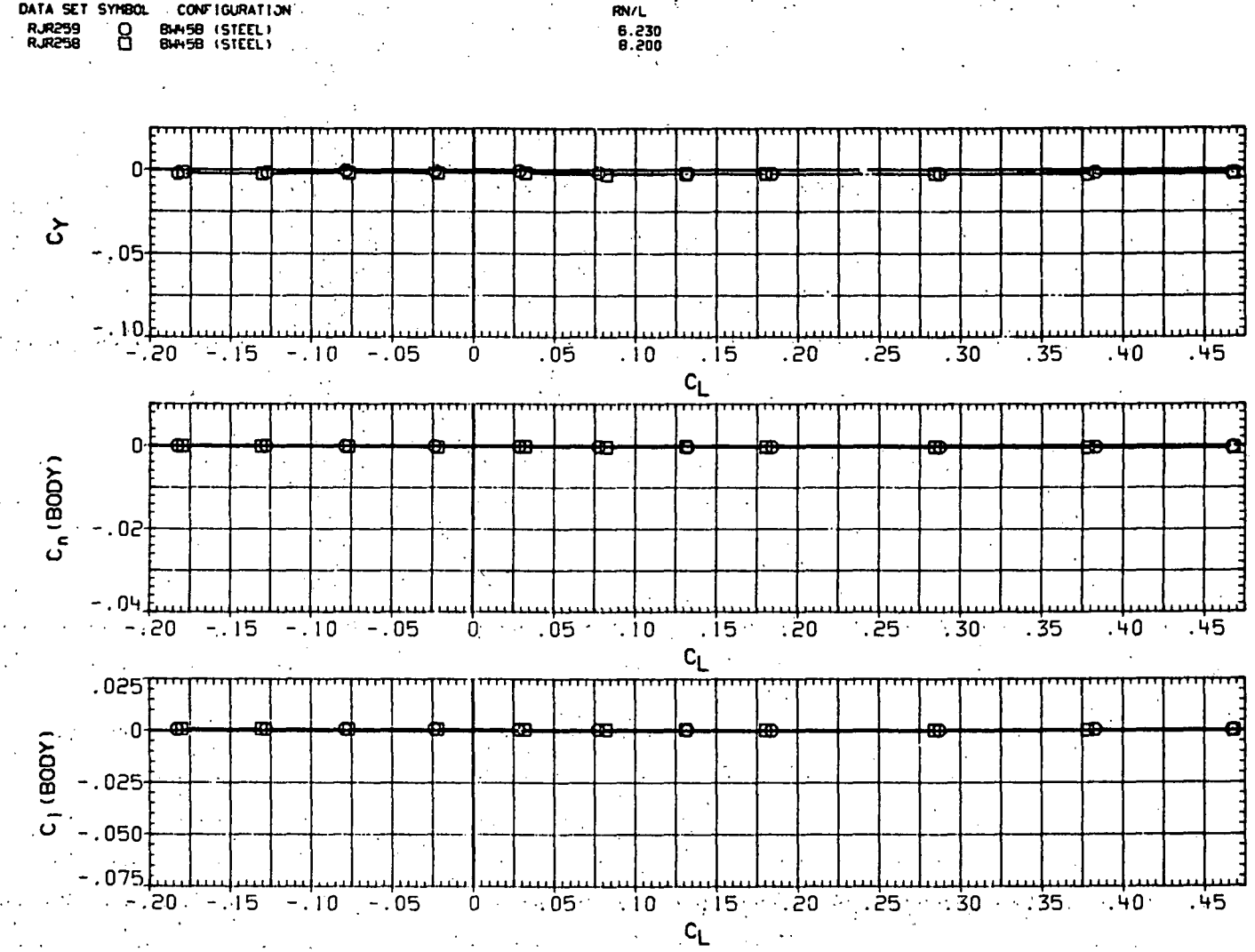

(e) C_Y, C_n and C_ℓ vs C_L.

Figure 97.– Concluded.

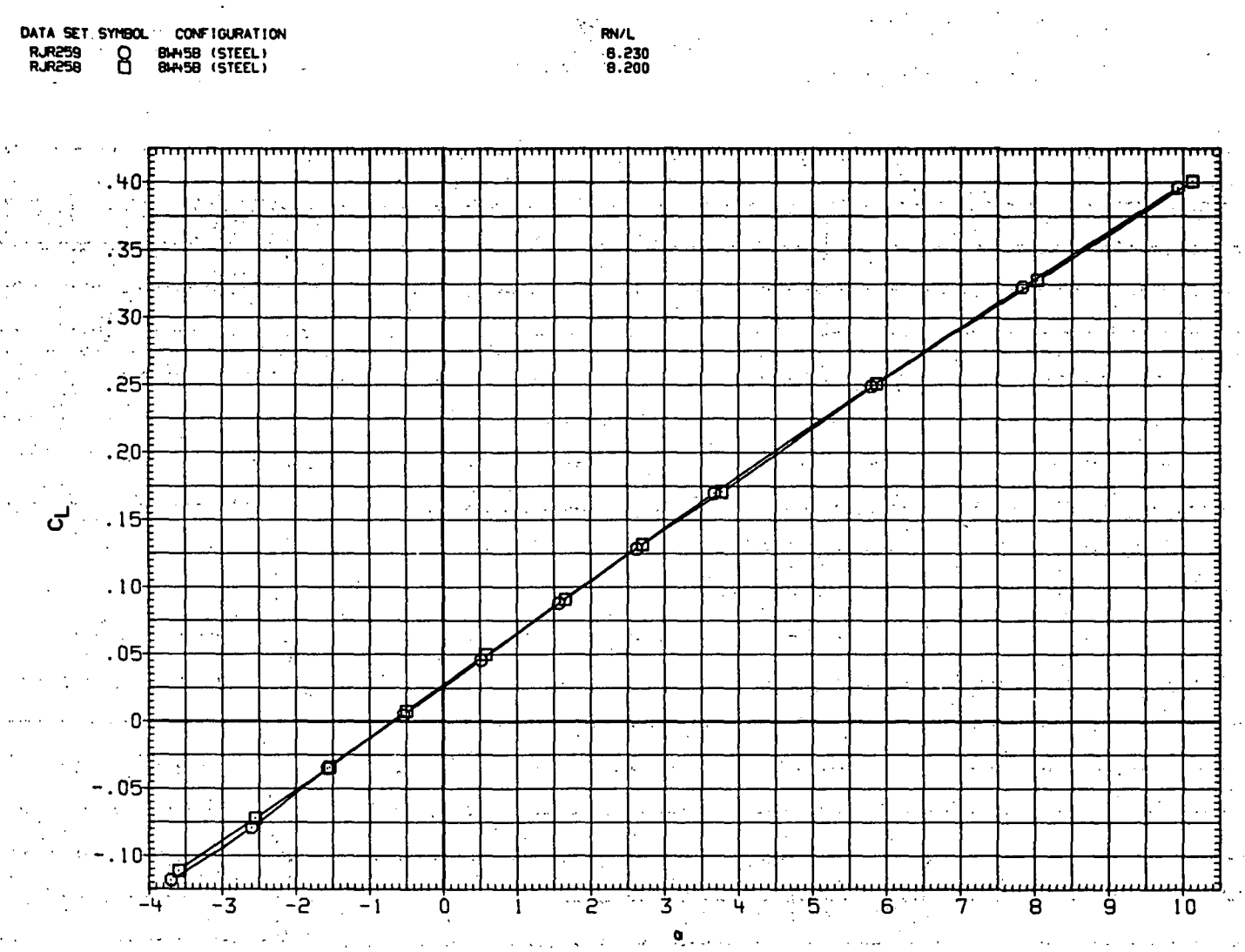

(a) C_L vs α.

Figure 98.— Reynolds-number effects on the aerodynamic characteristics of the steel swept wing-body combination (M = 2.0 and the NACA 65A204 airfoil).

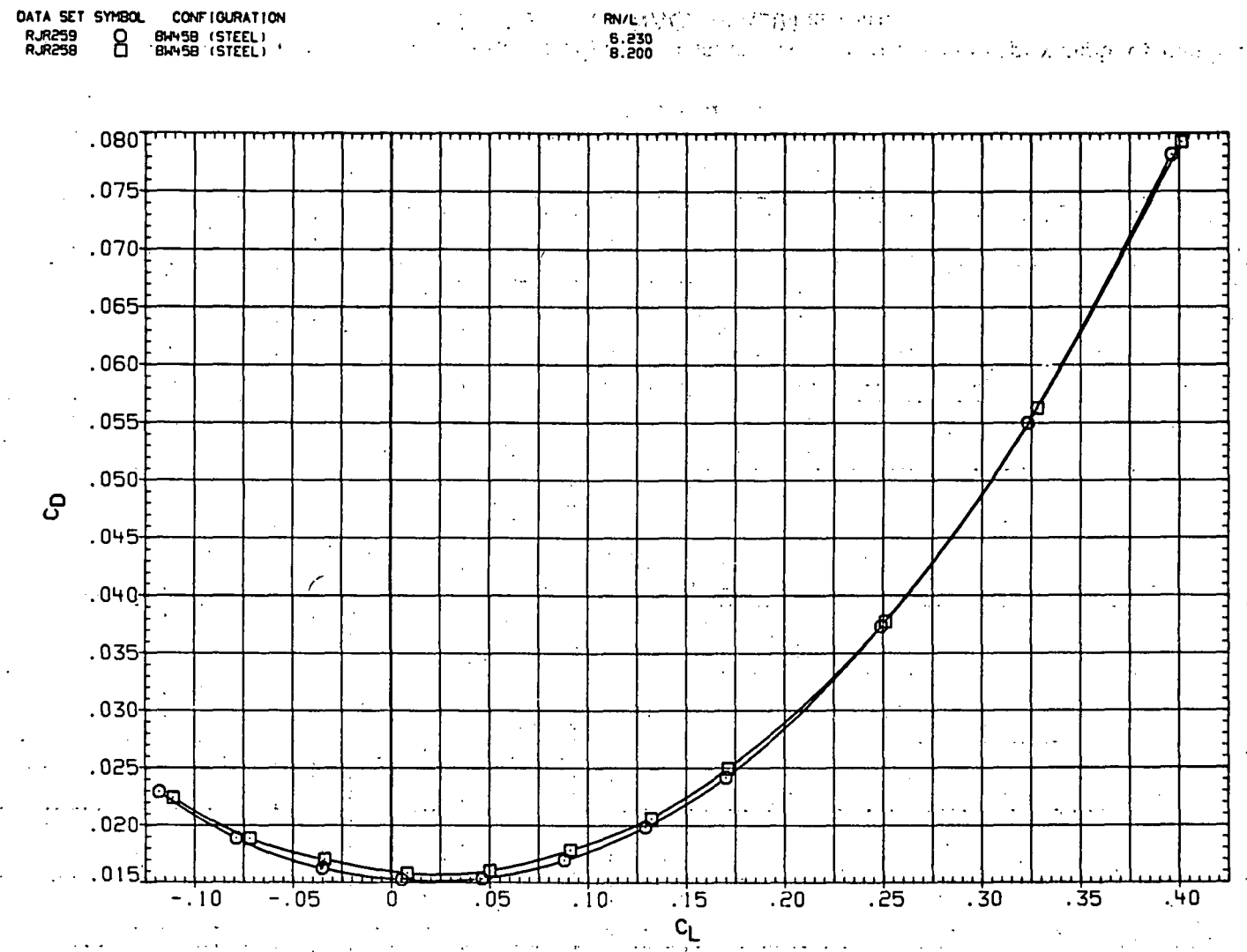

(b) C_D vs C_L.

Figure 98.– Continued.

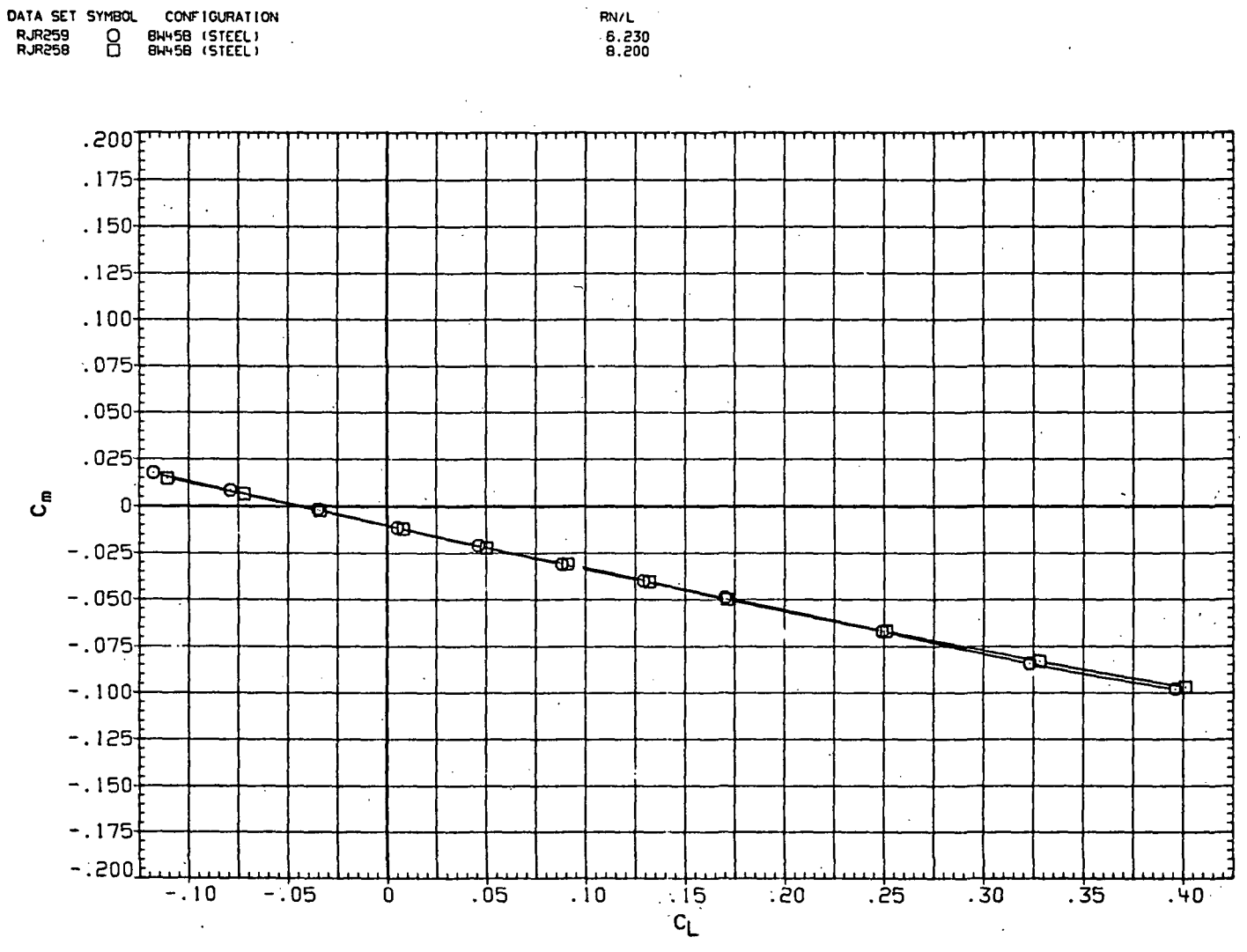

(c) C_m vs C_L.

Figure 98.– Continued.

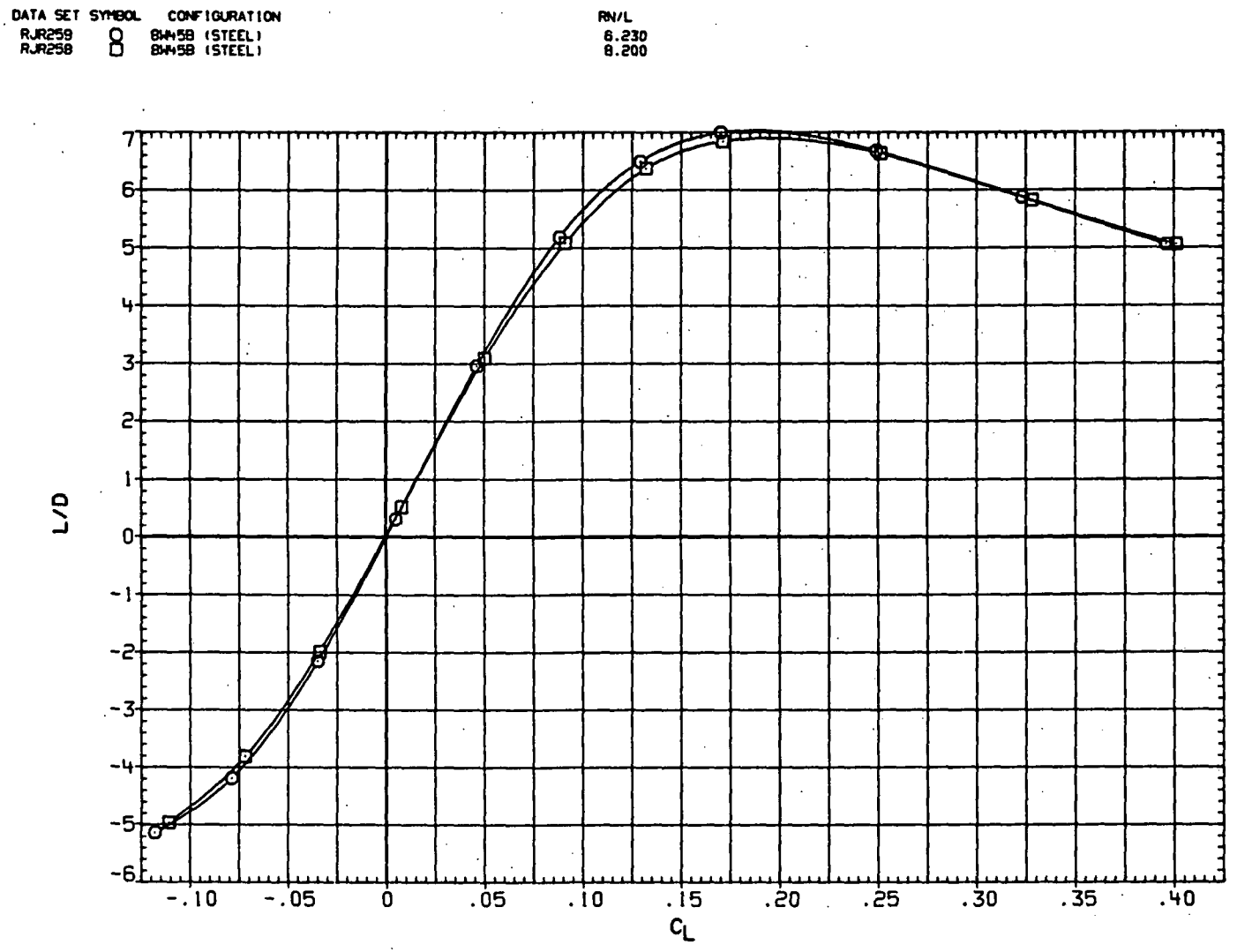

(d) L/D vs C_L.

Figure 98.– Continued.

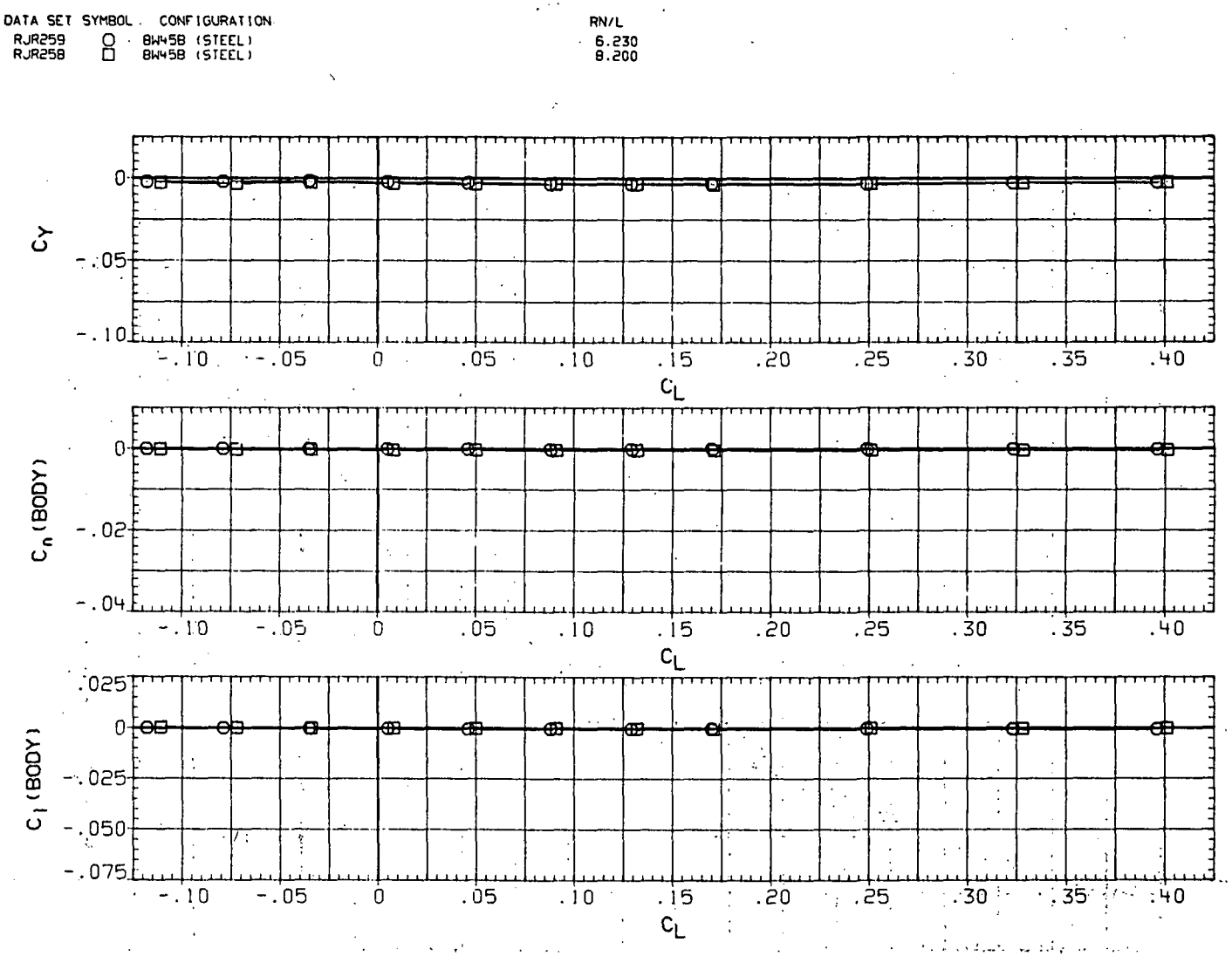

(e) C_Y, C_n and C_ℓ vs C_L.

Figure 98.– Concluded.

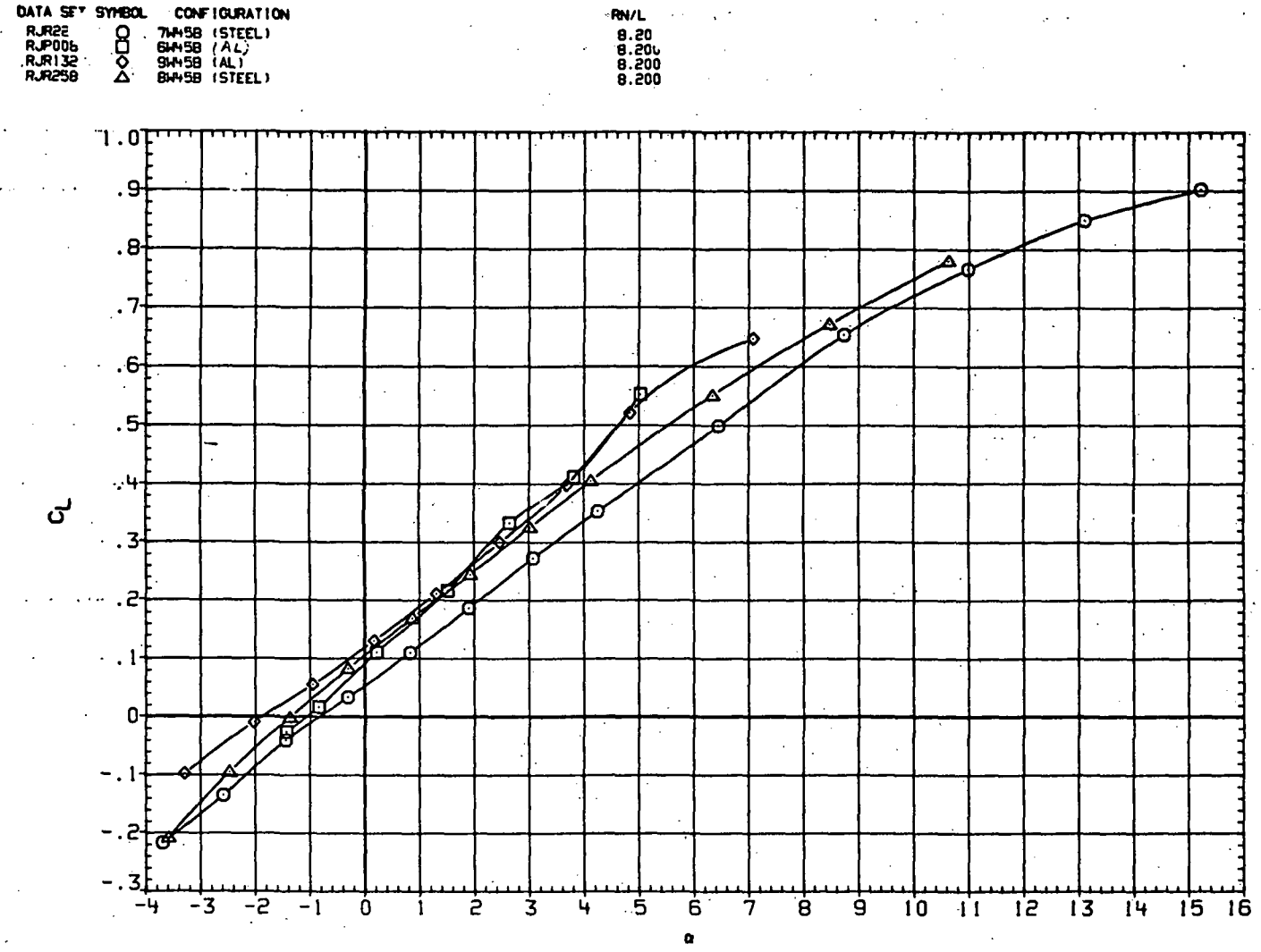

(a) C_L vs α.

Figure 99.– Flexibility effects, airfoil modification effects and planform effects on the aerodynamic characteristics ($\Lambda = 45°$ and $M = 0.95$).

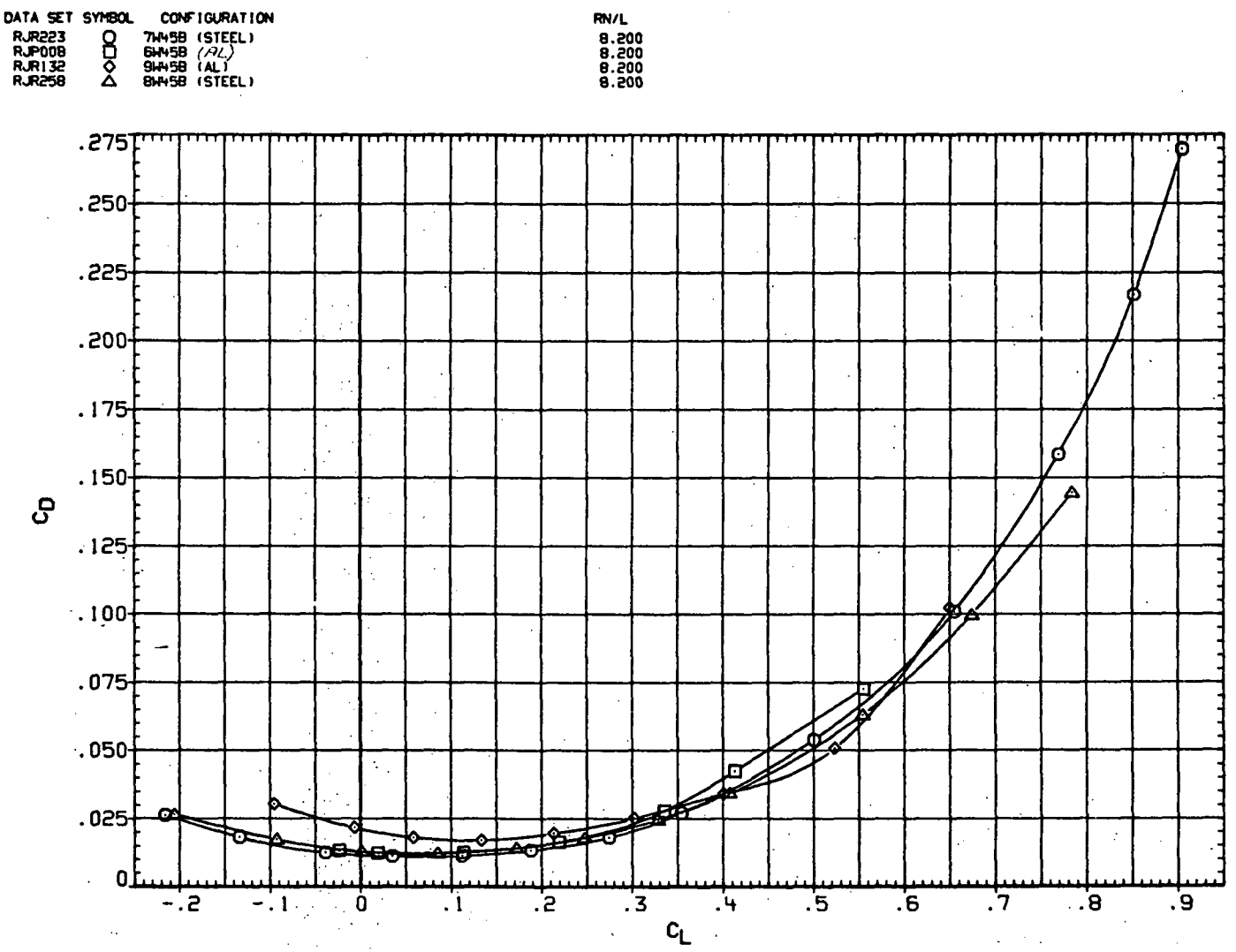

(b) C_D vs C_L.

Figure 99.– Continued.

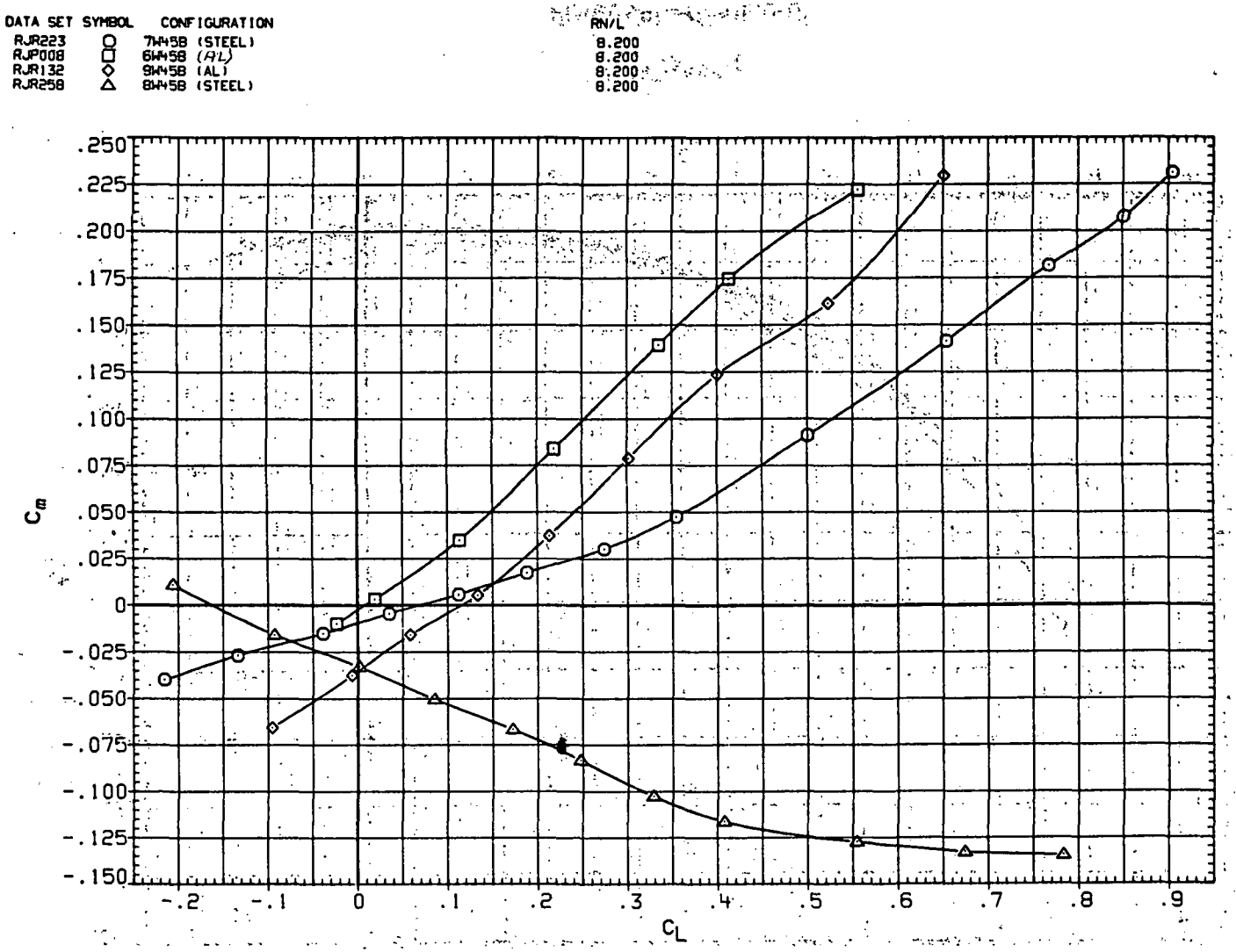

(c) C_m vs C_L.

Figure 99.– Continued.

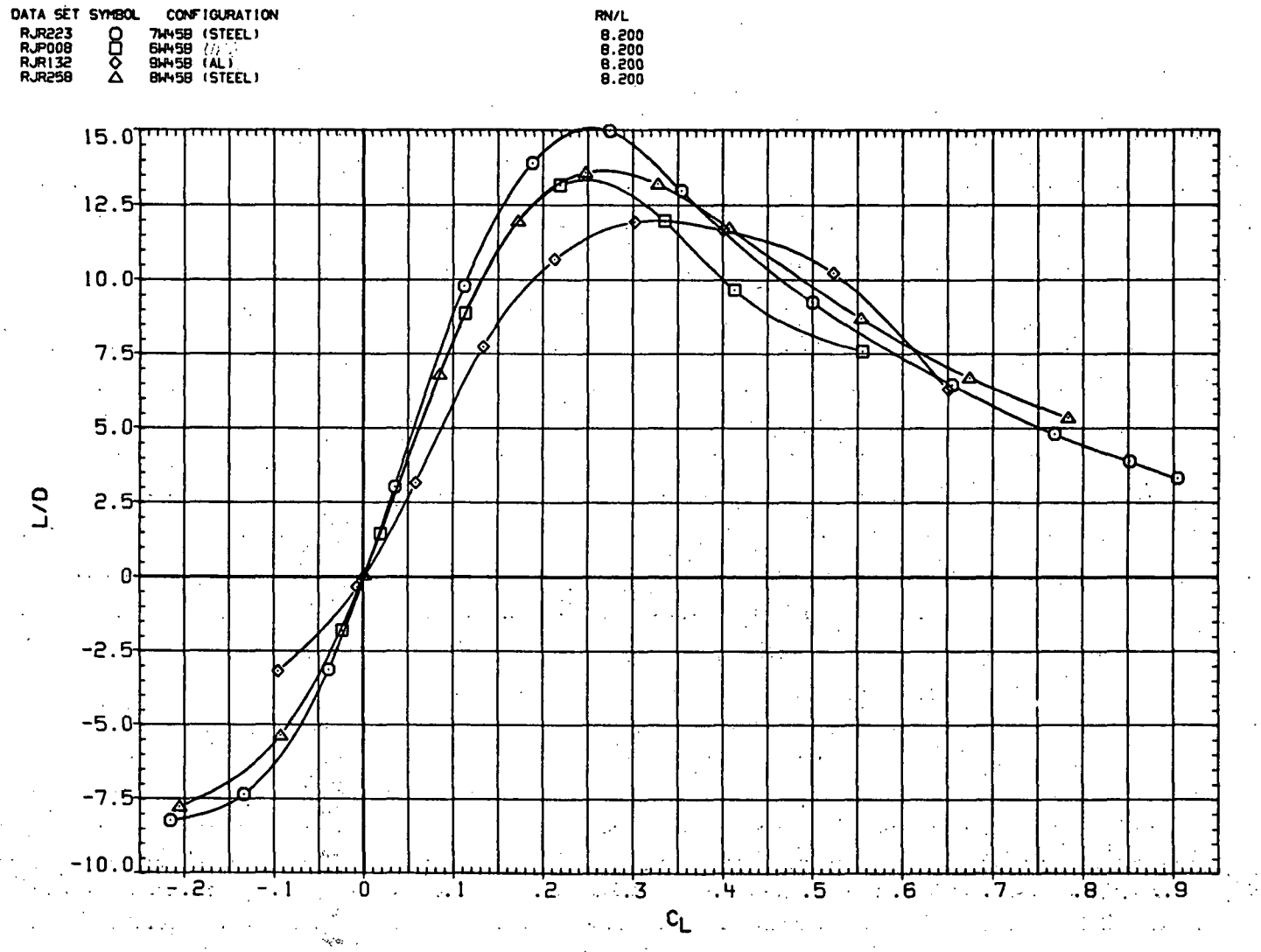

(d) L/D vs C_L.

Figure 99.– Continued.

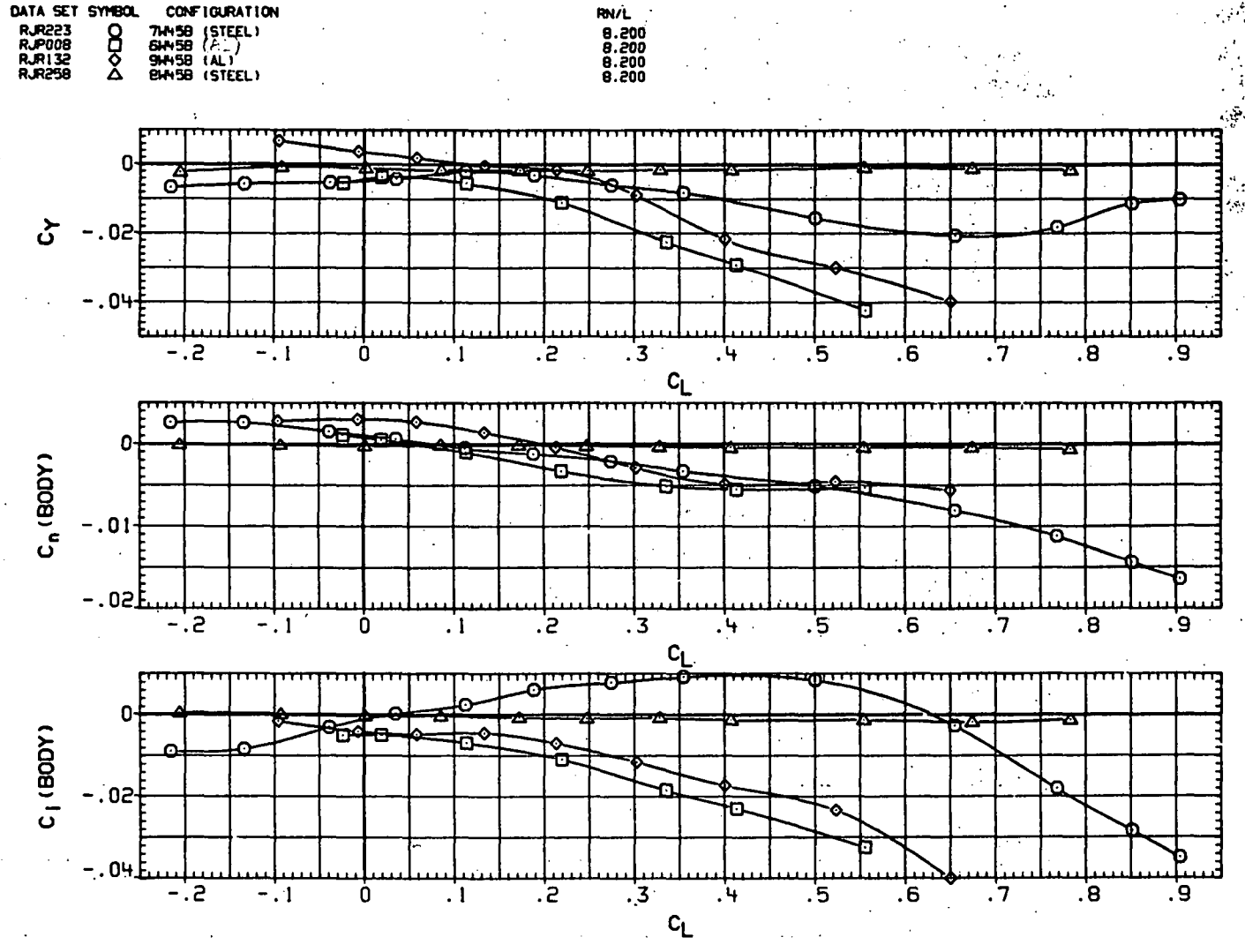

(e) C_Y, C_n and C_ℓ vs C_L.

Figure 99.– Concluded.

*U.S. GOVERNMENT PRINTING OFFICE: 1977 - 735-004/14

NATIONAL AERONAUTICS AND SPACE ADMINISTRATION
WASHINGTON, D.C. 20546

OFFICIAL BUSINESS
PENALTY FOR PRIVATE USE $300

SPECIAL FOURTH-CLASS RATE
BOOK

POSTAGE AND FEES PAID
NATIONAL AERONAUTICS AND
SPACE ADMINISTRATION
451

U.S.MAIL

POSTMASTER: If Undeliverable (Section 158 Postal Manual) Do Not Return

"The aeronautical and space activities of the United States shall be conducted so as to contribute . . . to the expansion of human knowledge of phenomena in the atmosphere and space. The Administration shall provide for the widest practicable and appropriate dissemination of information concerning its activities and the results thereof."

—NATIONAL AERONAUTICS AND SPACE ACT OF 1958

NASA SCIENTIFIC AND TECHNICAL PUBLICATIONS

TECHNICAL REPORTS: Scientific and technical information considered important, complete, and a lasting contribution to existing knowledge.

TECHNICAL NOTES: Information less broad in scope but nevertheless of importance as a contribution to existing knowledge.

TECHNICAL MEMORANDUMS: Information receiving limited distribution because of preliminary data, security classification, or other reasons. Also includes conference proceedings with either limited or unlimited distribution.

CONTRACTOR REPORTS: Scientific and technical information generated under a NASA contract or grant and considered an important contribution to existing knowledge.

TECHNICAL TRANSLATIONS: Information published in a foreign language considered to merit NASA distribution in English.

SPECIAL PUBLICATIONS: Information derived from or of value to NASA activities. Publications include final reports of major projects, monographs, data compilations, handbooks, sourcebooks, and special bibliographies.

TECHNOLOGY UTILIZATION PUBLICATIONS: Information on technology used by NASA that may be of particular interest in commercial and other non-aerospace applications. Publications include Tech Briefs, Technology Utilization Reports and Technology Surveys.

Details on the availability of these publications may be obtained from:

SCIENTIFIC AND TECHNICAL INFORMATION OFFICE

NATIONAL AERONAUTICS AND SPACE ADMINISTRATION

Washington, D.C. 20546